Can geodiversity help to save the soil archives?

Seijmonsbergen, A.C.; van den Ancker, J.A.M.; Jungerius, P.D.; Norder, S.J.

DOI
10.1016/B978-0-444-64108-3.00008-2

Publication date
2019

Document Version
Final published version

Published in
Reading the soil archives

DEVELOPMENTS IN **QUATERNARY SCIENCE** 18
SERIES EDITOR: JAAP J.M. VAN DER MEER

READING THE SOIL ARCHIVES

UNRAVELING THE GEOECOLOGICAL CODE OF PALAEOSOLS AND SEDIMENT CORES

EDITED BY
JAN M. VAN MOURIK AND JAAP J.M. VAN DER MEER

ELSEVIER

READING THE SOIL ARCHIVES

This page intentionally left blank

Developments in Quaternary Science

Volume 18

READING THE SOIL ARCHIVES

UNRAVELING THE GEOECOLOGICAL CODE OF PALAEOSOLS AND SEDIMENT CORES

Edited by

JAN M. VAN MOURIK
Institute for Biodiversity and Ecosystem Dynamics (IBED), University of Amsterdam, the Netherlands

JAAP J.M. VAN DER MEER
School of Geography
Queen Mary
University of London
London, United Kingdom

ELSEVIER

Elsevier
Radarweg 29, PO Box 211, 1000 AE Amsterdam, Netherlands
The Boulevard, Langford Lane, Kidlington, Oxford OX5 1GB, United Kingdom
50 Hampshire Street, 5th Floor, Cambridge, MA 02139, United States

Notices
Knowledge and best practice in this field are constantly changing. As new research and experience broaden our understanding, changes in research methods, professional practices, or medical treatment may become necessary.

Practitioners and researchers must always rely on their own experience and knowledge in evaluating and using any information, methods, compounds, or experiments described herein. In using such information or methods they should be mindful of their own safety and the safety of others, including parties for whom they have a professional responsibility.

To the fullest extent of the law, neither AACCI nor the Publisher, nor the authors, contributors, or editors, assume any liability for any injury and/or damage to persons or property as a matter of products liability, negligence or otherwise, or from any use or operation of any methods, products, instructions, or ideas contained in the material herein.

Library of Congress Cataloging-in-Publication Data
A catalog record for this book is available from the Library of Congress

British Library Cataloguing-in-Publication Data
A catalogue record for this book is available from the British Library

ISBN: 978-0-444-64108-3

ISSN: 1571-0866

Publisher: Candice Janco
Acquisition Editor: Amy Shapiro
Editorial Project Manager: Charlotte Rowley
Production Project Manager: Selvaraj Raviraj
Cover Designer: Miles Hitchen

Typeset by TNQ Technologies

Contents

Contributors

D.J.G. Braekmans Cranfield Forensic Institute, Cranfield University, Cranfield, United Kingdom

S.P.C. de Goede Department of Ecosystem and Landscape Dynamics, Institute for Biodiversity and Ecosystem Dynamics, University of Amsterdam, Amsterdam, the Netherlands

S.J. de Vet Naturalis Biodiversity Center, Leiden, the Netherlands

I.K. de Wolf Institute for Biodiversity and Ecosystem Dynamics, University of Amsterdam, Amsterdam, the Netherlands

M. Doorenbosch Faculty of Archaeology, University Leiden, The Netherlands

M.J. Roces Hernandez Universidad Politécnica de Cartagena, Cartagena, Spain

H. Hooghiemstra Department of Ecosystem and Landscape Dynamics, Institute for Biodiversity and Ecosystem Dynamics, University of Amsterdam, Amsterdam, the Netherlands

B. Jansen Department of Ecosystem and Landscape Dynamics, Institute for Biodiversity and Ecosystem Dynamics, University of Amsterdam, Amsterdam, the Netherlands

P.D. Jungerius Geoheritage NL, Ede, the Netherlands

K. Land Institute for Biodiversity and Ecosystem Dynamics, University of Amsterdam, Amsterdam, the Netherlands

C.N.H. McMichael Institute for Biodiversity and Ecosystem Dynamics, University of Amsterdam, Amsterdam, the Netherlands

S.J. Norder Theoretical and Computational Ecology (TCE), University of Amsterdam, Amsterdam, the Netherlands; Centre for Ecology, Evolution and Environmental Changes (cE3c)/Azorean Biodiversity Group, Faculdade de Ciências, Universidade de Lisboa, Lisboa, Portugal

T. Reimann Soil Geography and Landscape Group & Netherlands Centre for Luminescence Dating, Wageningen University, Wageningen, the Netherlands

A.C. Seijmonsbergen Theoretical and Computational Ecology (TCE), University of Amsterdam, Amsterdam, the Netherlands

J. Sevink Institute for Biodiversity and Ecosystem Dynamics (IBED), Faculty of Science, University of Amsterdam, Amsterdam, the Netherlands

H.J. Streurman Centre for Isotope Research, University of Groningen, Groningen, the Netherlands

J.A.M. van den Ancker Geoheritage NL, Ede, the Netherlands

J.J.M. van der Meer School of Geography, Queen Mary, University of London, London, United Kingdom

J. van der Plicht Centre for Isotope Research, University of Groningen, Groningen, the Netherlands

J.M. van Mourik Institute for Biodiversity and Ecosystem Dynamics (IBED), Faculty of Science, University of Amsterdam, Amsterdam, the Netherlands

J. Wallinga Soil Geography and Landscape Group & Netherlands Centre for Luminescence Dating, Wageningen University, Wageningen, the Netherlands

This page intentionally left blank

Dedication

Technicians and laboratory assistants are vital to our work; they spend time with us in the field and have skills and time to do all the routine lab work that we as scientists don't have time for. They must absolutely be acknowledged for their contribution.

For the research of soil archives support by professional technicians is indispensable. They are responsible for the production of thin sections, pollen and phytoliths preparation and chemical analysis. We express our gratitude to

- Cees Zeegers, Frans Bakker (thin section grindery, UvA) and Adrian Palmer (RHUL) for the production of thin sections (Chs. 1, 2, 3, 4, 6)
- Annemarie Philip (palaeo-botanical laboratory, UvA) for the production of pollen and phytoliths slides in the IBED pollen lab (Chs. 2, 3, 4, 5, 6, 7)
- Leo Hoitinga (soil chemical laboratory, UvA) for soil chemical analysis (Ch. 6)
- Piet Wartenberg (soil chemical laboratory, UvA) for the preparation of the soil organic carbon fractions (Ch. 3)
- Joke Westerveld (soil chemical laboratory, UvA) for the production of biomarker extracts (Ch. 5)
- Roel van Elsas (Mineral Separation Laboratory, Free University Amsterdam, VU) for the heavy mineral separations (Ch. 6).
- Ruud Hendrikx (Materials Science and Engineering of Delft University of Technology, TUD) for the X-ray analysis (Ch. 6).
- Jan van Arkel (digital illustrator IBED, UvA) for the upgrade of older and creation of new illustrations (Chs. 1, 2, 3, 4, 5, 6).

This page intentionally left blank

Introduction

The earth's surface is subject to endogenic and exogenic processes that create landforms and soils. Scientists of ancient civilizations have already tried to explain the essentials of the planet earth system and during the last few centuries disciplines like geology, physical geography, geomorphology, pedology, hydrology, geoecology and archaeology developed and contributed to the understanding of the processes responsible for the dynamics of ecosystems and landscapes.

In the 19th century, Charles Darwin and Alexander von Humboldt stimulated earth surface science by the introduction of the concepts of evolution and zonality of landscapes. William Davis developed the principle of landform evolution and Von Humboldt was the instigator of the zonal soil map. Physical maps of the earth's surface (e.g., climate, vegetation, geomorphology and soils) were produced and the research focused on the explication of zonal differentiation and landscape evolution. Mapping was at that time a scientific discipline. Maps give people a lot of information about their livelihood but then the demand increased to understand more about the potentials and risks of land use.

The oldest analytical technique concerned the microscopic determination of rocks and minerals. This knowledge was highly appreciated by society because of the economic value of jewels, ore and raw materials. The invention of the microscope stimulated mineralogy and in the 19th century textural and mineral analyses of soil and sediment became common research methods. The study of earth surface materials came in and accelerated in the 1950s when innovative analytical techniques became available (Fig. 1).

FIGURE 1 Professor Jan Pieter Bakker introduced sample analysis and founded the Laboratory for Physical Geography and Soil Science of the University in Amsterdam (UvA) in 1963.

The editors of this book are alumni of the UvA where J.P. Bakker founded the Laboratory of Physical Geography and Soil Science. Bakker added the analysis of earth surface materials to quantify the impact of landscape-forming processes to traditional landscape description and mapping in physical geography. He stimulated the measurement of, for instance, 'regular'

abiotical soil parameters, the analysis of light and heavy minerals, X-ray diffraction of clay minerals and embraced other upcoming new techniques. Starting after World War II in a provisional utility he opened a fully equipped brand-new laboratory in 1963 and over several decennia this laboratory was trendsetting in northwest Europe in the field of physical geography.

Bakker stimulated his students to study an optional technique somewhere else and then apply this new expertise in his laboratory. In this way he created a group of researchers specializing in mineralogy, clay mineralogy, pollen analysis, diatom analysis and soil micromorphology. The physical geographical tradition of Bakker's lab at the UvA has been described by Jungerius (2004). Reorganizations of the system of higher education in the Netherlands had an impact on the departments of physical geography. At UvA, the physical geography department moved from the faculty of geographical sciences to the brand-new Institute for Biodiversity and Ecosystem Dynamics and consequently the cooperation with human geography and archaeology came to an end. The integration with biology and environmental chemistry was supposed to keep earth surface science as part of environmental research (van Mourik, 2004). Most of the new techniques, which over several decennia developed as an academic discipline (similar to soil mapping and geomorphological mapping), survived as 'not more than a scientific tool'.

It is thus not surprising that alumni of Bakker learned to translate a research question or hypothesis concerning the development of landscape and soil in a research proposal, including mapping, profile selection and sampling for multiproxy analysis.

Between 1970 and 2010 most of the traditional manual lab procedures were replaced by autoanalysers and new techniques like electron microscopy became available. Master students, continuing as PhD students and postdocs, improved their research by applying these new analytical possibilities. For some of them it was a challenge to resample polycyclic soil profiles (natural soil archives) to apply new techniques and achieve more insight into their genesis. Actually, the ongoing introduction of techniques creates cyclical research (Fig. 2). The first editor of this book was such a student and during the last decennia he took the opportunity to advocate this approach in several sessions of the European Geosciences Union (EGU).

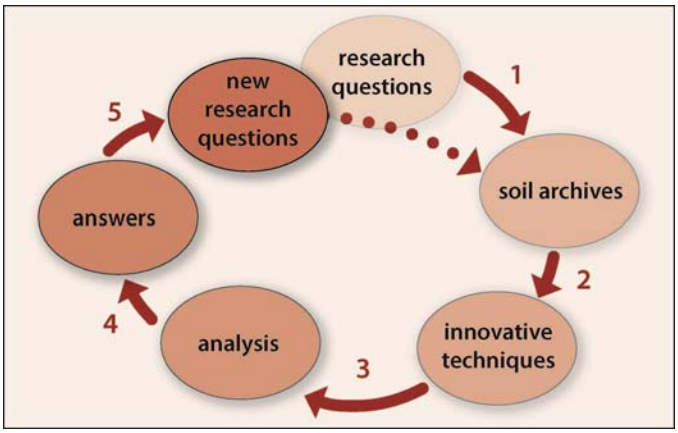

FIGURE 2 Back to the soil archives for the application of innovative techniques to find new answers.

During the General Assembly 2012 of the EGU the subdivision Soils as a Record of the Past (in 2015 renamed as Soils as Records in Time and Space) was founded (Kluiving et al., 2015). The main mission of this subdivision was to create oral and poster sessions focusing on the results of studies utilizing soils as natural archives. The subdivision focused on:

1. Soils and palaeosols that provide information related to soil genesis and landscape evolution;
2. Results of analysis of soil records that may be relevant for disciplines such as soil science, geomorphology, archaeology and landscape ecology;
3. Various analytical techniques that are available to 'read' the soil records;
4. Bringing together disparate information from various soil records to contribute effectively to studies of the evolution of natural and cultural landscapes;
5. Environmental change, whether caused by natural or by human processes, that impact on landscape evolution. Environmental change can be recorded in sediments, especially peat and lake deposits, but also in (palaeo)soils. Consequently, soils and palaeosols may contain geoecological and geoarchaeological archives;
6. The results of soil archive analysis are helpful in sustaining the studies of earth surface processes, global change and archaeological reconstructions.

In 2016 we decided to write this book *Reading the Soil Archives* to advocate the techniques and the scientific proceeds of multiproxy analysis of soil archives. This book aims to inform students and researchers in earth surface sciences about the multiproxy analysis of soil archives. A successful study of soil archives requires knowledge of the sample material, knowledge of analytical techniques and knowledge of the complexity of the interpretation of results.

- Chapter 1 is dedicated to the principles of soil micromorphology, a technique mainly developed since the 1960s. The case studies demonstrate the value of soil micromorphology in finding answers to pedological and geomorphological questions.
- Chapter 2 is dedicated to soil pollen analysis. Pollen analysis of limnic deposits and peat was introduced at the beginning of the 20th century, but the first results of pollen analysis of soils appeared in the 1960s. Without knowledge of the processes of infiltration and conservations of pollen in soil, achieved by micromorphological analysis, a reliable interpretation of soil pollen spectra is not possible.
- Chapter 3 is dedicated to the radiocarbon dating of soil organic carbon, a technique that was introduced around 1950. Interpretation of ^{14}C dates of soil samples is complicated and requires not only detailed knowledge of the dating process itself but also of the properties of the sampled profile and the extraction methods of soil organic carbon from soil samples.
- Chapter 4 is dedicated to optically stimulated luminescence dating. This technique became available in the 1990s. Also for this dating technique it is valid that detailed knowledge of the technique and the sample properties are crucial for the interpretation of the dates. The case studies of polycyclic driftsand deposits and plaggic Anthrosols demonstrate the differences in ages of organic and mineral fractions of soil samples and how to interpret this in the context of soil genesis.
- Chapter 5 is dedicated to biomarker analysis of soil archives, introduced in earth surface studies in the first decennium of the 21st century. This technique is still in a juvenile stadium of development and the interpretation of the biomass spectra requires more references, but the first results are promising. Biomarker analysis, applied to

samples of soil archives, provides relevant information as an extra to pollen analysis.
- Chapter 6 is dedicated to pedogenic provenance analysis. The case studies demonstrate how techniques like SEM-EDX and WD-XRF are helpful to answer questions about the provenance of elements and soil materials.
- Chapter 7 is dedicated to phytoliths analysis. This technique developed in biological and ecological science and was introduced to earth surface studies like archaeology in the 1980s. In soil archives where pollen is absent due to humification and mineralization, phytoliths analysis is a promising method to generate information on the vegetation that played a role during soil genesis.
- Chapter 8 is dedicated to soil archives as part of the geoheritage. Techniques are available to make multidisciplinary inventories of the geodiversity, and areas with a specific geodiversity can be indicated as potential geoparks. The question that arises is whether the soil archives are safe in such parks or need more local and legal protection. It is important that scientists convince politicians to take care of our geoheritage not only for the conservation of unique landscapes, including the soil archives, but also for future geoecological research to unravel the remaining secrets of the geoecological code.

Jan M. van Mourik
Jaap J.M. van der Meer

References

Jungerius, P.D., 2004. De Fysisch Geografische traditie. In: Knippenberg, H., Schendelen, van M. (Eds.), Alles Heeft Zijn Plaats. Askant, Amsterdam, pp. 457–481.

Kluiving, S.J., van Mourik, J.M., Zaccone, C., 2015. Man versus nature: natural and anthropogenic footprints recorded in the soil archives. Catena 132, 69–71.

van Mourik, J.M., 2004. Nieuwe perspectieven voor de fysische geografie binnen IBED? In: Knippenberg, H., Schendelen, van M. (Eds.), Alles Heeft Zijn Plaats. Askant, Amsterdam, pp. 483–529.

CHAPTER

1

Soil micromorphology

J.J.M. van der Meer[a,*], *J.M. van Mourik*[b]

[a]School of Geography, Queen Mary, University of London, London, United Kingdom; [b]Institute for Biodiversity and Ecosystem Dynamics (IBED), Faculty of Science, University of Amsterdam, Amsterdam, the Netherlands

*Corresponding author. jjmvdmeer@gmail.com

1.1 Introduction

When studying soils or palaeosols in the field, we are limited by our eyes as to what we can see. A hand lens will help, but because the soil is usually moist and the soil particles and constituents cover each other, we can only see so much. From the beginning there has always been a desire and a need to see more, and researchers started to take samples into laboratories. Separating the samples into fractions and cleaning them allowed the mineralogy of individual particles to be determined. What this does not allow is to establish the relations between particles. For this reason, Kubiena (1938, 1956) established a method of impregnating undisturbed samples with a resin and − after curing −preparing thin sections from them. Studying the thin sections under a low-powered microscope (plane light and crossed polarizers) allowed scientists to study (1) the composition of the material, (2) the spatial relations between particles and (3) the temporal relations (stratigraphy) between particles. Initially, micromorphology developed as an instrument to support soil classification. By fully describing the thin sections a proper understanding of the make-up of that soil, as well as the processes that are or have been active within it, can be achieved. After WWII the use of thin sections became first a 'science' in itself, before it developed into a standard research technique. By now many major soil groups had been described and analysed, although not completely and not exhaustively. There is still a lot of work to do (Stoops, 2010). The technique has also been applied in archaeology (Courty et al., 1989) and sedimentology (van der Meer and Menzies, 2011).

In this chapter we will describe the technique and provide examples, while applications of micromorphology will appear throughout this volume.

1.1.1 Sampling for micromorphology

Although sampling for micromorphology entails taking samples to the lab, it is still considered a non-destructive research method. This is because samples are collected as cohesive blocks and never taken apart. To prevent samples from falling apart they are collected in containers. Traditionally, these containers consist of stainless steel or messing, but cardboard has been

Reading the Soil Archives
https://doi.org/10.1016/B978-0-444-64108-3.00001-X

used as well. The containers are made up of a hinged or flexible frame with two removable lids. The frame preferably has a cutting edge on one side. Without applying pressure the container is gradually cut into the soil profile until it is flush with the surface. Once it is cut free it is properly documented as to orientation and wrapped up for transport. It is important to retain field moisture conditions in the sample to prevent desiccation and collapse.

Because of the time it takes to prepare a thin section (see later) and the cost involved it is important to develop a sampling strategy. Depending on the purpose it may be enough to take only a sample of the B horizon, for instance, when wanting to establish the amount of clay illuviation. But if one wants to study the genesis of the whole profile it is imperative to sample all horizons as well as boundaries and transitions, including the parent material (Fig. 1.1.1), which allows for the production of either a horizontal or a vertical thin section, or both.

1.1.2 Thin section preparation

Over time the production of thin sections has changed. Keeping pace with the development of health and safety regulations, production changed from open labs to contained production in fume boards. Initially, samples were left to dry before impregnation because water impedes the penetration of resin into the sample. The downside of this was that clay-rich samples cracked extensively. To overcome this problem the alcohol replacement technique was developed. Because the resins used for impregnation are niche products for chemical companies, different resins have been used by the different laboratories.

Following impregnation the samples need to dry, and although heating the sample speeds up drying time, it also leads to cracking of the sample and thus curing is usually left to itself. Overall the production of a thin section from field to final product takes between 6 and 9 months.

1.1.3 Analysis

Thin sections are best described under a relatively low magnification. This way one can see the structure instead of just individual grains. In case the latter need to be studied, one changes to a microscope with higher resolution.

Analysis starts with macroscopic characterization. This way, larger structures are noted, because one can lose the overview when using the microscope. Microscopic description consists of several sections. The first concerns the skeleton, subdivided into lithic and humic components. The

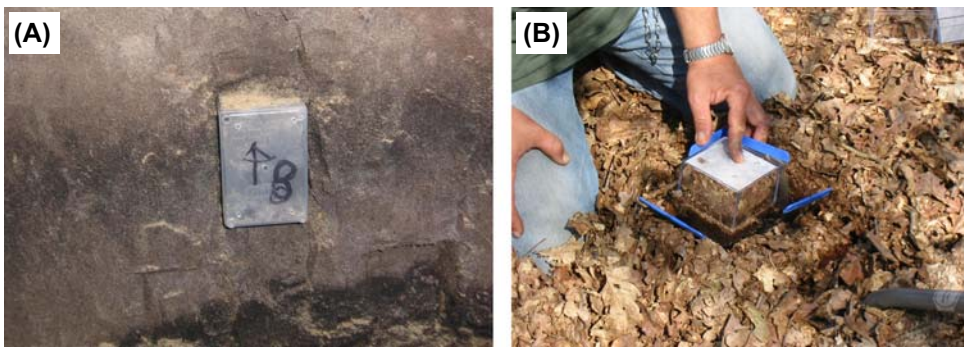

FIGURE 1.1.1 Sampling for micromorphology. (A) Vertical sampling of the 3Ah horizon of profile Defensiedijk 1. (B) Surface sampling of the Mormoder of profile Nabbegat (which allows for the production of either a horizontal or a vertical thin section, or both).

second is the plasma, in fact this material is smaller than the thickness of the thin section (c.26 μm) because the particles cannot be seen individually. Next are the voids and related distribution pattern. For all of these note is taken of the size, shape, distribution and where applicable composition. The last section deals with special features like coatings, crystallaria, faecal pellets, etc.

Only after a full description is made of all the thin sections of one profile can the analysis begin.

When studying the micromorphological literature it must be realized that there has been a substantial change in terminology. The terminology that is currently in use was published by Bullock et al. in 1985 and standardized by Stoops (2003). Prior to that the terminology of Brewer (1964) was in use.

1.2 Micromorphological features

Because there is an extensive volume on micromorphology of soils and regoliths (Stoops et al., 2018) we will try not to summarize it here. Instead, we will highlight the groups in which micromorphological features can be distinguished. These features are the result of a number of processes.

1.2.1 Sedimentation

Sediment accumulates in a number of different environments, like glacial, aeolian and marine. Each environment produces sediments in a variety of ways, from bedded or laminated to massive. Furthermore, most environments sort sediments by grain size, from homogeneous to mixed. Thus all sediments possess micromorphological features (van der Meer and Menzies, 2011), most certainly an arrangement of particles, the fabric. Depending on the stresses that have acted on the sediment, sediments can also have a striated B-fabric (Fig. 1.2.1). This can be due to static loading, in which the particles in clay beds will become oriented when the sediment pile grows. If, in addition to loading, there is also a horizontal component, different types of B-fabrics can develop. A horizontal component can be present because of slope movement, faulting or drag underneath a glacier. Because sediments are not chemically inert, there can also be translocation of material like carbonates, iron compounds and clay particles.

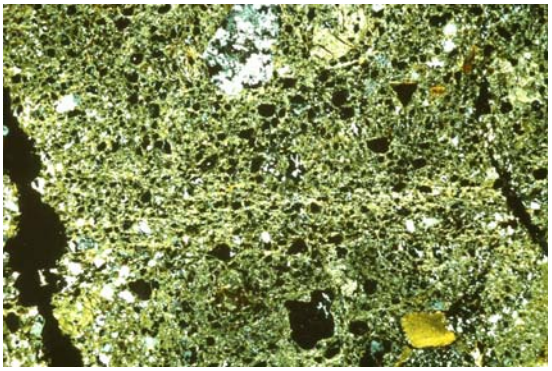

FIGURE 1.2.1 Striated B-fabrics in a Saalian till in the Netherlands, demonstrating that sediments contain micromorphological features prior to soil formation. Xpol, horizontal field of view (hfov) 18.0 mm.

Before soil formation starts in sediments the latter possess a wide variety of micromorphological features; soil formation does not start on a blank canvas. Depending on the age of soils, inherited, sedimentary micromorphological features can still be present. Unfortunately, in many micromorphological descriptions the C horizon has not been included, which precludes detecting inherited features in the soil.

1.2.2 Stresses

Soils are subject to all kind of stresses. As such we can mention stresses caused by slope movement, compaction, swelling and shrinking, frost, crystal growth, etc. These stresses affect especially the orientation of clay particles. Clay particles have a high birefringence but are too small

to be seen individually in thin section. Through (re-)orientation by stresses the clay particles align and thereby oriented domains become visible under crossed polarizers. The oriented domains occur in different parts of the soil, although they are rare in the A horizon. Lower down they can occur dispersed throughout the groundmass, along voids or parallel to skeleton grains. Particular orientation patterns cannot uniquely be assigned to particular processes because different processes can result in the same distribution pattern. Almost all soils will show striated B-patterns, but the strength and frequency are highly variable. In the first place it depends on the amount of clay; if there is only a small amount of clay in a soil it is difficult for the particles to form domains that are large enough to be seen. Furthermore, the strength of the stresses and their duration play a role. Finally, in calcareous soils they may be present but difficult to detect because carbonates undo the polarizing effect of the microscope.

1.2.3 Solution and (re)deposition

There are quite a few soluble components in soils like salts or metal compounds. Depending on conditions like pH these components can go in solution and be moved around within or out of the soil with percolating groundwater. This means that movement can be in any direction, although it is usually downward or downslope. While some components (like NaCl) are not widespread, carbonates are. Many sediments contain carbonates which then become incorporated in the developing soil. When carbonates go into solution, they will move until the local conditions change and they precipitate again. In this way nodules or coatings are formed. The same goes for Fe or Mn compounds, which mottle the soil upon fallout and tend to obscure visibility in the thin section.

Apart from components in solution, particles can also be moved within and out of the soil system. Clay particles can be chemically separated and are small enough to be transported through voids by percolating water. Once the water drains into the groundmass the clay particles are plastered against the wall of the void and form a coating. Because the clay particles are aligned in the coating they are highly visible because of their birefringence (Fig. 1.2.2). It is not just clay particles that can be moved, silt particles can also move under the right circumstances and they do not need to be chemically separated. Silt coatings are known to form under periglacial conditions (van Vliet-Lanoë, 2010), not just in sediments but also in soils. In the latter they can also occur in arable lands under the

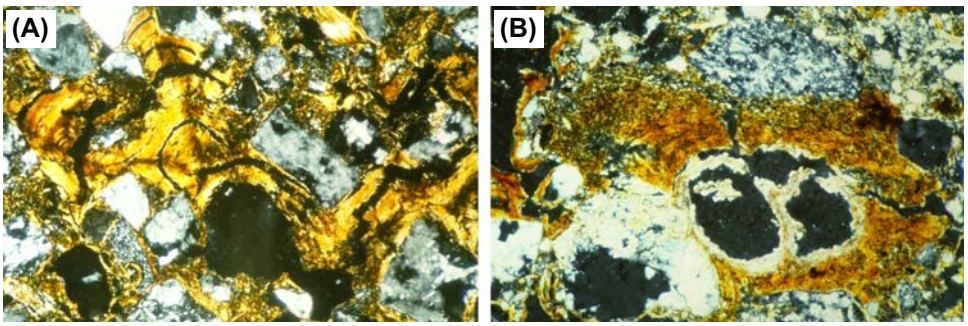

FIGURE 1.2.2 (A) Clay coating in an orthic Luvisol on a Late Glacial beach barrier dune north of Lake Neuchatel, Switzerland. (B) Carbonate coating on a clay coating in a calcaric Phaeozem on a Holocene beach barrier north of Lake Neuchatel, Switzerland. Hfov for both is c.0.9 mm.

right physical conditions. Furthermore, humic material can be translocated and form coatings around skeleton grains.

1.2.4 Weathering

Alteration of bedrock leads to the formation of soils in situ, although slope movement ensures that the weathering products do not necessarily lead to soil in the same spot. But weathering is not restricted to bedrock; sediments will weather as well. Apart from breaking up bedrock, weathering also leads to the transformation of minerals and the liberation of nutrients. None of the processes above could occur without weathering.

1.2.5 Future developments

Micromorphology is essentially 2D, but there is a need for 3D information on structures, especially voids, because of, for instance, connectivity. It has been thought that this could be achieved by making multiple parallel thin sections from the same impregnated block. However, because with each cut one loses a minimum of 3 mm, it is difficult to follow the same structure from one thin section to the next. More recently, μCT-scanning has become available, whereby multiple X-rays produce a complete 3D record of a sample (for instance, Ngom et al., 2011). Of course, one cannot use optical properties of minerals, but density differences between the different components of the sample reveal the structure. Because the whole scan exists in digital form, one can do volumetric calculations. Combining a thin section with the scan determines which mineral gives which grey tone in the scan. Because the scan shows the position of dense minerals relative to voids, one can assess the potential for, for instance, the release of heavy metals.

There are many applications of micromorphology in pedological studies.

1.3 Soil micromorphology supports reconstructing geomorphological development

When mapping soils in a part of the western Swiss Plateau, one of the emerging problems was whether there was systematically enough clay illuviation to mark soils as Luvisols instead of Cambisols (FAO, 1968). All of this area was glaciated during the last glacial, which left tills and slope deposits derived thereof as the parent material for soil formation. Soils started to form in the lateglacial and continued throughout the Holocene.

Studying soils in profile pits only occasionally allowed classification on the basis of macroscopic observations. Obviously, granular analysis does not help because it does not separate illuviated clay from clay content of the parent material. But it did show that in 12 analysed profiles, clay content of the B horizon varied between 13.5% and 27.5%, thus there is no shortage of clay. Micromorphology was a standard technique in this study and thin sections were prepared for most profiles. To get a better grip on clay illuviation it was decided to use point count analysis, and by using an ocular fitted with a Σ pattern with tics, 1000 points were counted in each thin section. Each tic on the pattern records what is underneath, in this case coating, matrix, skeleton, void and others. The result was that in 13 profiles the percentage illuviated clays varied between 1.2 and 31.5 (van der Meer, 1982). The next question that arose concerned the relation between time and clay illuviation. Were the soils with the highest percentage illuviated clay the oldest with the longest continuous translocation process or did they occur because of favourable conditions? Fortunately, an age could be assigned to some profiles because they were on archaeological sites or because pollen analysis allowed the soil to be bracketed (for instance, by analysing peat on either side of a beach barrier; van der Meer,

1976). It quickly appeared that in the soil with the highest percentage illuviated clay (Fig. 1.2.2) the surface could be dated to the Allerød and besides had a high permeability, which is a favourable condition. Although the outcome of the study was that in general – all other factors being equal – older soils have a higher percentage of illuviated clay, there was no linear trend. Another outcome was that the percentage of clay determined by granular analysis showed no relation to percentage of illuviated clay in thin section. Neither was there any relation between the depth of the peak percentage of clay in a profile and the peak in illuviated clay in thin section. In some profiles the peak in illuviated clay in thin sections was higher up in the profile than the peak in clay content, while in others it was reversed.

All of this seems fairly straightforward because the study area appears to be fairly uniform. However, to the east the Sarine river flows in an over 100 m deep box canyon (Fig. 1.3.1), which, given the full glaciation of the area, begs the question of the age of the canyon. It could have been incised throughout the Holocene to reach its current depth but for the presence of two fluviatile terraces in its deeper part (Fig. 1.3.1). The terraces are respectively 15 and 10 m above the valley floor. Soils on the terraces and in the valley floor were studied and it was clear that the soil on the lower terrace and certainly the soil in the valley floor were young to very young. However, the soil on the higher terrace showed evidence of a much higher age; with 15.8% illuviated clay in the thin section it could not be of a relatively young Holocene age (Fig. 1.3.2). Because of the level of soil development it was concluded that it must have started forming during the Older Dryas, i.e., around 11,800 BP. The Older Dryas is the first period in which valley aggradation can be surmised. As a consequence the box canyon cannot be of Holocene age, but must either have been present as a subglacial bedrock channel or must have formed rapidly in the few thousand years between deglaciation and the Older Dryas. The other possibility is that it is actually an older preglacial formation, which was subglacially filled with sediment and quickly

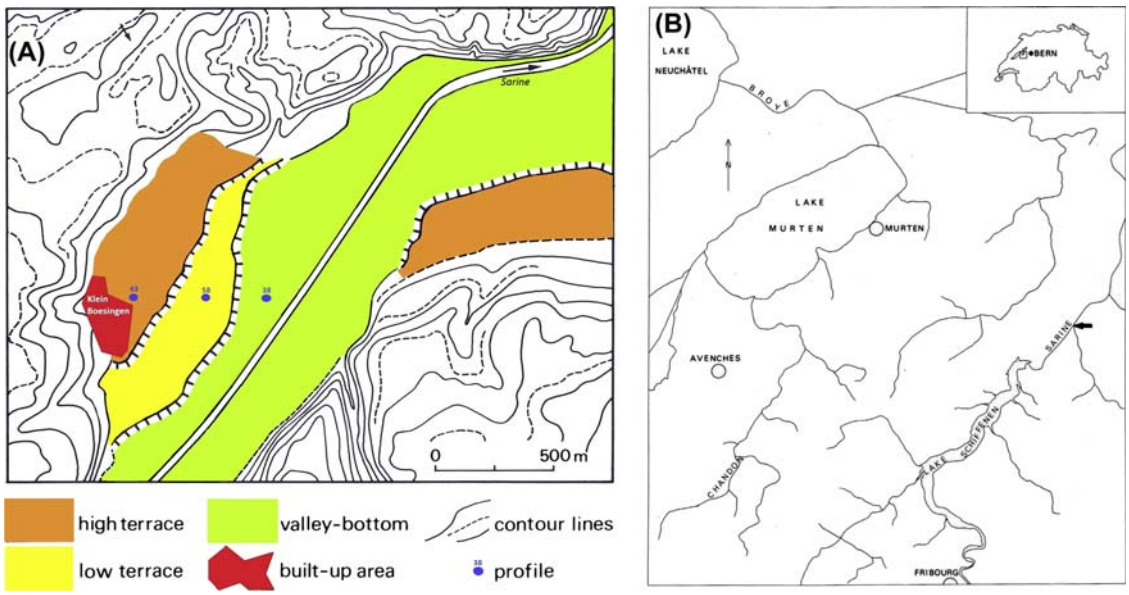

FIGURE 1.3.1 Location of soil profiles on terraces in the box canyon of the Sarine river, Switzerland.

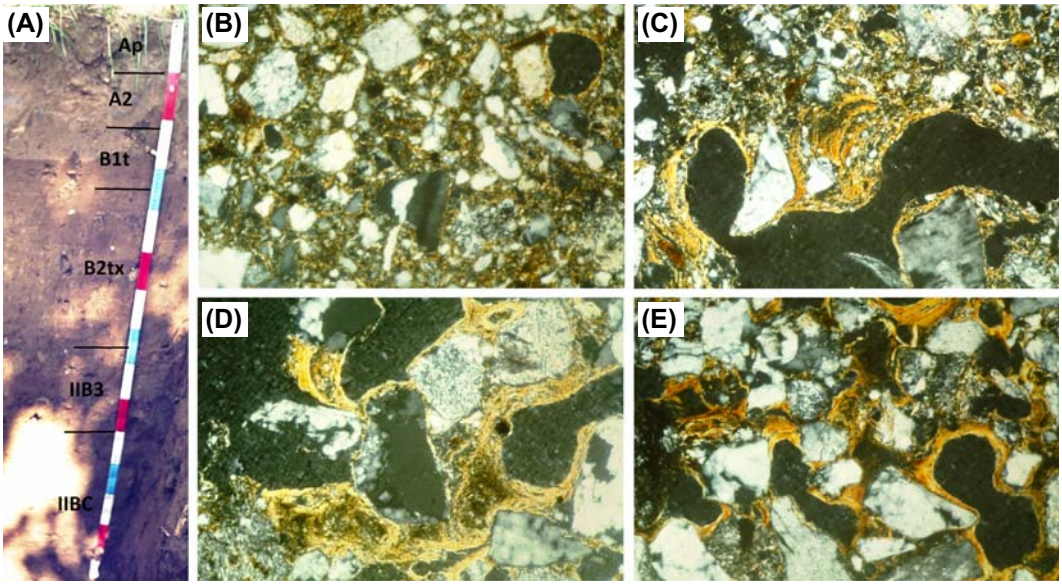

FIGURE 1.3.2 (A) Orthic Luvisol on a high terrace in the Sarine box canyon near Klein Boesingen, Switzerland. (B–E) Clay illuviation increases with depth: (B) 46 cm, (C) 65 cm, (D) 85 cm, (E) 114 cm. Xpol, hfov for all is c.0.9 mm.

cleared after deglaciation. Because there was no datable material around that could confirm the age of the terrace, the inferred age had to stand. There may be other terrace remnants in the upstream part of the canyon, but because it is largely flooded behind a series of barrier dams, they are inaccessible.

However, a couple of years ago, further upstream archaeologists found a site in the Sarine canyon consisting of a rock shelter on a comparable terrace that was assigned an early Mesolithic age and provided a ^{14}C date for the lowest hearth found of 8000 BP (Braillard and Mauvilly, 2008). These authors came to the conclusion that the box canyon must have formed in two phases of different speeds of incision: a lateglacial rapid phase, followed by a much lower rate after the canyon had become habitable.

We can conclude that it was soil development that first drew attention to the age problem of the canyon and that it was soil micromorphology that provided enough information to solve the problem.

1.4 Geogenic versus pedogenic clay translocation

Clay translocation is a common process in soils and consists of three steps: dispersion, transport and deposition. Dispersion, whereby clay particles are pried apart, is influenced by a number of properties like salt concentration, pH, Fe or Mn coating, clay minerals, for instance swelling or non-swelling clay, coarse or fine clay, etc. Once the clay particles are separated they can be transported by percolating water, either vertical in the profile or downslope. Transport is influenced by pore frequency, size and connectivity. Loss of water is one of the reasons why clay particles are deposited. Because this happens particle by particle and these are positioned parallel to and on top of each other, clay coatings become visible over time. Only when the coating is large enough can it be seen under the microscope, especially under crossed polarizers.

However, clay translocation is not exclusive to soils, but can also occur in sediments and in

bedrock. Under the right conditions, clay particles can be separated, albeit not by the same processes as in soils. Pressurized water can pry apart clay particles and if that water is moving it will transport these clay particles. When such sediments become subject to soil formations, such clay coatings or parts thereof can become incorporated in the soil and presumed to be due to pedogenic processes.

1.4.1 Rhine riverbed

Following devastating floods in 1953 the safety of the southwest Netherlands was secured by the construction of barriers across a number of major waterways. A side effect of this was that the Rhine started to build an 'internal' delta in many of these waterways, with sedimentation of up to 1 m per year. In the 1990s concern was raised about potential contamination (for instance, heavy metals) of these sediments and whether leaching might occur. Questions to be answered were, for instance, whether the sediments recorded continuous sedimentation or alternating sedimentation and erosion. There were also questions about the chemical stability of the sediments. A couple of cores were collected by Rijkswaterstaat (Office of Public Works) (Fig. 1.4.1A). The cores were all collected from open water with a permanent water depth of c.7 m. These sediments were always subaqueous and never exposed to air.

Altogether 20 mammoth thin sections (Fig. 1.4.1B) were prepared from these cores. The first answer to chemical stability came from thin section preparation: organic compounds within the sediments kept reacting with the resin, and curing of the samples only succeeded after gamma irradiation. Studying the thin sections it became clear that the sediments were chemically highly active with numerous neoformations like vivianite, gypsum, siderite and sulphide (van der Meer et al., 1994a,b). Nevertheless, it came as a surprise when in some of the samples carbonate coatings were observed in pores, while in one of the samples a clear clay coating was observed (Fig. 1.4.1C). At 7 m water depth and 3 m of sediment there must have been substantial hydrostatic pressure within the groundwater. However, for coatings to form the water must have been percolating as well. Fig. 1.4.1B shows a lot of pores, but it should be realized that many of these are related to the problematic preparation of the thin section and that actually pore connectivity is low. This may be the reason why only one example of a clay coating has been observed. Whereas the components for the neoformation are transported in solution, the clay particles are physically moved and need connected pores that are also wide enough.

1.4.2 Subglacial

Although hidden from view the subglacial environment must be rather wet. Streams emerge from it and anyone who has ever tried to walk up to a glacier with a sediment forefield will have been unpleasantly surprised how deep one can sink into that seemingly solid surface. Nevertheless, the general consensus is that a subglacial till is more or less impermeable and has a low hydraulic conductivity. Subglacial water is highly pressurized and can only go down and move toward the front, following the pressure gradient. There is also continuous production of meltwater and thus that water has to be evacuated. No one had ever looked at what was happening within the water-rich sediment underneath a glacier until micromorphology became applied as a common research tool. Now, we know that subglacial till is a highly complicated and well-structured sediment (Fig. 1.2.1; Menzies and van der Meer, 2018). It comes as no surprise that the highly pressurized water is capable of separating clay particles and transporting them. Today, many observations have been made of clay coatings in till

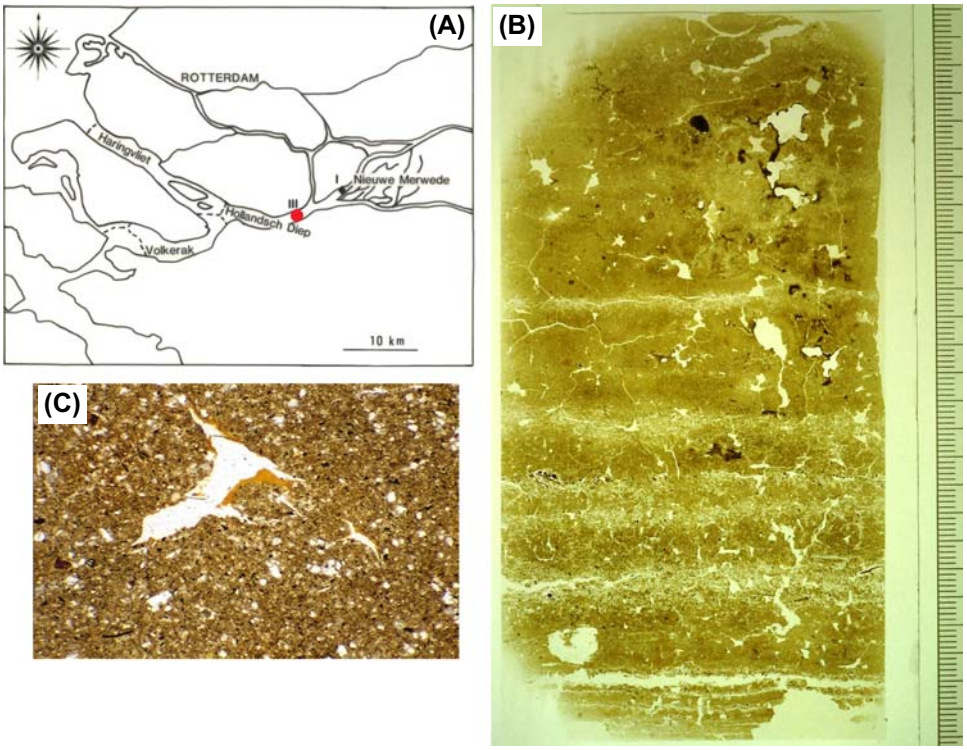

FIGURE 1.4.1 (A) Location map of Rhine riverbed cores in the southwest Netherlands. The *red dot* indicates the core from which this example comes. (B) Mammoth thin section from 300 to 315 cm depth in the core, scale in mm. (C) Clay coating in thin section (B). Hfov is 3.5 mm.

(Fig. 1.4.2), for instance, Rappol (1983). As the example in Fig. 1.4.2 shows, clay coatings forming in a subglacial till setting are continuously disrupted.

This is caused by the bed deforming as long as the overlying glacier is moving. Consequently, clay coatings are broken up and may even be completely obliterated and returned to the main

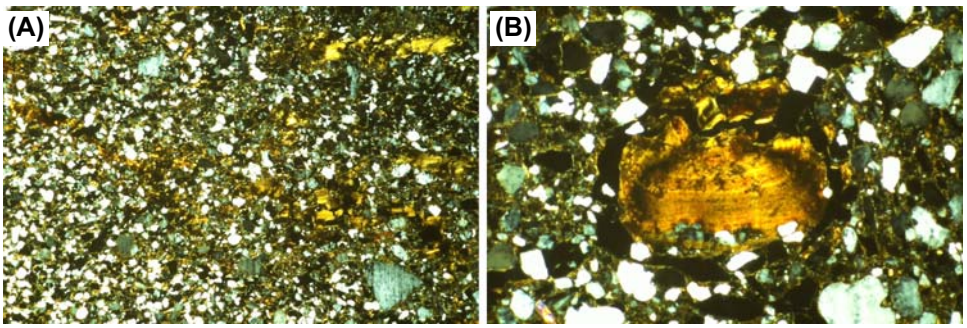

FIGURE 1.4.2 Subglacial till of Saalian age, Emmerschans, the Netherlands. (A) Zone with disrupted clay coatings. Xpol, hfov 11.2 mm. (B) Detached part of a clay coating incorporated in the till. Xpol, hfov 3.5 mm.

groundmass. Fig. 1.4.2B shows that such coating fragments can be very sturdy and should be able to survive the transition from sediment to soil.

When a glacier overlies bedrock the water becomes even more of a problem, depending on the permeability of the bedrock. If it is well fissured like a limestone, water can relatively easily dissipate and add to the groundwater body. But if the bedrock is denser or consists of very dense quartzites, different processes start to operate.

On the west coast of Ireland we recorded many sites where the bedrock (alternating quartzites and shales) is subglacially disrupted, i.e., glaciotectonized. One of these sites was Farrihy Bay, with a well-exposed coastal section (Fig. 1.4.3A). It shows on one end an upturned and curved slab of bedrock, while the other end appears to be unaffected and in situ. Close observations revealed that till had been squeezed in between bedrock layers. Alternatively, it could have formed more or less in situ by grinding the softer shale beds. With the help of an angle grinder it was possible to collect undisturbed blocks from which thin sections were made (Fig. 1.4.3B). The thin sections showed that the sample mainly consisted of rock fragments in an open frame network. In between

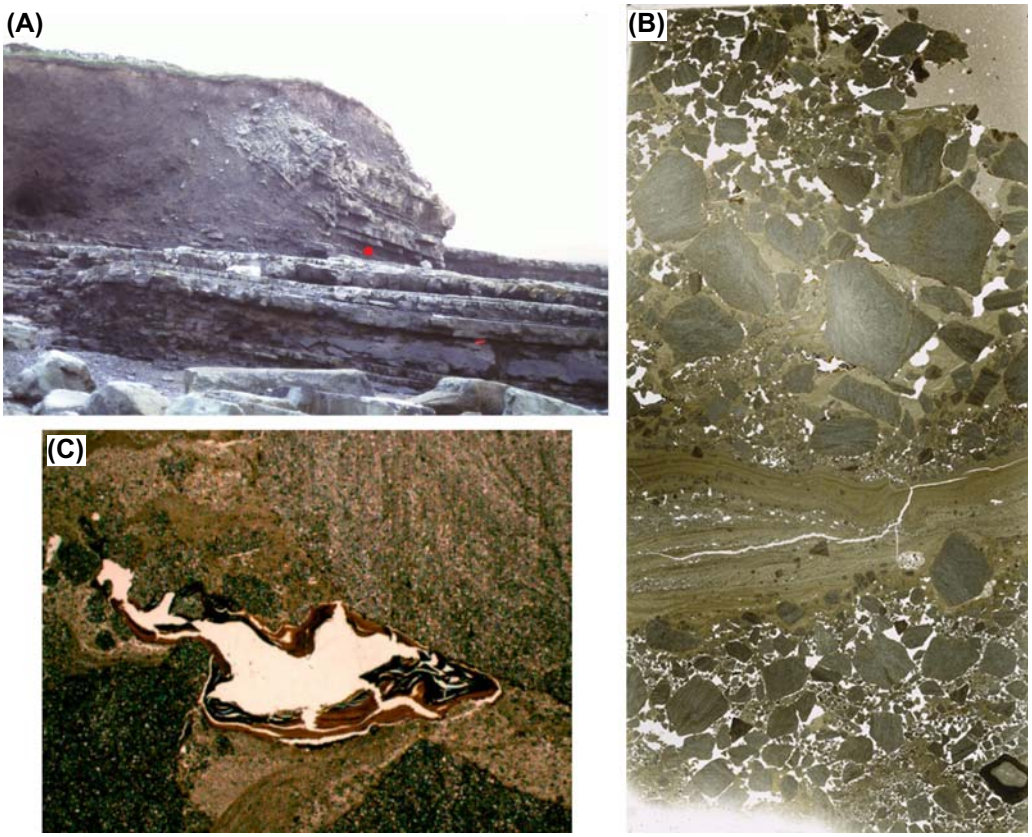

FIGURE 1.4.3 (A) Farrihy Bay, County Clare, west coast of Ireland. Glaciotectonized bedrock. The *red dot* is the thin section location. (B) Thin section of tectonized sediment formed between bedrock layers 14 cm high. (C) Clay coating with heavy Fe staining; from the center of (B). Hfov is 18.0 mm.

there were some fine-grained beds, some with current ripples. Most telling, however, were the widespread and heavily Fe-stained clay coatings in the pores (Fig. 1.4.3C). Samples were collected from more than one location and all showed the same features, demonstrating that pressurized subglacial water not only forms the clay coatings but is powerful enough to break up the bedrock.

1.4.3 Periglacial

It is well known that clays translocate easily under periglacial conditions (van Vliet-Lanoë, 2010 and references therein; van der Meer et al., 1992). This can be attributed to liquefaction at the surface and/or fast percolation of surface runoff after snowmelt (van Vliet-Lanoë, 2010). The low electrolyte content of snowmelt water seems to be able to disperse clay particles quickly. In northwest Europe, Saalian tills have been weathered to the extent that the residue is known as 'boulder sand' rather than boulder clay. Such weathering residues contain ample evidence of periglacial reworking with silt-droplet structure as well as clay coatings (van Beek, 1990), while there is no further evidence for soil formation and organic matter is completely absent.

Here we want to draw attention to a feature that so far has remained largely unknown. In the Allan Hills in the Antarctic, with a mean annual air temperature of −30°C, we observed the effects of running water (van der Meer and Barrett, unpublished data). All the observations pointed to the fact that under particular weather conditions, snow spots melted and the water ran off over the surface, not only over slopes forming small rills, but also as elongated drapes over vertical rock faces (Fig. 1.4.4A). The drapes on the

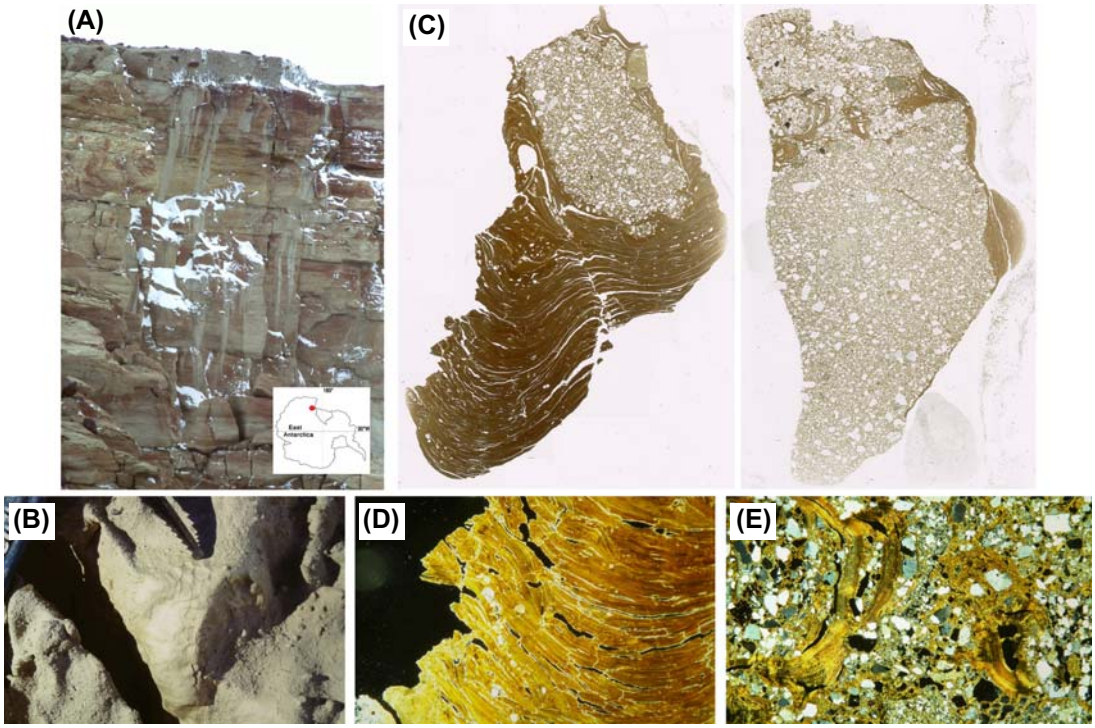

FIGURE 1.4.4 Clay coatings in the Allan Hills, Antarctica. The *red dot* in the inset map indicates the general location of the Allan Hills.

rock faces all stemmed from the overlying Tertiary Sirius tillite. Close-up inspection of the tillite surface showed it to be covered by a thick clay coating (Fig. 1.4.4B).

Thin sections have been prepared from blocks broken off the tillite/coating combination (Fig. 1.4.4C). What they show is that the coating on the surface consisted of multiple layers of clay (Fig. 1.4.4D), recording numerous events. However, they also showed that well-laminated clay coatings penetrated pores into the tillite matrix (Fig. 1.4.4E). Whereas the surface coatings are unlikely to survive transition to soil because they are most likely removed after a major change in climate, the in-pore coatings could easily become part of the soil and one would be hard put to tell the difference between geogenic and pedogenic coatings.

1.5 The micromorphological distinction between pedogenic and geogenic organic layers intercalated in polycyclic driftsand sequences

1.5.1 Introduction

Since medieval times, polycyclic driftsands have developed in cultural landscapes in northwestern Europe where the surface geology is dominated by lateglacial aeolian, medium fine, chemically poor coversands (Koster, 2010). During unstable periods in landscape evolution, sand drifting occurred, whereas during stable periods, soil formation took place. On sheltered sites, valuable soil archives arose in the form of polycyclic soils, consisting of inorganic sands intercalated with organic layers (Section 3.2). These provide unique palaeoecological records of alternating unstable (sand-drifting) and stable (soil-forming) phases in landscape evolution. The organic layers (or micropodzols) embedded in polycyclic sequences appear to be stratigraphic markers between various driftsand beds. Before we can use such layers as stratigraphic markers we must know if they are the result of local or regional processes and we must distinguish micropodzols as the result of soil formation during a stable phase and sedimentary organic layers as the result of eroded and redeposited organic horizons elsewhere. A complication is that recognition of pedogenic and sedimentary organic layers, intercalated in polycyclic sequences, cannot be based on field properties alone.

The study area of Weerterbergen (southeast Netherlands) is located a few kilometres southwest of the city of Weert (Fig. 1.5.1), and is part of an intensively studied driftsand landscape (van Mourik, 1988; van Mourik et al., 2012). In the Early Preboreal the aeolian activities were suppressed by vegetation development, starting with a pioneer steppe-like vegetation and succeeded by temperate deciduous forest (van Mourik et al., 2012). In prehistoric times the use of timber for fuel and for constructions, together with forest grazing and shifting cultivation, caused forest degradation and extension of partly degraded heaths. Local small-scale sand drifting, related to storms, forest fires and shifting cultivation, resulted in the deposition of pre-Medieval driftsand deposits. During the 11th–13th centuries, commercial logging of the remaining forests resulted in the first large-scale extension of the driftsand landscape and the deposition of medieval driftsands (van Mourik et al., 2012). Due to population growth the demand for food increased in the 18th century. Farmers started with the construction of larger stables and the use of heath sods to increase organic manure (Vera, 2011). This practice initiated the second large-scale extension of sand drifting and the deposition of post-Medieval driftsands. Holocene sand drifting transformed parts of the coversand landscape, consisting of coversand ridges, planes and valleys, into driftsand landscapes, consisting of deflation plains and complexes of sand covers and inland dunes. Polycyclic driftsand profiles consisting of various cycles of soil formation and deposition

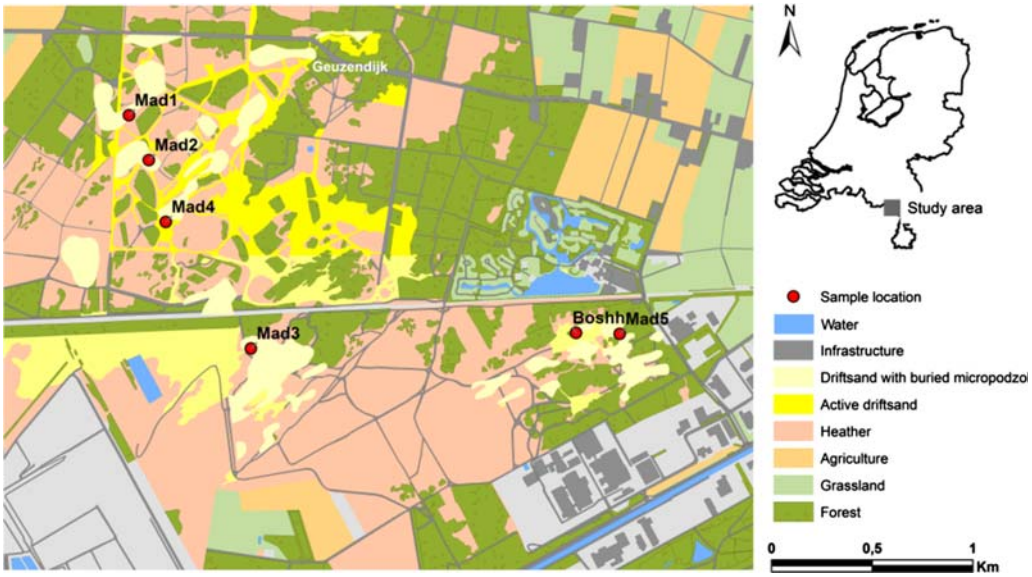

FIGURE 1.5.1 Distribution of sample sites in the study area of Weerterbergen, southeast Netherlands.

developed on sheltered locations and provided the soil archives that we can use for geoecological research. Such archives occur not only in the southeast Netherlands but also in other parts of northwestern Europe (Castel et al., 1989).

The area directly around the city of Weert was used for agriculture and plaggic Anthrosols developed there as a result of fertilization of the barren sandy soils with plaggic manure (Bokhorst et al., 2005; van Mourik et al., 2016). The area to the west of the arable fields was used for sheep grazing (van Mourik et al., 2010). Nowadays we find a restored 'natural' heath, planted pine forests and an as yet extensive area with active sand drifting. During the 20th century, sand drifting continued here as a consequence of heath degradation related to toxic pollution from a zinc smelter and its use as a military exercise ground (van Mourik and Hermans, 2011).

In Weerterbergen we selected six micropodzols in various polycyclic sequences to test with a multiproxy approach the reliability of humous intercalations as a chronological marker (Fig. 1.5.2). The sample schedule for soil micromorphology, ^{14}C and optically simulated luminescence (OSL) dating is presented in Fig. 1.5.2. The results of this pilot study have been published by Wallinga et al. (2013).

1.5.2 Development of micropodzols

Micropodzols (Green et al., 1993; Sevink and de Waal, 2010) are initial Podzols that develop in chemically poor substrates like driftsand deposits. Based on field characteristics, buried micropodzols are easily recognized, but a distinction between real pedogenic micropodzols and more sedimentary micropodzols must be based on micromorphological observations. In pedogenic micropodzols, in chemically barren sands the sequestration of soil organic carbon is mainly the result of in situ decomposition of litter in the ectorganic layer (Mormoder) or endorganic layer (Rhizomull) over a number of decades. In sedimentary micropodzols, in contrast, the accumulation of organic matter is

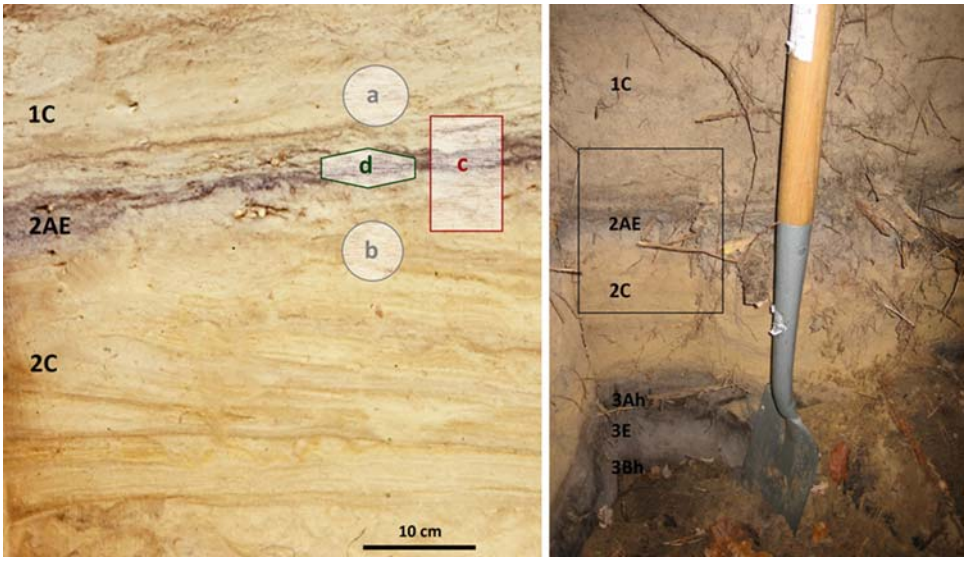

FIGURE 1.5.2 Profile Boshoverheide (overview of the polycyclic sequence *right* and detail of the micropodzol *left*) with the sample schedule. A pollen diagram of this sequence is published in Section 3.2. In the micropodzol the regular sequence of horizons was: 1C, laminated (medium fine) driftsand; 2AE, micropodzol, consisting of some organic and mineral micro horizons; 2C, laminated (medium fine) driftsand; and 3Ah/E/Bh, horizons of buried Podzol in coversand. The sample schedule of the micropodzol includes: a and b, optically simulated luminescence samples in pF rings; c, undisturbed sample in a Kubiena box for soil micromorphology; and d, 200 g soils for radiocarbon dating and pollen extraction. *First published in Wallinga, J., van Mourik, J.M., Schilder, L.M.L. 2013. Identifying and dating buried micropodzols in Subatlantic polycyclic driftsands. Quaternary International 306, 60–70.*

mainly due to redeposition of wind-transported soil organic matter originating from eroded humic soil horizons in the direct vicinity.

The controlling processes for micropodzol formation are organic carbon accumulation and sesqui (Al, Fe) mobilization (Dijkstra and van Mourik, 1996, Sevink and de Waal, 2010; Koster, 2010; van Mourik et al., 2010). Stabilizing driftsands will be colonized by plants in a specific succession (Sevink and de Waal, 2010; van Mourik and Jansen, 2013). Algae are the first colonizers, followed by lichens (e.g., *Cladonia*) and *Polytrigum*. The litter of these organisms will be decomposed by fungi and microarthropods and the humus form is restricted to a thin (<1 cm) Mormoder. After some years the microenvironment becomes less extreme in temperature and moisture fluctuations. At that point, *Corynephorus* will be the main successor and the humus form will transfer into a Rhizomull. After some decades, trees will establish (especially *Pinus* and *Betula*) or *Calluna* shrubs and the humus form will transfer into a thick (>1 cm) Mormoder. At that point also the characteristic albic E horizon will become obvious, due to leaching of sesquioxides (van Mourik, 1996; Sevink and de Waal, 2010).

A complication in soil development in driftsands is the rate of stabilization, because the stabilization of the driftsands was until recently never complete. Even in the ectorganic layer of an optimally developed Mormoder, blown-in mineral grains are present. In stabilized driftsand the formation of initial Podzol with a field differentiation [L-F-C] takes no more than one or two decades, with a field differentiation [L-F-H-AE-Bw-C] of eight to 10 decades (Paton et al., 1970; van Mourik et al., 2012).

1.5.3 The geochronology of micropodzols

In preliminary studies of the driftsands in Weerterbergen (van Mourik, 1988; van Mourik et al., 2010, 2012), micropodzols were used as stratigraphic markers between medieval and post-medieval driftsand deposits. However, it appeared to be problematical to date these markers accurately.

A first impression of the age of the micropodzols is provided by pollen spectra of the organic layers (Fig. 1.5.3). All the spectra show low percentages of *Quercus* and *Corylus* and high percentages of Ericaceae and Poaceae, indicating that the micropodzols developed after the transformation of the Subboreal deciduous forest in heaths. Besides, the percentages of *Pinus* pollen in Boshh and Mad-1 point to the presence of pine trees in the vicinity and consequently the burial of the micropodzol took place after 1850 CE. The first plantation of Scots pine trees was realized in the middle of the 16th century near the city of Breda in western Brabant as a commercial plantation of ship masts. Also, in other places, pine trees were used for mast production and as exotic park trees near cities. In the course of the 19th century, people started to plant pine trees to tackle sand drifting, and extensive reforestations with Scots pine accelerated after the abandonment of plaggic agriculture at the end of the 19th century (van Mourik, 1988; van Mourik and Dijkstra, 1995). The percentages of *Pinus* pollen in MAD-2, -3 and -4 are low and can be the result of long-distance transport, indicating a palynological age between 1550 and 1850. Mad-5 is free from *Pinus* pollen, indicating a palynological age of the organic matter of more than 500 years.

Based on pollen spectra it is not possible to identify the species plant rooting at the site during the stable period with initial podzolization because the aeolian pollen influx is a mix of pollen produced by onsite and distance plant species. Pollen grains in Mormoders occur in organic aggregates (Fig. 1.5.4A); the processes of infiltration and conservation of pollen grains in the soil are explained in Chapter 2. Another option for identifying onsite growing species is by phytoliths, microscopic structures made of silica, found in some plant tissues (especially leaves) and persisting after the decay of the plant. Plants take up silica from the soil, whereupon it is deposited within different intracellular and extracellular structures of the plant and the morphology of phytoliths is plant species specific (Piperno, 2006). In the thin sections of the Mormoders, some phytoliths have been

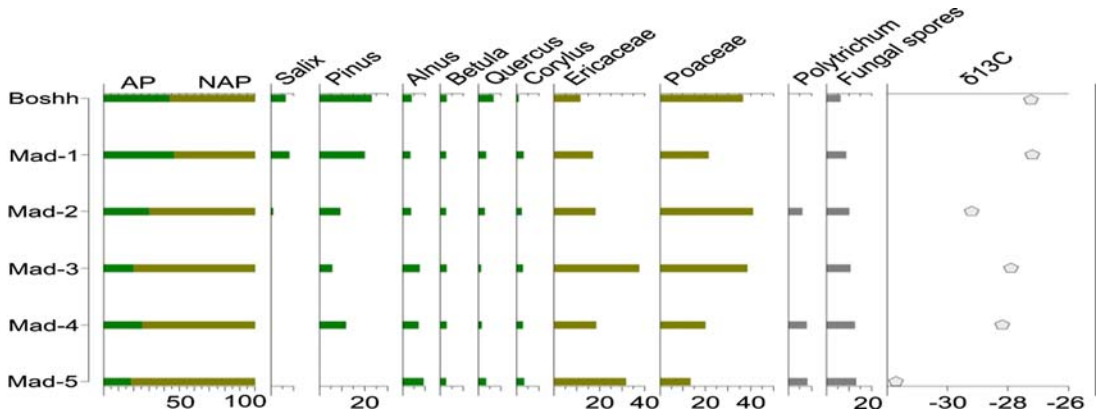

FIGURE 1.5.3 Pollen spectra and $\delta^{13}C$ values of the top of the organic (AE) horizon of the micropodzols.

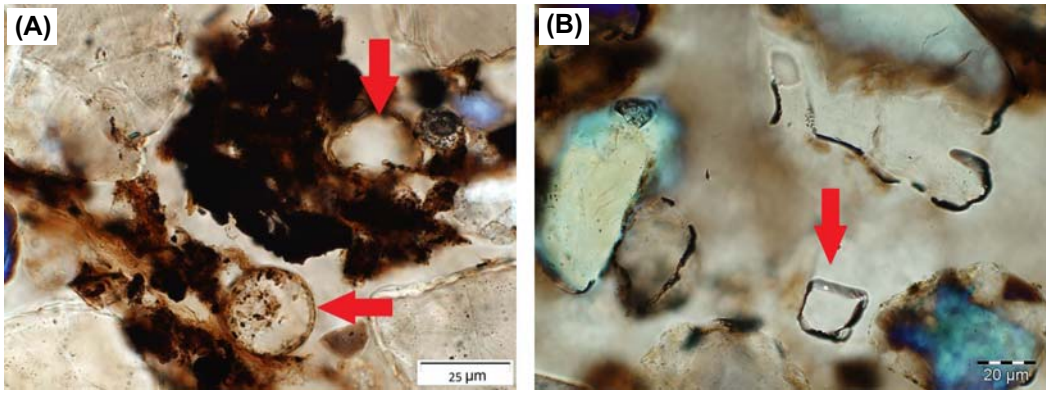

FIGURE 1.5.4 (A) Pollen grains, observed in the thin section of the 2AE in profile boshh. (B) Phytolith, observed in the thin section of the 2Ae in profile boshh.

identified (Fig. 1.5.4B). According to the overview of phytolith shapes (Piperno, 2006, pp. 30–31) key of Poaceae, pointing to the presence of grasses onsite during soil formation and absence of heath but such a conclusion, based on just observations in thin sections, is not very reliable; better results require analyses of phytolith extraction from soil samples as explained in Chapter 7.

The $\delta^{13}C$ values (Fig. 1.5.3) measured on the samples yield additional information on the measured material. Important species, responsible for organic carbon sequestration in the ectorganic horizon of micropodzols, are *Cladonia* (indirectly indicated in the spectra by fungal spores) and *Polytrigum*. The biomass of *Cladonia* and *Polytrigum* has a $\delta^{13}C$ value around −32. The biomass of *Corynephorus*, *Calluna*, *Betula* and *Pinus* has a $\delta^{13}C$ value around −27. Samples with a $\delta^{13}C$ value <−28 can be considered as affected by *Cladonia* and *Polytrichum* (Mad-2, -4 and -5). Sample $\delta^{13}C$ values around −27 point to a vegetation controlled by *Corynephorus* (Boshh, Mad-3) or *Calluna* (Mad-1). The decomposition of litter of *Cladonia* and *Polytrichum* promotes the development of a black, thin (<1 cm) Mormoder (F-H horizon), decomposition of *Corynephorus* roots promotes the development of a Rhizomull (AE horizon) and the decomposition of *Calluna* litter promotes the development of thicker (>1 cm) brown–black Mormoder (F-H-AH horizon).

A second impression of the age of micropodzols is provided by absolute dating (Table 1.5.1).

TABLE 1.5.1 OSL and ^{14}C dates (CE) of the six investigated micropodzols in Weerterbergen. Sample locations are indicated in Fig. 1.5.2.

Boshh	Mad-1	Mad-2	Mad-3	Mad-4	Mad-5	Horizon	Chronology
1957 ± 3	1916 ± 4	1980 ± 1	1994 ± 2	1937 ± 3	1783 ± 9	1C	OSL age of the bottom of younger driftsand
1574 ± 72	1092 ± 67	1315 ± 52	1955 ± 1	1365 ± 144	535 ± 92	2AE	^{14}C age of humic acids
1810 ± 9	1892 ± 5	1880 ± 6	1994 ± 3	1865 ± 6	1782 ± 10	2C	OSL age of the top of older driftsand

CE, Common Era; *OSL*, optically simulated luminescence.

First published in Wallinga, J., van Mourik, J.M., Schilder, L.M.L. 2013. Identifying and dating buried micropodzols in Subatlantic polycyclic driftsands. Quaternary International 306, 60–70.

Radiocarbon dating was applied to the humic acids extracted from the organic horizons. It is known from previous studies that radiocarbon ages of samples of soil organic carbon (first, the humin fraction but also the humic acids fraction) are not reliable (van Mourik et al., 1995, Section 3.2) and some radiocarbon ages were conflicting with the palynochronology.

For a better understanding of the origin and chronology of micropodzols we selected and sampled six polycyclic driftsand sequences at Weerterbergen in 2006. Based on the geogenetic landscape map of Weerterbergen (van Mourik, 1988) suitable sites were selected within the map unit 'driftsand with buried micropodzols' (Fig. 1.5.1). Each of these sites contains buried micropodzols at less than 100 cm depth, embedded between driftsand beds. The micropodzols were easily recognized in the field and sampled for soil pollen analysis, ^{14}C and OSL dating and soil micromorphology, according to the sample schedule in Fig. 1.5.2. The theory of radiocarbon dating is discussed in Section 3.1, and the theory of OSL dating in Section 4.1. The results of ^{14}C and OSL dating of the six micropodzols are summarized in Table 1.5.1.

The radiocarbon dating results (ranging from 500 CE to 1955 CE) indicate older ages than suggested by pollen evidence and OSL dating. These age overestimations are likely related to the incorporation of older, redeposited carbon as was also identified in the micromorphological analysis. We conclude that the radiocarbon ages are unreliable, and that radiocarbon dating of micropodzols in polycyclic soil sequences should be avoided.

The OSL data, on the other hand, agree well with the pollen evidence. The oldest micropodzol (Mad-5, OSL dated to 1782–1783 CE) shows a very low *Pinus* pollen contribution (4% of total pollen sum), indicating that pine planting may have commenced but was still minor. The fact that all results agree with stratigraphic order provides further evidence of the robustness of the results of OSL dating. Based on the differences in OSL age between the top of the older driftsand and the bottom of the younger driftsand it is possible to estimate the time, available during the stable phase for soil formation between two phases of active sand drifting (Fig. 1.5.5).

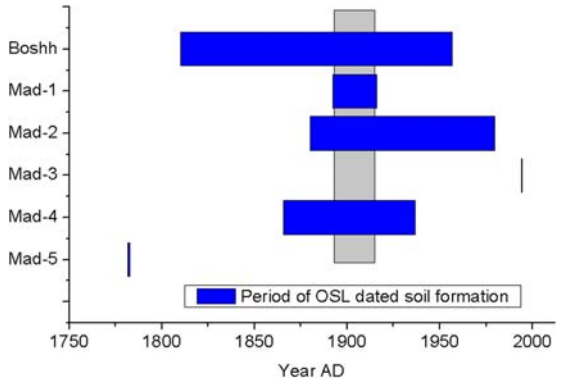

FIGURE 1.5.5 Duration of soil formation based on optically simulated luminescence dating *First published in Wallinga, J., van Mourik, J.M., Schilder, L.M.L., 2013. Identifying and dating buried micropodzols in Subatlantic polycyclic driftsands. Quaternary International 306, 60–70.*

1.5.4 Micromorphology of micropodzols

The morphological classification of micropodzols is summarized in Fig. 1.5.6, and the diagnostic micromorphological features of pedogenic and geogenic micropodzols are presented in Figs. 1.5.7 and 1.5.8.

Characteristic micromorphological features in pedogenic micropodzols are well-developed Mormoder layers (Fig. 1.5.7A and C), litter and root decomposition by humus inhabiting microarthropods (Fig. 1.5.7D and F) and aggregate decomposition (Fig. 1.5.7E) by soil fungi during active soil formation. Blown-in sand grains are regularly present in the Mormoder layers (Fig. 1.5.7C). The rather undisturbed geogenic lamination of the driftsand beds points to a very low rate of bioturbation. Humus inhabiting arthropods move hardly into the mineral horizon and there is no evidence of vertical transport

FIGURE 1.5.6 Three genetic types of micropodzols in field profile and thin section. (1) Monocyclic pedogenic micropodzol (*left*, Mad-1), clear ectorganic layer, overlying a mineral horizon with humic and albic properties. (2) Polycyclic pedogenic micropodzol (*middle*, Mad-2), the ectorganic layer is laminated. The soil formation was interrupted by short-lived sand drifting several times. The lower part of the older driftsand deposit is laminated, pointing to the result of a sequence of events; the colour differences are geogenic. (3) Geogenic micropodzol (*right*, Mad-3), showing a weakly developed Rhizomull with a sedimentary distribution pattern of organic particles. On the base of the humus form we can distinguish a discontinuous organic layer (decomposition of short-lived lichens/moss vegetation).

of mineral grains related to animal activity. Root channels in the AE are formed by plants living on the stabilized surface (*Corynephorus*, *Calluna*) during soil formation. Also, secondary root systems from plants, growing at the present surface, can reach, penetrate and disturb the structure of buried micropodzols. Growing plant roots cause friction around the root channel, and mineral grains will be somewhat replaced in the soil skeleton. But after root decomposition, mineral grains can move down several centimetres in fossil channels.

In polycyclic micropodzols the formation of the Mormoder layer was interrupted by short-lived sand drifting, resulting in the deposition of mineral layers. The vegetation was not completely buried and soil formation could continue (Fig. 1.5.6B).

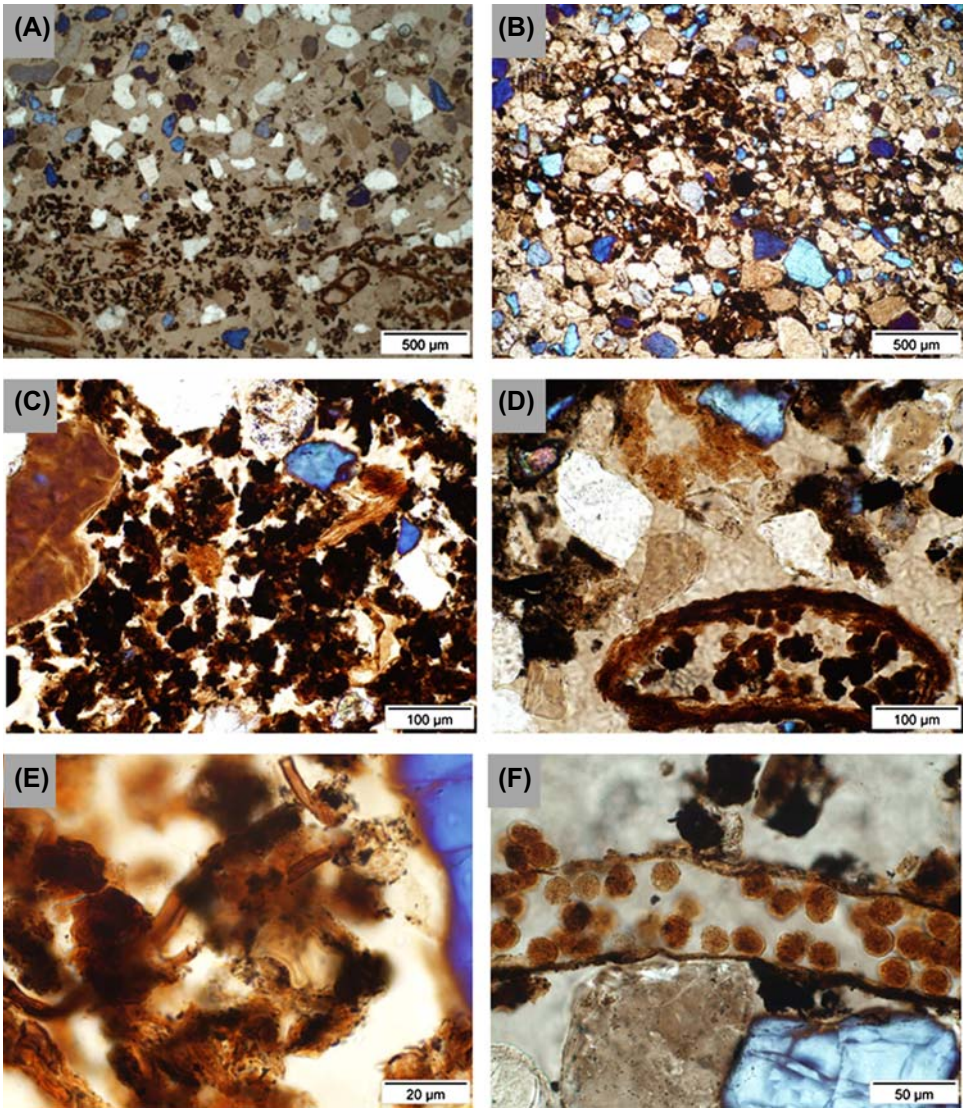

FIGURE 1.5.7 Pedogenic features in buried micropodzols. (A) Distribution pattern of organic aggregates in a buried AE horizon (Mad-1). (B) Micropodzol with organic (pedogenic) and mineral (sedimentary) lamina (Mad-2). (C) Pedogenic distribution of organic aggregates (faecal pellets) in the Mormoder layer with blown-in mineral gains (Mad-2). (D) Litter decomposition with in situ-produced faecal pellets in the Mormoder layer of a micropodzol by microarthropods (Mad-1). (E) Decomposition of organic aggregates (faecal pellets) by fungi in the Mormoder layer (Mad-2). (F) Decomposition of (laterally positioned, most probably of *Corynephorus*) roots in the AE (Rhizomull) by microarthropods (Mad-2).

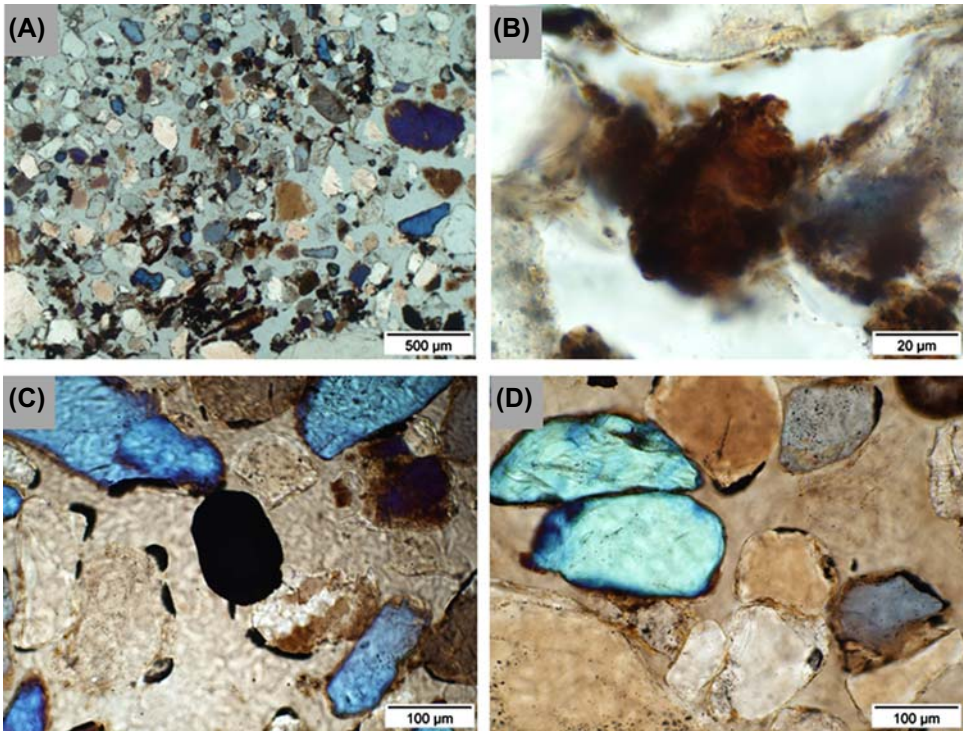

FIGURE 1.5.8 Sedimentary features in buried micropodzols. (A) Sedimentary distribution of organic particles in driftsand frame (2AE Mad-5). (B) Rounded, transported organic aggregate as part of the soil skeleton (2AE Mad-3). (C) Rounded (transported) charcoal particle as part of the soil skeleton (2AE Mad-3). (D) Humic cutans on quartz grains in the soil skeleton (2AE Mad-3).

Characterizing micromorphological features of sedimentary micropodzols are the sedimentary distribution of organic particles in the soil matrix (Fig. 1.5.8A), the occurrence of transported and rounded organic aggregates (Fig. 1.5.8B) and charcoal particles (Fig. 1.5.8C) and the occurrence of mineral grains with humic cutans (Fig. 1.5.8D), originating from spodic B horizons of elsewhere eroded Podzols. We note that all investigated samples contain contaminating organic elements such as charcoal particles (Fig. 1.5.8C) and humic cutans (Fig. 1.5.8D), originating from the erosion of eroded humic soil surfaces in the vicinity (Ah and Bh horizons of eroded Podzols and older micropodzols). These organic contaminants are not only found in the (sedimentary) micropodzols, but are dispersed throughout the driftsand matrix.

Based on soil micromorphological analyses, three types of micropodzols were identified (Fig. 1.5.6). Micropodzols at two sites (Mad-3 and Mad-5) were interpreted to be sedimentary micropodzols. The OSL data corroborate this interpretation, because the time for formation is determined to be 0 and 1 year for Mad-3 and Mad-5, respectively. Even when taking the uncertainties into account, the time for 'soil formation' would be less than 10 years (at 1 sigma). We conclude that the information from micromorphology and OSL dating is in good agreement; both point to a sedimentary origin of the organic layer in Mad-3 and -5.

The two soils that are interpreted as pedogenic micropodzols based on soil micromorphology were formed in 24 or 71 years. This

confirms that micropodzols can form rapidly, and do not need a long period of landscape stability (Paton et al., 1970; Sevink and de Waal, 2010). Finally, the two soils interpreted as polycyclic pedogenic micropodzols (BHH and Mad-2) were formed in 147 and 99 years. The longer period relative to the monocyclic pedogenic micropodzols reflects that the profiles contain several layers of initial soil formation.

1.5.5 Micropodzols as stratigraphic marker

Pedogenic micropodzols were identified at four of the six investigated sites. The micropodzols at Mad-3 and Mad-5 were identified as sedimentary micropodzols, and not considered here. The OSL ages obtained at different sites for driftsands both above and below the pedogenic micropodzol differ widely. The ages for driftsand below the micropodzol yield a *maximum* age for the start of micropodzol development. These ages range from 1810 CE (site BOH) to 1892 CE (Mad-1). The age of the sand on top of the micropodzol provides a *minimum* age for the end of soil formation. These ages range from 1916 CE (Mad-1) to 1980 CE (Mad-2).

Interestingly, the periods for soil development for each of the four pedogenic micropodzol sites overlap around 1900 CE (Fig. 1.5.5). Hence, our data may indicate a period of landscape stability around 1900 CE. OSL dating of the drifts and indicates that the period of stability was of different duration in the different sites, likely related to local differences in shielding and/or disturbance. We note that the period around 1900 CE coincides with the time when plaggic agriculture was abandoned, and precedes the period of toxic soil contamination and intensive military use of this area as a training field (Denneman et al., 1987; van Mourik and Hermans, 2011).

The results suggest that the pedogenic micropodzol can be used as a marker horizon to distinguish sand drifting before 1900 CE and sand drifting after 1900 CE. However, such inferences should be made with great care, because the pedogenic micropodzol may be absent. We expect the soil to be discontinuous because some parts of the landscape likely never stabilized sufficiently to allow development of this soil, whereas erosion may have removed the soil in other places. The absence of the soil at Mad-3 and -5 provides evidence for the discontinuous nature of the pedogenic micropodzol.

1.5.5.1 Conclusions

- This study highlights the value of polycyclic soil sequences as geological archives of landscape evolution in driftsand areas.
- Micropodzols in polycyclic sequence can form due to both sedimentary and pedological processes, and soil micromorphological analysis is necessary to distinguish the two types.
- Radiocarbon dating of the humic acid fraction cannot be used to determine the age of the overblowing of micropodzols, because all of the soils contain some older wind-blown organic material. As a consequence, radiocarbon ages are older than the age of the soil.
- OSL dating of the driftsands is a robust tool for determining the time of deposition and for bracketing periods of soil formation and landscape stability.
- The combination of palynology, soil micromorphology and OSL dating has shown that a period of landscape stability occurred in Weerterbergen around 1900 CE. The timing of this period is likely related to the absence of anthropogenic disturbance around that time.

1.6 Monitoring of initial soil development in an experiment on mine waste materials to promote soil regeneration

1.6.1 Introduction

Degraded landscapes associated with large deposits of mine waste materials from more than 2500 years of metal extractions are common in

southeast Spain. Utilization of these unproductive lands is risky because of environmental hazards such as potential leaching of metals into groundwater and high susceptibility to erosion by water and wind. Soils in these unsightly areas are quite inhospitable to plant growth because of low soil organic matter (<1 g carbon/kg soil), acidity (pH ≈ 2), high electrical conductivity (up to 20 dS/m) and high metal concentrations (e.g., lead = 5000–8000, zinc = 8000–22,000 mg metal/kg soil) (Conesa et al., 2007; Ottenhof et al., 2007). These large tracts of land need to be properly managed to prevent and/or minimize further environmental damage and to boost their economic value.

Southeast Spain generates an estimated 3.5 million m^3/year of wastes from the pork industry (Consejería de Agricultura, Agua y Medio Ambiente, 2007) and large amounts of marble wastes from extensive use of limestone materials for construction purposes. Pig manure and sewage sludge are potential soil amendments to enrich soil carbon and nitrogen, while marble wastes contain calcium carbonate (or calcite) to counteract high acidity. Typical pig manure generated by the pig industry in southeast Spain may contain 32%–34% organic carbon and 22–28 g/kg nitrogen, while municipal sewage sludge has 34% organic carbon and 50 g/kg nitrogen (Carmona et al., 2009; Zanuzzi et al., 2009). Animal manure, when added to soil, increases nitrogen concentrations and availability in many infertile soils and may prevent toxicities of dissolved metals (Bradshaw, 1987; Ye et al., 2002; Walker et al., 2004; Viventsova et al., 2005). Although a large portion of the organic carbon from organic amendments is decomposed by microbial activities within 4–5 weeks of the amendments, as reported in Zanuzzi et al. (2009).

The Cartagena-La Union Mining District covers an area of 50 km^2 on the eastern section of the province of Murcia in southeast Spain. Until 1991, this mining area was an important center for extraction of mineral ores such as sphalerite, galena, pyrite, pyrhotite and marcasite for more than 2500 years. We selected the Brunita tailings pond (Fig. 1.6.1) to represent a typical mine waste deposit characterized by low pH, high electrical conductivity and metal concentrations and very low carbon and nitrogen concentrations. The Brunita site lies on a slope and, like other tailing ponds, was formed from tailings discharged during metal extraction from copper, lead and zinc containing sulphate minerals. Plants in the study area are limited to isolated patches and consisted of millet rice (*Piptatherum miliaceum*), thatching grass (*Hyparrhenia hirta*), needle grass (*Stipa* sp.), sticky fleabane (*Dittrichia viscosa*), arinica (*Paronychia suffruticosa*), aster (*Helichrysum decumbens*), grey–green needle grass (*Lygeum spartum*), Mediterranean snow thistle (*Sonchus tenerrimus*), Mediterranean salt brush (*Atriplex halimus*), bean caper (*Zygophyllum fabago*) and rock phagnalon (*Phagnalon saxatile*) (Conesa et al., 2006; Zanuzzi et al., 2009).

FIGURE 1.6.1 Plants in the experimental grid on the balsa of Brunita; view to the southeast. In the background is a closed mine industry complex. Start of the experiment in 2007, sampled in 2012.

1.6.2 Field experiment

A detailed description of the field research is given in Zanuzzi et al. (2009). The results of

TABLE 1.6.1 Mean (and standard deviation) values of selected soil properties of marble waste + pig manure and marble waste + sewage sludge amended mine wastes and control samples ($n = 3$).[a]

Soil parameters	Marble waste + pig manure	Marble waste + sewage sludge	Control
pH in H_2O	6.0 (1.51)	5.8 (1.90)	2.8
Electrical conductivity (dS/m)	2.2 (0.28)	2.3 (0.09)	2.8
Total nitrogen (g/kg)	0.2 (0.042)	0.2 (0.026)	0.1
Total carbon (g/kg)	8.3 (10)	5.6 (2.4)	1.4
Total sulphur (g/kg)	18.7 (4.2)	16.0 (0.91)	25.7
Select total elements (mg/kg)			
Phosphorus	544 (31)	507 (37)	514
Potassium	4638 (491)	5028 (175)	4291
Sodium	551 (72)	619 (37)	451
Calcium	35,222 (34,658)	22,006 (11,145)	16,693
Magnesium	3818 (813)	4919 (407)	2177
Manganese	1957 (472)	2250 (278)	2083
Zinc	1428 (274)	1589 (192)	1447
Cadmium	BDL	BDL	BDL
Lead	1562 (331)	1697 (184)	1491
Copper	69 (4)	65 (6)	67
Strontium	52 (13)	45 (5)	47
Water-soluble metals (mg/kg)			
Zinc	0.32 (0.324)	1.61 (2.53)	4.03
Copper	0.27 (0.005)	0.35 (0.026)	0.66
Cadmium	BDL	BDL	BDL
Lead	0.13 (0.139)	0.45 (0.387)	0.79
DTPA-extractable metals (mg/kg)			
Zinc	6.4 (0.736)	5.7 (0.364)	5.5
Copper	0.53 (0.117)	0.44 (0.027)	0.82
Cadmium	0.018 (0.020)	0.023 (0.003)	0.003
Lead	15.6 (12.18)	19.0 (3.96)	3.7

BDL, Below detection limit; *DTAP*, diethylenetriaminepentaacetic acid.
[a] *Control has composite sample.*

chemical and micromorphological analyses have been published by Arocena et al. (2012).

In brief, a 4 m^2 plot was established in each of 20 experimental units subjected to blanket application of 160 t/ha of marble waste to raise the pH to 7 (Sobek et al., 1978). The following treatments were applied in three replications: control no amendment, marble waste + pig manure, and marble waste + sewage sludge. The quantities of pig manure were 6.25, 12.50 and 25 t/ha; the rates of sewage sludge were 5, 10 and 20 t/ha based on European and Spanish N legislations (Directive 91/676/EEC, 1991; Real Decreto 261/1996). The marble waste was applied, then allowed to dry for 24 h, after which it was annually mixed with the soil using a shovel to a depth of 0–15 cm. Organic amendments were then applied using the same procedure. After manual applications of the various soil amendments, the experimental plots were exposed to the semiarid climatic conditions (annual rainfall of 200–300 mm, mean annual temperature of 18°C) in the study area. All plants observed growing in the experimental units are pioneer species because the plots were never seeded or planted to assess the succession in any long-term natural plant colonization.

Composite soil samples from five subsamples (from the centre and four corners) were collected in each experimental plot 60 months after application of amendments. Each sample was ≈200 g and was taken from the 0–15 cm layer. Samples were air dried and passed through a 2 mm sieve prior to laboratory analyses conducted at the University of Amsterdam (the Netherlands) and Technical University of Cartagena (Spain). The methods of soil analysis are described in Arocena et al. (2012), and the results are summarized in Table 1.6.1.

1.6.3 Micromorphological analysis

One undisturbed soil sample was collected using Kubiena boxes from each treatment, including the control for a total of seven undisturbed samples. A thin section (5 × 7.5 cm) was prepared from each Kubiena box sample according to the technique described by Jongerius and Heintzberger (1975). Seven soil thin sections were described for micromorphological characteristics following the concepts and terms in Brewer (1976), Bullock et al. (1985) and Stoops (2003). Micromorphological features indicative of the evolution in soil structure and other manifestations of past and active soil-forming processes were recorded in more than 100 micrographs.

Noticeable differences in soil microstructure were observed between soil thin sections from the control and amended plots. A banded (or platy) microstructure was evident in the control plots (Fig. 1.6.1A). The thickness of the band (or plate) ranged from ~200 to 1000 mm. Areas outside and between these bands had single grain microstructure composed of coarse (>50 mm) particles of quartz, chlorite, iron oxides, gypsum and many dark-coloured and opaque minerals (Fig. 1.6.1B). Fine materials (B50 mm) were very few and limited to very thin coatings on coarse materials. Continuous simple packing voids (or interconnected pore space) between coarse fragments constituted the dominant type of porosity in the non-banded sections in the control plots. The porosity within the densely packed bands (or plates) was mostly isolated vugh-type voids (or pore spaces not connected with each other).

Mine wastes amended with pig manure, sewage sludge and marble waste had intergrain microaggregate soil microstructure (Fig. 1.6.1C and D). This type of structure is mostly composed of sand-sized materials (or coarse materials) with microaggregates of fine materials in between (Stoops, 2003). In some parts of the section, dark-coloured materials bridged the grains to form a bridged grain microstructure (Stoops, 2003). Coarse (>50 mm) grains were dominated by quartz, iron oxides and dark and opaque minerals. The aggregates between these coarse

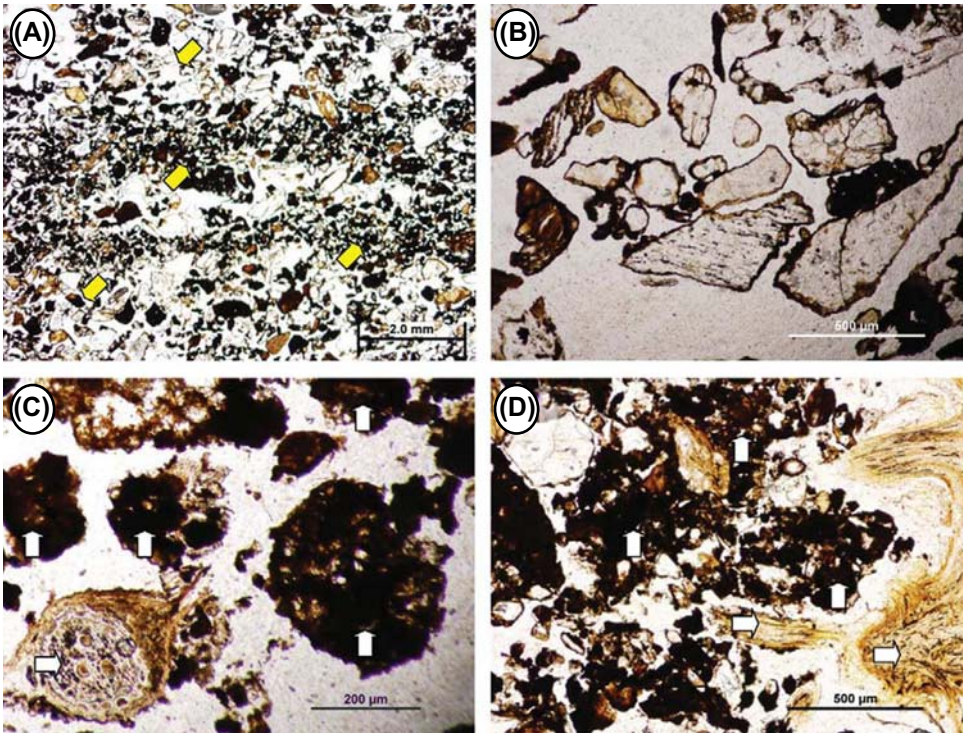

FIGURE 1.6.2 Microstructures in control and amended mine wastes. (A) Single grain (◇) and banded (or platy) (◇) soil microstructures dominated the control plot. (B) Close-up of single grain structure, control. (C and D) Granular soil structural units (⬠) were commonly observed near root fragments (⇨) in amended mine wastes. (C) Marble waste + sewage sludge. (D) Marble wastes + pig manure. *First published in Arocena, J.M., van Mourik, J.M., Faz Cano, A., 2012. Granular soil structure indicates reclamation of degraded to productive soils: a case study in southeast Spain. Canadian Journal of Soil Science 92, 243–251.*

grains were dark coloured and had a spherical shape with sizes ranging from ≈100 to 1000 mm. These aggregates were composed of monomorphic organic materials or amorphous organic fine materials with no recognizable vegetal or fungal structure according to Stoops (2003) and Bullock et al. (1985). The internal fabric of these aggregates showed dominantly dark-coloured and opaque materials intermixed with discrete mineral particles 10–50 mm in size. Aggregates were commonly observed around fragments of plant materials (e.g., roots) where they tended to coalesce to form large aggregates >1000 mm (Fig. 1.6.1D). Some of these aggregates became interconnected with each other, resulting in a predominantly compound type of packing void. Fragments of primary calcite from the blanket application of marble waste were often observed in thin sections of amended mine wastes. The sizes of these calcite particles ranged from B50 mm to as large as 2000 mm (Fig. 1.6.2A and B). In a few areas of thin sections in the pig manure, sewage sludge and marble waste plots, single grain microstructure similar to that in the control treatment was observed.

Pedofeatures are discrete fabric units that are recognizable from adjacent materials (Bullock et al., 1985; Stoops, 2003) and are micromorphological characteristics indicative of soil-forming processes that took place in the pedon. The accumulation of secondary calcium carbonates was one of the easily recognizable inorganic

pedofeatures in amended mine wastes. Common zones of secondary calcite precipitation included spaces between dark-coloured materials in the 0–5 cm part of the amended mine wastes and infillings in pore spaces between coarse fragments. Infillings of secondary calcite occurred in pore spaces as large as several hundred mm^2 area (Fig. 1.6.2C and D). Secondary calcite also precipitated on the surface of plant roots (Fig. 1.6.3A and B). Secondary calcite was not observed in the 2.5–5.0 cm section of any thin section collected from amended or control plots.

Pedofeatures of biological origins were observed in amended plots. Most of these pedofeatures were organisms and their faecal materials were composed of the aggregates in the intergrain microaggregate structure described earlier for amended soils. Remains of plant and soil organisms, including fungal hyphae (Fig. 1.6.4A and B), were commonly found near the zone of decomposing plant fragments (Fig. 1.6.4C). The aggregate in Fig. 1.6.4D was an example of excremental pedofeatures typical for enchytraeids (spring tails), a soil mesofauna. The faecal material consisted of dark-coloured organic matter intimately mixed with soil minerals. van Mourik (1999) referred to these coprogenic aggregates of soil animals as modexi. Other biological pedofeatures included fragments of roots (Fig. 1.6.3A–D). Plant roots were always observed in association with both primary and secondary calcite accumulations.

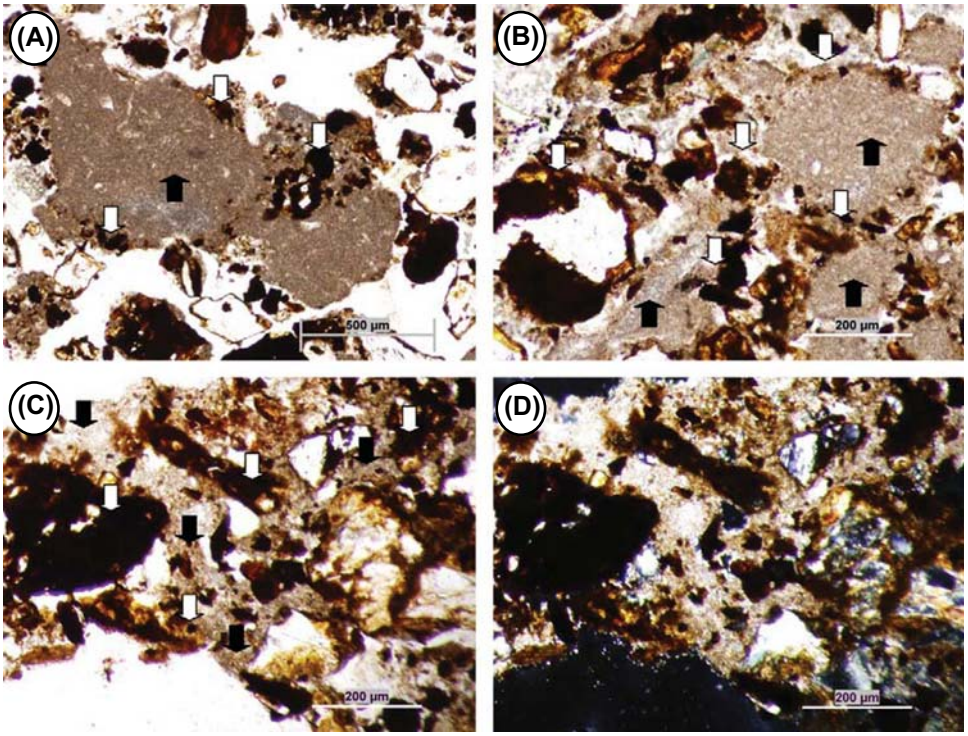

FIGURE 1.6.3 Calcium carbonates are sorption sites for monomorphic soil organic matter (⇩). Primary carbonates (⬆) in (A) marble waste + pig manure and (B) marble-waste + pig manure. Secondary (▮) carbonates in marble waste + sewage sludge plot in (C) plain polarized and (D) cross-polarized light. *First published in Arocena, J.M., van Mourik, J.M., Faz Cano, A., 2012. Granular soil structure indicates reclamation of degraded to productive soils: a case study in southeast Spain. Canadian Journal of Soil Science 92, 243–251.*

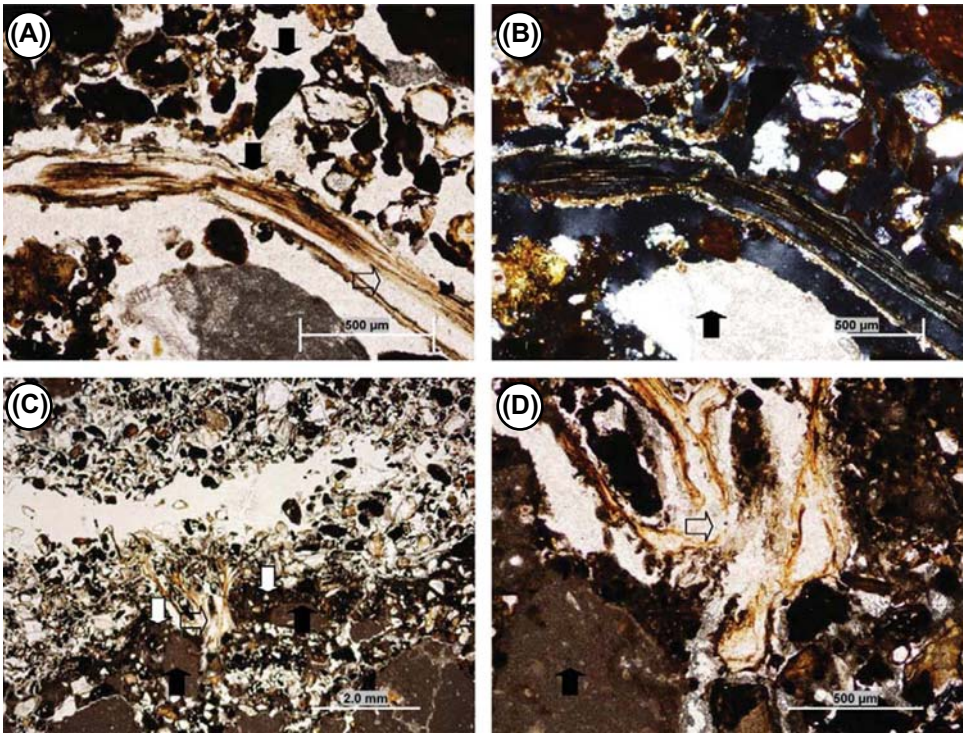

FIGURE 1.6.4 Roots grow (⇨) in the vicinity of calcium carbonates and monomorphic organic coatings (⇧). Secondary carbonates (▮) in marble waste pig + manure plot in (A) plain polarized light, (B) cross-polarized light and (C and D) primary carbonates (▮) in marble waste + sewage sludge. *First published in Arocena, J.M., van Mourik, J.M., Faz Cano, A., 2012. Granular soil structure indicates reclamation of degraded to productive soils: a case study in southeast Spain. Canadian Journal of Soil Science 92, 243–251.*

Monomorphic organic matter was consistently observed as coatings on the surface of these primary calcite particles or infillings in primary and secondary calcite-rich zones (Fig. 1.6.2A–D). Plant roots were commonly observed growing near accumulations of monomorphic coatings (Fig. 1.6.3C and D). Biological pedofeatures were not observed in the lower depths or bottom sections of control plots (Fig. 1.6.5).

1.6.4 Conclusions

- Addition of organic amendments such as pig manure and sewage sludge in combination with marble cuttings improved soil conditions in mine waste deposits in southeast Spain.
- Inorganic pedofeatures such as secondary calcite enhanced the accumulation of organic matter from organic amendments that promote initial biological activities in amended mine wastes.
- We conclude that accumulations of organic matter cappings on calcite promote the growth of soil microorganisms such as fungi and enchytraeids in amended mine wastes.
- The presence of aggregation (or granular structure) in soils often results in better aeration, water availability and increased sources of nitrogen and other essential nutrients.

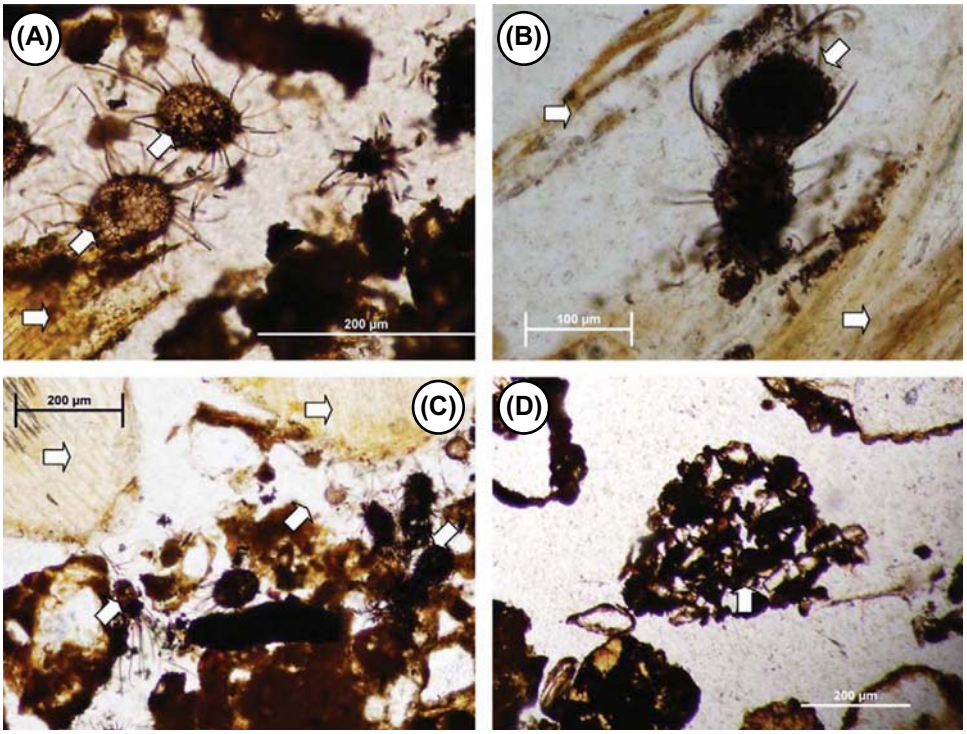

FIGURE 1.6.5 Soil organisms and excrements were commonly observed around decomposing plant materials (⇨) in mine wastes amended with organic and industrial wastes. (A, B, C) Fungal hyphae on spore-like plant remains (⇦). (B) Fungal hyphae on cell residue (⇦). (C) Marble waste−pig manure plot. (D) Faecal excrement of enchytraeids (⇩).

- Another benefit of the amendments is the decreased concentration of soluble zinc.
- We conclude that land reclamation approaches to mine wastes should focus on efforts that will lead to the development of granular soil microstructure.

References

Arocena, J.M., van Mourik, J.M., Faz Cano, A., 2012. Granular soil structure indicates reclamation of degraded to productive soils: a case study in southeast Spain. Canadian Journal of Soil Science 92, 243−251.

van Beek, E.P.L., 1990. Micromorfologische Kenmerken Van Subglaciale Tills. MSc Thesis, University of Amsterdam unpublished.

Bokhorst, M.P., Duller, G.A.T., van Mourik, J.M., 2005. Optically stimulated luminescence dating of a fimic anthrosol in the Southern Netherlands. Journal of Archaeological Science 32, 547−553.

Bradshaw, A.D., 1987. The reclamation of derelict land and the ecology of ecosystems. In: Jordan III, W.R., Gilpin, M.E., Aber, J.D. (Eds.), Restoration Ecology: A Synthetic Approach to Ecological Research. Cambridge University Press, Cambridge, pp. 53−74.

Braillard, L., Mauvilly, M., 2008. Morphogenesis of the Sarine canyon in the Plateau Molasse, Switzerland: new data from an archaeological site. Geographica Helvetica 63, 181−187.

Brewer, R., 1964. Fabric and Mineral Analysis of Soils. Wiley, New York, p. 470.

Brewer, R., 1976. Fabric and Mineral Analysis of Soils. R.E. Krieger. Huntington, N.Y., p. 482.

Bullock, P., Fedoroff, N., Jongerius, A., Stoops, G., Tursina, T., 1985. Handbook for Soil Thin Section Description. Wayne Research Publ., Albrighton, 152pp.

Carmona, D.M., Faz Cano, A., Arocena, J.M., 2009. Accumulation of organic carbon from pig manure added to surface soil in mined areas, SE Spain. In: Cano, F., et al. (Eds.), Advances in Geoecology. 40 Land Degradation and Rehabilitation Dryland Ecosystems. Catena Verlag, Reiskirchen, pp. 37−52.

Castel, I.I.Y., Koster, E.A., Slotboom, R.T., 1989. Morphogenetic aspects and age of late Holocene drift sand in Northwest Europe. Zeitschrift für Geomorphologie, NF 33, 1–26.

Conesa, H.M., Faz Cano, A., Arnaldos, R., 2007. Initial studies for the phytostabilization of a mine tailing from the Cartagena-La Union Mining District (SE Spain). Chemo-sphere 66, 38–44.

Conesa, H.M., Faz, A., Arnaldos, R., 2006. Heavy metal accumulation and tolerance in plants from mine tailings of the semiarid Cartagena-La Union mining district (SE Spain). Science of the Total Environment 366, 1–11.

Consejeriá de Agricultura, Agua y Medio Ambiente, 2007. D. G. Ganaderiá. Registro de Explotaciones Porcinas de la Región de Murcia.

Courty, M.A., Goldberg, P., Macphail, R., 1989. Soils and Micromorphology in Archeology. Cambridge University Press, Cambridge, 344pp.

Denneman, W.D., Eijsackers, H.J.P., Faber, J.H., Ma, W.C., 1987. Zware metalen in de Kempen; ecologische aspecten. Landschap 187, 172–159.

Dijkstra, E.F., van Mourik, J.M., 1996. Reconstruction of forest dynamics based on pollen and micromorphological studies of young acid forest soil under Scotch pine plantations. Acta Botanica Neerlandica 45, 393–410.

Directive 91/676/EEC, 1991. Concerning the protection of waters against pollution caused by nitrates from agricultural sources. Ofic. J.L 375, 31.12. European Union, Brussels, Belgium.

FAO, 1968. Guidelines for Soil Profile Description. Rome, 53pp.

Green, R.N., Towbridge, R.L., Klinka, K., 1993. Towards a taxonomic classification of humus forms. Forest Science, Monograph 29, 49pp.

Jongerius, A., Heintzberger, G., 1975. Methods in Soil Micromorphology: Soil Survey Papers, 10. Wageningen, 48pp.

Koster, E.A., 2010. Origin and development of Late Holocene drift sands. In: Fanta, J., Siepel, H. (Eds.), Inland Drift Sand Landscapes. KNVV Publishing, Zeist, Netherlands, pp. 25–48.

Kubiena, W.L., 1938. Micropedology. Collegiate Press, Ames, p. 243pp.

Kubiena, W.L., 1956. The Soils of Europe. Th. Murby, London, p. 314pp.

van der Meer, J.J.M., 1976. Cartographie des sols de la région de Morat (Moyen-Pays suisse). Bulletin de la Société Neuchâteloise de Géographie 54, 5–52.

van der Meer, J.J.M., 1982. The Fribourg Area, Switzerland. A Study in Quaternary Geology and Soil Development. PhD Thesis, University of Amsterdam, p. 203pp.

van der Meer, J.J.M., Rabassa, J.O., Evenson, E.B., 1992. Micromorphological aspects of glaciolacustrine sediments in Northern Patagonia. Argentina. Journal of Quaternary Science 7, 31–44.

van der Meer, J.J.M., van Berghem, J.W., van Dreumel, P.F., 1994a. Microscopische waarnemingen aan waterbodems van de zuidrand van het noordelijke deltabekken. Grondboor and Hamer 48, 49–53.

van der Meer, J.J.M., Mücher, H.J., Höfle, H.C., 1994b. Observations in some thin sections of Antarctic glacial deposits. Polarforschung 62, 57–65.

van der Meer, J.J.M., Menzies, J., 2011. Micromorphology of unconsolidated sediments. Sedimentary Geology 238, 213–232.

Menzies, J., van der Meer, J.J.M., 2018. Micromorphology and microsedimentology of glacial sediments. In: Menzies, J., van der Meer, J.J.M. (Eds.), Past Glacial Environments. Elsevier, Amsterdam, pp. 753–806.

van Mourik, J.M., 1988. De ontwikkeling van een stuifzandgebied in de Kempen. Netherlands Geographical Studies 74, 363–370.

van Mourik, J.M., Dijkstra, E.F., 1995. Geen inheemse dennen rond de Oisterwijksche vennen; een palyno-ecologische studie. Nederlands Bosbouwtijdschrift 67, 51–59.

van Mourik, J.M., Wartenbergh, P.E., Mook, W.G., Streurman, H.J., 1995. Radiocarbon dating of palaeosols in aeolian sands. Mededelingen Rijks Geologische Dienst 52, 425–440.

van Mourik, J.M., 1999. The use of micromorphology in soil pollen analysis: the interpretation of the pollen content of slope deposits in Galicia, Spain. Catena 35, 239–257.

van Mourik, J.M., Nierop, K.G.J., Vandenberghe, D.A.G., 2010. Radiocarbon and optically stimulated luminescence dating based chronology of a polycyclic driftsand sequence at Weerterbergen (SE Netherlands). Catena 80, 170–181.

van Mourik, J.M., Hermans, P., 2011. Hoe Zuidoost-Brabant een milieuramp overleefde. Geografie 2011/1, 23–25.

van Mourik, J.M., Seijmonsbergen, A.C., Jansen, B., 2012. Geochronology of Soils and Landforms in Cultural Landscapes on Aeolian Sandy Substrates, Based on 14C and OSL Dating (Weert, SE Netherlands). InTech, Radiometric Dating, pp. 75–114.

van Mourik, J.M., Jansen, B., 2013. The added value of biomarker analysis in palaeopedology; reconstruction of the vegetation during stable periods in a polycyclic driftsand sequence in SE-Netherlands. Quaternary International 306, 14–23.

van Mourik, J.M., Wagner, T.V., de Boer, J.G., Jansen, B., 2016. The added value of biomarker analysis to the genesis of plaggic Anthrosols; the identification of stable fillings used for the production of plaggic manure. SOIL 2, 299–310.

Ngom, N.F., Garnier, P., Monga, O., Peth, S., 2011. Extraction of three-dimensional soil pore space from microtomography images using a geometrical approach. Geoderma 163, 127–134.

Ottenhof, C., Faz, A., Arocena, J., Nierop, K., Verstraten, J., van Mourik, J.M., 2007. Soil organic matter from pioneer

species and its implications to phytostabilization of mined sites in the Sierra de Cartagena (Spain). Chemosphere 69, 1341–1350.

Paton, T.R., Mitchell, P.B., Adamson, D., Buchanan, R.A., Fox, M.D., Bowman, G., 1970. Speed of podsolization. Nature 260, 601–602.

Piperno, D.R., 2006. Phytoliths, a Comprehensive Guide for Archaeologists and Palaeoecologists. Altamira Press, Rowman & Littlefield publishers.

Rappol, M., 1983. Glacigenic Properties of till. PhD Thesis. University of Amsterdam, p. 225pp.

Real Decreto 261/1996, 1996. De 16 de febrero. Protección de las aguas contra la contaminación producida por los nitratos procedentes de fuentes agrarias. BOENo 61 de 11 demarzo de 1996.

Sevink, J., de Waal, R.W., 2010. Soil and humus development in drift sands. In: Fanta, J., Siepel, H. (Eds.), Inland Drift Sand Landscapes. KNVV Publishing, Zeist, Netherlands, pp. 107–134.

Sobek, A.A., Schuller, W.A., Freeman, J.R., Smith, R.M., 1978. Field and Laboratory Methods Applicable to Overburdens and Minesoils. EPA-600/2-78-054.

Stoops, G., 2003. Guidelines for Analysis and Description of Soil and Regolith Thin Sections. Soil Science Society of America, Madison, p. 184pp.

Stoops, G., 2010. Micromorphology as a tool in soil and regolith studies. In: Stoops, G., Marcelino, V., Mees, F. (Eds.), Interpretation of Micromorphological Features of Soils and Regoliths. Elsevier, Amsterdam, pp. 1–13.

Stoops, G., Marcelino, V., Mees, F. (Eds.), 2018. Interpretation of Micromorphological Features of Soils and Regoliths. Elsevier, Amsterdam, 720pp.

Vera, H., 2011. 'dat men het goed van de ongeboornen niet mag verkoopen'; Gemene gronden in de Meierij van Den Bosch tussen hertog en hertgang 1000 – 2000. Uitgeverij BOXpress, Oisterwijk, Netherlands.

Viventsova, E., Kumpiene, J., Gunneriusson, L., Holmgren, A., 2005. Changes in soil organic matter composition and quantity with distance to a nickel smelter: a case study on the Kola Peninsula, NW Russia. Geoderma 127, 216–226.

van Vliet-Lanoë, B., 2010. Frost action. In: Stoops, G., Marcelino, V., Mees, F. (Eds.), Interpretation of Micromorphological Features of Soils and Regoliths. Elsevier, Amsterdam, pp. 81–108.

Walker, D.J., Clemente, R., Bernal, M.P., 2004. Contrasting effects of manure and compost on soil pH, heavy metal availability and growth of *Chenopodium album* L. in a soil contaminated by pyritic mine waste. Chemosphere 57, 215–224.

Wallinga, J., van Mourik, J.M., Schilder, L.M.L., 2013. Identifying and dating buried micropodzols in Subatlantic polycyclic driftsands. Quaternary International 306, 60–70.

Ye, Z.H., Shu, W.S., Zhang, Z.Q., Lan, C.Y., Wong, M.H., 2002. Evaluation of major constraints to revegetation of lead/zinc mine tailings using bioassy techniques. Chemosphere 47, 1103–1111.

Zanuzzi, A., Arocena, J.M., van Mourik, J.M., Faz Cano, A., 2009. Amendments with organic and industrial wastes stimulate soil formation in mine tailings as revealed by micromorphology. Geoderma 154, 69–75.

CHAPTER

2

Pollen analysis of soil archives

J.M. van Mourik[a,*], *M. Doorenbosch*[b]

[a]Institute for Biodiversity and Ecosystem Dynamics (IBED), Faculty of Science, University of Amsterdam, Amsterdam, the Netherlands; [b]Faculty of Archaeology, University Leiden, The Netherlands

*Corresponding author. j.m.vanmourik@uva.nl

2.1 Introduction

2.1.1 Summary of the development of soil pollen analysis

Modern palynology started at the beginning of the 20th century with the publication by *Lennart von Post* in 1916, which was the results of a study of peat deposits in Sweden (Manten, 1967). It took several decades to understand the problems concerning pollen morphology and determination, pollen production and distribution and pollen conservation and decay before pollen analysis developed from an innovative to a mature technique with applications in a broad scale of studies in biology, ecology, archaeology, climatology and earth sciences.

Studies of recent pollen morphology are based on grains removed from stamens, which are unaffected by any deterioration process. These studies resulted in handbooks with rules for pollen grain description and determination, as published by Moore et al. (1998) and Beug (2004).

A number of studies of the evolution of vegetation, climate, landscape and soil are based on ancient pollen spectra, extracted from aquatic sediments and peat bogs. Determination of ancient or fossil pollen grains is based on the comparison of characteristics of ancient with recent grains. Pollen diagrams of such deposits reflect, in general, changes in the pollen influx of the region around lakes and bogs and can be used for the description of regional vegetation development. The recognized pollen zones in such diagrams can also be used for palynological dating of the sediments.

Also, dry land surfaces are subjected to pollen influx and pollen grains can infiltrate into the soil. Consequently, the pollen content of soil horizons is post-sedimentary in contrast to the syn-sedimentary pollen in lake deposits and peat. Humous horizons of palaeosols contain microfossils like pollen and spores but macro remains are often absent with the exception of weathered root fragments. Pollen spectra, extracted from humous soil horizons, can provide interesting palynological fingerprints and can be of importance for archaeological and landscape ecological studies. But before we can interpret soil pollen spectra reliably, we must have a better understanding of the processes of soil infiltration and conservation of pollen grains. The development of soil pollen analysis has been summarized by van Mourik (1986, pp. 37–73) and the following are some milestones in the evolution of the technique:

Reading the Soil Archives
https://doi.org/10.1016/B978-0-444-64108-3.00002-1

1. Florschütz (1941) suggested that pollen precipitation occurs not only in lakes and peat bogs but also on dry land surfaces. He presented pollen spectra of the soil horizons of heathlands. He considered the pollen content as syn-sedimentary pollen in sandy deposits and because of that his interpretation resulted erroneously in palynological dating of soil horizons. Also Dimbleby (1957) reported the presence of pollen grains in terrestrial soils.
2. Guillet (1970) pointed to the presence of pollen in soil samples of Podzols in northeastern France; Havinga (1963) discovered a connection between pollen zoning in podzolic soils in coversand in the Netherlands and the retrogression of soil faunal activity during soil development.
3. Elsik (1971) and Havinga (1971, 1974) investigated the deterioration of pollen grains between liberation from the stamen to its incorporation into sediment or soil. The most common processes are corrosion, degradation and mechanical damage (Figs. 2.1.3–2.1.4). The microenvironment within sediments or soils can affect the preservation quality and even the types of pollen represented. Experiments on the deterioration of pollen grains in litter bags (Havinga, 1984) have shown that differences in the chemical composition of the exine affects their preservation potential. The percentage of resistant pollen species in soil increases relative to those more prone to deterioration, while some species do not fossilize at all. Summarized, pollen corrosion is caused by microbial attack, by fungi and bacteria, which results in perforation of the exine. Degradation is caused by chemical oxidation, which leads to thinning rather than perforation. Both corrosion and degradation are promoted by drainage and aeration of the host sediment or soil. Mechanical damage is caused by physical agents, like shrinkage and swelling of soil, which result in crumpling or rupturing of the exine. Damage also occurs during transport by wind and insects, and as a result of consumption and redistribution by soil invertebrates. Last but not least, the methods used to extract pollen and spores for study also contribute to their deterioration.
4. Benninghof (1962) introduced the method of absolute pollen counting, based on the addition of a known amount of exotic pollen or spores to the sample, used for pollen extraction. It is possible to use a homemade suspension with a known density of a pollen or spore type of your own choice (Hartman, 1968) or to use commercial tablets (Stockmarr, 1971). Pollen density can be used to estimate the sedimentation rate of peat and lake deposits but also to identify soil infiltration from stable (soil) surfaces. In general the pollen densities in soil profiles decrease logarithmically with depth (van Mourik, 1999).
5. van Mourik (1986, 1999) introduced the use of soil micromorphology in pollen analysis to microscopically identify the location of pollen grains in the soil matrix and the origin and

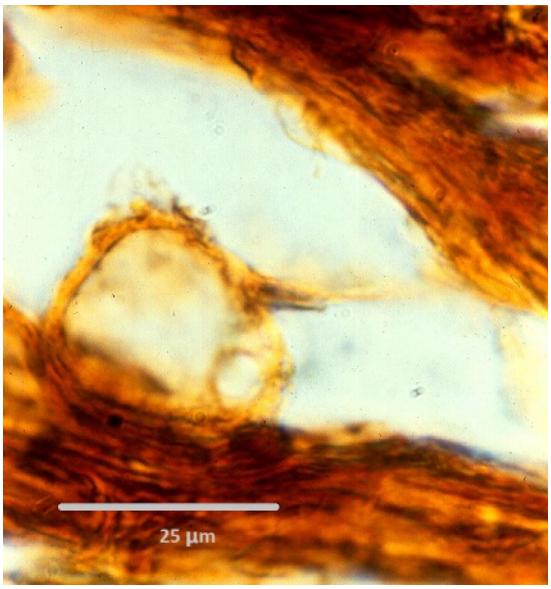

FIGURE 2.1.1 Free pollen grain embedded by tissue in a hydromorphic Histosol.

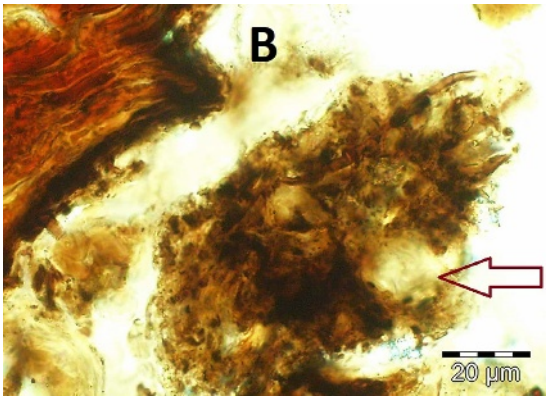

FIGURE 2.1.2 Pollen grain enclosed in an organic aggregate in a xeromorphic humous soil horizon.

properties of the embedding and conserving soil materials (Figs. 2.1.1–2.1.2).

The combination of concepts such as pollen infiltration, retrogressive bioturbation, pollen density distribution and pollen conserving microenvironment explains the characteristics of pollen profiles in mineral soils. Fig. 2.1.5 shows the relation between soil development and pollen zoning for sandy soils in northwestern Europe.

Phase 1: Fluvial and aeolian sediment may contain syn-sedimentary pollen (association I).

FIGURE 2.1.3 Pollen grain (*Quercus*) affected by mechanical corrosion.

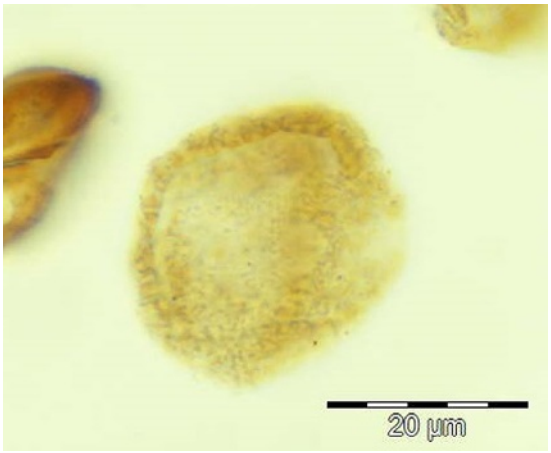

FIGURE 2.1.4 Pollen grain (*Quercus*) affected by microbial corrosion.

The pollen density curve (log *D*) is the result of the pollen influx and the sedimentation rate but in general the pollen curve in sediments (parent material for soil development) is linear. Not all sediments contain syn-sedimentary pollen. Lateglacial coversands are palynologically sterile and Holocene driftsand has a syn-sedimentary pollen content. Pollen is deposited on the soil surface and part of the litter layer of the humus forms. The quality of the humus form will control the process of pollen infiltration.

Phase 2: A herbaceous pioneer vegetation develops and produces litter, relatively rich in albumen and poor in lignin. The soil pH in this phase is 5–6 and the litter quality is eutrophic (C/N ratio <20). A large part of the organic matter added to the soil consists of underground, decomposing roots (Rhizomull humus form). After microbial attack the organic mass is consumed especially by arthropods. The excrements of these primary devourers are relatively rich in albumen and form together with other organic products (including pollen grains) the food secondary devourers as soil inhabiting earthworms with a low acid tolerance (Walch et al., 1970; Wallwork, 1976; Satchell, 1983). Earthworm species occurring in humid soils

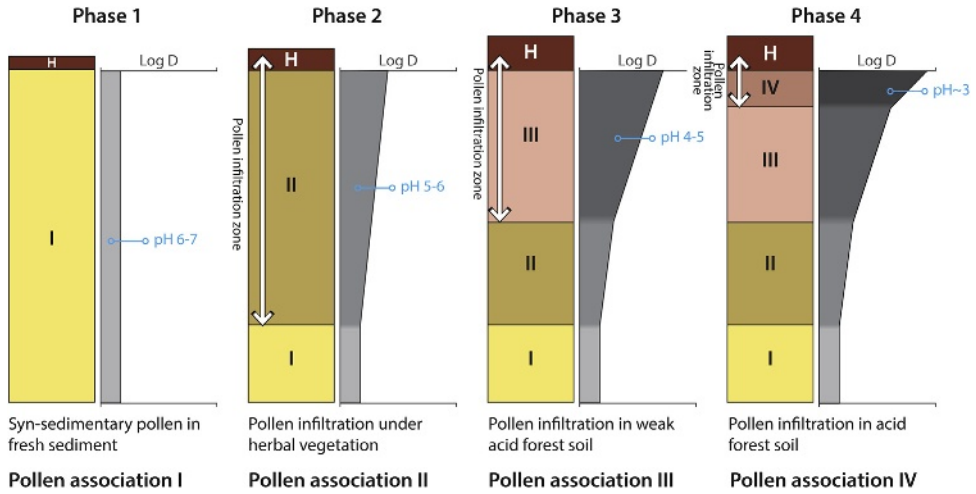

FIGURE 2.1.5 Pollen zoning in sandy soils as the result of pollen infiltration under changing pedological and biotical conditions. The *blue arrows* indicate retrogression of soil fauna activity.

(such as the *Allolobophora* and the Lumbricidae) are burrowing down to 100–150 cm deep in the soil. Their execrated aggregates are medium sized (100–300 μm) and consist of a mix of soil particles and vegetable debris (including pollen grains) saturated with intestinal secretion (Hayes, 1983). This secretion is poorly soluble in water, is even water repellent and consequently aggregate stabilizing. Because of that, the microenvironment in earthworm excrements is perfect for pollen preservation. Earthworms move vertically peristaltically and deposit their excrements in the soil or (by lack of space) on the soil surface. Thus earthworms are responsible for the infiltration of pollen grains into the soil and as long as this process stays active there is a continuous homogenization of older (infiltrated and syn-sedimentary pollen) and younger (association II) pollen. The pollen density curve is (logarithmically) decreasing with depth.

Phase 3: During the Early Holocene the vegetation developed from a herbaceous vegetation to a (weak acid) deciduous forest. The soil pH decreased to 5–4, the litter of the forest (*Quercetum mixtum*) has a C/N ratio of 20–30, dominant houmus forms are now the Mullmoder and the Mormoder, soil formation proceeded from Umbrisol to Podzol and the population of earthworms with a low acid tolerance is replaced by small-sized red pigmented earthworms with a higher acid tolerance. Most of them are not soil- but humus-inhabiting animals and burrow activity is restricted. Most of them are not burrowing their own pipes but follow the root holes. Their excrements are small (50–150 μm). Micromorphological observations show that these excrements do not contain mineral particles, in contrast to the excrements of the bigger, deep-burrowing worms (van Mourik, 1999). Pollen grains can be embedded and preserved in aggregates or clusters of such excrements (van Mourik, 2003). Pollen infiltration proceeds, but the infiltration depth decreases and the deeper part of the profile with the II association is no longer affected by homogenization by retrogressive soil fauna activity (Havinga, 1963). In the active infiltration zone, pollen association III develops.

Phase 4: Forest degradation and soil acidification are responsible for the next system change. Soil pH decreases to 3-4, the C/N value of the litter increases (>30), Mormoder is the dominant humus form and the umbric Podzols transform

to carbic Podzols. Earthworms are no longer present and arthropods are now the main decomposers of litter. They are humus inhabiting, not vertically burrowing. Aggregates of their excrements, embedding pollen, can move down in root holes and cracks. This phase is reflected in pollen association IV. Due to retrogression, the deeper part of association IV will fossilize.

Besides the presence of syn-sedimentary pollen in the sediment and the retrogressive infiltration of pollen from the surface, pollen grains are subjected to various forms of corrosion (Elsik, 1971). This means that the pollen densities of association A can decrease over time and also that the percentage of corrosion-resistant pollen can increase. The same is true for the fossilized parts of associations B and C. Pollen infiltration in deeper root holes and cracks 'contaminates' the older, fossilized associations.

2.1.2 The interpretation of soil pollen spectra

The interpretation of pollen spectra of soil samples requires understanding the processes of pollen incorporation into the soil and its subsequent preservation. The pollen content of peat and lake deposits is considered to be syn-sedimentary. In rain water-controlled moorlands the water table is relatively stable, and peat accumulates rapidly. Pollen is incorporated in water-saturated organic sediment, and deterioration is inhibited. In thin sections it can be observed how free pollen grains occur in the matrix, composed of mainly organic or skeleton particles. The water table of groundwater-controlled peat moors is relatively stable, resulting in more rapid decomposition of organic litter and greater deterioration of pollen by corrosion and degradation. The pollen content of lacustrine deposits is well preserved, while conditions remain water logged, but following drainage and aeration the grains oxidize completely.

The pollen content of terrestrial humous soil horizons is post-sedimentary. The aerobic conditions of well-drained soils promote fast corrosion and degradation of free pollen grains because the grains are not protected against oxygen. The interpretation of soil pollen spectra, extracted from soil samples, requires an understanding of the processes that control the infiltration, incorporation and preservation of pollen grains in the soil matrix. In thin sections of undisturbed soil, pollen and spores can be identified as spherical sporoid bodies. Taxonomic identification of pollen grains in thin sections is impossible because the surface of the exine is not cleaned by a pollen extraction technique, may even be hidden by fine organic and mineral plasma and most of the grains in 20–25 μm thick thin sections are dissected. The micromorphological setting of the pollen grains, however, gives information about the infiltration process into the soil and the conditions of preservation (van Mourik, 1999, 2003).

2.1.3 Pollen infiltration and conservation

Many pollen diagrams of well-drained soils seem to show a zonation that reflects local landscape-ecological change (Dijkstra and van Mourik, 1995; Davidson et al., 1999). Pollen is deposited as part of the aeolian organic litter influx on a soil surface. Water does not transport pollen into the soil because pollen grains have hydrophobic properties and the mean grain size (coarse silt) does not allow vertical transport of single grains through primary voids (van Mourik, 1999). Micromorphological observations show that pollen is present in faecal pellets produced by soil invertebrates, but never as single grains in voids or channels. Single pollen grains only occur in the ectorganic litter horizons of humus profiles (Dijkstra and van Mourik, 1995). After deposition, pollen grains are subjected to oxidation and microbial decomposition and consequently a part of the pollen influx will be lost, but another part will be consumed by grazing animals and the soil fauna and incorporated in faecal pellets. Depending on the source

vegetation, the litter may consist of a range of tissues with various C/N values, which are decomposed by different soil organisms at various rates.

In chemical-rich (eutrophic) soil systems, the protein content of the litter is high (C/N value <15). Deposition on the surface consists of litter and droppings of grazing animals. Fresh litter is fermented and decomposed by the soil fauna consisting of earthworms, microarthropods and microbes like bacteria and fungi. Earthworms consume and digest chemically rich litter, including bacterial mucus, fungi and pollen. The walls of pollen grains are not digestible and are incorporated into their excrements. This dense acidic microenvironment protects pollen against microbial attack and deterioration, but promotes mechanical damage. Earthworms consume in the litter layer but live and excrete in the mineral soil and are therefore of great importance for the dispersion of pollen through the soil profile (Walch et al., 1970). Earthworms promote the development of Vermimul humus forms, characterized by excremental aggregates and secreted in channels in the mineral soil. The internal fabric of such excrements consists of a mixture of fine organic particles (including pollen grains), fine mineral grains and (organic and mineral) plasma.

In chemically less-rich (mesotrophic) soil systems the protein content of the litter is lower ($15 < C/N < 30$), and the decomposition of litter is controlled by humus-inhabiting soil animals, mainly microarthropods and fungi. They produce excrements consisting of fine organic skeleton grains and organic plasma. For most of the microarthropods, pollen grains are too big to consume, but pollen grains are embedded and conserved in clusters of ageing faecal pellets. This activity results in the development of Mormoder humus forms. In thin sections, pollen grains can be observed in clustered organic aggregates (Fig. 2.1.2). Pollen containing aggregates can penetrate the mineral soil in root holes and cracks.

In chemically poor (oligotrophic) soil systems, low (C/N value >30), soil and humus animals are absent and litter decomposition is controlled by fungi. They do not produce pollen-embedding and -conserving excrements but an ectorganic layer, consisting of particles of fermenting tissue and organic plasma, including organic acids that will leach to the B horizon or even to the groundwater zone.

Some examples of the application of soil pollen analysis in pedology and geomorphology will be discussed in the next paragraphs: the infiltration and life cycle of pollen grains in the Mormoders of a forest soil (Drenthe, the Netherlands) in Section 2.2, the pollen distribution in polycyclic slope deposits (Galicia, Spain) in Section 2.3, the origin of pollen grains in colluvic Stagnosol (Gutland, Luxembourg) in Section 2.4 and the application of soil pollen analysis in archaeology in Section 2.5.

Other examples of soil pollen diagrams of the soil archives of plaggic Anthrosols, polycyclic Arenosols and initial and buried Podzols related to research questions concerning the genesis of plaggic Anthrosols and driftsand deposits in northwestern Europe (van Mourik et al., 2012, 2013) are included in Chapters 3,4,5 and 6.

2.1.4 Pollen extraction

Pollen analysis is a tool applied in many research institutions involved in earth and life sciences. Most of them developed their own laboratory manuals for sample treatment, extraction and preparation of pollen slides. Pollen extraction is based on a sequence of steps, potassium hydroxide digestion > hydrochloric acid treatment > hydrofluoric acid treatment > acetolysis. Useful information about treatment of samples and pollen extraction is found in Moore et al. (1991), Chapter 4 and Campbell et al., 2016. It is evident that punctuality during sampling and lab procedures is crucial for the quality of the results. Also, knowledge of the geoecological development of the soil archives and of the

sample composition promotes the quality of the results.

2.2 The distribution pattern of pollen grains in polycyclic slope deposits (Galicia, Spain)

2.2.1 Introduction

In a palynoecological study of Holocene slope deposits in Galicia, the combination of soil pollen analysis and soil micromorphology resulted in an acceptable reconstruction of the development of these polycyclic soil sequences. The investigated sites are indicated on the geomorphological map of Galicia (Fig. 2.2.1). In this section we discuss the results of profile Monte Pedroso, situated in the site Santiago. The results of all the sampled profiles are presented in van Mourik (1986).

The Galician area forms part of a Hercynian orogen composed of acid metamorphic phyllites and intrusive granites (Noon, 1969; de Galicia, 1984). During the Eocene, the relief obtained the character of a planation surface with isolated hills and mountain ranges (sierras) resulting from planation under humid tropical conditions. During the Miocene the orogen was uplifted. Tectonic activity continued into the Holsteinian. The Quaternary can be considered as a period during which climate and topography gave rise to slope processes which operated fast enough to inhibit or interrupt pedogenic profile differentiation, but not fast enough for unweathered rock to become exposed. During interpluvial periods the vegetation was probably well developed, resulting in soil development (Noon, 1969; Guitian Ojea and Carballas, 1968). During pluvial periods, degradation of the vegetation promoted mass movement. This resulted in erosion and some accumulation of solifluction deposits only on suitable downslope sites.

Soil erosion during the Late Holocene was responsible for truncation of soils on the slopes and for deposition of colluvium downslope and on valley bottoms. In sample area Escairon (site 1 in Fig. 2.2.1) we sampled colluvial deposits on the bottom of shallow valleys (Fluvisols). Radiocarbon dating pointed to a start of the deposition around calBC 680, just before the Roman Time (van Mourik, 1986).

Due to soil erosion, most soils on the hillslopes have been truncated, but on sheltered sites the soil in the Pleistocene solifluction deposit (ferralic Cambisol) was buried by Holocene colluvium. On this site we could sample valuable soil archives (van Mourik, 1986) for profile Avion (site 6 in Fig. 2.2.1), which is a good example of a hardly truncated buried Cambisol (Fig. 2.2.2A and B), and profile Buyo (site 3 in Fig. 2.1.1), which is a good example of a seriously truncated Cambisol, buried by Holocene colluvial deposits.

Truncation of a Cambisol in gravelly solifluction material results in the development of stone lines (Fig. 2.2.3A and B). Later, we present the results of the micromorphological and palynological analyses of profile Monte Pedroso (site 4 in Figs. 2.2.1 and 2.2.4).

Fig. 2.2.5 shows a schematic diagram of a sequence of slope deposits in the Galician landscape. On the upper slopes the regolith is very thin. The observed soils are associations of lithic and humic Leptosols. Downslope, especially in dell-shaped depressions and on concave foot slopes, the thickness of the regolith increases. The soils are associations of humic Leptosols and (buried) Cambisols.

The humic Leptosols on the middle slopes are seriously truncated ferralic Cambisols, transforming in colluvic humic Regosols. The local name for this specific profile is Ranker Atlantico (Guitian Ojea and Carballas, 1968). Due to the polygenetic character of slope deposits it is not possible to find a satisfactory corresponding soil unit name in the world soil classification (UNESCO/UNESCO, 1988).

Humous horizons of well-drained soil sequences such as polycyclic slope deposits

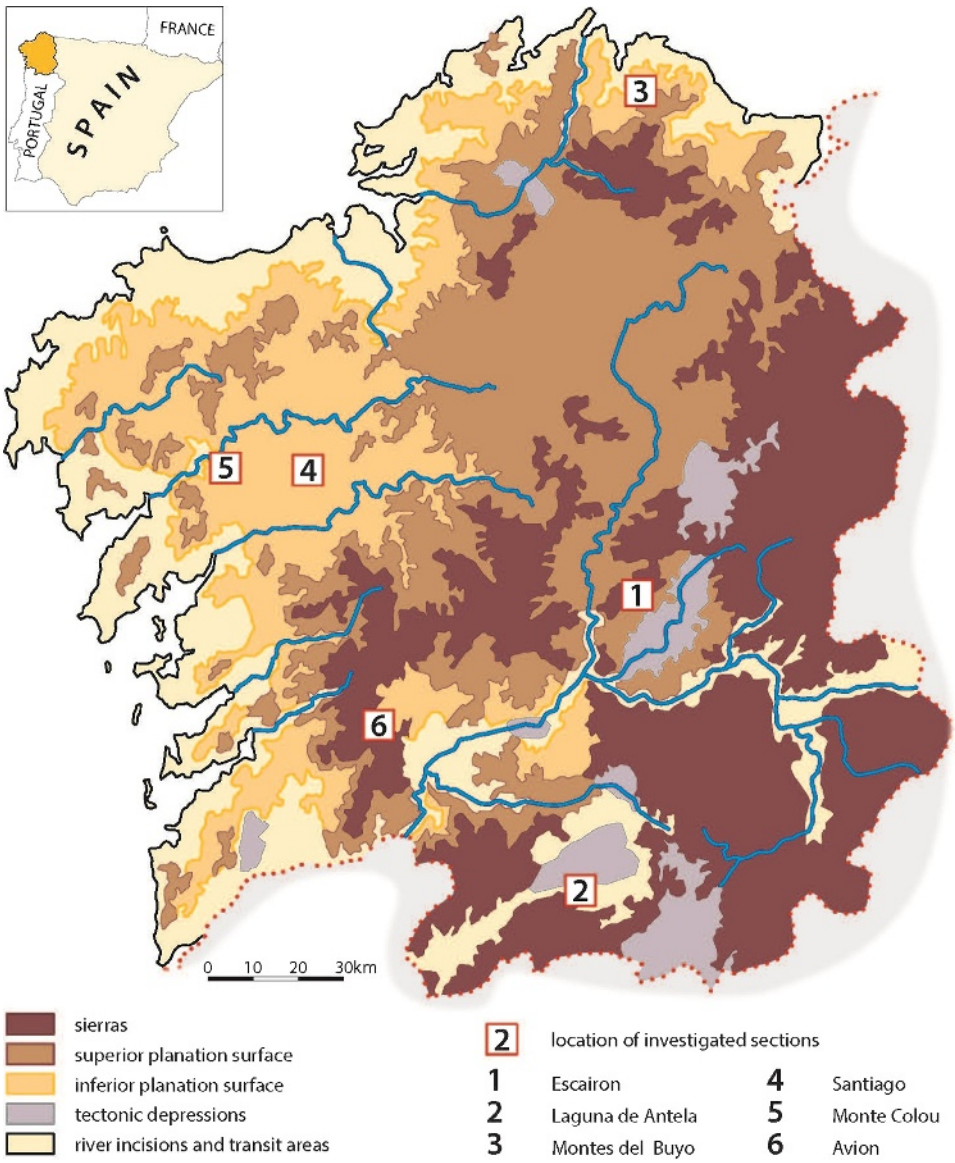

FIGURE 2.2.1 Simplified geomorphological map of Galicia with the locations of the investigated sample sites. *After J.M. van Mourik, Pollen Profiles of Slope Deposits in the Galician Area (N.W. Spain). Netherlands Georaphical Studies, KNAG Amsterdam, 12 (1986) 171 pp.*

contain pollen. Comparison of the pollen spectra of such profiles with the pollen zones of reference diagrams of peat deposits seems to offer palynoecological information, relevant for the reconstruction of the genesis of polycyclic slopes. But first we must explain how pollen grains infiltrate in the soil and stay conserved. In palynological studies of semi-terrestrial and aquatic

FIGURE 2.2.2 (A) Valley of the Rio Avia. (B) Profile Avion (colluvic ferralic Cambisol). Site 6.

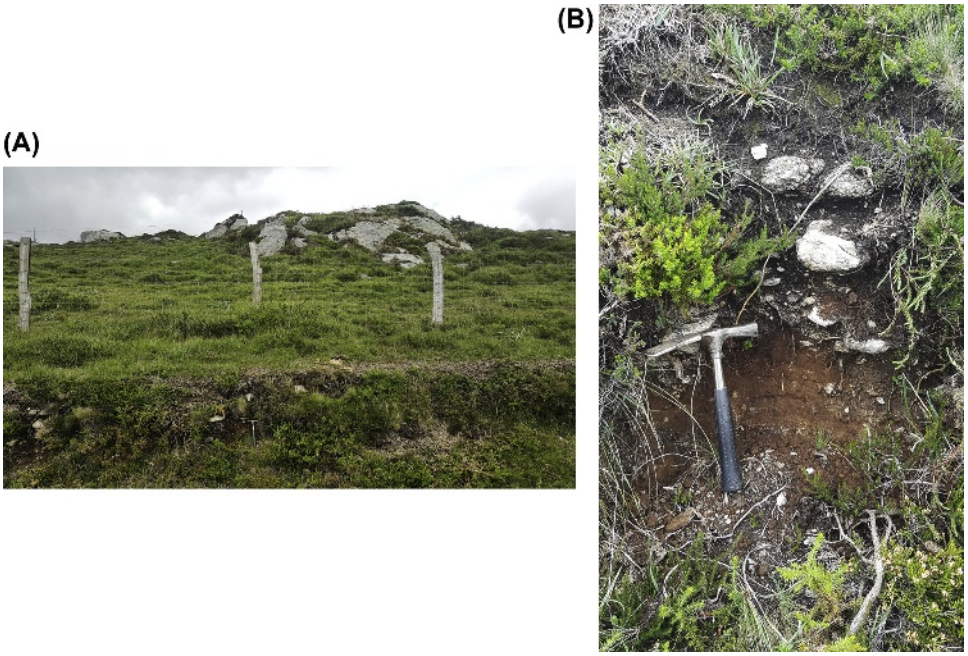

FIGURE 2.2.3 (A) Montes de Buyo. (B) Profile Buyo (humous colluvium, overlying stone lines and a truncated ferralic Cambisol). Site 3.

FIGURE 2.2.4 Soil profile Monte Pedroso (colluvium, stone line, overlying a truncated ferralic Cambisol). Site 4.

deposits, pollen is considered to be part of the sediment, and anaerobic conditions in water-saturated deposits promote its conservation. This is different for pollen grains in well-drained soils. Aerobic soil conditions promote bio-oxidation of unprotected pollen grains. A reliable interpretation of soil pollen spectra requires knowledge of the processes of post-sedimentary pollen infiltration and conservation of pollen grains into the soil. Micromorphology is an important technique to investigate these processes. This is demonstrated in a case study of polycyclic slope deposits in Galicia (Spain). The foot slopes of the granite hills are covered with Pleistocene solifluction deposits (Nonn, 1966). Soil development in such deposits tends to Cambisols and cambic and umbric Podzols. The thickness of the humous epipedon of the soils on slopes can increase to several decimetres. In the traditional local soil descriptions these soils were classified as 'Ranker Antlantico' (de Galicia, 1984) and it was not clear whether the growth of the humous epipedon was a pedogenic or a geogenic process (Guitian Ojea and Carballas, 1968). It was supposed that pollen analysis could provide evidence. For a reliable interpretation of soil pollen diagrams it was necessary to understand in which way pollen grains can survive in such well-drained soils. For this reason, thin sections of undisturbed samples were made for additional micromorphological research. In the next paragraphs the combined results of pollen analysis and micromorphology of one of the investigated slope profiles (Monte Pedroso) are presented. Results of the analysis of more slope profiles in Galicia have been published in van Mourik (1986).

2.2.2 Palynological references

In the palynological study of Galician slope deposits, a characteristic sequence of pollen associations was observed. ^{14}C dating of samples of such material are not reliable (Chapter 3) and therefore the associations recognized in slope profiles cannot be radiocarbon dated. But we can use palynological time markers, based on the description of the lateglacial and Holocene vegetation development of Spain by Mendez Amor and Florschütz (1961) and of some radiocarbon-dated Holocene diagrams of Histosols in Galicia: Torbero de Byo (site 3); Torbero de Brins (site 4); Torbero de Toiriz (sample 1); and Torbero de Antela (site 6) (van Mourik, 1986). The palynological zones are summarized in (Table 2.1.1).

Quercus, *Castanea* and *Pinus* are important palynological time markers. For soil pollen diagrams it counts more than for peat diagrams that the interpretation of the relative scores

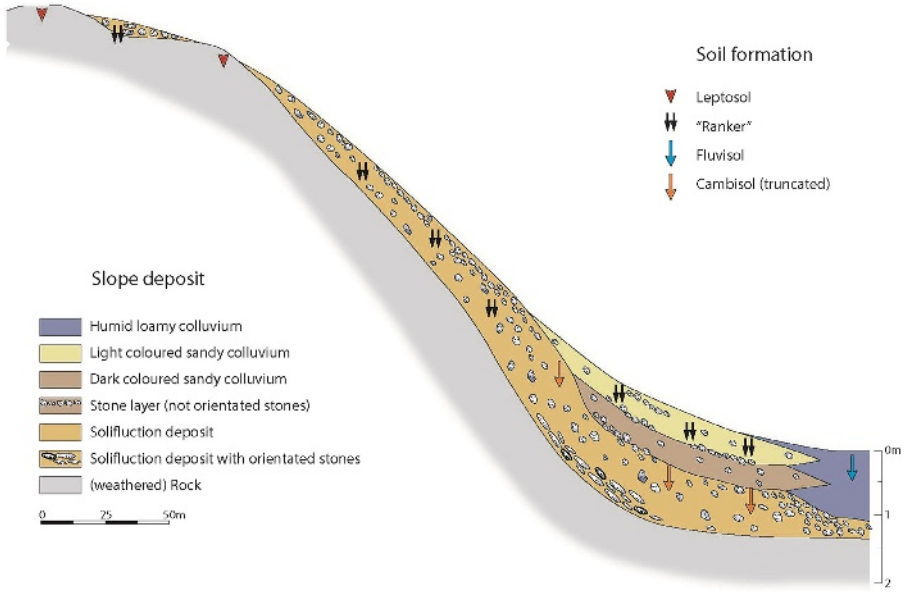

FIGURE 2.2.5 Catena of a granite hillslope in Galicia with slope deposits and soils. *After J.M. van Mourik, Pollen Profiles of Slope Deposits in the Galician Area (N.W. Spain). Netherlands Georaphical Studies, KNAG Amsterdam, 12 (1986) 171 pp.*

TABLE 2.1.1 Pollen associations used as regional palynological time markers.

Association	Chronozone	Palynological characteristics
L	Subatlantic	Pine plantation
K	Subatlantic	Chestnut plantation
J	Subatlantic	Heath, dominated by Ericaceae
H	Subatlantic	Cultivated land, dominated by Poaceae and Cerealia
G	Subatlantic	Deforestation; increase of *Castanea* and Cerealia
F	Subboreal/Subatlantic	First signs of deforestation; decrease of *Quercus*
E	Atlantic/Subboreal	Deciduous forest, dominated by *Quercus* and *Corylus*
D	Atlantic/Subboreal	Deciduous forest, dominated by *Quercus*
C	Boreal	Gradual displacement of the steppe by deciduous forest
B	Late Dryas/Preboreal	Steppe dominated by Poaceae and Asteraceae
A	Allerød	Steppe dominated by Poaceae and Asteraceae, scattered pine trees

After J.M. van Mourik, Pollen Profiles of Slope Deposits in the Galician Area (N.W. Spain). Netherlands Georaphical Studies, KNAG Amsterdam, 12 (1986) 171 pp.

requires knowledge about pollen dispersal. What is the abundance of tree growths onsite? What is a reflection of long-distance transport? Fig. 2.2.3 shows the relative scores of *Quercus*, *Castanea* and *Pinus* related to the distance of the sample site to the trees.

Slope deposits were sampled in the areas Buyo (3), Santiago (4), Colou (5) and Avion (6). The sequence of pollen zones in the slope profiles was similar but interpretation of soil pollen diagrams required evidence that the pollen content is more than 'contamination'. Micromorphological observation provides ideal evidence of the origin of pollen grains and the preservative microenvironment. The results of pollen analysis and micromorphology of profile Monte Pedroso (area 4) are presented as an example of the multiproxy analysis of slope deposits. Fig. 2.2.4 shows the profile description. The soil pollen diagram (Fig. 2.2.5) shows a sequence of the B associations infiltrated in the B and C horizons of the truncated palaeosol in the solifluction layer. The F, G, J and L associations are recognized in the overlying colluvial sediments. Fig. 2.2.7 shows the histogram of micromorphological observations.

2.2.3 Profile description

Profile Monte Pedroso is situated northwest of Santiago de Compostela (sample site 4 in Fig. 2.1.1, coordinates: 42°55′00″N/8°33′58″W). Fig. 2.2.6 shows the soil catena, Fig. 2.2.7 the soil description, Fig. 2.2.8 the diagram of micromorphological observations and Fig. 2.2.9 the pollen diagram. The nomenclature, used for micromorphological description (using magnification factor 78), is based on Bal (1973) and Brewer (1976). The names of the microenvironments (using magnification factor 780) of pollen grains was added by van Mourik (1986).

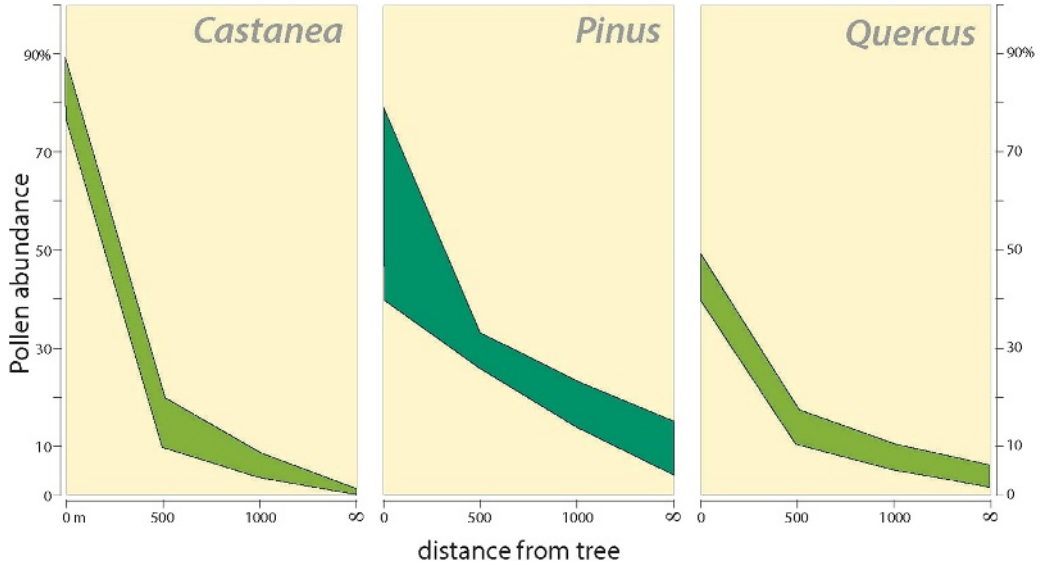

FIGURE 2.2.6 Pollen dispersal of *Castanea*, *Pinus* and *Quercus*; the relative scores in pollen spectra of 120 surface samples collected in the sample sites (Fig. 2.6). 1 = tree is present at the sample location; 2 = tree is present within a limit of 500 m; 3 = tree is present within a limit of 1000 m; 4 = tree is not present within the limit of 1000 m. *After J.M. van Mourik, Pollen Profiles of Slope Deposits in the Galician Area (N.W. Spain). Netherlands Georaphical Studies, KNAG Amsterdam, 12 (1986) 171 pp.*

Depth (cm)	Horizon	Ass.	%C	pH	Material
6	F	L	1.4	3.7	Fermented organic matter
13	Ah	L	8.3	3.7	Very dark grayish brown (10YR3/2) sandy loam; very weak crumbly, very friable; many roots
27	C1	J	4.5	3.9	Dark grayish brown (10YR4/2) sandy loam; slightly gravelly (2cm); structureless; many roots
29	S1	-	-	-	Dark brown (10YR4/3) sandy loam; very gravelly (2cm); structureless, loose; common roots
38	C2	G	6.3	4.0	Dark brown (10YR4/3) sandy loam; slightly gravelly (2cm); structureless, loose; common roots
39	S2	-	-	-	Very dark grey (10YR3/1) sandy loam; gravelly (2cm); structureless, loose; common roots
78	C3	F	6.9	4.0	Very dark grey (10YR3/1) sandy loam; slightly gravelly (2cm); very weak crumbly, loose; few roots
85	2S	F	3.0	4.2	Very dark grey (10YR3/1) sandy loam; very stony (20cm); weak crumbly, very friable; few roots
100	2B	B_*	0.7	4.2	Brown (10YR5/3) sandy loam; slightly gravelly (6cm); faint diffuse dark brown mottles (10YR4/5);structureless, very friable; very few roots
140	3C1	B_*	0.1	4.3	Light brownish grey (10YR6/2) sandy loam; slightly gravelly (4cm); faint diffuse brown mottles (10YR5/3); structureless, friable; very few roots
160	3C2	-	-	4.3	Light olive grey (5YR6/2) sandy loam; weathered granite, friable to firm; roots absent

FIGURE 2.2.7 Profile Monte Pedroso profile description. *After J.M. van Mourik, Pollen Profiles of Slope Deposits in the Galician Area (N.W. Spain). Netherlands Georaphical Studies, KNAG Amsterdam, 12 (1986) 171 pp.*

Many parts of the slopes have been subjected to soil erosion, but in sheltered zones, soil erosion was restricted and deposition took place. The accumulation of slope deposits can be interrupted by a short-lived erosion phase, recorded by stone lines in the sequences of deposits. The investigated slope profiles show a sequence of late Holocene colluvial layers, overlying a palaeosol developed in a lateglacial/Early Holocene solifluction layer, deposited on weathered granite.

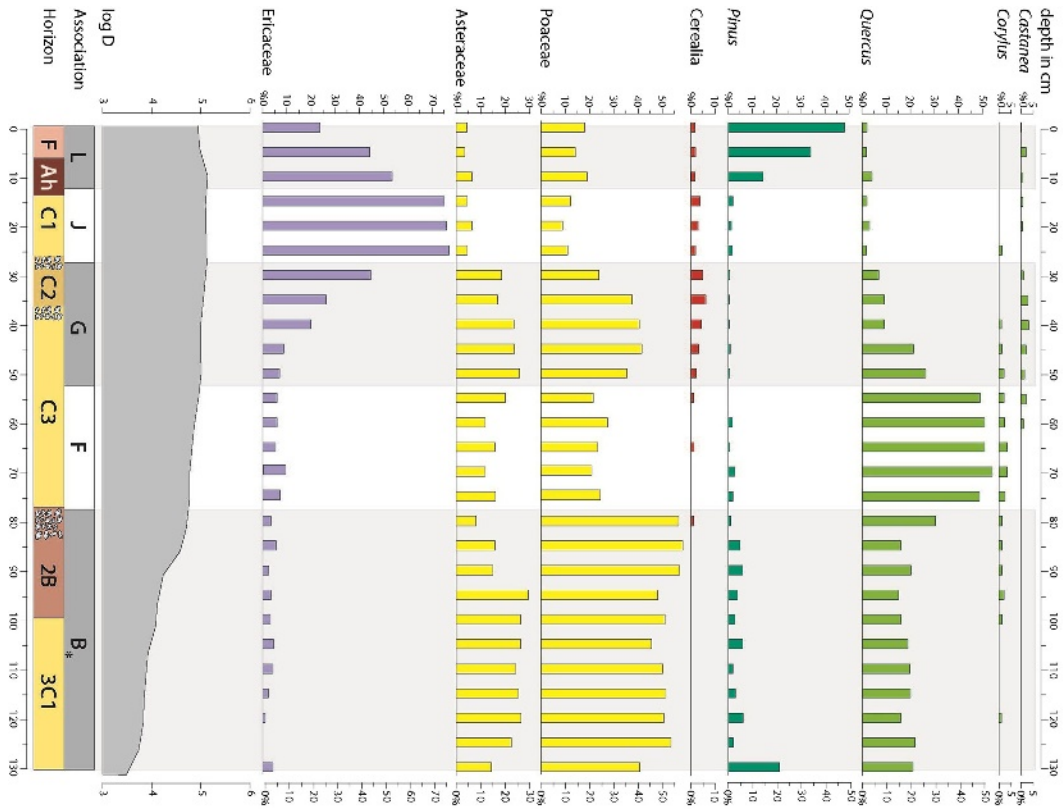

FIGURE 2.2.8 Profile Monte Pedroso pollen diagram. *After J.M. van Mourik, Pollen Profiles of Slope Deposits in the Galician Area (N.W. Spain). Netherlands Georaphical Studies, KNAG Amsterdam, 12 (1986) 171 pp.*

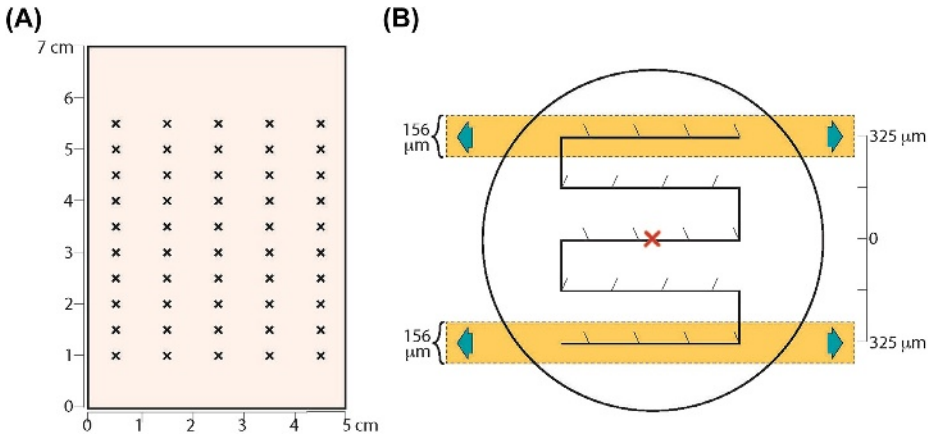

FIGURE 2.2.9 Strategy for observation of pollen grains in a thin section. *After J.M. van Mourik, Pollen Profiles of Slope Deposits in the Galician Area (N.W. Spain). Netherlands Georaphical Studies, KNAG Amsterdam, 12 (1986) 171 pp.*

Podzolation was the dominating soil-forming process in the solifluction deposits, resulting in Cambisols and cambic Podzols (in the local soil classification 'Tierra Parda'). In profile Monte Pedroso the soil in the solifluction layer is truncated. The Ah and the upper part of the B are reduced to a stone line.

Soil development in the colluvial layers is inhibited by continuous colluviation. The local soil classification indicates a dark-coloured epipedon, consisting of humous colluvium deposited on the Ah of the palaeosol 'Rankers Atlantico'.

Leptosols occur on the higher parts of the slope due to intense soil erosion. Downslope to the valley bottom the texture of the colluvium becomes loamy and here we find Fluvisols.

2.2.4 The identification of pollen grains in thin slope deposits

In thin sections, pollen grains can be identified as opaque organic skeleton grains with a spherical to elliptical shape, a diameter of about 15–30 mm and a smooth wall. As a rule, the living content has disappeared and only the exine remained. Identification of pollen grains in thin sections requires a magnification factor of at least 500 (van Mourik, 1986, 1999). The mean diameter of pollen grains in thin sections is systematically smaller than in normal pollen slides, because the chemical treatment to which the grains are submitted during extraction always causes some swelling. Furthermore, it is difficult to determine pollen grains in thin sections, since chemical treatment, including cleaning and swelling of the grains, did not take place, and because organic and mineral plasma, attached to the wall, hides properties like sculpture and aperture of the grains.

Pollen identification in thin sections was carried out in two steps (Fig. 2.2.9). The first involves a quantitative description of the fabric. For each search, 50 focusing points are inspected by means of a Leitz–Blaschke occular (magnification factor 78). Each focusing point determines the position of 20 observation points. Based on 1000 observations, a fairly reliable volumetric quantification of micromorphological objects can be achieved. The results are shown as percentages in the left-hand section of the micromorphological histogram. The next step is to search a limited sample volume section for identification and classification of pollen grains. For this purpose, a magnification factor 780 has been used. The sample volume consists of 20 bands, each having a length of 4 cm, a width of 0.0156 cm and a thickness of about 0.0020 cm. The position of the bands in the sections is determined by the location of the focusing points. The total sample volume amounts to 0.0025 mL. When a pollen grain has been identified it is necessary to record the microenvironment (magnification 78). The observed grains are expressed in absolute numbers in the right-hand section of the histograms. The amount of observed pollen grains in thin sections is a fraction of the total amount that should be present according to the pollen concentrations in the pollen slides. The results of the micromorphological analysis are summarized in Fig. 2.2.10.

The skeleton of the colluvial C horizons consists mainly of single grains and a small percentage of lithorelicts. These relicts are rounded and free from weathering skins, indicating transport of the material. The proportion of humiskel is low. Some melanons (glaebules, formed by melanosis) are present. They have sharp boundaries and are round in shape, which again indicates transport of the material. The fine material in the colluvial horizons consists of a mixture of fragmented and colloidal organic matter and some silt, which was described as silasepic mullicol. A part of the fine material is observed in spherical to elliptical aggregates with dimensions of 40–120 mm. These are coprogenic aggregates of soil animals which have preserved their shape after secretion (modexi). The internal fabric of these modexi is identical

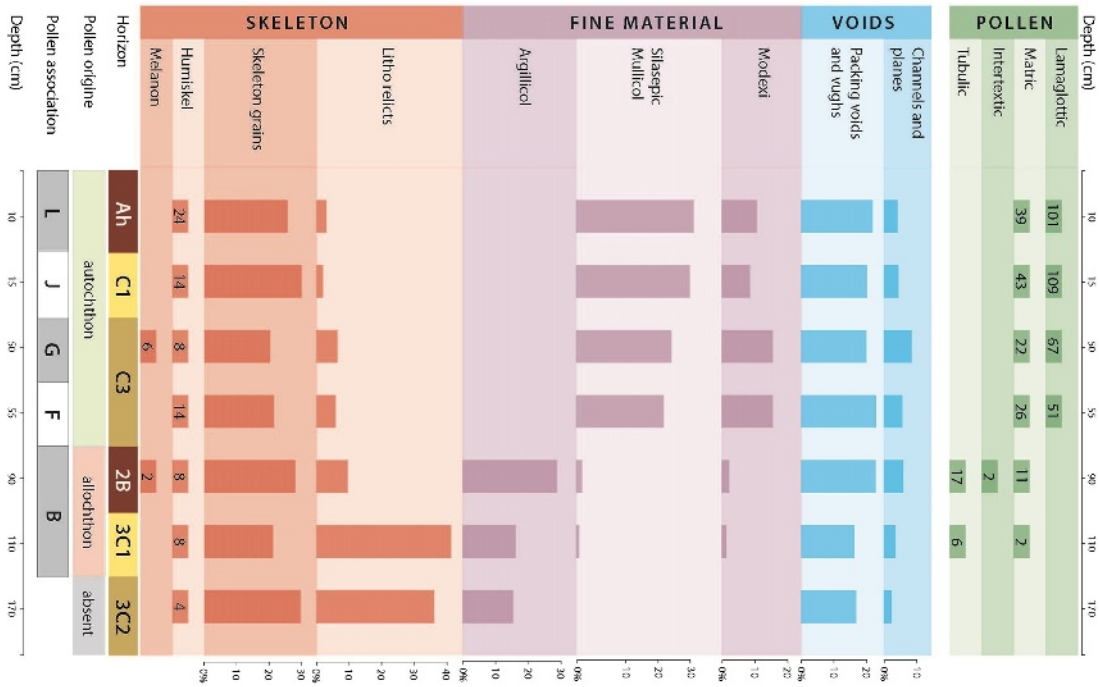

FIGURE 2.2.10 Profile Monte Pedroso micromorphological observations. *After J.M. van Mourik, Pollen Profiles of Slope Deposits in the Galician Area (N.W. Spain). Netherlands Georaphical Studies, KNAG Amsterdam, 12 (1986) 171 pp.*

to those of the remaining plasma, which is interpreted as an ageing product of modexi, or as an irregularly shaped mass secreted by soil animals. Characteristic is the presence of lamellar strings of modexi, visible only in thin sections, not in the field. The voids in the colluvial horizons are for the most part packing voids and vughs. The observed channels are mainly aged root channels. Skeleton, fine material and voids form a porphyroskelic to agglomeroplasmic basic structure. No differences can be defined between dark-coloured 'geologic' and light-coloured 'anthropogenic' colluvial C horizons. Pollen grains in the C layers are not present as free grains in voids but as lamaglottic grains (Fig. 2.2.11) in lamaglotically distributed aggregates and as matric grains embedded in silasepic mullicol (Fig. 2.2.12). These observations show that pollen infiltration does not occur with vertical water transport related to channels or planar voids. The downward movement of pollen grains is related to the colluvial downslope movement of modexi and the vertical migration in root holes. The modexi show a lamagglotic distribution pattern; they occur in laminae and agglomerates (Figs. 2.2.13 and 2.2.14). The lamagglotic modexi can be considered as syn-sedimentary. They have been transported laterally and deposited at the surface downslope. Consequently, the pollen grains in these modexi originate from the upslope vegetation.

In contrast to the syn-sedimentary pollen content of the colluvial horizons, the pollen content of solifluction deposits is post-sedimentary. Pollen grains infiltrate from the former stable slope surface until burial by colluvial layers. The various horizons of the buried palaeosols in solifluction material, deposited on weathered granite, show different characteristics.

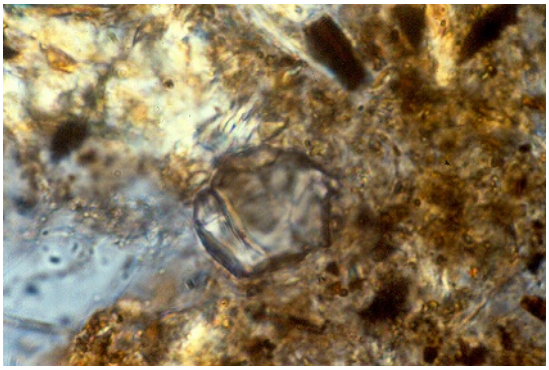

FIGURE 2.2.11 Microphotograph of a matric pollen grain identified in aggregated excremental matter, C2 horizon, 780×.

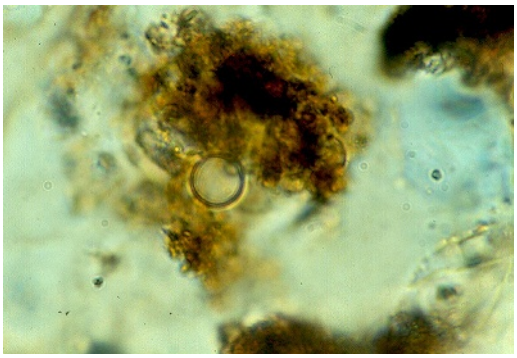

FIGURE 2.2.12 Microphotograph of a lamaglottic pollen grain, identified in a modexi (modelled excrement), C2 horizon, 780×.

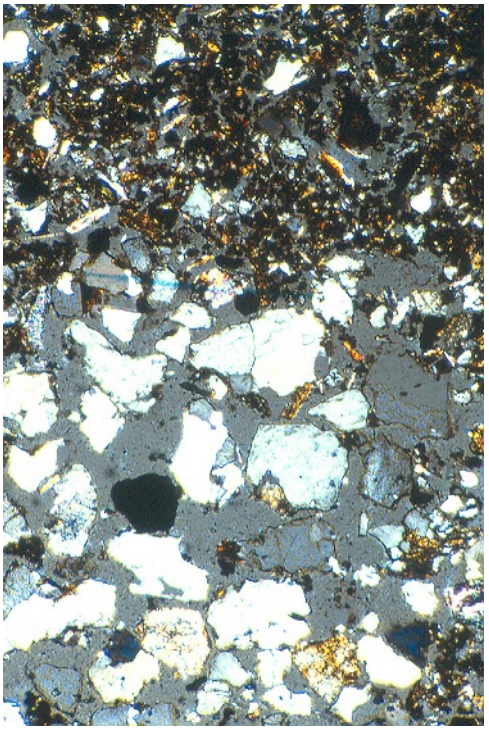

FIGURE 2.2.13 Laminated colluvial slope deposit C2 horizon, 60×.

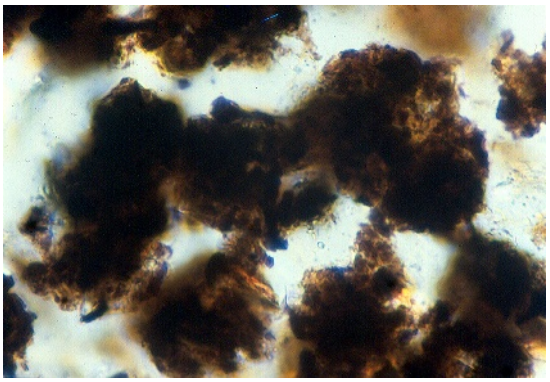

FIGURE 2.2.14 Microphotograph of lamagglotically distributed welded modexi in laminated slope deposits, 165×.

In profile Monte Pedroso the 2A horizon has been eroded and reduced to a dark-coloured stone line between the 2B horizon and the colluvial layers.

The basic structure of the cambic 2B horizon is intertextic to porphyroskelic. Argillicol is present in the cambic horizon and the percentage of modexi is lower than in the overlying horizons. Two types of modexi are observed. First, intertextic dark brown modexi consisting of mainly organic matter and light brown tubulic modexi with a high percentage of clay and silt. This type is similar to the modexi in the mineral horizon of an acid forest soil. Primary organic aggregates move downward in root holes from the ectorganic layer to the mineral horizons.

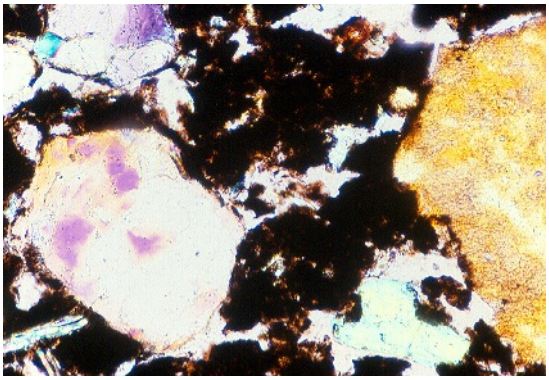

FIGURE 2.2.15 Microphotograph of intertextically distributed modexi, 2B horizon (*top*), 165×.

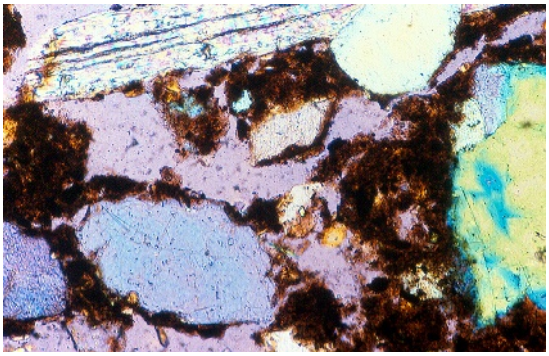

FIGURE 2.2.16 Microphotograph of intertextically distributed welded modexi, 2B horizon (*middle*), 165×.

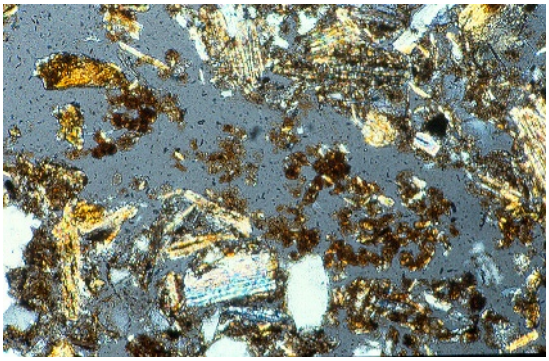

FIGURE 2.2.17 Microphotograph of tubucally distributed welded modexi, 2B horizon, magnification 60.

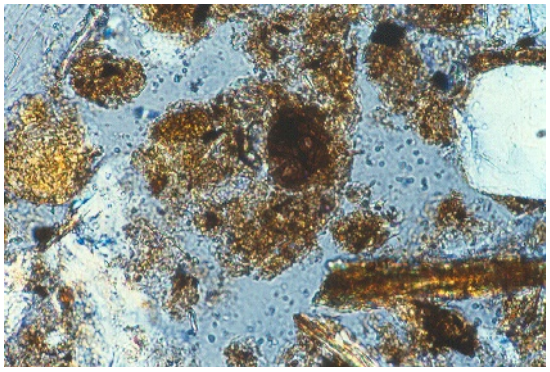

FIGURE 2.2.18 Pollen grain in ageing tubic modexi, magnification 500.

The aggregates are intercepted on contact points between minerals and gradually form bigger structures (Figs. 2.5.15–2.5.16) (Bal, 1973). The second type, found in and beside aggrotubules, is a relic of a stage in soil development with earthworm activity. The tubulic pollen content is related to the activity of saprophagous, deeply burrowing soil animals in an early Holocene period in which steppe-like vegetation dominated (Fig. 2.2.17, 2.2.18).

Comparison of the results of micromorphological and pollen analyses provides insight into the development of the slope sequence.

The pollen concentration curve shows high values in the colluvial (C1, 2, 3) layers and in the stone layer in the top of the 2B horizon. The pollen concentrations decrease logarithmically with depth in the truncated palaeosol, which is indicative for pollen infiltration.

Pollen infiltration reached the top of the weathered granite (3C1); the 3C2 is sterile.

In the 3C1 and 2B horizons, pollen grains were identified in matric and tubulic aggregates in aggrotubules, indicative for earthworm activity. The pollen spectra belong to zone B (dominated by Poaceae and Asteraceae), the reflection of an early Holocene steppe vegetation, in line with the observed tubulic aggregates and an indication that the solifluction layer dates from the lateglacial or the Preboreal.

In the top of the 2B horizon, some pollen grains were also identified in intertextic aggregates, associated with infiltration in the (truncated) 'Tierra Parda' under deciduous forest. The Ah horizon of profile Monte Pedroso was eroded and reduced to a stone line. It was not possible to produce a thin section of this stone line and as a result we do not have observations of the distribution of aggregates. But in similar Galician slope profiles (a good example is profile Brins, published in van Mourik, 1999) the 2Ah in solifluction material was not eroded and in the thin sections we found more intertextic-distributed aggregates pollen. The post-sedimentary pollen spectra of AH belongs to zone D/E, the reflection of Atlantic/Subboreal deciduous forest, dominated by *Quercus*.

In the colluvial C layers, pollen grains were identified in matric and lamagglotic aggregates. These aggregates are part of the sediment load originating from higher parts of the slope and deposited as colluvium on the foot slope. The pollen spectra of the colluvial layers reflect the Subatlantic vegetation development starting with deforestation, the extension of cultivated land with increase of *Castanea*, Cerealia and Ericaceae and finally the registration of reforestations with pine trees.

2.2.5 Conclusions

- The presence of pollen grains in well-drained slope deposits can be explained by micromorphological observations.
- Single pollen grains are not observed in packing voids or planar voids in thin sections of slope deposits with the exception of grains, partly released from ageing modexi. Pollen grains were identified in excremental aggregates and aged excremental material.
- In the young Holocene silty colluvial deposits, pollen grains were identified in excremental aggregates with a lamagglotic distribution pattern. Such aggregates are part of the slope sediment, deposited on the foot slope.
- In the old Holocene gravelly solifluction deposits, pollen grains were identified in intertextic- and tubulic-distributed aggregates. These aggregates were infiltrated by bioturbation under forest or steppe conditions.
- Based on palynological and micromorphological observations, a distinction could be made between a period of slope stability and soil development in the solifluction deposit followed by instability, soil erosion and deposition of colluviation.
- In the solifluction deposit we observe the tubulic modexi of earthworm activity under steppe conditions, followed by intertextic modexi of microarthropods, produced in the (weak) acid forest soil.
- Based on the appearance of culture indicators in the pollen spectra of the colluvial layers we can conclude that slope stability and soil development could continue until humans started forest degradation, resulting in soil erosion and colluviation.

2.3 Life cycle of pollen grains in a Mormoder humus form

2.3.1 Introduction

Soil pollen infiltration starts in the ectorganic horizon of the humus form of the soil. We must try to understand the life cycle of a pollen grain in a humus profile from the moment of deposition to the final decay. Pollen diagrams of humus forms show both pollen zoning and a specific pollen density distribution (Dijkstra and van Mourik, 1995, 1996). Validation of the palynological data of humus forms requires additional knowledge of the presence and distribution of pollen grains in the soil matrix.

In this case we present the results of analyses of a Mormoder humus form development under planted *Larix decidua* in the forestry Gieten in The Netherlands (52°57′27″N/6°46′18″O (O means, East); Figs. 2.3.1–2.3.3). Like most Dutch

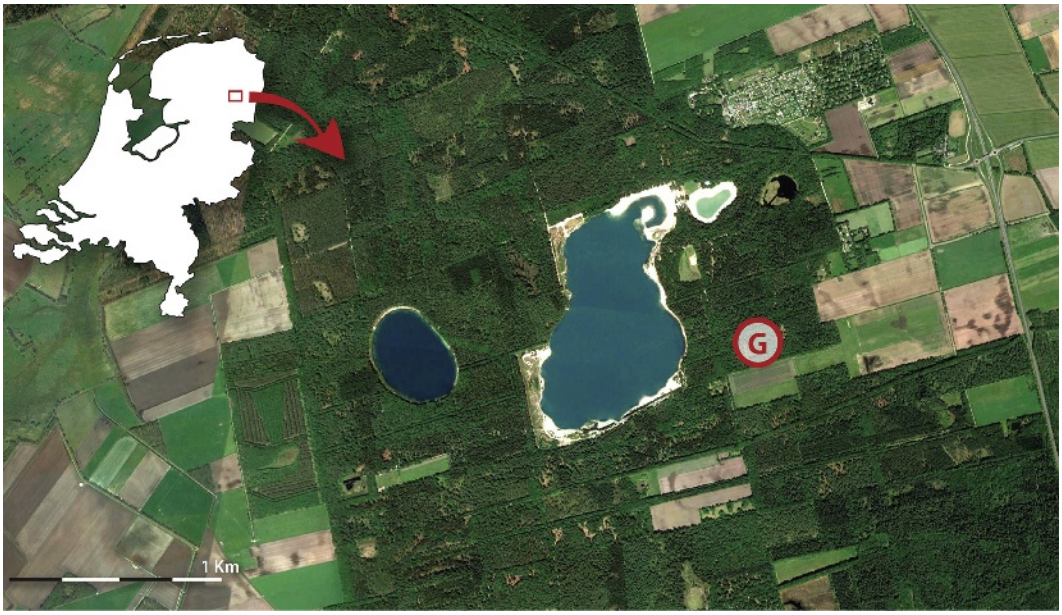

FIGURE 2.3.1 The sample site (G) in the forestry Gieten in The Netherlands

forests in the Pleistocene coversand district this concerns a reforestation on the former heath on coversand. Grazed heath area was part of the traditional plaggic agriculture system. The heath was important for the production of sheep manure but lost this function around AD 1900 due to the introduction of chemical fertilizers. Production of wood was one of the new functions. Before planting, the soil (in general, carbic Podzols) was deeply ploughed to prepare 'fresh' parent material for forest development. Since reforestation around AD 1930, the development of the forest soil is still restricted to the first decimetre and soil can be described as an initial Podzol with a well-developed Mormoder humus form in parent material that consists of chunks of the former top horizons of a ploughed carbic Podzol. This initial soil was sampled for pollen analysis and soil micromorphology. The observed pollen zonation and pollen density distribution of this profile confirms the results of preliminary investigations of humus forms under planted coniferous trees (Dijkstra and van Mourik, 1995; 1996).

2.3.2 Soil description

The sequence of horizons of the Mormoder is L-F-(H)-2ABp. The L (Litter) horizon is very thin and consists of scattered fresh needles. The F (Fermentation) horizon is loose and consists of litter fragments, single and clustered excrements and organic matter without a clearly developed structure, originating from the decomposition of needles and roots of grasses. The distinction between the F1 (loose, coarse fragmented litter) and F2 (dense, matted, fine fragmented litter) is based on a sudden increase in living roots. The brown–black H (Humus) horizon is clearly but discontinuously developed. It consists of fine organic material with a very fine granular structure. In the 2ABp horizon, structures are lacking and the concentration of leached mineral grains increases.

FIGURE 2.3.2 Picture of the sampled Mormoder under *Larix*.

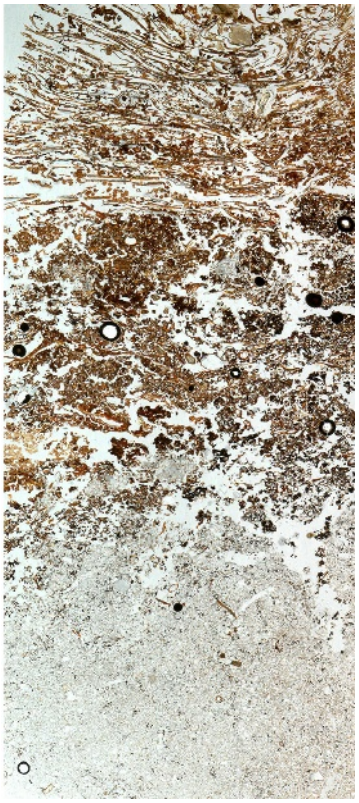

FIGURE 2.3.3 Thin section of the sampled Mormoder under *Larix* (450/850 mm).

2.3.3 Pollen diagram of the Mormoder

The pollen diagram (Fig. 2.3.4) reflects the transition from the former heath to the present *Larix* forest. The Ericaceae—Poaceae association of the mineral horizons reflects the former heath. The ectorganic part of the humus form shows a pollen stratification that reflects three phases in forest development. The pioneer phase is represented by the temporal increase in *Betula*. The first succession phase is reflected in the increase in *Larix* and other planted trees in the surroundings. The second succession phase is represented by a slight decrease in *Larix* and an increase in Poaceae.

The pollen density curve shows maximal values in the lower part of the F2 and H horizons. This is caused by a relative increase of the resistant pollen grains in the organic residue during litter decomposition. The pollen concentrations decrease sharply in the mineral horizons.

The pollen content of the AE and 2ABp horizons is mainly a relic of the former heath. The pollen density in this zone is low. It must be taken into account that this part of the profile has been disturbed by ploughing during preparation of the former heath soil before forest plantation.

The stratification and density distribution of the pollen profile point to a low rate of vertical bioactivity in this Mormoder humus form.

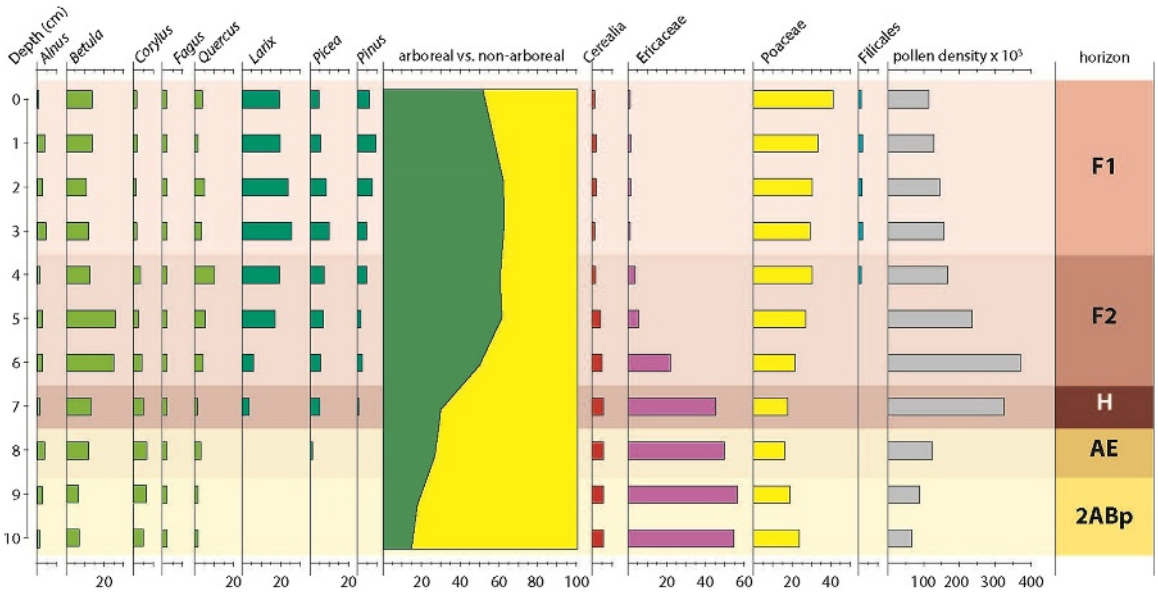

FIGURE 2.3.4 Pollen diagram of the Mormoder under *Larix*. *After J.M. van Mourik, Life cycle of pollen grains in mormoder humus forms of young acid forest soils: a micromorphological approach. Catena 54 (2003) 651–663.*

2.3.4 Micromorphological observations

Bal (1970) published the first detailed description of the micromorphology of humous soil horizons. His research was focused on decomposition processes of organic matter in the organic horizons, but infiltration and distribution of pollen grains in the humus form remained outside the scope of his study. Bal used magnifications between 20 and 100, common at that time in micromorphological descriptions of thin sections of soils but insufficient to identify fossil pollen grains.

The input of organic matter in the forest soil system is mainly controlled by aeolian deposition of organic litter (including pollen grains) on the soil surface and decaying roots in the soil profile. Litter and roots form the basic food for various soil biota living in various horizons of the humus form. Microbial synthesized polysaccharides also contribute to nutrient storage, and are available for decomposition by soil fauna (Dijkstra et al., 1998). The chemical quality of litter controls the composition of soil biota involved in the decomposition of organic matter (Coleman and Crossley, 1996). Litter with a low (<20) C/N ratio promotes earthworm activity, resulting in the development of mull humus forms. A C/N ratio >20 is a limiting factor for earthworm activity but stimulates arthropods and soil fungi, resulting in the development of Mormoder humus forms.

The acidity of the ectorganic layer under *Larix* (pH ≈ 3) hampers the decomposition of litter and the most important consumers are microarthropods. The low decomposition rate results in the development of a thick fermentation (F) horizon. During the fermentation of litter the concentration of small excrements and less consumable particles like pollen grains increases. Pollen can be incorporated in secondary organic aggregates and the anaerobic properties inside these aggregates protect the pollen grains against oxidation. Continuous litter accumulation results in the development of pollen zonation in the ectorganic horizons.

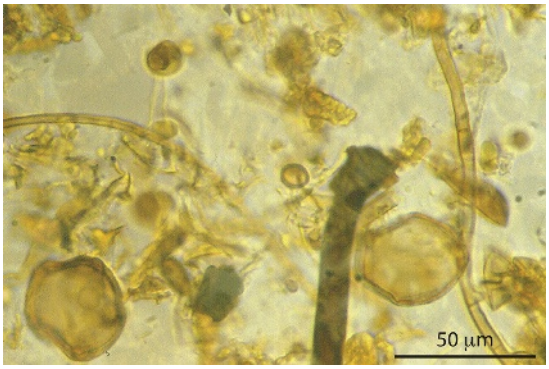

FIGURE 2.3.5 Pollen grains and fungal remains in a pollen slide of the F1.

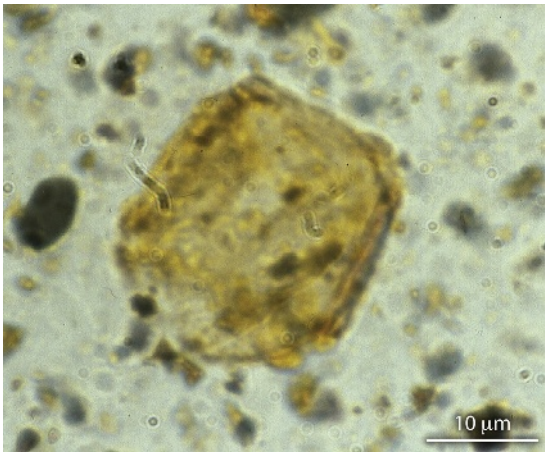

FIGURE 2.3.6 Decayed pollen grains (by microbial consumption) in a pollen slide of the AE.

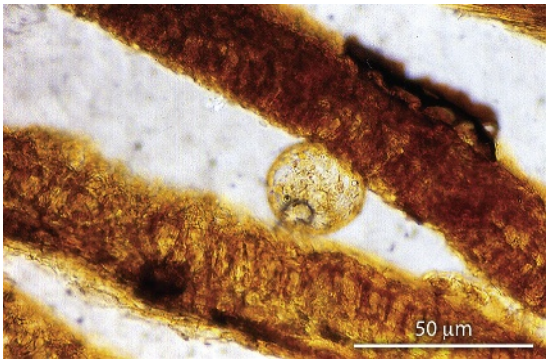

FIGURE 2.3.7 Free pollen grain in fresh litter in the F1.

In the field study of ectorganic layers, hyphae of fungi could hardly be observed, but the pollen extractions show high concentration of hyphae fragments and fungus spores (Fig. 2.3.4). This indicates a systematic underestimation of fungal activity in the ectorganic layers and of the role of fungi in the decomposition process. Samples of the endorganic mineral horizons also contain pollen grains. Most of them are in a bad state due to corrosion (Fig. 2.3.5). The Pleistocene sandy sediments were originally free of pollen. Holocene pollen infiltration from the land surface into the endorganic mineral horizons is controlled by soil fauna activity (van Mourik, 1999, 2001). Validation of pollen zonation of humus forms requires evidence of the processes, responsible for incorporation, preservation, transport and decay of pollen and spores in the various soil horizons. Observations in thin section enable the reconstruction of the life cycle of pollen grains in a Mormoder.

In the upper part of the F1 horizon, free pollen grains occur between litter fragments (Fig. 2.3.6). Fresh litter is affected by microbial activity. Soil fungi are responsible for the decomposition of the epidermis of the needles (Fig. 2.3.7). Fungal attack is followed by the consumption of the content of needles by soil fauna. Microarthropods and enchytraeidae are involved in this phase of decomposition of litter in acid in well-drained forest soils with a high (>25) C/N ratio (Wallwork, 1976). They consume soft litter tissue but also fresh biomass produced by the soil fungi (Coleman and Crossley, 1996). Most of the excrements are dropped inside or just outside the space of the consumed leaf tissue. They are small (Ø 50–100 µm) and consist of small black organic particles and black–brown organic plasma (Fig. 2.3.7). Pollen is not present in such excrements because these small soil animals cannot consume such big grains (Davidson et al., 1999).

Initially, litter fragments dominate the soil matrix of the F1. As a result of the decomposition, the macroporosity of the matrix decreases and voids are filled with ageing excrements, embedding original free pollen grains. This process results in pollen containing organic aggregates. The microenvironment in these aggregates offers the embedded pollen grains perfect protection against microbial decay (Fig. 2.3.8). This process is confirmed in a study by Davidson et al. (1999) to explain pollen distribution in acid soils in the United Kingdom.

The soil matrix of the F2 horizon is composed of fragmented litter particles and organic aggregates. The matrix of the H horizon is dominated by organic aggregates. This part of the ectorganic profile is characterized by high root density and fungal attack of organic aggregates. Decomposition of the aggregates is responsible not only for the release of nutrients but also for the incorporated pollen grains (Figs. 2.3.9 and 2.3.10), which are again exposed to possible decay. There is no evidence of consumption of the content of the decomposing aggregates by soil fauna. However, the biomass of the fungi together with decaying root tissue is consumed by the same microarthropods and enchytraeidae as in the F1 horizon. This results in the supply of fresh small-sized excrements (Fig. 2.3.11). Previously released pollen is re-embedded by fine organic

FIGURE 2.3.9 Small excrements produced by the consumption of decayed leaf tissue in the F1.

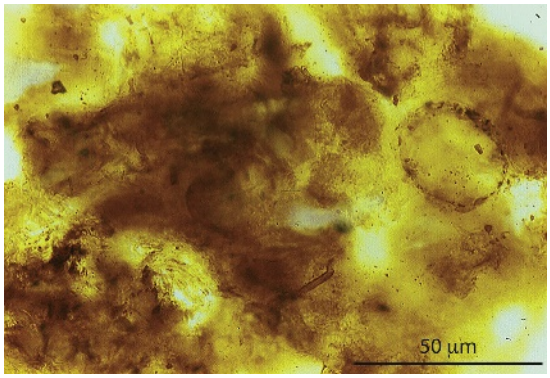

FIGURE 2.3.10 Pollen grain incorporated in an organic aggregate in the F2.

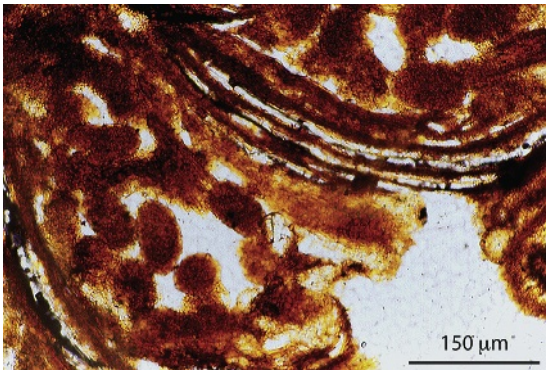

FIGURE 2.3.8 Free pollen grain on a litter fragment attacked by fungi in the F1.

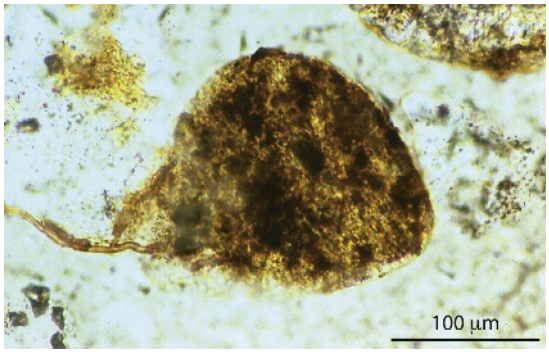

FIGURE 2.3.11 Fungal attack of an organic aggregate in the H.

matter and finally reincorporated and conserved in secondary aggregates composed of ageing excremental particles.

Sand grains dominate the soil matrix of the endorganic AE horizon. Black organic aggregates are randomly distributed in the voids. The density of fresh and decaying roots is low. Most of the organic aggregates look stable, and a few are attacked by soil fungi.

It is important to realize that most of these aggregates are inherited from the former heath soil system. Incidentally released pollen grains from ageing aggregates are present. In thin sections it is impossible to observe features of decay of the pollen wall, due to contamination of the grains. But after extraction, the grains are cleaned and the effects of decay can be observed in the pollen slides (Elsik, 1971). Many pollen grains show traces of mechanical damage. The process of embedding, incorporation, release, re-embedding and reincorporation promotes this type of damage. Some grains also show traces of microbiological damage. The final process of decay is mineralization of the pollen wall by bacterial consumption (Fig. 2.3.12). The mineralization rate of various pollen types is different and the composition of pollen spectra in soil horizons with released grains can be affected by selective corrosion (Havinga, 1984). The rate of degradation of organic aggregates in acid mineral soil horizons is low and soil pollen can survive in the protecting microenvironment of organic aggregates for thousands of years (van Mourik, 1986, 1999).

FIGURE 2.3.12 Release of pollen grains in the H.

2.3.5 Conclusions

In thin sections of the Mormoder profile, free pollen grains can only be observed in the L and the upper part of F1 horizons. Furthermore, the distribution of pollen in the humus form is controlled by the development and degradation of organic aggregates, incorporating and protecting pollen grains. The life cycle of pollen grains in a Mormoder profile can be summarized by the following steps:

- The influx of pollen in a terrestrial soil system is part of the aeolian organic litter deposit on the soil surface in the Litter horizon.
- Single pollen grains are present in the upper part of the F1 horizon between somewhat weathered litter fragments. In the lower part of the F1 horizon, pollen grains are embedded in clustering small excrements and are incorporated into organic aggregates. The small-sized excrements are produced by microarthropods. These humus-inhabiting soil animals consume decayed leaf tissue and soil fungi.
- In the next phase, soil fungi attack organic aggregates. This results in the release of incorporated pollen grains. In the F2 and H horizons, roots consuming microarthropods produce small-sized excrements, and previously released pollen from primary aggregates can be re-embedded by small ageing excrements and reincorporated and survive in secondary organic aggregates.
- Non-reincorporated released pollen grains will mineralize, due to microbial consumption.
- Micromorphological features contribute to the explanation of the observed pollen zonation and pollen density distribution of the analyzed Mormoder and validate the use of pollen spectra of humus forms for palynoecological reconstructions.

2.4 Palynological dating of mardels on the Gutland plateau (Luxembourg)

2.4.1 Introduction

Characteristic for the geomorphology of the Gutland plateau in Luxembourg is the occurrence of mardels, which are small closed depressions (diameter 10–50 m; depth 1–3 m). The surface geology of the Gutland plateau is dominated by Luxembourger sandstone, Strassen marls and Keuper marlstone (Fig. 2.4.1) (Lucius, 1948). Podzolization is the dominating soil process in weathered sandstone resulting in umbric Podzols; clay leaching is the dominating soil-forming process under deciduous forest on the Lias and Keuper marlstone (Cammeraat and Kooijman, 2009) resulting in stagnic Alisols (ISRIC/UNESCO, 2006).

The landforms of mardels are rather similar to pingo's and dolines. However, periglacial ring walls, characteristic of pingos, are absent and in contrast to funnel-shaped dolines they have flat bottoms (Slotboom, 1963). Most of the mardels occur in clusters in forests; mardels in pastures are exceptional. It is assumed that outside the forests, mardels may have been masked out by agricultural levelling (Poeteray et al., 1984). In mardels, deposition of clayey colluvium causes water stagnation, resulting in the development of colluvial Stagnosols. In the present landscape, mardels are fens and wetlands which potentially contribute to the biodiversity of the landscape. Cores of sedimentary mardel fillings are valuable soil archives for the reconstruction of Late Holocene landscape evolution of the Gutland (Slotboom and van Mourik, 2015; van Mourik and Slotboom, 2017).

The genesis of mardels has been the subject of many studies inside and outside Luxembourg. Papers published before 2010 suggested a natural genesis of mardels (Lucius, 1941, 1948; Slotboom, 1963; Braque, 1966; Poeteray et al., 1984; Barth, 1996; Gauthier, 2000; Thoën and Hérault, 2006). These authors ascribed the genesis of the majority of the mardels on Keuper marlstone in Luxembourg and Lorraine to subsurface solution of gypsum, followed by collapse and subsidence of the overlying beds.

The inventory of mardels on the Gutland plateau of Schmalen (2002) includes, besides mardels on the Keuper marlstone (Steinmergelkeuper, unit Km3 on the national geological map) (Lucius, 1948), also mardels on Lias marlstone (Strassen marl formation, unit Li3 on the national geological map). The Li3 is a formation without soluble inclusions, which means that the genesis cannot be explained by the solution of gypsum lenses. In other studies of mardels in Lorraine the natural genesis of mardels was contradicted (Etienne et al., 2011). These authors suggested that the investigated mardels were formed in a relatively short time period during the younger Iron Age and the Roman Time in a partially deforested, open landscape. This was based on the post-Roman palynological dating of the sediment cores of all the investigated mardels. The Roman occupation of Luxembourg lasted from 53 BC until AD 406; the Romans controlled land management, constructed settlements and created a dense road network (Thill, 1977).

On the Gutland plateau, depressions on the Luxembourger sandstone (Li2) also occur. The distribution of these mardels is associated with the pattern of tectonic crevasses in the sandstone beds. In these depressions, sedimentation of clayey colluvium does not occur.

To understand the process of colluviation in mardels on the Gutland plateau we have to study the soil development and slope processes around them. The soils under deciduous forests in weathered Strassen marlstone and Steinmergelkeuper were classified as stagnic Alisols (ISRIC/UNESCO, 2006) with a Vermimul humus form (Green et al., 1993). The current dominating soil process is lateral leaching of clay by overland flow and piping, triggered by the dispersion of

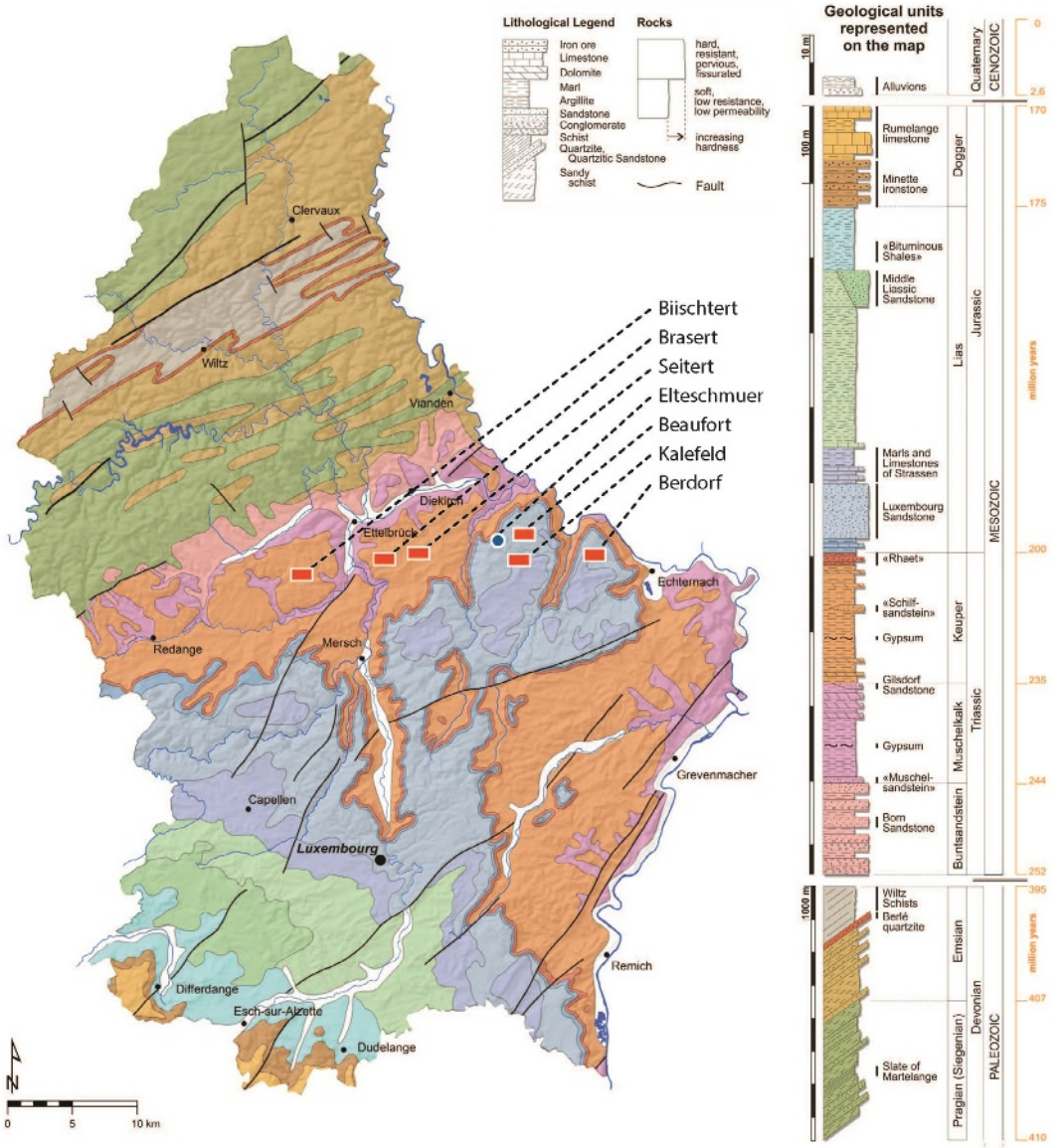

FIGURE 2.4.1 The location of investigated mardels on the Gutland plateau. *After van Mourik (2017).*

clayey earthworm droppings (Cammeraat, 2006; Cammeraat and Kooijman, 2009). Earthworms defecate on the ectorganic layer (Fig. 2.4.2), but by rainfall, dispersed clay is leached through the litter layer to the top of the mineral Ah horizon and will be subjected to soil erosion (Fig. 2.4.3). This process results in a sharp transition in grain size on the boundary between the E and Bg horizons of the profile. Most of the leached clay will finally reach the rivers (after rainfall we can observe a cloud of lutum in the river) but a small part is caught in the mardels.

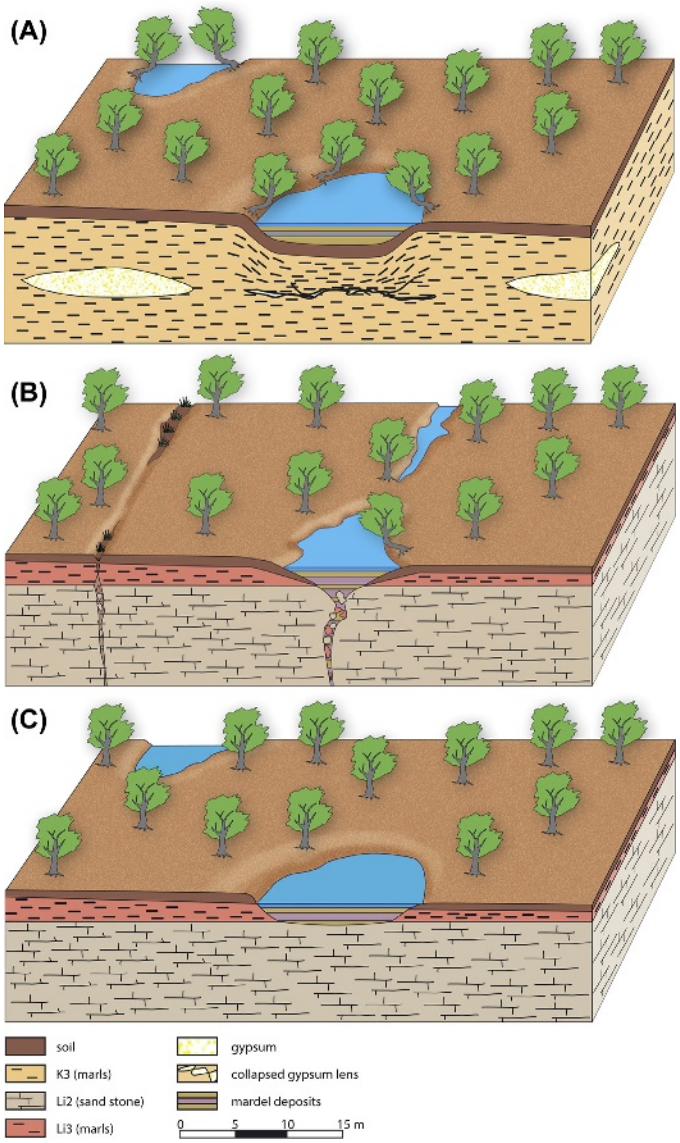

FIGURE 2.4.2 Typology of mardels on the Gutland plateau. (A) Mardels in the Strassen marls (Li3) in depressions, related to joint patterns in the Luxembourger sandstone; historical quarries (clay excavations), filled with clayey colluvium. (B) Mardels in the Luxembourger sandstone (Li2), depressions determined by faults or joints, filled with sandy colluvium and peat. (C) Mardels in the Steinmergelkeuper (Km3) in subsidence basins caused by subsurface solution of gypsum lenses, filled with clayey colluvium. *After van Mourik (2017).*

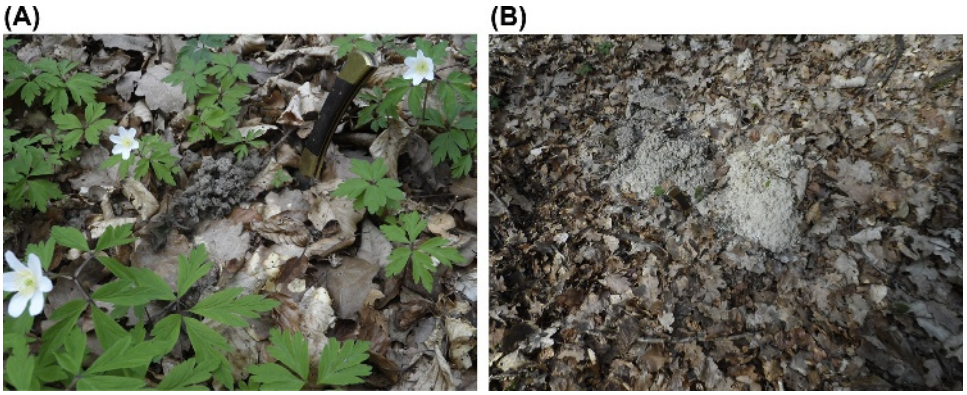

FIGURE 2.4.3 (A) Fresh earthworm droppings on the surface of the F horizon of the forest soil (May 2014). (B) Aged earthworm droppings after rainfall; here the leaching of dispersed clay starts (October 2013).

The earthworm droppings include excrements consisting of clay, silt and consumed organic matter, including pollen grains. This means that the influx of pollen in mardels is a mix of the regular regional and local pollen grain with pollen included in the soil material, eroded upslope and deposited in the mardels.

The soils in the surroundings of depressions on the Luxembourger sandstone are Podzols. In contrast to the soils in marls, earthworms and earthworm droppings are absent.

To show the potential of the mardel soil archives, we discuss the pollen diagrams of mardel Beaufort on the Strassen marls and Brasert on the Keuper marls. Palynological dating must be based on absolute dated reference diagrams. We can use the pollen diagram Elteschmuer of the peat in an elder carr on the Luxembourger sandstone. The observed palynological time markers, sustained by reliable ^{14}C dates, agree with the results of other reference diagrams, particularly Roudbaach and Dauwelsmuer (van Mourik, 2017). Useful palynological time markers are:

- The Late Subboreal transfer of the *Quercetum mixtum* into *Fageto Quercetum* (reflected by deciduous tree species) and start of the anthropogenic deforestation and extension of agriculture (reflected by herbal species and cultural indicators) (Slotboom and van Mourik, 2016).
- The four Subatlantic Fagus peaks (Slotboom, 1963).
- The appearance of extension of Cerealia in the Celtic/Roman Time (Slotboom and van Mourik, 2016).
- The appearance of *Fagopyrum* after AD 1450 (Leenders, 1987).
- The expansion of *Picea* and *Pinus* after AD 1800 (Slotboom and van Mourik, 2015).

If we want to identify time markers in pollen diagrams of mardel cores we have to consider a number of biological and sedimentological factors that have an impact on the reliability of the spectra of the cores.

First, the interpretation of the percentages of arboreal pollen. The Late Subboreal transfer in the forest composition is based on the scores of *Quercus*, *Tilia* and *Fagus*. *Quercus* is a wind-pollinated species and for that reason overrepresented in pollen spectra; *Tilia* is an insect-pollinated species and underrepresented. Furthermore, the share of *Quercus* and *Fagus* to the forest composition can be very different in time and space. Pollen production of a monoculture of *Quercus* is around 35×10^6 grains/ha,

and of Fagus around 20×10^6 grains/ha (Andersen, 1970). Consequently, a displacement of *Fagus* by *Quercus* inside a forest stand can result in an increase in the score of arboreal pollen, which cannot be translated into forest extension (Faegri and Iversen, 1989). Optimal environmental conditions for the *Fageto–Quercetum* are base-rich substrates, mean annual temperature of 7–9°C, annual precipitation of 600–800 mm and a topographical altitude of 200–550 m. Fluctuations in temperature and precipitation affected the ratio between *Quercus* and *Fagus* trees. Colder and wetter climate during the Migration Period and the Little Ice Age promoted the extension of *Quercus* trees at the expense of *Fagus*; warmer and moister conditions during the Roman Time and Middle Ages promoted the extension of the *Fagus* trees. The results of the research of Loehle (2006) confirm these climatic oscillations.

Second, the pollen content of peat is supposed to be syn-sedimentary and reliable for palynochronology. The pollen composition of the colluvial sediments, however, is a mix of the regular regional aeolian pollen precipitation and pollen grains present in eroded and transported slope material. Consequently, the pollen spectra are a mix of species present in the regular influx and species infiltrated in the soil upslope and transported by soil erosion to the mardel. The real age of the pollen grains of the second fraction is older than the real age of the pollen on the first fraction. Due to this process of mixing, species occurring on slopes, subjected to soil erosion, can be overrepresented in pollen extractions of mardel cores. Moreover, the top of the profile of the colluvic Stagnosols is subjected to bioturbation, especially in the relatively dry summer season. Therefore boundaries between pollen in diagrams of mardel cores zones are never sharp but always gradual or even diffuse.

2.4.2 Reference pollen diagram Elteschmuer of a Histosol in an elder carr on the Luxembourger sandstone

The elder carr Elteschmuer is situated in Esselbur (49°50′28″N/6°15′82″E; altitude 410 m), 400 m east of the cuesta front. A linear range of wetlands has developed in an elongated subsidence basin parallel to the cuesta front. Considering the vicinity of the cuesta front it is likely that the shape is associated with patterns of tectonic crevasses. It is also likely that water infiltration in the crevasses stagnated by sediment jam and wetlands (muers) could develop. The actual wetland vegetation is dominated by *Betula*, *Alnus*, *Molinia* and *Sphagnum* (Fig. 2.4.4). The water in the carr is stagnating rain water with a low alkalinity and a very low inorganic carbonate concentration (van Mourik and Slotboom, 2018). Therefore radiocarbon dates of the peat samples are hardly affected by reservoir effects (Mook and Streurman, 1983; Slotboom and van Mourik, 2015) and can be used for reliable radiocarbon dating. The pollen diagram Elteschmuer (Fig. 2.4.5) and the radiocarbon dates (Table 2.4.1) will be used as reference material because they offer absolute dated palynological

FIGURE 2.4.4 The elder carr Elteschmuer on the Luxembourger sandstone.

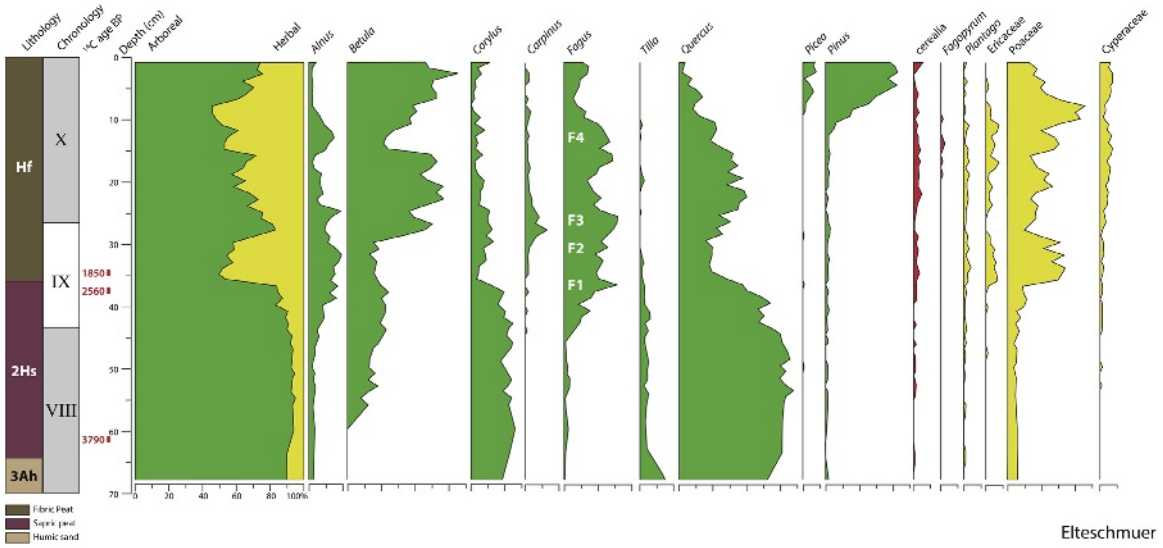

FIGURE 2.4.5 Pollen diagram Elteschmuer. *After van Mourik (2017).*

TABLE 2.4.1 Radiocarbon dates of the Histosol Elteschmuer.

Gr-code	Depth	Material	Year BP	Calendric age	Firbas zone
GrN-26042	34 cm	Humin	1990 ± 120	BC 13 ± 146	IX
GrN-26043	38 cm	Humin	2620 ± 130	BC 734 ± 175	VIII
GrN-26044	60 cm	Humin	4330 ± 200	BC 2986 ± 294	VIII

BP, Before present.

time markers that we need for the chronological interpretation of pollen diagrams of mardel fillings. Radiocarbon dates of colluvial sediments are not reliable, due to the contaminating effect of transported (older) organic carbon originating from upslope eroded soils.

The pollen spectra of Zone VIII (Subboreal) from the sandy layer are dominated by arboreal pollen, *Quercus*, *Corylus* and *Tila*. It is likely that the pollen content of the sandy substrate was the result of soil pollen infiltration under forest into an at-that-moment well-drained soil (van Mourik, 2001). Rejuvenation of the pollen composition by infiltration could continue until the start of peat accumulation around 3800 BC. Likely, the lowering of the temperature in the Subboreal and subsequently the decrease of evapotranspiration by forest was responsible for soil wetting at that time.

The accumulation of peat on the sandy (palaeo)sol started around 3800 BP. The oldest peat layer has sapric properties and consists of strongly decomposed plant tissues, indicating seasonal groundwater-level oscillations. *Betula*, not present in the sandy substrate, appears in the sapric peat horizon. Between 2560 and 1850 BP the character of the sediment changed from sapric into fibric peat indicating more stable groundwater levels. The increase in herbal pollen points to deforestation.

Zones IX and X (Subatlantic) are characterized by the decrease in *Tilia* and *Quercus* and increase in *Fagus*, which indicates the transformation of the *Quercetum mixtum* to *Fageto–Quercetum*. The palynological registration of human impact on landscape development is clearly expressed. Celtic/Roman cultivation is expressed by the extension of Cerealia in combination with a decrease in arboreal pollen (35–30 cm), the Migration Period (AD 400–AD 800) is reflected by temporal recovery of forest (30–25 cm) and the Middle Ages by deforestation and extension of agriculture (Cerealia and Poaceae). The appearance around AD 1350 of *Fagopyrum* is recorded (25–15 cm). The last two centuries are reflected by the extension of *Pinus* and the appearance of *Picea* (15–0 cm).

The *Fagus* curve in this record shows clearly four maxima in the Subatlantic, the first during the Roman Period from AD 0– to AD 200 (F1), the second from AD 700– to AD 800 (F2), the third around AD 1200 (F3) and the last from AD 1700– to AD 1900 (F4). These four maxima were also reported by Persch (1950), Slotboom (1963) and Daniels (1964) and usable as palynological chronomarkers.

2.4.3 Pollen diagram Beaufort of the colluvic Stagnosol in a mardel on the Strassen marls

Mardel Beaufort is situated in the Scheiwelterboesch (49°49′59″N/6°16′52″E; altitude 379 m), southwest of Beaufort under *Fageto–Quercetum*. It is one of a linear range of depressions, situated parallel to the border of the forest (Figs. 2.4.6–2.4.8). Most likely these mardels on the Lias marlstone developed in Roman quarries.

The lower part of the pollen diagram (horizons 4C, 5C, 5Cca) is characterized by very low pollen densities. The percentages are based on pollen sums <50 (exclusively the exotic marker). The occurrence of pollen grains of aquatics (the sum of the scores of *Myriophyllum*, *Typha*, *Menyanthes*, *Potamogeton* and *Thalictrum*) indicating wetland conditions on the floor of the excavation. Some pollen grains infiltrated in the 4C horizon (grey clay), a residual water-saturated loam bed on the bottom of the excavation, are probably due to the swirling of the saturated clay or in root channels of aquatic plants. Also, some pollen grains infiltrated into the 5C horizon (light grey silt loam with light pink and light blue mottles) are inherited from the weathered marlstone.

FIGURE 2.4.6 Picture of mardel Beaufort in the Strassen marls (sampled in May 2013, location indicated by the *white arrow*).

The pollen grains in these horizons are hardly damaged by any form of corrosion (Fig. 2.4.9), in contrast to the grains in the 2C and C horizons (Fig. 2.4.10). This confirms the theory that these pollen grains are not a relic of a former (truncated) soil in the Strassen marls, but that they infiltrated in the residual sediment on the floor of the abandoned excavation (Slotboom and van Mourik, 2015). Burial by the initial Histosol (3H) protected these pollen grains against corrosion.

Of all the investigated mardels this was the only one with a thin discontinuous peat layer (3H), deposited on the abandoned quarry floor. In contrast to organic matter extracted from colluvial deposits, the hardly decomposed leaves of moss and in the peat layer, including

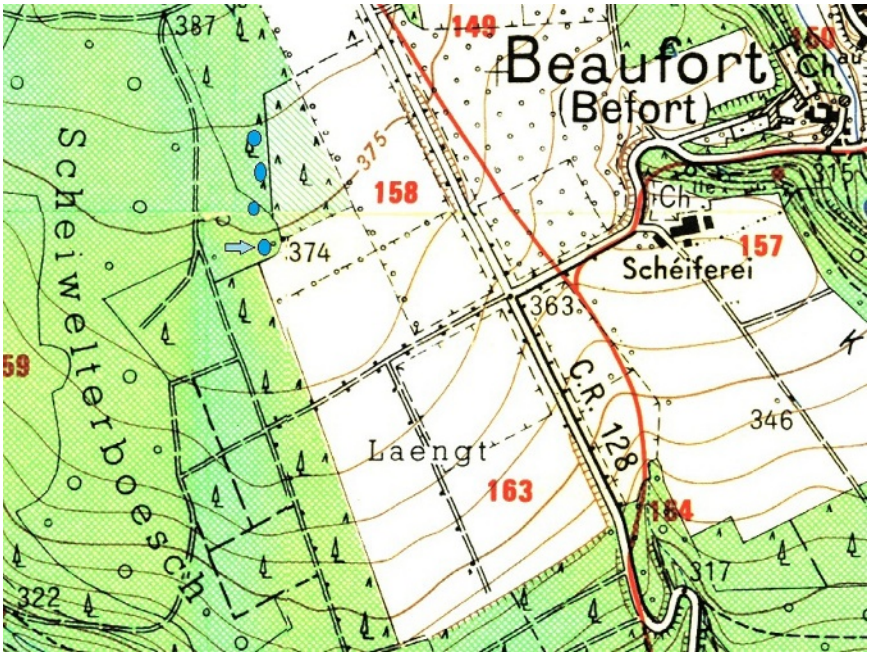

FIGURE 2.4.7 Fragment of the topographical map 1:20,000 (Larochette, 1980) with the mardel cluster in the Scheiwelterboesch; the sampled mardel is indicated by the *blue arrow*.

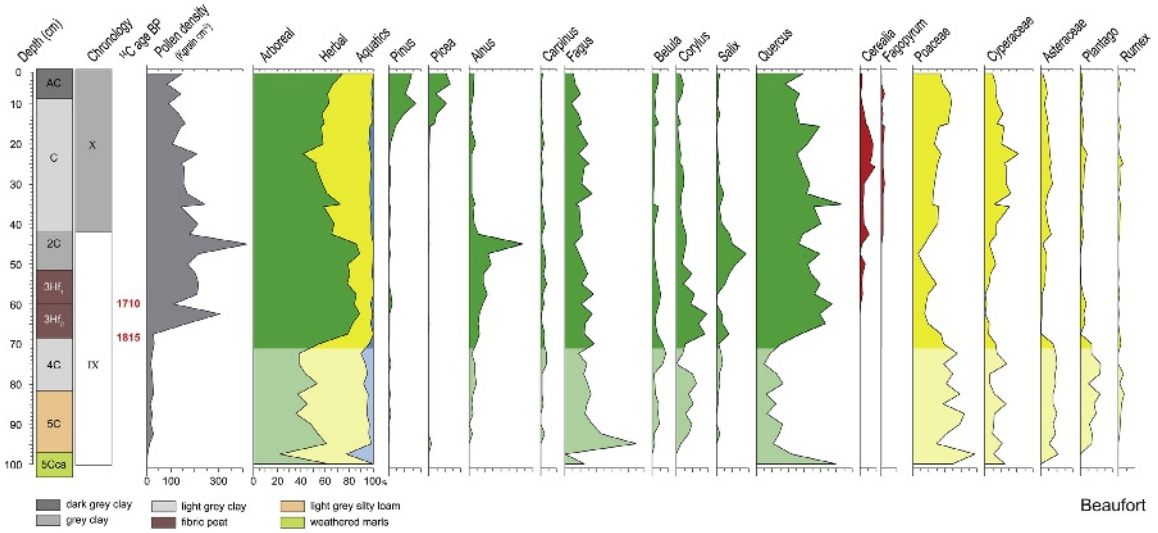

FIGURE 2.4.8 Pollen diagram Beaufort. Radiocarbon dates are specified in Table 2.3. *After van Mourik (2017).*

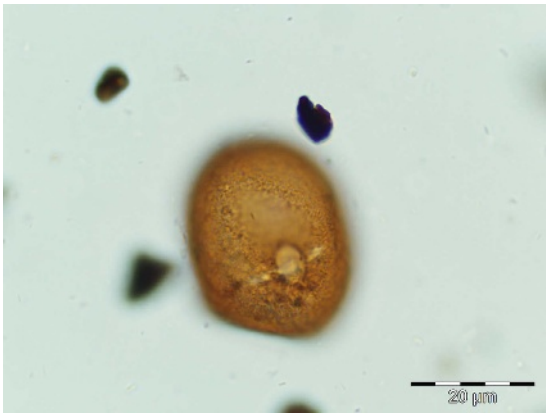

FIGURE 2.4.9 Profile Beaufort, pollen slide 90 cm; *Fagus* grain, hardly corroded.

FIGURE 2.4.10 Profile Beaufort, pollen slide 50 cm; severe and moderated corroded *Fagus* grains.

conserved fragments of leaves from the surrounding trees, could be used for radiocarbon dating (Table 2.4.2).

The accumulation of *Drepanocladus* peat ($3Hf_{1,2}$) started around 1800 BP. The $3Hf_2$ consists of pure laminated plant tissues, and the $3Hf_1$ consists of laminated loamy peat. Based on the radiocarbon dates (Table 2.4.2) the initial Histosol formed at the end of the Roman Period (Fig. 2.4.11).

The 2C horizon consists of grey loam and reflects the increasing soil erosion in the surroundings after the exit of the Romans. None of the peaks in the *Fagus* curve are clearly expressed. The pollen spectra of the 2C show high scores of *Alnus* and *Salix*, pointing to stabilizing trees around the mardel, and high pollen densities, pointing to a low sedimentation rate.

The Migration Period is also not clearly recorded in this diagram. Probably, soil erosion in the surroundings was minimal during a period of temporal recovery of the forest as reported in profile studies in Germany (Zolitschka et al., 2003). The location of this mardel, very close to the watershed, is probably responsible for a very low denudation rate under forest during the Dark Ages. The reduction in cereals at 42.5 cm is probably caused by decreasing agricultural production during the pest epidemic (AD 1325–AD 1350, Slicher van Bath, 1960).

The C horizon consists of grey clay loam and the pollen spectra reflect deforestation and extension of Cerealia. At 40 cm, *Fagopyrum*

TABLE 2.4.2 Accelerator mass spectrometry radiocarbon dates of the initial Histosol in profile Beaufort.

GrA code	Sample depth	Sample material	^{14}C age (BP)	Calibrated age (1-sigma)[a]
58611	60 cm	Leaf fragments	1710 ± 30	AD 270–AD 370
58612	65 cm	*Dreplanocladus* peat	1760 ± 35	AD 230–AD 310
58613	68 cm	Leaf fragments	1815 ± 30	AD 148–AD 228

BP, Before present.
[a] *Calibrated with OxCal version 4.2.4.*

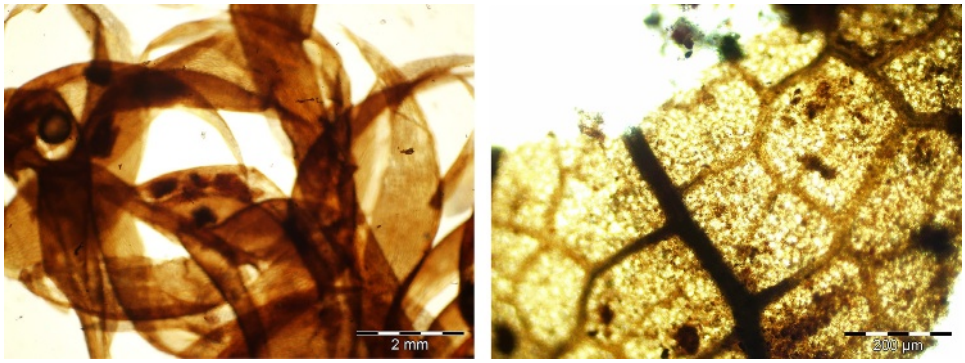

FIGURE 2.4.11 Materials, used for reliable accelerator mass spectrometry radiocarbon dating of the initial Histosol in profile Beaufort. Left tissue of *Dreplanocladus* (sample 65 cm); right leaf fragment of *Quercus* (sample 60 cm).

appears (≈AD 1500). The pollen densities are lower in comparison with the 2C, pointing to a higher sedimentation rate during the Little Ice Age. The appearance of *Picea* and the increase in *Pinus* reflect reforestations since AD 1800.

2.4.4 Pollen diagram Brasert of the colluvic Stagnosol in a mardel on the Strassen marls

The Brasert mardel (Figs. 2.4.12 and 2.4.13) is situated in the Brasert forest (49°49′42″N/6°08′48″E; altitude 356 m) on the Steinmergelkeuper under *Fageto–Quercetum*. Similar to mardel Seitert, the soil in the mardel filling is a Stagnosol (clayic, colluvic), and the soil around the mardel is a stagnic Alisol (clayic), developed in the regolithic cover of weathered Keuper marls.

The zoning of pollen diagram Brasert (Fig. 2.4.14) is rather similar to diagram Beaufort. Colluvial beds were deposited on a truncated surface with a residual bed (2Cca, 2C) in the weathered Keuper marls in which pollen had infiltrated. The pollen concentrations are very low, but the percentages of herbal pollen and (sub)aquatic species (in this diagram *Myriophyllum* and *Typha*) are relatively high. The faintly expressed F3 indicates that the colluvial

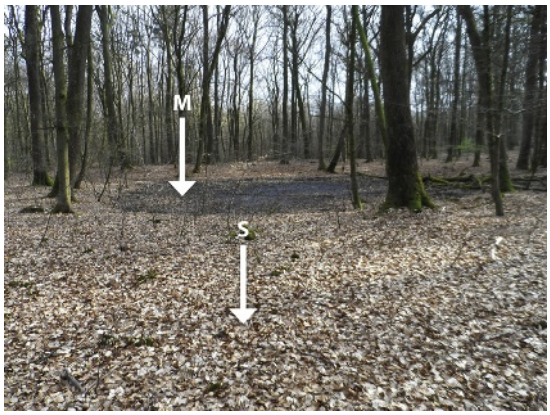

FIGURE 2.4.12 Picture of mardel Brasert on Keuper marls sampled in October 2013. The sample location is indicated with an *arrow*.

sedimentation of the C2 grey clay started before AD 1200 and continued until ≈AD 1500. The pollen spectra of this layer reflect the local recovering of the forest. The colluvial top layer (C1) was deposited ≈AD 1500 considering the palynological reflection of the appearance of *Fagopyrum*, the extension of Cerealia and the *Picea* plantations.

Similar pollen diagrams of mardel fillings, sampled at the locations Berdorf, Kalefeld, Seitert and Biischtert (Fig. 2.4.1), have been published in van Mourik (2017). Close to the mardel clusters

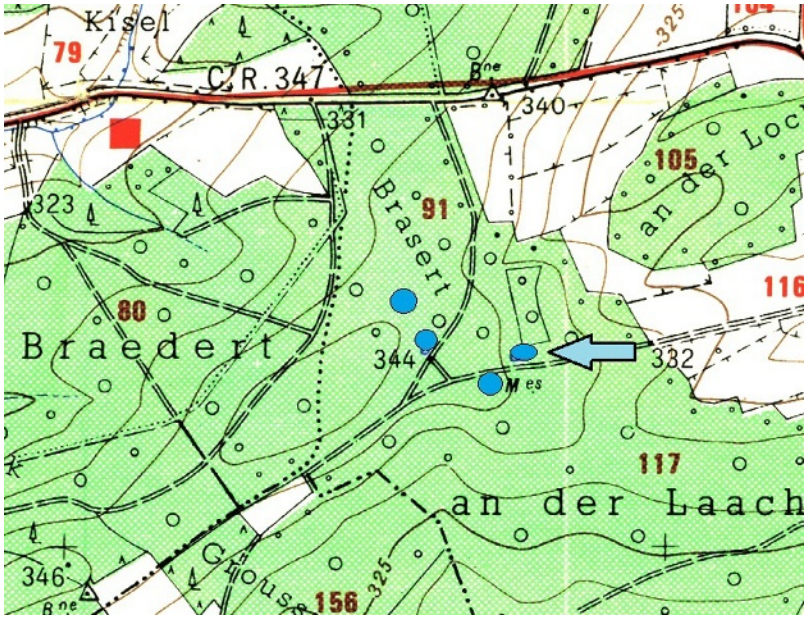

FIGURE 2.4.13 Fragment of the topographical map 1:20,000 (Larochette, 1980) with the mardel cluster in the Brasert forest (the sampled mardel is indicated with the *blue arrow*).

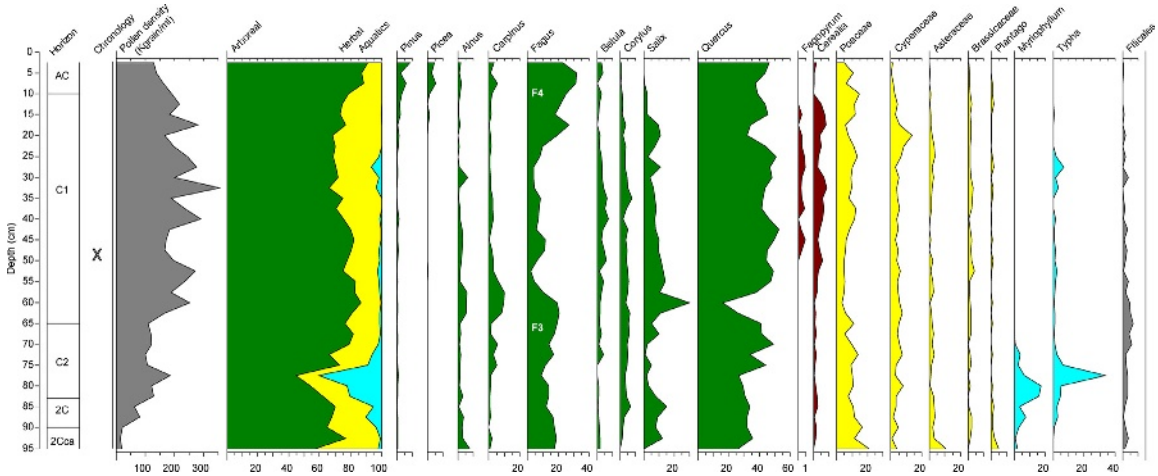

FIGURE 2.4.14 Pollen diagram Brasert. *After van Mourik (2017).*

Kalefeld and Biischtert, archaeologists found some Roman ceramics. Provenance analysis points to the use of mardel fillings for the production of these ceramics (Chapter 7, Section 7.2).

2.4.5 Conclusions

- Mardels on the Gutland plateau in the marl have a clayey colluvial filling.
- The colluvial layers were deposited on a truncated (palaeo)sol in marl, most probably the floor of an abandoned quarry.
- The pollen content of the colluvial sediments is a mix of the regular regional pollen precipitation (these pollen grains are just slightly corroded) and pollen grains provided by soil erosion (these grains are severely corroded).
- Based on the identified palynological markers in the pollen diagrams we can date the colluvial filling as post-Roman.
- The ages of anthropogenic depressions may rank from the Roman Period to the Middle Ages.
- Pre-Roman mardel fillings were never found in mardels on the Gutland plateau (Poeteray et al., 1984) or in Lorraine (Etienne et al., 2011), and consequently it is not possible to date the age of 'natural' depressions on the Gutland plateau; they may rank from Early to Late Holocene.
- Mardels are the result of natural and cultural processes and are part of the geoheritage of Luxembourg.

2.5 Reconstruction of the Dutch barrow landscape on the ancestral heaths, based on soil pollen analysis

2.5.1 Introduction

Archaeology is the study of prehistoric and historic humans and their activities through material remains. An important aspect in everyday life of past communities is the environment they lived in. For example, the environment determined where people could build settlements, what building materials were available to them and where to find and cultivate food. Not only had the environment an impact on humans, humans also altered the landscape by their activities. They cleared forests to create space for their settlements, grazing fields and crop cultivation, and used the wood as construction material and as fuel for fire. Understanding landscapes of the past in relation to human societies increases our knowledge of these processes.

The reconstruction of landscapes often involves multiple methods. Techniques incorporated into landscape reconstruction are, for example, the analysis of geographical information, sediment analysis, the analysis of macrobotanical remains such as seeds, fruits and wood and pollen analysis. As has been explained in the previous section, pollen that is present in the soil archives contains information about past vegetation in the regional and local surroundings of the sample location. Pollen analysis is therefore of great value in landscape reconstruction as well as for archaeological investigations. Palynology has, for example, shown that human pressure on the natural environment increased substantially from the Neolithic period onward, changing the character of the vegetation. Natural forests were cleared in many places, reflected by a decrease in arboreal pollen and an increase in herbal pollen in palynological diagrams, for example, from the southern part of the Netherlands, as has been published by Janssen and Ten Hove (1971) and Janssen (1974).

The intensification of crop cultivation and pasture became visible in palynological research in the form of cereal pollen grains and weeds from both agricultural and pasture (Louwe Kooijmans, 1974; Behre, 1986; Bakker, 2003; Out, 2009). Due to expanding (agri)cultural activities, the soil degraded and *Calluna* heath could establish itself at large scale, indicated by a significant increase in *Calluna* pollen during

the Medieval Period (Janssen and Ten Hove, 1971). Palynological analyses of features such as wells, pools and ditches in and near settlement sites can, for example, reveal animal grazing by the presence of spores from coprophilous fungi (Van Geel, 1978) and the processing of food by the presence of cereal pollen grains (Groenman-van Waateringe, 1992) and grains from herbs used for cooking (Zeven, 1997; Van Haaster, 2008). Also, in barrow research, pollen analysis has played an important role. This will be further explained and discussed in the next section.

2.5.2 The evolution of heathlands during the Holocene in the coversand district in the Netherlands

Based on the palaeoecological analyses of palaeosols (van Mourik et al., 2012) it was possible to reconstruct the changing economic and cultural management of heaths and the consequences for landscape and soils (Doorenbosch and van Mourik, 2016). Heaths are characteristic components of cultural landscape mosaics on sandy soils in the Netherlands. The natural habitat of heather species such as *Calluna vulgaris* and *Erica tetralix* was moorland. At first, natural events like forest fires and storms caused small-scale forest degradation; in addition, forest degradation accelerated due to cultural activities like forest grazing, wood cutting and shifting cultivation. Heather plants invaded degraded forest soils and heaths developed.

People learned to use the heaths for economic and cultural purposes. The impact of heath management on landscape and soils was registered in soil records of barrows, drift sand sequences and plaggic Anthrosols. Based on pollen diagrams of such records we can show that heaths were used for cattle grazing before the Bronze Age. During the late Neolithic, Bronze Age and Iron Age, people created barrow landscapes on the ancestral heaths. After the Iron Age, people probably continued with cattle grazing on heaths and plaggic agriculture until the early Middle Ages. Severe forest degradation because of the production of charcoal for melting iron during the Iron Age until the 6th and 7th centuries and during the 11th to 13th centuries for the wood trade resulted in extensive sand drifting, a threat to valuable heaths. The introduction of a deep, stable economy and heath sods digging in the course of the 18th century resulted in acceleration of the rise of plaggic horizons, severe heath degradation and again extension of sand drifting. At the end of the 19th century, heath lost its economic value due to the introduction of chemical fertilizers. The heaths were transformed into 'new' arable fields and forests, and due to deep ploughing, most soil archives were destroyed. Since AD 1980, the remaining relicts of the ancestral heaths have been preserved and restored in the framework of programs to improve regional and national geobiodiversity. Despite the realization of many heath restoration projects during the last few decades, the area of present heaths is just a fraction of the heath extension in AD 1900. Fig. 2.5.1 shows the maximal extension of heathland in the Netherlands.

2.5.3 Reconstructing the barrow landscape

Burial mounds (Fig. 2.5.2) are amongst the most numerous and important prehistoric monuments in Europe. Burial mounds, also called barrows, are prehistoric grave monuments and they were built from the 4th millennium BC until around 500 years BC. Although many barrows have disappeared over time, thousands of them are still visible in the landscape today. Many barrows have been the subject of archaeological research in the past decades, expanding our knowledge of barrows and prehistoric man, who built the barrows. It was shown that barrows were important ritual places with a specific cultural value (Arnoldussen and Fontijn, 2006;

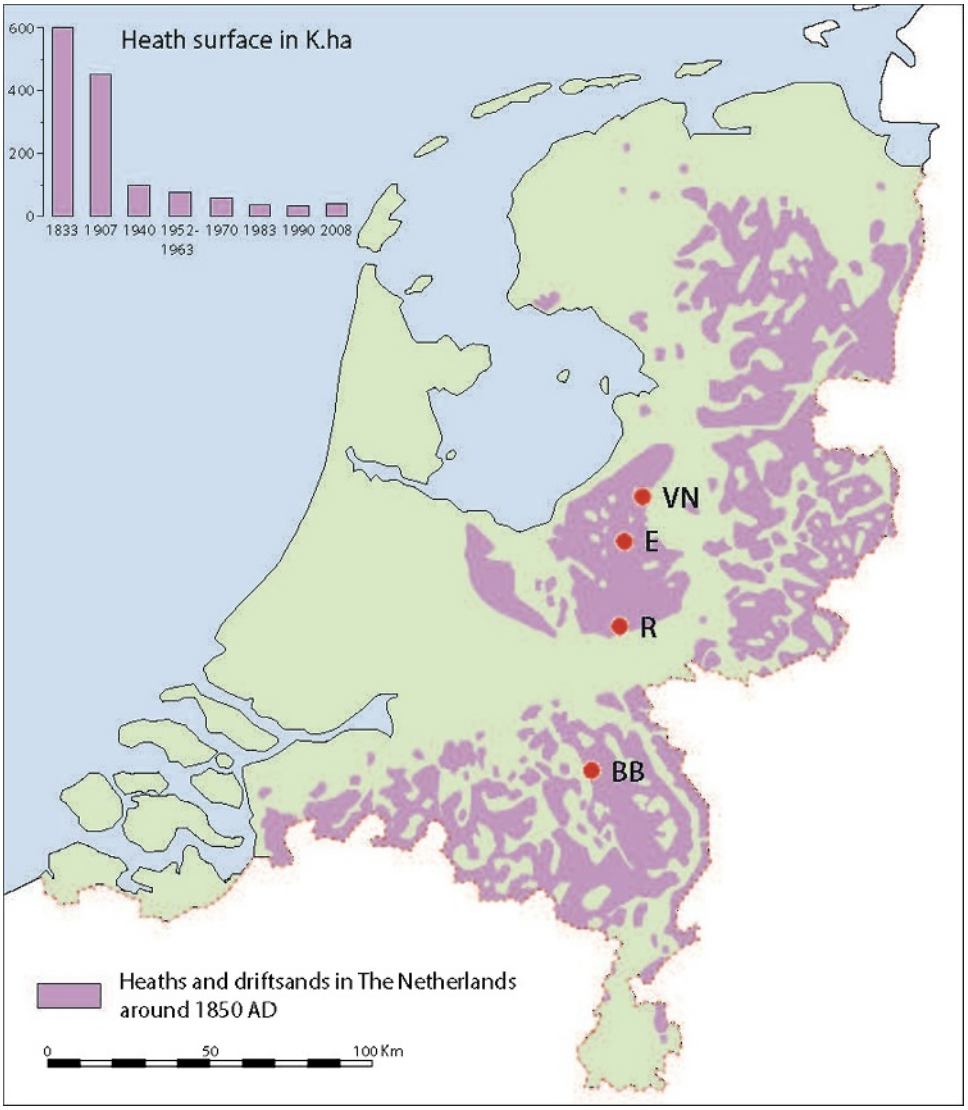

FIGURE 2.5.1 Extension of heather in the Netherlands around AD 1850 and the diminution of heaths between 1833 and 2008. The locations of the research sites Renkum stream valley and Echoput are indicated. *After M. Doorenbosch, J.M. van Mourik, The impact of ancestral heath management on soils and landscapes: a reconstruction based on paleoecological analyses of soil records in the central and southeastern Netherlands, SOIL 2 (2016) 311–324.*

Fontijn et al., 2011; Bourgeois, 2013). Not only the burial mound itself, but also the landscape in which it was situated played an important role for barrow builders, as has been concluded by the Ph.D. research of Doorenbosch (2013), by combining pollen data of nearly 100 barrows from the central and southern parts of the Netherlands.

For reconstructing the barrow landscape, palynological analysis has proven to be a

FIGURE 2.5.2 Soil archives of a barrow showing a palaeosol buried by a barrow, built with sods and dug in heathlands in the surroundings. *Photograph by Q. Bourgeois.*

suitable method (Waterbolk, 1954; Van Zeist, 1967; Casparie and Groenman-van Waateringe, 1980; Doorenbosch, 2011, 2013). Pollen grains that had precipitated onto the surface in the period just before the barrow was built represent the surrounding regional and local vegetation of that period. The construction of the barrow sealed the surface, creating suitable circumstances for the grains to be preserved and preventing additional pollen precipitation. Pollen analysis of the old surface beneath a barrow reveals in what kind of landscape the mound was built (Fig. 2.5.3).

Barrows were mostly constructed from sods. Sods are pieces of the upper soil that are piled up to construct a mound on top of a grave. Sods usually contain the old surface and part of the soil profile below. Similar to the soil beneath a barrow, pollen grains that are present in the old surface of the sod provide information about the vegetation surrounding the area where the sod was taken.

2.5.4 Soil pollen analysis

Pollen analysis of roughly 100 mounds in the central and southern part of the Netherlands has shown that the majority of barrows were raised in open heath vegetation surrounded by forest. Pollen spectra are available from two Iron Age barrows at Echoput near Apeldoorn (central Netherlands). The pollen spectra of both the palaeosol in the old surface (Fig. 2.5.4) and

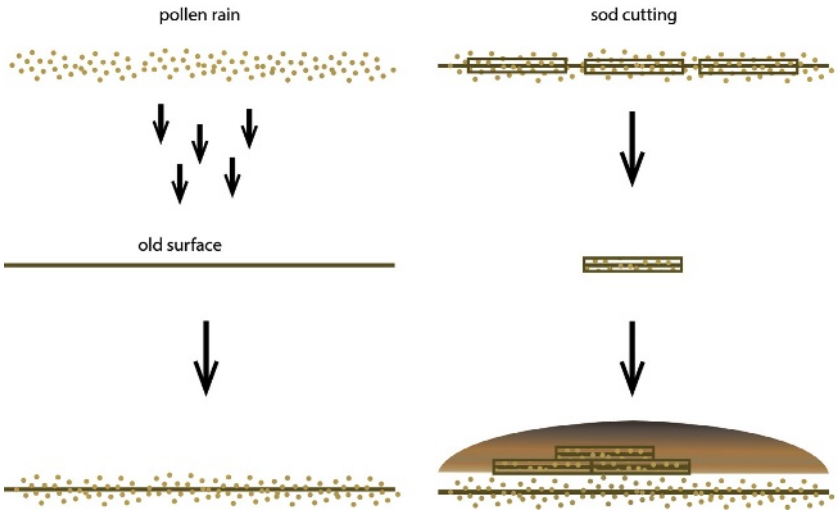

FIGURE 2.5.3 A schematic illustration of pollen precipitation and how pollen grains are preserved in the old surface underneath a barrow and in its sods. *After Fig. 4.1 M. Doorenbosch, Ancestral Heaths. Reconstructing the Barrow Landscape in the Central and Southern Netherlands. PhD thesis. University of Leiden (2013) p. 39.*

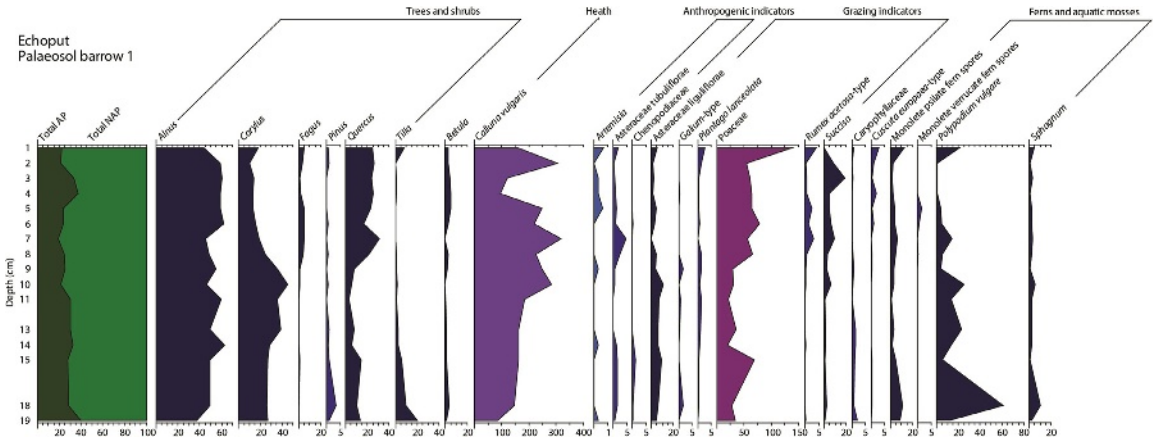

FIGURE 2.5.4 Pollen spectra from the sods and old surface samples taken from Echoput barrows 1 and 2. Spectra are given in % based on a tree pollen sum minus *Betula*. In the total AP, *Betula* is included. In the NAP, spores are included; non-pollen palynomorphs are excluded. Different scales have been used, indicated with different colours. *AP*, Arboreal pollen; *LIA*, Late Iron Age; *MIA*, Middle Iron Age; *NAP*, non-arboreal pollen. *After Fig. 8.6 M. Doorenbosch, Ancestral Heaths. Reconstructing the Barrow Landscape in the Central and Southern Netherlands. PhD thesis. University of Leiden (2013) p. 103.*

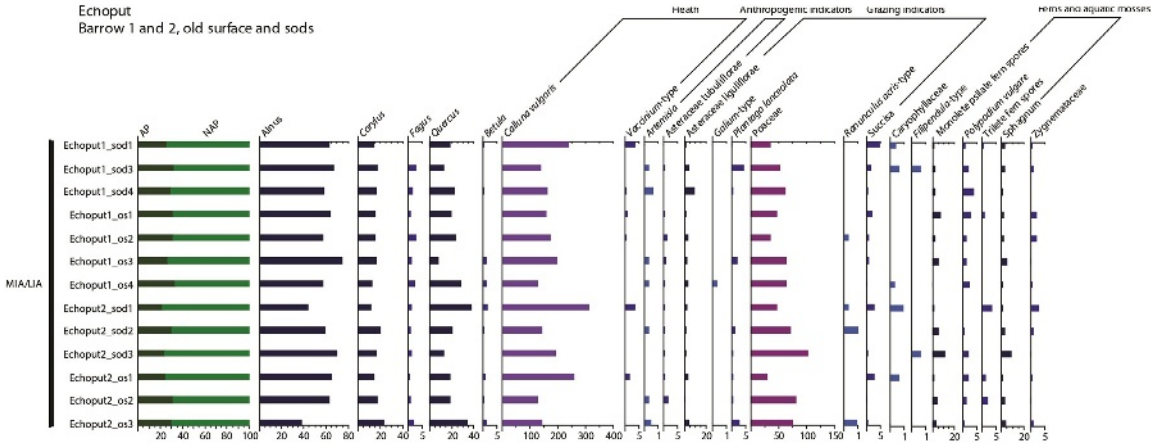

FIGURE 2.5.5 Pollen diagram derived from the series of samples taken under Echoput barrow 1. A relative diagram is shown, with percentages based on a tree pollen sum minus *Betula*. In the total AP, *Betula* is included. In the NAP, spores are included; non-pollen palynomorphs are excluded. Different scales have been used, indicated with different colours. *AP*, Arboreal pollen; *NAP*, non-arboreal pollen. *After Fig. 8.7 M. Doorenbosch, Ancestral Heaths. Reconstructing the Barrow Landscape in the Central and Southern Netherlands. PhD thesis. University of Leiden (2013) p. 106.*

sods (Fig. 2.5.5) are dominated by *Calluna vulgaris* (heather) and Poaceae (grasses). Since heather pollen tends not to spread outside the heathlands where the pollen is produced, it is implied that the Echoput barrows were built in an open spot covered with heath vegetation. The surrounding vegetation consists of forest that is dominated by *Corylus* (hazel) and *Quercus* (oak). Based on the ratio between arboreal and non-arboreal pollen the open spot was likely to

have an area with an average distance to the forest (ADF) of approximately 300 m (Doorenbosch, 2013, Chapters 7 and 8). The heath vegetation was probably already present some time before the barrows were built, shown by the pollen diagram of the soil profile underneath the barrow.

The landscape as shown by the pollen spectra from the Echoput is representative of nearly all investigated barrows. The size of the open space probably varied. The oldest barrows were mostly built in relatively small open spaces with an ADF of 50–100 m, while relatively young Middle to Late Iron Age barrows such as at the Echoput tend to be built in rather large open areas with an ADF of 300–500 m. In all cases, heath seemed to have been the main vegetation type locally present at the barrow site. Pollen diagrams showing the vegetation development in the period preceding the barrow building such as at the Echoput have not been produced for all barrows. However, since diverse heath vegetation was present in most cases, it is suggested that the area must have been open for some time, otherwise this vegetation would not have had the time to establish and develop. Barrows were numerous in the investigated areas and according to Bourgeois (2013), only a fraction of the barrows has been preserved; the original number of barrows in the Netherlands was much higher. This implies that the Dutch barrow landscape must have been dominated by patches of heathland.

Although heath patches seem to be small, many barrows were built close together and sometimes form alignments. It is very likely that many of these heath patches were clustered, forming open spaces that were long and narrow.

Fig. 2.5.6 shows the pollen spectra from barrows in the stream valley of Renkum in the southern part of the Veluwe. These barrows form part of an alignment with a length of at least 4.5 km (Bourgeois, 2013). Pollen spectra show that the investigated barrows were built in heath areas that were most likely connected to each other, possibly forming corridors in the landscape, as has been modelled in Fig. 2.5.7.

2.5.5 Ancestral heaths

Although heath can establish itself in a natural way, for example, in forest openings created

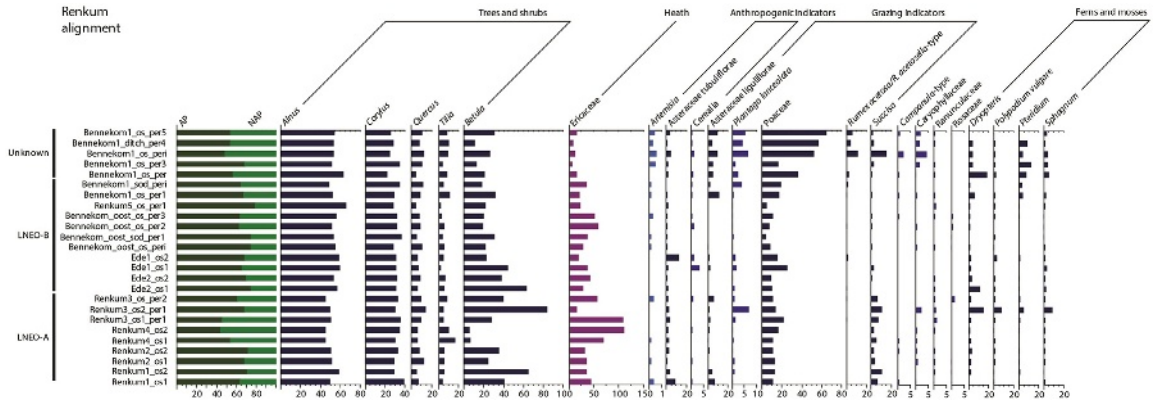

FIGURE 2.5.6 Pollen spectra from the samples taken from the barrows of the Renkum alignment. Spectra are given in % based on a tree pollen sum minus *Betula*. In the total AP, *Betula* is included. In the NAP, spores are included; non-pollen palynomorphs are excluded. Different scales have been used, indicated with different colours. *AP*, Arboreal pollen; *LNEO*, Late Neolithic; *NAP*, non-arboreal pollen. *After Fig. 9.2 M. Doorenbosch, Ancestral Heaths. Reconstructing the Barrow Landscape in the Central and Southern Netherlands. PhD thesis. University of Leiden (2013) p. 145.*

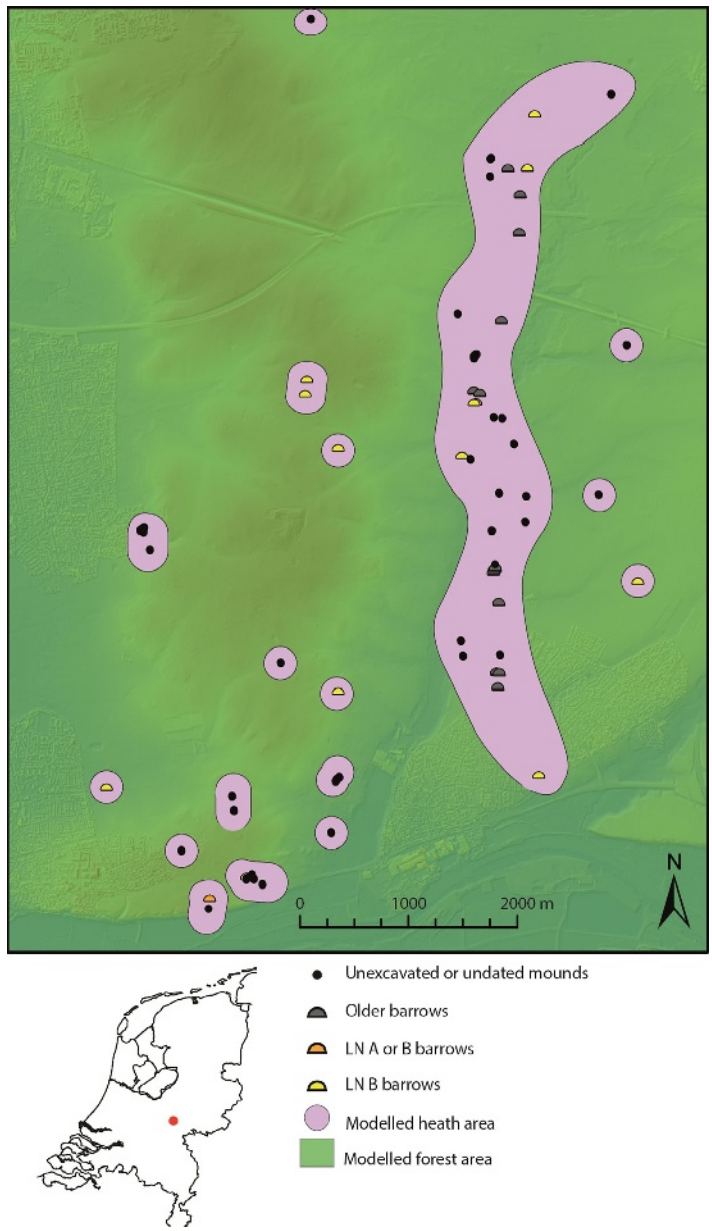

FIGURE 2.5.7 Barrow alignment of Renkum, situated in a (hypothetical) long-stretched heath area surrounded by forest. The vegetation reconstruction is based on palynological data from barrows. An exact reconstruction of the forest area is therefore not possible, since barrows are not present in those areas. *The figure is based on a digital elevation model of the AHN (copyright www.ahn.nl). After Fig. 13.1c M. Doorenbosch, Ancestral Heaths. Reconstructing the Barrow Landscape in the Central and Southern Netherlands. PhD thesis. University of Leiden (2013) p. 228.*

after a storm, heath vegetation cannot be maintained without some form of management. Since heath must have been present for long periods in areas where barrows were present it is very likely that heath management was conducted by the people living in the area. Methods of heath management can involve sod cutting, burning and grazing (or mowing) (Stortelder et al., 1996, p. 287). Sod cutting has taken place, since sods were used as building material for barrows. It is, however, not very likely that sod cutting alone was sufficient to maintain the barrow heath areas (Doorenbosch, 2013, p. 112). Charcoal present in small amounts could be the result of burning of heath; however, charcoal that could not be related to the burial itself has been found in only a few case studies. The most plausible method of barrow heath management is grazing. Grazing indicators were present in most barrow pollen spectra, indicating that the heathlands have been grazed (Hjelle, 1999).

As has been argued previously, barrow heathland must have been extensively present in the

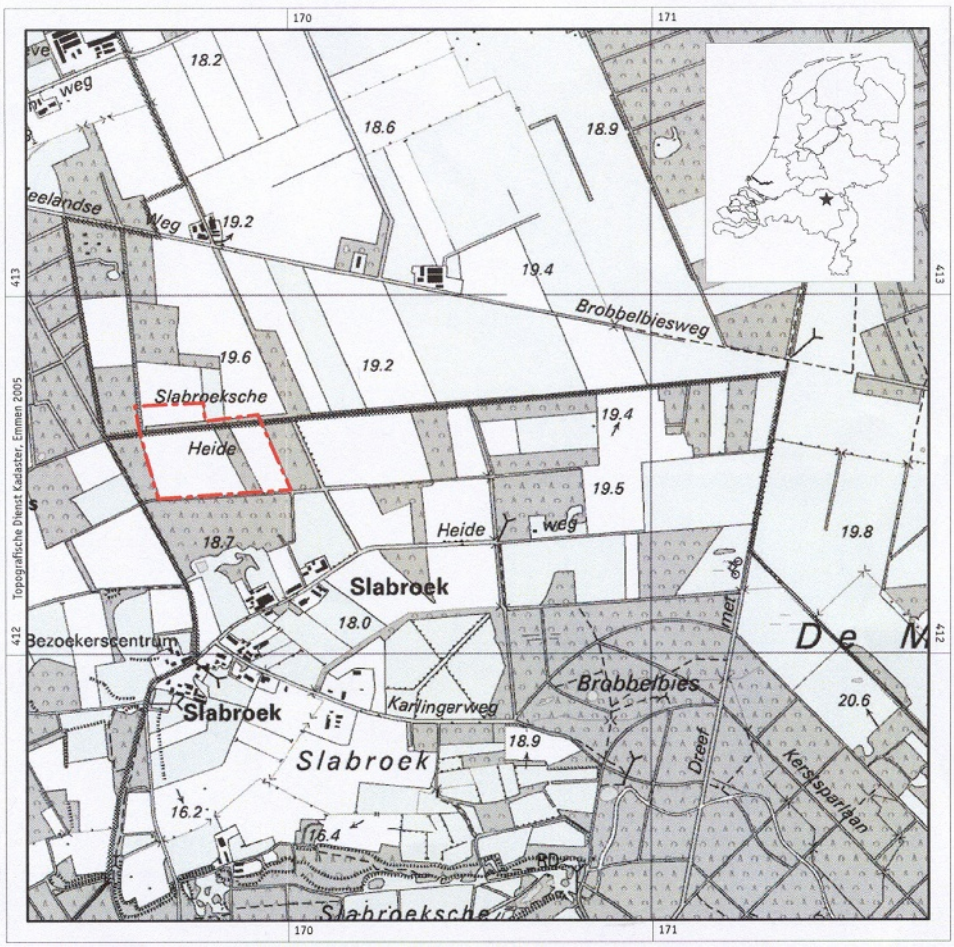

FIGURE 2.5.8 Location of the Bronze Age burial field on the Slabroekse Heide (Maashorst, Netherlands).

central and southern Netherlands. To maintain such areas of heathland, several households must have worked together, letting their cattle graze the heath. It cannot be concluded that these grazing activities have been practised by prehistoric man with the aim of managing the heath; they might just have been carried out by the barrow builders as part of their daily agricultural activity. Nevertheless, heath vegetation was a very important component of the barrow landscape and the barrow landscape played an important role in the daily life of the people living in the area, forming part of their economic zone. The heathland was already present before the barrows were built and most likely these heathlands have been in use as grazing grounds by the prehistoric communities living in the area, which might very well have been the ancestors of the barrow builders. The heathland areas where barrows were built can be considered as ancestral heaths; not only did they serve as burial places for ancestors, they had also been used by these ancestors as pastoral areas.

2.5.6 Palynological and absolute dating of the barrow of Slabroek

Archaeological finds in barrows may be helpful for dating, but such finds are always post-sedimentary and consequently not very accurate. The reconstruction of the Dutch barrow landscape is based on soil pollen analysis and palynological dating. Is it advisable to confirm palynological ages by absolute ^{14}C or optically stimulated luminescence (OSL) dates. But reliable absolute dating of palaeosols below barrows is problematic. A pilot study of the palaeosol below a barrow on the Slabroekse Heide (Fig. 2.5.8) will illustrate this problem (van Mourik, 2010).

Palynological dating of the 2Ah of the Slabroek barrow (Fig. 2.5.9–2.5.13) indicates that the pollen spectra of the 2Ah horizon (Fig. 2.5.14) are poor in pollen species. Grains of Ericaceae (*Calluna vulgaris*) dominate the spectra, which demonstrates that this barrow was built on existing heath. The scores of Poaceae are low, indicating a low degree of overgrassing. *Corylus* dominates the arboreal pollen. In pollen diagrams of palaeosols in the

FIGURE 2.5.9 Profile of the barrow, build on a palaeo carbic Podzol in coversand. The barrow was built with heath sods but the materials were subjected to secondary podzolization. The location of the burial field is indicated in Fig. 2.5.8; the locations for profile sampling are indicated. Micromorphological details of the samples are shown in Figs. 2.5.11–2.5.13. ▲ = ^{14}C dating and pollen analysis (2Ah and 2Bh); ● = optically stimulated luminescence dating (1C).

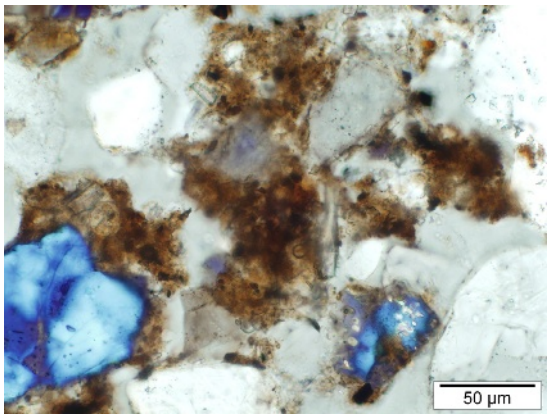

FIGURE 2.5.10 Micrograph of the distribution of organic matter and minerals in the C horizon, used for optically stimulated luminescence dating.

southeastern Netherlands this is indicative of the Bronze Age (van Mourik et al., 2012).

Radiocarbon dating of the humic acid fraction of the 2Ah and 2Bh of the palaeosol (Table 2.5.1; CIO, University Groningen) points to a burial of the palaeosol in the Iron Age. This is not in line with palynological dating. It is very likely that decomposed roots contaminated the organic content of the palaeosol and caused underestimation of the real age. The occurrence of charcoal particles in the organic aggregates also affects the reliability of the radiocarbon dating. Complications of the interpretation of radiocarbon dating of fractions of soil organic carbon are explained in Chapter 3. The impact of younger roots on the 'age' of soil organic carbon in buried humous horizons can be investigated with biomarker analysis, as explained in Chapter 5.

With the application of OSL dating of quartz grains (NCL, Wageningen University) from the base of the barrow sediments we can achieve better results. OSL ages are based on the luminescence signal of bleached mineral grains after burial (explained in Chapter 4). The OSL dating

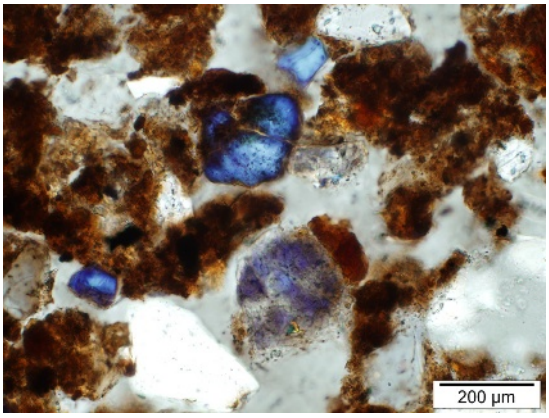

FIGURE 2.5.11 Micrograph of the distribution of minerals and organic matter in the 2Ah horizon, sampled for ^{14}C dating and pollen analysis.

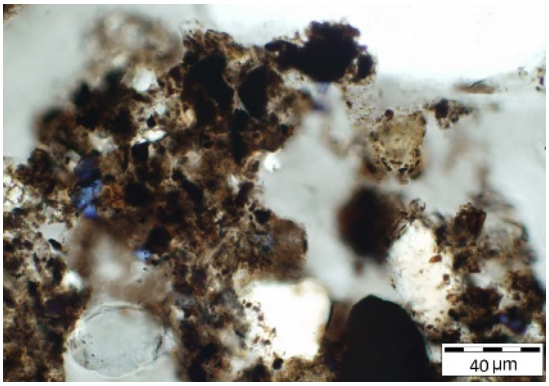

FIGURE 2.5.12 Micrograph of an organic aggregate in the 2Ah horizon. The internal fabric consists of aggregated fine organic particles (residual cellulose, lignin and charcoal) and plasma.

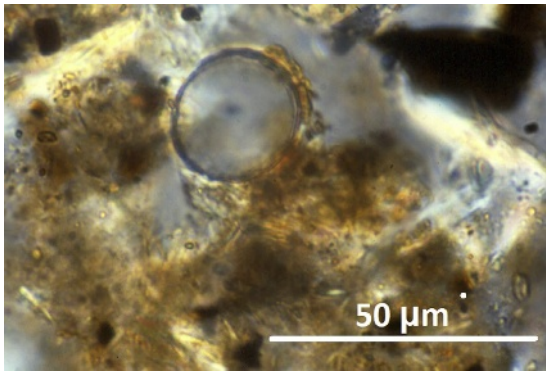

FIGURE 2.5.13 Micrograph of an organic aggregate in the 2Ah horizon, showing an embedded pollen grain and a charcoal fragment.

TABLE 2.5.1 Optically stimulated luminescence dating of the C horizon and ^{14}C datings of the humic acid fractions, extracted from the 2Ah and 2Bh horizons of the palaeosol.

NCL 5405031	C (bottom)	3800 ± 220 BP
GrN-29965	2Ah	2530 ± 90 BP
GrN-29966	2Bh	2560 ± 60 BP

BP, Before present.

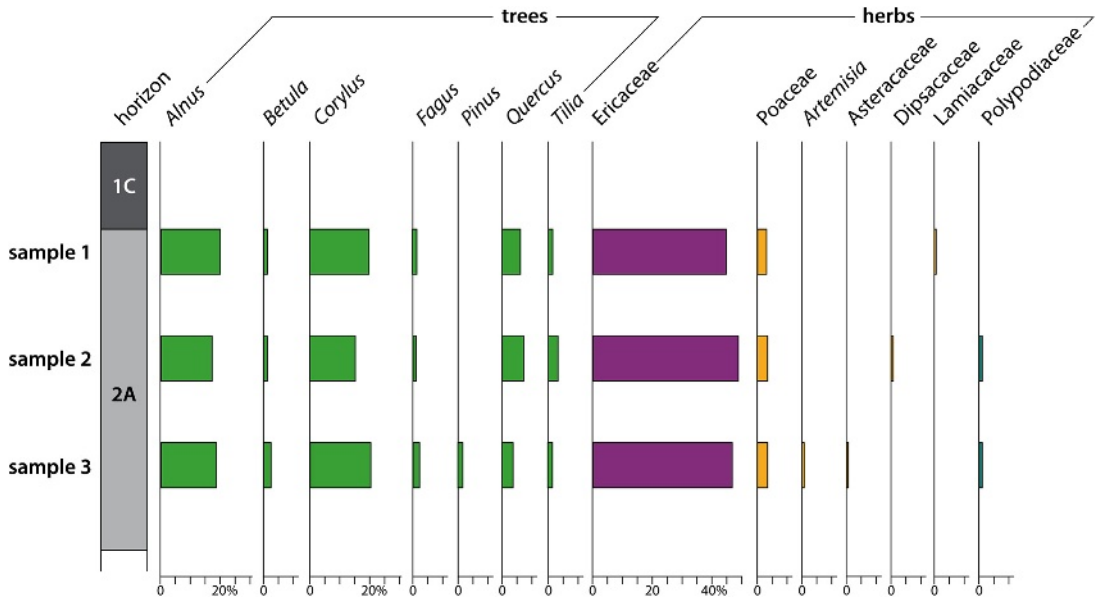

FIGURE 2.5.14 Pollen spectra of the 2Ah horizon. *After van Mourik (2010).*

of quartz grains from the base of the barrow (3.8 ± 0.22 Ky) points to a start of the accumulation of the barrow in the Early Bronze Age (in line with the palynological dating).

2.5.7 Conclusions

- Study of the reconstruction of the barrow landscape in the Dutch coversand district has proven the added value of soil pollen analysis to archaeological barrow research. It allowed a detailed reconstruction of the barrow landscape and increased our understanding of the important role heathlands played in the life of prehistoric people.
- Choice of the best dating method must be based on knowledge of landscape evolution, the properties of the samples and the specifications of the dating technique that can be used.
- In the pilot of the Slabroek barrow, the OSL date fit much better than the ^{14}C dating with the expected age of the barrow.

References

Andersen, S.T., 1970. The relative pollen productivity and pollen representation of North European trees. Danmarks Geologiske Undersøgelse R2 Nr 96, 1–99.

Arnoldussen, S., Fontijn, D., 2006. Towards familiar landscapes? On the nature and origin of Middle Bronze Age landscapes in the Netherlands. Proceedings of the Prehistoric Society 72, 289–317.

Bakker, R., 2003. The Emergence of Agriculture on the Drenthe Plateau. A Palaeobotanical Study Supported by High-resolution 14C Dating. University of Groningen.

Bal, L., 1973. Micromorphological Analysis of Soils, 6. Soil Survey Papers, Wageningen, 176 pp.

Barth, B., 1996. Mardellen im Lotharingischen Gipskeuper. Delattinia 22, 7–60.

Behre, K.E., 1986. Anthropogenic Indicators in Pollen Diagrams. Balkema, Rotterdam/Boston.

Beug, H.J., 2004. Leitfaden der Pollenbestimmung für Mitteleuropa und Angrenzende Gebiete. Verlag Friedrich Pfeil, München.

Bourgeois, Q.P.J., 2013. Monuments on the Horizon. The Formation of the Barrow Landscape throughout the 3rd and 2nd Millennium BC.. PhD thesis University of Leiden.

Braque, R., 1966. Observation sur les mardelles du plateau nivernais. Bulletin de l'Association française pour l'étude du quaternaire 3, 167–179. Numéro 3 - 1966.

Brewer, R., 1976. Fabric and Mineral Analysis of Soils. Krieger, Huntington, NY, 482 pp.

Cammeraat, L.H., 2006. Luxembourg. In: Boardman, J., Poesen, J. (Eds.), Soil Erosion in Europe. John Wiley & Sons, Chichester, pp. 427–438.

Cammeraat, L.H., Kooijman, A.M., 2009. Biological control of pedological and hydro-geomorphological processes in a deciduous forest ecosystem. Biologia 64 (3), 428–432.

Campbell, J.F.E., Fletcher, W.J., Hughes, P.D., Shuttleworth, E.L., 2016. A Comparison of Pollen Extraction Methods Confirms Dense-media Separation as a Reliable Method of Pollen Preparation. JQI.

Casparie, W.A., Groenman-van Waateringe, W., 1980. Palynological analysis of Dutch barrows. Palaeohistoria 22, 7–65.

Coleman, D.C., Crossley, D.A., 1996. Fundamentals of Soil Ecology. Academic Press, London/New York.

Daniels, A.G., 1964. A contribution to the investigation of the Holocene history of the Beech in the Eastern Netherlands. Acta Botanica Neerlandica 1, 66–74.

Davidson, D.A., Carter, S., Boag, B., Long, D., Tipping, R., Tyler, A., 1999. Analysis of pollen in soils: processes of incorporation and redistribution of pollen in five soil profile types. Soil Biology and Biochemistry 31, 643–653.

de Galicia, A., 1984. Cartografia y Diseno, Madrid, 127 pp.

Dijkstra, E.F., van Mourik, J.M., 1995. Palynology of young acid forest soils in the Netherlands. Mededelingen Rijks Geologische Dienst 52, 283–296.

Dijkstra, E.F., van Mourik, J.M., 1996. Reconstruction of forest dynamics based on pollen analysis and micromorphological studies of young acid forest soils under Scots pine plantations. Acta Botanica Neerlandica 45, 393–410.

Dijkstra, E.F., Boon, J.J., van Mourik, J.M., 1998. Analytical pyrolysis of a soil profile under Scots pine. European Journal of Soil Science 49, 295–304.

Doorenbosch, M., 2011. An environmental study of the Echoput barrows. In: Fontijn, D.R., Bourgeois, Q.P.J., Louwen, A. (Eds.), Iron Age Echoes. Prehistoric Land Management and the Creation of a Funerary Landscape – the " Twin Barrows" at the Echoput in Apeldoorn. Sidestone Press, Leiden.

Doorenbosch, M., 2013. Ancestral Heaths. Reconstructing the Barrow Landscape in the Central and Southern Netherlands. PhD thesis. University of Leiden.

Doorenbosch, M., van Mourik, J.M., 2016. The impact of ancestral heath management on soils and landscapes: a reconstruction based on paleoecological analyses of soil records in the central and southeastern Netherlands. SOIL 2, 311–324.

Elsik, W.C., 1971. Microbiological degradation of sporopollenin. In: Brooks, J., Grant, P.R., Muir, R., Van Gijzel, P., Shaw, G. (Eds.), Sporopollenin. Academic Press, London, pp. 480–511.

Etienne, D., Ruffaldi, P., Goepp, S., Ritz, F., Georges-Leroy, M., Pollier, B., Dambrine, E., 2011. The origin of closed depressions in Northeastern France: a new assessment. Geomorphology 126, 121–131.

Faegri, K., Iversen, J., 1989. Textbook of Pollen Analysis, fourth ed. John Wiley & Sons, Chichester.

FAO-UNESCO, 1988. Soil Map of the World. Revised Legend. World Soil Recourses Report 60. FAO, Roma, 138 pp.

Fontijn, D.R., Bourgeois, Q.P.J., Louwen, A. (Eds.), 2011. Iron Age Echoes. Prehistoric Land Management and the Creation of a Funerary Landscape – the " Twin Barrows" at the Echoput in Apeldoorn. Sidestone Press, Leiden.

Green, R.N., Trowbridge, R.L., Klinka, K., 1993. Towards a Taxonomic Classification of Humus Forms. Forest Science. Monograph 29. 49 pp.

Groenman-van Waateringe, W., 1992. Palynology and archaeology: the history of a plaggen soil from the Veluwe, The Netherlands. Review of Palaeobotany and Palynology 73 (1–4), 87–98.

Guillet, B., 1970. Etude palynologique des podzols. Pollen et Spores XII, 45–69.

Guitian Ojea, F., Carballas, T., 1968. Suelos de la zona humida espanola: III. Ranker atlantico. Anales de Edafologia y Agrobiologia XXVII, 57–73.

Havinga, A.J., 1963. A Palynological Investigation of Soil Profiles Developed in Cover Sand. Veenman, Wageningen.

Havinga, A.J., 1984. A 20-year experimental investigation into the differential corrosion susceptibility of pollen and spores in various soil types. Pollen and Spores 26, 541–558.

Hjelle, K.L., 1999. Modern pollen assemblages from mown and grazed vegetation types in western Norway. Review of Palaeobotany and Palynology 197, 55–81.

ISRIC-FAO, 2006. World Reference Base for Soil Recourses 2006. World Soil Resources Reports, 103.

Janssen, C.R., 1974. Verkenningen in de palynologie. Oosthoek, Scheltema & Holkema, Utrecht.

Janssen, C.R., Ten Hove, H.A., 1971. Some late-Holocene pollen diagrams from the Peel raised bogs (Southern Netherlands). Review of Palaeobotany and Palynology 11, 7–53.

Leenders, K.A.H.W., 1987. De boekweitcultuur in historisch perspectief. Geografisch Tijdschrift 21, 213–222 (with English summary).

Loehle, C., 2007. A 2000-year global temperature reconstruction based on non-treeing proxies. Energy and Environment 18 (7+8).

Louwe Kooijmans, L.P., 1974. The Rhine/Meuse Delta. Four Studies on its Prehistoric Occupation and Holocene Geology. PhD thesis. University of Leiden.

Lucius, M., 1948. Geologie Luxemburgs; Erläuterungen zu der Geologischen Spezialkarte Luxemburgs. Band V. Service Géologique de Luxembourg.

Manten, A.A., 1967. Lennart von Post and the foundation of modern palynology. In: Review of Palaeobotany and Palynology, 1, pp. 11–22.

Mendez Amor, J., Florschütz, F., 1961. Contribución al conocimiento de la historia de la vegetación en Espana durante al Cuaternario. Estudios Geologicos XVII, 83–99.

Mook, W.G., Streurman, H.J., 1983. Physical and chemical aspects of radiocarbon dating. In: First symposium on 14C and Archaeology, Groningen, PACT, 8, pp. 31–55.

Moore, P.D., Webb, J.A., Collinson, M.E., 1991. Pollen Analysis, second ed. Blackwell, Oxford. 216 pp.

Nonn, H., 1969. Evolution géomorphologique et types de relief en Galice occidentale et septentrionale. Revue de Géography Physique et de Géologie Dynamique XI, 31–53.

Out, W.A., 2009. Sowing the seed? Human impact and plant subsistence. In: Dutch wetlands during the Late Mesolithic and Early and Middle Neolithic (5500-3400 Cal. B.C.). Archaeological Studies Leiden University, Vol. 18. Leiden University Press, Leiden.

Persch, F., 1950. Zur postglazialen Wald- und Morentwicklung im Hohen Venn. Decheniana 104.

Poeteray, F.A., Riezebos, P.A., Slotboom, R.T., 1984. Rates of Subatlantic lowering calculated from mardel-trapped material (Gutland, Luxembourg). Zeitschrift für Geomorphologie 467–4821.

Schmalen, C., 2002. Einige Mardellen Luxemburgs auf den Keuper-und Liasschichten des Forstamtbezirks Zentrum. Diplomarbeit in Studiengang Umweltplanung an der Fachhochschule Trier. Standort Birkenfeld.

Slicher van Bath, B.H., 1960. De Agrarische Geschiedenis Van West Europa, 32. Uitgave Spectrum, Aula.

Slotboom, R.T., 1963. Comparative geomorphological and palynological investigation of the pingos (viviers) in the haute Fagnes (Belgium) and the Mardellen in the Gutland (Luxembourg). Zeitschrift für Geomorphologie 7, 193–231.

Slotboom, R.T., van Mourik, J.M., 2015. Pollen records of mardel deposits; the effects of climatic oscillations and land management on soil erosion in Gutland, Luxembourg. Catena 132 (2015), 72–88.

Stockmarr, J., 1971. Tablets with spores used in absolute pollen analysis. Pollen et Spores 13, 615–622.

Stortelder, A.H.F., de Smidt, J.T., Swertz, C.A., 1996. Callunoulicetea. In: Schaminée, J.H.J., Stortelder, A.H.F., Weeda, E.J. (Eds.), De vegetatie van Nederland. Deel 3. Plantengemeenschappen van graslanden, zomen en droge heiden. Opulus press, Leiden, pp. 287–316.

Thill, G., 1977. Vor- und Frühgeschichte Luxemburgs. Editions Bourg-Bourger, Luxembourg.

Thoen, D., Hérault, B., 2006. Flore, groups socio-écologique et typologie de mardelles forestières de Lorrainne belge et luxembourgeoise. Bulletin Societe Luxembourgeois 107, 3–25.

Van Geel, B., 1978. A palaeoecological study of Holocene peat bog sections in Germany and the Netherlands, based on the analysis of pollen, spores and macro- and microscopic remains of fungi, algae, cormophytes and animals. Review of Palaeobotany and Palynology 25, 1–120.

Van Haaster, H., 2008. Archeobotanica uit 's-Hertogenbosch. Milieuomstandigheden, bewoningsgeschiedenis en economische ontwikkelingen in en rond een (post)middeleeuwse stad. Groningen Archaeological Studies 6.

van Mourik, J.M., 1986. In: Pollen Profiles of Slope Deposits in the Galician Area (N.W. Spain). Netherlands Georaphical Studies, 12. KNAG, Amsterdam, 171 pp.

van Mourik, J.M., 1991. Spuren von Plaggenlandbau im Gebiet der Schleswiger Landenge. Offa 47, 169–176.

van Mourik, J.M., 1999. The use of micromorphology in soil pollen analysis. Catena 35, 239–257.

van Mourik, J.M., 2001. Pollen and spores, preservation in ecological settings. In: Briggs, E.G., Crowther, P.R. (Eds.), Palaeobiology II. Blackwell, Oxford, pp. 315–318.

van Mourik, J.M., 2003. Life cycle of pollen grains in mormoder humus forms of young acid forest soils: a micromorphological approach. Catena 54, 651–663.

van Mourik, J.M., 2010. Resultaten van het dateringsonderzoek van hrafheuvel 39 op de Slabroekse Heide. In: van Wijk en, I.M., Jansen, R. (Eds.), Het Urnenveld Slabroekse Heide op de Maashorst. Archol 72, Leiden, The Netherlands, pp. 67–73.

van Mourik, J.M., Slotboom, R.T., 2018. Palynological reconstruction of the effects of Holocene climatic oscillations and agricultural history on soils and landforms in Luxembourg. In: Kooijman, A.H., Cammeraatand, L.H., Seijmonsbergen, A.C. (Eds.), The Luxembourger Landscape. Springer, pp. 39–72.

van Mourik, J.M., Seijmonsbergen, A.C., Slotboom, R.T., Wallinga, J., 2012. The impact of human land use on soils and landforms in cultural landscapes on aeolian sandy substrates (Maashorst, SE Netherlands). Quaternary International 265, 74–89, 2012a.

Van Zeist, W., 1967. Archaeology and palynology in the Netherlands. Review of Palaeobotany and Palynology 4, 45–65.

Walch, K.M., Rowley, J.R., Norton, N.J., 1970. Displacement of pollen grains by earth worms. Pollen et Spores XII, 39–45.

Wallwork, J.A., 1976. The Distribution and Diversity of Soil Fauna. Academic Press, London/New York.

Waterbolk, H.T., 1954. De praehistorische mens en zijn milieu. Een palynologisch onderzoek naar de menselijke

invloed op de plantengroei van de diluviale gronden in Nederland. University of Groningen.

Zeven, A.C., 1997. De introductie van onze cultuurplanten en hun begeleiders van het Neolithicum tot 1500 AD. Vereniging voor landbouwgeschiedenis, Wageningen.

Zolitschka, B., Behre, K.E., Schneider, J., 2003. Human and climatic impact on the environment as derived from colluvial, fluvial and lacustrine archives examples from the Bronze Age to the Migration Period, Germany. Quaternary Science Reviews 22, 81–10.

CHAPTER

3

Radiocarbon dating of soil archives

J. van der Plicht[a,*], *H.J. Streurman*[a], *J.M. van Mourik*[b]

[a]Centre for Isotope Research, University of Groningen, Groningen, the Netherlands; [b]Institute for Biodiversity and Ecosystem Dynamics (IBED), Faculty of Science, University of Amsterdam, Amsterdam, the Netherlands

*Corresponding author.

3.1 The theory of radiocarbon dating of soil organic matter

3.1.1 Introduction

This chapter reviews the radiocarbon method with an emphasis on dating soil organic matter and its intrinsic difficulties. Both ^{14}C measurement techniques (conventional and accelerator mass spectrometry (AMS)) are presented and discussed. This includes the present state of the art of the radiocarbon dating method on timescale calibration, sample quality aspects and sample pretreatment. In addition, the stable isotope ^{13}C can be used as a tracer for geochemical processes. Applying both carbon isotopes in soil science is illustrated by selected case studies.

The radiocarbon (^{14}C) dating method was developed around 1950 (Libby, 1952; Taylor et al., 1992). The method enables direct dating of organic remains back to about 50,000 years ago. Since that time, several 'revolutions' have improved the method considerably. Amongst the most significant are the introduction of AMS in the 1980s, and calibration of the ^{14}C timescale to obtain absolute dates.

AMS enables small (milligram size) sample analysis (Tuniz et al., 1998; Jull, 2013). This is a factor of 1000 less than the original so-called conventional method based on radiometry (Cook and van der Plicht, 2013). AMS therefore enables ^{14}C dating of precious fossils, such as archaic human bones and artefacts, as well as intrinsically small samples, such as botanical remains (macrofossils and seeds) and fragments (e.g., Wagner et al., 2018).

Calibration now enables absolute dating back to 50,000 years ago (Reimer et al., 2013), i.e., the complete dating range. In turn, this has spawned 'revolutions' in applications, amongst which are archaeology, palaeontology and Quaternary geology. Radiocarbon provides a 'yardstick of time', enabling the measurement of past time by scientific means, independent of associations and assumptions. This enables synchronization and chronological comparison of different areas at excavation sites and also between sites and regions. This is essential for proper interpretation of archaeological or stratigraphical layers and association with data from other fields (e.g., van der Plicht and Bruins, 2001).

Reading the Soil Archives
https://doi.org/10.1016/B978-0-444-64108-3.00003-3

While the method is basically simple, it is complex in detail and errors in matters concerning both fieldwork and technical laboratory aspects. Therefore stringent quality control is necessary to build up reliable ^{14}C chronologies. This involves regular laboratory intercomparisons, duplicate measurements of samples, issues such as conventional dating versus AMS, sample selection, association and others (van Strydonck et al., 1999; Scott et al., 2010). In addition to ^{14}C dating, the content of the stable carbon isotope ^{13}C of the sample is also measured. For some applications this is complemented by the stable isotope ^{15}N (Fry, 2008). Both stable isotopes provide insight into topics such as palaeoecological conditions and geochemical processes. Also, the stable isotope ^{18}O is a geochemical tracer, in particular for carbonates and aquatic reservoirs (Mook, 2006).

In this section, a short review of the principles of the ^{14}C method and conventions is given. The application discussed here is dating of soil organic matter. This category of samples shows intrinsic problems. The use of the stable isotope ^{13}C in soil science is illustrated as well. Selected case studies will be discussed.

3.1.2 The ^{14}C dating method

The element carbon consists of three naturally occurring isotopes: ^{12}C, ^{13}C and ^{14}C with abundances of ca. 98.9%, 1.1% and 10^{-10}%, respectively. The isotope ^{14}C (radiocarbon) is continuously produced in the earth's atmosphere by cosmic radiation. Radiocarbon is radioactive and decays with a half-life of 5730 ± 40 years (Godwin, 1962). A stationary state of production, distribution between the main carbon reservoirs (atmosphere, ocean and biosphere) and decay result in a more or less constant ^{14}C concentration in atmospheric CO_2 and the terrestrial biosphere (e.g., Mook and Waterbolk, 1985; Mook and van de Plassche, 1986). Upon the death of an organism, the radioactive ^{14}C decays, and by measuring the amount of remaining ^{14}C in the sample its time of death can be derived. For accurate radiocarbon dating, only the ^{14}C that was part of the organism when it died should be measured. This requires so-called pretreatment of the sample.

It has been known for some time that the ^{14}C concentration of atmospheric CO_2 has not always been the same. In tree rings, natural variations of atmospheric $^{14}CO_2$ abundance were discovered on a timescale of one decade to a few centuries (de Vries, 1958). Later, it was discovered that these variations can be attributed to variations in solar activity (Stuiver, 1965), which in turn influence the production of ^{14}C in the atmosphere. Also, changes in the geomagnetic field strength influence the production of ^{14}C in the atmosphere (Bucha, 1970). This is understood because both solar activity and geomagnetic field strength determine the amount of cosmic radiation impinging on the earth (van der Plicht, 2013). In addition, atmospheric $^{14}CO_2$ concentration also depends on exchange between the atmosphere and ocean.

Because of these variations in the natural ^{14}C concentration, the ^{14}C clock runs at a varying pace, different from real clocks: ^{14}C time is not equivalent to calendar time. Therefore the ^{14}C timescale has been defined and needs to be calibrated to establish the relationship between ^{14}C time and historical time.

This definition is known as the 'radiocarbon convention' (Mook and Streurman, 1983; van der Plicht and Hogg, 2006; Mook and van der Plicht, 1999). The definition states that ^{14}C radioactivity is always measured relative to that of a standard (oxalic acid with a radioactivity of 0.226 Bq/gC), representing modern natural radiocarbon, which corresponds to AD 1950. From this measured radioactivity the 'radiocarbon age' is calculated using a half-life of 5568 years. This value was used in the early days of ^{14}C dating and is not correct; the proper value was later established as the aforementioned 5730 years. However, it is still used to

avoid confusion; the error in the 'date' that is introduced this way is corrected by calibration (see later).

Other complications arise from the differences in processes in nature and the laboratory for the different isotopes, caused by their different masses. This is known as 'fractionation'. For example, in biological pathways, lighter isotopes are taken up preferentially, reducing the proportion of ^{14}C in a sample making it seem older. The proportion of ^{13}C is also changed. This isotope is stable, i.e., its concentration is constant throughout time. Therefore the ratio of the stable isotopes ^{13}C and ^{12}C in a sample can be used to estimate the fractionation effect of ^{14}C. The radiocarbon convention implies that the fractionation correction must be to a standardized value for the $^{13}C/^{12}C$ ratio (to $\delta^{13}C = -25‰$; the δ values are introduced later, and see Mook, 2006).

In the following we will use the 'activity ratio' ^{14}a. This is defined as the ^{14}C radioactivity of the sample relative to that of the standard, and taking into account the convention. Thus for the oxalic acid standard, $^{14}a = 1$ or 100%; for a sample with a (conventional) half-life of 5568 years, $^{14}a = 0.5$ or 50% (Mook and van der Plicht, 1999).

The defined conventional ^{14}C timescale is expressed in the unit BP. This originally meant 'Before Present'. The expression 'Present', originally taken as AD 1950, should not be taken literally, because the relation between the ^{14}C timescale and the calendar timescale is complex. This relation is determined by calibration.

3.1.3 Timescale calibration

Calibration involves measuring samples by both the ^{14}C method (reported in BP by the convention) and another method. Ideally, this other method has to be independent from ^{14}C, yielding absolute dates (in AD/BC), and the samples have to be from the terrestrial (or atmospheric) reservoir. The paired dates (BP and AD/BC) then are used to construct a calibration curve, which gives the relationship between both timescales. For the dates calibrated using this curve, the chosen convention values for half-life and fractionation correction are taken into account.

The unit calBP is used as well; this is defined as calendar years relative to AD 1950 (calBP = AD − 1950).

The ideal samples for calibration are tree rings, because they can be dated absolutely by means of dendrochronology. Following the early work of Suess (1980), the ^{14}C community distributed special issues of the journal *Radiocarbon* with calibration curves based on a variety of available records. These issues are updated regularly. The main data are tree rings dated by both ^{14}C and dendrochronology. Beyond the available absolutely dated dendrochronological dataset, records from varves (laminated sediments containing botanical remains), plus corals/foraminifera and speleothems, which are also dated by isotopes in the uranium decay chain, are used. The main varved record is from the terrestrial sediment of Lake Suigetsu in Japan (Bronk Ramsey et al., 2012).

Using these datasets, the calibration curve named IntCal13 has been constructed. It is the presently recommended calibration curve, and is shown in Fig. 3.1.1. It will be replaced shortly by IntCal20 (Reimer et al., 2020). Significant changes will be implemented for the oldest part of the curve. The dendrochronological part and the part derived from other records are indicated, separated at 13,900 calBP (Reimer et al., 2013).

The long-term (millennia scale) trend of the calibration curve is explained by the changing geomagnetic field. On this long-term trend, modulations on the century/decennium scale (known as 'wiggles') can be seen, which are caused by fluctuations in solar activity. There was significantly more ^{14}C present in nature millennia ago, causing ^{14}C ages to be 'young': 46,000 ^{14}C years ago (in BP) corresponds to

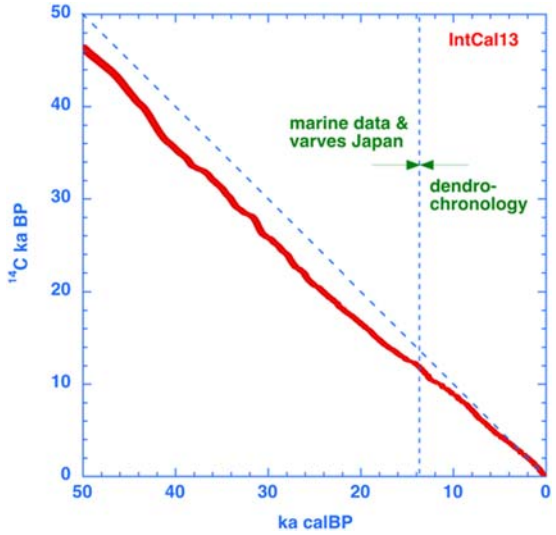

FIGURE 3.1.1 The calibration curve IntCal13, to be used for transferring ^{14}C dates (vertical, BP) into calendar ages (horizontal, calBP = AD − 1950).

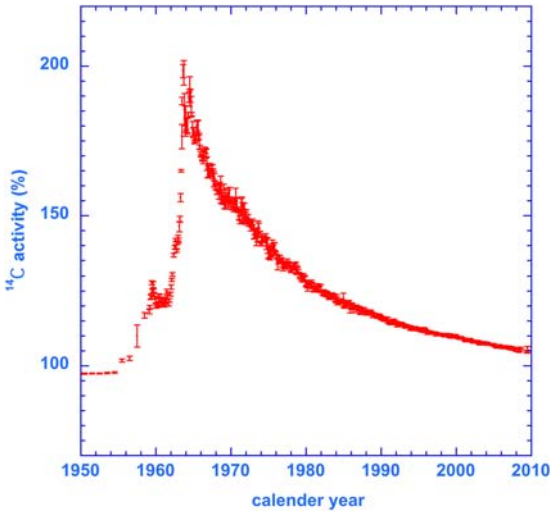

FIGURE 3.1.2 Measurements of atmospheric ^{14}C content for modern times, showing the 'bomb peak'.

about 50,000 calendar years ago (in calBP). This is obviously important for the interpretation of Pleistocene samples.

In modern times, the ^{14}C content in nature is influenced by anthropogenic effects. First, in the atmosphere and terrestrial samples, the greenhouse gas emissions (which are of geological age and thus do not contain ^{14}C) have diluted the natural atmospheric $^{14}CO_2$ content since around AD 1900. This is known as the Suess effect, which is also apparent in terrestrial samples like tree rings (Stuiver and Quay, 1981). Furthermore, after the Second World War, test explosions of nuclear bombs in the atmosphere produced extra ^{14}C. In the Northern Hemisphere this increased the ^{14}C concentration by a factor of two in 1963 (Fig. 3.2.2).

Since 1963 atmospheric explosions no longer occurred (except for a few small bomb tests), so the ^{14}C content decreased in the atmosphere and increased in the oceans by exchange of $^{14}CO_2$ (e.g., Levin and Hesshaimer, 2000). The atmospheric ^{14}C signal for the years 1950−2010 is shown in Fig. 3.1.2. It shows what is generally known as the 'bomb peak' and is valid for the Northern Hemisphere (Hua et al., 2013). At present, the interplay of ^{14}C in the global carbon cycle (bomb peak, fossil fuels and the reservoirs' atmosphere, biosphere and the oceans) causes natural ^{14}C content in the atmosphere close to 'normal', defined as $^{14}a = 100\%$ (Graven, 2015).

Examples of 'bomb dating' of soil organic carbon can be found in Trumbore et al. (1989). The ^{14}C isotope can be used as a tracer for carbon (geo)chemistry.

3.1.4 Measuring carbon isotopes

For accurate ^{14}C dating, only the ^{14}C that was part of the organism when it died should be measured. Therefore the first task is to remove any foreign carbon that entered the sample since that time. Such contamination comes principally from the burial environment. This is done by a mixture of physical and chemical means using pretreatment protocols. These procedures also isolate a stable chemical fraction of a sample − for example, collagen from bone, or cellulose

from wood. The treatment of soil organic matter is discussed later. For a complete description of sample pretreatment aspects we refer to Mook and Streurman (1983) and Mook and van de Plassche (1986).

The next stage in dating is combustion of the isolated and purified datable fraction of the sample to produce CO_2. This CO_2 gas contains the ^{14}C from the sample; dating is the measurement of this amount of ^{14}C.

For the conventional method, the ^{14}C radioactivity in the CO_2 is measured by radiometry. This ^{14}C radioactivity is extremely low. Therefore special counters in a low-background setup are required, designed to shield the natural radioactivity. This method typically requires a litre of CO_2 gas, roughly equivalent to a gram of carbon, or grams of sample material. The conventional radiometric method was developed around 1950. For more technical details of the conventional method we refer to Mook and Streurman (1983) and Cook and van der Plicht (2013).

AMS is a form of mass spectrometry which measures the ^{14}C content directly instead of those ^{14}C atoms which decay by radioactivity. Mass spectrometry is much more efficient than radiometry, which enables a very significant reduction (by a factor of 1000) in sample size to typically 1 mg of carbon. The AMS technique was developed in the 1980s (Tuniz et al., 1998; Bayliss et al., 2004; Jull, 2013).

For AMS, the principles of chemical/physical pretreatment are the same as for the conventional method. However, for AMS, one extra step is needed: the CO_2 gas needs to be reduced to graphite (Aerts et al., 2001). The graphite is pressed into targets, mounted in a sample wheel before it is loaded into the ion source of the machine.

Using a high voltage, the AMS accelerates the C ions to high energies. A set of magnets separates this high energy beam of C ions according to mass: 12, 13 and 14 for the isotopes ^{12}C, ^{13}C and ^{14}C, respectively. The ^{12}C and ^{13}C beams are measured by current meters, and from this the ratio $^{13}C/^{12}C$ is determined. This is used for fractionation correction, necessary for ^{14}C dates. A particle detector measures the ^{14}C counts, so that the $^{14}C/^{12}C$ ratio can also be determined. Further technical details, performance and status reports of the Groningen AMS facility can be found in van der Plicht et al. (2000) and references therein. From all of this, the ^{14}C ages in BP are calculated (Mook and van der Plicht, 1999). Note that both ^{14}C measuring methods (radiometry and mass spectrometry) yield numbers in BP, which have the same meaning.

For conventional dates, the CIO laboratory code GrN is used; for AMS dates, this is GrA.

Stable isotope concentrations are measured by conventional mass spectrometry based on molecular gases. The stable carbon isotope (^{13}C) content of the sample is measured in CO_2 by isotope ratio mass spectrometry upon combustion of the pretreated ^{14}C sample material (such as collagen, prepared from fossil bone). Thus the same CO_2 is used for both isotope measurements, ^{13}C and ^{14}C dating – either by AMS or by the conventional method.

The stable isotopic content of the samples is expressed in delta (δ) values, which are defined as the deviation (expressed in per mil) of the rare to abundant isotope ratio from that of a reference material:

$$\delta^{13}C = (^{13}C/^{12}C)_{sample}/(^{13}C/^{12}C)_{reference} - 1(\times 1000‰)$$

The absolute isotope content of the reference materials has been measured very accurately (Mook, 2006 and references therein). For ^{13}C, the reference material is Pee Dee Belemnite carbonate, the carbonate from a belemnite found in the Cretaceous Pee Dee formation of North America (Mook, 2006; Fry, 2008).

Apart from fractionation correction for ^{14}C dating, the stable isotope ratio $\delta^{13}C$ has merit by itself. As will be shown in selected case

studies, this isotope can be used as a tracer for geochemical processes (Michener and Lajtha, 2007; Fry, 2008).

3.1.5 Chemical aspects of samples

Not all types of material are equally suitable for radiocarbon dating. For example, from a geophysical point of view, a sample has a certain degree of association with the event to be dated (Mook and Streurman, 1983; Olsson, 1989; van Strydonck et al., 1999). From a physical point of view, ^{14}C ages may have different degrees of reliability because, for example, the original ^{14}C age of the sample is not well known (which is the case for groundwater). From a chemical point of view, the sample may contain foreign carbon having a different ^{14}C content (for example, humic substances of plant roots from stratigraphically lower depths).

In general, the contaminant has a higher (often 'modern') ^{14}C concentration, which will result in a date which is too young. On the other hand, admixture of zero-activity bituminous products or graphite ('dead') in the sample will result in a date which is too old. Both are known to happen.

One can calculate how much contamination is needed to explain aberrant dates. It obviously depends on the age of the contaminant, which theoretically can be any age between modern and fossil. Let us assume here modern contamination, then a contamination of 1% modern carbon in a sample of 50,000 BP will be measured as 35,000 BP. Further examples can be found in Mook and Streurman (1983) and Mook and van de Plassche (1986). These articles were written for the conventional dating method, using large samples. For our example, 1% foreign carbon for a 1 g sample is 10 mg, which is relatively large. The same calculations apply to AMS but the samples are much smaller. Here, a contamination of 1% foreign carbon for a 1 mg sample is only 10 μg; AMS is obviously much more sensitive for contamination (Lanting and van der Plicht, 1994).

Samples to be dated need pretreatment to remove contaminants. The form and intensity of pretreatment depend on the type, quality and quantity of the sample. An example of physical pretreatment is the removal of subrecent plant roots. Chemical pretreatment is designed to isolate the pure datable fraction of the sample. The standard chemical recipe is the so-called acid-alkali-acid (AAA) method, also known as acid-base-acid. This is applied to most sample materials. The sample material is subjected to the following extraction steps:

1. A 4% HCl solution to remove soil carbonate and infiltrated humic (fulvic) acids;
2. A 4% NaOH solution to remove components like tannic acids and lignin;
3. A 4% HCl to remove any CO_2 absorbed during step 2.

Standard usually means also a temperature of 80°C for 24 h for each step; however, this is often too rigorous, so that too much sample material will dissolve. A lower temperature, duration and/or a more diluted acid/base can be applied in such cases. Pretreatment by step 1 only is referred to as A treatment.

3.1.6 Soil organic carbon

In mineral humous soil horizons, no plant remains are recognizable. The mineral matrix may be sand, clay or löss. The organic content consists mainly of fulvic and humic acids and humin (see later).

Plants and wood have an organic carbon content of about 50% (Mook and Streurman, 1983). Compared with such sample materials, that of soils can be very low, often below 5%. Therefore the relative contribution of contaminants can be considerable. The organic content of the sample can be as follows:

1. Autochthonous carbon, formed during deposition; this is generally the datable fraction;
2. Allochthonous carbon, which was part of the deposited matrix prior to the formation of the autochthonous carbon; this carbon causes older ages;
3. Reworked or eroded allochthonous organic matter, usually older, which is redeposited in the dated layer;
4. Younger carbon from stratigraphically lower depths, like fulvic and humic acids;
5. Rootlets from higher, younger levels.

After the removal of roots and coarse sands by sieving (physical pretreatment), soil samples undergo chemical pretreatment to isolate the datable fraction and to remove contaminants (Mook and Streurman, 1983).

Based on their solubilities, the organic compounds are generally subdivided into fulvic acids (soluble in alkaline and in acids) and humic acids (soluble in alkaline, precipitating in acids). A residual fraction (often referred to as humin) is insoluble in both acids and alkaline. The latter organic molecules, originating from the decomposition of organic matter, are relatively resistant against further degradation. This humin fraction is therefore considered the allochthonous organic matter.

Fulvic acids represent a very unstable phase of humic components, which is highly mobile and moves relatively quickly through a profile. Since in general there is net water transport downward, this means that they usually show a younger age than other fractions at the same depth. Nevertheless, for soils, humic acid is the most reliable datable fraction.

Generally, a consistent date for both humin and alkaline fraction (the humic acid) is a quality check for the homogeneity of the sample. This is then considered as a good indication of the relative integrity of the material selected for dating.

A schematic illustration of the pretreatment is shown in Fig. 3.1.3. For the datable fraction (the humic acid) the carbon content C_v is about 60% for good quality samples (C_v is defined later; see also Mook and Streurman, 1983).

3.1.7 Reservoir effects

The ^{14}C convention is defined for terrestrial material, which is in equilibrium with atmospheric CO_2. Reservoirs like oceans, rivers and

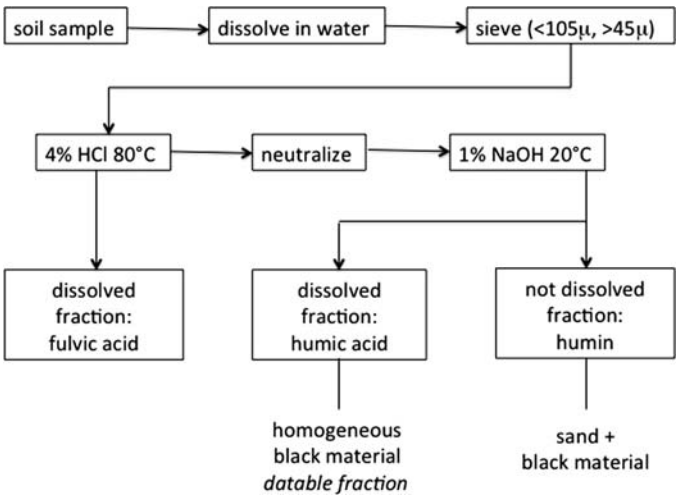

FIGURE 3.1.3 Scheme for pretreatment of soil samples for ^{14}C dating.

lakes generally contain less ^{14}C than the atmosphere. This causes apparent ages for organisms acquiring their carbon from these reservoirs: the so-called 'reservoir effect'.

For the marine reservoir, the size of this effect is 400 years. The activity of the ^{14}C standard can be taken as $^{14}a^0 = 100\%$, representing the activity of modern atmospheric material (Mook and van der Plicht, 1999). A difference of 400 years corresponds to 5% in activity, so that modern marine plants show a recent activity of 5% less than the standard (thus their $^{14}a^0 = 95\%$).

For non-marine aquatic reservoirs the size of the effect depends on the chemical/physical conditions. Obviously, for the purpose of ^{14}C dating, knowledge of the size of the reservoir effect is essential. For plant material that forms the constituent of soil organic matter, the stable isotope value $\delta^{13}C$ can be used to obtain information on the reservoir effect for ^{14}C.

For example, submerged plants show typical $\delta^{13}C$ values of about $-38‰$ in running water, and between -22 and $-15‰$ for stagnant water. These $\delta^{13}C$ values correspond to recent activities of $^{14}a^0 = 85\%$ and 100%, respectively. This in turn corresponds to reservoir effects of 1300 and 0 years, respectively (van der Plicht et al., 2001/2002; Olsson, 1983). The number 85% is generally valid for the Holocene but for the (Late) Glacial it can be much lower (Meadows, 2005).

3.1.8 Carbon isotopes in different types of deposits

We briefly summarize here various types of soil, with characteristic values for the carbon isotopes: $\delta^{13}C$ and $^{14}a^0$. This is based on laboratory experience based on many dating projects during the last six decades.

Gyttjas show typical $\delta^{13}C$ values of $-15‰$ (stagnant) and $-38‰$ (running); for $^{14}a^0$ this corresponds to 100% and 85%, respectively. The latter leads to a significant reservoir effect.

Lake sediments show typical $\delta^{13}C$ values between -22 and $15‰$ and $-38‰$. Because this concerns submerged aquatic plants, ^{14}C dates do show reservoir effects.

Soils show typical $\delta^{13}C$ values between $-26‰$ (from vegetation living under dry conditions) and $-30‰$ (from vegetation living under wet conditions). Sometimes inversion of ^{14}C dates is observed, depending on the amount of allochthonous carbon in the soil and the dry/wet conditions during soil formation, as well as on redeposition of organic material. Usually, there are no reservoir effects (no aquatic plant material is involved).

Note also that redeposition itself plays an important role in the aberrant ^{14}C dates obtained for (micro)podzols.

Vegetation horizons do not show reservoir effects or inversions of ^{14}C dates; some redeposition is possible. The $\delta^{13}C$ values are typically -25 to $-27‰$.

Coastal peat does not show significant reservoir effects or inversion of ^{14}C dates. The $\delta^{13}C$ values are typically between -26 and $-30‰$.

Peat bogs show hummocks ('horsten') or hollows ('slenken'), depending on dry or wet zones in the bog.

The driest conditions result in $\delta^{13}C$ values around $-28‰$. There are no reservoir effects.

The wettest conditions result in $\delta^{13}C$ values around $-19‰$. In this case, reservoir effects are possible by bacterial methanogenesis. Methane (CH_4) is very depleted in ^{13}C ($\delta^{13}C \approx -70‰$); the $\delta^{13}C$ of the resulting CO_2 can be as high as $\delta^{13}C = +10‰$. The $\delta^{13}C$ value of atmospheric CO_2 is about $-7‰$; mixing with $+10‰$ obviously results in higher $\delta^{13}C$ values after photosynthesis by the plants. This may cause reservoir effects or inversions.

In marine sediments (coastal) in coastal regions there is a mixture between marine and riverine influence. Marine plants have a $\delta^{13}C$ value of $-17‰$; the older river sediments have a $\delta^{13}C$ value of about $-28‰$. The mixed value is then $\delta^{13}C = -22‰$. The mixing ratio

also determines the magnitude of the reservoir effect.

In marine sediments (sea and ocean) there is no influence from rivers, so here only the marine reservoir effect of 400 years applies.

3.2 Radiocarbon dating of polycyclic soil sequences in Late Glacial and Holocene aeolian sand deposits (profile Weerterbergen, southeast Netherlands)

3.2.1 Introduction

The landscape of Weerterbergen between the cities of Weert and Budel (southeast Netherlands) is an example of an inland dune landscape in the Pleistocene coversand district. Coversand is chemically poor medium fine aeolian sand deposited in the Weichselian Late Glacial and dominates the surface geology of an extensive part of northwest Europe (Castel et al., 1989; van Mourik et al., 2012a,b).

During the Preboreal the area stabilized under a pioneer vegetation, consisting of herbal species, and the first phase of foil formation was an Umbrisol. After the Preboreal, warmer and moist climatic conditions promoted the development of forests and in the course of the Boreal and Atlantic, a deciduous forest covered the area and the soils evolved to umbric Podzols.

In prehistoric and early historical times, forest grazing, wood cutting and shifting cultivation gradually transformed the forest into heath. Subsequently, the use of the heath for the production of sheep manure during the period of plaggic agriculture (from the early Middle Ages to the introduction of chemical fertilizers around AD 1900), but especially commercial deforestations during the 11th–14th centuries, resulted in the local remobilization of coversands and led to major phases of sand drifting (Vera, 2011). Locally, the coversand landscape transformed into a driftsand landscape with characteristic new landforms and soils (van Mourik, 1988, 2012a,b).

Interesting soil archives in these cultural landscapes are polycyclic driftsand sequences, geoecological records of a succession of cycles of alternating unstable and stable phases in landscape development. As a representative example we present the results of profile Defensiedijk-1, one of the most complete soil archives of driftsand landscapes in the southeast Netherlands situated in the Weerterbergen (Fig. 3.2.1). The sequence consists of three complete geomorphological cycles. The profile is shown in Fig. 3.2.2.

Soil pollen analysis provides information as to whether such alternating periods of landscape stability and instability were caused by changing climatic conditions or by land use. But soil archives also need to have their chronology established by absolute dating. Traditionally, radiocarbon dating of soil organic matter extracted from buried humic (Ah) horizons was used to date individual cycles of the polycyclic sequence. However, this approach has two disadvantages.

First, extracted soil organic matter from buried humic horizons has a complicated composition in terms of chemical characteristics and ages (Goh and Molloy, 1978; Ellis and Matthews, 1984; Stevenson, 1985). This must be considered when interpreting the ^{14}C results.

Second, every geomorphological cycle reflects a period of landscape instability (sand drifting) and landscape stability (soil development). The ^{14}C ages of buried soil horizons identify aeolian deposition phases, but they do not separate within one cycle the time used for sand deposition and time available for soil formation.

The interpretation of the radiocarbon dates of the 'bulk' samples of the buried Ah horizons was problematic. Therefore we decided to resample the buried Ah and Bh horizons to perform fractionated dating to evaluate the reliability of radiocarbon dating of such soil archives (van Mourik et al., 1995).

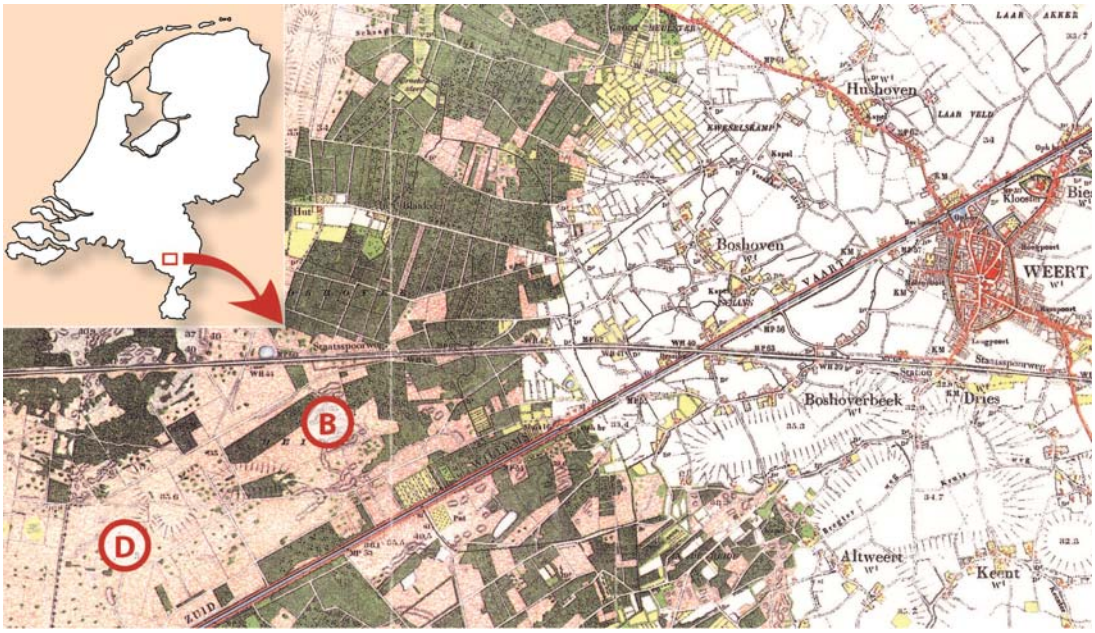

FIGURE 3.2.1 Part of the historical topographical map (scale 1:25.000) showing the location of the profiles Defensiedijk-1 (D) and Boshoverheide-1 (B). The map shows the landscape around the city of Weert in 1901 AD with the distribution of arable fields (*white*), heath and driftsand (*pink*) and the first reforestation with Scotch Pine (*green*). *After van Mourik, J.M., Seijmonsbergen, A.C., Jansen, B., 2012a. Geochronology of Soils and Landforms in Cultural Landscapes on Aeolian Sandy Substrates, Based on Radiocarbon and Optically Stimulated Luminescence Dating (Weert, SE-Netherlands). Intech Radiometric dating, 75–114; van Mourik, J.M., Seijmonsbergen, A.C., Slotboom, R.T., Wallinga, J., 2012b. The impact of human land use on soils and landforms in cultural landscapes on aeolian sandy substrates (Maashorst, SE Netherlands). Quaternary International 265, 74–89.*

The pollen diagram for Defensiedijk-1 (Fig. 3.2.3) shows a record of several cycles in landscape development. The technique of pollen extraction and determination is according to Moore et al. (1991). Based on the pollen density curve (log *D*) it is possible to recognize periods with sand deposition (with a synsedimentary pollen content) and periods with soil formation (with a post-sedimentary pollen content). The unstable phases with sand drifting and deposition are indicated with the code D (2D, 3D, 4D, 5D). Phase 1D concerns Late Weichselian coversand; this sediment is palynologically sterile and not registered in the pollen record. The stable phases with soil formation are indicated with the code S (1S, 2S, 3S, 4S).

The pollen spectra of cycle 1S show high percentages of deciduous trees, mainly *Corylus*, *Alnus* and *Quercus*; the percentages of Ericaceae are increasing. Pollen infiltration took place from the beginning of the Preboreal until burial around 3615 BP. Consequently, the older pollen spectra do not show a record of the vegetation development from 9000 to 3600 BP, because the older pollen content is continuously erased by younger pollen. But pollen spectra with high percentages of *Corylus* and *Quercus* and upcoming heath are indicative for the Bronze Age and early Iron Age, which is consistent with the radiocarbon age of the HAC fraction of the 4Ah horizon (3615 BP). At that time, soil formation in coversand reached the stage of carbic Podzol.

FIGURE 3.2.2 Picture of profile Defensiedijk-1, sampled in 1984.

Cycle 2 starts with deposition of the pre-Medieval driftsand (D2). The pollen densities are low; the pollen content is syn-sedimentary. There is a slight increase of Poaceae, indicating some degradation of heath in the surroundings. Zone 2S shows the vertical distribution, indicative for pollen infiltration during the formation of the carbic Podzol. The spectra are dominated by Ericaceae. The ^{14}C date of the humic acids fraction of the 3Ah (1365 BP) is pre-Medieval.

Cycle 3 starts with the deposition of Medieval driftsand (D3). The sedimentary pollen concentrations of the driftsand layers indicate a relatively low sedimentation rate. The pollen spectra are still dominated by Ericaceae, but Poaceae are rising, pointing to increasing degradation of the heath. During the next stable period (3S), an initial Podzol (micro-Podzol) developed. The 2A horizon of the micro-Podzol shows pollen spectra with increasing percentages of *Pinus*. Reforestation with pine trees to stabilize driftsand landscapes started in the Netherlands after AD 1550. This is consistent with the ^{14}C date of the humic acid fraction (410 BP) of the 2Ah horizon.

Cycle 4 starts with the sedimentation of the post-Medieval driftsand (D4). Since 1995 the area stabilized under a vegetation of grasses and lichens. This stable period is too short for soil formation and is in the initial phase of a Rhizomull humus form.

Based on radiocarbon dates of humic acid fractions of buried Ah horizons we can make a distinction in three periods characterized by instability and sand drifting: pre-Medieval, Medieval and post-Medieval. In the next paragraph we explain why dates of the humic acids fractions instead of the bulk samples are used.

Based on the pollen diagram we can conclude that there are no palynological indications that climatic change was responsible for unstable periods with sand drifting. Human influence, forest degradation and heath management seem to be the dominant factors.

3.2.2 Fractionated radiocarbon dating of profile Defensiedijk-1

The results of the radiocarbon dating of bulk samples of the three buried Ah horizons collected in 1984 were not reliable for establishing the chronology of the cycles. Especially, the dating of the 2H2 horizon was 'too old'. Therefore we resampled the profile in 1986 for fractionated radiocarbon dating. The results are shown in Table 3.2.1.

Some micrographs (terminology based on Brewer, 1976) are shown to illustrate complications in the composition of organic matter in soils (Figs. 3.2.4–3.2.9).

For each sample (with the exception of the bulk samples), three chemical fractions were

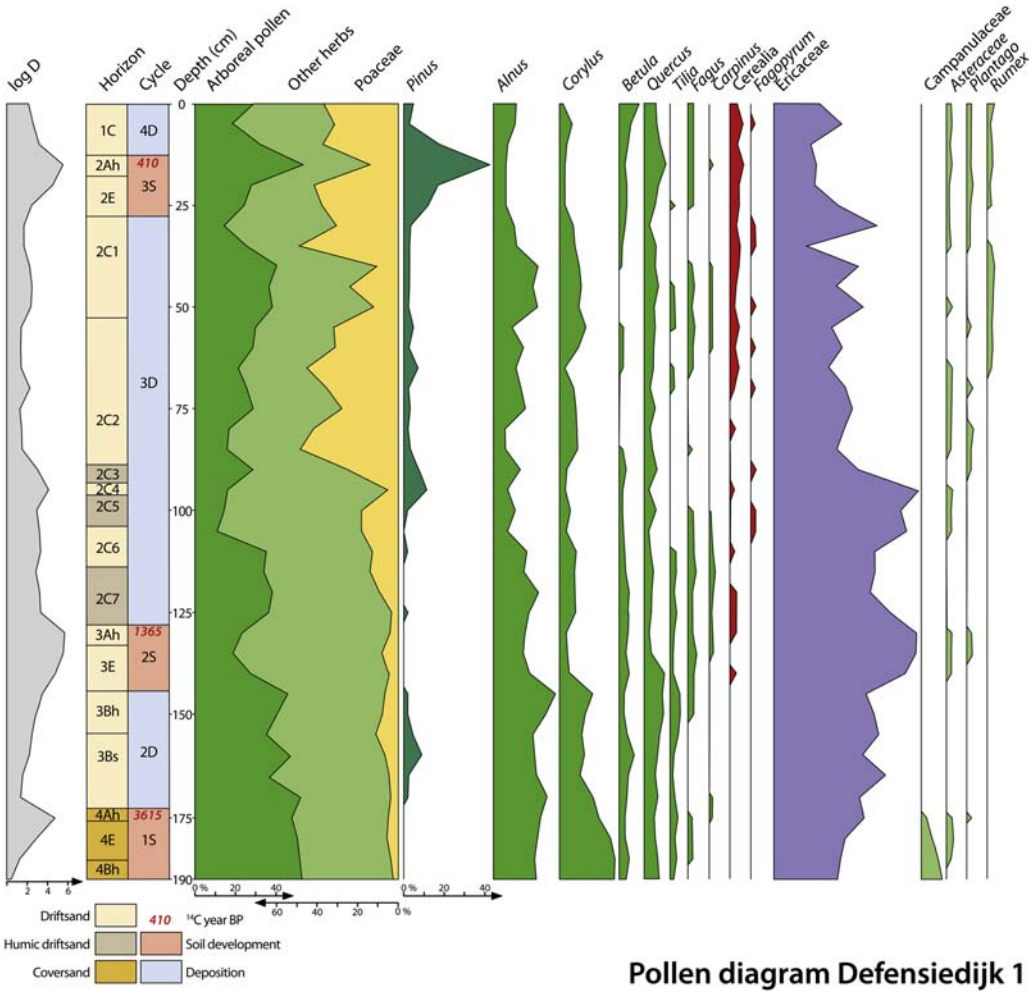

FIGURE 3.2.3 Pollen diagram Defensiedijk-1. The ^{14}C dates are based on the humic acid fraction of the buried Ah horizons. *After van Mourik, J.M., Seijmonsbergen, A.C., Jansen, B., 2012a. Geochronology of Soils and Landforms in Cultural Landscapes on Aeolian Sandy Substrates, Based on Radiocarbon and Optically Stimulated Luminescence Dating (Weert, SE-Netherlands). Intech Radiometric dating, 75–114; van Mourik, J.M., Seijmonsbergen, A.C., Slotboom, R.T., Wallinga, J., 2012b. The impact of human land use on soils and landforms in cultural landscapes on aeolian sandy substrates (Maashorst, SE Netherlands). Quaternary International 265, 74–89.*

prepared and dated: fulvic acids, humic fraction and residue. For all fractions, the amount of sample (in grams) is shown, as well as the amount of carbon extracted. The C_v is determined as (amount of C)/(amount of sample minus amount of ash) * 100%. The Cpr is the relative amount of carbon after pretreatment; the C_v is the relative amount of the organic fraction (Mook and Streurman, 1983). For each fraction, the ^{14}C age is measured and shown in BP with its 1-sigma measurement uncertainty, as well as the $\delta^{13}C$ value.

TABLE 3.2.1 List of radiocarbon dates and sample compositions of profile Defensiedijk-1.

Lab code	Horizon	Depth (cm)	Fraction	Sample (g)	C (g)	Cpr (%)	Cv (%)	^{14}C age (BP)	Sigma	δ^{13}C (‰)
GrN-12804	2Ah	025–027	Bulk	55.0	1.03	38	53	1130	60	−27.68
GrN-14833			Humin	96.2	0.67	<1	50	3230	110	−27.98
GrN-14458			Humic	3.00	1.43	48	53	410	45	−27.00
GrN-14759			Fulvic	0.95	0.33	35	50	110	110	−26.84
GrN-12805	3Ah	127–129	Bulk	206.0	7.35	29	54	1075	30	−27.78
GrN-14837			Humin	95.8	1.57	2	33	1350	45	−27.19
GrN-14459			Humic	14.5	7.41	51	56	1365	25	−27.31
GrN-14760			Fulvic	1.20	0.43	36	44	850	100	−26.36
GrN-14838	3Ah	129–131	Humin	120.0	0.53	<1	26	1900	110	−28.87
GrN-14694			Humic	8.50	3.43	40	44	1675	30	−27.33
GrN-14774			Fulvic	0.73	0.23	32	41	1200	130	−26.03
GrN-14695	3B2h	147–148	Humin	18.5	9.00	49	54	1820	25	−29.84
GrN-14765			Fulvic	1.29	0.48	37	40	1160	90	−27.45
GrN-14696	3B2h	149–150	Humic	17.0	6.71	39	44	1670	25	−28.70
GrN-14772			Fulvic	1.85	0.65	35	42	1160	70	−27.22
GrN-14843	3B2h	147–150	Humin	256.0	1.00	<1	18	1445	60	−28.62
GrN-14841	3B2h	151–152	Humin	133.5	0.36	<1	14	1900	140	−26.43
GrN-14697			Humic	7.50	3.58	48	54	1700	30	−28.34
GrN-14770			Fulvic	2.35	0.98	42	52	1480	60	−27.50
GrN-12806	4Ah	173–174	Bulk	269	2.71	16	53	3920	40	−29.72
GrN-14836			Humin	133.3	0.75	<1	36	4110	90	−26.27
GrN-14460			Humic	7.30	3.15	48	63	3615	35	−28.02
GrN-14761			Fulvic	1.20	0.25	21	30	2200	170	−27.60
GrN-14840	4Ah	175–176	Humin	137.9	0.50	<1	26	4430	160	−27.94
GrN-14698			Humic	5.20	1.96	38	44	3965	40	−28.34
GrN-14775			Fulvic	1.18	0.36	30	36	3010	140	−27.11
GrN-14699	4B2h	185–186	Humic	9.90	3.18	32	37	3985	35	−27.32
GrN-14768			Fulvic	1.74	0.48	28	40	2900	100	−26.96
GrN-14700	4B2h	187–188	Humic	11.5	3.85	33	38	3730	35	−28.04
GrN-14767			Fulvic	1.91	0.44	23	32	2890	110	−26,58

(*Continued*)

TABLE 3.2.1 List of radiocarbon dates and sample compositions of profile Defensiedijk-1.—cont'd

Lab code	Horizon	Depth (cm)	Fraction	Sample (g)	C (g)	Cpr (%)	Cv (%)	^{14}C age (BP)	Sigma	δ^{13}C (‰)
GrN-14701	4B2h	189–190	Humic	10.7	4.00	37	44	3700	50	−26.10
GrN-14766			Fulvic	2.37	0.96	40	40	2830	110	−27.01
GrN-14849	4B2h	185–190	Humin	395.0	0.80	<1	14	3550	80	−27.59

Cpr, relative amount of carbon after pretreatment; *Cv*, (amount of C)/(amount of sample minus amount of ash) * 100%.

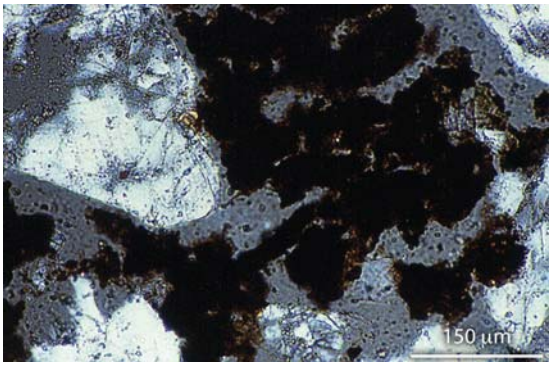

FIGURE 3.2.4 Micrograph of intertextic distributed organic aggregates (3Ah horizon).

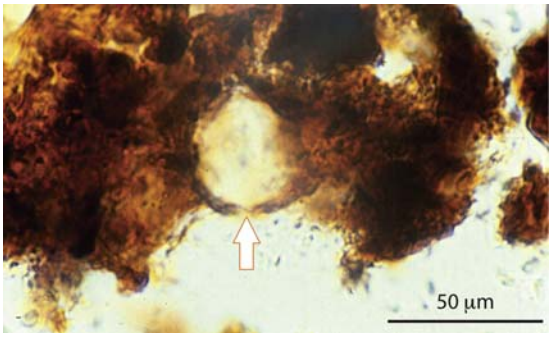

FIGURE 3.2.5 Micrograph of the internal fabric of an intertextic aggregate (in the centre is an embedded pollen grain).

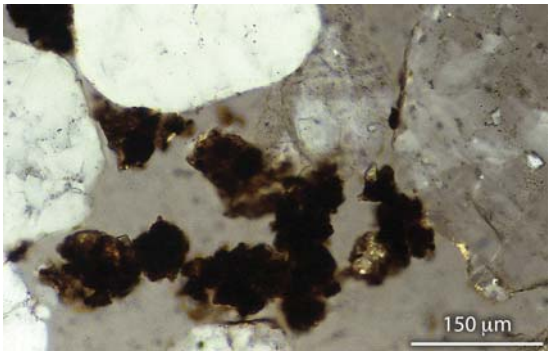

FIGURE 3.2.6 Micrograph of a root hole with (down-moving) organic aggregates in the 3E horizon.

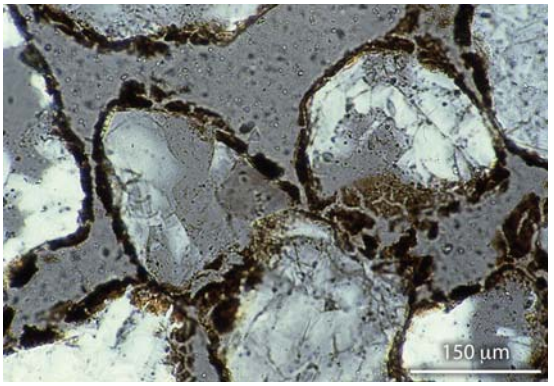

FIGURE 3.2.7 Micrograph of organic cutans in the 3Bh horizon.

As explained earlier, fulvic acids represent the mobile fraction, humic acid is considered to be the datable fraction and the humin fraction contains the older material. When the dates of humic acid and the humin fraction are the same within mutual uncertainty, the ^{14}C date can be considered reliable. An example is sample 3Ah (127–129 cm depth).

As can be seen from Table 3.2.1, fulvic acids are much younger than the other fractions. This

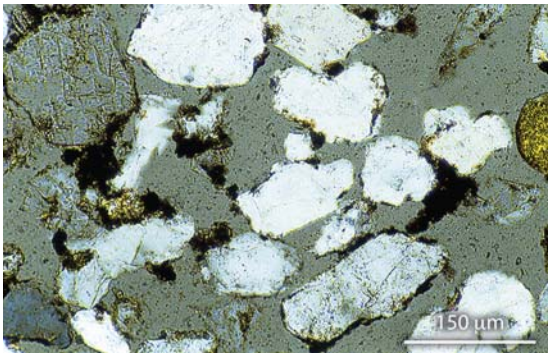

FIGURE 3.2.8 Micrograph of organic particles (including charcoal) in the 2C horizon.

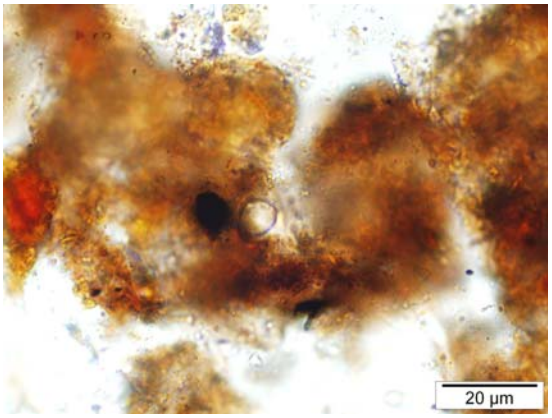

FIGURE 3.2.9 Micrograph of the internal fabric of welded aggregates (including pollen and charcoal) in the 2A horizon.

shows that this fraction is not the correct ^{14}C datable material. The humic fraction shows a more or less reliable stratigraphy for this soil sequence. Radiocarbon dates of other polycyclic profiles with similar results have been published in van Mourik et al. (2012a,b).

The general conclusion is that the humic acid fractions are the best datable fractions for ^{14}C, as expected. The stratigraphic order is correct. There is no significant inversion. Only GrN-14695 shows a very negative $\delta^{13}C$ value. This can be an indication of wetter conditions at the time of soil formation, resulting in a change in type of vegetation.

3.2.3 Radiocarbon dating of Boshoverheide

A second polycyclic profile Boshoverheide-1 was sampled in a small plateau dune, 1750 m northeast of profile Defensiedijk-1 (Figs. 3.2.10 and 3.2.11). The pollen diagram is shown in Fig. 3.2.12, and the dates in Table 3.2.2.

In this profile the cycle of deposition and podzolation in pre-Medieval driftsand is missing. Pre-Medieval drift deposits are very local small-scale features and the result of natural events such as storms and forest fires, and cultural degradation by shifting cultivation (van Mourik, 1988). Other cycles related to regional Medieval and post-Medieval sand drifting are recorded. The pollen zoning of Boshoverheide-1 (Fig. 3.2.12) and the series of radiocarbon dates show similar trends to profile Defensiedijk-1 (Table 3.2.1).

The palynological age (dominance of *Alnus* instead of *Corylus*) and the ^{14}C dates of the buried Podzol, developed in coversand, point to a Middle Subatlantic age. This means that the development of the carbic Podzol of the

FIGURE 3.2.10 Small plateau dune on the Boshoverheide.

FIGURE 3.2.11 Profile Boshoverheide-1.

oldest cycle (1S) was continuous from the deposition of coversand (Late Glacial/Preboreal) until about AD 1200.

The burial of the Palaeopodzol by Medieval driftsand took place after AD 1200. This is still consistent with the period of forest clearing as reported by Vera (2011).

Cycle 2S in profile Boshoverheide-1 was included in a study of initial Podzols in the Weerterbergen to answer the question whether these initial Podzols (Mormoders) were indicative for a regional or only a local phase of landscape stability by applying both ^{14}C and optically stimulated luminescence (OSL) dating (Wallinga et al., 2013). The sampling strategy is shown in Fig. 3.2.13; the OSL dates from the top of 2C and the bottom of 1C are presented in Table 3.2.2.

The time available for the development of the initial Podzol (2S), representing the stable phase with soil formation between the depositions of D2 and D3, was less than 150 years (based on OSL dates). The radiocarbon ages of the carbon fractions extracted from the 2AE appear too old. The OSL age of the base of the C horizon (driftsand and phase D3) fits with the second regional extension of sand drifting related to the overexploitation of the heaths during the 18th century.

Parts of the soil organic matter of Holocene driftsand deposits (the parent material for soil development) are eroded and transported (older) organic particles of former vegetation layers, grains with organic cutans originating from Podzols eroded elsewhere and charcoal fragments affecting the results of the ^{14}C dating (Figs. 3.2.14 and 3.2.15).

Since the Late Neolithic, people occupied the landscape and caused degradation of vegetation and soil. The oldest relics in the Weerterbergen are small-scale sand drifts, related to shifting cultivation as recorded in the Defensiedijk profiles. A second group of relics are barrows from the Bronze Age and Iron Age. More degradation and extensive sand drifts were caused by deforestations in the 11th–13th centuries and the overexploitation of the heaths in the 18th century.

The Boshoverheide is nowadays an archaeological reserve containing several restored barrows. Fig. 3.2.16 shows a barrow close to the investigated profile of Boshoverheide-1. The profile is shown in Fig. 3.2.17. The ^{14}C dating of a bulk sample of the buried Ah horizon (GrN-13515, 2400 $\pm$ 60 BP) and the palynological age of the 2Ah Podzol buried by the barrow fit with 1S of Boshoverheide-1 (van Mourik, 1988). The ^{14}C dates of the 2Ah horizons below five other barrows range from 2460 to 2610 BP (Groenman-van Waateringe, 1988). Consequently, the pre-Medieval driftsands of Defensiedijk-1, the Medieval sand dune of Boshoverheide-1 and the barrows on

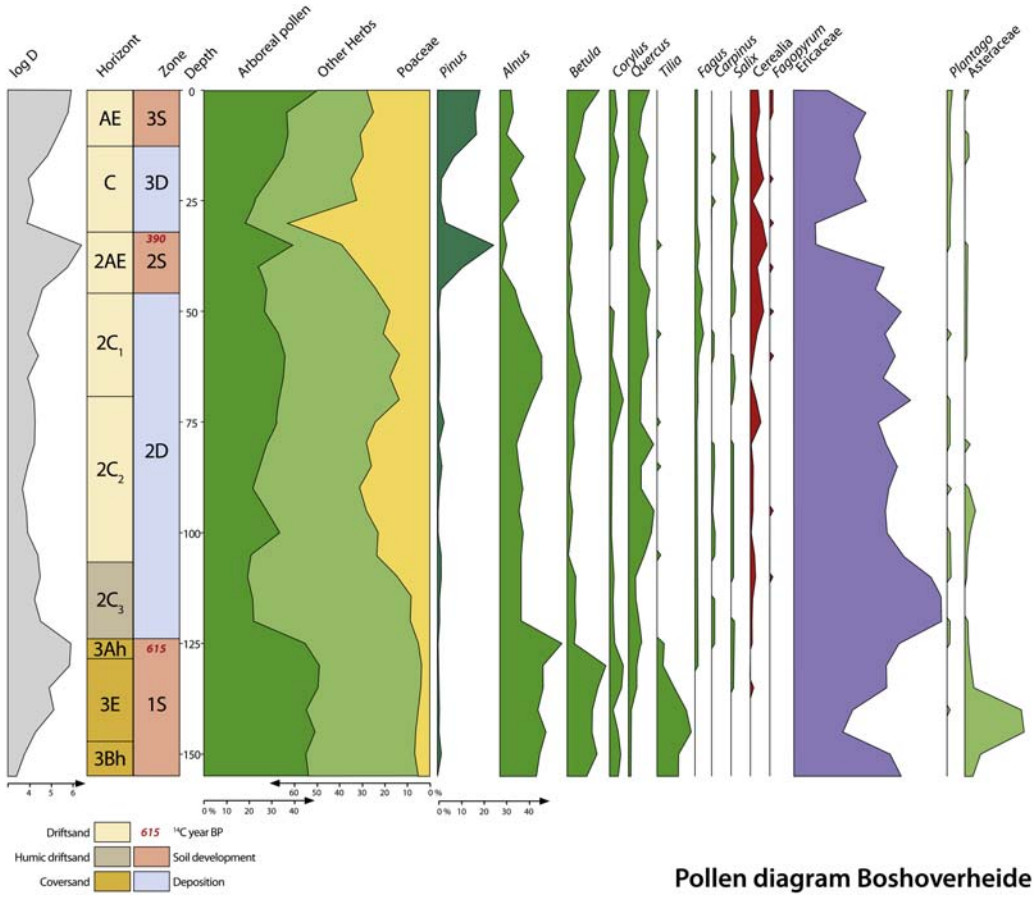

FIGURE 3.2.12 Pollen diagram Boshoverheide-1.

the Boshoverheide came into existence on the same surface, a podzolic soil, developed in coversand. Podzolation could continue until burial by pre-Medieval driftsand covers, barrows, Medieval and post-Medieval driftsand covers and land dunes. The accuracy of the dating methods determines the details of our knowledge of the geochronology of these relics.

The next step in the study of the geochronology of sequences of aeolian sand deposits was the application of luminescence dating of mineral grains (Chapter 4). In 1989 the Aberystwyth Luminescence Research Laboratory was founded and a promising technique (thermoluminescence (TL) dating) became available for the dating of sandy deposits. As a pilot, the sand deposits of the cycles of profile Defensiedijk-1 were resampled for TL application.

Every geomorphological cycle started with an unstable period with sand deposition, followed by a stable period with soil formation. The research question was whether we could determine the duration of the unstable periods and the remaining time for soil

TABLE 3.2.2 ^{14}C and OSL dating of profile Boshoverheide-1.

Number	Horizon	Depth (cm)	Fraction	^{14}C age (BP)	Calibrated ^{14}C age (AD)	$\delta^{13}C$ (‰)	OSL age (AD)
NCL 5106010	1C	027–032	Quartz				1957 ± 3
GrN-12869	2AE	033–035	Bulk	265 ± 30	1539 ± 58		
GrN-14834	2AE		Humin	1710 ± 35	321 ± 53	−26.87	
GrN-14461	2AE		Humic acids	390 ± 25	1521 ± 67	−26.90	
GrN-14762	2AE		Fulvic acids	240 ± 80	1694 ± 125	−26.77	
NCL 5106011	2C	035–040	Quartz				1810 ± 9
GrN-12870	3A	125–127	Bulk	1190 ± 30	829 ± 42	–	
GrN-14835	3A		Humin	830 ± 60	1172 ± 70	−28.49	
GrN-14462	3A		Humic acids	615 + 45	1344 ± 40	−28.04	
GrN-14763	3A		Fulvic acids	490 ± 70	1410 ± 68	−27.30	
GrN-14839	3A	127–129	Humin	1460 ± 90	556 ± 85	−26.59	
GrN-14702	3A		Humic acids	840 ± 45	1182 ± 52	−27.68	
GrN-14773	3A		Fulvic acids	835 ± 55	1172 ± 67	−27.62	
GrN-14703	3Bh	148–149	Humic acids	1100 + 45	935 ± 44	−28.62	
GrN-14771	3Bh		Fulvic acids	910 + 70	1118 ± 71	−27.03	
GrN-14704	3Bh	150–153	Humic acids	1230 ± 70	790 ± 82	−26.88	
GrN-14769	3Bh		Fulvic acids	1020 + 60	1026 ± 76	−26.83	
GrN-14705	3Bh	152–190	Humic acids	1115 + 35	908 ± 37	−28.12	
GrN-14764	3Bh		Fulvic acids	1058 + 45	960 ± 47	26.90	
GrN-14845	3Bh	148–153	Humin	1235 ± 85	792 ± 91	−27.61	

formation, which was not possible using radiocarbon dating alone. It was worthwhile approaching this question with TL dating. The TL dates were published by Dijkmans et al. (1992).

The results are presented in Table 3.2.3. In 1993 the luminescence dating laboratory of the University of Ghent was established, and in 2002 profile Defensiedijk-2 was resampled, now for a pilot of the application of OSL dating of coversand and driftsand (van Mourik et al., 2010).

Table 3.2.3 shows the results of the TL and OSL dating of deposits and the ^{14}C dates of the humic acids of the buried Ah horizons. The ^{14}C dates are also calibrated; the results are shown at the 1-sigma confidence level. The TL and OSL dates of 1C, 2C and 4C correspond reasonably well with each other, but the TL ages of 3E are significantly younger than the OSL age. Also, the duration of the phases with soil formation between the phases with sand depositions are not really similar. Especially, the ^{14}C date of 4Ah is too old compared to the OSL date.

FIGURE 3.2.13 Photograph of the initial Podzol (2AE) in profile Boshoverheide-1 with the sample locations for optically stimulated luminescence dating (*yellow rings*), micromorphology and ^{14}C dating (*grey box*).

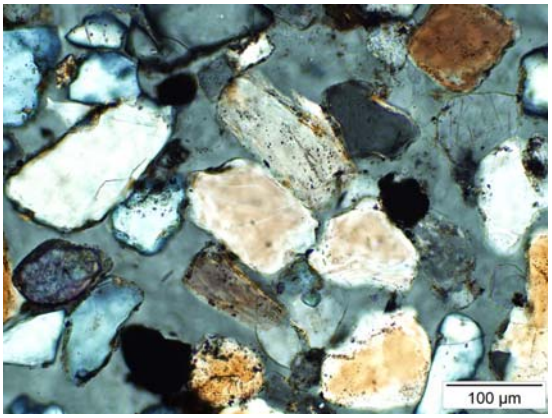

FIGURE 3.2.14 Micrograph of the 2AE horizon (Boshoverheide-1) showing charcoal and organic cutans, originating from elsewhere-eroded Podzols.

The interpretation of dates requires detailed knowledge of processes during active soil formation or sand deposition, but also of the processes after the burial of soils.

Fig. 3.2.18 shows bioturbation (by soil animals or in root holes) that can pollute mineral samples with grains with a younger (downward transport) or older (upward transport) signal. Decomposing roots cause rejuvenation of soil organic matter.

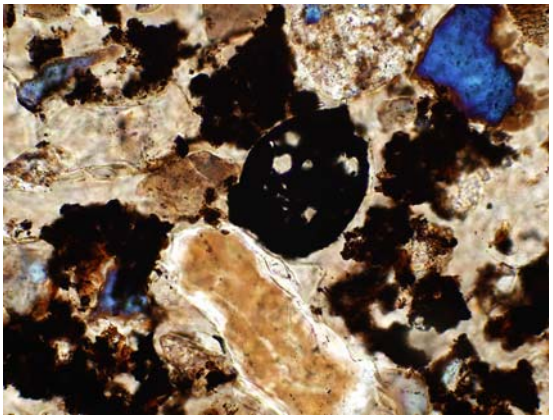

FIGURE 3.2.15 Micrograph of the 2AE horizon (Boshoverheide-1) with (rounded) organic aggregates and charcoal particles.

FIGURE 3.2.16 View of the examined barrow on the Boshoverheide.

FIGURE 3.2.17 Soil profile of the barrow and the buried palaeosol.

TABLE 3.2.3 TL, OSL and ^{14}C dating of the polycyclic sequence Defensiedijk-1.

	(Aberystwyth)	(Gent)	(Groningen)	
Sample	TL age (ka) (feldspar fraction)	OSL age (ka) (quartz fraction)	^{14}C age BP (humic acid fraction)	Calibrated ^{14}C age (calBP)
1C top		0.08 ± 0.01		
1C middle		0.10 ± 0.01		
1C bottom	0.2 ± 0.1	0.09 ± 0.01		
2AE			410 ± 45	335–515
2C top	0.8 ± 0.2	0.59 ± 0.05		
2C middle	0.4 ± 0.2	0.67 ± 0.06		
2C bottom		1.3 ± 0.1		
3Ah			1675 ± 30	1545–1610
3 EC top	3.1 ± 0.3	5.8 ± 0.5		
3 EC bottom	3.1 ± 0.3	4.7 ± 0.4		
4Ah			3615 ± 35	3880–3975
4C top	7.7 ± 0.6	9.2 ± 0.8		
4C (bottom)	9.6 ± 0.8			

FIGURE 3.2.18 Detail of the deepest buried Podzol of profile Defensiedijk-1, showing evidence of (palaeo)bioturbation through the 3Ah horizon (profile 1984).

3.3 Absolute and relative dating of the Gasserplatz soil archives (Vorarlberg, Austria) and the reservoir effect

3.3.1 Introduction

The Late Glacial is a period of rapid climate change that marks the transition from the last Glacial to the Holocene. It can be subdivided into stadial and interstadial phases, which were clearly recognized in the Greenland ice core records (Johnsen et al., 2001). These changes in climate are also recognized in pollen diagrams of Late Glacial deposits on the Gasserplatz (Austria, Vorarlberg).

Gasserplatz is a shallow basin in the rather flat confluence area of the former glaciers of the rivers Rhine and Ill (Simons, 1985;

de Graaff et al., 1989). This area became ice free during the Feldkirch stadium (around 15,500 calBP) and developed as a tiny ice-marginal lake in a sheltered position at an elevation of 559 m above sea level. During the Late Glacial, lacustrine carbonate (calcareous gyttja) with some interbedded initial Histosols was deposited in the accumulated Holocene peat. To deduce information about Late Glacial environmental oscillations, pollen analysis, radiocarbon dating and isotope analyses have been applied to the Late Glacial lacustrine carbonates.

The Gasserplatz sampling site is indicated on the geomorphological map of the area (Fig. 3.3.1). The first sediment core was taken in 1989 with a Dachnowsky sampler from the surface down to 510 cm. Samples from depths of 300–465 cm (vertical sampling distance 2 cm) have been used for pollen and isotope analysis and radiocarbon dating (Gasserplatz-1).

The second core was taken in 2002 very close to the first site using a mechanical auger from the surface down to a depth of 590 cm (Fig. 3.3.2). Samples from depths of 330–530 cm (vertical sampling distance 2 cm) have been used for extractions for (absolute) pollen and isotope analysis (Gasserplatz-2). Also, thin sections have been produced to observe the presence of Laacher See Tephra (LST) (Riede, 2008) and to assess the quality of the limnic carbonates and the initial Histosols (Figs. 3.3.3–3.3.8).

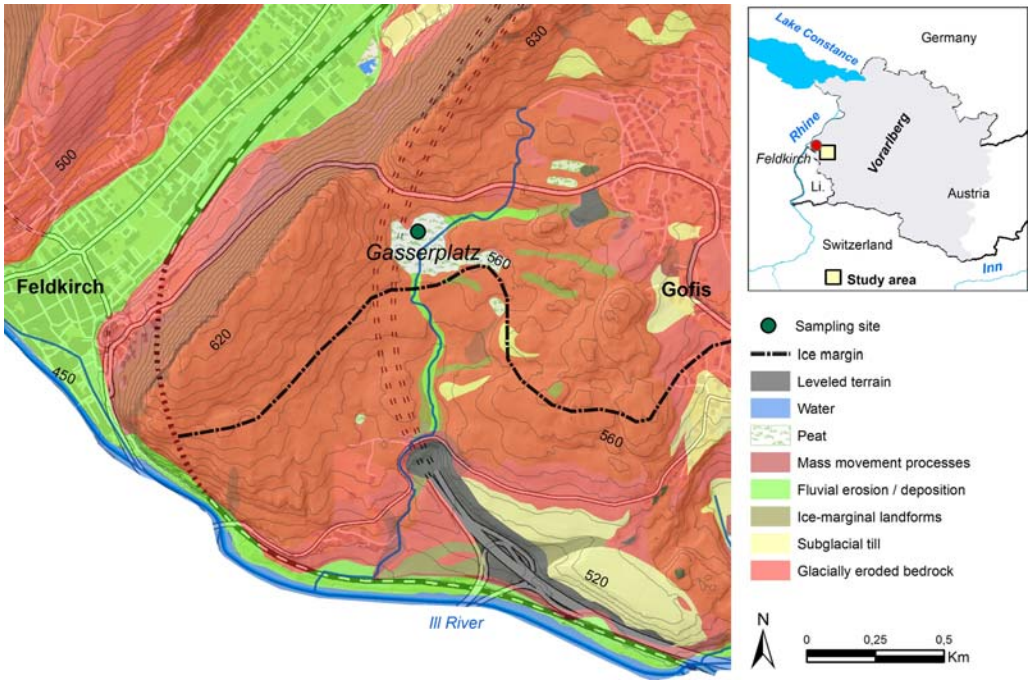

FIGURE 3.3.1 Geomorphological map of the Gasserplatz with the location of the sample site. *After van Mourik, J.M., Slotboom, R.T., van der Plicht, J., Streurman, H.J., Kuijper, W.J., Hoek, W.Z., de Graaff, L.W.S., 2013. Geochronology of Betula extensions in pollen diagrams of Alpine Late-glacial lake deposits: a case study of the Late-glacial deposits of the Gasserplatz soil archives (Vorarlberg, Austria). Quaternary International 306, 3–13.*

FIGURE 3.3.2 Picture of the Gasserplatz with the mechanical auger (March 2002).

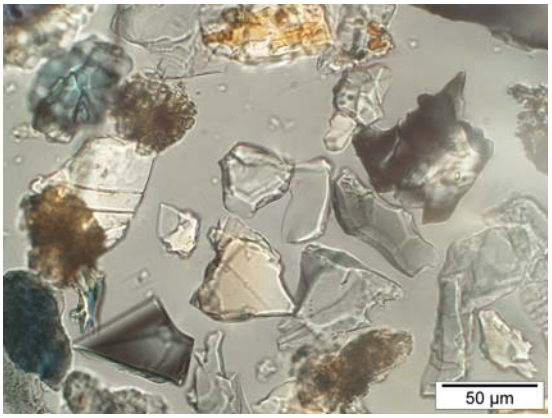

FIGURE 3.3.3 Gasserplatz-2, 383 cm; micrograph of extracted tephra shards.

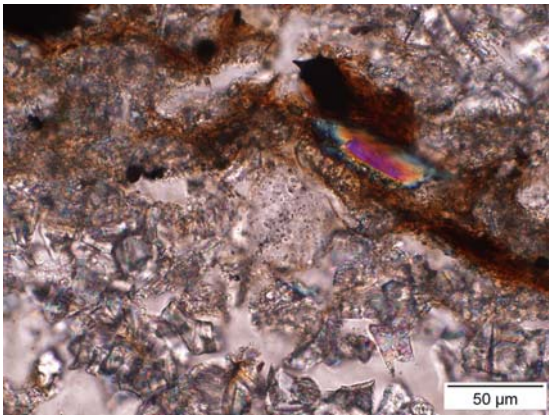

FIGURE 3.3.4 Gasserplatz-2, 383 cm; micrograph of tephra shards in a thin section (*arrow*), deposited in a winter lamella.

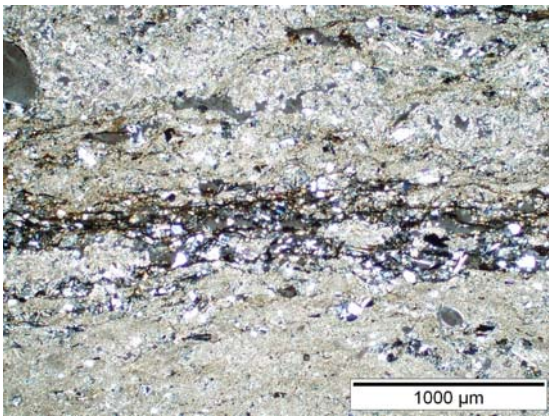

FIGURE 3.3.5 Gasserplatz-2, 505 cm; laminated calcareous gyttja used for ^{14}C dating; light-coloured lamella are winter deposits, rich in organic matter summer deposits. The $\delta^{13}C$ value of the carbonate is $-3.1‰$.

In the Oldest Dryas, lake sedimentation started with clay (glacier milk), followed by the cyclic deposition of calcareous clay and humic calcareous gyttja. The sediment core Gasserplatz-2, sampled with a mechanical auger,

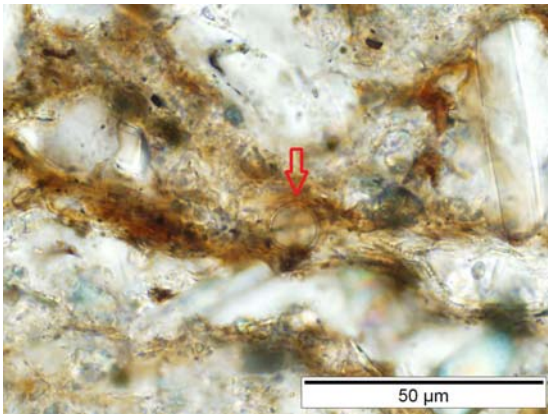

FIGURE 3.3.6 Gasserplatz-2, 505 cm; detail of a humic summer lamella with pollen grain (*arrow*). The $\delta^{13}C$ of the organic fraction is −38.00‰, indicative of biomass produced by aquatic plants.

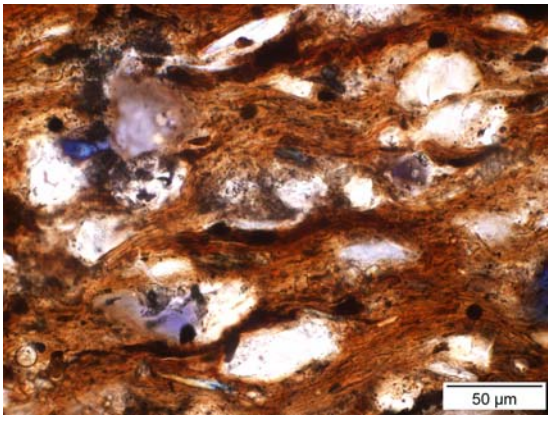

FIGURE 3.3.7 Gasserplatz-2, 386 cm; micrograph of the matrix of the initial Histosols used for ^{14}C dating. The $\delta^{13}C$ value of the peat is −32.4‰, indicative of a mixture of biomass produced by subaqueous and subaerial plants.

allowed the accurate distinguishing of various initial Histosols, a lithological reflection of short-lived periods with relatively low water levels. During the Holocene the lake transferred into a peat bog (Figs. 3.3.9 and 3.3.10).

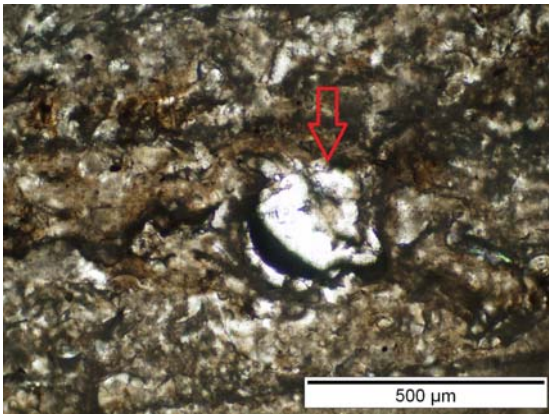

FIGURE 3.3.8 Gasserplatz-2, 468 cm; micrograph of a mollusc in laminated calcareous gyttja used for ^{14}C dating (*arrow*). The $\delta^{13}C$ of a mollusc is around −8.5‰.

3.3.2 Pollen analysis

In the pollen diagrams of Gasserplatz-1 and -2 (previously published in van Mourik et al., 2013), several chronozones can be recognized. They are well expressed in the pollen and isotope stratigraphy and are described next.

Zone I-a, Oldest Dryas. The sedimentation of white laminated calcareous gyttja on sterile blue−grey clay started during the Oldest Dryas. The pollen concentrations of the white gyttja are very low (<200 grains/mL). In the relative pollen diagrams, the Oldest Dryas is dominated by non-arboreal pollen (mainly *Artemisia*, Cyperaceae, *Helianthemum*, Poaceae). The low pollen concentrations indicate that pollen precipitation was mainly the result of long-distance transport. Biomass production in and around the Gasserplatz lake was very low, considering the relatively high $\delta^{13}C$ values.

Zone I-b, Bølling. In the $\delta^{18}O$ curves this interstadial is clearly recognized as a relatively warm period. The deposition of white gyttja with low pollen concentrations continued until a depth of 485 cm. The relative pollen diagrams show a first increase of *Betula* after the

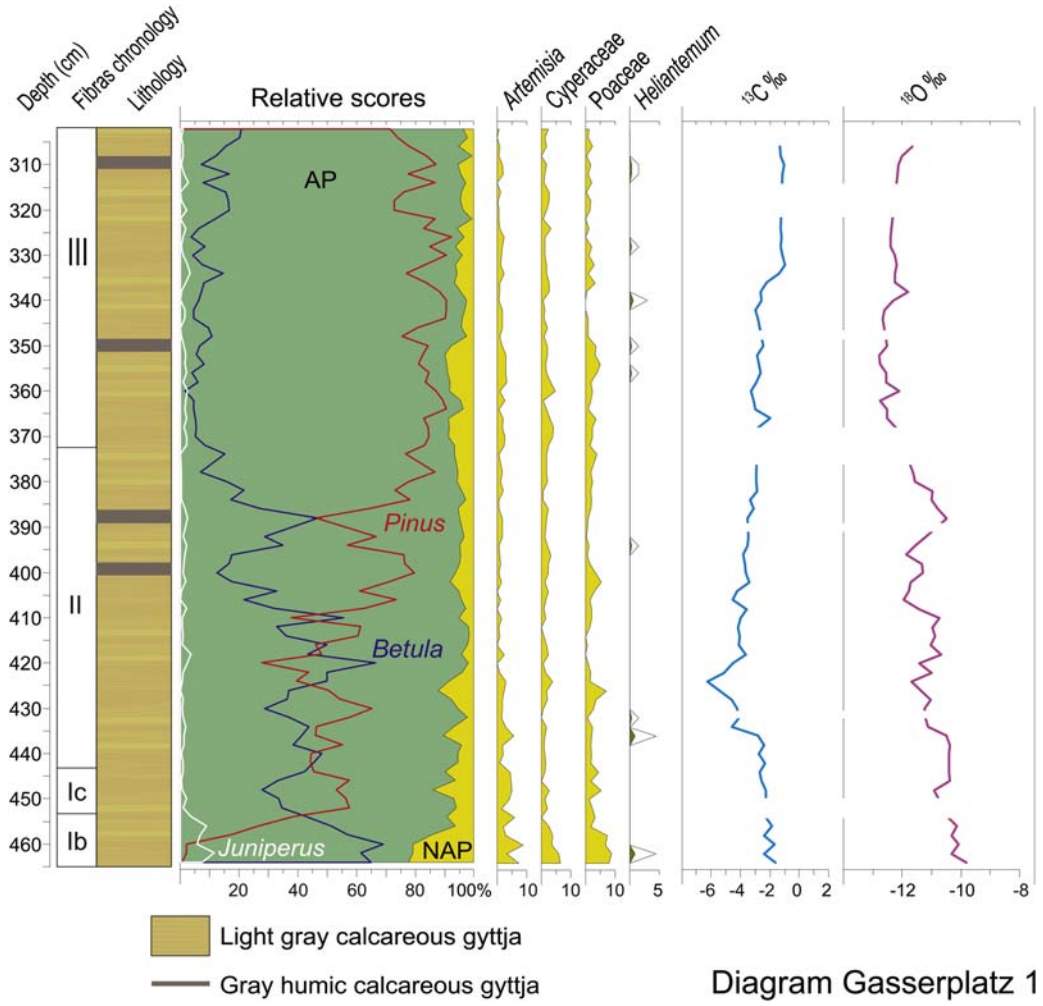

FIGURE 3.3.9 Pollen and isotope diagram Gasserplatz-1, sampled in 1989. *After van Mourik, J.M., Slotboom, R.T., van der Plicht, J., Streurman, H.J., Kuijper, W.J., Hoek, W.Z., de Graaff, L.W.S., 2013. Geochronology of Betula extensions in pollen diagrams of Alpine Late-glacial lake deposits: a case study of the Late-glacial deposits of the Gasserplatz soil archives (Vorarlberg, Austria). Quaternary International 306, 3–13.*

beginning of the Bølling, followed by an expansion of *Juniperus*. The pollen concentration curve of *Betula* provides additional information. Together with the start of deposition of light grey humic gyttja and decreasing $\delta^{13}C$ values from 485 cm, the pollen concentrations increase drastically. This means that the first *Juniperus* arrived in the Gasserplatz area, followed by *Betula* and later by *Pinus*, and started to contribute to local pollen production and dispersion. Consequently, the oldest peak in the relative pollen diagrams must be considered a reflection of a *Betula* expansion on distance; evidently it took time after the deglaciation before *Juniperus*, followed by *Betula* and *Pinus*, first arrived at the Gasserplatz site.

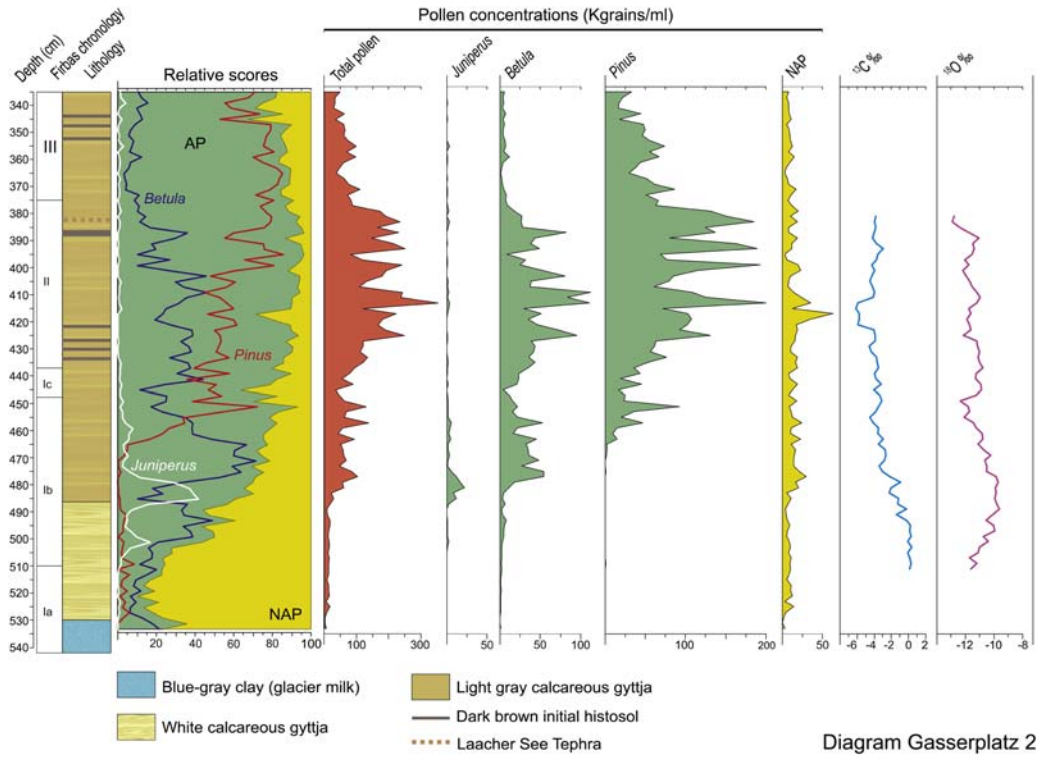

FIGURE 3.3.10 Pollen and isotope diagram Gasserplatz-2, sampled in 2002. *After van Mourik, J.M., Slotboom, R.T., van der Plicht, J., Streurman, H.J., Kuijper, W.J., Hoek, W.Z., de Graaff, L.W.S., 2013. Geochronology of Betula extensions in pollen diagrams of Alpine Late-glacial lake deposits: a case study of the Late-glacial deposits of the Gasserplatz soil archives (Vorarlberg, Austria). Quaternary International 306, 3–13.*

Zone I-c, Older Dryas. This zone is reflected in the diagrams by a decrease in *Betula* and $\delta^{18}O$ as well as an expansion of non-arboreal pollen.

Zone II, Allerød. During the Allerød we can distinguish three oscillations in the *Betula* and $\delta^{18}O$ curves, reflecting three periods with expansion and retreat of *Betula*, likely in reaction to a change in temperature. During these oscillations we observe also a response in the lithology: the deposition of calcareous gyttja is interrupted by the formation of initial Histosols. The characterization of such initial soils was based on a $\delta^{13}C$ value of around −32‰ (Table 3.3.1), suggesting a combination of subaqueous and subaerial conditions.

Zone III, Allerød. During the Allerød, three oscillations in the *Betula* and $\delta^{18}O$ curves are observed, reflecting three periods with expansion and retreat of *Betula*, likely in reaction to a change in temperature. During these oscillations we observe also a response in the lithology: the deposition of calcareous gyttja is interrupted by the formation of initial Histosols. The characterization of such initial soils was based on a $\delta^{13}C$ value of around −32‰ (Table 3.3.1), pointing to a combination of subaqueous and subaerial conditions.

Zone IV, Younger Dryas. During the Younger Dryas, we can distinguish two phases with a short-lived increase in temperature, separating three colder periods, as recorded in the $\delta^{18}O$

TABLE 3.3.1 Results of radiocarbon measurements. GrN: conventional; GrA: AMS.

Lab code	Material	Depth (cm)	^{14}C age (BP)	Sigma (BP)	Calibrated age (calBP)	δ^{13}C (‰)
GrN-32143	Peat	41	1800	60	1820–1630	−28.1
GrN-32144	Peat	65	3370	35	3690–3490	−27.9
GrN-32145	Peat	99	3780	50	4240–4020	−28.8
GrN-15918	Peat	256	8650	70	9675–9540	−27.6
GrN-15919	Peat	283	9500	200	11,125–10,570	−27.8
GrN-31212	Carbonate	309	11,480	100	13,420–13,260	−1.2
GrN-31208	Carbonate	353	11,780	180	13,790–13,440	−2.6
GrN-31206	Carbonate	364	11,920	110	13,890–13,660	−3.1
GrN-31656	Peat	386	11,300	100	13,270–13,120	−32.4
GrA-11476	Snails	468	12,790	70	15,200–15,090	−8.5
GrA-11479	Carbonate	468	13,010	70	15,840–15,240	−3.1
GrN-31210	Carbonate	505	16,840	120	19,790–19,450	+1.1

AMS, Accelerator mass spectrometry; *BP*, Before Present;*, not calibrated.

curve and reflected as a slight increase in the *Betula* curve.

Similar oscillations in pollen diagrams of Late Glacial lake deposits in the Alpine region have been published by Bortenschlager (1984).

3.3.3 Radiocarbon stratigraphy

Radiocarbon dating of calcareous gyttja is problematic because it easily overestimates ages due to reservoir effects (Mook and Streurman, 1983), which are difficult to quantify. We could obtain reliable dates for a few (bulk) peat samples of Gasserplatz core 2, in addition to two 'anchor points' (the onset of the Younger Dryas and the LST) to obtain a reliable chronology.

Various samples of Gasserplatz core 1, consisting of peaty gyttja, calcareous gyttja and molluscs, were selected for radiocarbon dating. The results are shown in Table 3.3.1 and Fig. 3.3.11. The peat sequence (red in Fig. 3.3.11) shows a linear relation with time (calibrated ^{14}C dates).

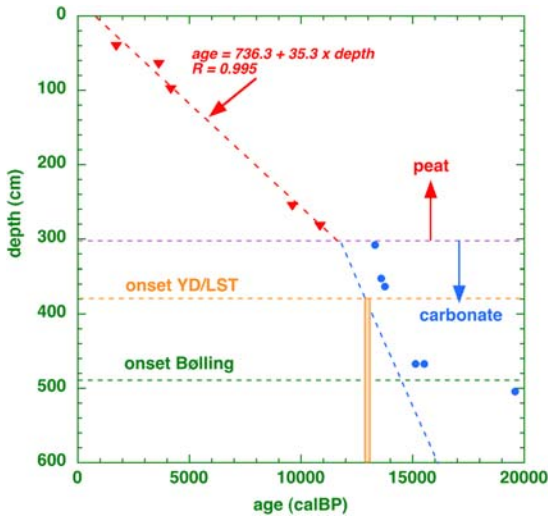

FIGURE 3.3.11 Calibrated ^{14}C dates as a function of depth for Gasserplatz. *After van Mourik, J.M., Slotboom, R.T., van der Plicht, J., Streurman, H.J., Kuijper, W.J., Hoek, W.Z., de Graaff, L.W.S., 2013. Geochronology of Betula extensions in pollen diagrams of Alpine Late-glacial lake deposits: a case study of the Late-glacial deposits of the Gasserplatz soil archives (Vorarlberg, Austria). Quaternary International 306, 3–13.*

The starting time of the peat is at a depth of 306 cm, corresponding to a calibrated age of 11,550 calBP. This point is also the end point of the carbonate set of dates obtained from the gyttja.

The timeline for the carbonates can be constructed from this point and the other horizons as 'anchor points': the onset of the Younger Dryas (YD) and Laacher See Tephra (LST) at 380 and 383 cm, respectively, and the onset of Bølling (490 cm depth, 14,500 calBP).

LST is identified in the sequence at a depth of 383 cm. From the laminated Meerfelder Maar sequence in the Eifel, it appears that LST was deposited some 190 years before the onset of the Younger Dryas (Brauer et al., 1999).

All carbonates (blue in Fig. 3.3.11) are subjected to reservoir effects, as can be seen from their deviation from the deposition line. Even a peat sample at 386 cm depth shows a (small) reservoir effect. It shows a very negative $\delta^{13}C$ value of −32.4‰ caused by submerged plants.

3.3.4 Stable isotope stratigraphy

For both Gasserplatz series, the stable isotope ratios ($\delta^{13}C$ and $\delta^{18}O$) of the carbonate fractions are shown in Fig. 3.3.12A and B as a function of depth. They overlap, and the Younger Dryas cold reversal is clearly visible. These data lead to the following observations.

In general terms, the organic production (plant growth) determines the $\delta^{13}C$ of the carbonate in the system, and thus the size of the reservoir effect for ^{14}C dates. Plants are in isotopic equilibrium with the carbonates. Further biological production leads to higher CO_2 concentration and consequently a more negative $\delta^{13}C$ for submerged plants and carbonates. For example, for the sample at a depth of 422 cm, the $\delta^{13}C$ for the organic material was −38‰, and for the carbonate −6‰.

There is a clear relationship between $\delta^{13}C$ and $\delta^{18}O$ (Fig. 3.3.12A and B). Lower temperatures (lower $\delta^{18}O$ values) correlate with more negative

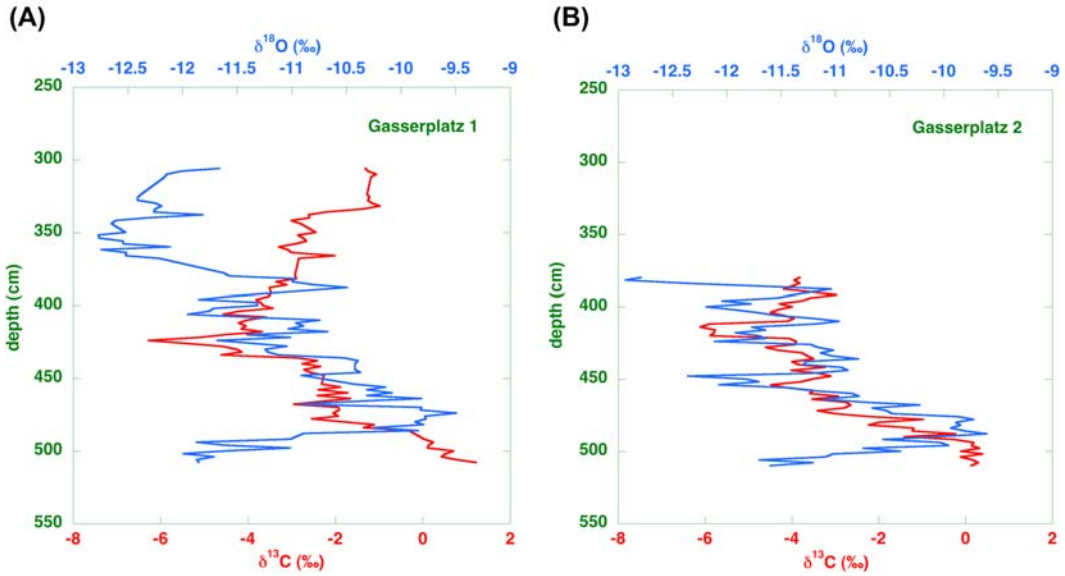

FIGURE 3.3.12 (A). Isotope stratigraphy of Gasserplatz-1. (B). Isotope stratigraphy of Gasserplatz-2. *After van Mourik, J.M., Slotboom, R.T., van der Plicht, J., Streurman, H.J., Kuijper, W.J., Hoek, W.Z., de Graaff, L.W.S., 2013. Geochronology of Betula extensions in pollen diagrams of Alpine Late-glacial lake deposits: a case study of the Late-glacial deposits of the Gasserplatz soil archives (Vorarlberg, Austria). Quaternary International 306, 3–13.*

$\delta^{13}C$ values, and are related to higher water levels caused by higher rain- and groundwater input. In contrast, the warmer periods mean less water input, a lower water level and evaporation, yielding more positive $\delta^{13}C$ and $\delta^{18}O$ values. During the cold period before 16,000 there is no biological activity in the system, which is consistent with the observation of higher reservoir effects (Fig. 3.3.11).

The oxygen isotope stratigraphy shown in Fig. 3.3.12B is consistent with the one shown in Fig. 3.3.12A. The climate proxy signals show a similar trend in both cores. Together with the ^{14}C-derived deposition plot, the stratigraphic framework of the stable isotopes is used to support the chronology of the Late Glacial section of the Gasserplatz records. This approach has been used successfully at other locations (Von Grafenstein et al., 1999; Schwander et al., 2000; Hoek and Bohncke, 2001; Lotter et al., 1992, 2012).

We conclude that the pollen records of the Gasserplatz show a clear registration of Late Glacial oscillations, probably caused by climatic oscillations. Radiocarbon dates overestimate the age of calcareous lake sediments and cannot be used to establish the geochronology of these climatic oscillations. This is caused by reservoir effects, for which the stable isotopes $\delta^{13}C$ and $\delta^{18}O$ of the carbonate fraction provide information.

The oxygen isotope chronology of the Gasserplatz records correlates with the *Betula* oscillations and with the oxygen isotope stratigraphy of the Greenland ice cores.

3.4 Dating of vegetation horizons

Similar to soils, for vegetation horizons, the humic acid fraction is the best datable fraction for radiocarbon dating. As an example we consider the Schildmeer (in the province of Groningen, the Netherlands). A series of dates is shown in Tables 3.4.1 and 3.4.2 for two locations named S230 and S123.

Only two separate layers (named I and II) are observed in clay above a peat layer, which is very common in the region (Schoute, 1985).

The data are a summary based on the observations made by Schoute (1985). In general, the C content is low for these samples. Therefore

TABLE 3.4.1 Dating fractions from vegetation horizons from Schildmeer (S230).

Type	Lab code	Fraction	Sample (g)	Ash (g)	Carbon (g)	Cpr (%)	Cv (%)	^{14}C age (BP)	Sigma	$\delta^{13}C$ (‰)
Clay	GrN-9520	Humic acid	4.02	0.25	1.90	47	50	2260	50	−27.35
Clay	GrN-9519	Humin	185.6	172.4	3.11	2	24	2395	35	−27.46
Top vh I	GrN-9516	Humic acid	100.0	72.0	14.0	14	50	1975	20	−27.29
Top vh I	GrN-9515	Humin	152.0	138.0	6.79	45	48	2150	30	−26.70
Bottom vh I	GrN-9514	Humic acid	43.4	31.3	5.71	13	47	2350	30	−25.68
Bottom vh I	GrN-9513	Humin	198.0	187.9	2.55	1	25	2845	50	−26.71
Clay	GrN-9518	Humic acid	7.7	3.10	2.26	29	49	2815	55	−24.52
Clay	GrN-9517	Humin	160.0	143.2	4.81	3	28	2800	30	−27.41

Cpr, relative amount of carbon after pretreatment; *Cv*, (amount of C)/(amount of sample minus amount of ash) * 100%.

TABLE 3.4.2 Dating fractions from vegetation horizons from Schildmeer (S123).

Type	Lab code	Fraction	Sample (g)	Ash (g)	Carbon (g)	Cpr (%)	Cv (%)	^{14}C age (BP)	Sigma	δ^{13}C (‰)
Clay	GrN-9502	Humic acid	1,4	0.2	0.6	42	49	1280	60	−26.90
Clay	GrN-9501	Humin	242.0	22.9	2.9	1	22	1355	45	−26.69
vh II	GrN-8981	Humic acid	92.4	80.8	4.57	5	39	1665	25	−29.18
vh II	GrN-8980	Humin	282.7	270.0	2.12	1	17	2050	60	−28.18
Top vh I	GrN-8979	Humic acid	40.3	31.3	4.71	12	52	2015	25	−26.89
Top vh I	GrN-8978	Humin	162.0	155.2	2.04	1	30	2200	60	−27.43
Bottom vh I	GrN-8977	Humic acid	43.3	28.8	4.71	11	32	2210	25	−27.17
Bottom vh I	GrN-8976	Humin	144.0	133.6	4.16	3	40	2410	80	−27.58
Clay	GrN-9500	Humic acid	3.8	0.05	1.9	51	51	2935	55	−24.58
Clay	GrN-8982	Humin	219.0	203.0	3.0	1	19	2730	60	−25.69

Cpr, relative amount of carbon after pretreatment; *Cv*, (amount of C)/(amount of sample minus amount of ash) * 100%.

the risk for contamination is large. The humin fraction contains the allochthonous carbon, mostly from marine clay sediment consisting of fine particles of reworked peat.

As a function of depth we observe the following for S123:

GrN-9502/9501 is taken from clay, GrN-8981/8980 the upper vegetation horizon (VH2); for the lower vegetation horizon (VH1) GrN-8979/8978 is from the top and GrN-8977/8976 is from the bottom. The next clay layer yields GrN-9500/9501. For the region, the underlying peat is dated to ca. 2600 BP (GrN-8961/8960) (not shown in the table).

The vegetation horizons above the peat show a reasonable stratigraphy for the humic acid fraction; the humin dates appear to be unreliable. The lowest clay fraction also yields an impossible date.

For S230, also as a function of depth:

GrN-9520/9519 is taken from clay; GrN-9516/9515 and 9514/9513 represent the top and bottom of VH1. Also here, the underlying peat is dated to ca. 2600 BP (GrN-8961/8960) (not shown in the table).

3.5 Dating of bog peat

Raised bogs from the eastern Netherlands (Meerstalblok, Engbertsdijkveen and others) have been studied extensively. This concerns botanical analysis as well as ^{14}C dating and interpretation of δ^{13}C values (Blaauw, 2003 and references therein).

Fig. 3.5.1 shows the δ^{13}C values of aboveground remains from several bog plant species. It illustrates the influence of wet/dry conditions quite well. *Sphagnum cuspidatum* represents wet conditions, with high δ^{13}C values. Plants representing dry conditions (like *Calluna vulgaris*) show low δ^{13}C values; wetter conditions correspond to higher δ^{13}C values. For more details we refer to Blaauw et al. (2004).

The datable fraction for peat bogs is the humin fraction; the humic acids generally show rejuvenation. Organic matter from peat bogs is chemically pretreated by the standard AAA method (Mook and Streurman, 1983). Note that soils are the exception for this procedure. Contamination problems do play a role for

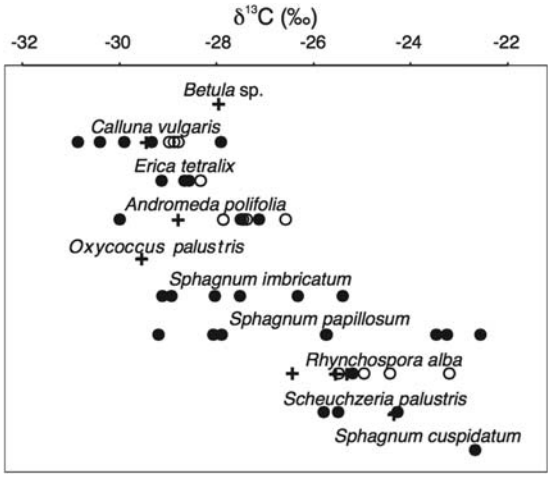

FIGURE 3.5.1 The $\delta^{13}C$ values of raised bog plant species. *From Blaauw, M., 2003. An Investigation of Holocene Sun-Climate Relationships Using Numerical ^{14}C Wiggle Match Dating of Peat Deposits. PhD thesis, University of Amsterdam.*

dating of peat, in particular the Pleistocene age (e.g., van der Plicht, 2012).

Bulk peat sample dating was the only possibility during the conventional era. The introduction of AMS enabled ^{14}C dating of small samples, which for peat can be translated into selected macrofossils or seeds (Blaauw, 2003 and references therein). This solved dating problems caused by mobile organic fractions, and the consensus that *Sphagnum* plant fragments should be used in ^{14}C dating of peat (e.g., Nilsson et al., 2001).

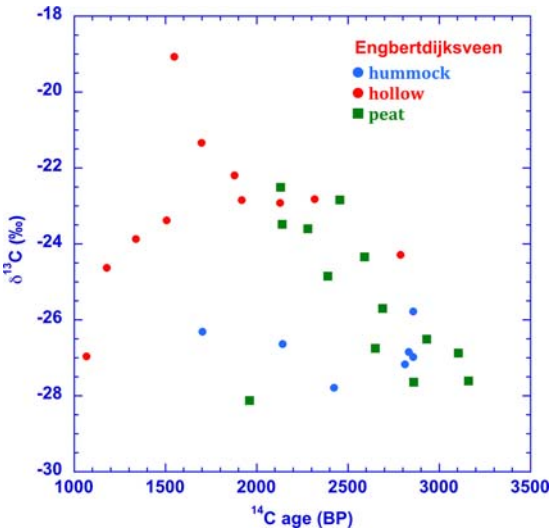

FIGURE 3.5.2 The $\delta^{13}C$ values of hummocks and hollows for the peat bog Engbertdijksveen.

Fig. 3.5.1 shows results for species-specific plants. Bulk dates (not species specific) of peat bogs show different $\delta^{13}C$ values of hummocks and hollows determined by dry/wet conditions. An example for Engbertdijksveen is shown in Fig. 3.5.2, which shows such $\delta^{13}C$ values between 1000 and 3500 BP. The data and references can be found in Blaauw (2003).

3.6 Conclusions

Radiocarbon dating of organic samples is usually very successful, provided the correct datable fraction is prepared and contamination is removed. Soil organic carbon is complicated matter for dating.

In general, the humic acid fraction is considered the correct datable fraction for soil organic carbon but also the humin fraction provides information about the development of soil and landscape.

The stable isotope ^{13}C can be used as a tracer for soil formation processes. The $\delta^{13}C$ value yields information on aquatic plants and wet/dry conditions, depending on type of organic deposit. Application of both carbon isotopes in soil science is illustrated by selected case studies showing the interpretation of fractionated radiocarbon dating and the added value of the $\delta^{13}C$ data.

References

Aerts, A.T., van der Plicht, J., Meijer, H.A.J., 2001. Automatic AMS sample combustion and CO_2 collection. Radiocarbon 43, 293–298.

Bayliss, A., McCormac, A.G., van der Plicht, J., 2004. An illustrated guide to measuring radiocarbon from archaeological samples. Physics Education 39, 1–8.

Blaauw, M., 2003. An Investigation of Holocene Sun-Climate Relationships Using Numerical ^{14}C Wiggle Match Dating of Peat Deposits. PhD thesis. University of Amsterdam.

Blaauw, M., van der Plicht, J., van Geel, B., 2004. Radiocarbon dating of bulk peat samples from raised bogs: non-existence of a previously reported reservoir effect? Quaternary Science Reviews 23, 1537–1542.

Bortenschlager, S., 1984. Die Vegetationsentwicklung im Spätglazial. Das Moor beim Lanser See III, ein Typprofil für die Ostalpen. Dissertationes Botanicae 72, 71–79.

Brauer, A., Endres, C., Gunter, C., Litt, T., Stebich, M., Negendank, J.F.W., 1999. High resolution sediment and vegetation responses to Younger Dryas climate change in varved lake sediments from Meerfelder Maar, Germany. Quaternary Science Reviews 18, 321–329.

Brewer, R., 1976. Fabric and Mineral Analysis of Soils. Robert E. Krieger Publishing Company, Huntingon, New York, 482pp.

Bronk Ramsey, C., Staff, R.A., Bryant, C.L., Brock, F., Kitagawa, H., van der Plicht, J., Schlolaut, G., Marshall, M.H., Brauer, A., Lamb, H.F., Payne, R.L., Tarasov, P.E., Haraguchi, T., Gotanda, K., Yonenobu, H., Yokoyama, Y., Tada, R., Nakagawa, T., 2012. A complete terrestrial radiocarbon record for 11.2 to 52.8 kyr BP. Science 338, 370–374.

Bucha, V., 1970. Influence of the Earth's magnetic field on Radiocarbon dating. In: Olsson, I.U. (Ed.), Radiocarbon Variations and Absolute Chronology. Proceedings of The 12th Nobel Symposium. Wiley, pp. 501–511.

Castel, I.I.Y., Koster, E.A., Slotboom, R.T., 1989. Morphogenetic aspects and age of late Holocene drift sand in northwest Europe. Zeitschrift für Geomorphologie, Neu Folge 33, 1–26.

Cook, G.T., van der Plicht, J., 2013. Radiocarbon dating. In: Encyclopedia of Quaternary Science, second ed. Elsevier, Amsterdam, pp. 305–315.

de Graaff, L.W.S., Kuijper, W.J., Slotboom, R.T., 1989. Schlussvereisung und spätglaziale Entwicklung des Moorgebietes Gasserplatz (Feldkirch-Göfis, Vorarlberg). In: Jahrbuch der Geologischen Bundesanstalt, Band, vol. 132, pp. 397–413.

de Vries, H., 1958. Variation in concentration of radiocarbon with time and location on earth. Proceedings KNAW B61, 1–9.

Dijkmans, J.W.A., van Mourik, J.M., Wintle, A.G., 1992. Thermoluminescence dating of aeolian sands from polycyclic soil profiles in the Southern Netherlands. Quarternary Science Reviews 11, 85–92.

Ellis, S., Matthews, J.A., 1984. Pedogenetic implications of a 14C-dated paleopopodzolic soil at Haugabreen, Southern Norway. Arctic and Alpine Research 16, 77–91.

Fry, B., 2008. Stable Isotope Ecology. Springer.

Godwin, H., 1962. Halflife of radiocarbon. Nature 195, 984.

Goh, K.M., Molloy, B.P.J., 1978. Radiocarbon dating of paleosols using soil organic matter components. Journal of Soil Science 29, 567–573.

Graven, H.D., 2015. Impact of fossil fuel emissions on atmospheric radiocarbon and various applications of radiocarbon over this century. Proceedings of the National Academy of Sciences United States of America 112, 9542–9545.

Groenman-van Waateringe, W., 1988. Palynologisch onderzoek van het urnenveld te Weert. KNAG Netherlands Geographical Studies 74, 139–156.

Hoek, W.Z., Bohncke, S.J.P., 2001. Oxygen-isotope wiggle-matching as a tool for correlation of ice-core and terrestrial records over termination I. Quaternary Science Reviews 20, 1251–1264.

Hua, Q., Barbetti, M., Rakowski, A.Z., 2013. Atmospheric radiocarbon for the period 1950–2010. Radicoarbon 55, 2059–2072.

Johnsen, S.J., Dahl-Jensen, D., Gundestrup, N., Steffensen, J.P., Clausen, H.B., Miller, H., Masson-Delmotte, V., Sveinbjornsdottir, A., White, J., 2001. Oxygen isotope and palaeotemperature records from six Greenland ice core stations: camp century, GRIP, GISP2, Renland and NorthGRIP. Journal of Quaternary Science 16, 299e307.

Jull, A.J.T., 2013. AMS method. radiocarbon dating. In: Elias, S.A. (Ed.), Encyclopedia of Quaternary Science, second ed. Elsevier, Amsterdam, pp. 2911–2918.

Lanting, J.N., van der Plicht, J., 1994. 14C-AMS: pros and cons for archaeology. Palaeohistoria 35/36, 1–12.

Levin, L., Hesshaimer, V., 2000. Radiocarbon, a unique tracer of global carbon cycle dynamics. Radiocarbon 42, 69–80.

Libby, W.F., 1952. Radiocarbon Dating. University of Chicago Press.

Lotter, A.F., Eicher, U., Siegentahler, U., Birks, H.J., 1992. Late-glacial climatic oscillations as recorded in Swiss lake sediments. Journal of Quaternary Science 7, 187–204.

Lotter, A.F., Heiri, O., Brooks, S., van Leeuwen, J.N., Eicher, U., Ammann, B., 2012. Rapid summer temperature changes during termination 1a: high resolution multi-proxy climate reconstructions from Gerzensee (Switzerland). Quaternary Science Reviews 36, 103–113.

Meadows, J., 2005. The younger Dryas episode and the radiocarbon chronologies of the lake Huleh and Ghab valley pollen diagrams, Israel and Syria. The Holocene 15, 631–636.

Michener, R., Lajtha, K.R., 2007. Stable Isotopes in Ecology and Environmental Science. Blackwell, Oxford.

Mook, W.G., 2006. Introduction to Isotope Hydrology: Stable and Radioactive Isotopes of Hydrogen, Oxygen and Carbon. Taylor and Francis, London.

Mook, W.G., Streurman, H.J., 1983. Physical and chemical aspects of radiocarbon dating. PACT Publications 8, 31–55.

Mook, W.G., Waterbolk, H.T., 1985. Handbooks for Archaeologists No.3: Radiocarbon Dating. European Science Foundation. ISBN 2-903148-44-9.

Mook, W.G., van de Plassche, O., 1986. Radiocarbon dating. In: van de Plassche, O. (Ed.), Sea Level Research: A Manual for the Collection and Evaluation of Data. Geo Books. Norwich525-560.

Mook, W.G., van der Plicht, J., 1999. Reporting 14C activities and concentrations. Radiocarbon 41, 227–239.

Moore, P.D., Webb, J.A., Collinson, M.E., 1991. Pollen Analyses. Blackwell, Oxford, p. 216.

Nilsson, M., Klarqvist, M., Bohlin, E., Possnert, G., 2001. Variation in 14C age of macrofossils and different fractions of minute peat samples dated by AMS. The Holocene 11, 579–586.

Olsson, I.U., 1983. Dating non-terrestrial materials. PACT Publications 8, 277–294.

Olsson, I.U., 1989. The 14C method, its possibilities and some pitfalls. PACT Publications 24, 161–177.

Reimer, P.J., Bard, E., Bayliss, A., Beck, J.W., Blackwell, P.G., Bronk Ramsey, C., Buck, C.E., Edwards, R.L., Friedrich, M., Grootes, P.M., Guilderson, T.P., Haflidason, H., Hajdas, I., Hatté, C., Heaton, T.J., Hoffmann, D.L., Hogg, A.G., Hughen, K.A., Kaiser, K.F., Kromer, B., Manning, S.W., Niu, M., Reimer, R.W., Richards, D.A., Scott, E.M., Southon, J.R., Staff, R.A., Turney, C.S.M., van der Plicht, J., 2013. IntCal13 and Marine13 Radiocarbon age calibration curves 0-50,000 years cal BP. Radiocarbon 55, 1869–1887.

Reimer, P.J., Austin, W.E.N., Bard, E., Bayliss, A., Blackwell, P.G., Bronk Ramsey, C., Butzin, M., Cheng, H., Edwards, L., Friedrich, M., Grootes, P.M., Guilderson, T.P., Hajdas, I., Heaton, T.J., Hogg, A.G., Hughen, K.A., Kromer, B., Manning, S.W., Muscheler, R., Palmer, J.G., Pearson, C., van der Plicht, J., Reimer, R.W., Richards, D., Scott, E.M., Southon, J.R., Turney, C.S.M., Wacker, L., Adophi, F., Büntgen, U., Capano, M., Fahrni, S., Fogtmann-Schulz, A., Friedrich, R., Kudsk, S., Miyake, F., Olsen, J., Reinig, F., Sakamoto, M., Sookdeo, A., Talamo, S., 2020. The IntCal20 Northern Hemisphere radiocarbon calibration curve (0-55 kcal BP). Radiocarbon (in press).

Riede, F., 2008. The Laacher See-eruption (12,920 BP) and material culture change at the end of the Allerød in northern Europe. Journal of Archaeological Science 35, 591–599.

Schoute, J.F.T., 1985. Vegetation Horizons and Related Phenomena. PhD thesis, VU, Amsterdam.

Schwander, J., Eicher, U., Ammann, B., 2000. Oxygen isotopes of lake marl at Gerzensee and Leysin (Switzerland), covering the Younger Dryas and two minor oscillations, and their correlation to the GRIP ice core. Palaeogeography, Palaeoclimatology, Palaeoecology 159, 203e214.

Scott, E.M., Cook, G.T., Naysmith, P., 2010. The Fifth International Radiocarbon Intercomparison (VIRI): an assessment of laboratory performance in stage 3. Radiocarbon 52, 859–865.

Simons, A.L., 1985. Geomorphologische und glazialgeologischeUntersuchungen in Vorarlberg, Österreich. In: Schriften des VorarlbergerLandesmusums, Reihe A, Band, vol. 1, p. 57.

Stevenson, F.J., 1985. Geochemistry of soil humic substances. In: Humic Substances in Soil Sediment and Water. Wiley, New York, pp. 13–53.

Stuiver, M., 1965. Carbon-14 content of 18th- and 19th-century wood: variations correlated with sunspot activity. Science 149, 533–534.

Stuiver, M., Quay, P., 1981. Atmospheric 14C changes resulting from fossil fuel CO_2 release and cosmic ray flux variability. Earth and Planetary Science Letters 53, 249–362.

Suess, H.E., 1980. The radiocarbon record in tree rings of the last 8000 years. Radiocarbon 22, 200–209.

Taylor, R.E., Long, A., Kra, R.S., 1992. Radiocarbon after Four Decades: An Interdisciplinary Perspective. Springer Verlag, New York.

Trumbore, S.E., Vogel, J.S., Southon, J.R., 1989. AMS measurements of fractionated soil organic matter: an approach to deciphering the soil carbon cycle. Radiocarbon 31, 644–654.

Tuniz, C., Kutschera, W., Fink, D., Herzog, G.F., Bird, J.R., 1998. Accelerator Mass Spectrometry: Ultrasensitive Analysis for Global Science. CRC press. ISBN 9780849345388.

van der Plicht, J., 2012. Borderline radiocarbon. Netherlands Journal of Geosciences 91, 257–261.

van der Plicht, J., 2013. Variations in atmospheric 14C. In: Elsevier Encyclopedia of Quaternary Science, 2nd, revised edition, pp. 329–335.

van der Plicht, J., Bruins, H.J., 2001. Radiocarbon dating in Near-Eastern Mediterranean contexts: confusion and quality control. Radiocarbon 43, 1155–1166.

van der Plicht, J., Hogg, A., 2006. A note on reporting radiocarbon. Quaternary Geochronology 1, 237–240.

van der Plicht, J., Wijma, S., Aerts, A.T., Pertuisot, M.H., Meijer, H.A.J., 2000. The Groningen AMS facility: status report. Nuclear Instruments and Methods B 172, 58–65.

van der Plicht, J., Streurman, H.J., Bottema, S., Mook-Kamps, E., 2001/2002. Wildervank: an investigation using natural isotopes. Palaeohistoria 43/44, 35–42.

van Mourik, J.M., 1988. De ontwikkeling van een stuifzandgebied. KNAG Netherlands Geographical Studies 74, 5–42.

van Mourik, J.M., Wartenbergh, P.E., Mook, W.G., Streurman, H.J., 1995. Radiocarbon dating of palaeosols in aeolian sands. Mededelingen Rijks Geologische Dienst 52, 425–440.

van Mourik, J.M., Nierop, K.G.J., Vandenberghe, D.A.G., 2010. Radiocarbon and optically stimulated luminescence dating based chronology of a polycyclic driftsand sequence at Weerterbergen (SE Netherlands). Catena 80, 170–181.

van Mourik, J.M., Seijmonsbergen, A.C., Jansen, B., 2012a. Geochronology of Soils and Landforms in Cultural Landscapes on Aeolian Sandy Substrates, Based on Radiocarbon and Optically Stimulated Luminescence Dating (Weert, SE-Netherlands). Intech Radiometric dating, pp. 75–114.

van Mourik, J.M., Seijmonsbergen, A.C., Slotboom, R.T., Wallinga, J., 2012b. The impact of human land use on soils and landforms in cultural landscapes on aeolian sandy substrates (Maashorst, SE Netherlands). Quaternary International 265, 74–89.

van Mourik, J.M., Slotboom, R.T., van der Plicht, J., Streurman, H.J., Kuijper, W.J., Hoek, W.Z., de Graaff, L.W.S., 2013. Geochronology of Betula extensions in pollen diagrams of Alpine Late-glacial lake deposits: a case study of the Late-glacial deposits of the Gasserplatz soil archives (Vorarlberg, Austria). Quaternary International 306, 3–13.

van Strydonck, M., Nelson, D.E., Combré, P., Bronk Ramsey, C., Scott, E.M., van der Plicht, J., Hedges, R.E.M., 1999. What's in a 14C date. In: Proceedings Third Conference on 14C and Archaeology, pp. 433–440. Lyon (France).

Vera, H., 2011. 'Dat men het goed van de ongeboornen niet mag verkoopen'; Gemene gronden in de Meierij van Den Bosch tussen hertog en hertgang 1000 – 2000. Uitgeverij BOXpress, Oisterwijk, Netherlands (with english summary).

von Grafenstein, U., Erlenkeuser, H., Brauer, A., Jouzel, J., Johnsen, S.J., 1999. A mid-European decadal isotope-climate record from 15,500 to 5000 years BP. Science 284, 1654–1657.

Wagner, T.V., Mouter, A.K., Parsons, J.R., Sevink, J., van der Plicht, J., Jansen, B., 2018. Molecular characterization of charcoal to identify adsorbed SOM and assess the effectiveness of common SOM-removing pre-treatments prior to radiocarbon dating. Quaternary Geochronology 45, 74–84.

Wallinga, J., van Mourik, J.M., Schilder, M.L.M., 2013. Identifying and dating buried micropodzols in Subatlantic polycyclic drift sands. Quaternary International 306, 60–70.

This page intentionally left blank

CHAPTER

4

Luminescence dating of soil archives

J. Wallinga[a,*], *J. Sevink*[b], *J.M. van Mourik*[b], *T. Reimann*[a]

[a]Soil Geography and Landscape Group & Netherlands Centre for Luminescence Dating, Wageningen University, Wageningen, the Netherlands; [b]Institute for Biodiversity and Ecosystem Dynamics (IBED), Faculty of Science, University of Amsterdam, Amsterdam, the Netherlands
*Corresponding author.

4.1 Principles of soil archive exploration through luminescence dating

4.1.1 Introduction

Luminescence dating methods determine the last light exposure of quartz and feldspar minerals, which are the primary constituents of sediments and mineral soils. The method was conceived in archaeology, where thermoluminescence methods were developed to determine the baking time of pottery (Daniels et al., 1953). These methods were first applied to sediments in the 1970s and have rapidly evolved since the introduction of optically stimulated luminescence (OSL) methods in the 1980s (Huntley et al., 1985). The development of reliable single-aliquot regenerative dose (SAR) methods for quartz were a major catalyst (Murray and Wintle, 2000), and applications in earth sciences has strongly increased over the last few decades (e.g., Preusser et al., 2008; Rhodes, 2011).

Although application of luminescence dating to (palaeo)soils is not straightforward, luminescence dating is now increasingly used to explore soil archives. In this chapter we set out to introduce the basic principles of luminescence dating to non-specialists, followed by a brief review of considerations and applications relevant to soil archives. Then, three case studies are presented to illustrate the possibilities and limitations of luminescence dating for enlightening soil archives.

4.1.2 The luminescence dating method

Natural quartz and feldspar minerals are semiconductors with imperfect crystal structures. They have the natural ability to act as dosimeters, similar to radiation badges worn by radiation workers in hospitals. In their natural environment, minerals are exposed to background radiation – naturally occurring ionizing radiation arising from the decay of radioactive elements (K^{40} and several nuclides in the U and Th chains) and cosmic radiation. This energy may excite electrons within the crystal, and part of these electrons become trapped at higher energy levels. If such electron traps are stable over geological time, the number of electrons in these traps will increase in time due to continued

https://doi.org/10.1016/B978-0-444-64108-3.00004-5

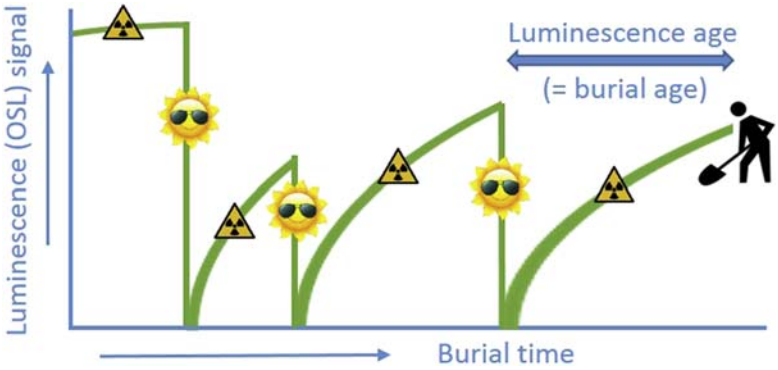

FIGURE 4.1.1 Conceptual diagram showing the principle of luminescence dating. Luminescence signals increase during burial in response to absorption of ionizing radiation. Upon light exposure the luminescence signal is reset. Luminescence dating determines the last resetting event — usually the time of deposition and burial at the sample location. This is referred to as luminescence age or burial age. *OSL*, Optically stimulated luminescence.

exposure to ionizing radiation. Exposure to daylight will liberate electrons from the light-sensitive traps, resetting the amount of trapped charge within seconds at full sunlight exposure.

The cycle of gradual trap filling during burial and rapid resetting during erosion and transport may be repeated over and over again (Fig. 4.1.1), resembling the charging and discharging of a battery. The degree of filling of electron traps depends on: (1) the local background radiation flux; (2) the time since last daylight (or heat) exposure; and (3) the properties of the crystal and trap.

When trapped charge is released, it may give rise to a minute light signal, referred to as luminescence. The brightness of the luminescence signal is proportional to the amount of trapped charge, and can be used to infer the burial age of the mineral. To do so, two properties need to be determined. First, the amount of absorbed radiation needed to produce the luminescence signal, referred to as equivalent dose (unit Gy; J/kg). The equivalent dose is determined by comparison of the natural luminescence signal with a signal induced by laboratory irradiation using a calibrated radiation source, usually a beta source (Fig. 4.1.2). Widely used SAR methods monitor and correct for luminescence sensitivity changes during the measurement procedure (e.g., Murray and Wintle, 2003). Second, the annual dose received by the mineral grains during burial needs to be established. Toward this, radionuclide (activity) concentrations of the sample (including surrounding material) are determined, and a depth-dependent contribution of cosmic rays is taken into account. Because water and organic matter have a shielding effect for radiation, the average water and organic contents

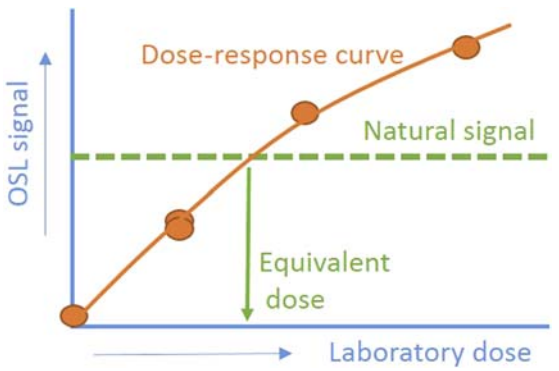

FIGURE 4.1.2 To obtain the equivalent dose (on small subsamples, aliquots or single grains) the natural optically stimulated luminescence (OSL) signal (*green dashes*) is compared to OSL signals induced by laboratory irradiation (*orange dots*). The projection of the natural signal on the constructed dose–response curve (*orange line*), provides the equivalent dose estimate (*green arrow*).

of the sample during the period of burial also need to be taken into account. The annual dose is referred to as dose rate, and is expressed in Gy/a (or often per 1000 years: Gy/ka). The burial age of a mineral is then obtained by dividing the equivalent dose by the dose rate:

$$\text{Age (ka)} = \frac{\text{Equivalent dose (Gy)}}{\text{Dose rate (Gy/ka)}} \qquad (4.1.1)$$

Although all luminescence methods are based on this principle, users should be aware that luminescence dating is not a straightforward technique with prescribed procedures. Different minerals can be used for analysis, and for each of these minerals, different luminescence signals can be probed depending on parameters selected in sample preparation and measurement. Which method is most suitable depends on many aspects, including the depositional environment, provenance of the material, luminescence characteristics of the minerals and depositional age. Successful luminescence dating in soil sciences requires close collaboration of a dating specialist and soil scientists, or involvement of a specialist covering both fields. Methods adopted at a site should be validated through a range of tests, and successful application at one site does not necessarily imply that the same methods are applicable to other sites.

4.1.3 Luminescence of quartz and feldspar minerals

Both quartz and feldspar minerals can show luminescence, and both are used for dating. Quartz is usually the mineral of choice, because its luminescence signal is rapidly reset upon light exposure, and the trapped charge is stable over geological timescales. Disadvantages of quartz OSL is that the signal saturates at relatively low doses (usually limiting the age range to the last 100 ka) and highly varying luminescence sensitivity. The latter often precludes OSL dating of quartz from settings where the quartz is derived from plutonic or metamorphic bedrock (Guralnik et al., 2015) and has experienced few erosion–deposition cycles.

Luminescence from K-feldspar minerals is usually sampled using infrared stimulation, giving rise to infrared stimulated luminescence (IRSL; Hütt, 1988). Compared to quartz OSL, this signal is less light sensitive and less stable. Yet, its advantages are that it saturates at higher doses, often allowing dating up to 500 ka, and that most grains show bright luminescence signals, largely regardless of geological history of the mineral. Problems with regard to signal instability ('anomalous fading') have been to a great extent overcome using post-IR IRSL (pIRIR) methods (Buylaert et al., 2012; Kars et al., 2012).

In summary, quartz OSL is still the method of choice when quartz luminescence properties at the site are suitable and the deposit of interest is within the accessible age range (see 4.1.5). Feldspar pIRIR provides an interesting alternative in other cases, or if information from individual grains is needed.

4.1.4 The importance of sample (aliquot) size

Ideally, all grains within a sample carry the same information: they all had their luminescence signal reset prior to burial, and were exposed to identical dose rate. This assumption may well hold for uniform deposits of aeolian material (e.g., sand dunes), but for other settings and in particular soil archives it may well be violated. Below we discuss three mechanisms causing grain-to-grain differences in equivalent dose, and graphically illustrate these in Fig. 4.1.3. Understanding the nature of spread in equivalent-dose distributions is crucial to select suitable approaches for measurement and analysis.

First, there may be slight deviations in dose rate between grains, caused by inhomogeneous distribution of radionuclides. As a consequence, equivalent doses of the grains will also be more spread out than expected based on measurement uncertainties (Fig. 4.1.3A). This additional

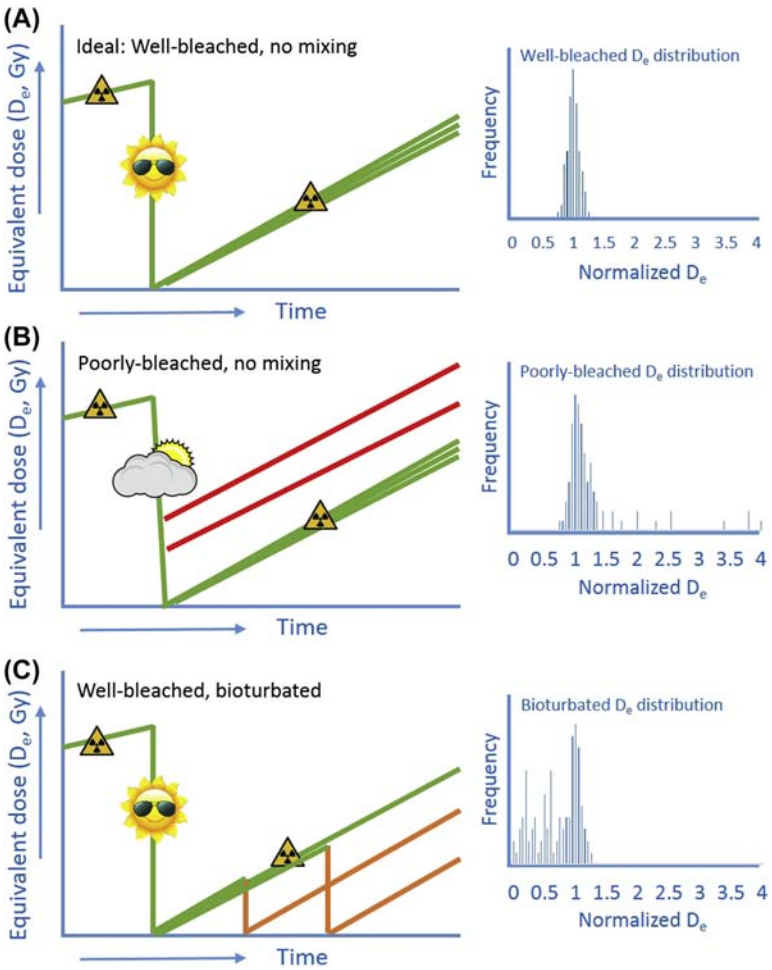

FIGURE 4.1.3 Conceptual graph showing potential causes for spread in equivalent doses between grains. (A) In the ideal case, the luminescence signal of all grains is reset at the last light exposure, and all grains yield similar equivalent doses. Slight grain-to-grain variations in dose rate will result in some spread in equivalent doses. (B) If light exposure is limited, signals may not be reset in all grains. Lowest equivalent doses (*green*) will reflect the true burial dose, while other equivalent doses may overestimate the burial dose (*red*). (C) If part of the grains is exposed to daylight after initial deposition and burial, luminescence signals in these grains are reset. The time of deposition is reflected by the greatest equivalent doses (*green*), while lower equivalent doses provide information on soil mixing (*orange*).

spread is referred to as overdispersion. Overdispersion has no significant effect on the result obtained, and uncertainties can be reduced by repeating measurements on many subsamples ('aliquots').

Second, if light exposure prior to deposition and burial was limited, the luminescence signals of some grains may not have been completely reset. Those grains possess a 'remnant' age at the time of deposition and burial, and the luminescence age would overestimate the true burial age (Fig. 4.1.3B). As light exposure will not be identical for all grains, remnant ages will differ as well, giving rise to additional scatter in

equivalent dose. This phenomenon is referred to as heterogeneous bleaching. Provided that part of the grains was exposed to sufficient light to have their luminescence signal completely reset, the burial age can still be obtained if only equivalent doses of the subset of 'bleached' grains is used. These are the grains providing the lowest equivalent doses.

A third consideration, which is particularly important for soil archives, is that grains may be exposed to light after deposition and burial through mixing processes. Bioturbation through animals (e.g., burrowing, mounting) and plants (e.g., uprooting) may bring grains to the surface, after which they mix with the soil matrix again (e.g., Bateman et al., 2007). This process may continuously rejuvenate the top of a soil until it becomes buried below new deposits. Deeper in the soil profile, recently light-exposed grains may be mixed with a matrix of non-exposed grains (Fig. 4.1.3C). Interpreting luminescence signatures from such settings allows inferences on the age of the deposit, the duration of soil formation and the intensity of soil reworking. In more complex settings consisting of multiple depositional units of different age, grains from different depositional units may become mixed yielding highly complicated luminescence profiles (e.g., Deeben et al., 2010).

Above we discussed three potential causes of grain-to-grain differences in equivalent dose. The average equivalent dose may provide a reasonable estimate of burial dose in the absence of poor bleaching or mixing. However, insight into equivalent-dose distributions is needed to identify additional unexplained spread in equivalent dose. Moreover, insight into the deposition environment (i.e., bleaching circumstances) and soil processes (i.e., potential post-depositional mixing) is required to interpret the equivalent-dose distribution and select suitable approaches for analysis.

Identifying grain-to-grain differences in equivalent dose requires measurement of small aliquots, ideally consisting of a single grain. Especially for quartz, true single-grain measurements are cumbersome because only a very small fraction of grains (often <5%) yields bright enough luminescence to allow analysis. For this reason, measurements on 'small aliquots', containing tens of grains, may in many cases provide a pragmatic alternative to obtain 'single grain' information (Cunningham et al., 2011, 2015). Deriving a burial dose from a heterogeneously bleached single-aliquot equivalent-dose distribution requires advanced statistical methods that take into account other sources of spread (e.g., dose-rate heterogeneity). The minimum age model (Galbraith et al., 1999) and subsequently developed bootstrapped versions (Cunningham and Wallinga, 2012) are widely used for this purpose, but other statistical approaches are also used (e.g., Thomsen et al., 2007). Obtaining meaningful information on soil mixing (rates) requires true single-grain data; for this reason, feldspar rather than quartz may be more suitable for such investigations (Reimann et al., 2017). This aspect is discussed in detail in Section 4.4.

4.1.5 Age range and precision

Luminescence methods have been successfully applied to deposits ranging from a few years (Madsen and Murray, 2009) to about half a million years (Wallinga and Cunningham, 2015). At the lower limit, full resetting of luminescence signals becomes highly important. As quartz OSL is more rapidly reset than luminescence signals of feldspar, quartz is usually the mineral of choice for samples of Holocene age. Due to saturation of the quartz OSL signal at relatively low doses, the method is usually limited to the last 100 ka although in low dose rate settings much older ages have been obtained (e.g., Schokker et al., 2005). Feldspar IRSL signals saturate at higher doses, and stable signals may be obtained using pIRIR methods that allow dating up to 500 ka (e.g., Joordens et al., 2015).

In ideal settings, luminescence ages yield uncertainties of ~5% of the age (at 1-sigma); systematic uncertainties in machine calibration and conversion factors prevent much greater precision. In less ideal settings, e.g., poorly-known water content or burial history, uncertainties will be (much) greater (see Wallinga and Cunningham, 2015). OSL ages are usually expressed in ka (kilo year) relative to the time of sampling. Throughout this chapter we use Gregorian calendar ages to facilitate comparison with other age information (e.g., historical maps, radiocarbon chronologies). We use the notations of CE (Common Era) and BCE (Before Common Era) as academic alternatives to the Dionysian AD and BC notations. Uncertainties are given as 1-sigma confidence intervals, and include random and systematic uncertainties in both equivalent dose and dose rate estimates.

An aspect that is often ignored in luminescence dating is the possibility of changes in dose rate during burial due to weathering, eluviation and illuviation. These processes are common in soils, and may alter radionuclide activity concentrations over time, while calculations assume that present concentrations are representative of the entire burial history. As radionuclide concentrations in silt and clay fractions are usually larger than in sand fractions, eluviation is likely to result in dose rate lowering. This implies that the present dose rate is lower than the time-averaged dose rate, resulting in an age overestimation. In contrast, ignoring the effects of illuviation could result in age underestimation when the illuviation layer is sampled. These aspects have been given very little attention so far, and further research is needed to quantify potential inaccuracies.

4.1.6 Reading soil archives through luminescence dating

Luminescence dating offers a wide range of applications to explore soil archives. A conventional application is the determination of the age of a deposit to establish soil chronosequences (e.g., Nielsen et al., 2010). In such cases, samples should be obtained from below the level of active soil mixing to avoid age underestimation due to mixing effects (Bateman et al., 2007). Luminescence dating can also be used to determine deposition ages of stacked depositional units, with soils formed during stable landscape phases. In Section 4.2, Jan Sevink outlines such an application for the Laarder Wasmeer (LWM) region in the central Netherlands, based on previous publications (Sevink et al., 2013, 2018).

For the LWM, periods with landscape instability alternate with periods of soil formation. In other cases, both processes may occur at the same time. In hilly landscapes, for instance, convex settings may be prone to erosion, and sediments are displaced laterally downslope to concave settings where they settle (e.g., Heimsath et al., 2002). Luminescence dating has been widely applied to date such deposits (e.g., Fuchs and Lang, 2009). Soil mixing through ploughing has often been ignored in these studies, but agricultural use and in particular ploughing is likely to play an important role in inducing and/or enforcing erosion processes in such settings. Van der Meij et al. (2019) presented a novel approach combining OSL dating of deposits and historical information on plough depth to infer landscape evolution for an agricultural hilly setting in northeast Germany. OSL dating proved to be a powerful tool here, although advanced statistical methods were needed to unravel the different processes (lateral transport and vertical mixing).

In Section 4.3, Jan van Mourik describes the application of OSL dating to determine the timing of plaggen soil development in the southern Netherlands. Here, too, ploughing causes intense mixing up of the upper layer, and OSL ages inform when sediments are buried below this ploughed layer. This section is based on previous publications on the different sites (van Mourik et al., 2011, 2012a,b; Doorenbosch and van Mourik, 2016).

In Section 4.4, Tony Reimann describes novel applications of luminescence dating to determine soil mixing rate and soil mixing intensity. This section is based on detailed investigations of samples from a hillslope catena in Spain; the section summarizes the main findings from three recent publications resulting from those investigations (Reimann et al., 2017; Román-Sánchez et al., 2019a,b).

4.2 OSL dating of polycyclic palaeosols in driftsands: a case study from the LWM area near Hilversum, the Netherlands

4.2.1 Introduction

In the Netherlands, for a long time driftsands were supposed to be initiated by agricultural overexploitation of the Pleistocene sand landscapes during the Middle Ages, while earlier driftsand phases would be of very marginal importance, if occurring at all (see, e.g., Koster et al., 1993; Riksen et al., 2006; Koster, 2009; Jungerius and Riksen, 2010; Groenman-van Waateringe and Spek, 2016). The driftsand complexes regularly hold more-or-less complex podzolic palaeosols, reflecting alternating phases in stability and instability. A problem was that Podzols were considered to require relatively long periods of time to develop, as was, for example, concluded from the studies of Podzols in coversands or similar Pleistocene deposits (see Waterbolk, 1964), and this theory is still rather widely held (Groenewoudt, 2012; Jongmans et al., 2012; Groenman-van Waateringe and Spek, 2016). Therefore, at first sight, the occurrence of quite well-developed Podzols in driftsand complexes would point against a medieval or younger age of the sands concerned, and suggest an earlier start of sand drifting. An explanation was sought in the provenance of the driftsand: it would be mainly derived from the highly weathered and leached topsoils of earlier formed Podzols in Pleistocene aeolian sands, and thus be apt to fast podzolization (see, e.g., Dalsgaard and Odgaard, 2001). van Mourik et al. (2012a) and Wallinga et al. (2013) convincingly demonstrated that in such driftsands, podzolization may indeed proceed rapidly.

In earlier studies, when reliable dating techniques were not available, ages of driftsand phases and intercalated palaeosols often remained uncertain, but there was a strong tendency to assume that these were medieval or younger (see, for example, Koster, 2009). The conventional radiocarbon dating technique was unsuited for dating such phases, since radiocarbon dating of organic fractions from podzolic soils turned out to produce disputable results (e.g., Goh and Molloy, 1978; Geyh et al., 1983; Wallinga et al., 2013) and sequences rarely contained plant remains or charcoal of sufficient dimensions to allow for reliable conventional radiocarbon dating. Attempts to use soil organic matter fractions to obtain reliable datings (see, e.g., van Mourik et al., 1995) later on turned out to be rather unsuccessful (van Mourik et al., 2010).

The dating of driftsands greatly improved with the introduction of the OSL dating technique, while the AMS radiocarbon dating technique enhanced the possibilities for dating even minute charcoal and macroplant remains. Their application in studies of Dutch driftsands rapidly showed that these driftsands may have a far more complex history than earlier assumed (e.g., van Mourik et al., 2012a; Sevink et al., 2013) and that sand drifting started even before the Neolithic (Sevink et al., 2018). This is fully in line with recent archaeology-based studies on sand drifting (Willemse and Groenewoudt, 2012) and with studies in neighbouring countries (e.g., Tolksdorf and Kaiser, 2012; Nicolay et al., 2014), which described landscape instability leading to sand drifting to have already started during the Mesolithic. From the review by Pierik et al. (2018) it is now clear that, in the Netherlands, this history of sand drifting and polycyclic soil development stretches far back into the Holocene. The sequences may comprise

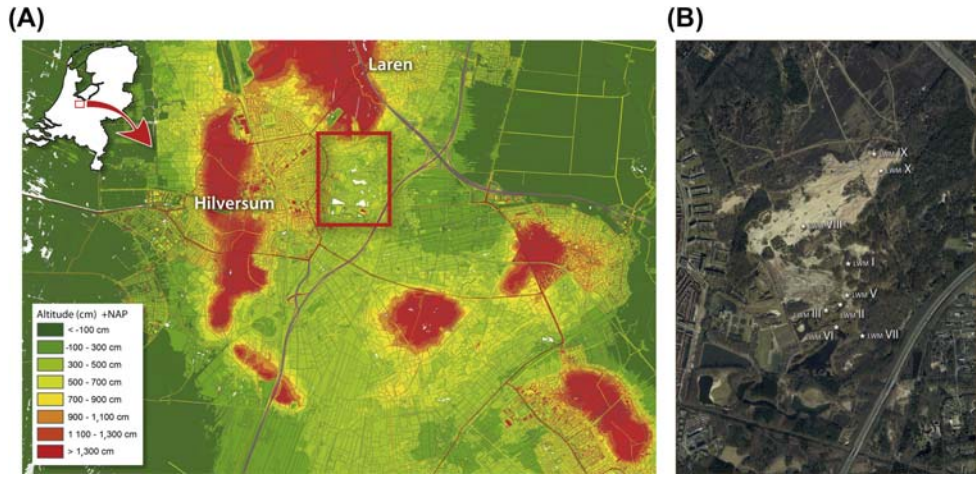

FIGURE 4.2.1 (A) Location of the Laarder Wasmeren (LWM) area; (B) location of the various sites within the LWM area. *NAP*, Normaal Amsterdams Peil or Dutch Ordnance Datum.

up to four phases of landscape stability with distinct Podzols, as was observed in the LWM area (Fig. 4.2.1). The studies performed in this area demonstrate the power of the OSL technique in unravelling the history of complex driftsand landscapes and are summarized in this chapter. Following a description of this area, general results, based on a combination of OSL and ^{14}C dating, and pollen analysis, are described. This is followed by a more in-depth discussion and description of the individual phases, with emphasis on the OSL dating results. Finally, some general conclusions are drawn regarding the use of OSL dating in studies of driftsand landscapes.

4.2.2 Study area and previous research

The LWM area near Hilversum, the Netherlands (52°13′30″N, 50°12′40″E), is a nature reserve with driftsands and several lakes that originally were fens or bogs. It is set in a large glacial meltwater valley, cut through the ice-pushed ridges of 'het Gooi' formed during the Saalian glaciation. The valley has a thick Late Pleistocene fill, topped by Late Weichselian coversands and Holocene driftsands. The area was heavily polluted as a result of long continued discharge of urban waste waters in the 20th century, which ultimately necessitated a large-scale soil remediation project that started in 2007 and was completed in 2011. The project involved the removal of heavily polluted sludge that occurred as a more-or-less continuous layer in the lakes and on the adjacent land surface, and as infill of an intricate network of ditches and canals (Sevink et al., 2008; Sevink, 2010). Upon its removal the underlying soils and sediments were exceptionally well exposed over large areas and to a considerable depth (up to 3 m), allowing for detailed observations on the complex of Late Weichselian and Holocene sandy deposits with often complex palaeosol sequences. Simultaneously, in the area to the north, over large tracts the existing forest vegetation was removed to reactivate driftsands, which also led to the exposure of large sections with some exceptional palaeosol sequences.

In this LWM area, Sevink et al. (2013, 2018) distinguished four Holocene inland driftsand phases, with often prominent Podzols that developed during intermediate phases of landscape stability. The earliest driftsand covers a podzolic palaeosol with common pine-derived

charcoal in Younger Coversand II, which in turn rests on a palaeosol in Younger Coversand I, which developed during the Allerød interstadial. The latter palaeosol is generally known as the Usselo layer (Van Geel et al., 1989) and is noted for the rather abundant occurrence of pine-derived charcoal and its incipient podzolization. Identification of the early palaeosol in the LWM area as the Usselo layer was based on its distinct cryoturbation, deviating granulometry (loamy layer) and prominent occurrence of pine-derived charcoal. The driftsand complex exhibits two lacustrine phases, of which the earlier results from a temporary high groundwater level around 3000 BCE and the later from stagnation on a Podzol that had become impervious over time and induced the formation of the fens, which still exist today. Lastly, abundant late medieval and early modern cart tracks were found, buried underneath driftsands from the latest phase.

The stratigraphy and chronology of this sequence was reconstructed using a combination of OSL dating of selected palaeosol sequences, AMS radiocarbon dating (particularly of charcoal contained in the early palaeosols), microfossil analysis and a detailed field study of a large series of sections. Analytical methods used in the quartz OSL dating of multigrain aliquots were extensively described in the papers by Sevink et al. (2013, 2018), to which reference is made for details. The same holds for the AMS ^{14}C dating, performed on samples pretreated using the standard acid-base-acid (Brock et al., 2010) extraction sequence. In a separate study, the reliability of such AMS dating of charcoal from these palaeosols was investigated, paying particular attention to the role of sample pretreatment (Wagner et al. 2018). Plant microfossil assemblages were studied to assess changes in vegetation over time and their relation to the phases of landscape instability (Sevink et al., 2013), while detailed palynological studies of some sections were published by Doorenbosch (2013).

4.2.3 Driftsands and palaeosols in the LWM area

During the Holocene, parts of the LWM area were deflated, while in other parts the deflated sand was deposited in the form of smaller or larger dunes. Overall trends are deflation in the southwest and deposition in the northeast. Some dunes in the northeast sector exhibit complex sequences of driftsands and intercalated palaeosols, which are best developed in the higher central part of these dunes and can be described as a complex of monogenetic palaeosols, i.e., more-or-less prominently developed Podzols, separated by distinct C horizons. The various phases laterally grade into more polygenetic sequences or even apparently monogenetic soils that seem to have developed in Pleistocene coversand. In the latter cases, it is often only in the Ah and E horizons that indications are found for the presence of more recent Holocene driftsand in these topsoil horizons.

The site LWM-X, in the northeastern part of the area, represents the most complex sequence of stacked Podzols separated by C horizons (Fig. 4.2.2). The Usselo layer is well developed, with a clearly cryoturbated incipient Podzol and a distinctly loamy topsoil, containing abundant pine-derived charcoal. It is overlain by a relatively thin sheet of Younger Coversand II (less than about 1 m) that in cross-section is wedge shaped. In this sheet a palaeosol was encountered, marked by a well-developed dark Ah horizon with bleached sand grains, a rather incipient E horizon and a distinct spodic Bs horizon. Characteristic for this soil is the abundant occurrence of charcoal, which appeared to largely consist of pine cone fragments, very much like the underlying Usselo layer.

In the central part of the dune, this podzolic palaeosol (Podzol 1) is abruptly overlain by a thick layer of aeolian sand in which a second, much more pronounced Podzol (Podzol 2) is developed. Its spodic horizon (Bh) does not reach Podzol 1. Toward the flanks of the dune,

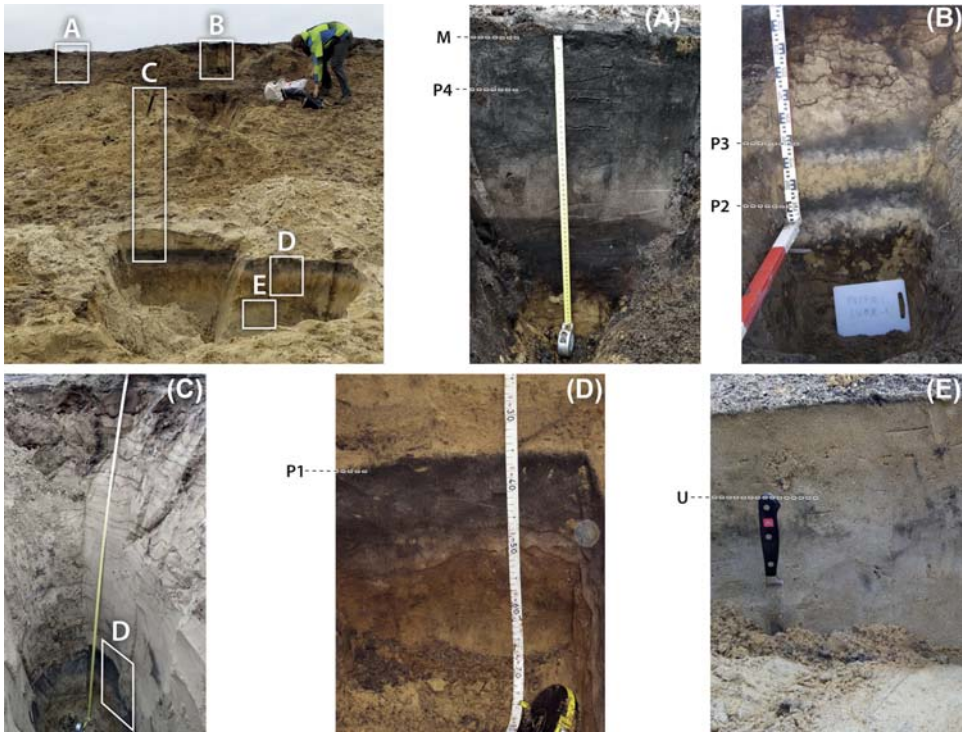

FIGURE 4.2.2 Palaeosols at LWM-X. Overviews (*left upper and lower*) and details (A, B, D, E). U = Usselo layer; P1 = Podzol 1; P2 = Podzol 2; P3 = Podzol 3; P4 = Podzol 4; M = Modern driftsand.

where this driftsand layer wedges out, the Podzols increasingly overlap and the upper boundary of Podzol 1 becomes irregular and more gradual, testifying that bioturbation linked to the pedogenesis that produced Podzol 2 reached into the top of the underlying palaeosol and Younger Coversand II. Podzol 3 is far less prominent and developed in a rather thin driftsand sheet, whereas Podzol 4 is strongly developed and the driftsand layer is thicker with a clearly distinguishable C horizon over Podzol 3. This Podzol 4 is partly buried by medieval to modern driftsands. In the northern outer flank of the dune the various Podzols merge into a single Podzol with its Ah and E horizons in a thin sheet of aeolian sand over a hard and thick spodic B in gravelly fluvioperiglacial deposits.

A more-or-less similar multiphase sequence was encountered in the mideastern part of the LWM area (LWM-II). The section is shown in Fig. 4.2.3 and strongly resembles LWM-X, though the various driftsand layers are thinner and the palaeosols are more overlapping. In this section, the lowest soil — Podzol 1 — is rather weakly developed, resembling Podzol 1 in section LWM-X. It is covered by a thin layer of driftsand, in which later podzolization merely led to the development of an Ah and prominent E horizon (Podzol 2), thus producing a distinctly polygenetic complex Podzol with two stacked Ah and E sequences. Podzol 3 is also rather weakly developed — as in LWM-X — and is buried underneath driftsand with a very strongly developed Podzol 4. Its topsoil was marked by cart tracks and, like the section

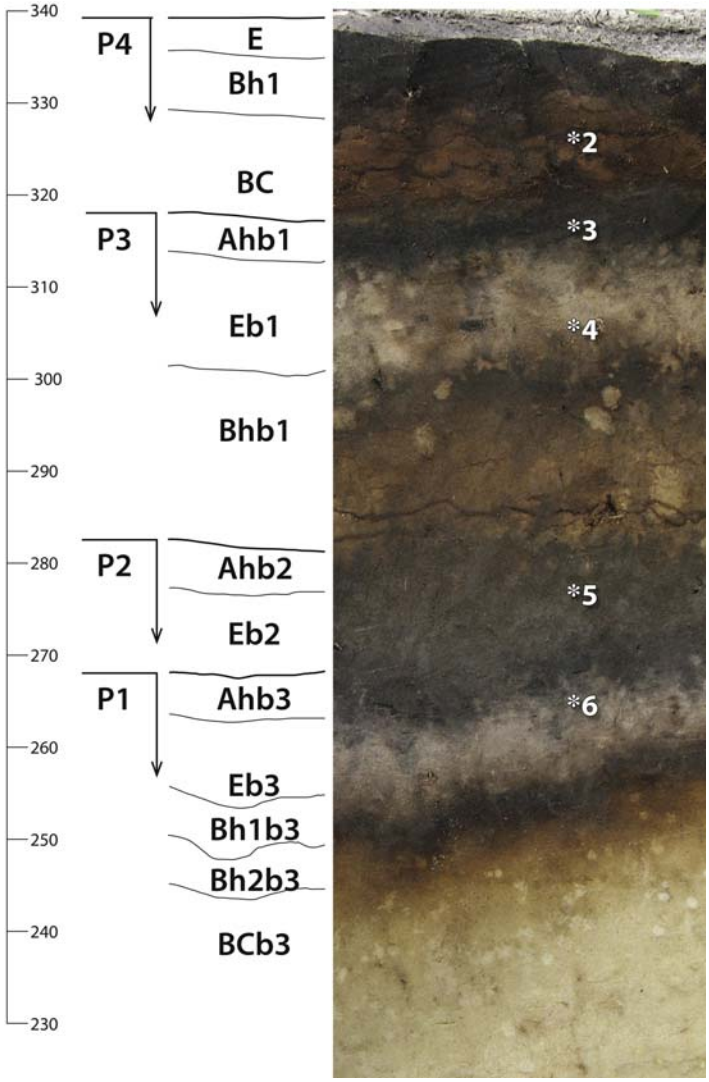

FIGURE 4.2.3 Palaeosols at LWM-II with soil horizons and elevation over Dutch Ordnance Datum in cm. P1 = Podzol 1; P 2 = Podzol 2; P3 = Podzol 3; P4 = Podzol 4. Locations of OSL samples are indicated with an *.

LWM-X, was partly covered by medieval and recent driftsands.

Complex sequences like LWM-X and LWM-II are relatively rare and in most exposures a lesser number of palaeosols and driftsand phases were observed: commonly, two pronounced Podzols (Fig. 4.2.4). Generally, the stratigraphies are too fragmented to allow for reliable correlation of individual palaeosols and driftsands with one or more of the phases distinguished in the complex stratigraphies observed at the sites LWM-X and -II. However, some of these have features allowing for tentative attribution, examples of which are given later.

FIGURE 4.2.4 Characteristic double Podzol in a trench.

LWM-I is a large exposure with a very strongly developed, presumably polygenetic, Podzol covering an incipient Podzol (Fig. 4.2.5). The latter soil contains abundant charcoal, dominantly composed of pine cone scales. It resembles Podzol 1 at LWM-X and differs from the Usselo layer in that it does not show any sign of cryoturbation, nor is it loamy. This is in contrast with LWM-VIII (Fig. 4.2.6), which also holds charcoal but exhibits clear cryoturbation and has a distinctly loamy Ah horizon. Correlations of the Late Pleistocene and Early Holocene palaeosols based on similarity in sedimentological characteristics are obvious, but remain tentative, as will be illustrated by the description of the characteristics and presumed age of the various phases distinguished, which is the topic of the next section. In that section, less attention is paid to LWM-X, since that major sequence was found relatively recently and dating results are not yet available.

4.2.4 Palaeosols, driftsands and other landscape genetic phases: characteristics and age

The chronologies in this section are largely based on OSL and radiocarbon ages presented in Table 4.2.1 and 4.2.2, respectively.

4.2.4.1 Usselo layer and early Holocene palaeosols

As described before, palaeosols holding abundant carbonized pine cone scales are common in the LWM area. The Usselo layer in addition exhibits distinct cryoturbation, evidencing its Pleistocene age. The identification of a specific palaeosol as an Usselo layer is based on these characteristics, as well as its overall stratigraphic position. Remarkably, our absolute dates for the presumed Usselo layer that we encountered is not fully consistent: the age obtained for charcoal from the distinctly cryoturbated LWM-VIII was 12,670−12,420 calBP, whereas the OSL dates were 11.5 ± 0.7 ka for the E horizon (below the charcoal-containing Ah horizon) and 11.2 ± 0.7 ka for the sand above this Ah horizon, respectively. Our ^{14}C age is very much in line with ages found for charcoal in other Usselo layers (see van Hoesel et al., 2012) and truly confirms the identification of this palaeosol as the Usselo layer. The apparent offset between the ^{14}C and OSL data is somewhat problematic, but might be explained by a later onset of aeolian activity leading to the deposition of the Younger Coversand II (see, e.g., Bateman and Van Huissteden, 1999), eventually preceded by some bioturbation, explaining the slightly younger age of the top of the Younger Coversand II, relative to the ^{14}C age of the Ah horizon. Alternatively, it could be argued that the OSL and ^{14}C evidence is not in conflict, because the 2-sigma uncertainty ranges overlap. The 95% confidence interval for OSL ages extends back to 12.9 and 12.6 ka, respectively, in agreement with the ^{14}C results.

As to Podzol 1, the situation is more complex. At LWM-II the top of Podzol 1 is OSL dated at

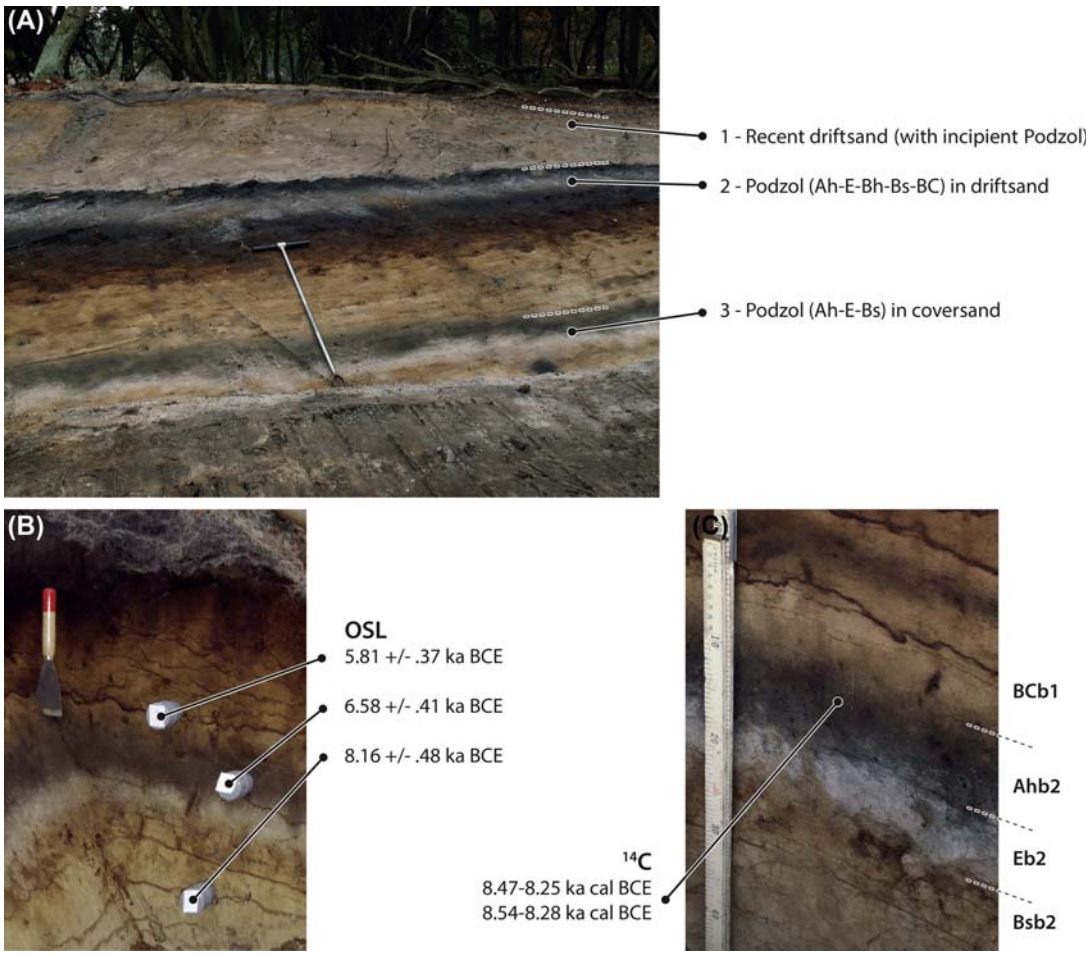

FIGURE 4.2.5 (A) Palaeosols at LWM-I; (B) lower palaeosol with locations of optically stimulated luminescence samples; (C) location of ^{14}C samples.

8.8 ± 0.4 ka. Since the sample is from the top of the palaeosol, which exhibits distinct bioturbation, this age has to be considered as the 'time of burial'. In other words, it reflects the time at which the driftsand covering this palaeosol was deposited, thereby setting a terminus ante quem for the genesis of Podzol 1. At LWM-I, charcoal in the lower Podzol was extensively studied for the impact of sample pretreatment on ages obtained by ^{14}C dating (Wagner et al., 2018), resulting in very precise dating of this charcoal (pine cone scales): roughly around 10.3 ± 0.1 ka calBP. This is in excellent agreement with the OSL age obtained on the C horizon; the sand in which the Podzol is developed (10.2 ± 0.5 ka). However, the Ah horizon gave an OSL age of 8.6 ± 0.4 ka, which is nearly 2 ka later than the age obtained for the charcoal. Moreover, driftsand covering the Ah horizon was OSL dated at 7.8 ± 0.4 ka (Fig. 4.2.5).

Though the OSL dates for the topsoils at LWM-1 and LWM-II are nearly identical, there

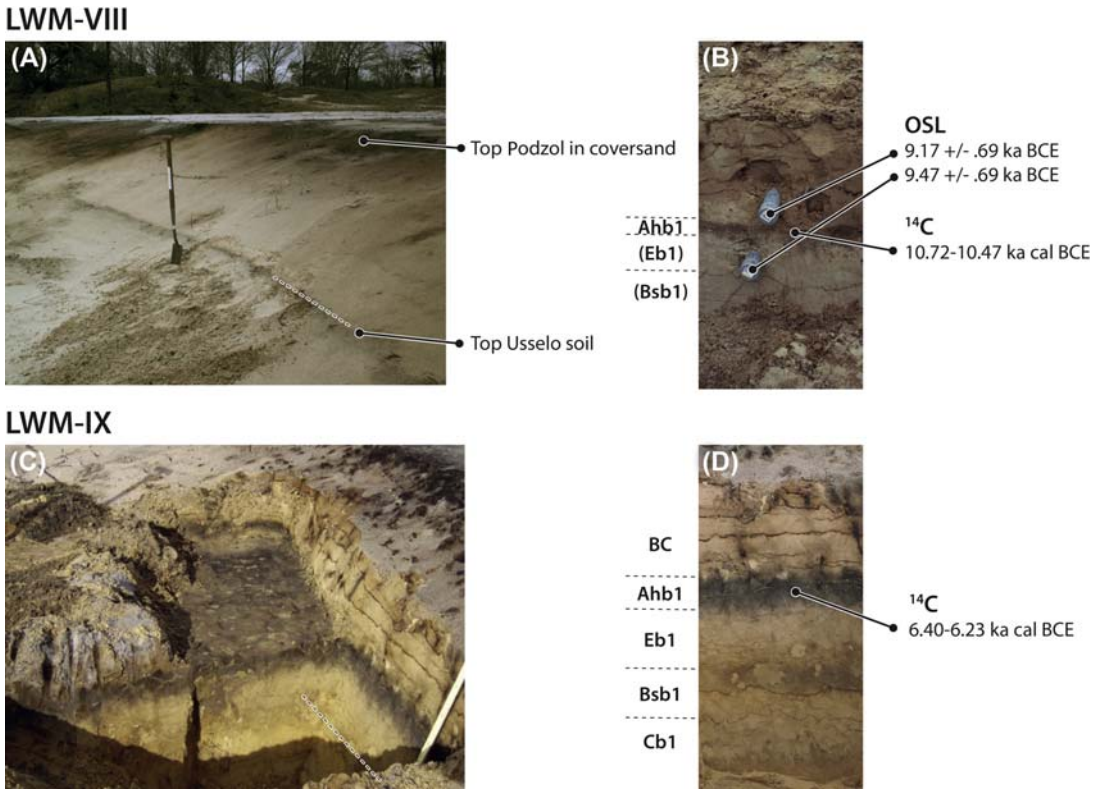

FIGURE 4.2.6 LWM-VIII (A and B) and LWM-IX (C and D): overviews and profiles with location of samples and ages.

are doubts whether the date for LWM-I truly represents the time at which the palaeosol was buried. The abundant pine cone scales in the topsoil are extremely well conserved and lack any sign of post-formational transport. It is highly improbable that these fragile charred scales were exposed to soil formation over prolonged periods of time, i.e., nearly 2 ka. An explanation may be found in bioturbation following deposition of the overlying driftsand, as suggested by the upward decline in OSL age of this sand, but also by the common presence of animal burrows (probably insects) that reach down from the strongly developed Podzol above into the lower Podzol (Fig. 4.2.5). Brussaard and Runa (1984), for example, described bioturbation by scarab beetles, reaching a depth of 1 m in Podzols developed in Pleistocene aeolian sands and assume a mainly Preboreal and post-Atlantic age for this disturbance.

That the time at which the early Holocene Podzols were buried under driftsands may indeed vary within the LWM area, reflecting spatial and temporal variations in landscape instability, is further supported by data from another site − LWM-IX − where a similar Podzol, also containing abundant pine charcoal, was observed (Fig. 4.2.6). This charcoal was dated at 8348−8180 calBP. Evidently, in the area concerned, forest fires repeatedly occurred (see also Sevink et al., 2018), but this ^{14}C dating also sets a terminus post quem for the later driftsand, which is clearly younger than at the sites LWM-I and -II.

TABLE 4.2.1 Quartz optically stimulated luminescence ages obtained on Laarder Wasmeren (LWM) samples.

Sample	NCL code	Location		Depth (m)	Palaeo-dose (Gy)	Overdis-persion (%)[a]	Age model[b]	Dose rate (Gy/ka)	Water content (weight%)	Organic content (weight%)	Age		
		x	y								(ka)	(BCE (−)/CE)	Validity
LWM-I-3	NCL-7309040	521,339	51259	1.03	7.59 ± 0.27	15 ± 2	CAM	0.97 ± 0.03	9.4 ± 2.3	1.6 ± 0.3	7.82 ± 0.37	−5812 ± 374	Ok
LWM-I-2	NCL-7309039	521,339	51259	1.13	8.30 ± 0.30	16 ± 2	CAM	0.97 ± 0.03	8.1 ± 2.0	1.0 ± 0.2	8.59 ± 0.41	−6586 ± 413	Ok
LWM-I-1	NCL-7309038	521,339	51259	1.38	10.0 ± 0.3	14 ± 2	CAM	0.99 ± 0.03	12.1 ± 3.0	0.6 ± 0.1	10.2 ± 0.5	−8162 ± 479	Ok
LWM-II-2	NCL-7208034	143,227	470,811	0.35	5.03 ± 0.17	15 ± 2	CAM	1.04 ± 0.03	6.5 ± 1.6	2.3 ± 0.5	4.85 ± 0.22	−2838 ± 224	Ok
LWM-II-3	NCL-7208035	143,227	470,811	0.45	5.45 ± 0.28	22 ± 3	CAM	0.94 ± 0.03	7.6 ± 1.9	2.8 ± 0.6	5.78 ± 0.35	−3774 ± 349	Questionable
LWM-II-4	NCL-7208036	143,227	470,811	0.55	6.01 ± 0.21	13 ± 2	CAM	1.03 ± 0.03	7.4 ± 1.9	1.0 ± 0.2	5.84 ± 0.28	−3831 ± 277	Ok
LWM-II-5	NCL-7208037	143,227	470,811	0.73	6.06 ± 0.26	20 ± 3	CAM	0.94 ± 0.03	5.0 ± 1.3	1.5 ± 0.3	6.48 ± 0.35	−4470 ± 350	Ok
LWM-II-6	NCL-7208038	143,227	470,811	0.83	8.36 ± 0.24	13 ± 2	CAM	0.95 ± 0.03	8.7 ± 2.2	0.8 ± 0.2	8.82 ± 0.38	−6812 ± 383	Ok
LWM-III-9	NCL-7308046	143,165	470,780	0.40	4.88 ± 0.19	16 ± 3	CAM	0.93 ± 0.03	10.0 ± 2.5	0.5 ± 0.1	5.23 ± 0.27	−3220 ± 268	Ok
LWM-III-10	NCL-7308047	143,165	470,780	0.48	4.73 ± 0.17	14 ± 2	CAM	0.95 ± 0.03	10.0 ± 2.5	0.4 ± 0.1	4.97 ± 0.24	−2966 ± 241	Ok
LWM-III-11	NCL-7308048	143,165	470,780	0.60	4.93 ± 0.16	14 ± 2	CAM	0.98 ± 0.03	10.0 ± 2.5	0.5 ± 0.1	5.04 ± 0.23	−3036 ± 233	Ok
LWM-III-12	NCL-7308049	143,165	470,780	0.75	4.75 ± 0.19	16 ± 2	CAM	0.84 ± 0.03	13.5 ± 3.4	0.6 ± 0.1	5.66 ± 0.30	−3655 ± 303	Ok
LWM-III-13	NCL-7308050	143,165	470,780	0.95	10.0 ± 0.5	26 ± 3	CAM	0.88 ± 0.03	18.2 ± 4.5	1.3 ± 0.3	11.4 ± 0.7	−9368 ± 688	Questionable
LWM-V-1	NCL-7208043	143,296	470,874	0.45	5.23 ± 0.18	15 ± 2	CAM	0.99 ± 0.03	5.0 ± 1.3	0.9 ± 0.2	5.30 ± 0.23	−3290 ± 235	Ok
LWM-V-2	NCL-7208044	143,296	470,874	0.70	6.26 ± 0.23	14 ± 2	CAM	0.98 ± 0.03	5.0 ± 1.3	1.2 ± 0.2	6.37 ± 0.31	−4357 ± 306	Ok
LWM-VI-15	NCL-7408052	143,317	470,770	0.15	0.11 ± 0.02	40 ± 8	BS MAM	0.70 ± 0.03	19.2 ± 4.8	2.2 ± 0.4	0.16 ± 0.03	1843 ± 32	Likely ok
LWM-VI-16	NCL-7408053	143,317	470,770	0.15	0.12 ± 0.01	38 ± 10	BS MAM	0.65 ± 0.03	28.9 ± 7.2	3.1 ± 0.6	0.19 ± 0.02	1820 ± 22	Likely Ok
LWM-VII-18	NCL-7408058	143,453	470,588	0.50	0.57 ± 0.04	42 ± 7	BS MAM	0.92 ± 0.03	10.4 ± 2.6	3.3 ± 0.7	0.62 ± 0.04	1391 ± 44	Questionable
LWM-VII-19	NCL-7408059	143,453	470,588	0.65	1.85 ± 0.07	16 ± 2	CAM	0.78 ± 0.03	10.0 ± 2.5	0.7 ± 0.1	2.37 ± 0.12	−362 ± 119	Ok
LWM-VII-20	NCL-7408060	143,453	470,588	0.80	5.67 ± 0.21	17 ± 2	CAM	0.86 ± 0.04	23.4 ± 5.9	4.2 ± 0.8	6.61 ± 0.37	−4606 ± 371	Ok
LWM-VIII-1	NCL-7511085	143,102	471,340	0.55	11.3 ± 0.6	20 ± 2	CAM	1.01 ± 0.04	8.0 ± 4.0	0.5 ± 0.1	11.2 ± 0.7	−9168 ± 690	Ok
LWM-VIII-2	NCL-7511086	143,102	471,340	0.75	12.0 ± 0.5	19 ± 3	CAM	1.04 ± 0.04	15.0 ± 5.0	0.4 ± 0.1	11.5 ± 0.7	−9468 ± 690	Ok

BCE, Before Common Era; *CE*, Common Era; *NCL*, Netherlands Centre for Luminescence dating.

[a] *Overdispersion was obtained through the Central Age Model (CAM) (Galbraith et al., 1999), after iterative removal of equivalent doses outside 3 standard deviations from the sample mean.*

[b] *CAM refers to Central Age Model (Galbraith et al., 1999), after removal of outliers (see footnote a).* BS MAM refers to the bootstrapped Minimum Age Model (Cunningham and Wallinga, 2012), using a sigmab of 14.9 ± 0.4 determined using the approach of Chamberlain et al. (2018).

TABLE 4.2.2 Radiocarbon ages obtained on Laarder Wasmeren (LWM) samples.

Sample	GrA number	Age BP	Sigma	% C	$\delta^{13}C$ PDB	Age cal. BP	Age cal.
LWM-1-Ah	39939	9305	35	57.2	−25.10	10,647–10,305	8698–8356 BCE
LWM-1-E	39954	9670	45	58.5	−25.28	11,207–10,792	9258–8843 BCE
LWM-1-Bs	39940	9260	35	52.5	−24.92	10,556–10,296	8607–8347 BCE
LWM-1a.ps	61960	9120	50	59.6	−25.23	10,418–10,197	8469–8248 BCE
LWM-1b.ps	61959	9155	50	61.8	−24.29	10,486–10,227	8537–8278 BCE
LWM-VII	47532	2030	40	n.a.	n.a.	2,113–1,894	164 BCE–57 CE
LWM-VIII	49935	10,575	50	59.7	−25.93	12,670–12,420	10,721–10,471 BCE
LWM-IX	45652	7435	40	67.3	−25.90	8,348–8,180	6399–6231 BCE

BCE, Before Common Era; *BP*, Before Present; *cal*, calibrated; *calBP*, calibrated years before the present; *CE*, Common Era; *n.a.*, not available; *PBD*, Pee Dee Belemnite.

4.2.4.2 Podzols 2, 3 and 4, and related driftsands

Correlations of these palaeosols and intercalated driftsands seem to be more straightforward than those for the earlier palaeosols. In LWM-II the top of Podzol 2 was OSL dated at 6.5 ± 0.4 ka and a similar age − 6.4 ka ± 0.3 ka − was found in another sequence (LWM-V, Fig. 4.2.7), setting its burial at around 6.5 ka ago or slightly younger. Dating the driftsand in which Podzol 2 developed, which is the first driftsand phase that can be distinguished, is more problematic. At LWM-II it postdates Podzol 1 (c.8.8 ka) and at LWM-I its lower age is not clear, since its onset may range between c.8.6 and c.10 ka (see earlier). OSL dating of driftsands from the recently found site LWM-X will most likely provide further detailed information on its age. At this site it occurs as a distinct dune of which only the upper part is affected by soil formation (Fig. 4.2.2), allowing for more precise OSL dating of its deposition.

Podzol 3 is a weakly developed palaeosol that was only encountered at LWM-II and LWM-X. At LWM-II its top was dated at 5.8 ± 0.4 ka (Ah horizon), suggesting that it was buried by driftsand shortly thereafter. This is in line with the OSL date for the base of the aeolian sands that were deposited in a lacustrine environment at the nearby site LWM-III, which is 5.7 ± 0.3 ka (see sample 12, Fig. 4.2.8 and Table 4.2.1). Driftsand deposition (phase 2), which is of limited magnitude (see both sections LWM-II and -X), and soil development together would cover a period of 0.7 ka or slightly less, based on OSL dating. Such short period is in line with the presumed fast podzolization in pre-weathered driftsands.

Podzol 4 is a prominent Podzol, developed after the next phase of driftsand (phase 3), and is encountered throughout the area. The driftsand was deposited from about 5.5 ka onward. Evidence thereof consists of the OSL dating of various sections: LWM-II, -III and -V. At LWM-II the underlying Podzol 3 was buried around 5.8 ka and the OSL date at limited distance above this boundary was 4.9 ± 0.2 ka, and at LWM-V an OSL date of 5.3 ± 0.2 ka was obtained for the basal part of this driftsand. At LWM-III, the earliest part of this phase dated to c.5.7 ka when driftsand was deposited in a shallow lake, filling in this lake. Deposition continued until about 5.0 ka and reached a thickness of about 1 m, as in the other sections.

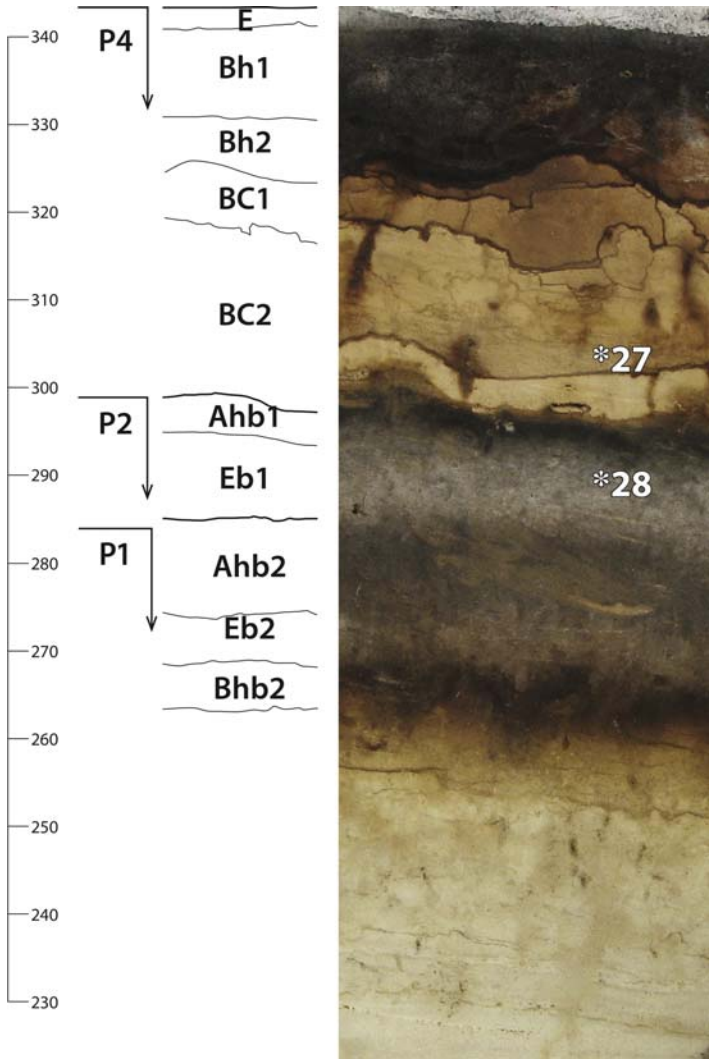

FIGURE 4.2.7 LWM-V: Podzols, soil horizons and location of optically stimulated luminescence samples.

4.2.4.3 *Recent driftsand*

The age of the recent driftsands might conform to the earlier general concept of the origin of driftsands, i.e., medieval or more recent, but here too the situation appears to be more complex. Cart tracks are common in the LWM site and generally consist of multiphase tracks that were successively filled with driftsand, composed of deflated Ah and E horizons. The occurrence of these tracks is of particular interest because ancient transport paths are often described as a major cause for the generation of driftsands (Pierik et al., 2018). An example of such tracks is given in Fig. 4.2.9. One of these fills (Fig. 4.2.9A, LWM-VI) was dated by OSL to respectively 0.16 ± 0.03 and 0.19 ± 0.02 ka, which might point to a relatively late date for these tracks and potentially associated drift-sands. However, the cart tracks were

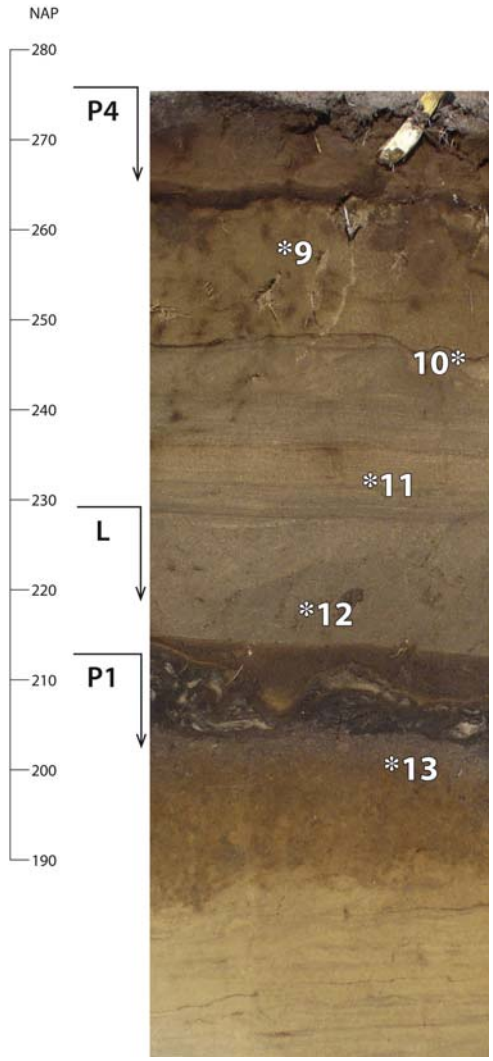

FIGURE 4.2.8 LWM-III, with lacustrine sediment (L), overlying a palaeosol (P1) in Younger Coversand II exhibiting heavy load casting. The transition from lacustrine to aeolian sands is at ±230 cm. Locations of optically stimulated luminescence samples are indicated with an *.

also found to run along the Groot Wasmeer and to disappear underneath driftsands that, along its southern border, had been blown into the fen and became intercalated in more-or-less peaty layers that formed in the fen (Fig. 4.2.9B). In this border zone, section LWM-VII was studied (Fig. 4.2.10). The aeolian sand, blown into the lake and covering a pronounced stagnative Podzol at its base, provided an OSL age of 2.4 ± 0.1 ka (363 ± 119 BCE). Higher up in the sequence, an OSL date was found of 0.62 ± 0.04 ka (1391 ± 44 CE), while AMS ^{14}C dating of the intermediate peat layer resulted in an age of 20 ± 40 BCE. Upward, the driftsand graded into the characteristic yellowish driftsand that to the south of the Groot Wasmeer today forms a pronounced dune landscape, with active sand drifting until the last century. The cart track in the southern border zone ran at the medieval level, which would be in line with the known age of the early roads and tracks in the area. Interestingly, the base of the driftsand, blown into the lake, is of considerably earlier age (2.4 ± 0.1 ka), which in historical terms is even Pre-Roman. The presumed recent sand drifting in fact thus already started in Pre-Roman times, as was also found in nearby fens (Monnikenberg; Sevink et al., 2017).

4.2.5 General conclusions

Due to the excellent visibility of the driftsands and their palaeosols, and through the ample application of OSL dating, we were able to establish that the LWM area holds a multiphased complex of Holocene inland driftsands and podzolic palaeosols that already started in the Early Holocene. Thus far this seems to be rather unique for the Netherlands (see Pierik et al., 2018). Whether it is truly unique is not yet clear, since several other recent studies suggest a far wider occurrence of early driftsands and associated palaeosols (see, e.g., van Mourik et al., 2012a,b). This would be fully in line with studies from adjacent countries (Tolksdorf and Kaiser, 2012; Nicolay et al., 2014; Baker et al., 2013), where such multiphased complexes are fairly common.

The often prominent podzolisation exhibited by the Holocene palaeosols studied is striking and evidences the low acid neutralizing capacity of these inland driftsands and their associated

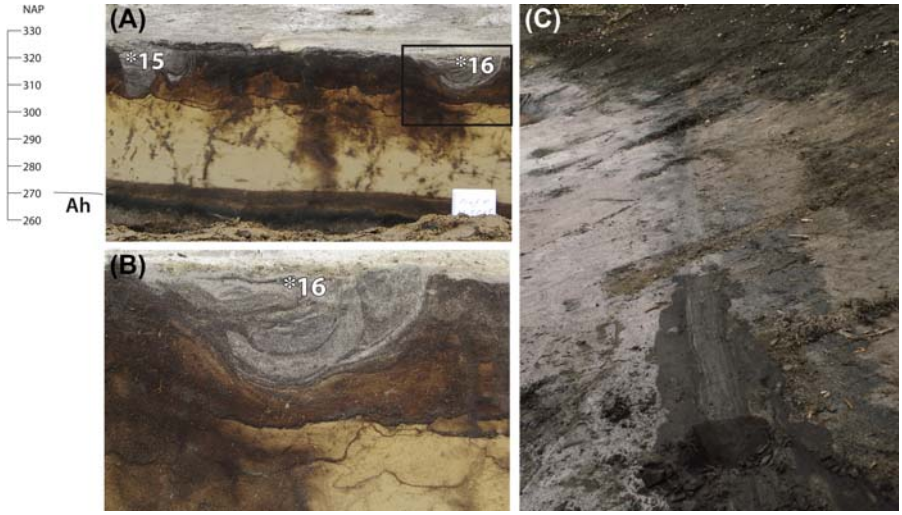

FIGURE 4.2.9 Cart tracks and location of optically stimulated luminescence samples at site LWM-VI (A and B) and cart track in the border zone of the Groot Wasmeer, buried by later driftsand (C).

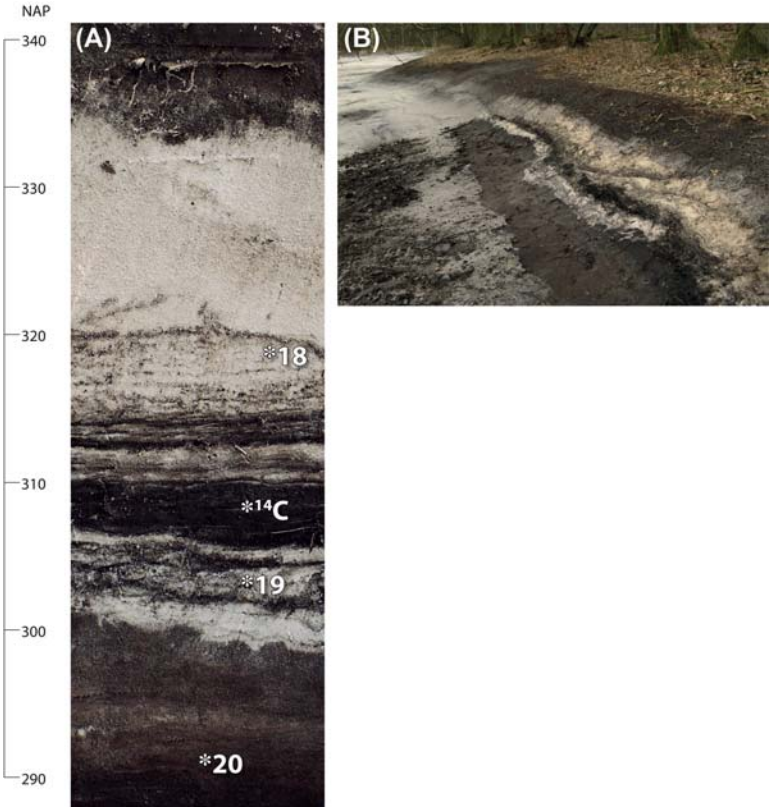

FIGURE 4.2.10 Sections in the southern border zone of the Groot Wasmeer, with a strongly developed Podzol, buried underneath lacustrine deposits (at c.300 cm + Dutch Ordnance Datum (NAP)) and driftsand (at 320 cm), respectively. * = location of optically stimulated luminescence samples; *^{14}C = location of ^{14}C sample.

rapid leaching and acidification, required for podzolization to occur (Van der Salm and Verstraten, 1994). However, it is also evident that for distinct Podzols to develop in driftsand that was not pre-weathered and leached, and of which individual grains were still coated by iron–clay complexes (see, for example, LWM-X), indeed significant time is required. This is fully in line with recent OSL-based studies on soil development rates in similar materials (Nielsen et al., 2010) and illustrates the important role of the driftsand characteristics, i.e., the extent to which they have been pre-weathered during earlier soil-forming phases.

The Younger Coversand II encountered in the LWM area is a typical example of the aeolian sands deposited during the Younger Dryas in the Netherlands, which in terms of their mineralogy have a rather uniform composition, with only slight local and regional variation in their content of weatherable minerals, which overall is very low (e.g., Crommelin, 1964; Sevink et al., 2017). Therefore our results additionally demonstrate that the concept of Dutch Podzols having only been formed upon replacement of forest by heathland as a result of human impacts, notably the introduction of agriculture during the Neolithic (see, e.g., Jongmans et al. 2012; Groenman-van Wateringe and Spek, 2016), is outdated. This hypothesis may hold for substrates such as the Pre-Saalian so-called 'brown sands' of the ice-pushed ridges and similar fluvial sediments that hold somewhat higher amounts of weatherable minerals, but certainly not for the quartzitic aeolian sands, which cover a large part of the Netherlands. Lastly, from the plant macrofossil study it appeared that heathlands already existed long before the introduction of agriculture (Sevink et al., 2013, 2017; Doorenbosch, 2013), which is in line with results from several recent studies elsewhere in the Netherlands (e.g., Hamburg et al. 2012; Doorenbosch and van Mourik, 2016).

The multigrain quartz OSL technique formed an important tool in unravelling the complex history of the area, but some of its limitations were clearly seen. Ideally, OSL ages obtained reflect the 'time of deposition', presuming that a specific driftsand layer was rapidly buried under newly deposited aeolian sand. This was the case in LWM-III and -VII (lacustrine sands), and also in LWM-X (the driftsand of phase 1, underneath Podzol 2). However, soil formation often goes together with bioturbation, which may even occur after deposition of a thin layer of driftsand and affect the palaeosol in the underlying, next older driftsand phase. OSL ages obtained on topsoils in such cases will reflect 'time of burial' rather than 'time of deposition'. Information on bioturbation in Podzols is scant and largely1 limited to scarab beetle activity (Brussaard and Runia, 1984). Tree uprooting is also sometimes mentioned as a possible cause for bioturbation, but this phenomenon is even less well studied (e.g., Schaetzl et al., 1990; Šamonil et al., 2010). In our study it is often not clear to what extent bioturbation controls the OSL age, and additional reliable AMS dating would be needed to assess its role. Typical examples of such situations are the Early Holocene soil in LWM-I and the various phases in LWM-II.

'Reliable' AMS dating requires the presence of plant macro remains or charcoal, which rarely occur in the more recent Mid- to Late Holocene Podzols (see Section 4.3). An alternative might be offered by single-grain OSL, presuming that this technique allows for 'filtering out' of the effect of bioturbation (see Section 4.4). The driftsand and palaeosol complex of the LWM area offers excellent opportunities for testing this method.

4.3 OSL dating of plaggic Anthrosols

4.3.1 Introduction

Plaggic Anthrosols (soil classification according to ISRIC-FAO, 2006) occur in cultural landscapes, developed on coversands, Late Glacial

aeolian chemically barren sand deposits. The development of these soils is closely connected with historical land management, thus providing interesting soil archives for archaeologists, historical geographers, geomorphologists and soil scientists. Plaggic Anthrosols developed in areas where heath sods were used as stable filling, mixed with cattle dung and then used to fertilize arable land. Application of this material on the fields for centuries resulted in elevated fields with thick organic-rich A horizons and excellent soil properties. This land use system was practised until the late 19th century, when chemical fertilizers became available.

The distribution area of plaggic Anthrosols in northwestern Europe is indicated in Fig. 4.3.1. The first map of the distribution of plaggic agriculture in northwestern Europe was published by Pape (1972). Bastiaens and van Mourik (1994) found traces of intensification and extension of this area in Vlaanderen (Belgium). van Mourik (1991) reported plaggic Anthrosols in Schleswig-Holstein (Germany). Beside the area with 'real' plaggic Anthrosols, Spek (2004, p. 724) summarized information on the occurrence of soils with some evidence of the application of plaggic manure in the Atlantic coastal zones of Norway, Denmark, France, Spain, Scotland and Ireland.

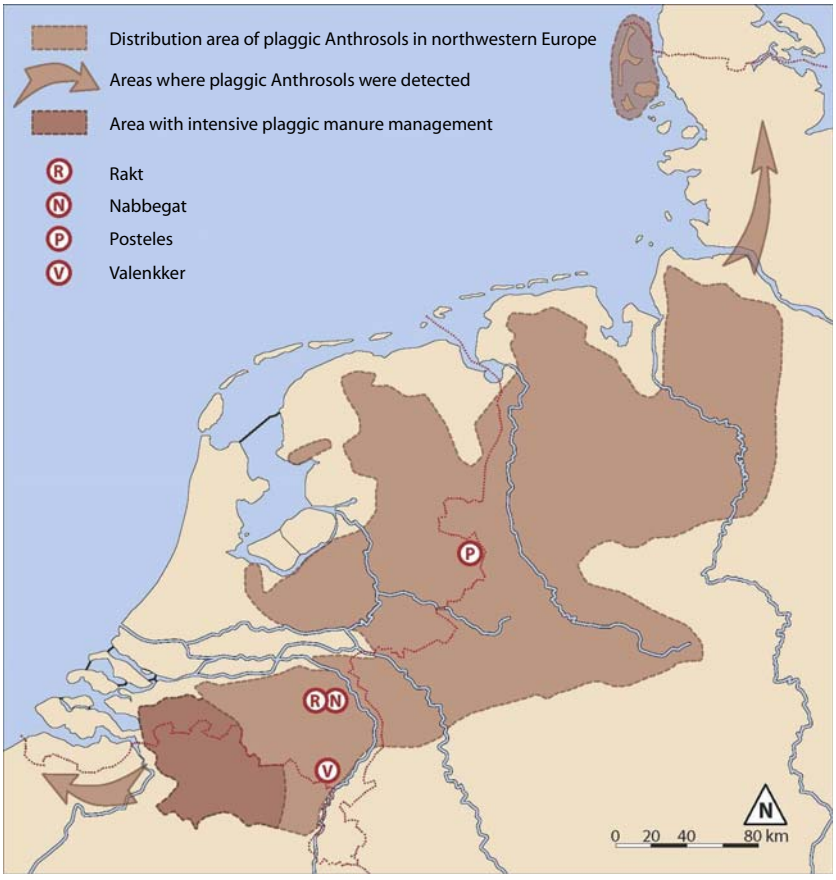

FIGURE 4.3.1 Distribution area of the plaggic agriculture in northwestern Europe according to Pape (1974). The locations of the profiles, sampled for optically stimulated luminescence dating, are indicated: Valenakker, Nabbegat, Rakt and Posteles.

Here we illustrate how OSL dating can provide insight into the development of plaggic Anthrosols. We build on results obtained from four plaggic Anthrosols in the Netherlands with an undisturbed plaggic horizon: Valenakker, Nabbegat, Rakt and Posteles (Fig. 4.3.1). These profiles were previously investigated using a range of conventional methods and by OSL dating. In subsequent sections we present details on results obtained on each of the profiles, including references to the original publications. Prior to that we briefly describe the Holocene evolution of Dutch coversand landscapes, the development of plaggic Anthrosols and the OSL methods used.

4.3.2 The Dutch coversand landscape and plaggic Anthrosols

Fig. 4.3.2 shows a simplified pollen diagram of the Late Glacial and Holocene vegetation development of Pleistocene Netherlands according to Janssen (1974). During the Late Glacial, a steppe vegetation with scattered trees (*Betula* and *Pinus*) colonized and stabilized the coversands. After the Preboreal, *Betula* and *Pinus* were displaced by deciduous forest and during the Atlantic the region was covered by forest. Around 5000 BP, humans entered the region and due to silvopastoralism and shifting cultivation the forest degraded and extension of the heath was started. Heaths have played a role in ancestral communities since the Late Neolithic (Doorenbosch and van Mourik, 2016). Traces of sedentary agriculture (like Celtic fields) have been found in soil archives from around 3000 BP (Spek, 2004, p. 146–148; Jansen and van der Laan, 2011). Logging of trees (particularly *Quercus*) for the production of charcoal, necessary for the melting of iron, started in the Iron Age but accelerated in Early Medieval times due to intensification of iron production (Laban et al., 1988; Beukenkamp and Sevink, 2005). During the 11th–13th centuries the remaining forests were logged for the exportation of timber to rich Flemish cities (Vera, 2011).

Increased population pressure, with associated deforestation and extending road networks,

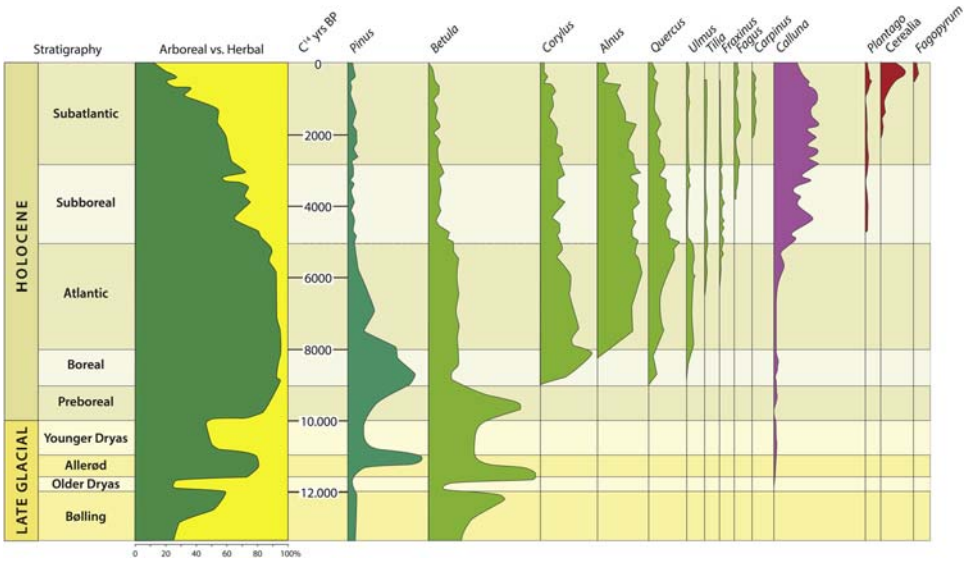

FIGURE 4.3.2 Simplified pollen diagram of Late Glacial and Holocene vegetation development in Pleistocene Netherlands according to Janssen (1974).

caused the first regional extension of sand drifting around 900 CE (Pierik et al., 2018). After the Middle Ages a deforested landscape remained with extended heaths and driftsands. On the Pleistocene sands, plaggic agriculture became the dominant form of land use. This form of sedentary agriculture created a landscape consisting of arable fields in the vicinity of hamlets and extensive heaths, used for shepherding and the production of stable manure, needed as fertilizer for the crop fields. It was assumed that the surface level of the fields was raised due to the mineral fraction in the manure, originating from sods, dug on the heaths. Around 8–10 ha heathland was required for the production of plaggic manure for 1 ha arable land (Pape, 1972). The heaths reached their maximal extension around 1850 CE (Smits and Noordijk, 2013; Fig. 2.5.1). Afterward the plaggic agriculture ended due to the invention of chemical fertilizers at the end of the 19th century, allowing transformation of heaths into agricultural areas. A substantial part of the plaggic Anthrosols disappeared during the 20th century by agricultural modernization and urban expansion. However, at some sites the soil archives of plaggic Anthrosols remained quite undamaged and such sites have been used for archaeological and geoecological research.

Archeological research demonstrated that plaggic horizons show some pollen stratification and can be rich in ceramics and other finds that can be used for dating (van der Hammen, 1965,; Bakels, 1988). Palaeopedological studies of plaggic Anthrosols in the Netherlands (van Mourik and Ligtendag, 1984; Mücher et al., 1989) unlocked information from the archives through soil pollen analysis.

Several types of stable fillings have been used such as litter from forest soils, sods from grasslands and heaths and straw from crop species (van Mourik et al., 2016).

The use of litter from forest soils as stable filling must have been strongly reduced in the 11–13th centuries because of commercial logging, as recorded in archived documents (Vera, 2011). This deforestation caused sand drifting and the farmers and shepherds had to protect their valuable heaths against this 'historical environmental catastrophe', as recorded in historical documents of the Belgium Kempen and the Dutch Campina (Burny, 1999; van Mourik, 1987, 1988; de Keyzer, 2014).

In the course of the 18th century, population growth resulted in increasing food demand and a deep stable economy was introduced (Vera, 2011). Better material became available to construct deeper and bigger stables and resulted in the intensification of manure production and farmers starting to use heath sods as (additional) stable filling (Spek, 2004). This caused heath degradation and initiated the second regional extension of sand drifting, potentially aided by climatic conditions during the Little Ice Age (Pierik et al., 2018). As said before the use of sods came to an end after the introduction of chemical fertilizers at the end of the 19th century.

Because of the accumulation of humin in an active furrow of the fields and the occurrence of charcoal fragments in the soil matrix (Fig. 4.3.7), ^{14}C dating is not reliable for the determination of the age of plaggic deposits, but just indicative for the age of extracted soil organic matter (Chapter 3; Mook and Streurman, 1983; van Mourik et al., 1995). This has been the main reason to revisit the soil archives once OSL dating became available (for the principles of OSL dating, see Section 4.1). We assumed mineral grains to be light exposed prior to deposition (transfer of the sods from the heather), but also after deposition (through ploughing). This light exposure is expected to bleach the quartz OSL signal of the grains allowing determination of burial age.

4.3.3 OSL dating methods

Details of sample preparation and measurement are provided in the original publications (van Mourik et al., 2011 – Posteles; van Mourik

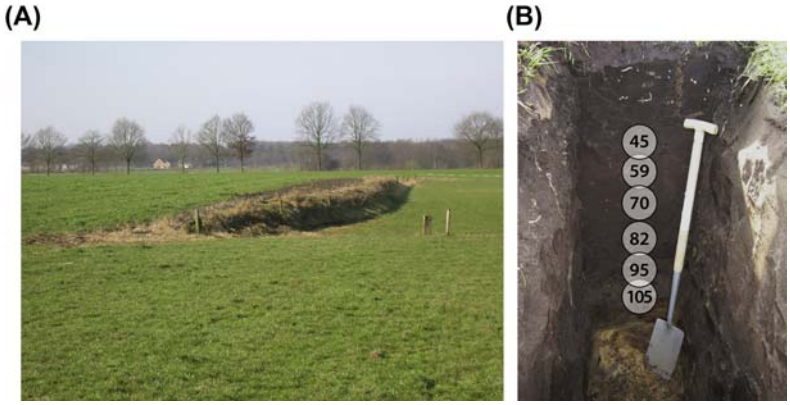

FIGURE 4.3.3 Picture of the Posteles (A, *left*) and the sampled profile (B, *right*). Location of the OSL samples is indicated with *white circles* (depth in cm). *First published in van Mourik, J.M., Slotboom, R.T., Wallinga, J., 2011. Chronology of plaggic deposits; palynology, radiocarbon and optically stimulated luminescence dating of the Posteles (NE-Netherlands). Catena 84, 54–60.*

et al., 2012b – Valenakker; van Mourik et al., 2012a – Rakt and Nabbegat). Sand-sized quartz grains were collected from bulk samples through sieving and chemical preparation. OSL measurements were performed on small aliquots (2–3 mm diameter) using the SAR procedure for equivalent dose determination. Dose rates were determined based on thick-source alpha counting and beta counting (Valenakker) or radionuclide activity concentrations as measured by gamma-ray spectrometry (other sites), and taking into account attenuation by water and organics and a contribution from cosmic rays.

In the original publications, palaeodoses were obtained from equivalent dose distributions by calculating the unweighted mean on a cleaned dataset (omitting equivalent doses deviating more than two standard deviations from the sample mean). A more sophisticated approach has been proposed, using the bootstrapped Minimum Age Model (Cunningham and Wallinga, 2012). This requires an assessment of expected overdispersion (sigmab), which was obtained on the dataset following the procedure of Chamberlain et al. (2018). This approach was not feasible for the archival data of all sites, because necessary information was not available. For the Rakt dataset we had the information, and investigated whether this would further improve the ages obtained. We found that nearly identical ages were obtained as with the initial approach, rendering support to the robustness of the published ages.

4.3.4 Profile Posteles

Profile Posteles (Fig. 4.3.3) is a plaggic Anthrosol overlying a ploughed umbric Podzol. The soil archives at the site are well preserved, because cultivation during the last century was restricted to traditional ploughing of the upper 18 cm (van Mourik et al., 2011 – based on oral information from the Scholten family, owner of the Posteles for at least three generations). Mücher et al. (1989) compared pollen diagrams of the Posteles with those from a nearby Late Holocene peat profile (van der Woude, 1983). The researchers found a similarity in pollen zoning and introduced a palynological-based chronology for the plaggic horizon that can be considered an excellent foundation for the evaluation of ^{14}C and OSL dating results of the plaggic deposits of the Posteles. For this purpose, profile Posteles was resampled in 2007 for pollen, ^{14}C, OSL dating and micromorphology (van Mourik et al., 2011).

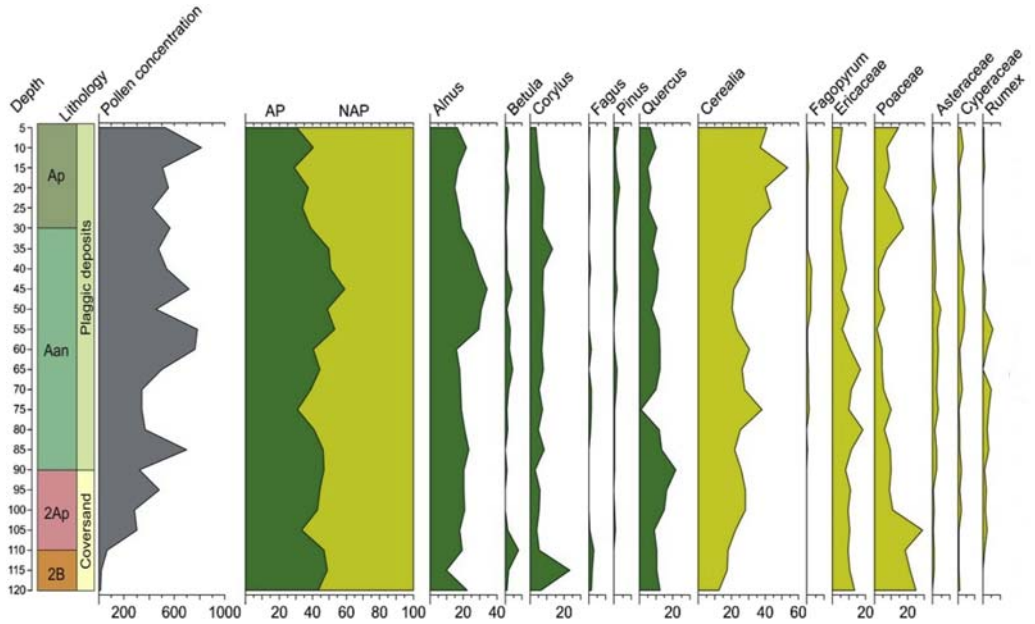

FIGURE 4.3.4 Pollen diagram Posteles; pollen density in kgrain/mL. *First published in van Mourik, J.M., Slotboom, R.T., Wallinga, J., 2011. Chronology of plaggic deposits; palynology, radiocarbon and optically stimulated luminescence dating of the Posteles (NE-Netherlands). Catena 84, 54–60.*

The pollen diagram (Fig. 4.3.4) and the ages obtained through ^{14}C and OSL (Table 4.3.1) reflect a development of at least 1200 years. Ericaceae and Cerealia dominate all the pollen spectra. *Fagopyrum* is considered a palynological time marker, because it was introduced around 1450 CE (Leenders, 1996). In the spectrum, *Fagopyrum* pollen appears in the diagram from 90 cm upward. *Zea mays*, a crop species introduced in the area around 1955 CE, is present only in the upper 15 cm of the profile, corroborating the oral information on ploughing restricted to

TABLE 4.3.1 Optically stimulated luminescence (OSL) and ^{14}C dating results of profile Posteles.

Horizon	Depth (cm)	Sample code	Calendric ^{14}C ages – humin (CE)	Calendric ^{14}C ages – humic acids (CE)	Calendric OSL ages (CE/BCE)
Aan	45	NCL-5204004	–	–	1758 ± 14
Aan	59	NCL-5204005	–	–	1711 ± 20
Aan	70	NCL-5204006 GrN-28782/83	1132 ± 68	1172 ± 51	1651 ± 31
Aan	82	NCL-5204007	–	–	1626 ± 20
Aan	95	NCL-5204008 GrN-28784/85	884 ± 82	861 ± 85	1517 ± 31
2ABp	105	NCL-5204009	–	–	−2035 ± 450

BCE, Before Common Era; *CE*, Common Era.

the upper 18 cm (the actual Ap) in the last century. The active plough horizon is further palynologically characterized by peak percentages of Cerealia, a slight extension of *Pinus* (planted on the abandoned heath after 1900 CE). The pollen content of the buried ploughed Podzol (2Ap, 2B) is post-sedimentary infiltrated and reflects evidence of agriculture (Cerealia) in a deforested landscape (low percentages of *Alnus*, *Quercus* and *Fagus*). The pollen density for the 2B horizon is extremely low.

The calibrated radiocarbon age of the base of the plaggic deposits (95 cm) is 861 ± 85 CE, significantly older than the palynological age (around 1450 CE at 90 cm depth). The age obtained higher in the profile (70 cm; 1172 ± 51 CE) is much younger than expected. These inconsistencies underscore the difficulties related to the presence of soil organic matter of different origins and ages in soil horizons, as discussed in Chapter 3.

The six OSL ages are all in stratigraphic order, with ages for the plaggic Aan horizon ranging from 1517 ± 31 CE at the bottom (95 cm) to 1758 ± 14 CE for the uppermost sample (49 cm). The former is similar to the expected age based on palynological evidence. The OSL age of the 2Ap (105 cm) is 2035 ± 450 BC, 3500 years older than sample 95. The depositional age of this coversand unit is expected to be much older (Late Glacial); likely the age reflects the effects of bioturbation near the palaeosol surface (see Section 4.4) and/or the inclusion of some grains that were brought to the surface by ploughing (discussed later).

The equivalent-dose distributions of the Posteles samples are shown in Fig. 4.3.5. Equivalent-dose distributions for all but the lower two samples of our study indicate tight, symmetrical distributions with few outliers, suggesting that the vast majority of grains were exposed to sufficient light to erase the quartz OSL signal prior to burial below the plough horizon. This corroborates preliminary results on plaggic deposits of profile Dijkerakker (Limburg) by Bokhorst et al. (2005). We expect the ages on these samples (ranging from 1626 ± 20 CE to 1758 ± 14 CE, all in stratigraphic order) to accurately reflect the time of burial below the plough horizon.

The lower two samples (top and bottom of the 2ABp horizon) show more scatter in their equivalent-dose distribution. For the 95 cm depth sample, the distribution is slightly wider than those from the overlying samples obtained from the Aan horizon. Also, there are more outliers at the higher end of the distribution, indicating that not all grains were exposed to light shortly before mixing of this layer ceased (Fig. 4.1.3). As a consequence, we cannot exclude the possibility that the OSL age of this sample (1517 ± 31 CE) slightly overestimates the true burial age below the ploughing layer. The lowermost sample shows a much wider distribution, with all aliquots returning doses greater than the average equivalent dose determined for each of the overlying samples. This may be caused by the mixing of sand grains of two layers of different age (the top of the coversand deposit and the bottom of plaggic deposits) without light exposure or it may reflect natural bioturbation of the palaeosol, which is much less intense and occurs at a slower rate than mixing due to ploughing. The luminescence age of this sample (around 2000 BCE) should be seen as an artefact, and does not reflect the burial age.

4.3.5 Profile Valenakker

The Valenakker is a plaggic Anthrosol (Aan), overlying a ploughed umbric Podzol (2ABp, 2Bs) that is well preserved in the urban environment of Weert on the sports field of a college and has not been ploughed for over 100 years (van Mourik and Horsten, 1995). The oldest historical evidence of the Valenakker as a complex of arable fields is a historical map dating from 1550 CE.

The pollen diagram shows two phases in the landscape development (Fig. 4.3.6; OSL datings in Table 4.3.2). The older phase is recorded in

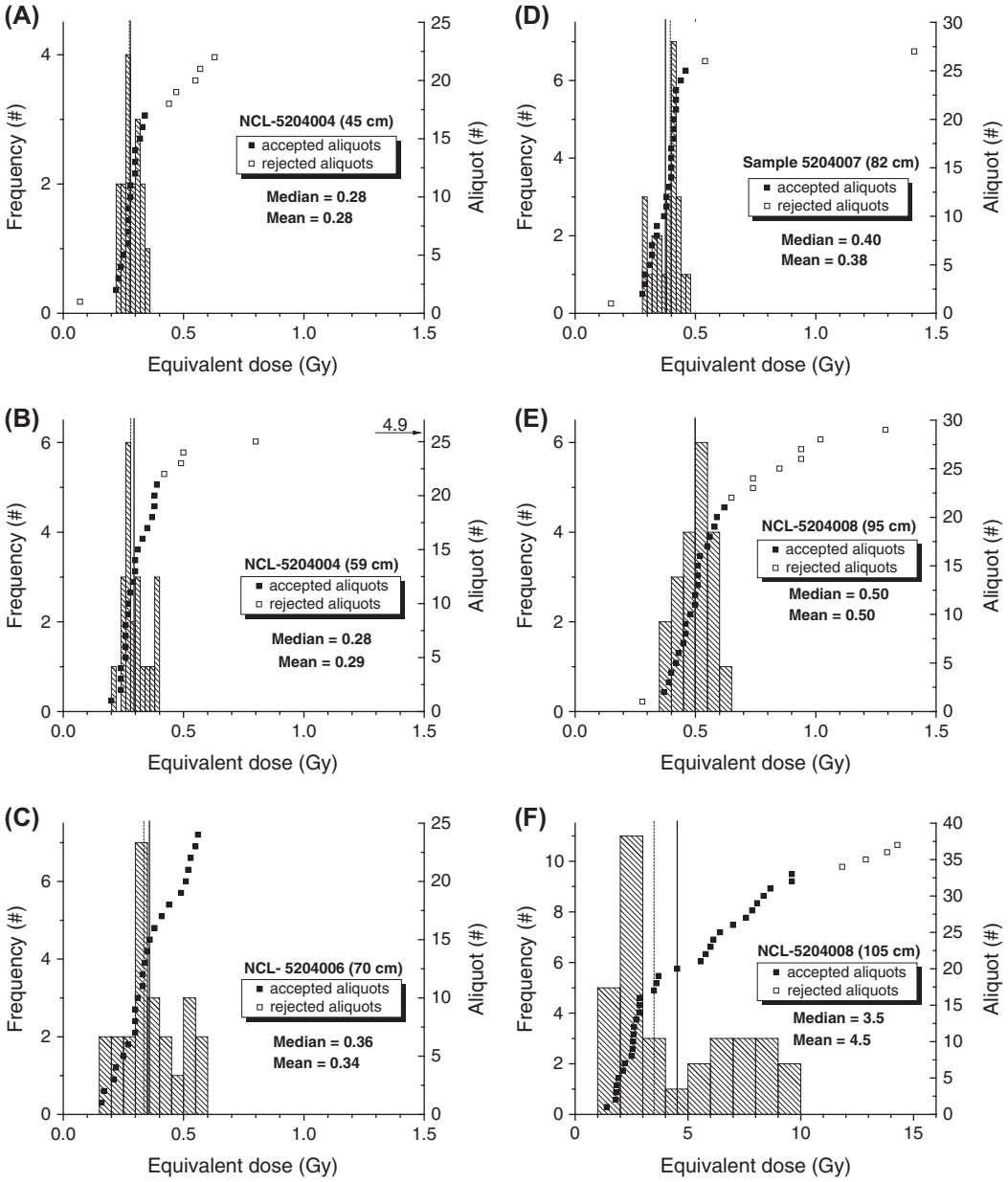

FIGURE 4.3.5 The equivalent dose distributions of the six samples of Posteles. *First published in van Mourik, J.M., Slotboom, R.T., Wallinga, J. 2011. Chronology of plaggic deposits; palynology, radiocarbon and optically stimulated luminescence dating of the Posteles (NE-Netherlands). Catena 84, 54–60.*

FIGURE 4.3.6 Picture of the sports field on the Valenakker (A, *left*) and the sampled plaggic Anthrosol (B, *right*). The location of the optically stimulated luminescence samples are indicated with *white circles* (depth in cm). *First published in van Mourik, J.M., Seijmonsbergen, A.C., Jansen, B. 2012b. Geochronology of Soils and Landforms in Cultural Landscapes on Aeolian Sandy Substrates, Based on Radiocarbon and Optically Stimulated Luminescence Dating (Weert, SE-Netherlands). InTech, Radiometric Dating, 75–114.*

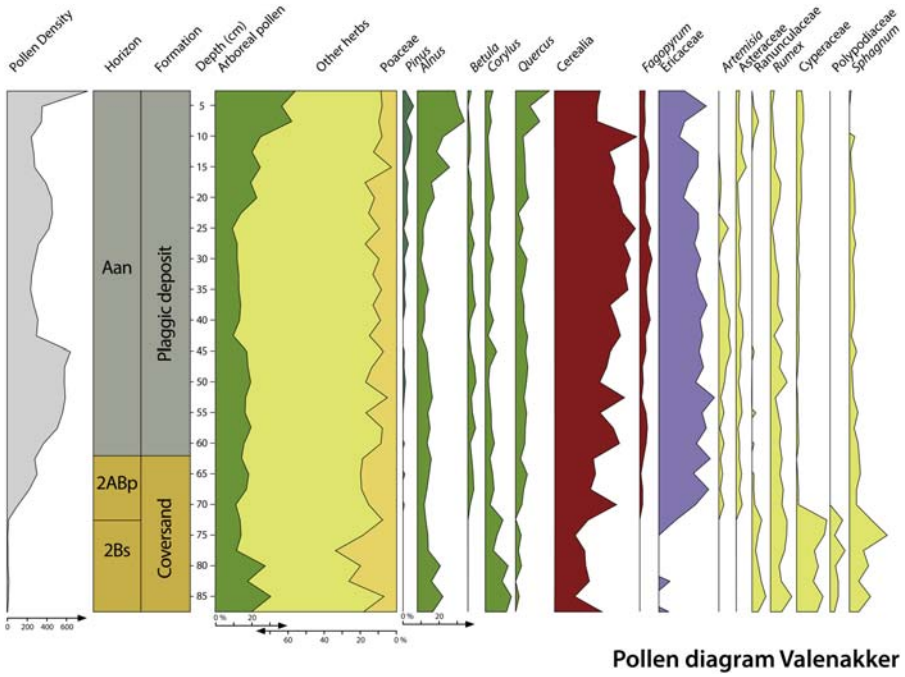

FIGURE 4.3.7 Pollen diagram Valenakker. Pollen density in kgrains/mL. *First published in van Mourik, J.M., Seijmonsbergen, A.C., Jansen, B. 2012b. Geochronology of Soils and Landforms in Cultural Landscapes on Aeolian Sandy Substrates, Based on Radiocarbon and Optically Stimulated Luminescence Dating (Weert, SE-Netherlands). InTech, Radiometric Dating, 75–114.*

TABLE 4.3.2 Optically stimulated luminescence (OSL) and ^{14}C dating results of profile Valenakker.

Horizon	Depth (cm)	Sample code	Calendric ^{14}C ages − humin	Calendric ^{14}C age humic − acids	Calendric OSL age
Aan	20	NCL-5104001	–	–	1775 ± 20 CE
Aan	40	NCL-5104002 GrN21233/34	771 ± 92 CE	1049 ± 78 CE	1635 ± 30 CE
Aan	60	NCL-5104003 GrN21235/36	595 ± 61 CE	698 ± 54 CE	1565 ± 30 CE

CE, common era.

the buried palaeosol. The pollen density curve indicates soil pollen infiltration in coversand. The presence of Poaceae, Cyperaceae, *Rumex* and Ranunculaceae reflects a period of pasture in a deforested landscape with hedgerows with *Corylus* and *Quercus*, characteristic for the landscape with degrading forest in the Bronze/Iron Age. The scores of Cerealia in the palaeosol indicate a form of sedentary agriculture before the start of plaggic agriculture. The younger phase is recorded in the plaggic horizon. The pollen spectra of the Aan are dominated by Cerealia and Ericaceae. Also, *Fagopyrum* is present in all the spectra, indicating an age younger than 1450 CE (Leenders, 1996). The increase in arboreal pollen in the youngest spectra reflects the reforestations on driftsands after 1900 CE.

Micromorphological observations (Figs. 4.3.8 and 4.3.9) of the plaggic deposits show the complexity of soil organic matter, mostly concentrated in intertextic distributed aggregates with the internal fabric of earthworm excrements (Fig. 4.3.8). The provenance of decomposing organic material is extremely diverse: regular litter precipitation (including pollen, Fig. 4.3.9), decomposing roots of crop species, organic manure, plaggic sods and charcoal. This composition affects the reliability of ^{14}C dating (Chapter 3).

^{14}C dating indicates a carbon age of the base (60 cm) of the Aan horizon of 1000−1500 years, with ages of the humic acids fraction younger than the ages of the humin fraction (Chapter 3). The OSL ages are significantly younger

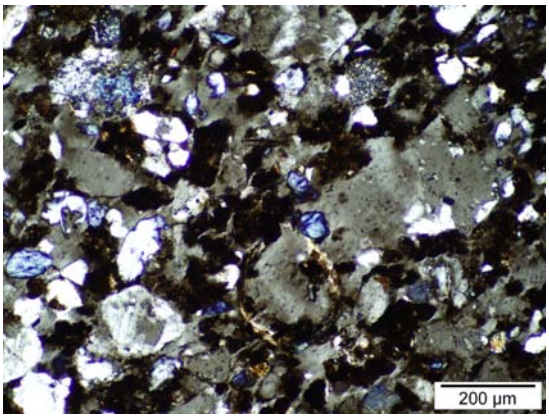

FIGURE 4.3.8 Distribution pattern of organic aggregates in a thin section of the Aan of Valenakker (40−50 cm).

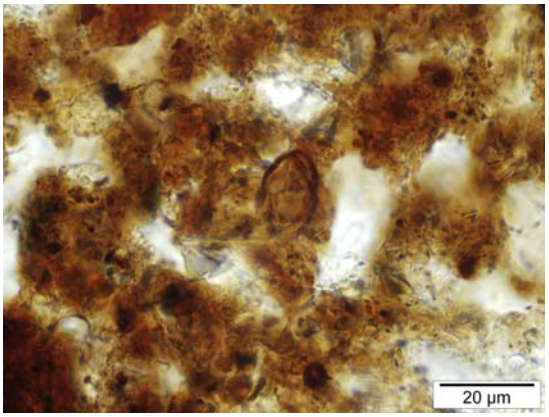

FIGURE 4.3.9 A pollen grain, visible in one of the aggregates of Fig. 4.3.8.

(1565 ± 30 to 1775 ± 20 CE) and in line with the occurrence of *Fagopyrum* pollen and historical evidence. We conclude that a phase of agricultural land use with accumulation of soil organic matter must have preceded the development of the plaggic horizon; the Aan then developed from the 16th century until the end of plaggic agriculture around 1900 CE.

4.3.6 Profile Nabbegat

Profile Nabbegat is a haplic Arenosol (with Mormoder humus form), overlying a plaggic Anthrosol, overlying a ploughed umbric Podzol (Fig. 4.3.10). The old fields of Nabbegat are part of a complex of arable fields on the Maashorst (Fig. 4.3.1). The western border of this agricultural complex was buried by driftsand around 1800 CE (van Mourik et al., 2012a).

The pollen diagram (Fig. 4.3.11) and the absolute dates (Table 4.3.3) reflect a soil development of ≈3000 years. The post-sedimentary pollen spectra of the 3ABp reflect the start of agriculture (increase in Cerealia) on a former heath (decrease in Ericaceae) in a surrounding with coppice hedges (*Quercus*, *Corylus*). Based on radiocarbon dates, agricultural activities started before 1000 BCE, while the OSL dates point to deposition of plaggic material from the 17th century. The large difference between radiocarbon and OSL ages indicates that the farmers used organic matter with a limited mineral admixture for a long time. OSL ages show that the arable field was overblown by driftsand around 1800 CE, shortly after the introduction of the deep stable economy (Vera, 2011). This may suggest that the use of heath sods resulted in heath degradation and sand drifting (van Mourik et al., 2012a).

4.3.7 The soil archives of Rakt and the Bedafse Bergen

Profile Rakt is part of the soil archives of the Bedafse Bergen (Fig. 4.3.12). At the east side of this dune ridge, the western edge of the fields of Rakt has been overblown by younger driftsand. The profile shows (similar to profile Nabbegat) a pedological sequence of a ploughed carbic Podzol in coversand, overlain by plaggic deposits and capped with younger driftsand with an initial Podzol (Mormoder humus form).

Also, zoning in the pollen diagram Rakt (Fig. 4.3.14) is rather similar to the diagram of Nabbegat. In Rakt we can distinguish a light

FIGURE 4.3.10 Picture (to the east) of the landscape (A, *left*) and the buried plaggic Anthrosols Nabbegat (B, *right*). The location of the optically stimulated luminescence samples are indicated with *white circles* (depth in cm). *First published in van Mourik, J.M., Seijmonsbergen, A.C., SLotboom, R.T., Wallinga, J., 2012a. Impact of human land use on soils and landforms in cultural landscapes on aeolian sandy substrates (Maashorst, SE-Netherlands). Quaternary International 265, 74–89.*

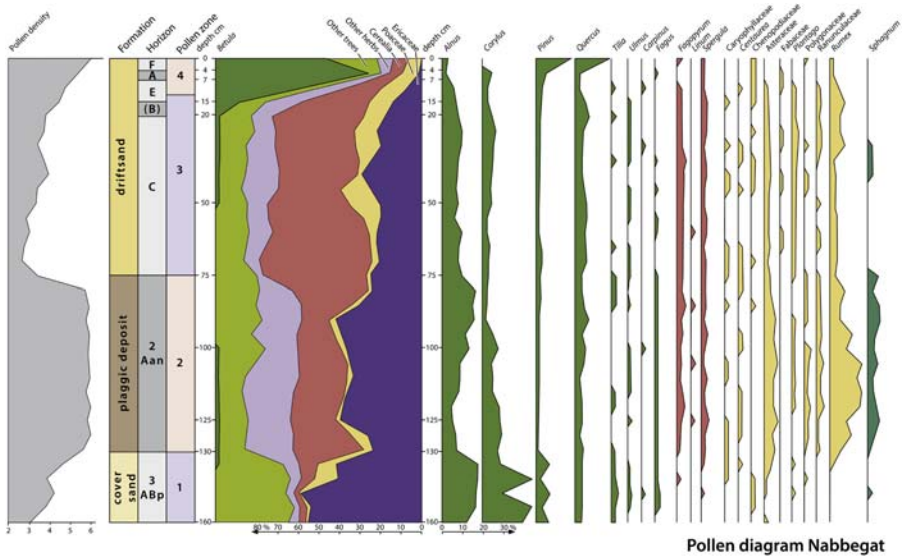

FIGURE 4.3.11 Pollen diagram Nabbegat; pollen density in kgrain/mL. *First published in van Mourik, J.M., Seijmonsbergen, A.C., SLotboom, R.T., Wallinga, J., 2012a. Impact of human land use on soils and landforms in cultural landscapes on aeolian sandy substrates (Maashorst, SE-Netherlands). Quaternary International 265, 74–89.*

grey 2Aan1 (37–80 cm) with rather low pollen densities and a grey 2Aan2 (80–144 cm) with higher pollen densities. The OSL ages obtained for profile Rakt (Table 4.3.4) show a development closely resembling that of the Nabbegat profile. Results for the lower two samples are less reliable, because they likely contain grains registering different events (see discussion for Posteles). The plaggic deposits are dated from the 16th century, while driftsand deposits buried the arable field around 1800 CE. The OSL ages show an increase in the deposition rate of plaggic deposits around 1700 CE; the 2Aan2 developed roughly between 1500 and 1700 CE, and the 2An1 between 1700 and 1800 CE. We deduce that during the deposition of the 2Aan1, sand

TABLE 4.3.3 Optically stimulated luminescence (OSL) and ^{14}C dating results of profile Nabbegat.

Horizon	Depth (cm)	Sample codes	Calendric ^{14}C ages – humin	Calendric ^{14}C ages – humic acids	Calendric OSL ages
C	70	NCL-5306087	–	–	1803 ± 12 CE
2An	80	NCL-5308088 GrN-17362/63	428 ± 107 CE	626 ± 45 CE	1770 ± 11 CE
2An	105	GrN-17359/60	37 ± 133 BCE	3 ± 101 CE	–
2An	130	NCL-5308089 GrN-17358/59	1182 ± 139 BCE	811 ± 101 BCE	1676 ± 14 CE
3ABp	140	GrN-17357	–	1299 ± 78 BCE	–
3ABp	150	GrN-17355	–	1385 ± 72 BCE	–

BCE, Before Common Era; *CE*, Common Era.

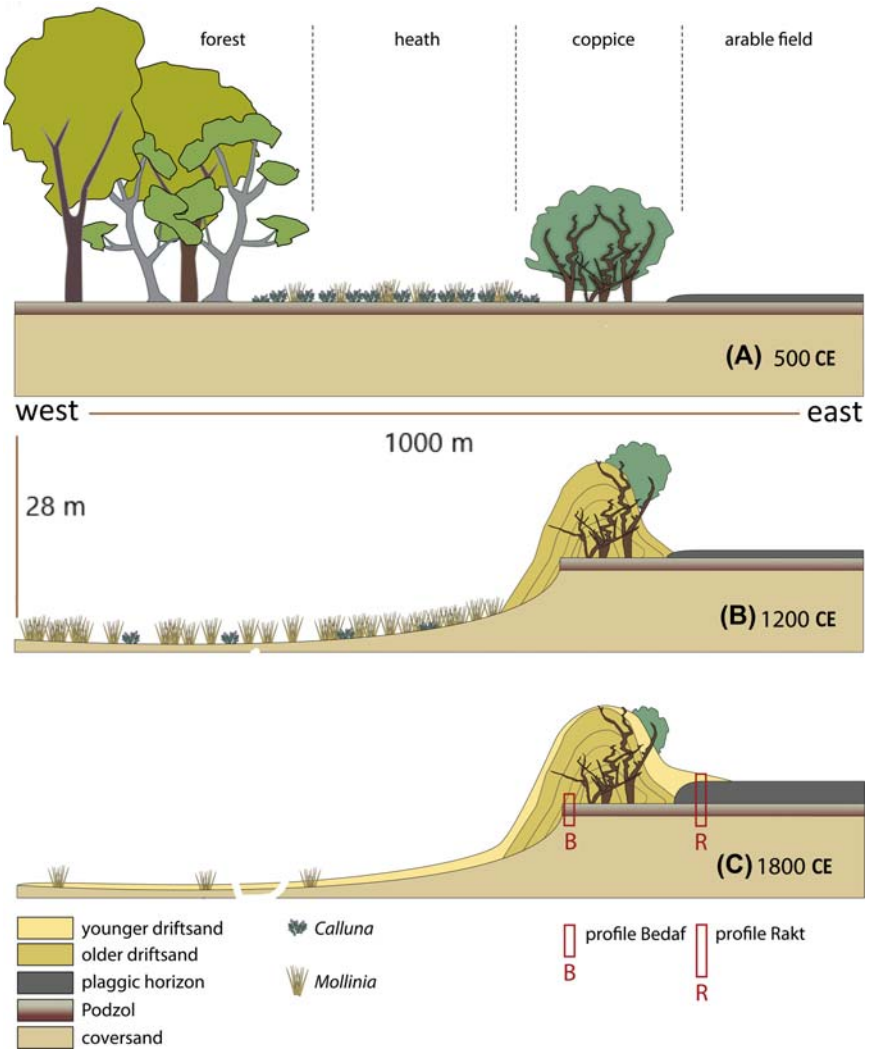

FIGURE 4.3.12 Three phases in the development of the soil archives of the Bedafse Bergen. *Modified after Doorenbosch, M., van Mourik, J. M., 2016. The impact of ancestral heath management on soils and landscapes: a reconstruction based on paleoecological analyses of soil records in the central and southeastern Netherlands. SOIL 2 (3), 311–324. https://doi.org/10.5194/soil-2-311-2016.*

drifting started at the western side of the Bedafse Bergen and provided extra input of sand grains on the fields of Rakt, ploughed into the plaggic horizon. Around 1800 CE the supply of driftsand reached a level that urged farmers to abandon the fields at the foot of the dune ridge. Most likely sand drifting at the west side of the Bedafse Bergen stopped around 1900 CE after plaggic agriculture was abandoned. At the profile location Rakt the vegetation recovered and an initial Podzol developed.

Profile Bedafse Bergen is a haplic Arenosol overlying a buried carbic Podzol (Fig. 4.3.15). The pollen spectra of the top horizons of the

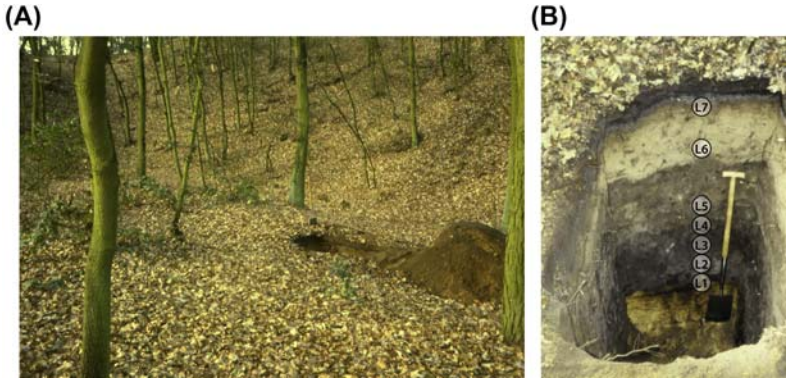

FIGURE 4.3.13 Landscape at the eastern footslope of the Bedafse Bergen (A, *left*) with the sampled buried plaggic Anthrosol Rakt (B, *right*). The locations for optically stimulated luminescence samples are indicated with *white circles*.

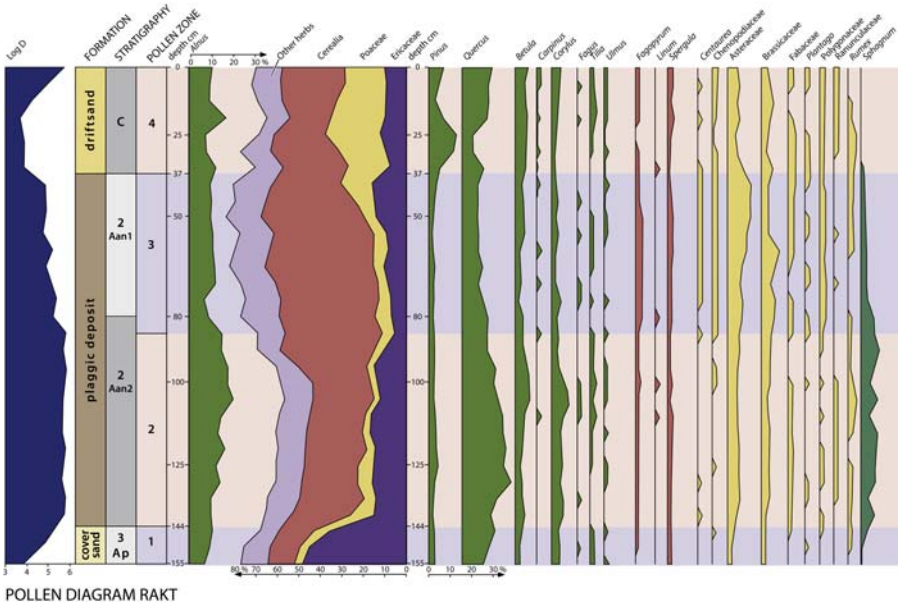

FIGURE 4.3.14 Pollen diagram Rakt pollen density in kgrain/mL. *First published in van Mourik, J.M., Seijmonsbergen, A.C., SLotboom, R.T., Wallinga, J., 2012a. Impact of human land use on soils and landforms in cultural landscapes on aeolian sandy substrates (Maashorst, SE-Netherlands). Quaternary International 265, 74–89.*

buried Podzol (Fig. 4.3.16) are characterized by high percentages of Ericacea (this points to pollen infiltration under heather) and *Quercus* and *Corylus* (this points to the presence of deciduous forest in the vicinity), which is in line with the pollen content of the oldest spectra of the 2An2 and 3Ap of profile Rakt. The pollen spectra in the basal layers of the (older) driftsand show a decrease in arboreal pollen and Ericaceae and an increase in Poaceae. This points to deforestation and grassing over (or even degradation) of the heath. We applied ^{14}C dating on humic acids

TABLE 4.3.4 Optically stimulated luminescence (OSL) ages of profile Rakt (Fig. 4.3.13 *right*).

Horizon	Ring	Depth (cm)	Sample codes	OSL ages
C top	L7	9.5	NCL-5207116	1808 ± 8 CE
C bottom	L6	32.5	NCL-5207117	1812 ± 9 CE
2Aan1 bottom	L5	57.5	NCL-5207118	1781 ± 9 CE
2Aan2 top	L4	77.5	NCL-5207119	1685 ± 14 CE
2Aan2 middle	L3	97.5	NCL-5207120	1593 ± 17 CE
2Aan2 bottom	L2	132.5	NCL-5207121	1417 ± 37 CE
3Ap	L1	144.5	NCL-5207122	69 ± 89 CE

CE, Common Era.
First published in van Mourik, J.M., Seijmonsbergen, A.C., SLotboom, R.T., Wallinga, J., 2012a. Impact of human land use on soils and landforms in cultural landscapes on aeolian sandy substrates (Maashorst, SE-Netherlands). Quaternary International 265, 74–89.

extracted from the 3Ah, and OSL dating on the basic layers of the older driftsand deposits.

^{14}C dating (Table 4.3.5) of the 3Ah horizon of the buried Podzol yields an age of 725 ± 39 CE. This indicates the start of deposition of driftsand after ≈725 CE. However, it is known that the results of ^{14}C dating of soil organic carbon may overestimate the age due to the accumulation of relatively resistant organic particles during active soil formation (van Mourik et al., 1995). OSL ages were obtained from the oldest driftsand layers (Table 4.3.5); the lowermost of these (L1) indicates that the deposition of older driftsand started in the 14th century (or a little bit earlier because the lower driftsand layer was too thin for sampling), i.e., after commercial deforestations (Vera, 2011).

Based on results for the two profiles Rakt and Bedafse Bergen and additional mapping (van Mourik et al., 2012a), a cross-section was reconstructed of the development of the Bedafse Bergen (Doorenbosch and van Mourik, 2016). Unique for the soil archives of the Bedafse Bergen is the possibility of linking the development of the plaggic horizon of Rakt to the main phases (Medieval and post-Medieval) of sand drifting. Three phases were recognized in the development (Fig. 4.3.12). During the first phase (around 500 CE), arable fields in the vicinity of the hamlet of Rakt were surrounded by oak coppice. Shepherding took place on the heaths west of the hamlet and organic manure was used for fertilizing the fields of Rakt. Because this fertilizer

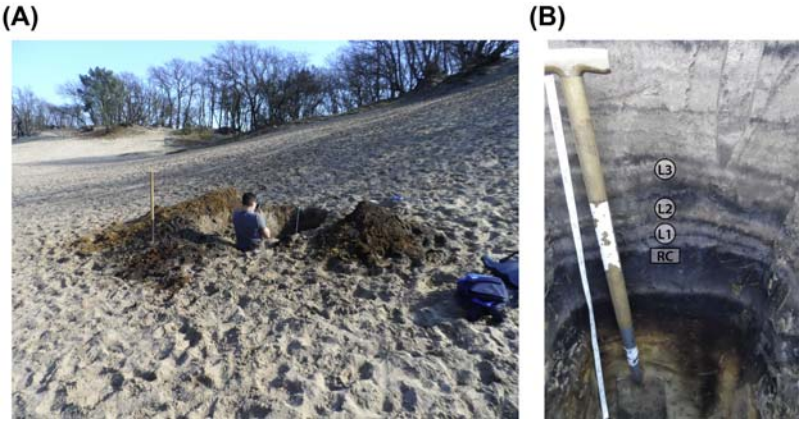

FIGURE 4.3.15 Landscape at the western footslope of the Bedafse Bergen (A, *left*) with the sampled buried carbic Podzol (B, *right*). The locations for optically stimulated luminescence samples are indicated with *rings*, and the location of the ^{14}C sample with a *white box*.

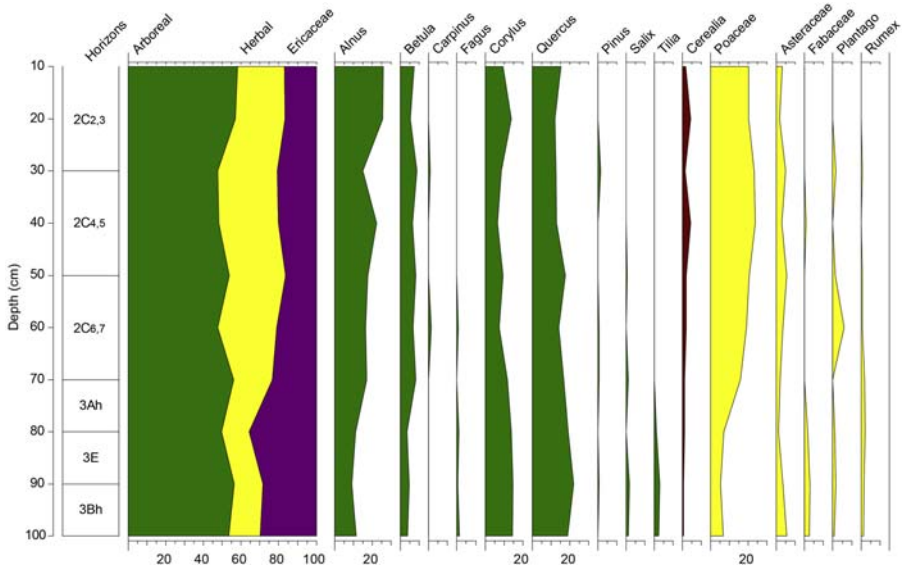

FIGURE 4.3.16 Pollen diagram Bedafse Bergen. *First published in Doorenbosch, M., van Mourik, J. M., 2016. The impact of ancestral heath management on soils and landscapes: a reconstruction based on paleoecological analyses of soil records in the central and southeastern Netherlands. SOIL, 2 (3), 311–324. https://doi.org/10.5194/soil-2-311-2016.*

TABLE 4.3.5 Radiocarbon and optically stimulated luminescence (OSL) dating results for profile Bedafse Bergen.

Horizon	OSL ring/^{14}C box	Sample code	OSL dating	^{14}C humic acids
2C2,3	L3	NCL-1113087	1473 ± 40 CE	
2C4,5	L2	NCL-1113088	1425 ± 40 CE	
2C6,7	L1	NCL-1113124	1365 ± 40 CE	
3Ah	RC	GrA-55401		725 ± 39 AD

CE, Common Era.

lacked a mineralogical component, the land surface was not significantly raised during this time. Deforestation during the 11th until the 13th centuries (Vera, 2011; van Mourik, 2001) triggered the first regional extension of (older) sand drifting. Prevailing westerly winds transported sand to the east and drifting sand grains were captured by the coppice surrounding the fields of Rakt. This initiated the development of the (biogenic) dune ridge – the Bedafse Bergen ('Bedaf – mountains'). Population growth in the 18th century and the increasing need for food resulted in the enlargement of manure production in deeper stables and the application of heath sods (Vera, 2011). Overdigging of heath sods initiated the second extension of (younger) sand drifting and due to the mineral fraction of heath sods the rise of the surface of the fields accelerated (Section C in Fig. 4.3.12). In fields close to the dune ridge, driftsand covered the plaggic Anthrosol around 1800 CE. This closely resembled the development at Nabbegat, as described earlier.

4.3.8 Conclusions

- Pollen diagrams of plaggic Anthrosols show a pollen zoning that reflects aspects of the Late Holocene agricultural landscape evolution but palynological time markers are not reliable for the dating of the plaggic deposits and consequently the rise of the land surface of the fields.
- ^{14}C dating results of extracted soil organic carbon from plaggic deposits are indicative for the age of the organic fraction and the start of agricultural land use, but due to mixing of organic matter of different ages the method is not suitable to determine when plaggic horizons developed.
- OSL dating results are related to (bleached) mineral grains in the plaggic deposits and are reliable for the determination of the age of the plaggic deposits. The OSL ages indicate the time of burial of the sampled grains below the ploughing layer. The method is highly suitable when the land surface is rapidly elevated though addition of a mineral component. Continued mixing of the soil layer by ploughing prohibits use of the method to record when people started to apply organic additions to the soil.
- Our multidisciplinary investigations have shown that in plaggic horizons an older soil organic matrix is suspended in the voids of a younger mineral soil skeleton. This is a typical characteristic of plaggic soils.

4.4 Reconstructing soil mixing and transport using single-grain luminescence methods

4.4.1 Background

The soil mantle facilitates critical ecosystem services such as food, clean water or biodiversity, which are of eminent importance for the future development of human societies (e.g., Keesstra et al., 2016). To secure and promote sustainable ecosystem functioning and provision of ecosystem services, it is key to be able to evaluate the resilience of the soil mantle. This requires profound understanding of the response of soils to changing environmental conditions. Yet, surprisingly little is known about the rates of many fundamental processes of soil formation (e.g., bioturbation or soil production) and its interaction with landscape evolution (e.g., through soil formation and erosion). Gaining deeper, i.e., more quantitative, understanding of these fundamental processes is a genuine task for soil scientists and geomorphologists.

On relatively short timescales (days to years), instrumental observations (e.g., remote sensing techniques) and field experiments of earth surface processes are able to provide valuable insights into process interrelations and rates of rapid earth surface processes (e.g., gullying). However, important soil geomorphological processes such as bioturbation, soil production or soil creep are typically characterized by lower dynamics, such that we need to integrate over longer time periods to reliably capture corresponding rates. Here, we discuss the possibilities of luminescence dating methods for capturing these soil geomorphological processes on a time resolution of decades to millennia, potentially bridging between short-scale instrumental inventories and very large-scale ($>10^{3-4}$ years) geological reconstructions using terrestrial cosmogenic nuclides (TCNs).

Concentrations of TCN are frequently used in hillslope or soil geomorphology to determine long-term averaged rates of soil production (Heimsath et al., 1997; review: Stockmann et al., 2014) or catchment-wide denudation rates (Bierman and Steig, 1996; review: Von Blanckenburg, 2005). In the theoretical framework papers of Furbish et al. (2018a,b), TCN and luminescence inventories are compared to each other regarding their properties for tracing particle transport and mixing in the soil mantle. They point out that TCN tracers track trajectories bottom up as they enter the soil system from

bedrock with zero TCN concentration, while luminescence age–depth profiles trace particle trajectories top down as the luminescence signal is reset at the surface (Furbish et al., 2018b).

Several studies applied commonly used luminescence dating methods to quantify soil mixing by bioturbation and/or soil creep particle transport along hillslopes (e.g., Heimsath et al., 2002; Wilkinson and Humphreys, 2005; Madsen et al., 2011; Stockmann et al., 2013; Johnson et al., 2014; Huisman et al., 2018). These studies indicate that bioturbation can be reconstructed using luminescence-based methods because this process is manifested as a vertical flux of soil particles exhuming grains to the surface where they are exposed to daylight and thus have their luminescence signal reset before reburial. In turn, active soil bioturbation leads to a detectable overprinting of the original bedrock or depositional luminescence age which was recognized already in many previous soil luminescence studies (e.g., Bateman et al., 2003, 2007; Kristensen et al., 2015; Gliganic et al., 2016).

In most settings, single-grain resolution is required to differentiate between grains that yield luminescence ages associated with the original soil parent material from those that provide insights into post-parent material modifications caused by typical soil processes such as bioturbation (Bateman et al., 2003). Only in cases with very high bioturbation intensities, i.e., close to complete mixing of the entire soil matrix, for example by lugworm bioturbation in a tidal flat, can meaningful mixing rates be established from multiple grain luminescence measurements (Madsen et al., 2011).

The vast majority of soil luminescence studies applied quartz single-grain OSL methods to differentiate between different grain populations (e.g., Heimsath et al., 2002). However, single-grain quartz OSL is usually very tedious and labour intensive, and typically restricted in its application possibilities (e.g., Reimann et al., 2012). Especially in settings where the quartz is directly sourced from close proximity plutonic and/or metamorphic bedrock (e.g., granitic or gneissic saprolites), quartz luminescence properties are typically poor (e.g., Preusser et al., 2006; Guralnik et al., 2015). As a consequence, quartz-based OSL dating in such settings is highly challenging, and single-grain OSL dating often impossible. These limitations of the conventional single-grain quartz OSL methodology might be an important reason why OSL techniques were never widely embraced in studying soil geomorphological processes.

To overcome these shortcomings we proposed and tested an alternative luminescence method for quantifying soil mixing rates based on feldspar single grains (Reimann et al., 2017). This alternative method makes use of sand-sized single-grain pIRIR measurements of K-rich feldspars, a method that was originally developed (Thomsen et al., 2008) and validated (Reimann et al., 2012) for conventional Quaternary dating applications (e.g., Van Gorp et al., 2013; Smedley et al., 2016; Brill et al., 2018). In our paper we could demonstrate that feldspar pIRIR measurements were well suited for granitic saprolite settings, and that they are more time and labour efficient than conventional single-grain quartz OSL techniques (Reimann et al., 2017).

The new feldspar-based luminescence approach also quantifies the percentage of surface visiting grains, the so-called non-saturation factor (NSF; Reimann et al., 2017). This factor is based on the simple idea that sand particles that never reached the surface since their introduction into the soil matrix at the interface between mobile regolith and the saprolite yield luminescence ages above the upper dating limit (saturation ages) in agreement with the geological age of the bedrock, whereas grains with a surface exposure history yield finite luminescence ages. Interestingly, Furbish et al. (2018a,b) in their theoretical framework papers also independently recognized the number of grains with finite luminescence ages, which is similar to our NSF, as a valuable proxy for the

concentration of luminescence tracers in the soil and they modelled this tracer concentration down a steady-state soil profile for different soil mixing intensity scenarios (Furbish et al., 2018b, their Fig. C1).

Luminescence NSF–depth profiles tracing surface visiting grains down the soil profile can substitute TCN concentration depth profiles because they mirror the TCN-determined bottom-up particle motion (Román-Sánchez et al., 2019a). Furthermore, NSF–depth profiles inform on the mobile regolith–saprolite boundary that separates the mechanically active mobile regolith from the saprolite. Together with the feldspar single-grain luminescence age–depth profiles this provides the prospect to measure two complementary OSL proxies (i.e., OSL age, NSF) from exactly the same grains. This provides a clear advantage of using feldspar-based OSL tracers in future soil geomorphological studies because they yield the prospect of simultaneously constraining soil bioturbation rates (e.g., Heimsath et al., 2002; Reimann et al., 2017) and rates of soil erosion and production on the same material (Román-Sánchez et al., 2019a,b).

In three studies we demonstrated that single-grain feldspar luminescence inventories are able to trace soil particle motions along a specific Mediterranean hillslope catena and thus provide valuable insights into fundamental earth surface processes (Reimann et al., 2017; Román-Sánchez et al., 2019a,b). Here, we combine insights from these technical papers to improve accessibility for non-luminescence experts, and promote application and further development of this promising new technology.

4.4.2 Luminescence tracing of soil particles along the hillslope catena – basic concept

The Mediterranean hillslope catena that was investigated for this proof of concept is located at the Santa Clotilde Critical Zone Observatory (SC-CZO). The SC-CZO is situated in the Cordoba province, southwest Spain, in the Martin Gonzalo headwater catchment (latitude 38.12′N, longitude 4.17′W), with altitudes between 660 and 740 m above sea level. The study area is characterized by a Mediterranean climate, Bsk according to the Köppen-Geiger system, and natural forest (mainly oaks) with very low to negligible grazing intensities. The parent material in the area consists of granitic rock and the resulting soils are classified as Regosol, Cambisols and Phaeozems according to the FAO-UNESCO World Reference Base (IUSS Working Group, 2014). More information on the field settings of the SC-CZO and the specific sampling locations can be found in Román-Sánchez et al. (2017, 2019a).

In Fig. 4.4.1 the soil geomorphological situation (soil scale and hillslope scale) of the SC-CZO hillslope catena, including the dominating earth surface processes, is illustrated. Soil is produced from granite bedrock and continuously mixed by soil bioturbation (see soil column scale, Fig. 4.4.1). Sand grains directly derived from the granitic bedrock yield infinite single-grain feldspar luminescence ages (Reimann et al., 2017) in agreement with the geological age of the granitic bedrock. Bioturbation results in an upward particle flux; infinitively old sand grains may reach the surface where they are exposed to daylight and particle luminescence ages are reset. Subsequently, grains are reburied and a new (finite) luminescence age accumulates until the stochastic mixing process brings the grains to the surface again. The combined effect of the net upward movement and stochastic mixing is that the average luminescence age of finite-age grains increases with depth. The fraction of surface-visiting grains, i.e., grains that reach the surface at least once and thus yield a finite age, decreases with depth. We previously proposed to express this as an NSF. The slope of this NSF decrease with soil depth is expected to be inversely proportional to the bioturbation intensity. Both inventories, i.e., single-grain

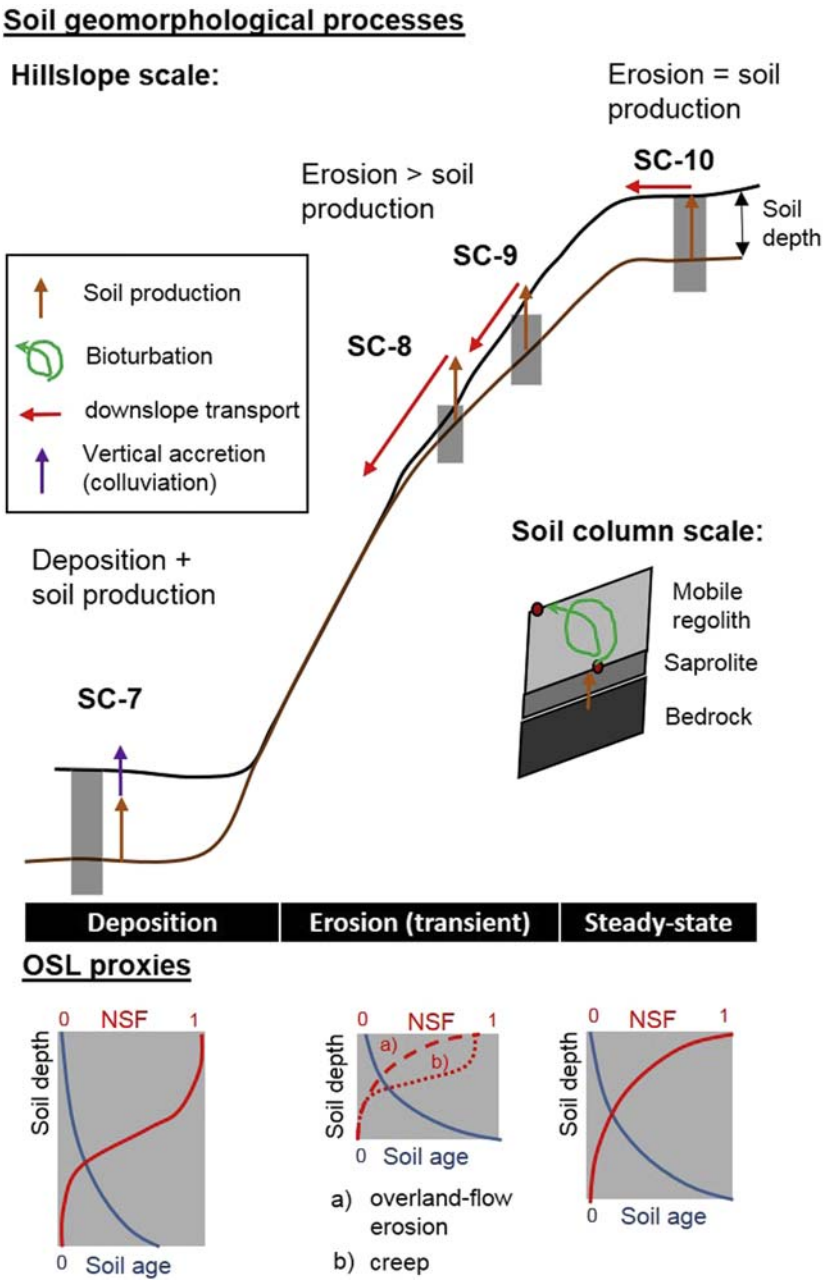

FIGURE 4.4.1 Conceptual model of soil particle motion along a hillslope catena and how it is captured in two proxies (age, NSF) extracted from feldspar single-grain luminescence analyses. Detailed explanations are provided in the main text. *NSF*, Non-saturation factor; *OSL*, optically stimulated luminescence. *This figure is based on the conceptual ideas presented in Román-Sánchez, A., Reimann, T., Wallinga, J., Vanwalleghem, T., 2019a. Bioturbation and erosion rates along the soil-hillslope conveyor belt, part 1: insights from single-grain feldspar luminescence. Earth Surface Processes and Landforms. doi: 10.1002/esp.4628.*

luminescence age versus depth and NSF versus depth, are censored at the upper dating limit of the dating method, which is ~300 ka for feldspar luminescence dating using the pIRIR signal (Buylaert et al., 2012; Kars et al., 2012).

At the hillslope scale, soil particle motions are in the vertical direction (soil production + bioturbation) and the lateral direction (downslope transport) as indicated in Fig. 4.4.1 as brown and red arrows, respectively. We assumed that soil production and bioturbation are spatially uniform and thus constant for all four soil profiles along the SC-CZO catena and that the erosion rate increases with slope (SC-8 > SC-9 > SC-10). At the hill base, deposition of colluvial material occurs (violet arrow; 'negative erosion rate'). Thus we can identify three different geomorphic situations along the hillslope catena: steady-state (erosion = soil production) at the hillcrest, a transient erosional (erosion > soil production) and depositional (deposition + soil production). In our study we have sampled four profiles: SC-10 is from the hillcrest and characterized as a steady-state profile, whereas SC-9 or SC-8 are located in either a gently or quickly eroding position, respectively. The soil profile at the hill base SC-7 is located in the depositional area.

In the lower part of Fig. 4.4.1 we illustrate the expected variation of the two luminescence-based proxies (age, NSF) with soil depth and geomorphic position. These expectations are based on the conceptual model developed in Román-Sánchez et al. (2019a). In the following we briefly illustrate our conceptual anticipations for each of the three geomorphic positions:

- Steady state: the steady-state profile SC-10 is the reference profile located at the hillcrest position. Here, material loss through erosion, either by overland-flow at the ground surface or soil creep below the ground surface, is compensated for by soil production at the mobile regolith–saprolite interface. Bioturbation presumably causes a constant and exponentially decaying depth-dependent vertical flux of soil particles resulting in an exponential increase in the average luminescence soil age and at the same time an exponential decrease in surfaced grains (i.e., NSF) with soil depth. The interface between saprolite and the mobile regolith is reached where NSF = 0, indicating no soil particle exchange with the surface below this point and thus no active mechanical mixing. The NSF proxy can in turn be utilized to objectively constrain soil depth (Reimann et al., 2017).
- Transient erosional: at eroding geomorphic positions (e.g., SC-8,9), soil production rates cannot keep up with erosion such that soil thickness will be reduce compared to the steady-state reference profile, indicated by NSF = 0 at shallower soil depth. This is the case for both erosion processes considered here: (1) overland flow erosion at the surface and (2) soil creep just below the surface. Both processes will result in a truncation of the luminescence age–depth and NSF–depth profiles at the surface caused by exhumation of 'old' grains and non-surfaced grains. At each depth the apparent age is expected to increase compared to the steady-state reference profile. If erosion is caused by soil creep, soil particles will not be removed at the surface but over the face of the entire vertical profile (subscenario (2)), which contrary to overland flow erosion will not directly result in daylight exposure and thus luminescence signal resetting during lateral transport. This subscenario will also cause surface lowering and won't affect the age–depth profile. However, we postulate that creep will add surface-visiting grains (finite age) laterally (i.e., sourced uphill) to the soil profile resulting in an increase in NSF compared to the overland erosion (subscenario (1)). This increase in NSF will be more pronounced near the surface, where creep velocities are typically higher.

- Depositional: for this geomorphic position the soil profile is accreting due to addition of upslope material. Soil thickness will increase, which can be recognized by the downward migration of the NSF = 0 threshold. Addition of 'bleached' upslope material will manifest in steeper and more stretched luminescent age–depth profile and the slope of this profile will predominantly reflect the rate of the colluvium deposition, which can be determined by conventional luminescence dating approaches (reviewed by Fuchs and Lang, 2009). However, these sedimentation processes will in many cases be moderated by bioturbation (this case) or anthropogenic soil mixing processes (e.g., Van der Meij et al., 2019). Addition of 'bleached grains' from upslope areas will further cause an increase in the number of surface-visiting grains reflected by increasing NSF values for the upper part of the soil profile that is dominated by sedimentation.

In the next subsections we will present the feldspar single-grain luminescence age versus depth and NSF versus depth results from our investigation at the SC-CZO (Fig. 4.4.2) and discuss them in the context of the conceptual considerations outlined earlier.

4.4.3 Luminescence age and NSF–depth profiles along the hillslope catena

In Fig. 4.4.2, single-grain feldspar luminescence age–depth and NSF–depth trends for all four soil profiles along the hillslope catena age are shown (data from Román-Sánchez et al., 2019a). Based on field and luminescence observations we identified the thickness of the soil by field mapping the mobile regolith–saprolite boundary according to Schoeneberger (2012). This field boundary is illustrated as a black dashed line, while the luminescence NSF-based upper and lower boundary are displayed as red-dotted and dashed-dotted lines,

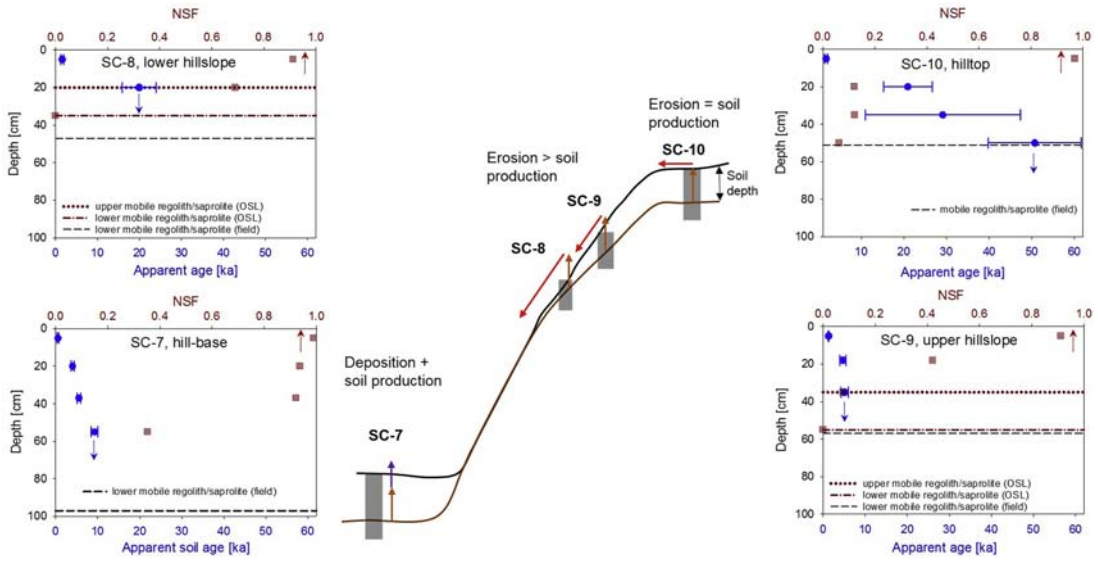

FIGURE 4.4.2 Feldspar single-grain luminescence age versus depth (*blue circles*) and NSF versus depth (*red squares*) results for four profiles along the Santa Clotilde Critical Zone Observatory hillslope catena. Detailed explanations are provided in the main text. The original feldspar single-grain luminescence data (age, NSF) are presented in Román-Sánchez et al. (2019a). *NSF*, Non-saturation factor.

respectively. Based on this we could order the four soil profiles according to their soil thickness as follows: SC-7 > SC-10 > SC-9 > SC-8, which is well in line with our expectations based on our conceptual model (Fig. 4.4.1). The depositional hill base profile SC-7 provides the thickest soil, while the two eroding hillslope positions SC-8 and -9 show truncated soil profiles (Fig. 4.4.2) resulting in a thinner mobile regolith. Interestingly, the NSF-based soil thickness estimates of the two eroding hillslope profiles (SC-8 and -9) are more in line with the soil geomorphic position of the two profiles than the corresponding field observations. This suggests that the luminescence-based proxy might provide a more objective manner to recognize the mechanically altered thickness of soils than field methods (Román-Sánchez et al., 2019a).

The luminescence age–depth distribution of all four soil profiles confirms this first observation. The depositional hill base luminescence age–depth profile SC-7 is stretched and shows a steep sublinear upper part reflecting the addition of colluvium from uphill areas. The steady-state hilltop profile SC-10 in contrast shows an exponentially slower decaying age–depth profile (Fig. 4.4.2) clearly in line with a dominance of bioturbation. The larger age errors compared to the hill-base soil reflect the higher age heterogeneity of the corresponding samples, which also hints at in situ bioturbation as the dominating grain-surfacing process. The exponentially decaying luminescence age versus depth profile of the lower hillslope position SC-8 is truncated reflecting erosion of soil material. The age versus depth trend of the upper hillslope soil SC-9 is less obvious. For this soil profile the sample at ~35 cm depth shows a relatively young age, which is not in line with the expected truncation of the luminescence age–depth profile. However, the number of surfaced grains that record this age trend is very small (NSF of 0.075 corresponding to 7.5% surfaced grains). Considering the gentler slope determined for the upper hillslope position compared to the lower hillslope it was concluded that SC-9 is at a moderately eroding position, while soil profile SC-8 is located at a more intensively eroding position (Román-Sánchez et al., 2019a). This interpretation could clarify the differences observed in SC-8 and SC-9 OSL age versus depth profiles. Overall the luminescence age versus depth trends observed along the SC-CZO hillslope catena can be well explained by process considerations outlined in our conceptual model (Fig. 4.4.1).

The NSF–depth profiles record the number of surfaced grains as a function of soil depth. Also, here we observe a stretched and steeper NSF versus depth trend for the depositional profile SC-7 at the hill base presumably reflecting the lateral addition of reworked grains from the uphill area. The hilltop soil SC-10 shows a clear exponential increase in NSF with decreasing soil depth reflecting the increasing intensity of bioturbation in increasing proximity to the ground surface. However, even at 55 cm depth, 6.2% (NSF = 0.062) of surfaced grains are detected suggesting that the profile is not truncated because erosion is balanced by soil production at the mobile regolith–saprolite interface. The two profiles at the hillslope positions show shorter and thus truncated NSF–depth profiles (Fig. 4.4.2). This truncation is more pronounced for the lower hillslope profile SC-8 than for the upper hillslope profile SC-9. This again confirms the field hypothesis that SC-8 is located at a more intensively eroding part of the hillslope than SC-9 (also see earlier). Furthermore, the NSF versus depth profiles provide valuable information on the erosional process itself. The NSF of the eroding soils SC-8 and SC-9 at shallow depth (~20 cm) yield values of 62% and 42%, respectively, indicating a significantly larger number of surfaced grains compared to the reference steady-state hilltop soil profile SC-10 (12%). This increase in NSF at shallow soil depth points to soil creep as the dominating lateral soil particle transport process along the hillslope catena (Fig. 4.4.1 and previous section).

4.4.4 From qualitative trends to quantitative rates

By combining the luminescence age versus soil depth information with the NSF versus depth information we can also calculate effective soil reworking rates (SR_{eff}) for individual samples based on a simple equation (Reimann et al., 2017):

$$SR_{eff} = \frac{\text{sample depth [mm]}}{\text{apparent burial age [a]}} \times \text{NSF}$$

The soil reworking rate SR_{eff} provides a useful first approximation of the combined effect of vertical and lateral mixing of particles at a certain sample position. The SR_{eff} estimate can be used to numerically compare samples from different bioturbation regimes (e.g., ant versus gopher bioturbation) with each other (Román-Sánchez et al., 2019a). However, it is important to point out that SR_{eff} is still a linear mixing measure of a process that has in fact two spatial dimensions. In the following we outline two possible paths to overcome this oversimplification.

In a companion paper (Román-Sánchez et al., 2019b) we use the luminescence data from the SC-CZO hillslope catena (previous subsection) and propose an analytical solution for the diffusion–advection equation. With this we are able to simultaneously calculate both the diffusivity constant (i.e., bioturbation) and erosion–deposition rate from the same dataset. The diffusivity constant at the surface varies between 11.4 and 81.9 mm^2/a for the hilltop and hill base profile, respectively, and from 7.4 to 64.8 mm^2/a at a soil depth of 50 cm (Román-Sánchez et al., 2019b). The uncertainties of corresponding erosion–deposition rates are too high to make firm statements. However, we also think that this reflects the dominance of the bioturbation process in the investigated SC-CZO settings and furthermore we are confident that the precision of the erosion–deposition rates can be improved in future research by a denser sampling scheme.

An alternative model to the diffusion–advection equation has been proposed by Furbish et al. (2018a,b). Their model describes soil particle trajectories as non-uniform two-dimensional motions with superimposed depth-dependent mixing using an Eulerian–Lagrangian algorithm. They characterize the mixing intensity by a Péclet number that incorporates the speed at which the soil particle enters the soil mantle at the saprolite–mobile regolith boundary, the thickness of the mobile regolith and the diffusivity at the surface. If we now compare the NSF soil depth trends presented in Fig. 4.4.2 with the model predictions of Furbish et al. (2018b, their Fig. C1) our field observation for the steady-state profile SC-10 is best described with a weak to moderate mixing scenario (corresponding to Péclet numbers 10 to 1). The shape of the NSF–depth trend for the depositional profile SC-7, on the other hand, better agrees with an intensive mixing scenario (with Péclet number < 1), nicely capturing the addition of well-mixed material from upslope areas.

4.4.5 Conclusion

Luminescence dating methods provide a new tool to gain a quantitative understanding of vertical and lateral soil mixing processes. This requires measurement of luminescence signals from single grains. Where most previous investigations were based on quartz OSL, we recently showed the great potential of single-grain feldspar luminescence methods for this application. This method determines what fraction of grains has reached the surface at least once during soil formation (the NSF) as well as information on mixing rates from the luminescence ages of individual grains. By combining both measures, the mixing intensity and possibly residence time of soil particles can be quantified. We expect this tool to be valuable for improved understanding of soil mantle responses to environmental conditions.

References

Bakels, C.C., 1988. Pollen from plaggen soils in the province of North Brabant. Man-made soils, BAR international Series 410, 35–54.

Baker, C.A., Bateman, M., Bateman, P., Jones, H., 2013. The aeolian sand record in the Trent Valley. The Mercian Geologist 18 (2), p108–118.

Bastiaens, J., van Mourik, J.M., 1994. Bodemsporen van beddenbouw in het zuidelijk deel van het plaggenlandbouw areaal. Historisch Geografisch Tijdschrift 12, 81–90.

Bateman, M.D., Van Huissteden, J., 1999. The timing of last-glacial periglacial and aeolian events, Twente, eastern Netherlands. Journal of Quaternary Science 14 (3), 277–283.

Bateman, M.D., Boulter, C.H., Carr, A.S., Frederick, C.D., Peter, D., Wilder, M., 2007. Preserving the palaeoenvironmental record in Drylands: bioturbation and its significance for luminescence-derived chronologies. Sedimentary Geology 195, 5–19.

Bateman, M.D., Frederick, C.D., Jaiswal, M.K., Singhvi, A.K., 2003. Investigations into the potential effects of pedoturbation on luminescence dating. Quaternary Science Reviews 22, 1169–1176.

Beukenkamp, P.C., Sevink, J., 2005. Natuur en landschap. In: Beukhof, H., van Essen, F., Pelzers, E., Sevink, J. (Eds.), Natuur en kunst 'De Hoge Veluwe'. Waanders Uitgevers, Zwolle, pp. 38–97.

Bierman, P., Steig, E.J., 1996. Estimating rates of denudation using cosmogenic isotopes abundances in sediment. Earth Surface Processes and Landforms 21, 125–139.

Bokhorst, M.P., Duller, G.A.T., van Mourik, J.M., 2005. Optically stimulated luminescence dating of a fimic anthrosol in the southern Netherlands. Journal of Archaeological Science 32, 547–553.

Brill, D., Reimann, T., Wallinga, J., May, S.M., Engel, M., Riedesel, S., Brückner, H., 2018. Testing the accuracy of feldspar single grains to date late Holocene cyclone and tsunami deposits. Quaternary Geochronology 48, 91–103.

Brock, F., Higham, T., Ditchfield, P., Ramsey, C.B., 2010. Current pretreatment methods for AMS radiocarbon dating at the Oxford Radiocarbon Accelerator Unit (ORAU). Radiocarbon 52 (1), 103–112.

Brussaard, L., Runia, L.T., 1984. Recent and ancient traces of scarab beetle activity in sandy soils of the Netherlands. Geoderma 34 (3–4), 229–250.

Burny, J., 1999. Bijdrage tot de historische ecologie van de Limburgse Kempen (1910–1950), Natuurhistorisch Genootschap in Limburg XLII(1) (Maastricht).

Buylaert, J.P., Jain, M., Murray, A.S., Thomsen, K.J., Thiel, C., Sohbati, R., 2012. A robust feldspar luminescence dating method for Middle and Late Pleistocene sediments. Boreas 41, 435–451.

Chamberlain, E.L., Törnqvist, T.E., Shen, Z., Mauz, B., Wallinga, J., 2018. Anatomy of Mississippi Delta growth and its implications for coastal restoration. Science Advances 4, eaar4740.

Crommelin, R.D., 1964. A contribution to the sedimentary petrology and provenance of Young Pleistocene coversand in the Netherlands. Geologie en Mijnbouw 43 (9), 389–402.

Cunningham, A.C., Wallinga, J., 2012. Realizing the potential of fluvial archives using robust OSL chronologies. Quaternary Geochronology 12, 98–106.

Cunningham, A.C., Wallinga, J., Minderhoud, P.S.J., 2011. Expectations of scatter in equivalent-dose distributions when using multi-grain aliquots for OSL dating. Geochronometria 38, 424–431.

Cunningham, A.C., Wallinga, J., Hobo, N., Versendaal, A.J., Makaske, B., Middelkoop, H., 2015. Re-evaluating luminescence burial doses and bleaching of fluvial deposits using Bayesian computational statistics. Earth Surface Dynamics 3, 55–65.

Dalsgaard, K., Odgaard, B.V., 2001. Dating sequences of buried horizons of podzols developed in wind-blown sand at Ulfborg, Western Jutland. Quaternary International 78 (1), 53–60.

Daniels, F., Boyd, C.a., Saunders, D.F., 1953. Thermoluminescence as a research tool. Science 117, 343–349.

de Keyzer, M., 2014. The Common Denominator; the Survival of the Commons in the Late Medieval Campine Area. University Antwerpen, Department of History, Belgium.

Deeben, J., Hiddink, H., Huisman, D.J., Müller, Schokker, J., Wallinga, J., 2010. Middle Palaeolithic artefact migration due to periglacial processes; a geological investigation into near-surface occurrence of Palaeolithic artefacts (Limburg – eastern Brabant coversand region, the Netherlands). Netherlands Journal of Geosciences – Geologie en Mijnbouw 89, 35–50.

Doorenbosch, M., 2013. Ancestral Heaths: Reconstructing the Barrow Landscape in the Central and Southern Netherlands. Sidestone Press.

Doorenbosch, M., van Mourik, J.M., 2016. The impact of ancestral heath management on soils and landscapes: a reconstruction based on paleoecological analyses of soil records in the central and southeastern Netherlands. SOIL 2 (3), 311–324.

Fuchs, M., Lang, A., 2009. Luminescence dating of hillslope deposits – a review. Geomorphology 109, 17–26.

Furbish, D.J., Roering, J.J., Almond, P., Doane, T.H., 2018a. Soil particle transport and mixing near a hillslope crest: 1. Particle ages and residence times. Journal of Geophysical Research: Earth Surface 123, 1052–1077.

Furbish, D.J., Roering, J.J., Keen-Zebert, A., Almond, P., Doane, T.H., Schumer, R., 2018b. Soil particle transport and mixing near a hillslope crest: 2. Cosmogenic nuclide

and optically stimulated luminescence tracers. Journal of Geophysical Research: Earth Surface 123, 1078–1093.

Galbraith, R.F., Roberts, R.G., Laslett, G.M., Yoshida, H., Olley, J.M., 1999. Optical dating of single and multiple grains of quartz from jinmium rock shelter, northern Australia, part 1, experimental design and statistical models. Archaeometry 41, 339–364.

Geyh, M.A., Roeschmann, G., Wijmstra, T.A., Middeldorp, A.A., 1983. The unreliability of 14 C dates obtained from buried sandy podzols. Radiocarbon 25 (2), 409–416.

Gliganic, L.A., Cohen, T.J., Slack, M., Feathers, J.K., 2016. Sediment mixing in aeolian sand sheets identified and quantified using single-grain optically stimulated luminescence. Quaternary Geochronology 32, 53–66.

Goh, K.M., Molloy, B.P., 1978. Radiocarbon dating of paleosols using soil organic matter components. Journal of Soil Science 29 (4), 567–573.

Groenewoudt, B.J., 2012. History continuous: drowning and desertification. Linking past and future in the Dutch landscape. Quaternary International 251, 125–135.

Groenman-van Waateringe, W., Spek, T., 2016. Heathland and palynology of prehistoric barrows. Reflections on the interrelation between soil formation and pollen infiltration. Palaeohistoria 58, 55–62.

Guralnik, B., Ankjaergaard, C., Jain, M., Murray, A.S., Muller, A., Walle, M., Lowick, S.E., Preusser, F., Rhodes, E.J., Wu, T.S., Mathew, G., Herman, F., 2015. OSL-thermochronometry using bedrock quartz: a note of caution. Quaternary Geochronology 25, 37–48.

Heimsath, A.M., Chappell, J., Spooner, N.A., Questiaux, D.G., 2002. Creeping soil. Geology 30, 111–114.

Heimsath, A.M., Dietrich, W.E., Nishiizumi, K., Finkel, R.C., 1997. The soil production function and landscape equilibrium. Nature 388, 358–361.

Huisman, H., de Kort, J.-W., Ketterer, M., Reimann, T., Schoorl, J., van der Heiden, M., van Soest, M., van Egmond, F., 2018. Erosion of Archaeological Sites: quantifying the threat using OSL and fall out isotopes. Geoarchaeology 1–17.

Huntley, D.J., Godfrey-Smith, D.I., Thewalt, M.L.W., 1985. Optical dating of sediments. Nature 313, 105–107.

Hütt, G., Jaek, I., Tchonka, J., 1988. Optical dating – K-feldspars optical-response stimulation spectra. Quaternary Science Reviews 7, 381–385.

ISRIC-FAO, 2006. World Reference Base for Soil Recourses. In: World Soil Resources Reports, vol. 103. FAO, Rome.

IUSS Working Group, 2014. World Reference Base for Soil Resources 2014. In: International Soil Classification System for Naming Soils and Creating Legends for Soil Maps, third ed. FAO, Rome.

Jansen, R., van der Laan, K. (Eds.), 2011. Verleden van een bewogen landschap, landschaps- en bewoningsgeschiedenis van de Maashorst. Matrijs, Utrecht.

Janssen, C.R., 1974. Verkenningen in de Palynologie. OOsthoek, Scheltema and Holkema, Utrecht.

Johnson, M.O., Mudd, S.M., Pillans, B., Spooner, N.A., Fifield, L.K., Kirkby, M.J., Gloor, M., 2014. Quantifying the rate and depth dependence of bioturbation based on Optically-Stimulated Luminescence (OSL) dates and meteoric 10Be. Earth Surface Processes and Landforms 39, 1188–1196.

Jongmans, A.G., Van den Berg, M.W., Sonneveld, M.P.W., 2012. Landschappen van Nederland: geologie, bodem en landgebruik. Wageningen Academic Publishers.

Joordens, J.C.A., d'Errico, F., Wesselingh, F.P., Munro, S., de Vos, J., Wallinga, J., Ankjaergaard, C., Reimann, T., Wijbrans, J.R., Kuiper, K.F., Mucher, H.J., Coqueugniot, H., Prie, V., Joosten, I., van Os, B., Schulp, A.S., Panuel, M., van der Haas, V., Lustenhouwer, W., Reijmer, J.J.G., Roebroeks, W., 2015. Homo erectus at Trinil on Java used shells for tool production and engraving. Nature 518. 228-U182.

Jungerius, P.D., Riksen, J.P.,M., 2010. Contribution of laser altimetry images to the geomorphology of the Late Holocene inland drift sands of the European Sand Belt. Baltica 23/1, 59–70.

Kars, R.H., Busschers, F.S., Wallinga, J., 2012. Validating post IR-IRSL dating on K-feldspars through comparison with quartz OSL ages. Quaternary Geochronology 12, 74–86.

Keesstra, S.D., Bouma, J., Wallinga, J., Tittonell, P., Smith, P., Cerdà, A., Montanarella, L., Quinton, J.N., Pachepsky, Y., van der Putten, W.H., Bardgett, R.D., Moolenaar, S., Mol, G., Jansen, B., Fresco, L.O., 2016. The significance of soils and soil science towards realization of the United Nations Sustainable Development Goals. SOIL 2, 111–128.

Koster, E.A., Castel, I.Y., Nap, R.L., 1993. Genesis and sedimentary structures of late Holocene aeolian drift sands in northwest Europe. Geological Society, London, Special Publications 72 (1), 247–267.

Koster, E.A., 2009. The "European Aeolian Sand Belt": geoconservation of drift sand landscapes. Geoheritage 1 (2–4), 93–110.

Kristensen, J.A., Thomsen, K.J., Murray, A.S., Buylaert, J.-P., Jain, M., Breuning-Madsena, H., 2015. Quantification of termite bioturbation in a savannah ecosystem: application of OSL dating. Quaternary Geochronology 30, 331–334.

Laban, C., Kars, H., Heidinga, A., 1988. IJzer uit eigen bodem. Grondboor en Hamer 42/1, 1–11.

Leenders, K.A., 1996. De boekweitcultuur in historisch perspectief. Geografisch Tijdschrift 21, 213–227.

Madsen, A.T., Murray, A.S., 2009. Optically stimulated luminescence dating of young sediments: a review. Geomorphology 109, 3–16.

Madsen, A.T., Murray, A.S., Jain, M., Andersen, T.J., Pejrup, M., 2011. A new method for measuring bioturbation rates in sandy tidal flat sediments based on luminescence dating. Estuarine, Coastal and Shelf Science 92, 464–471.

Mook, W.G., Streurman, H.J., 1983. Physical and chemical aspects of radiocarbon dating, first symposium on 14C and archaeology, Groningen. PACT 8, 31–55.

Mücher, H.J., Slotboom, R.T., ten Veen, W.J., 1989. Palynology and micromorphology of a man made soil. A reconstruction of the agricultural history since Late-Medieval Times of the Posteles in the Netherlands. Catena 17, 55–67.

Murray, A.S., Wintle, A.G., 2000. Luminescence dating of quartz using an improved single-aliquot regenerative-dose protocol. Radiation Measurements 32, 57–73.

Murray, A.S., Wintle, A.G., 2003. The single aliquot regenerative dose protocol: potential for improvements in reliability. Radiation Measurements 37, 377–381.

Nicolay, A., Raab, A., Raab, T., Rösler, H., Bönisch, E., Murray, A.S., 2014. Evidence of (pre-) historic to modern landscape and land use history near Jänschwalde (Brandenburg, Germany). Zeitschrift für Geomorphologie 58 (2), 7–31. Supplementary Issues.

Nielsen, A.H., Elberling, B., Pejrup, M., 2010. Soil development rates from an optically stimulated luminescence-dated beach ridge sequence in Northern Jutland, Denmark. Canadian Journal of Soil Science 90, 295–307.

Pape, J.C., 1972. Oude bouwlandgronden in Nederland. Boor en Spade 18, 85–115.

Pierik, H.J., van Lanen, R.J., Gouw-Bouman, M.T., Groenewoudt, B.J., Wallinga, J., Hoek, W.Z., 2018. Controls on late-Holocene drift-sand dynamics: the dominant role of human pressure in the Netherlands. The Holocene 28 (9), 1361–1381.

Preusser, F., Degering, D., Fuchs, M., Hilgers, A., Kadereit, A., Klasen, N., Krbetschek, M., Richter, D., Spencer, J.Q.G., 2008. Luminescence dating: basics, methods and applications. Eiszeitalter und Gegenwart – Quaternary Science Journal 57, 95–149.

Preusser, F., Ramsmeyer, K., Schlüchter, C., 2006. Characterisation of low OSL intensity quartz from New Zealand Alps. Radiation Measurements 41, 871–877.

Reimann, T., Thomsen, K.J., Jain, M., Murray, A.S., Frechen, M., 2012. Single-grain dating of young sediments using the pIRIR signal from feldspar. Quaternary Geochronology 11, 28–41.

Reimann, T., Román-Sánchez, A., Vanwalleghem, T., Wallinga, J., 2017. Getting a grip on soil reworking e single-grain feldspar luminescence as a novel tool to quantify soil reworking rates. Quaternary Geochronology 42, 1–14.

Rhodes, E.J., 2011. Optically stimulated luminescence dating of sediments over the past 200,000 years. Annual Review of Earth and Planetary Sciences 39, 461–488.

Riksen, M., Ketner-Oostra, R., van Turnhout, C., Nijssen, M., Goossens, D., Jungerius, P.D., Spaan, W., 2006. Will we lose the last active inland drift sands of Western Europe? The origin and development of the inland drift-sand ecotype in the Netherlands. Landscape Ecology 21 (3), 431–447.

Román-Sánchez, A., Reimann, T., Wallinga, J., Vanwalleghem, T., 2019a. Bioturbation and erosion rates along the soil-hillslope conveyor belt, part 1: insights from single-grain feldspar luminescence. Earth Surface Processes and Landforms 44, 2051–2065.

Román-Sánchez, A., Laguna, A., Reimann, T., Giráldez, J.V., Peña, A., Vanwalleghem, T., 2019b. Bioturbation and erosion rates along the soil-hillslope conveyor belt, part 2: quantification using an analytical solution of the diffusion-advection equation. Earth Surface Processes and Landforms 44, 2066–2080.

Román-Sánchez, A., Vanwalleghem, T., Peña, A., Laguna, A., Giráldez, J.V., 2017. Controls on soil carbon storage from topography and vegetation in a rocky, semi-arid landscapes. Geoderma.

Šamonil, P., Král, K., Hort, L., 2010. The role of tree uprooting in soil formation: a critical literature review. Geoderma 157 (3–4), 65–79.

Schaetzl, R.J., Burns, S.F., Small, T.W., Johnson, D.L., 1990. Tree uprooting: review of types and patterns of soil disturbance. Physical Geography 11 (3), 277–291.

Schoeneberger, P.J., Wysocki, D.A., Benham, E.C., Soil Survey Staff, 2012. Field book for describing and sampling soils, Version 3.0. In: Natural Resources Conservation Service. National Soil Survey Center, Lincoln, NE.

Sevink, J., Vlaming, M.C., Van den Berg, W.J., Khodabux, E.R., Landsmeer, D., Stoeten, G.J., 2008. De sanering van het Laarder Wasmerengebied. Bodem 5, 8–11.

Sevink, J., 2010. Precisiewerk bij bodemsanering. aandacht voor venherstel en aardkundige waarden bij sanering Laarder Wasmeren. Vakblad Natuur Bos Landschap 9, 26–29.

Sevink, J., Koster, E.A., van Geel, B., Wallinga, J., 2013. Drift sands, lakes, and soils: the multiphase Holocene history of the Laarder Wasmeren area near Hilversum, the Netherlands. Netherlands Journal of Geosciences 92 (4), 243–266.

Sevink, J., Bergsma, H., Koopman, S., Prins, M.A., 2017. Het (Jonger) dekzand in het Gooi: deel 2: geochemie en herkomst. Grondboor en Hamer 71.

Sevink, J., van Geel, B., Jansen, B., Wallinga, J., 2018. Early Holocene forest fires, drift sands, and Usselo-type paleosols in the Laarder Wasmeren area near Hilversum, the Netherlands: implications for the history of sand landscapes and the potential role of Mesolithic land use. Catena 165, 286–298.

Schokker, J., Cleveringa, P., Murray, A.S., Wallinga, J., Westerhoff, W.E., 2005. An OSL dated Middle and late quaternary sedimentary record in the roer valley Graben (southeastern Netherlands). Quaternary Science Reviews 24, 2243–2264.

Smedley, R.K., Glasser, N.F., Duller, G.A.T., 2016. Luminescence dating of glacial advances at Lago Buenos Aires (~46 °S), Patagonia. Quaternary Science Reviews 134, 59–73.

Smits, J., Noordijk, J., 2013. Heidebeheer, Moderne Methoden in een Eeuwenoud Landschap (KNNV uitgeverij).

Spek, T., 2004. Het Drentse Esdorpenlandschap, vol. 2. Een historisch-geografische studie, Matrijs, Utrecht, pp. 725–967 part vol. I.

Stockmann, U., Minasny, B., McBratney, A.B., 2014. How fast does soil grow? Geoderma 216, 48–61.

Stockmann, U., Minasny, B., Pietsch, T.J., McBratney, A.B., 2013. Quantifying processes of pedogenesis using optically stimulated luminescence. European Journal of Soil Science 64, 145–160.

Thomsen, K.J., Murray, A.S., Bøtter-Jensen, L., Kinahan, J., 2007. Determination of burial dose in incompletely bleached fluvial samples using single grains of quartz. Radiation Measurements 42, 370–379.

Thomsen, K.J., Murray, A.S., Jain, M., Bøtter-Jensen, L., 2008. Laboratory fading rates of various luminescence signals from feldspar-rich sediment extracts. Radiation Measurements 43, 1474–1486.

Tolksdorf, J.F., Kaiser, K., 2012. Holocene aeolian dynamics in the European sand-belt as indicated by geochronological data. Boreas 41 (3), 408–421.

van der Hammen, T., 1965. De Klokkenberg bij Denekamp: een geologisch-palynologisch onderzoek van een Twentse es. Tijdschrift KNAG. Tweede Reeks 82, 123–134.

Van der Meij, W.M., Reimann, T., Vornehm, V.K., Temme, A.J.A.M., Wallinga, J., van Beek, R., Sommer, M., 2019. Reconstructing rates and patterns of colluvial soil redistribution in agrarian (hummocky) landscapes. Earth Surface Processes and Landforms 44, 2408–2422.

Van der Salm, C., Verstraten, J.M., 1994. Acid neutralization mechanisms in three acid sandy soils. Geoderma 63 (3–4), 227–243.

Van Geel, B., Russell Coope, G., Van Der Hammen, T., 1989. Palaeoecology and stratigraphy of the Lateglacial type section at Usselo (the Netherlands). Review of Palaeobotany and Palynology 60 (1–2), 25–129.

Van Gorp, W., Veldkamp, A., Temme, A.J.A.M., Maddy, D., Demir, T., van der Schriek, T., Reimann, T., Wallinga, J., Wijbrans, J., Schoorl, J.M., 2013. Fluvial response to Holocene volcanic damming and breaching in the Gediz and Geren rivers, western Turkey. Geomorphology 201, 430–448.

van Hoesel, A., Hoek, W.Z., Braadbaart, F., van der Plicht, J., Pennock, G.M., Drury, M.R., 2012. Nanodiamonds and wildfire evidence in the Usselo horizon postdate the Allerod-Younger Dryas boundary. PNAS 109, 7648–7653.

van Mourik, J.M., 1987. Het Stuifzand Van Heeswijk-Dinther, vol. XXI. Geografisch Tijdschrift, pp. 327–337.

van Mourik, J.M., Ligtendag, W.A., 1988. De overstoven enk van Nabbegat. Geografisch Tijdschrift XXII, 412–420 (with English summary).

van Mourik, J.M., 1991. Spuren von Plaggenlandbau im Gebiet der Schleswiger Landenge. Offa 47, 169–176.

van Mourik, J.M., 2001. Pollen and spores, preservation in ecological settings. In: Briggs, E.G., Crowther, P.R. (Eds.), Palaeobiology II. Blackwell Science, pp. 315–318.

van Mourik, J.M., Horsten, F., 1995. De Paleogeografie van de Valenakker. Weerter Jaarboek 10, 105–118.

van Mourik, J.M., Wartenbergh, P.E., Mook, W.J., Streurman, H.J., 1995. Radiocarbon dating of palaeosols in eolian sands. Mededelingen Rijks Geologische Dienst 52, 425–439.

van Mourik, J.M., Nierop, K.G.J., Vandenberghe, D.A.G., 2010. Radiocarbon and optically stimulated luminescence dating based chronology of a polycyclic driftsand sequence at Weerterbergen (SE Netherlands). Catena 80 (3), 170–181.

van Mourik, J.M., Slotboom, R.T., Wallinga, J., 2011. Chronology of plaggic deposits; palynology, radiocarbon and optically stimulated luminescence dating of the Posteles (NE-Netherlands). Catena 84, 54–60.

van Mourik, J.M., Seijmonsbergen, A.C., SLotboom, R.T., Wallinga, J., 2012a. Impact of human land use on soils and landforms in cultural landscapes on aeolian sandy substrates (Maashorst, SE-Netherlands). Quaternary International 265, 74–89.

van Mourik, J.M., Seijmonsbergen, A.C., Jansen, B., 2012b. Geochronology of Soils and Landforms in Cultural Landscapes on Aeolian Sandy Substrates, Based on Radiocarbon and Optically Stimulated Luminescence Dating (Weert, SE-Netherlands). InTech, Radiometric Dating, pp. 75–114.

van Mourik, J.M., Wagner, T.V., de Boer, J.G., Jansen, B., 2016. The added value of biomarker analysis to the genesis of Plaggic Anthrosols; the identification of stable fillings used for the production of plaggic manure. SOIL 2, 299–310. www.soil-journal.net/2/299/2016/.

Vera, H., 2011. Dat men het goed van den ongeboornen niet mag verkoopen, Gemene gronden in de Meierij van Den Bosch tussen hertog en hertgang 1000–2000. Uitgeverij BOXpress, Oisterwijk, Netherlands (with English summary).

Von Blanckenburg, F., 2005. The control mechanisms of erosion and weathering at basin scale from cosmogenic

nuclides in river sediment. Earth and Planetary Science Letters 242, 224–239.

Wagner, T.V., Mouter, A.K., Parsons, J.R., Sevink, J., van der Plicht, J., Jansen, B., 2018. Molecular characterization of charcoal to identify adsorbed SOM and assess the effectiveness of common SOM-removing pretreatments prior to radiocarbon dating. Quaternary Geochronology 45, 74–84.

Wallinga, J., Cunningham, A.C., 2015. Luminescence dating, uncertainties, and age range. Encyclopedia of Scientific Dating Methods 440–445.

Wallinga, J., van Mourik, J.M., Schilder, M.L.M., 2013. Identifying and dating buried micropodzols in Subatlantic polycyclic drift sands. Quaternary International 306, 60–70.

Waterbolk, H.T., 1964. Podsolierungserscheinungen bei Grabhügeln. Palaeohistoria 10, 87–102.

Wilkinson, M.T., Humphreys, G.S., 2005. Exploring pedogenesis via nuclide-based soil production rates and OSL-based bioturbation rates. Soil Research 43, 767–779.

Willemse, N.W., Groenewoudt, B.J., 2012. Resilience of metastable landscapes? The non-linear response of Late Glacial aeolian landforms to prehistoric reclamation along Dutch river valleys. eTopoi. Journal for Ancient Studies 3 (special volume), 245–255.

CHAPTER

5

Biomarker analysis of soil archives

B. Jansen, H. Hooghiemstra, S.P.C. de Goede, J.M. van Mourik*

Department of Ecosystem and Landscape Dynamics, Institute for Biodiversity and Ecosystem Dynamics, University of Amsterdam, Amsterdam, the Netherlands

***Corresponding author. B.Jansen@uva.nl**

5.1 Principles of biomarker analysis

The last few decades have seen a dramatic increase in the application of biomarkers as molecular proxies in environmental reconstructions (Jansen and Wiesenberg, 2017). The term 'biomarker' is not very strictly defined and in its broadest sense refers to the use of specific molecular characteristics of organic matter that 'may be diagnostic of specific organisms, classes of organism, or general biota that contribute organic matter to the atmosphere, aqueous or sedimentary environment' (Peters et al., 2005). Biomarkers are used in many different fields of science. For instance, in medical science they encompass, inter alia, molecules that indicate the presence of a disease or response to treatment (Brennan et al., 2013; van Bon et al., 2014); in forensic science they establish a link between a crime scene and a suspect (Concheri et al., 2011); in limnology they are used to study the development over time of the conditions in a lacustrine environment (Castañeda and Schouten, 2011); and in organic geochemistry they can trace oil formation and translocation in rocks (Curiale, 2002). A biomarker can be a specific molecule, the presence of which is indicative of a certain process or effect. An example is the presence of cholesterol in the topsoil as biomarker evidence for the movement of a human body in a forensic context (Luong et al., 2018). However, a biomarker can also be a unique concentration ratio of two or more otherwise ubiquitous compounds, for instance, a shift in the ratio of the concentration of certain molecules in natural oil as an indicator of oil-to-gas cracking during fossil fuel formation (Chen et al., 2016).

This chapter will focus on the application of biomarkers preserved in palaeosols, or related archives such as peat deposits, as palaeoecological proxies in environmental reconstructions. When considered in this context, biomarker applications are still vast and diverse, but cluster in a limited number of main themes: reconstruction of changes in vegetation composition over time (e.g., Pautler et al., 2013; Buggle and Zech, 2015); reconstruction of changes in climate, i.e., mean annual precipitation and/or temperature over time (e.g., Schreuder et al., 2016; van den Bos et al., 2018); tracing input, transformation and/or decomposition of soil organic matter over time (e.g., Amelung et al., 2008; Li et al., 2018); and as evidence or to reconstruct impact

https://doi.org/10.1016/B978-0-444-64108-3.00005-7

over time of human settlement or environmental alteration, e.g., in the form of human-induced biomass burning, agricultural practices or animal husbandry (e.g., Dungait et al., 2010; Collins et al., 2017). Often, one or more areas of reconstruction are combined, for instance, when (combinations of) biomarkers are used to simultaneously reconstruct shifts in vegetation and climate (e.g., van den Bos et al., 2018).

5.1.1 Compounds used as biomarkers

Within the four mentioned domains of the main applications of biomarkers, there are many molecules, or features thereof, that are commonly used as biomarkers, virtually all of them belonging to the compound class of lipids (Jansen and Wiesenberg, 2017). Here we describe the main subclasses of components within the lipids that are commonly used as biomarkers, their origin, as well as the type of environmental reconstruction for which they are most commonly used.

5.1.1.1 Plant wax lipids

Terrestrial higher plants contain *n*-alkanes, *n*-alcohols and *n*-fatty acids of higher chainlengths (c. C_{20}–C_{36}) as part of the protective waxes of their leaves and roots (Kolattukudy et al., 1976). These lipids occur in typical odd-over-even chainlength predominance for the *n*-alkanes, and even-over-odd chainlength predominance for the *n*-alcohols and *n*-fatty acids (Kolattukudy et al., 1976). They are commonly used as biomarkers to estimate terrestrial biomass input and/or unravel (shifts in) past vegetation composition based on the premise that they occur in plant-specific concentration patterns that can be unravelled into (groups of) originating species (e.g., Marseille et al., 1999; Zhang et al., 2006; Zeng et al., 2011). For this the entire concentration pattern can be used, but often simple ratios such as the average chainlength (ACL), carbon preference index (CPI) or the relative abundance of two or three dominant chainlengths are applied (Jansen and Wiesenberg, 2017).

Like the *n*-alkanes, *n*-alcohols and *n*-fatty acids, plant sterols and pentacyclic triterpenoids originate from plant waxes (Dinel et al., 1990) and are used as biomarkers in vegetation reconstructions (e.g., Volkman, 2005; Jansen et al., 2007; Lavrieux et al., 2011). In contrast to the *n*-alkanes, *n*-alcohols and *n*-fatty acids, for the plant sterols and pentacyclic triterpenoids, mostly unique individual compounds indicative of (a group of) plant species or simply of terrestrial versus aquatic biomass are sought as biomarkers (e.g., Killops and Frewin, 1994; Otto and Simpson, 2005; Pautler et al., 2013).

5.1.1.2 Plant-derived lipid biopolymers

Lignin is a generic label for a large group of biopolymers that are part of plant cell walls of secondarily thickened cells (Vanholme et al., 2010). Lignin gives the cells rigidity and protects cell wall polysaccharides from microbial degradation (Vanholme et al., 2010). The three main groups of monomer units from which the lignin polymer is constructed are (1) *p*-hydroxyphenyl or cinnamyl, (2) guaiacyl or vanillyl and (3) syringyl, which occur in different relative abundances in different types of plants (Vanholme et al., 2010). Based on this the relative abundance of monomer units from the three groups has been used as biomarkers to separate organic matter input, particularly from gymnosperms, angiosperms and grasses (e.g., Spielvogel et al., 2007; Simpson, M. J. and Simpson, 2012).

Two other biopolymers with frequent biomarker application are cutin and suberin. Cutin occurs predominantly in plant leaves where it constitutes the molecular frame of the plant cuticle (Kögel-Knabner, 2002). In contrast, suberin is a cell wall component of cork cells that is found mainly on the outside of woody plant stems and roots, and in the endodermis and bundle sheet cells of grasses (Kögel-Knabner, 2002). The occurrence of cutin and suberin in different plant compartments forms the basis

of their application as biomarkers, which is mainly to differentiate aboveground from belowground biomass input into the soil (e.g., Mendez-Millan et al., 2011; Hamer et al., 2012). Separation is based on the general observation that in soil organic matter, long-chain even-numbered C_{20}–C_{30} ω-hydroxy fatty acids and α,ω-alkanedioic acids mainly originate from suberin, whereas shorter-chained C_{16} and C_{18} ω-hydroxy fatty acids mainly derive from cutin (Mendez-Millan et al., 2011).

5.1.1.3 Molecules of animal or microbial origin

Molecules of animal origin, in particular those linked to manure, are often used as biomarkers of past human impact in the form of agriculture or animal husbandry. Any number of compounds can be used, but predominantly the presence of compounds produced during digestion, such as coprostanol, 5β-stigmastanol, sitosterol and their epimers, is applied to infer the occurrence and/or intensity of such human practices (e.g., D'Anjou et al., 2012; Birk et al., 2012).

In environmental reconstructions, lipids of microbial origin are used to reconstruct palaeotemperature. Glycerol dibiphytanyl glycerol tetraethers (GDGTs) are microbial membrane lipids that originate from planktonic, methanogenic and methanotrophic species of Thaumarchaeota and Euryarchaeota, as well as from soil bacteria and archaea (Schouten et al., 2013). The exact soil bacterial origin is as yet unknown, although several researchers indicate that Acidobacteria are the most likely source (Schouten et al., 2013). In addition, the biosynthetic origin of GDGTs is not yet entirely clear (Meador et al., 2014) although recent studies determined a heterotrophic lifestyle of their source organisms and close relation to roots especially below the surface soil layer (Weijers et al., 2010; Huguet et al., 2012, 2013). In lake and sea water, the relative distribution of isoprenoid GDGTs produced by Crenarchaeota, as expressed in the TetraEther index of 86 carbon atoms (TEX86), serves as a proxy for sea surface temperature (Schouten et al., 2007; Blaga et al., 2009; Powers et al., 2010). In soils, the cyclization ratio of branched tetraethers, non-isoprenoid GDGT lipids produced by anaerobic terrestrial bacteria, coupled with the methylation index of branched tetraethers functions as a proxy for soil pH and past continental mean annual air temperature (Weijers et al., 2007).

Other applications of microbial lipids as biomarkers include the use of phospholipid fatty acids as a proxy for microbial biomass as part, for instance, of the reconstruction of soil organic matter input and/or turnover (e.g., Kramer and Gleixner, 2006; Kindler et al., 2009; Ngosong et al., 2012; Malik et al., 2013).

5.1.1.4 Compound-specific stable isotope signals as biomarkers

The previous paragraphs described the application of the concentration (ratio) or presence of various molecules as biomarkers in environmental reconstructions. In addition, the stable isotope signal of the same molecules can often be used as a biomarker as well. Specifically, this involves the use of the $\delta^{13}C$, $\delta^{15}N$ and/or $\delta^{2}H$ signal of (some of) the mentioned molecules. For instance, the $\delta^{13}C$ signal can be used to discern vegetation shifts from plants with a C_3 photosynthetic pathway to those with a C_4 photosynthetic pathway or vice versa, or track carbon transformations in the soil (e.g., Feng et al., 2010; Mendez-Millan et al., 2014). The $\delta^{15}N$ signal can be used to reconstruct (past) land management (e.g., Bol et al., 2005; Griepentrog et al., 2015). Finally, the $\delta^{2}H$ signal can be used to reconstruct palaeoelevation and palaeoprecipitation (e.g., Peterse et al., 2009; Luo et al., 2011; Sachse et al., 2012). Using both a molecule as well as its compound-specific isotopic composition potentially enables a direct coupling of the phenomena for which, respectively, the molecule itself and its isotopic composition are a biomarker, for instance, when a plant-specific set of *n*-alkanes

is used as vegetation biomarker and the δ^2H signal of the same molecules as precipitation biomarker (van den Bos et al., 2018).

5.1.2 Challenges for the use of biomarkers in environmental reconstructions

The application of biomarkers as a molecular proxy in environmental reconstructions, although very valuable, comes with several challenges (Jansen and Wiesenberg, 2017). Broadly, these challenges fall into three categories that will each be briefly discussed here.

A first challenge is the variability in composition of a biomarker in their source. The most prominent issue is variability in concentration of one or more lipids that alone or together are used as vegetation biomarkers. This applies to differences between different specimens of the same plant species or parts of the same plant as a result of genetic or life-stage variations and/or external factors such as climate or seasonality (Jansen and Wiesenberg, 2017). For instance, the composition of plant cuticular waxes and lignin of plant species has been found to vary with climatic influences (e.g., Shepherd and Griffiths, 2006; Bélanger et al., 2015; Moingt et al., 2016). This means that biomarker patterns reported in the literature for a certain climate zone cannot be used for reconstructions in another climate zone without considering possible climatic influences on the patterns.

A second challenge, specifically in palaeosols, is the input pathway of biomarkers, in particular input of biomarkers from roots versus leaves. This is particularly an issue with the plant wax lipids, because their composition differs between leaves and roots, although biomass from both sources enters the soil. To what extent this influences or compromises biomarker-based vegetation reconstructions is the subject of ongoing debate. On the one hand, concentrations of lipids in leaf waxes are often orders of magnitude higher than in root waxes, whereas, on the other hand, root biomass input is often much larger than leaf biomass input (Jansen and Wiesenberg, 2017). Also, for cutin and suberin, leaf versus root input in the soil can be an issue. These compounds, as explained, are explicitly used as biomarkers for leaf versus root biomass input. However, several publications challenge the universal applicability of such general observations, indicating instead that genetic variability results in many exceptions. For instance, Hamer et al. (2012) found that $\omega C_{22:0}$, $\omega C_{24:0}$ and $\omega C_{26:0}$ hydroxy fatty acids that are assumed to be suberin and thus root derived occurred in several species also in the shoots. In addition, they found that $\omega C_{16:0}$ and $\omega C_{18:0}$ fatty acids, which are assumed to be cutin derived, also occurred in the roots of several species they studied (Hamer et al., 2012).

Finally, a third challenge, as with any proxy, is degradation of a biomarker or some of the compounds that together constitute a biomarker, once deposited in the soil (or similar archive) (Jansen and Wiesenberg, 2017).

5.1.3 Multiproxy reconstructions and introduction to the case studies

Any proxy applied in environmental reconstructions comes with its own opportunities and challenges. This also holds for the application of biomarkers as explained earlier. Therefore biomarkers should not be seen as a cure-all proxy to replace other proxies, or be applied indiscriminately. Instead, the challenges mentioned should be taken into account and measures taken to counter them if possible, for instance, by using biomarker signals obtained from present-day analogue species from as similar as possible an environment that is to be reconstructed. In addition, wherever possible, biomarkers should be combined with multiple other proxies to obtain a much more rigorous reconstruction.

The opportunities and challenges of the application of biomarkers as one of several proxies in environmental reconstructions will be further explored through three case studies. These case

studies focus on the application of biomarkers to reconstruct upper forest line (UFL) migration in the Ecuadorian Andes (Section 5.2); unravel soil organic matter input sources used in historic plaggen agriculture in the Netherlands (Section 5.3); and explore the potential to jointly reconstruct vegetation and precipitation shifts in the Dominican Republic (Section 5.4).

5.2 Reconstruction of upper forest line migration in the Ecuadorian Andes

5.2.1 Introduction

The highest parts of the Northern Andes, between the UFL at c. 3200–3500 m above sea level (asl) and the snow line at c. 4800 m asl, consist of grass- and shrublands characterized by a high biodiversity (Luteyn, 1999). This tropical alpine ecosystem is known as páramo (Vareschi, 1970; Guhl, 1982; Luteyn, 1999; Sklenar et al., 2005). Here we focus on the Ecuadorian páramo (Acosta Solis, 1984; Vasconez et al., 2001) and we present a synthesis of an integrated study of current elevational vegetation distribution and past vegetation change based on analyses of pollens and biomarkers left in the soils by past vegetation.

The lowermost páramos and uppermost montane forests are mainly inhabited by indigenous populations that rely entirely on subsistence use of the natural resources provided by these ecosystems. Páramo grasslands, humid montane rainforest and cloud forests where ascending air masses cause an almost continuous fog, originally covered large stretches from Venezuela to northern Peru (Serrano Gine and Galarraga Sanchez, 2015). These biodiverse ecosystems fulfil important environmental functions, such as supply of drinking water and irrigation water, carbon storage (in the context of lowering atmospheric pCO_2 levels), agricultural production and tourism.

Although agriculture started in the Ecuadorian Andes some 3000 years ago (Bellwood, 2005; Scarre, 2013), agricultural land use has strongly expanded during the last few decades due to an expanding population and upscaling of agricultural production. Usage of inappropriate techniques often leads to rampant landscape degradation (e.g., Anthelme et al., 2014; Serrano Gine and Galarraga Sanchez, 2015). Natural upper montane forests and páramo grasslands have been widely replaced by potato fields and tree plantations, whereas páramo grasslands are in many places overexploited by grazing and burning (e.g., Hofstede et al., 2002; Buytaert et al., 2006). In the remaining natural forests, deforestation is responsible for a lowering of the natural UFL, i.e., the uppermost contour of continuous forest (e.g., Villota et al., 2012). However, also, natural factors such as shifts in soil water content, precipitation patterns and wind patterns, e.g., as a result of climate change, have been identified as drivers of a downward shift of the UFL (e.g., Peters et al., 2014). To complicate matters further, global warming causes upward shifts of the Andean UFL (e.g., Price, 1999; Bush et al., 2015).

Although the factors underlying the modern elevational position of the UFL are not fully understood (Körner, 1999; Körner and Paulsen, 2004; Körner et al., 2016), temperature has been identified as a major component in establishing the modern UFL position (Van der Hammen, 1974; Flenley, 1979). Also in palaeoecological studies, temperature is accepted as the main driver of past UFL shifts (e.g., Hooghiemstra, 1984; Groot et al., 2011). Factors driving the transitions between the shrubpáramo, grasspáramo and superpáramo are poorly understood (Hooghiemstra et al., 2012).

Establishing the position of the UFL under modern natural conditions as well as in the recent past has a great societal relevance with respect to support for conservation and restoration of montane forests under Reducing Emissions from Deforestation and forest Degradation-plus-driven activities aimed at a net CO_2 emission reduction (Dulal et al., 2012). Triggered by this incentive, in the period

2003–09 the Institute for Biodiversity and Ecosystem Dynamics of the University of Amsterdam performed an interdisciplinary research programme entitled Reconstruction of the Upper Forest Line in Ecuador (RUFLE) in cooperation with various organizations in the Andean region (Jansen et al., 2009). The RUFLE programme aimed at developing a reconstruction of the elevational position of the natural UFL in the northern Ecuadorian Andes. We studied the UFL dynamics during an interval long enough to reach the period that significant human interference was absent. In the Ecuadorian Andes, almost undisturbed conditions prevailed up to c.3000 years before present (BP) when early civilizations expanded (Bellwood, 2005; Bakker et al., 2008; Scarre, 2013).

A challenge of the RUFLE programme was reconstructing the natural UFL position in northern Ecuador with enough elevational precision to ecologically guide new tree plantations along the elevational gradient, as well as to assess the validity of past and present reforestation/afforestation activities (Bakker et al., 2008). Degradation of the natural forest, especially within the Central Valley, has been taking place for such a long time that the natural UFL position often cannot be recognized, or valley slopes are even fully deforested (Fig. 5.2.1). In such cases, palaeoecological research clarifying landscapes of the past may lead to useful answers. Also in the study area near the Guandera Biological Reserve (Fig. 5.2.1), human interference was reported to have significantly influenced the UFL position since the 18th century (Wille et al., 2002).

In the Guandera Biological Reserve, estimates of the natural position of the UFL ranged from

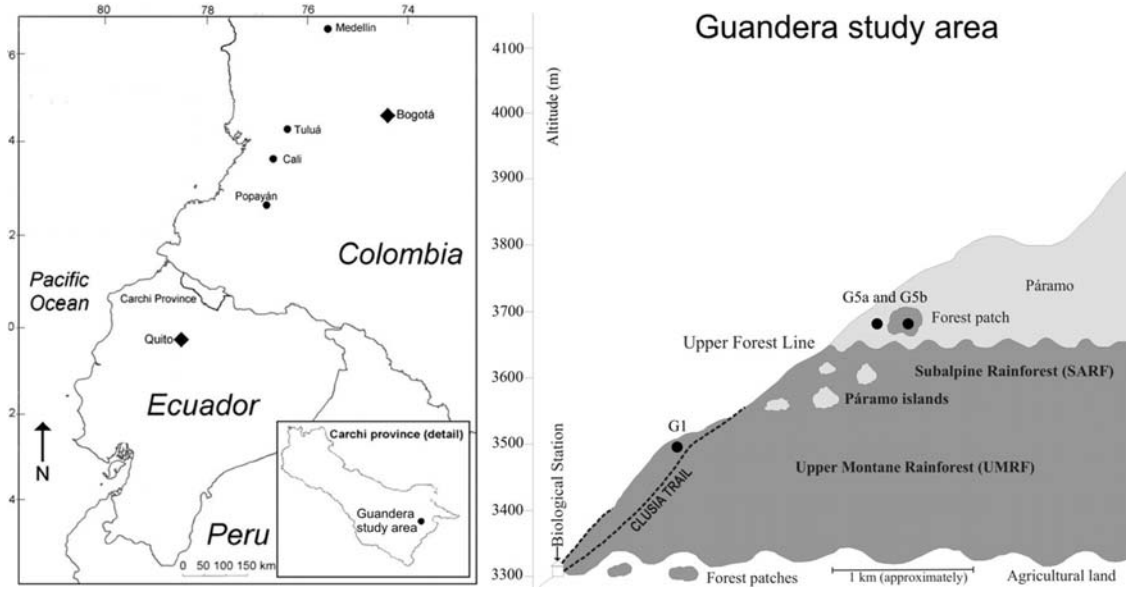

FIGURE 5.2.1 Schematic representation of the study area showing the elevational vegetation distribution. Land below c. 3300 m asl is deforested and almost completely transformed into agricultural land. *From Jansen, B., De Boer, E.J., Cleef, A.M., Hooghiemstra, H., Moscol-Olivera, M., Tonneijck, F.H., Verstraten, J.M., 2013. Reconstruction of late Holocene forest dynamics in northern Ecuador from biomarkers and pollen in soil cores. Palaeogeography, Palaeoclimatology, Palaeoecology 386, 607–619. Reprinted with permission © 2013, Elsevier Science B.V. License Number: 4590271293457.*

the present-day position of c. 3600 m asl to a hypothesized 4000 m asl (Laegaard, 1992; Wille et al., 2002) (Fig. 5.2.1). The uncertainty about the UFL position relates to the proxies used to reconstruct past elevational vegetation change, the most common ones being analysis of fossil pollen, plant macrofossils and stable carbon isotopes preserved in lacustrine or peaty sediments (e.g., Mayle et al., 2000; Clark and McLachlan, 2003). Aspects of fossil pollen analysis that are challenging the accuracy of establishing the position of the UFL include: (1) uncertainties in the calibration of the arboreal pollen percentage to the position of the UFL; (2) wind-blown upslope dispersal of arboreal pollen into the páramo prior to deposition that limits the elevational resolution of the pollen signal (e.g., Hicks, 2006; Crausbay and Hotchkiss, 2012); and (3) plant families with important arboreal as well as herbaceous species around the UFL, the Asteraceae in particular (Moscol-Olivera and Cleef, 2009a,b), without the pollen-morphological possibility of identifying beyond the family level (Hooghiemstra, 1984).

To reach the highest reliability in UFL reconstructions we used biomarkers preserved in soil monoliths together with fossil pollen analysis and vegetation analysis as a novel combination of proxies to reconstruct the character (trees versus herbs) of the in situ vegetation. Biomarkers as well as plant macrofossils are not wind transported and are both a source of information for the strictly local environmental conditions. However, in the absence of plant macrofossils in our sedimentary archives, biomarkers offer a challenging alternative proxy for which a methodology had to be developed. This approach reflects an innovative combination of techniques derived from soil science, molecular organic geochemistry, palynology and vegetation ecology to identify vegetation dynamics during the last millennia along altitudinal transects crossing current and potential past UFL positions in the study area. Here we synthesize the results of biomarker analysis as part of a multiproxy UFL reconstruction of the last millennia with special focus on the technical application of biomarkers, as well as the merits and drawbacks.

5.2.2 Description of the study area

The study area is located in the Guandera Biological Reserve in northern Ecuador, close to the Colombian border. It lies on the inner flanks of the Eastern Cordillera at approximately 11 km from the town of San Gabriel (Fig. 5.2.1). The area currently has a humid equatorial alpine climate with an annual precipitation of c. 1700 mm (Moscol-Olivera and Cleef, 2009b). Strong diurnal temperature fluctuations range from 4 to 15°C but annual temperature fluctuations are low (monthly means of maximum temperature vary between 12 and 15°C; Di Pasquale et al., 2007). Variation in temperature and precipitation is mainly forced by the annual migration of the Intertropical Convergence Zone (Haug et al., 2001). The Guandera Biological Reserve protects c. 10 km^2 of páramo grassland as well as areas of relatively undisturbed montane cloud forest located between 3300 and 3640 m asl. It consists at lower elevations of upper montane rainforest (UMRF) and changes at higher elevations into a small elevational band of subalpine rainforest (SARF), characterized by dwarf forest, before the UFL is reached. Under natural conditions the UFL is not a sharp transition but over a 50 m vertical interval the height of the trees gradually decreases (Moscol-Olivera and Cleef, 2009b). Around 3550 m asl, isolated patches of páramo vegetation occur within the forest, whereas above 3640 m, isolated patches of dwarf forest, mainly including asteraceous genera and the rosaceous *Polylepis*, occur in the páramo (Moscol-Olivera and Cleef, 2009a,b). In the study area the highest peaks reach c. 4100 m asl. This location was chosen as our study area because it constitutes the last remaining stretch of cloud forest of appreciable size and serves as a biodiversity hotspot. It was identified by Myers (1988) as part of the 'tropical Andes hotspots',

characterized by exceptionally high levels of plant endemism. At present the area suffers from serious levels of habitat loss.

5.2.3 The multiproxy approach of RUFLE

In its multiproxy approach, the RUFLE programme aimed at a full integration of various proxy-based reconstructions to identify past changes in vegetation distribution, elevational shifts of UFL position in particular, going back to conditions just predating the period of increasing human interference. Such a recent natural undisturbed setting serves as a reference and is called the 'baseline'.

5.2.3.1 Present-day vegetation analysis

Present-day vegetation composition of the UMRF, SARF and páramo was characterized during extensive vegetation surveys (Moscol-Olivera and Cleef, 2009a,b). Vegetation communities were described and the UFL was characterized in floristic and physiognomic terms. Such studies are the ideal basis for palaeoecological reconstructions. In this particular case, vegetation analysis allowed the selection of the most important plant species responsible for biomass input into soils and peat deposits and identification of their photosynthetic pathway. The leaf and root wax lipid composition could be assessed in pursuit of potential vegetation biomarkers in the context of UFL reconstruction (Jansen et al., 2006a).

5.2.3.2 Fossil pollen analysis

Compared to earlier palynological studies in volcanic soils (Salomons, 1986) we improved pollen-based UFL reconstructions from volcanic ash soils and peat sections significantly by calibrating improved radiocarbon-dated pollen records to robust vegetation surveys and characterization of soil organic matter in different elevational intervals (Tonneijck et al., 2008; Moscol-Olivera et al., 2009). We assessed the vertical distribution of pollen grains in the soil column related to activity of soil fauna by micromorphological observations in thin sections of undisturbed soil samples (Tonneijck and Jongmans, 2008). These observations also helped to understand the preservation of pollen grains within soil aggregates composed of organic matter and mineral particles, improving the interpretation of pollen records from soils.

5.2.3.3 Biomarker analysis

Within the context of the research aims of the RUFLE programme, biomarker analysis initially considered three potential categories of biomarkers preserved in soils along the altitudinal transect:

1. The use of lignin monomers preserved in soils to separate organic matter input from angiosperms (dominant in SARF and UMRF) and organic matter input from herbs, grasses in particular (abundant in the páramo) (e.g., Spielvogel et al., 2007; Simpson and Simpson, 2012);
2. The use of a difference in the $\delta^{13}C$ signature of the bulk soil organic matter and/or species-specific biomarkers to differentiate between hypothesized C_3-dominated SARF and UMRF vegetation and C_4-dominated poaceous taxa from the páramo (e.g., Feng et al., 2010; Mendez-Millan et al., 2014);
3. The use of straight-chain lipids and/or isoprenoids preserved in soils that are either unique or occur in unique combinations of concentration patterns that can be linked to (groups of) plant species characteristic of SARF, UMRF or páramo vegetation (e.g., Zeng et al., 2011; Lavrieux et al., 2011).

Along the altitudinal transects in the study area it was shown that lignin was not preserved to any significant extent (Nierop and Jansen, 2009). However, exceptionally large carbon stocks were found, almost doubling the global average for volcanic ash soils (Tonneijck et al., 2010). At that time this result was remarkable, but today fits well within the recently introduced

new paradigm of soil organic matter preservation. It includes the notion that a complex molecular composition does not necessarily lead to prolonged preservation (Schmidt et al., 2011; Lehmann and Kleber, 2015). It also meant that lignin monomers could not be used as biomarkers for UFL reconstruction.

With respect to the $\delta^{13}C$ signature, the analysis of present-day vegetation showed that grass species of the páramo use a C_3 photosynthetic pathway (Moscol-Olivera and Cleef, 2009a,b). The same is true for the species of SARF, whereas UMRF species consist of a mixture of species using C_3 and facultative Crassulacean Acid Metabolism photosynthetic pathways (Moscol-Olivera and Cleef, 2009a,b). As a result, using the $\delta^{13}C$ signature of soil organic matter as a biomarker for reconstructing the UFL position proved impossible as well.

The third biomarker option proved more promising. Along the altitudinal transect the molecular characterization of soil organic matter in the soils showed a strong accumulation of aliphatic compounds containing isoprenoids as well as straight-chain lipids (Nierop et al., 2007; Nierop and Jansen, 2009). As elaborated later in more detail, molecular analysis of the leaves and roots of 19 plant species — identified as responsible for the dominant biomass input in the soils and peat deposits in the study area — revealed that the *n*-alkanes and *n*-alcohols showed great potential to be applied as biomarkers for UFL reconstruction (Jansen et al., 2006a). Of the isoprenoids, only ubiquitous ones were abundantly present, preventing their use as biomarkers (Jansen et al., 2007).

These results underline the relevance of considering and testing several potential biomarkers in a given reconstruction, as well as a detailed analysis of the vegetation and pollen records and the main plant species producing the biomarkers conserved in the soils to reconstruct past UFL positions. In the next section we focus on the application of *n*-alkanes and *n*-alcohols as feasible biomarkers to reconstruct the elevational position of the UFL, emphasizing also the general procedure followed in such a biomarker-based reconstruction.

5.2.4 Measuring the biomarker signal

The straight-chain lipid classes of *n*-alkanes and *n*-alcohols that were ultimately used as biomarkers are part of the lipid fraction that can be extracted from soil and vegetation samples by an organic solvent, often dichloromethane (DCM) (Bianchi and Canuel, 2011). Such extraction will also liberate other lipid classes potentially applicable as biomarkers, for example, *n*-fatty acids (Bianchi and Canuel, 2011), which were considered but appeared inapplicable as a biomarker for our aim (Jansen et al., 2006a, 2007). Various methodologies exist to perform organic solvent extractions to liberate lipids from a soil matrix (Bianchi and Canuel, 2011). Traditionally, Soxhlet extraction was often used for our purpose, but we successfully tested and subsequently applied the automated technique of accelerated solvent extraction (ASE) to obtain the extractable lipids (Jansen et al., 2006b). The ASE technique is now commonly used for lipid extraction, but also other methodologies ranging from simple shaking with a solvent to sonification are sometimes applied (see Bianchi and Canuel, 2011).

Subsequent analysis of biomarkers normally takes place by gas chromatography/mass spectrometry (GC/MS). The use of this technique to analyse organic compounds, including extractable lipids, has been reviewed in detail elsewhere (Sneddon et al., 2007). Briefly, the methodology consists of a polarity-based separation of compounds in the gas phase on a column of a certain length using a specific carrier gas, often H_2 or He (Sneddon et al., 2007). Compounds in solution, such as extracted lipids, are brought into the gas phase through injection in a heated injector. Subsequent separation is normally aided through application of temperature programming of the column (Sneddon et al., 2007). Upon separation, the compounds are detected on a mass spectrometer, where they

are fragmented into characteristic mass/charge (m/z) fragments that are normally identified by comparison with known fragments in a database (Sneddon et al., 2007).

5.2.5 Interpretation of the biomarker signal

The *n*-alkane composition in the leaves of plant species most responsible for the bulk of biomass input into the soil and peat bogs is used as biomarkers. Fig. 5.2.2 serves as an illustration of a typical example of a higher plant-derived biomarker signal (Jansen et al., 2006a). Fig. 5.2.2 also shows it is not the presence of individual *n*-alkanes but the unique concentration patterns of a set of *n*-alkanes within a certain range of carbon chainlengths which is characteristic of a plant species. In some instances the concentration pattern seems very species specific, while the patterns of other species look more alike (Fig. 5.2.2). Upon consideration of several classes of straight-chain lipids the combination of the *n*-alkane + *n*-alcohol concentration patterns in leaves of the studied species allowed a meaningful clustering of the species into relevant plant associations, (SARF, UMRF, páramo and peat bog associations) from where they originate (Jansen et al., 2006a).

For the interpretation of the biomarker signal in the soil and peat sediments the usual requirements for a reliable proxy apply, such as an adequate and chronological preservation of the biomarker compounds in the sedimentary archive. However,biomarkers in the form of *n*-alkanes and *n*-alcohols are mixed upon their

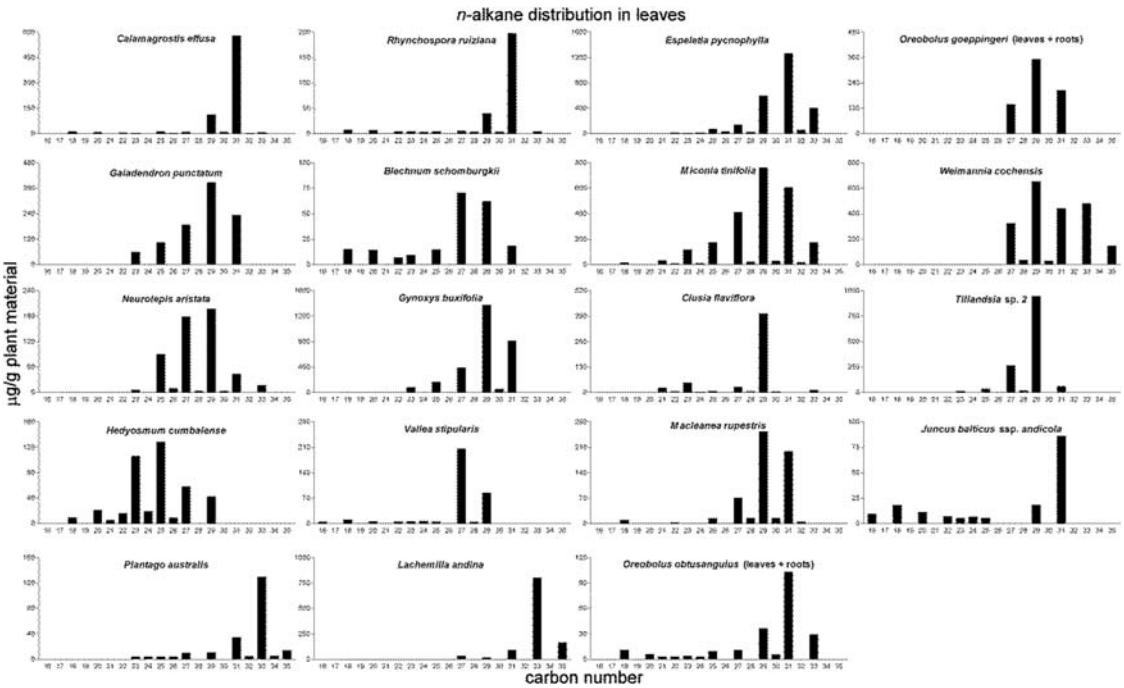

FIGURE 5.2.2 *n*-Alkane distribution in the leaves of the plant species responsible for the bulk of biomass input in the soils and peat bog sediments in the study area in the northern Ecuadorian Andes. *After Jansen, B., Nierop, K.G.J., Hageman, J.A., Cleef, A., Verstraten, J.M., 2006a. The straight-chain lipid biomarker composition of plant species responsible for the dominant biomass production along two altitudinal transects in the Ecuadorian Andes. Organic Geochemistry 37, 1514–1536; Jansen, B., Nierop, K.G.J., Kotte, M.C., De Voogt, P., Verstraten, J.M., 2006b. The application of accelerated solvent extraction (ASE) to extract lipid biomarkers from soils. Applied Geochemistry 21, 1006–1015.*

input into the archive. Since it is the concentration patterns of *n*-alkanes and *n*-alcohols rather than the individual compounds that constitute the plant-specific biomarker, a mixed signal of otherwise ubiquitous compounds is preserved in the archive. This mixed signal must somehow be unravelled into the most likely plant-specific sources.

In a first attempt to unravel the mixed biomarker signals we considered shifts in the ratio of concentrations of the dominant chainlengths of *n*-alkanes and *n*-alcohols (Jansen et al., 2008). The *n*-alkane concentration patterns (Fig. 5.2.3) in the deeper parts of the soils vary along the altitudinal transect in the study area (Fig. 5.2.1). The age of the organic matter in the soil samples (Fig. 5.2.3) ranges from c.1750 cal yr BC to 300 cal yr BC, predating the period of anthropogenic impact on the natural vegetation and the UFL position (Jansen and Nierop, 2009). When looking at the ratios of concentration values of the main chainlengths, i.e., C_{29} versus C_{31} *n*-alkane, there is a shift from a dominance of the former to a dominance of the latter between sampling sites G5a and G5b (Figs 5.2.1 and 5.2.3). This shift reflects a shift in the vegetation from forest (G1–G5a) to páramo (G5b–G9) (Fig. 5.2.3). Moreover, a dominance of C_{29} *n*-alkane over C_{31} *n*-alkane coincides with the ratio of concentration values dominantly present in tree species (*Clusia flaviflora*, *Miconia tinifolia*), whereas the reverse coincides with the ratio of concentration values dominantly present in poaceous species *Calamagrostis effusa* (Figs. 5.2.2 and 5.2.3). From these results it may be concluded that the shift in concentration ratios of prominent carbon numbers of *n*-alkanes offers a useful way of quickly assessing substantial shifts in vegetation composition in the study area (Jansen et al.,

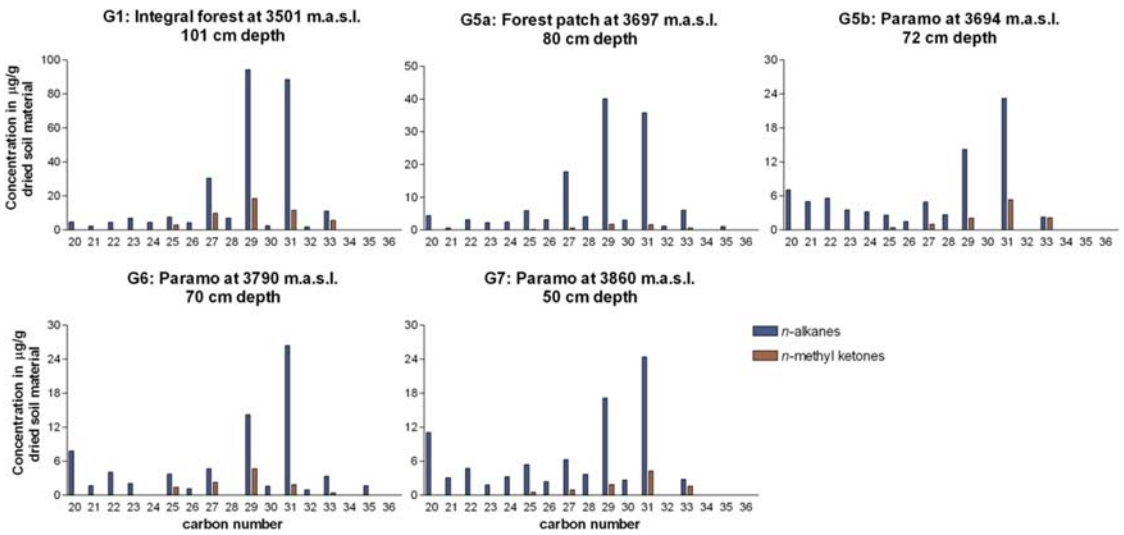

FIGURE 5.2.3 Soil *n*-alkane and *n*-methyl ketone distribution along an altitudinal transect from 3500 to 3860 m asl in the northern Ecuadorian Andes. *n*-Methyl ketones are the primary degradation product of *n*-alkanes in these soils. *After Jansen, B., Nierop, K.G.J., 2009. Me-ketones in high altitude Ecuadorian andisols confirm excellent conservation of plant-specific n-alkane patterns. Organic Geochemistry 40, 61–69.*

2008). It also offers the first indication that the present-day UFL position may be close to its position under natural undisturbed conditions (Jansen et al., 2008).

However, using simple ratios of *n*-alkanes of dominant chainlengths means that only a fraction of the biomarker information captured in the suite of straight-chain lipids is used. In addition, the ratio approach does not consider possible input of straight-chain lipids from sources other than leaves, such as roots, that may represent a substantial portion of the total influx, particularly in soils (Jansen and Wiesenberg, 2017).

We therefore developed a more systematic approach to unravel the mixed straight-chain lipid biomarker patterns encountered in a sediment archive that would include all chainlengths and the possibility to combine multiple classes of components. This led to the development of the Vegetation Reconstruction with the Help of Inverse modelling and Biomarkers (VERHIB) model (Jansen et al., 2010). The VERHIB model is a linear regression model that describes the way the development of vegetation composition over time at a particular location of interest has resulted in the accumulation of biomarkers (Jansen et al., 2010). By using inverse modelling, changes in past vegetation composition are then reconstructed with the biomarker signals (Jansen et al., 2010).

Several assumptions are required with respect to the input of the biomarkers in the sediment archive, which translates into several parameters in the model. The current version of VERHIB is configured to consider the individual or simultaneous input of *n*-alkanes, *n*-alcohols and/or *n*-fatty acids within a range of carbon numbers to be specified by the user (Jansen et al., 2010). In addition to input of biomarkers from leaves, the model explicitly considers biomarker input from roots. For both leaves and roots, a database must be provided of the ratios of biomarker concentration values in leaves and roots of modern analogues of the plant species to be considered in the reconstruction. The selection of plant species may be guided by the present-day vegetation composition, or based on the results of other sources of information of past vegetation change (e.g., fossil pollen or phytoliths) (Jansen et al., 2010).

Furthermore, explicit parameters must be provided, or estimated, that describe the distribution of input of biomarkers from leaves and roots in the sediments, as well as the ratio root/leaf biomass input (Jansen et al., 2010). All individual processes of the VERHIB model for a biomarker-based palaeovegetation reconstruction are shown in a flow chart (Fig. 5.2.4). The VERHIB model was ultimately applied to make biomarker-based vegetation reconstructions using the *n*-alkane and *n*-alcohol signals from leaves and

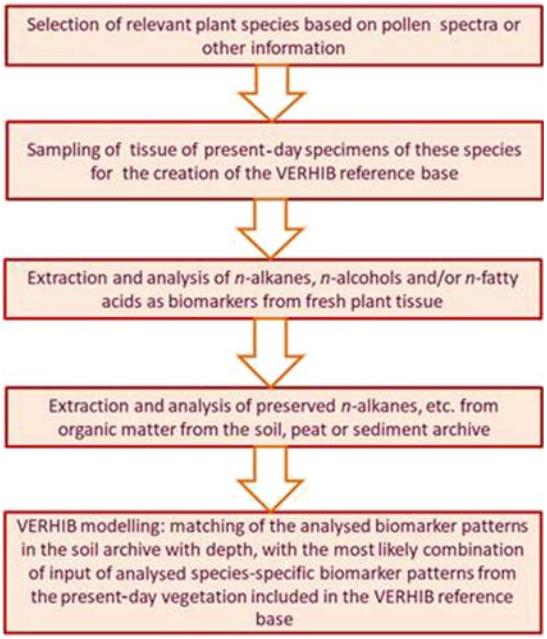

FIGURE 5.2.4 Flow chart of a biomarker-based vegetation reconstruction using the Vegetation Reconstruction with the Help of Inverse modelling and Biomarkers (VERHIB) model. *After van Mourik, J.M., Wagner, T.V., De Boer, J.G., Jansen, B., 2016. The added value of biomarker analysis to the genesis of plaggic anthrosols; the identification of stable fillings used for the production of plaggic manure. Soil 2, 299–310.*

roots of the plant species responsible for the bulk of biomass input into the soil and peat bogs as elaborated in the following section (Fig. 5.2.2).

5.2.6 Sediment archives and biomarker reference database

The sediment archives used for the reconstruction of past UFL positions are listed in Table 5.2.1, and their locations are shown in Fig. 5.2.2. The studied archives consisted of a peat core G15 located in the páramo, as well as three soil profiles located in, respectively, the UMRF (G1), a patch of SARF in the páramo (G5a) and in the adjacent páramo at some 20 m distance (G5b) (Table 5.2.1). Age models based on radiocarbon ages showed that all sediment archives had a linear age–depth relationship. The records

TABLE 5.2.1 Concise description of the sediment archives used for the pollen and biomarker-based vegetation reconstructions.

Archives	Horizon	Horizon depth (cm)	Sample depth (cm)	C_{org} (%)
Peat core G15 Páramo – 3400 m	Not applicable			
Soil core G1 Forest – 3500 m Folic, hemic, endo-aluandic, endofulvic Histosol[a]	L	+1–0	0	53
	F	1–40	10	54
	F		30	53
	H	40–75	50	52
	Ah	75–87	82	21
	1/2Bw	87–115	100	9.0
	2Ahb	115–145	125	13
	3BChb	145–160	150	4.0
	3BCb	160–241	160	0.5
Soil core G5a Forest patch – 3695 m Folic, hemic, aluandic, endomelanic Cambisol[a]	L	+4–0	0	50
	F	0–35	15	50
	Ah	35–75	45	18
	Ah		60	14
	Bw	75–92	85	9.0
	1/2Bw	92–120	95	10
Soil core G5b Páramo – 3695 m Aluandic, melanic, umbric Andosol[a]	L	+1–0	0	42
	Ah	0–45	15	20
	Ah		35	15
	Bw1	45–65	55	9.0
	1/2Bw2	65–116	75	8.0
	1/2Bw2		95	9.0

[a] *Soil classification according to the World Reference Base (FAO, 2006).*

For a more detailed description of the soil archives, see Jansen et al. (2013). For a more detailed description of the peat core, see Bakker et al. (2008).

reflected the last 6760 cal yr BP in G15, the last 7040 cal yr BP in G1, the last 4320 cal yr BP in G5a and the last 3710 cal yr BP in G5b (Bakker et al., 2008; Jansen et al., 2013); all ages rounded off at the nearest multiple of 10.The species of which the *n*-alkane and *n*-alcohol composition of leaves and roots was included and used in the reconstruction with the VERHIB model are presented in Table 5.2.2. For the *n*-alkane and *n*-alcohol patterns themselves, the reader is referred to Jansen et al. (2006a).

5.2.7 Results of UFL reconstruction

Results for fossil pollen and biomarkers from the peat archive and the three soil archives allowed an adequate vegetation reconstruction (Jansen et al., 2010, 2013) with focus on the presence of forest versus páramo (Figs 5.2.5). More detailed results about plant species (groups) can be found in the original publications by Bakker et al. (2008) and Jansen et al. (2010, 2013).

From Fig 5.2.5 it is clear that the biomarker-based reconstruction with the VERHIB model and the fossil pollen-based reconstruction show similar temporal trends in the proportions of forest versus páramo. Focusing first on the reconstruction from the peat archive (Fig. 5.2.5), the fossil pollen-based reconstruction provided an averaged signal of the regional shifts in vegetation composition. In the open páramo, wind-blown pollen originating from lower elevations is included in the sediment archive and diluting a sharp UFL signal (Jansen et al., 2010). The biomarker-based reconstruction is related to the local influx of biomarkers from leaves, and potentially aerosols to a limited extent, thus providing a more local vegetation signal (Jansen et al., 2010; Jansen and Wiesenberg, 2017). In this sense, the biomarker-based vegetation reconstruction is more akin to a reconstruction based on plant macro-remains (Mauqouy and Van Geel, 2007). Although both proxies have their limitations, the combination of both helps compensate for the imperfections in either proxy. The biomarker-based reconstruction with VERHIB may theoretically provide identifications of plants at the species level (Jansen et al., 2010), but in reality is sensitive to genotypic plasticity in the biomarker composition per species, in particular for species that have very similar patterns (Jansen et al., 2010; Jansen and Wiesenberg, 2017). Similarly, fossil pollen-based reconstruction with respect to the Asteraceae suffers from plant identifications at the family level

TABLE 5.2.2 Species included in the biomarker reference database.

Family	Species
Asteraceae	*Espeletia pycnophylla* Cuatrec.
Asteraceae	*Gynoxys buxifolia* (Kunth) Cass.
Blechnaceae	*Blechnum schomburgkii* (Klotzsch) C.Chr.
Bromeliaceae	*Tillandsia bakeri* L.B. Smith
Chloranthaceae	*Hedyosmum cumbalense* H. Karst
Clusiaceae	*Clusia flaviflora* Engl.
Cunoniaceae	*Weinmannia microphylla* Ruiz & Pav. (syn. *W. cochensis* Hieron.)
Cyperaceae	*Oreobolus cleefii* L.E. Mora

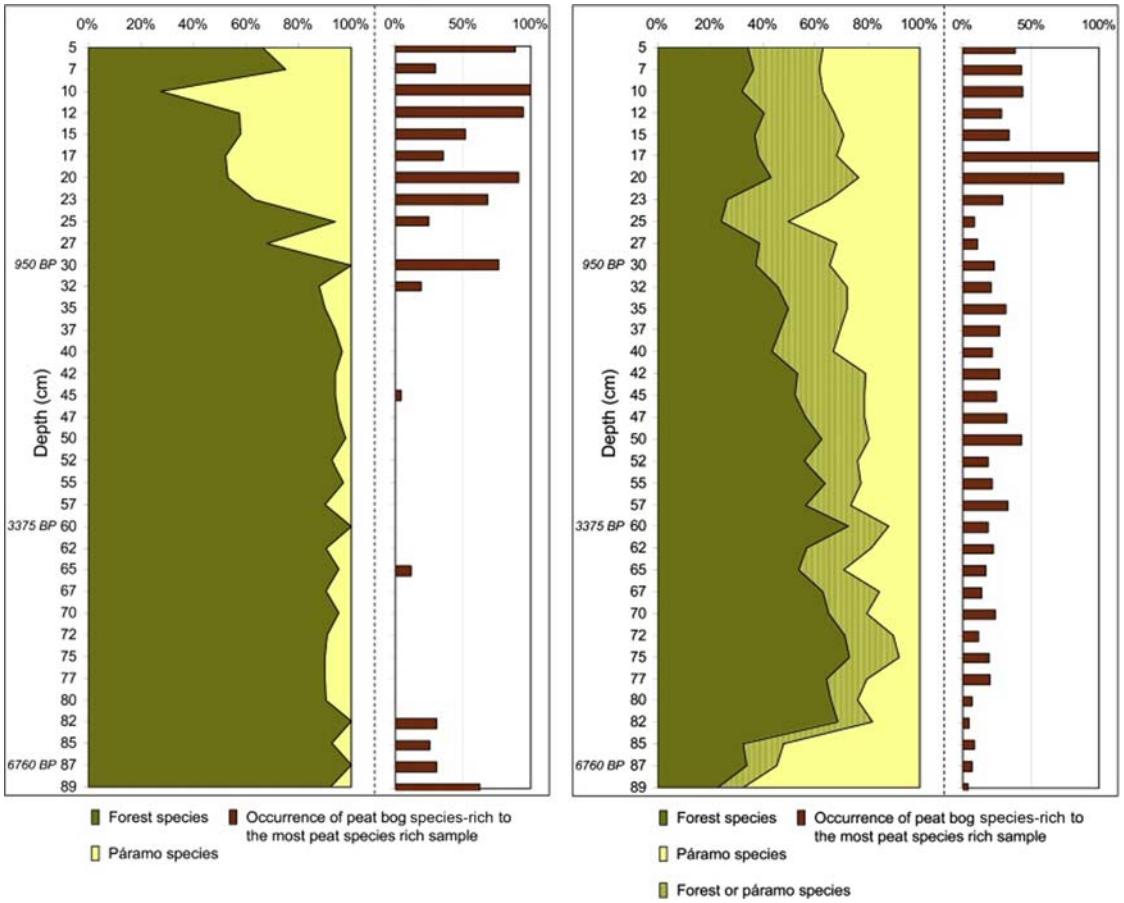

FIGURE 5.2.5 Reconstruction of proportions of forest versus páramo species in radiocarbon-dated peat core G15 based on biomarkers (*left*) and fossil pollen (*right*). *After Jansen, B., Van Loon, E.E., Hooghiemstra, H., Verstraten, J.M., 2010. Improved reconstruction of palaeo-environments through unravelling of preserved vegetation biomarker patterns. Palaeogeography, Palaeoclimatology, Palaeoecology 285, 119–130.*

at best reflecting trees and páramo herbs as well. Therefore the proportion of Asteraceae cannot be assigned unambiguously to forest or páramo vegetation (Jansen et al., 2010).

From a biomarker perspective, a peat archive-based vegetation reconstruction has the advantage that biomarker input by roots is absent, with the exception of the peat-forming plants themselves. For both fossil pollen and biomarkers, preservation in the anoxic conditions of a peat bog can be expected to be good. However, peat bogs have a restricted geographical occurrence (located in shallow basins where water is stagnating) potentially limiting the spatial resolution of data points. Fortunately, the soils in the RUFLE study area provided good preservation conditions for biomarkers. Preservation of fossil pollen grains was also good in these high-elevation soils (Salomons, 1986; Jansen et al., 2013). Comparing the biomarker-based and fossil pollen-based

vegetation reconstructions, a lag in timing of the incursion of forest is obvious in soil archive G1 in particular. This lag of some two millennia can be attributed to upslope aeolian arboreal pollen transport suggesting a too early arrival of forest at the coring site compared to the vegetation reconstruction based on leaf wax biomarker signals (Jansen et al., 2013). This observation shows that fossil pollen and biomarkers are complementary proxies, the combination of which provided information that could not have been attained by either method alone (Jansen et al., 2013). In using biomarkers from soil archives a specific challenge is the mixture of *n*-alkanes and *n*-alcohols from leaves and roots, potentially complicating the signal and disturbing its chronology. Designed to unravel such potential disturbance, the VERHIB model proved capable of filtering out the root signal in the soil archives (Jansen et al., 2013).

5.2.8 Implications for the use of biomarkers in vegetation reconstructions

In mountain areas the vertical component of vegetation change, the elevational position of the UFL in particular, sensitively responds to temperature change (mainly temperature, Groot et al., 2011) as well as to human impact on the landscape (Flantua et al., 2016a,b). In forested landscapes, pollen grains travel shorter distances than in open landscapes where pollen grains from herbaceous vegetation may be wind transported over larger distances (Hooghiemstra et al., 1986; Moore et al., 1991). Moreover, pollen-receiving sites (soils, peat bogs) in an open landscape accumulate pollen grains from a larger area than pollen-receiving sites in small forest openings (Moore et al., 1991; Bogotá-A et al., 2011). Therefore at the UFL, changes in pollen signals and their calibration to the actual vegetation are apparent (Moscol-Olivera and Cleef, 2009a). In the absence of plant macroremains in volcanic soils in the high Ecuadorian Andes, pollen analysis is missing information about the vegetation directly surrounding the site. As a consequence, the pollen signal from sites located in the grass páramo suggests prematurely that the UFL has reached the coring site, caused by upslope wind-blown arboreal pollen (Jansen et al., 2013). Biomarker analysis of leaves and roots in palaeosols using the VERHIB model proved highly successful in its application to reconstruct elevational changes of the UFL. This success was largely due to the combined application of biomarker analysis with traditional fossil pollen analysis, as both proxies yielded complementary information. Sufficient preservation of proxies in a sediment column is applicable to all palaeoecological proxies. With respect to the application of lipid biomarkers using the VERHIB model, shortcomings can be summarized as follows:

- Input of root-derived biomarkers may complicate the reconstruction from soil archives;
- A biomarker-based reconstruction using VERHIB is limited to the selected plant species available in the reference database of the biomarker patterns of present-day analogues. Moreover, the biomarker composition of modern analogues and of the species responsible for the biomass input in the past may differ, potentially leading to a biased interpretation;
- The biomarker composition of different species, combined with genotypic plasticity of the biomarker signal, may complicate an ecological interpretation of the signal.

To compensate for these potential pitfalls, we recommend applying the VERHIB model in biomarker reconstructions because of its design to filter out the biomarker input from roots and use the entire set of biomarkers rather than simple ratios. In addition, we recommend combining a biomarker-based reconstruction with adequate vegetation analysis to determine the plant species to be included in the VERHIB calibration database, and to sample and analyse

their modern analogues from an environmental setting that is as similar as possible to the one to be reconstructed to limit the influence of genotypic plasticity. Finally, we strongly recommend applying biomarker analysis as part of a multiproxy approach, for instance, with fossil pollen analysis.

5.3 Applications of biomarker analysis in palaeopedology

5.3.1 Introduction

So far we showed that multiproxy analysis of soil archives can provide valuable information for the benefit of geoecological reconstruction of landscape evolution. Complementary to pollen diagrams from peat and lacustrine deposits, pollen diagrams from soils provide relevant information from dry land surfaces.

The studies, presented in the preceding sections, clarify the advantages of pollen analysis in soils. Pollen grains are microfossils that can infiltrate into the soil and survive processes such as digestion and humification. The composition of pollen spectra from soils is influenced by processes such as selective corrosion and bioturbation. In addition, buried organic-rich soil horizons usually lack macroremains. These properties explain why pollen spectra from soils offer useful palynological fingerprints for the description of local environmental developments but are less appropriate for a reliable reconstruction of vegetation development.

The chronology of phases in palaeoecological development, identified in pollen diagrams, can be based on palynological time markers. However, a robust chronology must be based on absolute dating (Flantua et al., 2016a,b). ^{14}C dating of soil organic matter, extracted from organic-rich (buried) horizons, was for a long time the best option but the results were uncertain due to the complexity of the composition of soil organic matter. Since the 1990s we can apply optically stimulated luminescence (OSL) dating to aeolian and fluvial deposits. Assuming that the mineral grains were completely bleached during transport and (re)deposition, the dating results are more reliable than radiocarbon dating. In this respect it is important to realize that ^{14}C dating is connected to the organic soil matrix and OSL dating with the mineral skeleton of the soil. As a result, both can have different developments. The reliability of the combination of organic and mineral dating of soil archives depends on the knowledge of the properties of the samples and insight into the evolution of landscape and soil.

At the beginning of the 21st century the technique of biomarker analysis became operational and with this approach open questions regarding the development of polycyclic Podzols and plaggic Anthrosols could potentially be answered.

One question concerns the composition of vegetation during soil formation in stabilized driftsand beds, resulting in (initial) Podzols. Which plants species were responsible for carbon sequestration in the Podzols? The pollen spectra from soils cannot give a decisive answer because they consist of species of various source areas. Absence of plant macrofossils in the sediments might be compensated by biomarker analysis allowing to identify which plant taxa occurred in situ and which taxa at greater distance. A pilot study of the buried Podzols in profile Defensiedijk-1 showed the added value of biomarker analysis in the reconstruction of onsite vegetation during the stable phases in the development of the polycyclic sequence of driftsand deposits (van Mourik and Jansen, 2013).

Another question concerns the use of stable filings in the practices of plaggic agriculture, resulting in the formation of plaggic Anthrosols. The pollen spectra from plaggic deposits indicate the use of heath sods, but the historical archives deny sods digging before the 18th century. The results of a pilot study of plaggic Anthrosols

demonstrated that the identification of stable fillings, used for the production of plaggic manure, could be better based on information from biomarkers rather than from pollen grains (van Mourik et al., 2016).

In the following paragraphs the results of these pilot studies will be further elaborated to demonstrate the added value of biomarker analysis in palaeopedology.

5.3.2 The identification of plant species responsible for carbon sequestration in podzolic soils during stable phases in a polycyclic sequence of sand deposits

Here we highlight the results of a study where we examined the potential of using biomarkers to unravel pedogenesis in polycyclic driftsand sequences (van Mourik et al., 2012). The pollen diagram of profile Defensiedijk-1 (Chapter 4, Fig. 3.2.3) provides clear information about the presence and fluctuations of arboreal and herbaceous species during the various phases of sedimentation and soil formation. The phases of sand accumulation and soil formation have been ^{14}C and OSL dated. The pollen spectra from soils indicate that the phases of sand drifting took place in the early Holocene due to deforestation and extension of heathlands. However, the composition of pollen precipitation at the soil surface of the profile site (and consequently also of the composition of soil pollen spectra) is a mixture of pollen grains from species rooting at the sample location and growing at further distances. Therefore it is impossible to accurately identify the composition of the local vegetation during the stable phases in the build-up of the polycyclic sequence. Potentially, identification of these species might be possible by application of biomarker analysis.

In 2008 we resampled profile Defensiedijk-1 (Fig. 5.3.1) very close to the sample location of 2002 (Fig. 3.2.1). Samples for the extraction of pollen grains and biomarkers were taken from the organic-rich minerals 2AE, 3Ah and 4Ah horizons and the organic rich driftsand layers 1C3, 1C5 and 2C3 to compare pollen and biomarker spectra. Also, plant tissues were collected to create the required biomarker reference base.

Based on the pollen spectra, plant species potentially involved in carbon sequestration during active soil formation included *Pinus*, *Betula*, *Quercus*, *Calluna*, *Molinia*, *Corynephorus*, *Polytrichum* and *Cladonia*. The biomarker spectra of the reference species are shown in Figs 5.3.2

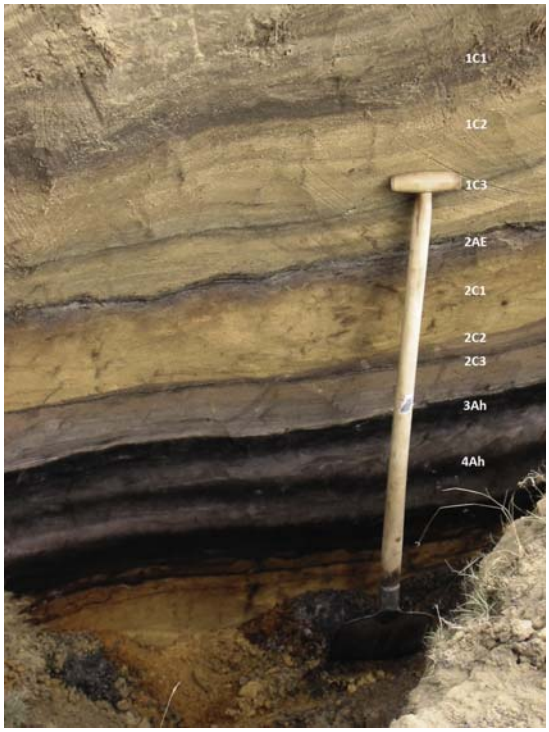

FIGURE 5.3.1 Profile Defensiedijk-1, resampled in 2006 for optically stimulated luminescence dating and 2008 for biomarker analysis. The location of Defensiedijk-1 is indicated in Fig. 3.2.1. *After van Mourik, J.M., Seijmonsbergen, A.C., Jansen, B., 2012. Geochronology of soils and landforms in cultural landscapes on aeolian sandy substrates, based on radiocarbon and optically stimulated luminescence dating (Weert, SE-Netherlands). In: Danuta, M.N. (Ed.), Radiometric Dating. In Tech, Rijeka, Croatia, pp. 75–114.*

and 5.3.3A andB, and the spectra of the soil samples are shown in Fig. 5.3.4. Biomarkers in this study consisted of the *n*-alkanes of higher chain-length that derive from the wax layers on plant leaves and roots (see also Section 5.1).

Fig. 5.3.4 shows the combined results of pollen and biomarker analysis of samples from the Ah horizons of the buried Podzols and some organic-rich C layers (representing deposition of organic-rich sand originating from eroded soils in the vicinity).

The pollen spectrum of the 4Ah horizon of the oldest palaeosol is dominated by Ericaceae, *Corylus* and *Alnus*, and micromorphological observations indicate an undisturbed soil matrix. Pollen grains could be extracted from organic aggregates with a modexal internal fabric and an intertextic distribution pattern. However, no biomarkers derived from Ericaceae or *Corylus* were present. Instead, in the biomarker-based reconstruction, *Pinus* and Poaceae are dominant. Pine trees were not introduced to the area until the 19th century and given the results of ^{14}C dating of 4Ah it is unlikely that they were present in the onsite vegetation at the time that the 4Ah horizon was formed. Instead, the dominance of *Pinus* biomarkers most likely represents 'contamination' of the soil organic carbon content in this horizon with younger decomposition products from roots of this deep-rooting species. At the same time, the low abundance of Ericaceae in the biomarker spectrum most likely indicates that this species was locally rare to absent. Its abundance in the pollen records is related to wind-blown pollen dispersal from surrounding areas. A cover dominated by grass and moss species, as inferred by the biomarker reconstruction, seems more likely.

The pollen spectrum of the 3Ah horizon is dominated by Ericaceae. The micromorphological structure is similar to the 4Ah; the biomarker spectrum is now dominated by Ericaceae and *Pinus*. The ^{14}C dating of the 3Ah makes clear also that the active formation of the 3Ah took place before the introduction of pine trees, and once more the abundance of *Pinus* biomarkers is caused by the input of decomposed younger roots. The presence of *Calluna* in both pollen and biomarker spectra points to a heath vegetation at the time during the formation of the 3Ah horizon. It is plausible that Ericaceae were already present in the vicinity, as indicated by their presence in the pollen spectra of the 4Ah horizon, and had now reached the sampling site causing their presence in the more local biomarker-based reconstruction.

During the active formation of the 2Ah horizon, the site was most likely covered by heather and lichens, the former being present in the pollen spectra as well as the biomarker reconstruction, whereas lichens are palynologically not visible. Only fungal spores are present in the pollen spectra but it could not be established which fungal taxa are associated with the lichens on driftsand and heath (*Cladena* and *Cladonia*) (Fig. 5.3.5). *Pinus* is now present in both pollen and biomarker spectra and must have been present in the onsite vegetation. Roots from this level reached the (moist and relative nutrient-rich) underlying 3Ah and 4Ah horizons and contaminated the soil organic matter, causing underestimation of the ^{14}C ages.

The ochric (A) horizon, developed in the youngest driftsand deposit, forms the present surface. The pollen spectrum is dominated by *Pinus* and Poacae; the biomarker spectrum by lichens (Fig. 5.3.4). The actual vegetation is dominated by *Cladonia* and *Polytrichum* (Fig. 5.3.6). Poaceae are present in the surroundings, *Corynephorus* on dry driftsands and inland dunes and *Molinia* in moist depressions (Fig. 5.3.6). The biomarkers from grasses, specific for dry soil conditions (*Corynephorus canescens*, *Deschampsia flexuosa*) and for moist soil conditions (*Molinia caerulea*) are distinctive in biomarker spectra in contrast to the pollen grains of these species.

The pollen spectra of the sampled driftsand layers 2C3, 1C5 and 1C3 are dominated by Poaceae and Ericaceae. Based on biomarkers, we can

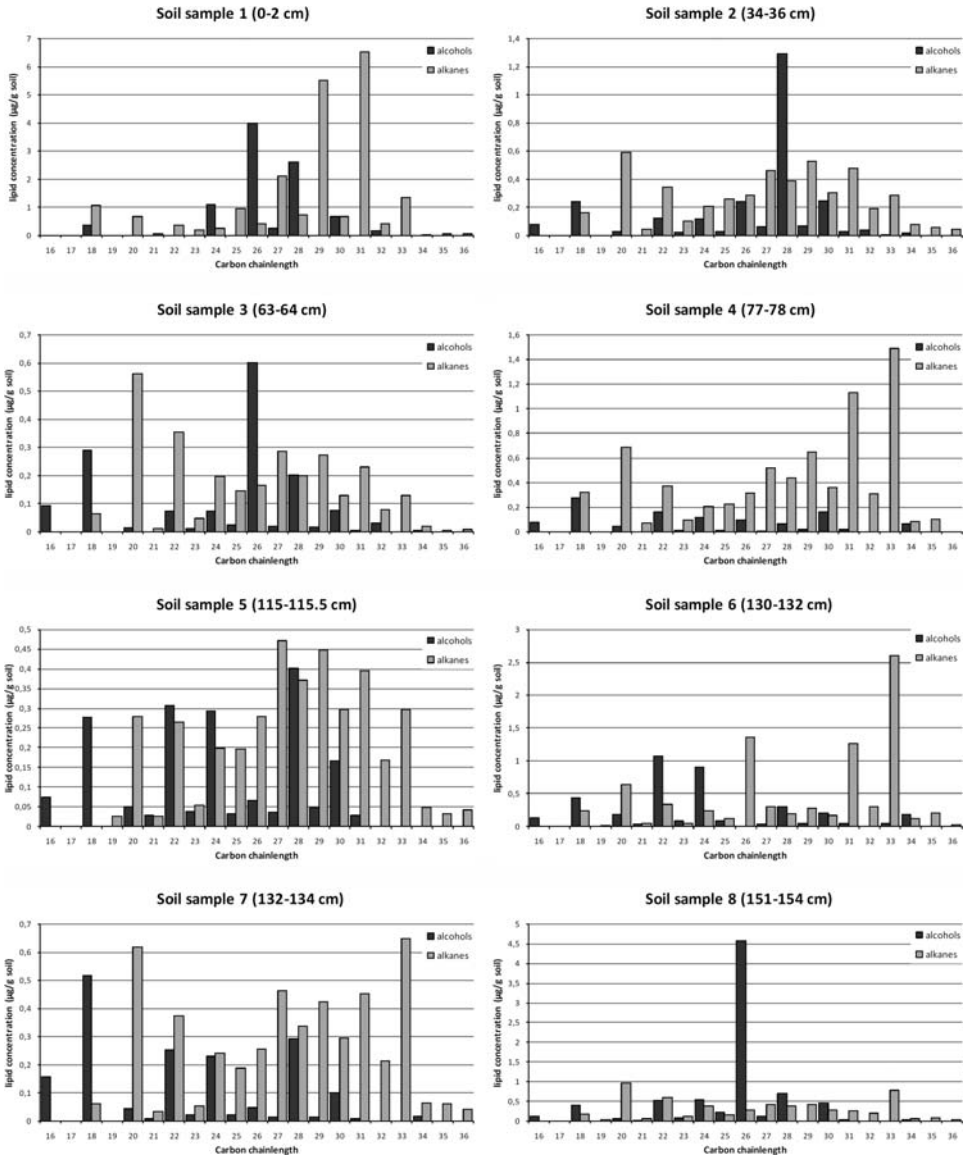

FIGURE 5.3.2 Biomarker spectra of the soil samples from the Defensiedijk profile. *After van Mourik, J.M., Jansen, B., 2013. The added value of biomarker analysis in palaeopedology; reconstruction of the vegetation during stable periods in a polycyclic driftsand sequence in SE-Netherlands. Quaternary International 306, 14–23.*

identify that the humus in the 1C5 horizon originated from an eroded soil under a vegetation of lichens and dry grasses (probably *Deschampsia*), and in the 1C3 horizon from an eroded site under lichens and *Molinia*. The biomarker spectra of these C layers are dominated by *Polytrichum*

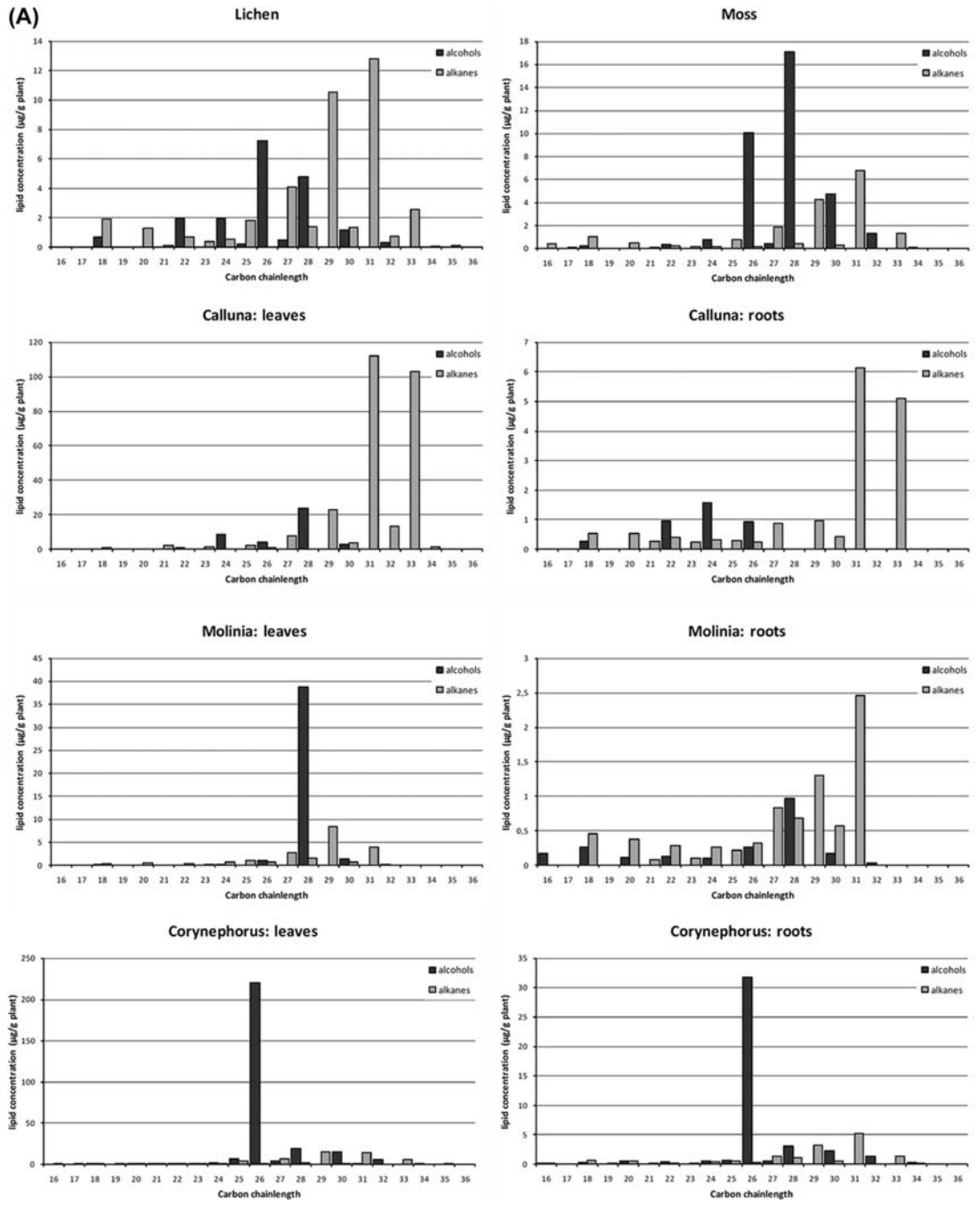

FIGURE 5.3.3 (A) Biomarker spectra of tissues of reference species. (B) Biomarker spectra of tissues of reference species (continuation). *van Mourik, J.M., Jansen, B., 2013. The added value of biomarker analysis in palaeopedology; reconstruction of the vegetation during stable periods in a polycyclic driftsand sequence in SE-Netherlands. Quaternary International 306, 14–23.*

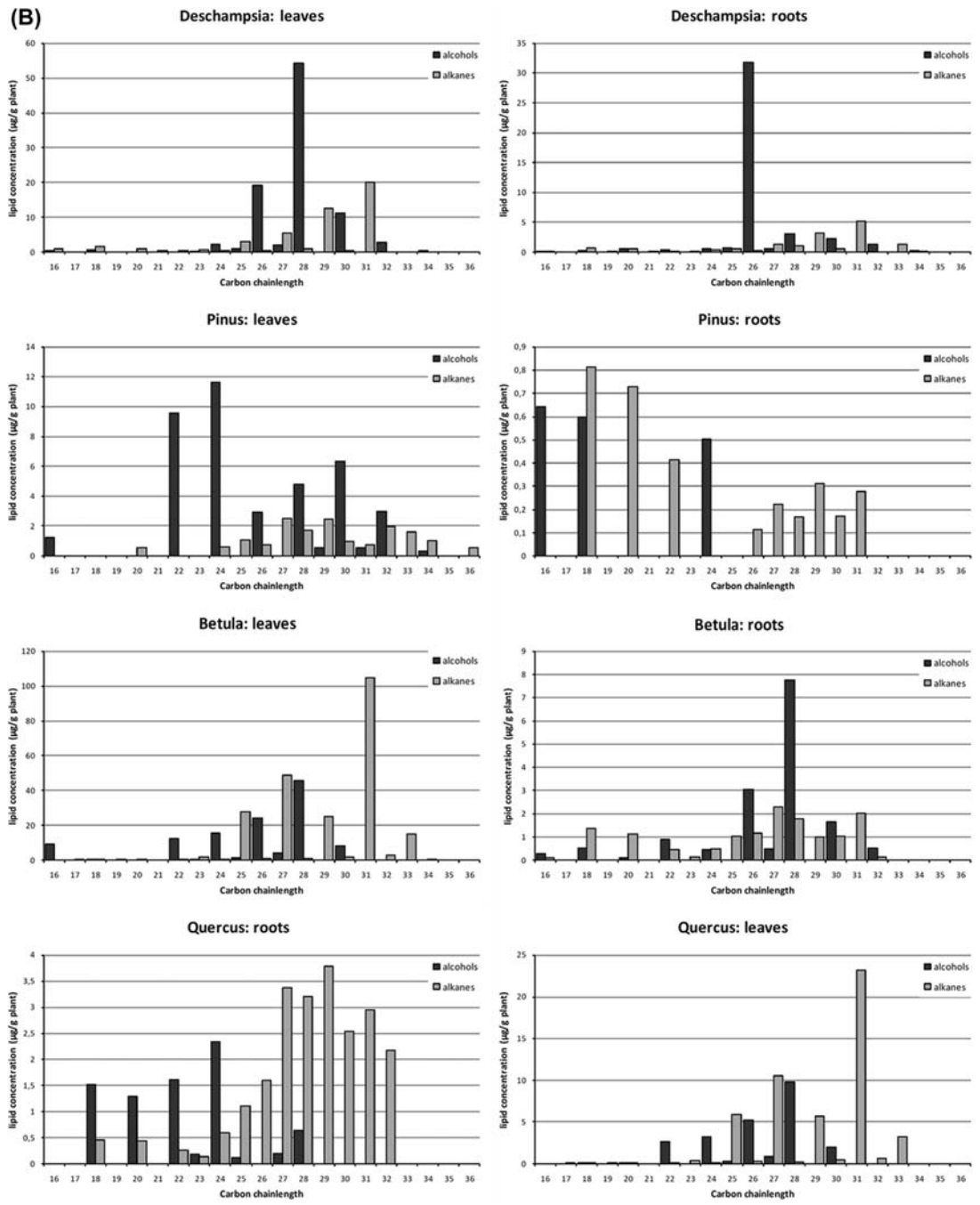

FIGURE 5.3.3 Continued.

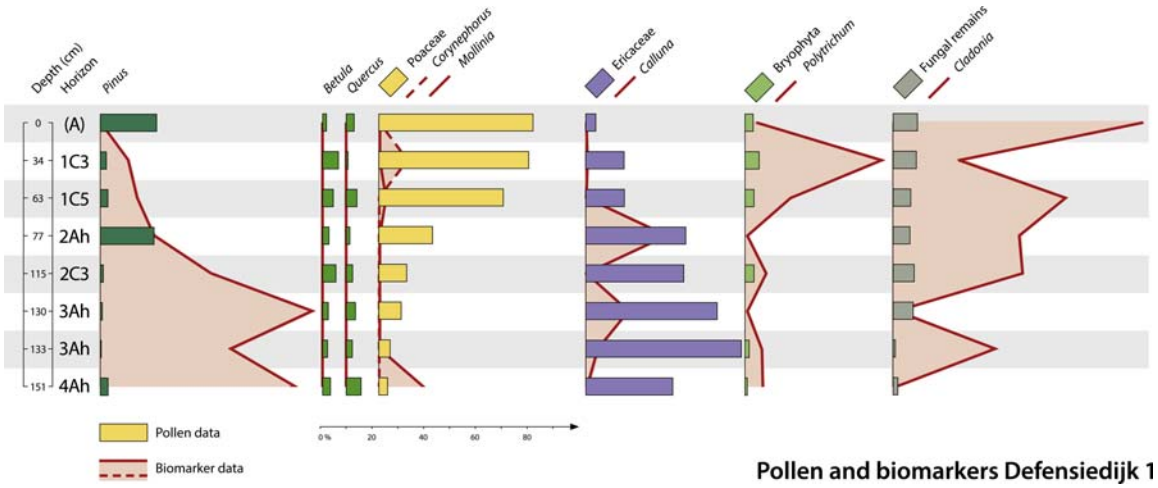

FIGURE 5.3.4 Pollen and biomarkers from the organic-rich horizons of profile Defensiedijk-1 (resampled in 2008, close to the sample location of 1986). *After van Mourik et al. (2013).*

and *Cladonia*; markers of *Calluna* are absent. This points to a pioneering initial vegetation consisting of mosses and lichens.

The comparison between the biomarker and pollen-based vegetation reconstructions allows for more decisive conclusions to be drawn about the in situ presence of species, given that biomarker input is largely in situ, while pollen spectra reflect a wider source area (Fig. 5.4.5).

This gives rise to identifying the following three hypothetical scenarios:

1. Pollen grains and biomarkers both indicate the presence of a species at a certain interval. This implies that the species was present at the site of interest, with the biomarker signal deriving from litter decomposition.
2. Pollen grains indicate the presence of a species at a certain interval, but biomarkers do not. This implies that the species was present in the vicinity of the site, but not at the actual location of the site.
3. Biomarkers indicate the presence of a species at a certain interval, but pollen do not. This implies that the species was present, but not in this particular interval. Instead, the biomarkers originate from younger root input from a higher (younger) soil surface of the sequence.

5.3.2.1 *Conclusions*

1. Biomarker analysis may be useful to distinguish between pollen taxa of local and regional relevance. Based on the combination of pollen and biomarker spectra we can select the plant species that form the local vegetation.
2. The results of biomarker analysis explain the contaminating impact of roots on the composition of soil organic matter used for ^{14}C dating of palaeosols.

5.3.3 The identification of stable fillings used for the production of plaggic manure

Here we highlight the results of a study where we examined the potential of using biomarkers to identify stable fillings utilized in the production of plaggic manure (van Mourik et al., 2016).

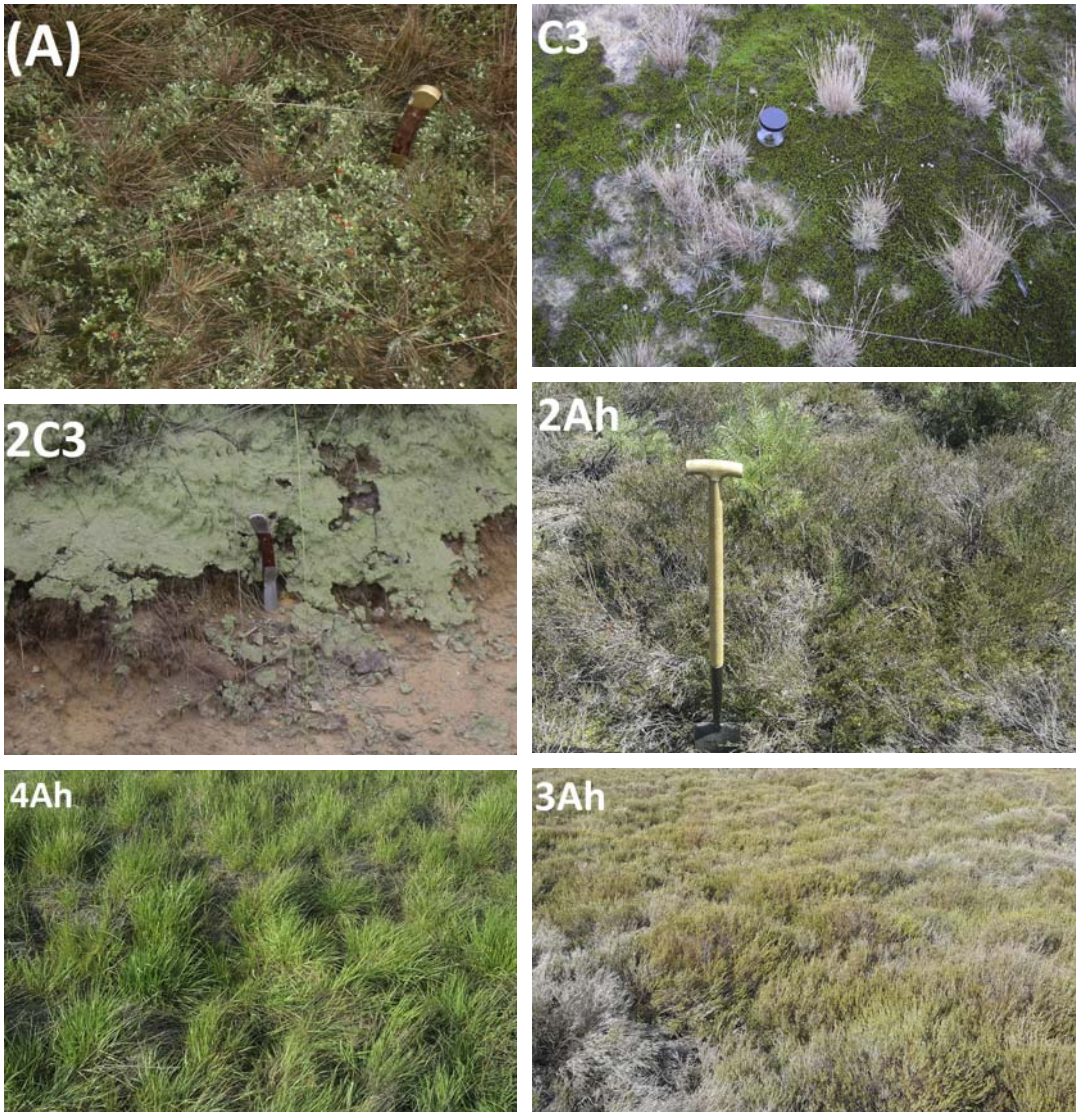

FIGURE 5.3.5 Modern vegetation types around the site Defensiedijk, which potentially could have occurred during the various phases of soil formation. (A) *Corynephorus and Cladonia*. (1C3) *Corynephorus and Polytrychum*. (2C3) *Algae* and *Cladonia*. (2Ah) *Calluna* and *Pinus*. (3Ah) *Calluna*. (4Ah) *Molinia*.

Plaggic Anthrosols are the result of plaggic agriculture, a historical form of land management in cultural landscapes on chemically barren sandy substrates in northwestern Europe. Anthrosols have been studied by historical and physical geographers (Chapter 4.4). The research questions were focused on the age of the plaggic horizons of Anthrosols, the practices of sods digging and the supposed relation between heath management and sand drifting (Chapter 4.4).

Through the combination of OSL and ^{14}C dating, historical records and fossil pollen

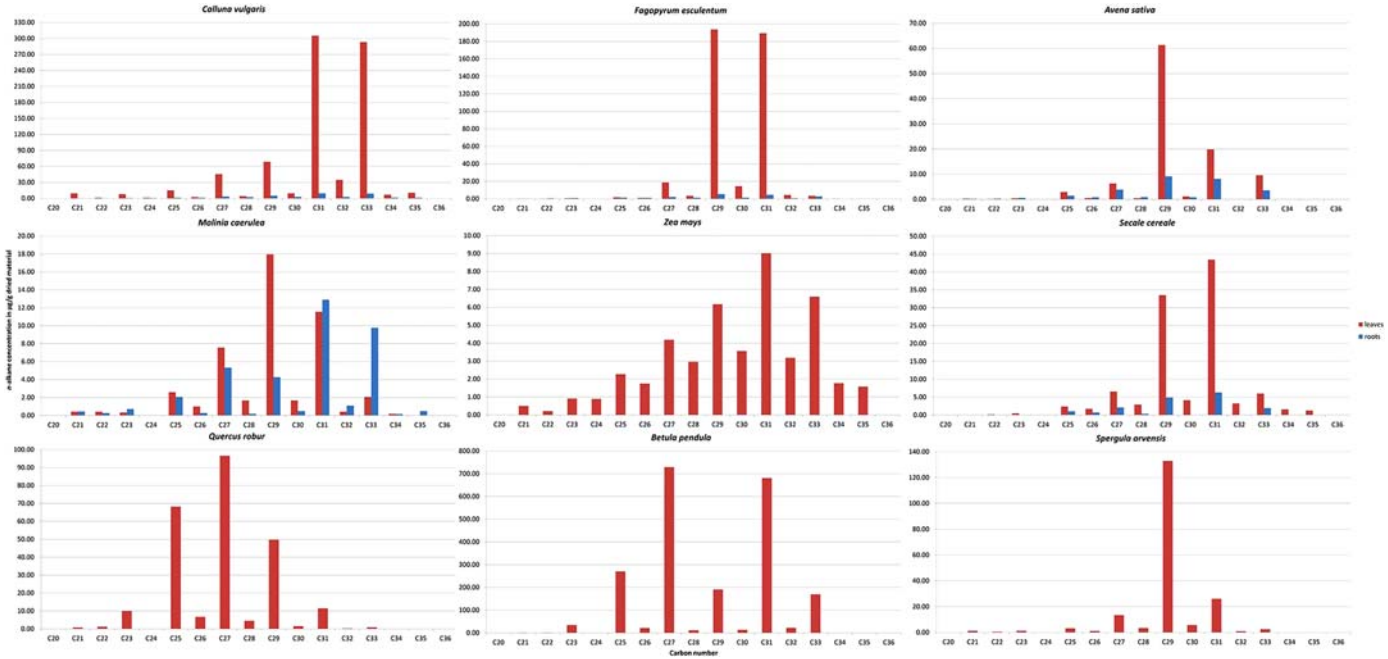

FIGURE 5.3.6 The *n*-alkane biomarker distribution in leaves (red) and/or roots (blue) of species making up the reference collection of this pilot study. *After van Mourik, J.M., Wagner, T.V., De Boer, J.G., Jansen, B., 2016. The added value of biomarker analysis to the genesis of plaggic anthrosols; the identification of stable fillings used for the production of plaggic manure. Soil 2, 299–310.*

analysis we have a good impression of the palaeoecological environment and the age of plaggic deposits. However, it remains problematic to reconstruct the combination of crop residues and various materials used by farmers as stable filling to produce the stable manure, which are together responsible for the rise of the surface of Anthrosols. This is also hindering a detailed interpretation of the agricultural practices and shifts therein related to the plaggic agriculture system, and specifically the timing of the onset of the intensive heath sod-driven deep stable agriculture with which plaggic Anthrosols are most commonly associated.

The combination of pollen diagrams and ^{14}C dates pointed to the start of agriculture around 1000 years BP. But in spite of the long period of traditional land use, OSL dates from the plaggic horizon made clear that the rise of the land surface of the old arable fields by deposition of plaggic deposits was not started before the 16th century but accelerated in the 18th century (Chapter 4.4).

The mineral fraction present in heath sods might have been responsible for the growth of the plaggic horizons and this seems to be confirmed by the presence of *Calluna* (Ericaceae) in all pollen spectra from the plaggic deposits. Based on historical documents of land management on barren sandy soils in the Flemish region and southeastern Netherlands (Burny, 1999; Vera, 2011; Doorenbosch, 2013; De Keyzer, 2014) it is known that farmers respected many rules to protect the heaths, the basis at that time for sustainable agricultural production. Digging of sods was scarcely permitted. Besides, the farmers were already aware that due to the acidity and the very low concentration of nutrients, *Calluna* sods were not a profitable adjustment to manure. Mowed *Calluna* was only used as stable filling, but more frequently as fuel and roofing. It was also known that an addition of sand to the manure could improve the quality, but not leached sand grains from heath sods or from shepherd`s tracks and sand driftings. In the course of the 18th century the situation changed due to the growth of the population, the increasing need for food production and consequently the need for more arable land and manure. Progress in the quality of construction materials made it possible to construct better, deeper and bigger stalks (the deep stable economy) and this all resulted in overdigging of heath sods, heath degradation, sand drifting and loss of heathlands (Vera, 2011). So, if the farmers did not use heath sods as stable filling before the 18th century, it is interesting to investigate what the alternatives were.

To identify the stable fillings used by the farmers in the course of time we applied biomarker analysis to samples of plaggic horizons of the Anthrosols Posteles, Nabbegat and Valenakker (Chapter 4.4) (van Mourik et al., 2016).

The first step in the flow diagram of biomarker analysis is the identification of potentially involved plant species, based on their presence in pollen spectra from plaggic deposits (Chapter 4.4). The sources of pollen grains may be various:

1. Pollen grains from the regional pollen rain-reflecting taxa of the surrounding vegetation. Because these species did not grow on the arable field they did not contribute to the composition of soil organic matter in the plaggic horizon.
2. Pollen grains originating from flowering local crop species. The decomposing roots of crop species contribute to the composition of soil organic matter in the plaggic horizon.
3. Pollen in sods and straw used as stable filling to produce stable manure. The organic content of applied organic stable filling contributes to the composition of soil organic matter in the plaggic deposits.

The second step is sampling of (fresh) plant tissues, potentially involved in the production of stable manure for the creation of the

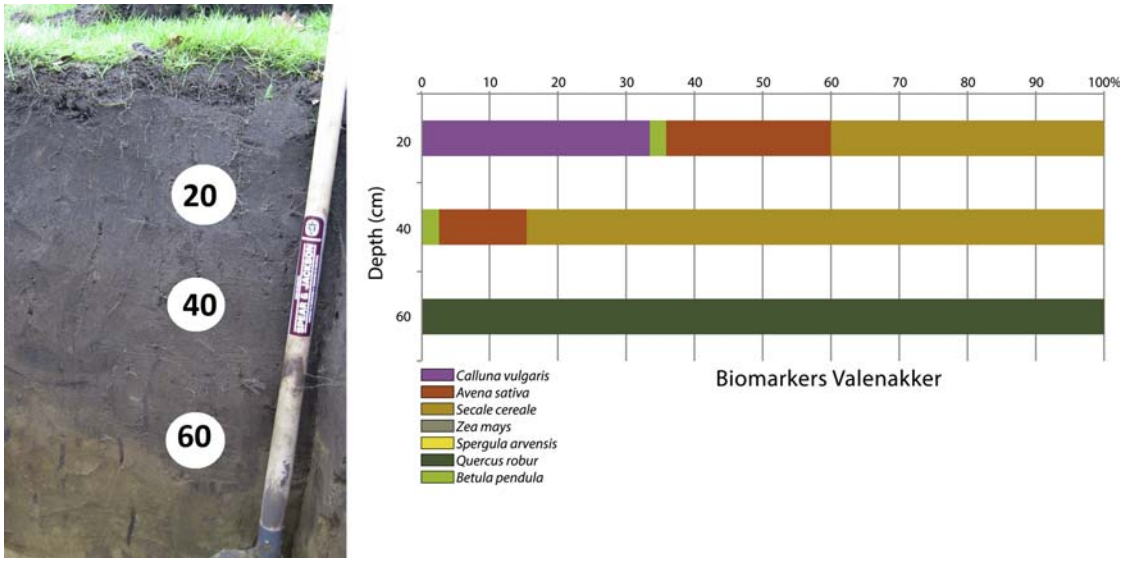

FIGURE 5.3.7 Biomarker diagram of the plaggic horizon of profile Valenakker. Optically stimulated luminescence ages indicated with the rings: (20) AD 1775 ± 20; (40) AD 1635 ± 30; (60) AD 1565 ± 30. *After van Mourik, J.M., Wagner, T.V., De Boer, J.G., Jansen, B., 2016. The added value of biomarker analysis to the genesis of plaggic anthrosols; the identification of stable fillings used for the production of plaggic manure. Soil 2, 299–310.*

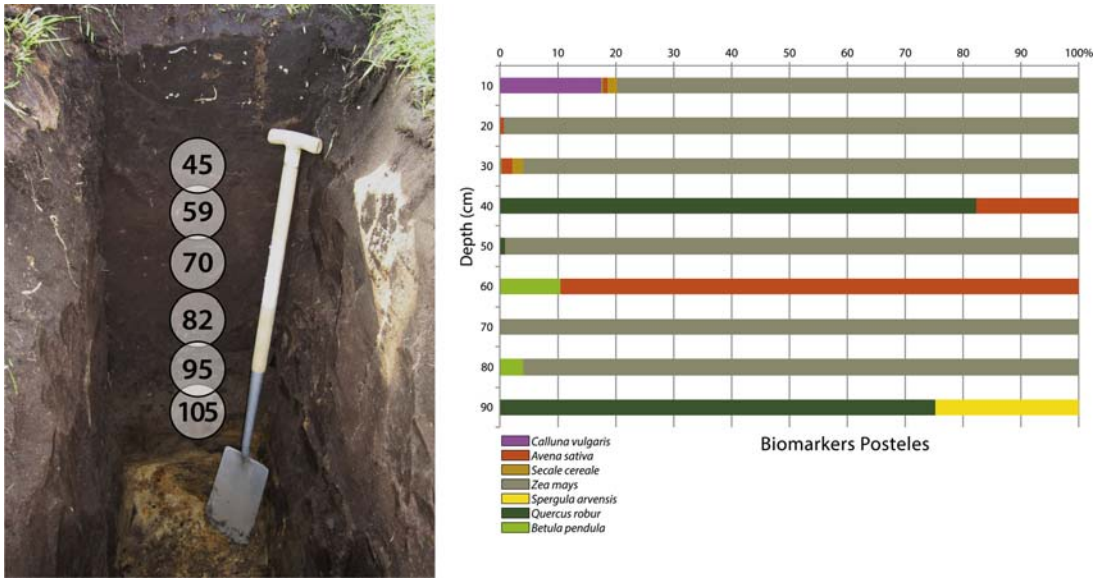

FIGURE 5.3.8 Biomarker diagram of the plaggic horizon of profile Posteles. Optically stimulated luminescence ages: (45) AD 1758 ± 14; (59) AD 1711 ± 20; (70) AD 1651 ± 31; (82) AD 1626 ± 20; (95) AD 1517 ± 31; (105) 2035 ± 450 BC. *After van Mourik, J.M., Wagner, T.V., De Boer, J.G., Jansen, B., 2016. The added value of biomarker analysis to the genesis of plaggic anthrosols; the identification of stable fillings used for the production of plaggic manure. Soil 2, 299–310.*

biomarker reference base. Two groups of species can be recognized:

1. A group of selected plant species reflecting the main sources of stable fillings used for manure production: fermented litter from deciduous forest soils (*Quercus robur*, *Betula pendula*), grass sods from brook valleys (*M. caerulea*) and mowed heath or heath sods (*Calluna vulgaris*).
2. The second group concerned crop species. Close to the educational Field Study Centre Orvelte (Drenthe) is a traditional plaggic field where cultivation of traditional crop species was continued. There we sampled *Fagopyrum esculentum*, *Spergula arvensis*, *Avena sativa* and *Secale cereale.* Modern crop species like *Zea mays* (corn) and *Solanum tuberosum* were sampled on the Posteles.

The next steps in the analysis are sampling of the three plaggic horizons, extraction of biomarkers of the tissue and soil samples and matching with the VERHIB application. The biomarker spectra of nine relevant tissue species are shown in Fig. 5.3.3. The results of the biomarker analysis of the plaggic horizons are shown in Figs 5.3.7–5.3.9. Biomarkers in this study consisted once more of the higher chain-length *n*-alkanes deriving from the wax layers on plant leaves and roots.

In previous studies the origin of stable fillings, used in plaggic agriculture, was reconstructed on the basis of pollen diagrams (Spek, 2004; van Mourik et al., 2012). Pollen spectra of plaggic horizons show low scores of deciduous trees and are dominated by Ericaceae and Poaceae. The presence of Ericaceae pollen may indicate the use of heath sods, the presence of Poaceae pollen suggests the use of grassland sods and the rise of the land surface by utilization of plaggic manure is caused by the mineral fraction in sods.

The biomarker spectrum of the base of the plaggic horizon of the Valenakker is dominated by *Quercus* (Fig. 5.3.7). Because oak trees are

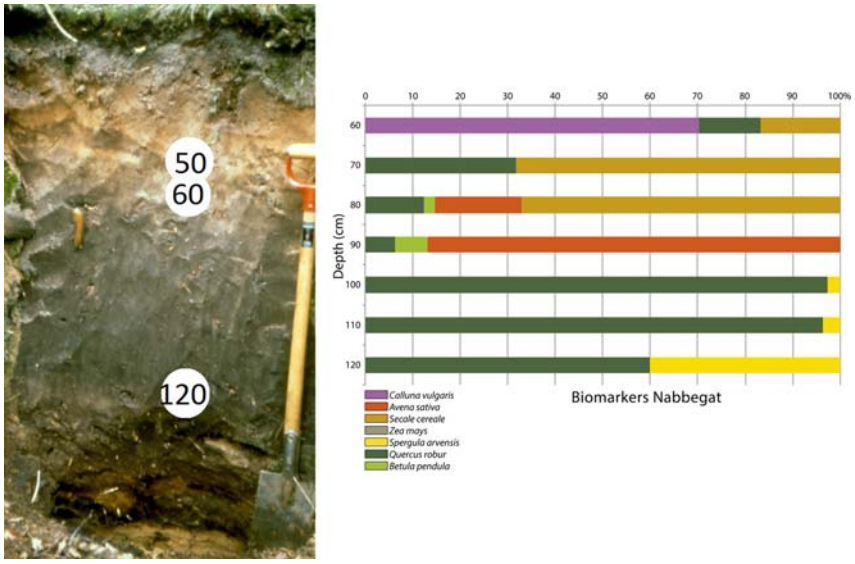

FIGURE 5.3.9 Biomarker diagram from the buried plaggic horizon of profile Nabbegat. Optically stimulated luminescence ages indicated with the rings: (50) AD 1803 ± 12; (60) AD 1770 ± 11; (120) AD 1676 ± 14. *After van Mourik, J.M., Wagner, T.V., De Boer, J.G., Jansen, B., 2016. The added value of biomarker analysis to the genesis of plaggic anthrosols; the identification of stable fillings used for the production of plaggic manure. Soil 2, 299–310.*

not growing on the arable field it is very likely that farmers used litter from the forest soil as stable filling. The middle spectrum is dominated by biomarkers of *Avena* and *Secale*. Partly, the source of these markers can be decomposing roots of these crop species, but more important was the use of straw from these species as stable filling. The upper spectrum biomarkers of *Calluna* are present together with *Avena* and *Secale*. *Calluna* did not grow on the field, so this points to the use of mowed heath or heath sods as additional stable filling during the last phase in the development of the plaggic horizon.

Just as in Valenakker (Fig. 5.3.7) the lowest spectrum (90) of Posteles is dominated by markers of *Quercus*, indicating the use of forest litter during the development of this part of the plaggic horizon. The biomarkers of the crop species *Spergula* will originate from decomposed roots. The spectra from 10, 20, 30, 50, 70 and 80 cm depths are dominated by biomarkers from roots of *Z. mays* (Fig. 5.3.8). This (deep-rooting) crop species was introduced around AD 1950, but the markers of decomposed *Zea* roots seem to suppress all the other species (this not the case in the profiles Valenakker and Nabbegat where *Z. mays* was never a crop species). Spectrum 40 is (again) dominated by *Quercus*; spectrum 60 is dominated by *Avena*. *Calluna* is only present in the youngest part of the plaggic horizon. In the past, stable fillings, composed of forest litter and straw only in the youngest phase heath sods or mowed heath, have been used.

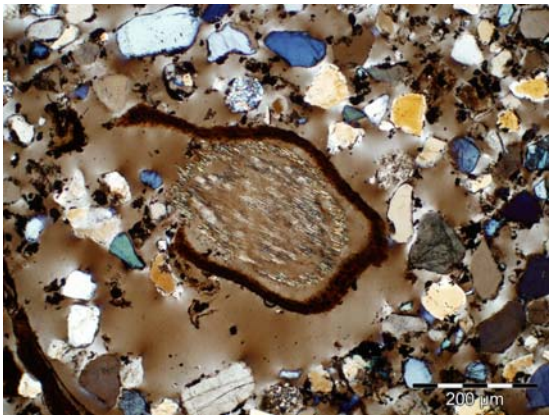

FIGURE 5.3.10 Cross-section of a tree root in the thin section (70–80 cm) of the buried plaggic horizon of profile Nabbegat. *After van Mourik, J.M., Wagner, T.V., De Boer, J.G., Jansen, B., 2016. The added value of biomarker analysis to the genesis of plaggic anthrosols; the identification of stable fillings used for the production of plaggic manure. Soil 2, 299–310.*

Polycyclic soil profile Nabbegat is a haplic Arenosol in driftsand, overlying a plaggic Anthrosol, overlying a ploughed umbric Podzol in coversand (Fig. 5.3.9). The plaggic horizon was buried around AD 1800 by driftsand and as a result it has not been disturbed by reallotment projects in the 20th century and by industrial and urban pollution. From c.1000 BC until AD 1500 farmers must have used organic matter with limited mineral 'contamination' because the land surface did not rise significantly in the period preceding the plaggic agriculture. Based on OSL dating, the rise of the plaggic horizon did not start before the 16th century. The dominance of *Quercus* in the oldest biomarker spectra (at 130, 120 and 110 cm depth) of the plaggic horizon points to the use of litter from the forest soil as stable filling (Fig. 5.3.9). *Spergula* must have been the main crop species during this phase and the markers must originate from decomposing roots of this species. The spectra of the middle part of the plaggic horizon (at 100, 90 and 80 cm depth) are dominated by biomarkers of *Avena* and *Secale*, partially originating from decomposing roots, partially from decomposing straw. During this phase in the development of the plaggic horizon, straw has mostly been used as stable filling. The spectrum at 70 cm

depth belonging to the youngest part of the plaggic horizon is dominated by *Calluna*, indicating the use of heath sods or mowed heath during the last phase of the development of the plaggic horizon (Fig. 5.3.10).

Biomarkers of *Quercus* occur not only (dominantly) in the oldest spectra, but also (low percentages) in the younger spectra. Most likely this is due to roots of young *Quercus* trees that colonized the driftsand deposit. In thin sections of the top of the buried plaggic horizon of Nabbegat, living and decomposing roots were observed (Fig. 4.4.11). Characteristic is the double fringing of the (living) root tissue. Such roots were only found in the upper part of the plaggic horizon of Nabbegat. Roots of crop species were not found in the thin sections of plaggic horizons; most likely they decompose rather quickly compared with tree roots. In the detailed description of root distribution of a similar soil profile (Rakt), roots from seedlings of *Quercus* and *Betula* colonizing a driftsand layer overlying a plaggic Anthrosol were found to reach the top of the buried plaggic deposits (Gocke et al., 2016).

5.3.3.1 The origin of sand grains in plaggic deposits

The mineral component of stable manure, applied on the fields, was responsible for the thickening of the plaggic horizon. Ploughing of the furrow will bleach the OSL signal of the mineral grains until the moment that the grains are no longer part of the active soil furrow. For that reason, OSL dating of the plaggic horizon provides reliable ages of the plaggic deposits (Bokhorst et al., 2005). The OSL dates of the profiles Valenakker, Nabbegat and Posteles indicate a start of the thickening c.AD 1550.

In the three biomarker diagrams we find *Quercus* as a dominant marker in the lowest part of the plaggic A horizon, indicating the use of forest litter (Figs 5.3.7–5.3.9). In Nabbegat, *Quercus* markers can also originate from roots of the colonized *Quercus* seedlings on the driftsand deposit. The middle part of the plaggic A horizon is dominated by biomarkers of *Avena* and *Secale*, indicating the use of straw as stable filling. Only in the top of the plaggic horizons are biomarkers of *Calluna* present, indicating the use of heath sods or mowed heath as stable filling only during the last phase of the development of the plaggic horizons. This fits with observations on the use of heaths in historical archives (Vera, 2011).

The question rises regarding heath management before the introduction of the deep stable economy. Some researchers point to careful heath management before the 19th century. In interviews with farmers born before 1950, Burny (1999) collected essential information about historical heath management in the Belgian Kempen. Before the 19th century, heath sods were never dug on the dry *Calluna* heath, only on the moist *Erica* heath. These organic sods were not used as stable filling but as fuel for the furnace. Burning of *Calluna* heaths was the most important management action to rejuvenate the heath. This is relevant, since juvenile heath is food for cows. Sods digging was a discouraged action due to the resistance and incoherence of these dry sods and also the long recovery period. Mowing of older *Calluna* shrubs took place. Twigs were used for roofs, burning and also as stable filling (Burny, 1999). Because of the very low nutrient contribution to the manure of mowed *Calluna*, farmers preferred the use of twigs of broom (*Genista*).

When conducting a biomarker-based analysis of plaggen deposits, an important issue to consider is the possibility of vegetation biomarkers being present in sheep droppings. According to Simpson et al. (1999), biomarkers survive the congestion process and stay in the manure. As such it is relevant to consider which plants sheep consume. Grazing sheep are very selective in collecting food and prefer grasses (*Molinia*, *Festuca* and *Corynephorous*) (Oom et al., 2008; Smits and Noordijk, 2013). Only late in the season do they eat shoots of *Calluna*, at that time nourished with high concentrations of Ca and Mg but no P. If it is true that *Calluna*

heath sods were dug only in the 18th and 19th centuries, how can we explain the mineral component in the plaggic manure responsible for the rise of the land surface before that time?

According to Smits and Noordijk (2013) there are several sources of minerals. First, an amount of mineral grains will be incorporated in the manure during emptying of manure from the stable. Second, farmers had the knowledge that the addition of sand could improve the fertility of the soil, not the leached and acid sand from heath sods, but leached sand dug on sheep walks and in blown-out depressions in nearby drift-sand landscapes.

5.3.3.2 *Conclusions*

- We can identify various stable fillings used, based on the vertical distribution of biomarkers.
- The biomarker spectra of the base layer of the plaggic horizon are dominated by biomarkers of deciduous tree litter (dominated by *Quercus*), indicating the use of organic matter from the forest floor.
- The biomarker spectra of the middle part of the plaggic deposits are dominated by crop species (*Avena*, *Secale*), indicating the use of straw from these species as stable filling over a relatively long time.
- Only the top spectra of the plaggic horizons are dominated by *Calluna*, indicating that heath sods were used as stable filling only during the last phase in the development of the plaggic horizon.

5.4 Simultaneous reconstruction of vegetation and precipitation shifts in the Dominican Republic

5.4.1 Introduction

The archipelago of Caribbean islands covers a vast and geographically diverse area in between the continents of North and South America. Despite a recent increase in studies on Holocene palaeoenvironmental change, both the number of studied sites and variety in applied proxies remain limited. Consequently, for many Caribbean islands the impact of past climate variability on the environment and its inhabitants is poorly understood. One of the causes is the scarcity of freshwater lakes and peat bogs that usually contain carbon-rich palaeoarchives. Caribbean soils are often calcareous and hence have a poor long-term preservation of organic matter, especially in combination with a semi-arid climate. Moreover, records of the past millennia are likely to bear the imprint of human activity obscuring natural processes (Castilla-Beltrán et al., 2018; Hooghiemstra et al., 2018). For terrestrial sites, palaeoenvironmental reconstructions mainly rely on evidence from fossil pollen, charcoal, grain size distributions and stable carbon and oxygen isotopes, whereas plant leaf wax-derived lipids as biomarkers are rarely used.

Effective precipitation is considered to be one of the most important environmental variables in the Caribbean during the Holocene (Douglas et al., 2012). Reconstructions of past changes in precipitation/evapotranspiration are often based on $\delta^{18}O$ values of ostracods, or other carbonate- or silica-producing organisms (Douglas et al., 2012), or inferred from fossil pollen records (Castilla-Beltrán et al., 2018; Hooghiemstra et al., 2018). However, these are not always sufficiently abundant or well preserved in palaeoarchives to establish reliable records of regional relevance. Recent years saw the development of a biomarker method for palaeohydrological reconstructions using the compound-specific isotopic composition of hydrogen (δ^2H or δD) in individual sedimentary wax lipid molecules originating from photosynthesizing organisms (Sachse et al., 2012). Various studies have demonstrated that δD values of such deposited lipid biomarkers are highly correlated with those of source waters used by their respective organisms (Sachse et al., 2012 and references cited therein). Successful application of plant wax lipid (e.g., *n*-alkanes)

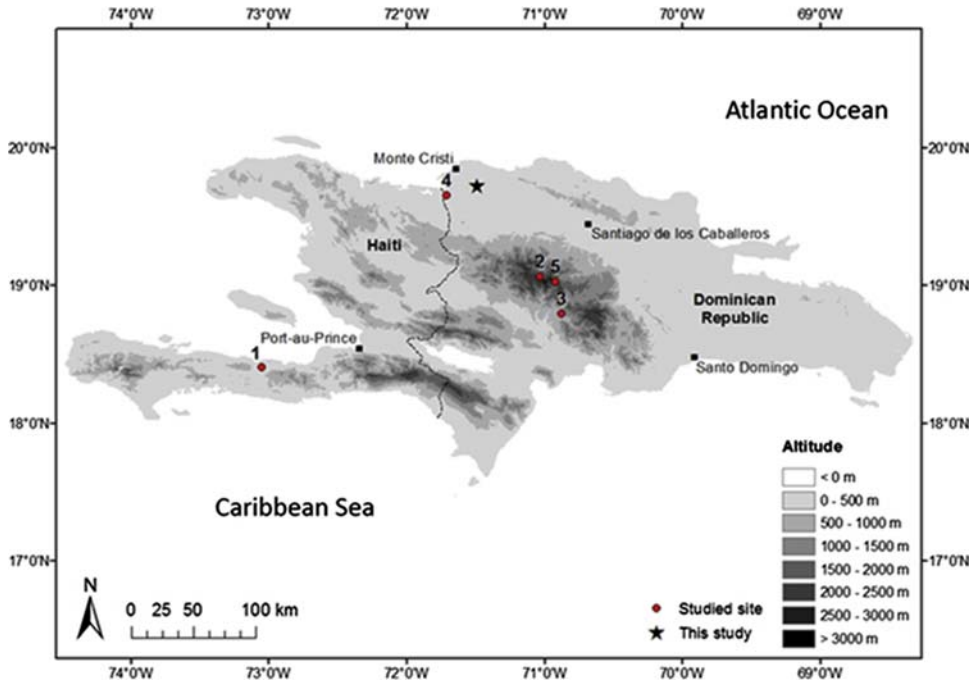

FIGURE 5.4.1 Map of Hispaniola, including elevation and published palaeoenvironmental studies focusing on the Holocene. The *black star* marks the location of the site investigated in this study.

δD values to reconstruct hydrological changes in various environments show great promise for it to be applied in the Caribbean, combined with a simultaneous vegetation reconstruction using the same compounds.

Here, a case study is presented that explores the application of the combined use of sedimentary wax lipids and their associated hydrogen-isotopic composition. The Dominican Republic was used as the study location because it is one of the main areas investigated within the European Research Council-Synergy project NEXUS 1492, which aims to rewrite and draw attention to the era of first encounters between European colonizers and indigenous Caribbean cultures and societies (http://nexus1492.eu).

5.4.2 Environmental setting

5.4.2.1 Geography

Hispaniola (c. 19°N, 71°W), now including the Dominican Republic and Haiti, was first discovered by Europeans during the first voyage of Christopher Columbus in 1492. Research will focus here on the Monte Cristi Province (19°51′N, 71°39′W) in the northern section of the Dominican Republic. The Rio Yaque del Norte is the major river of the province and originates from the Cordillera Central, the highest mountain chain of the Caribbean Islands with peaks over 3000 m asl (Fig. 5.4.1). The flats around the river and at its mouth into the Atlantic Ocean are made up of Quaternary sediments, while surrounding topography reflects

post-Eocene marine strata (French and Schenk, 1997; Reyna et al., 2012). The river is embedded between the Cordillera Central to the south and the Cordillera Septentrional to the north. The current mouth of the river is just south of Monte Cristi, the main centre of population in the generally sparsely populated province.

5.4.2.2 Climate

The positioning of the study area in between two mountain ranges has a large impact on the local climate. It is sheltered from the predominant supply of precipitation coming from the Atlantic Ocean by northeasterly trade winds (Lane et al., 2009; Cano Carmona et al., 2010; Caffrey et al., 2015). This makes the study area one of the driest regions of the Dominican Republic, receiving on average <800 mm of annual precipitation. This is in sharp contrast to the more than 2000 mm that falls in other parts of the country, all caused by the highly variable topography (Izzo et al., 2010; Reyna et al., 2012). Most of the precipitation falls in autumn and early winter (WMO, 2017) and is delivered by storms associated with polar outbreaks from the north, locally known as *nortes* (Horst, 1992; Lane et al., 2011). Mean annual air temperature in the city of Monte Cristi is 31.5°C, with low seasonal variability (Cano Carmona et al., 2010; Caffrey et al., 2013). Combined with the low amounts of precipitation this leads to a water deficit, and a classification of the area as semi-arid (Izzo et al., 2010). In general, climate in Hispaniola is primarily determined by large-scale, interacting climate phenomena such as the Intertropical Convergence Zone, El Niño-Southern Oscillation, North Atlantic Oscillation and the Azores High (Giannini et al., 2000; Lane et al., 2009; Izzo et al., 2010; Reyna et al., 2012; Caffrey et al., 2013; Flantua et al., 2016a and references cited therein).

5.4.2.3 Vegetation

Most of the region is classified as subtropical dry forest with many cactaceous and leguminous plant species (Van Royen, 1938; Reyna et al., 2012; Caffrey et al., 2013; Cano-Ortiz et al., 2015). Durland (1922) classified the area around Rio Yaque del Norte, west of the city of Santiago, as thorn forest, having 'many species of trees and shrubs strongly armed with needle-like and piercing spines and prickles'. The coastal zones contain mangrove forests and some lagoons of which a large section is protected in Parque Nacional Monte Cristi (e.g., Reyna et al., 2012). Most of the flat area (north)west of Guayubín is converted to suit agricultural needs in the form of large rice paddies, banana plantations, cropping fields and pastures (Tactuk et al., 2015). Only smaller pockets of vegetation remain, as well as small strips along roads, the Rio Yaque del Norte and smaller streams and channels. The hills east of the city of Monte Cristi have a more extensive and dense vegetation cover. The limestone outcrop El Morro de Monte Cristi, just north of the city, is a geological landmark that is easily recognizable in the distance due to the otherwise flat topography.

5.4.3 Materials and methods

5.4.3.1 Site description and vegetation

The Castañuela II site (19°43′23″N, 71°29′32″W) is an abandoned meander of the Rio Yaque del Norte located just east of the small town of Castañuela, Monte Cristi Province. The meander is partially filled in with sediments, but at the time of coring still held water in the former main channel. The smallest distance between the sampling location and the Rio Yaque del Norte is c. 500 m, and the town and main road are present within a 1 km radius. The inner area of the meander was reached by a dirt road cutting through the meander; a second crossing was made c. 350 m to the southeast. The site is surrounded by banana plantations and a patch of grassland used for cattle (Figs 5.4.2 and 5.4.3). According to the landowners, the banana plantations were founded in c. 1973–74 and before pastoralism was likely practised. The

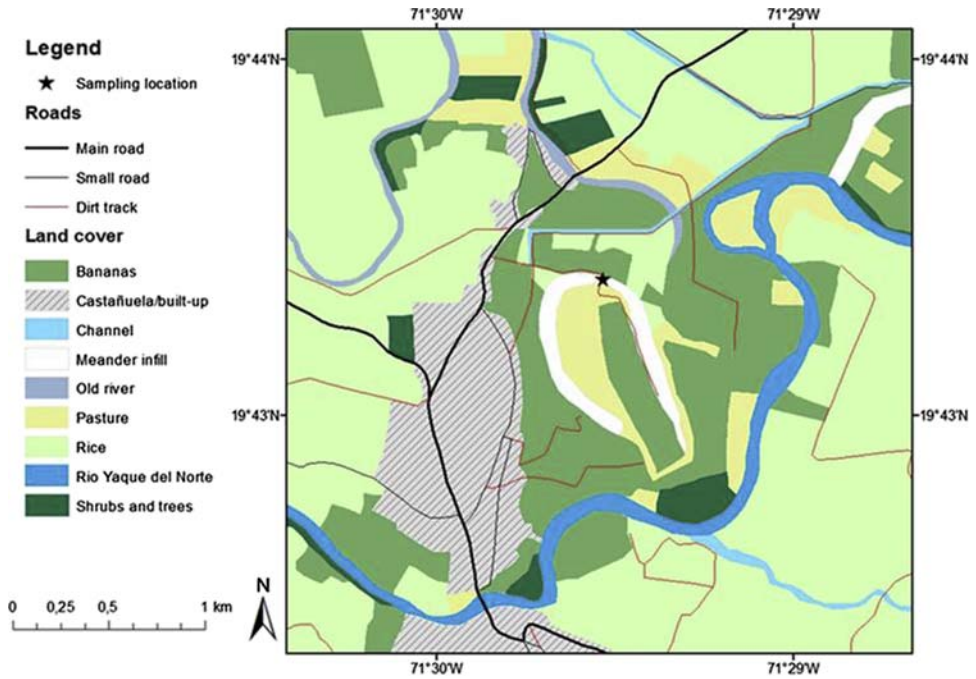

FIGURE 5.4.2 Land cover map of the area (c. 9 km^2) surrounding the Castañuela II site, an old meander of the Rio Yaque del Norte (Monte Cristi Province, Dominican Republic). The map is based on observations in the field and aerial imagery available in Google Earth and Esri ArcGIS, where the green areas are agricultural fields (mostly rice paddies and banana plantations).

presence of cattle was observed in the field, as well as their evidence in the form of dried-out manure, trampled soil and damaged vegetation. Some rice paddies were present in the direct vicinity of the coring location, and a bit further away larger paddies dominating the landscape. Large sections of the lake were covered with dense reed beds (*Typha domingensis*) and emergent water hyacinths (Pontederiaceae: *Eichhornia* sp.). Although less abundant, at shores were also present *Cyperus* spp., *Sagittaria lancifolia*, *Eleocharis interstincta* and *Hydrocotyle umbellata* (Areces-Mallea et al., 1999), as well as tall plants (c. 1.5 m height) that appeared to be *Zamia* sp.

Besides the banana plantations the area was very open, with only a few (groups of) trees and shrubs, mostly along the waterside and often containing vines (e.g., Convolvulaceae). *Albizia saman* (Fabaceae) was the most prominent tree species, and (prickly) shrubs were generally of the Fabaceae family. Other tree-like species included *Guazuma ulmifolia* (Malvaceae), tall palms (Arecaceae) and commercially interesting species such as mango (*Mangifera indica*) and tamarind (*Tamarindus indica*). In the grassland, numerous (flowering) forbs occurred, including the thistle *Argemone mexicana* (Papaveraceae), *Malachra* spp. (Malvaceae), *Ruellia tuberosa* (Acanthaceae), *Heliotropium indicum* and *Heliotropium curassavicum* (Boraginaceae), *Phylla* spp. (Verbenaceae) and *Achyranthes aspera* (Amaranthaceae), as well as some small shrubs (<1 m

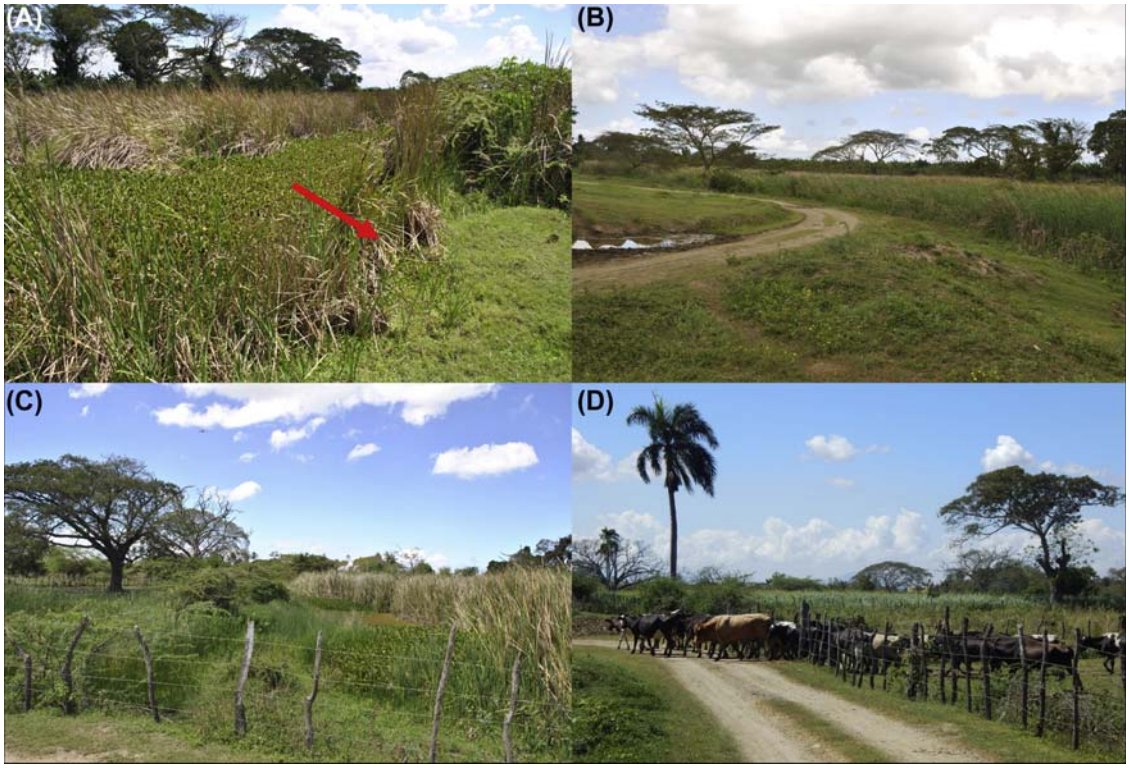

FIGURE 5.4.3 Pictures taken at Castañuela II (Monte Cristi Province, Dominican Republic), close to the sampling location, as is, for instance, indicated in Fig. 5.4.2. (A) Exact coring location (*red arrow*) with mostly *Eichhornia* sp. and dried-out *Typha domingensis* in the water. (B) Dirt road through a pasture just southeast of the coring site with a slightly sloping bank toward the water, which is full of *T. domingensis*. (C) From the coring location looking to the west, across the constructed crossing of the meander. (D) Looking to the south from the coring site, evidence of cattle and bananas in the background. *(A–C) By Steven de Goede. (D) By Eduardo Herrera Malatesta, C. All pictures taken in March 2015.*

height) like *Prosopis juliflora* (Fabaceae) and various Euphorbiaceae (e.g., *Jatropha gossypiifolia*).

5.4.3.2 Sampling and pretreatment

In March 2015, a sediment core of 1.5 m length was retrieved at Castañuela II using a Russian corer (ø50 mm). The core was taken in shallow water, covered by water hyacinths, a meter from a stretch of grass that was located of the side of the constructed crossing (Fig. 5.4.3). As a result, the core was taken in what would have been more or less the centre of the river flow, in the most outward position of the meander. Core halves were photographed and sealed immediately after collection, and after transport to Amsterdam sediment cores were stored refrigerated (4°C). Sediment subsamples were taken on two occasions, 12 at a time, within predescribed intervals of the core lithology (Table 5.4.1). The first set of samples acted as an explorative coarse-grid study to determine the presence and abundance of lipid biomarkers, to fine-tune the methodology and to determine the sampling strategy for the second set. The second set of samples had more emphasis on the bottom 50 cm, because this section appeared to be more heterogeneous and would be the oldest

TABLE 5.4.1 Description of the stratigraphy for a sediment core taken at Castañuela II, an infill of an old Rio Yaque del Norte meander.

Depth (cm)	Description
0–12	Dark grey, loose material with some plant remains
12–30	Lighter grey, dense/sticky clay material
30–45	Loose, fibrous organic matter, brown with dark grey mottles
45–63	More clayey material, with some smaller organic fibres
63–108	Grey clay with sandy intervals and small brown bands
108–126	Lighter, more clayey material
126–127	Darker, with some more poorly degraded OM
127–138	Clayey, more sand, some larger pieces of degraded OM
138–142	Darker, with some more poorly degraded OM
142–150	More sandy, loose material

OM, organic matter.

TABLE 5.4.2 List of sampled plant species at coring location Castañuela II in Monte Cristi Province (Dominican Republic), including short description of the plant species.

Family	Subfamily	Species	Description
Typhaceae		*Typha domingensis*	Tall reed
Typhaceae		*T. domingensis*	Tall reed; dead but standing, dried out
Musaceae		*Musa* sp.	Banana grown on plantation
Pontederiaceae		*Eichhornia* sp.	Emergent flowering water plant, forming large mats at water surface
Fabaceae	Caesalpinioideae	*Tamarindus indica*	Tree carrying pods used for consumption
Fabaceae	Mimosoideae	*Albizia saman*	Large tree carrying pods
Fabaceae	Mimosoideae	*Prosopis juliflora*	Prickly shrub
Malvaceae	Byttnerioideae	*Guazuma ulmifolia*	Evergreen tree with large leaves and many fruits

part. Subsamples were 1 cm-thick slices, or in some cases 2 cm to ensure enough material was available for analyses. Subsequently, subsamples were wrapped in aluminium foil and freeze dried for 48 h to complete dryness. Any obvious roots, stones and shells were removed, and samples were ground and stored in a desiccator awaiting further treatment, while a small portion (<0.5 g) was used to determine total carbon, nitrogen and sulphur (CNS) with an Elementar VarioEL CNS analyser. All previous sample treatments were carried out in a laboratory space

dedicated to natural abundance of stable isotopes, avoiding contact with (suspected) isotope-labelled materials.

From seven dominant plant species (Table 5.4.2), leaf material was collected to be used as a reference for biomarker analyses. These species were determined likely to be the producers of most of the biomass on the site.

From *T. domingensis* both living and dead specimens were sampled, because a lot of dead, dried-out standing reed was observed in the field. Collected leaf material was stored in aluminium foil while minimizing hand contact. Leaves were air dried prior to transport. Subsequently, plant samples were freeze dried for 48 h and ground to <0.2 mm. A small portion was used for CNS analysis, as was previously described.

5.4.3.3 Radiocarbon dating

Two freeze-dried sediment samples containing (decomposed) organic matter were selected for ^{14}C dating based on carbon content. One was taken at 39 cm containing poorly degraded plant material, and the other in the bottom section (126 cm) at an interval appearing to have a relatively high organic matter content. Samples were pretreated and subsequently radiocarbon dated with accelerated mass spectrometry. Radiocarbon ages were calibrated using CALIB 7.0.4 (Stuiver and Reimer, 1993) and CALIBomb (http://calib.org/CALIBomb) (Reimer et al., 2004; Hua et al., 2013) software packages with the intcal13 dataset (Reimer et al., 2013). As only two samples were analysed, no age–depth model was made and only linear sedimentation rates were calculated (cf. De Boer et al., 2014; Lane et al., 2014).

5.4.3.4 Extraction and fractionation of biomarkers

Lipid compounds to be used as biomarkers in this study were extracted by accelerated solvent extraction (ASE) using a Dionex 200 ASE extractor with DCM/MeOH, 93:7 v/v as the solvent (Jansen et al., 2006b). The amount (here 1–7 g) of sediment sample containing 0.15–0.20 g of organic carbon was weighed, to which internal standards (5α-androstan-3β-ol and 5α-androstane, 0.5 μg/μL per compound) were added, and the remaining space in the 11 mL extraction cells was filled with pure quartz sand (baked at 800°C). Extraction took place at 75°C (heating phase 5 min) and 1500 kPa, with a static extraction time of 20 min; the number of extraction cycles was set at three. Per four samples a blank containing only internal standards was added. Afterward, the solvent phase was evaporated to complete dryness under a gentle stream of pure N_2.

To prevent interference during stable isotope analysis, elemental sulphur was removed from the extracts (redissolved in DCM) with activated copper, and again evaporated to complete dryness (Schwab and Sachs, 2009; Günther et al., 2011; Prasad et al., 2014). Next, extracts were fractionated on self-made columns with activated silica gel (10 h at 450°C, deactivated 5% w/w ultrapure water) on top of glass wool in a glass syringe (e.g., De Rijke et al., 2015). Columns were conditioned using equal volumes of acetone, DCM and hexane, respectively, and subsequently dried at 50°C for >4 h. After initial rinsing with hexane, three fractions were created using different solvents: F1 contained *n*-alkanes and was eluted with hexane; F2 contained ketones and esters and was eluted with hexane/DCM (4:1 v/v); and F3 contained (amongst other things) *n*-alcohols and *n*-alkanoic acids and was eluted with DCM/methanol (9:1 v/v). F1 and F2 were evaporated to dryness under N_2, redissolved in 1 mL hexane and stored at 4°C awaiting analysis. For F3, dry extracts were redissolved in 1 mL DCM/2-propanol (2:1 v/v), of which 200 μL (or more) was derivatized with 50 μL *N,O*-bis(trimethylsilyl)trifluoroacetamide/trimethylchlorosilane (9:1 v/v) and 50 μL hexane. The mixture was heated for 1 h at 70°C to form trimethylsilyl (TMS) ethers at all free hydroxyl groups. After cooling and evaporation to complete dryness under N_2, the sample was

dissolved in hexane, the amount depending on the degree of concentration needed for good identification and quantification of *n*-alcohols. The protocol for plant samples slightly differed with 0.15 g used for ASE extraction, more internal standards to anticipate higher concentrations of lipids and two extraction cycles. The plant samples would not be analysed for compound-specific isotopes, and therefore the desulphurization step was skipped, whereas fractionation and derivatization were as described before.

5.4.3.5 Gas chromatography/mass spectrometry analysis

Measurements were carried out on a ThermoQuest TraceGC 2000 gas chromatograph linked to a Finnigan TraceMS quadrupole mass spectrometer (e.g., Jansen et al., 2010). A quantity of 1.0 μL of (derivatized) extract was injected cold on-column on a 30 m DB5 column with a diameter of 0.250 mm and film thickness of 0.1 μm. Helium was used as a carrier gas at constant flow (0.8 mL/min). The temperature programme was as follows: 50°C (held 2 min); 60°C/min to 80°C (held 2 min); 20°C/min to 130°C; 4°C/min to 350°C (held 10 min). Mass spectrometer detection was in full scan mode (m/z of 50–650) with an electron impact ionization set to 70 eV. The interface temperature was set to 300°C and the source to 250°C.

n-Alkanes were identified by comparison of retention times with an *n*-alkane standard mixture and relative abundance of mass fragments *m/z* 57, 71 and 85. Concentrations of *n*-alkanes were determined relative to the peak area of 5α-androstane using a calibration curve. Curves for *n*-C_{27} to *n*-C_{33} (most abundant chainlengths) were made by injecting a series of these *n*-alkanes in a concentration of 0–50 ng/μL; even-numbered *n*-alkanes had concentrations five times lower because these were less abundant. For shorter and longer chainlengths, curves of their corresponding nearest even- or odd-numbered *n*-alkanes were used. *n*-Alcohols were identified by *m/z* 75, a large fragment corresponding to the total molecular mass minus *m/z* 15, and comparison with a mixture containing several *n*-alcohols. Compounds in F3 (primarily *n*-alcohols) were quantified with 5α-androstan-3β-ol and a calibration curve for alcohol (TMS) *n*-C_{20} applied to all.

5.4.3.6 Analysis of hydrogen-isotopic composition of n-alkanes

For compound-specific hydrogen of *n*-alkanes in F1, the ratio of ^{2}H and ^{1}H (δD) was determined by coupled gas chromatography, temperature conversion and isotope ratio mass spectrometry at the University of Amsterdam. Samples were injected in splitless mode into an Agilent 7890A GC equipped with an Agilent 5075C MSD and a 30 m DB5 column (0.25 mm diameter, film thickness 0.25 μm). A constant helium flow was maintained of 0.9 mL/min and programmable temperature vaporizing was used as the injection method: 10 times 1.0 μL was injected at 40°C (held 1.6 min), then to 450°C at 720°C/min (held 4.5 min) and then held at 250°C until the end of the measurement. Compared to GC/MS, the temperature programme was optimized for this system: 40°C (held 3 min); 100°C/min to 90°C (held 2 min); 20°C/min to 130°C (held 0 min); 4°C/min to 315°C (held 14 min). Subsequently, the eluting compounds were quantitatively converted to H_2 in a high-temperature conversion furnace (Isoprime GC5 Interface, Elementar, UK) operated at 1000°C with a combustion tube filled with chromium oxide. Hydrogen isotopes were measured in an Isoprime 100 Vision Stable Isotope Analyzer (Elementar, UK). Data were processed in the accompanying software package ionOS. Samples were concentrated 5–8 times compared to GC/MS analysis to obtain a strong signal for reliable results. The H_3^+ factor was measured at the beginning and end of each sequence and was constant (mean 5.01; SD 0.09; $n = 16$) during the entire measurement period. A sequence typically consisted of six samples, before and after which the A5 Indiana

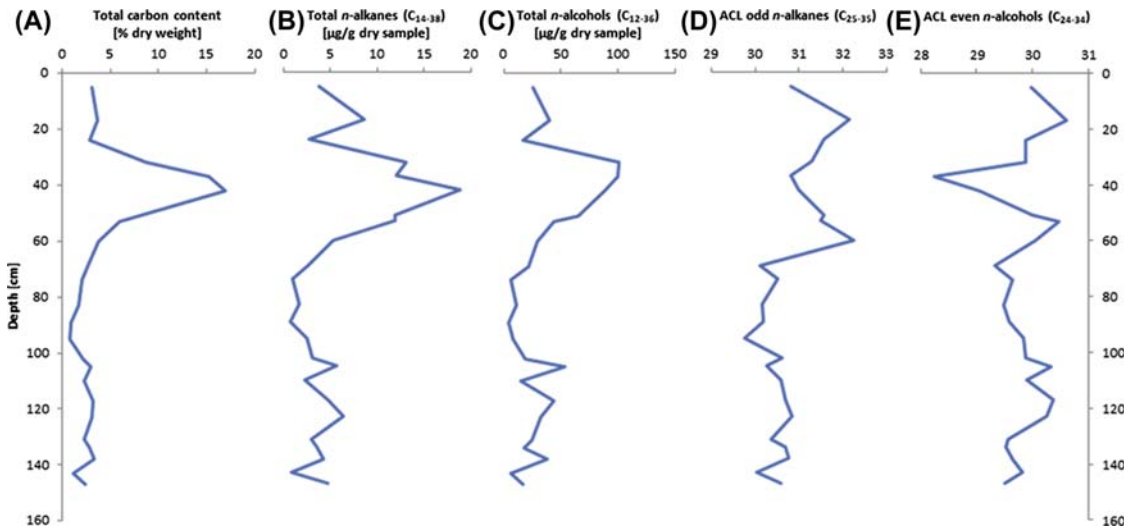

FIGURE 5.4.4 Castañuela II (core 1) records for carbon content and calculated wax lipid indices. (A) Total carbon content as proportion of dry weight. (B) Total *n*-alkane concentration for the range $C_{14–38}$ per gram of dry sample. (C) Total *n*-alcohol concentration for the range $C_{12–36}$ per gram of dry sample. (D) Average chainlength (ACL) of odd-numbered *n*-alkanes ($C_{25–35}$). (E) ACL of even-numbered *n*-alcohols ($C_{24–34}$). ACL is calculated as $\sum(C_n \times n)/\sum(C_n)$, where C_n is the concentration of the *n*-alkane or *n*-alcohol with *n* carbon atoms.

TABLE 5.4.3 Radiocarbon dates obtained through accelerated mass spectrometry ^{14}C measurements and calibrated ages for sediment samples from a core taken near Castañuela, Dominican Republic.

Lab code	Depth (cm)	$\delta^{13}C$ (‰)	Uncalibrated ^{14}C age (^{14}C yr BP)	Calibrated age range ±2σ (CE)	Area under probability curve
D-AMS 014349	39–40	−22.0	Modern (111.50%)	1955 CE	1.000
D-AMS 014350	126–127	−32.9	207 ± 24	1936–49 CE	0.126
				1761–1804 CE	0.476
				1737–58 CE	0.080
				1649–82 CE	0.318

BP, before present; *CE*, Common Era.

standard mix was measured and in between the B2 Indiana mix; samples and standards were all measured in triplicate. The A5 and B2 mixes (obtained from Arndt Schimmelmann, University of Indiana) contained *n*-alkanes C_{16}–C_{30} with off-line determined δD values expressed on the internationally agreed upon VSMOW (Vienna Standard Mean Ocean Water) scale. δD values of samples were normalized to VSMOW using the A5 mixes of each sequence, whereas B2 was used for cross-validation. Calculation and reporting of δD values and errors was inspired by the approach of Polissar and D'Andrea (2014), adapted for calibration with linear

regression. The mean standard deviation of all measured A mixes was 3.88‰ ($n = 180$), and of the targeted sedimentary *n*-alkanes 5.92‰ (C_{27}; $n = 13$), 2.71‰ (C_{29}; $n = 20$), 2.22‰ (C_{31}; $n = 21$) and 3.17‰ (C_{33}; $n = 19$).

5.4.4 Results and discussion

5.4.4.1 Stratigraphy and carbon content

The stratigraphical description (Table 5.4.1) is based on visual inspection of the core in the field and during subsampling in the laboratory. Roughly, the top half contained more (coarse) fibrous organic material and dense clay; the bottom half showed intervals with more sand and sometimes small organic fibres. Small (<3 mm) shells occurred between 24 and 53 cm. The total carbon content in the Castañuela II sequence varied around 3%, with two clear exceptions (Fig. 5.4.4).

Between 60 and 32 cm core depth the carbon content peaked toward almost 17% and the not very dense sediment clearly contained poorly degraded plant remains. On top of this an obviously more dense, lighter-coloured and clayey layer was deposited (30−12 cm core depth), followed by the surface sediment, which was darker and again contained plant remains and roots of *Eichhornia* (Table 5.4.2). It appears that the carbon-rich deposits were buried by a sudden influx of fine-grained sediments, probably due to the construction of the nearby road that crosses the meander infill, and further on-site developments possibly including removal of vegetation and increase in soil erosion. This interpretation is supported by radiocarbon dating of the buried layer at 39 cm revealing a modern date of 1955 CE (Table 5.4.3), together with local landowners stating that the

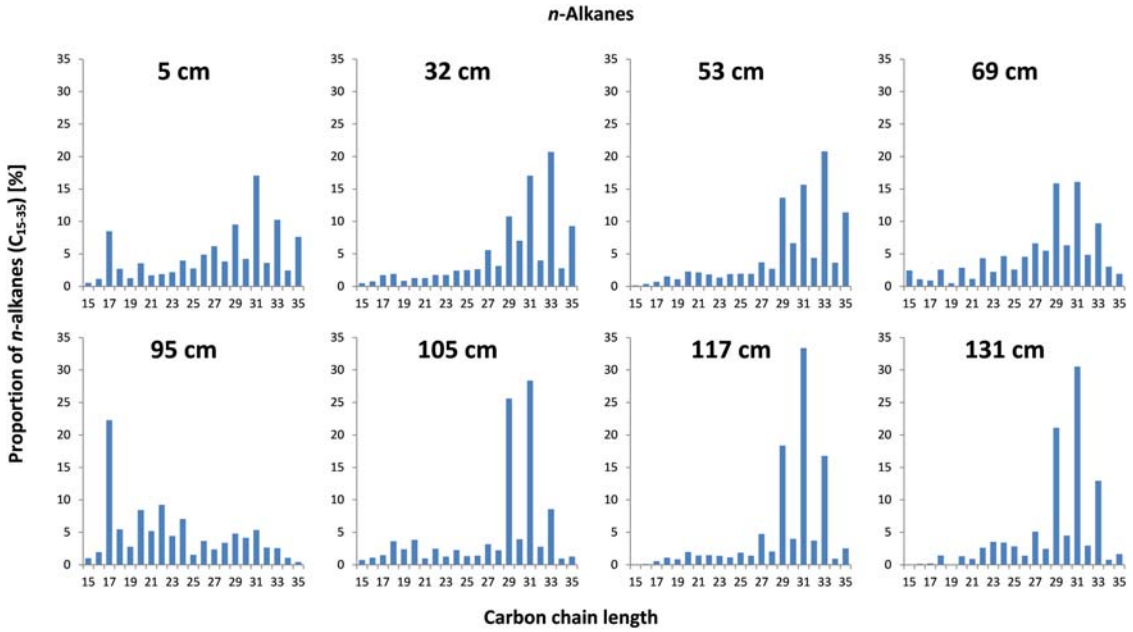

FIGURE 5.4.5 *n*-Alkane chainlength distributions of Castañuela II (core 1). A selection of histograms (%) from various depths for *n*-alkane carbon chainlengths $C_{15–35}$. Individual samples were selected as representative examples for their section in the core.

surrounding banana plantations were founded in the early 1970s.

This also reduces the possibility that the dated sample at 126 cm comes from the 1940s because it seems improbable that fine-grained (i.e., deposited in low-energy system), laminated sediments will be deposited in such a short timeframe. Therefore the samples between 30 and 12 cm should be treated with care because these can contain redeposited (older) organic matter. A decreased degree of degradation of the still relatively young organic materials below this section, due to increased protection, would (partially) explain the observed higher carbon content of these sediments. This should be sustained by a continuous presence of water in the meander infill or at least only very short dry spells, limiting the exposure to oxygen, which would enhance carbon mineralization. Possibly, the water table in the meander was kept artificially high (at some point) to serve as a reliable water reservoir for the surrounding agricultural fields.

Around 95 cm core depth carbon content dropped below 1% coinciding with some of the sandy intervals in this section of the core (Table 5.4.1). A lower sediment carbon content may have three reasons: (1) an increase in sediment input relative to the organic matter input, for instance, a decreased carbon content due to increased (soil) erosion in the watershed; (2) a decrease in total organic matter input related to total primary productivity, for example, decreased productivity due to deforestation or (over)grazing; and (3) an increase in organic matter degradation after deposition, for instance, due to a lower water table, exposing organic matter to the air. The *n*-alkane chainlength distribution (CLD) at 95 cm core depth showed a dominant *n*-C_{17} and a relative lack of long-chained uneven *n*-alkanes

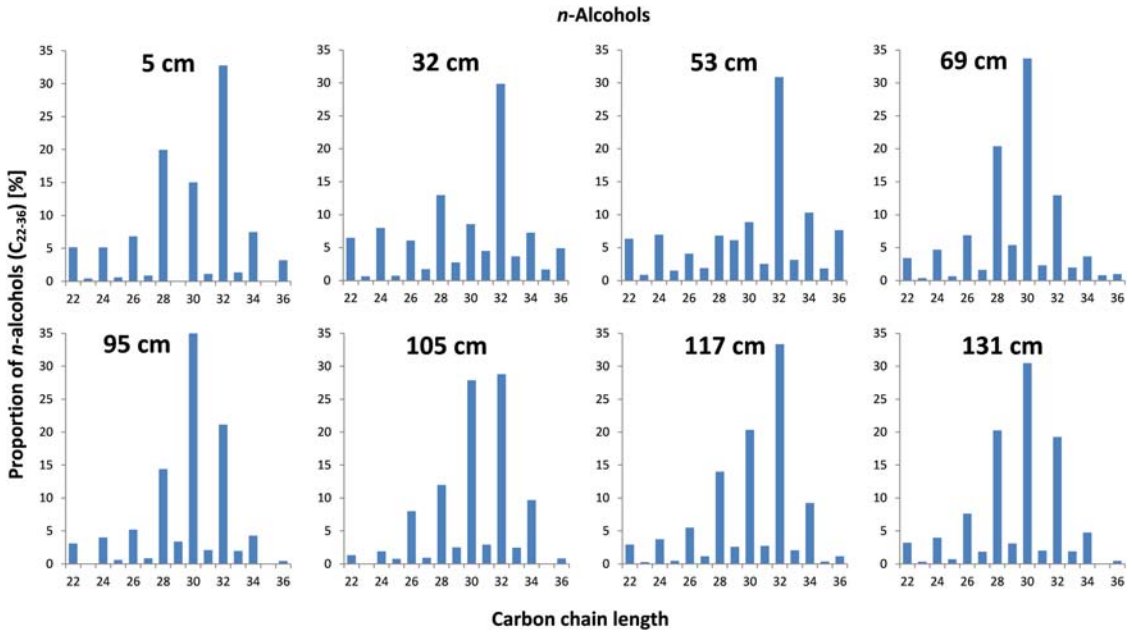

FIGURE 5.4.6 *n*-Alcohol chainlength distributions of Castañuela II (core 1). A selection of histograms (%) from various core depths for *n*-alcohol carbon chainlengths C_{22-36}. Individual samples were selected as representative examples for their section in the core.

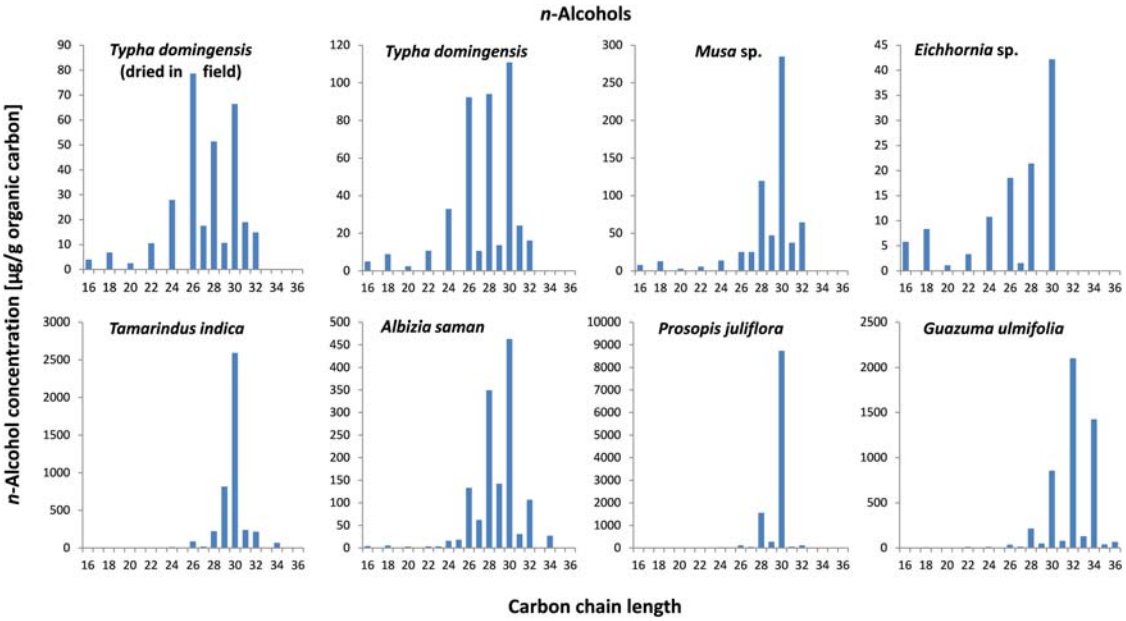

FIGURE 5.4.7 (A) *n*-Alkane and (B) *n*-alcohol chainlength distributions of leaves sampled from plants at Castañuela II. Note that the *y*-axes (lipid concentration in µg/g organic carbon) is different for each species.

(CPI_{ALK} <1) (Fig. 5.4.5). This pattern is typically associated with increased microbial activity (Cranwell, 1984; Meyers, 2003; Kristen et al., 2010), and consequently increased degradation of plant-derived organic matter. However, this does not explain the observed presence of layers containing more sand, and without a more detailed, quantitatively determined particle size distribution (cf. Van Hengstum et al., 2014, 2016) it will be challenging to formulate a more robust reasoning.

5.4.4.2 Disconnection of the meander from the river

It is difficult to conclusively determine the moment the meander has been disconnected from the river, based on the currently available sedimentological data and the two ^{14}C dates obtained. Most possibly the increase in organic matter content at 60 cm marks a continuous phase of stagnant water with the establishment of aquatic plants, meaning disconnection has taken place earlier as is the case in other studied meanders (Hooghiemstra et al., 2018; Castilla-Beltrán et al., 2018). Several brown bands with fibrous organic matter lower in the core (Table 5.4.1) indicate possible stagnant waters, suggesting either a disconnection below 147 cm or a phase of intermitting connection with the (main) river. The latter may very well be possible as the relatively slow flowing river in its lower catchment has not been confined to one stream channel, and may have been braided and/or repeatedly relaying its course in the past (Gabb, 1873; Morales et al., 2009). Some channels may have been temporarily blocked by debris (e.g., drift wood) or become dry during periods of reduced precipitation.

5.4.4.3 Preservation and origin of sedimentary lipid biomarkers

Throughout the Castañuela II core, *n*-alkanes with carbon chainlengths between 15 and 38 were observed (Fig. 5.4.5). Similarly, a

continuous *n*-alcohol signal was observed with carbon chainlengths between 14 and 36 (Fig. 5.4.6). *n*-Alkanes were most abundant in the range C_{27}–C_{35} with odd-numbered chains more dominant, and *n*-alcohols in the range C_{22}–C_{36} with even chains dominant. These straight-chain lipid biomarker patterns are commonly linked to an input of epicuticular waxes of vascular plants such as trees, shrubs and grasses (Eglinton and Hamilton, 1967; Rieley et al., 1991; Meyers, 2003; Eglinton and Eglinton, 2008). Additionally, *n*-alkane CPI values generally exceeded 2 and exceeded 5 for *n*-alcohols indicating a well-preserved terrestrial higher-plant signal.

5.4.4.4 Linking sedimentary biomarker patterns to vegetation

A mismatch seems to occur when comparing the *n*-alkane CLDs of the sampled plants (Fig. 5.4.7A) and the Castañuela II sequence (Fig. 5.4.5). Chainlengths longer than *n*-C_{29} were far less dominant in the plant samples, whereas these were very abundant in the core, especially in the upper half. For *n*-alcohols, issues are less clear but similar with chains >*n*-C_{30} being relatively more abundant in the core than in the sampled plant species (Fig. 5.4.5 versus Fig. 5.4.7B). Both *n*-alkane C_{31} and *n*-alcohol C_{32} were the most dominant in *G. ulmifolia*, a tall tree species that produces large quantities of lipids. However, it seems not very likely that this species was the main contributor to the sequence, especially for the top (most modern) section of the core, because currently just a few individuals are present at Castañuela II (versus dozens of *A. saman*) and the closest are over 200 m from the coring site. Moreover, *G. ulmifolia* does not explain the high abundance of *n*-alkanes C_{33} and C_{35}, whereas *n*-alcohol C_{34} was less abundant in the core than in the leaf sample. Still, *G. ulmifolia* is a species to be

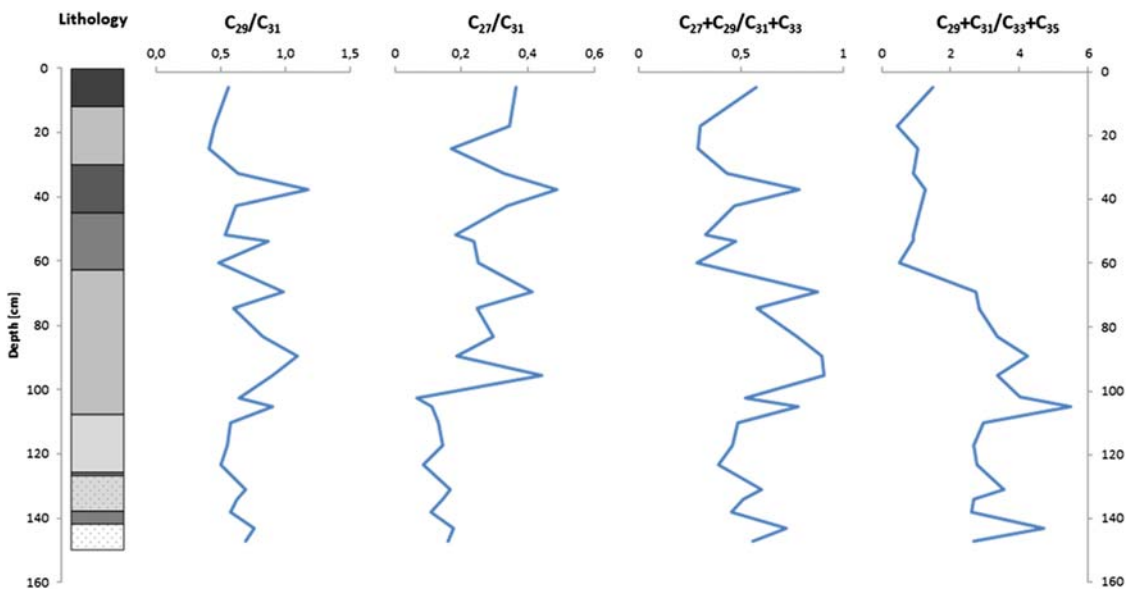

FIGURE 5.4.8 Site Castañuela II (core 1)-calculated *n*-alkane ratios (C_{29}/C_{31}, C_{27}/C_{31}, $[C_{27}+C_{29}]/[C_{31}+C_{33}]$, and $[C_{29}+C_{31}]/[C_{33}+C_{35}]$) to show changes in concentration patterns with depth. Lithological column on the left, matching the description given in Table 5.4.1 – in general: loose sediment with fresh plant litter (black), clay with decreasing organic matter content (from grey to white), increased sand content (*dotted*).

expected along streams and in disturbed areas, and can serve various purposes from providing timber to medicine (Janzen, 1982). As *Eichhornia* sp. and *T. domingensis* flourished on top of the borehole, it was expected that for the top sediment samples their CLDs (large n-C_{29} alkane, followed by n-C_{31} and n-C_{27}; and large n-C_{30} alcohol, followed by equal shares of n-C_{26} and n-C_{28}) would dominate, which is clearly not the case. Even more striking are the very low concentrations of n-alkanes from these two species compared to the terrestrial species (Fig. 5.4.7) but comply with n-alkane concentrations in emergent aquatic plants in other studies (Gao et al., 2011; Street et al., 2013). So, a first attempt to link plant and sediment biomarker data was apparently unsuccessful and more research is needed to determine the exact origin of the observed sedimentary wax lipids.

The discrepancy between CLDs of sampled plants and sediment can be explained by (a combination of) several reasons that are linked to the challenges related to biomarker-based vegetation reconstructions, as mentioned in the introduction to this chapter and elaborated in detail by Jansen and Wiesenberg (2017). Most likely reasons in the context of the current reconstruction are:

1. Important species were lacking from the reference database. Poaceous plants, making up most of the pastures in the area, were not sampled because we deemed it unlikely that they would be a major contributor to biomass

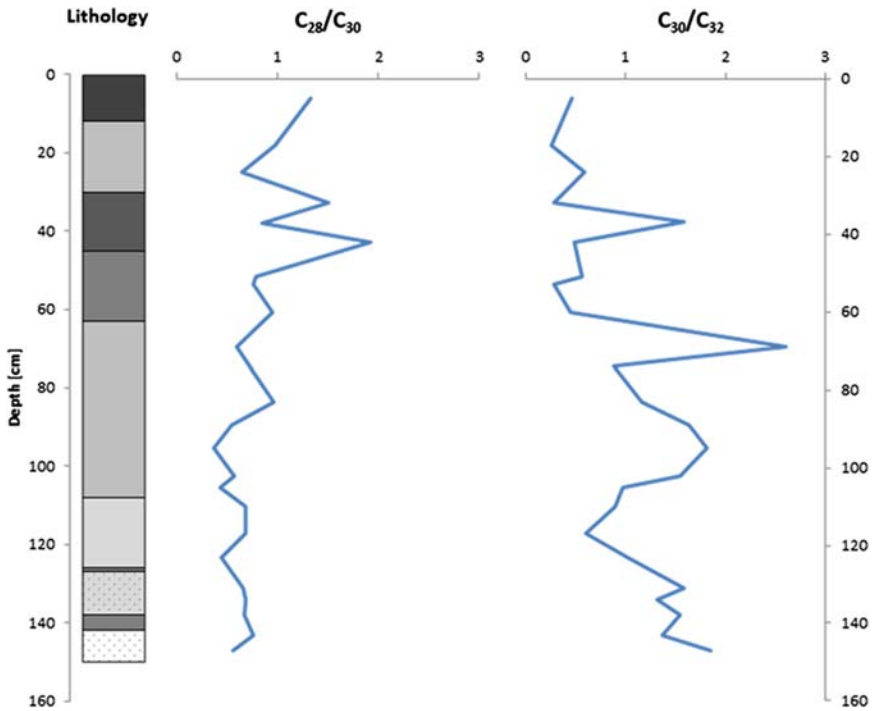

FIGURE 5.4.9 Site Castañuela II (core 1)-calculated n-alcohol ratios (C_{28}/C_{30} and C_{30}/C_{32}) to show changes in concentration patterns with depth. Lithological column on the left, matching the description given in Table 5.4.1 — in general: loose sediment with fresh plant litter (black), clay with decreasing organic matter content (from grey to white), increased sand content (*dotted*).

input in the archive. In addition, possibly at Castañuela II, different species were more important in the past, and therefore a more extensive analysis of local natural vegetation compositions at multiple similar sites is needed to infer possible changes.

2. Different input routes in addition to leaf input played an important role. While one would expect the main input into a riverine sediment to originate from leaves, the input from roots of species could have played a role (Jansen and Wiesenberg, 2017). In addition, input in the form of aerosols originating from species further away from the coring site may have had an influence (Jansen and Wiesenberg, 2017).

5.4.4.5 *Interpretation of the Castañuela II* n-*alkane and* n-*alcohol signals*

Several *n*-alkane quick ratios were calculated for the Castañuela II sequence (Fig. 5.4.8) to help detect changes in CLDs with depth. For C_{29}/C_{31}, the general dominance in the sequence is shown for *n*-C_{31} over *n*-C_{29}, especially in the intervals 150−100 cm and 50−0 cm, whereas between 100 and 50 cm the ratio approaches unity. *n*-C_{27} is far less dominant than *n*-C_{31} throughout the core, but is relatively even less abundant from 150 to 100 cm. When the abundant *n*-C_{33} is included to form the $(C_{27} + C_{29})/(C_{31} + C_{33})$ ratio, a pattern similar to C_{29}/C_{31} becomes apparent. Also, the ACL shows this three-phase pattern with a slightly shorter averaged chainlength from c. 100 to 50 cm (Fig. 5.4.4). The very long chains *n*-C_{33} and *n*-C_{35} clearly become relatively more abundant from 60 cm core depth to the top, coming from a low around 100 cm, as can be seen in the $(C_{29} + C_{31})/(C_{33} + C_{35})$ ratio and ACL. These two homologues were not represented in CLDs of studied local species (Fig. 5.4.7) and may have come from particular C_4 grasses that were not sampled during fieldwork (Rommerskirchen et al., 2006; Badewien et al., 2015). Conversely, instead of a changing vegetation composition around 50 cm, the production of longer *n*-alkanes in plants could be driven by changing environmental conditions like decreased water availability (Rommerskirchen et al., 2003; Sachse et al., 2006; Castañeda and Schouten, 2011; Vogts et al., 2012). This does not necessarily mean increased aridity due to decreased precipitation, but could also be related to site developments leading to decreased water retention or water extraction from the reservoir. The obtained $\delta^{13}C$ values of bulk sediment during radiocarbon dating (Table 5.4.3), which should be used with caution, also indicate an organic matter input of mainly C_3 plants in the bottom part and C_4 grasses in the top (e.g., Collister et al., 1994; Bi et al., 2005; Vogts et al., 2009b).

The *n*-alcohols C_{28}, C_{30} and C_{32} were the major homologues in the CLDs of the Castañuela II sequence (Fig. 5.4.6), and two quick ratios (C_{28}/C_{30} and C_{30}/C_{32}) were calculated to show changes in their relative proportions (Fig. 5.4.9). At the bottom, *n*-C_{30} was dominant, but toward 100 cm depth *n*-C_{32} was increasingly more prevalent. In the upper 70 cm of the core, *n*-C_{32} dominated the *n*-alcohol CLD, whereas *n*-C_{30} was often smaller relative to *n*-C_{28} (Fig. 5.4.9). Throughout the sequence the *n*-C_{26} homologue stays a bit behind, hovering around a relative abundance of 5% of mid- to long-chain alcohols, often surpassed by *n*-C_{34}. The even longer *n*-C_{36} alcohol is strikingly present in the top 50 cm, which usually falls outside the reported range for plants and sediments (e.g., Ficken et al., 2000; Xu and Jaffé, 2008; Vogts et al., 2009b; Schmidt et al., 2014), and is here only found in a leaf sample of the tree *G. ulmifolia* (Fig. 5.4.7). The observed *n*-alcohol CLDs (>*n*-C_{28} dominant) of this core from the hot and (semi-)arid northern Hispaniola clearly deviate from results from cooler and wetter regions in which the range *n*-$C_{22–28}$ is most abundant (e.g., Zheng et al., 2009; Zhou et al., 2010; Diefendorf et al., 2011; Pu et al., 2013). As for *n*-alkanes, this might suggest a climate effect through favouring plants (individuals and/or species) that produce longer chains under heat

and/or water stress (e.g., Jansen and Wiesenberg, 2017).

It should be stressed, however, that only using quick ratios or most abundant chainlength is too simplistic and important information is potentially lost. The ultimate goal should therefore be to have an approach that enables an ecologically meaningful and more robust interpretation, such as combining biomarker modelling and fossil pollen analysis to reconstruct past vegetation, as was done in Case study 2 presented in this chapter.

5.4.4.6 *Hydrogen-isotopic composition of sedimentary* n*-alkanes*

The hydrogen-isotopic composition of lipid biomarkers has been demonstrated to be a valuable tool for palaeohydrological reconstructions (e.g., Sachse et al., 2012 and references cited therein). The δD values of sedimentary lipids derived from higher plants correlate well with values of source waters, usually precipitation. The isotopic composition of source waters is mainly determined by temperature, the amount of precipitation, the travel history of the carrying air mass and evaporation (e.g., Gat, 1996). Plants incorporate the hydrogen from soil water (terrestrial plants) and lake water (aquatic plants) in their epicuticular waxes (e.g., *n*-alkanes, *n*-alcohols). However, as various fractionation steps take place before deposition of wax lipids in sedimentary archives, numerous secondary drivers will have affected the hydrogen-isotopic composition (Sachse et al., 2012). All these factors contributing to the overall net fractionation (also apparent fractionation, abbreviated as $\varepsilon_{l/w}$) of the plant are less well understood. Among these potential drivers are the plant's growing conditions (e.g., relative humidity, salinity), biosynthetic pathway of lipids, species-specific traits such as photosynthetic pathway (e.g., C_3 versus C_4) and lifeform (e.g., shrubs, trees, grasses) and processes related to integration of lipids in sediments.

In tropical regions, the amount of precipitation is the strongest primary determinant of the

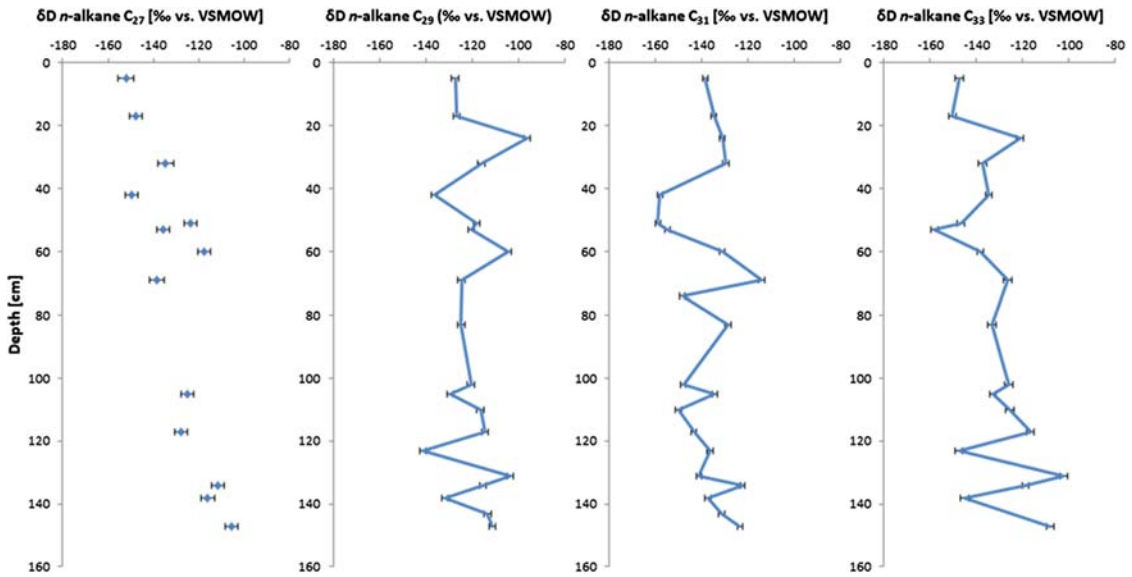

FIGURE 5.4.10 Site Castañuela II (core 1) records for the hydrogen-isotopic composition (δD) of sedimentary *n*-alkanes. The four selected *n*-alkanes (C_{27}, C_{29}, C_{31}, C_{33}) were the most abundant homologues and had the most complete sets of δD values. Errors bars (hardly visible) represent one standard error based on the overall analytical uncertainty per compound plus uncertainty of calibration to the VSMOW (Vienna Standard Mean Ocean Water) scale.

hydrogen-isotopic composition of meteoric (i.e., precipitation-fed) waters (Bowen, 2008). This will also be true for northern Hispaniola because of the limited temperature variability and the short distance the air mass carrying precipitation has travelled over land. Thus it is the amount of precipitation itself that mainly determines the isotopic composition (Sachse et al., 2012). Precipitation will be relatively enriched in heavier deuterium (D) relative to the water vapour in the air mass it originates from, because ^{1}HDO has a lower vapour pressure and condensates faster than $^{1}H_2O$. Relatively less D will be present (depleted) as the amount of precipitation increases, which eventually translates to lower (more negative) δD values, and hence higher δD values in the case of decreased precipitation rates. For (semi-)arid environments, like northern Hispaniola, evapotranspiration may even play a bigger role than precipitation itself (Feakins and Sessions, 2010; Douglas et al., 2012). A relative increase in evapotranspiration leads to a D enrichment of leaf, soil and/or surface water, yielding higher δD values as for lower precipitation amounts (Lane et al., 2014).

5.4.4.7 *Interpretation of Castañuela II* n-*alkane δD values*

The δD values of higher plant-derived *n*-alkanes C_{27}, C_{29}, C_{31} and C_{33} for the Castañuela II sequence are reported here (Fig. 5.4.10), all showing similar results. Partly due to persistent variability throughout the sequence, at least 40‰ for each *n*-alkane, no significantly different phases could be distinguished or shifts too gradual to be clearly observed. *n*-C_{27} appeared to have a trend toward gradually lower δD values at the top, but unfortunately many data points had to be removed because of unreliable results following low *n*-alkane concentrations. This was also the case for the other *n*-alkanes in the core interval of 102–60 cm, thereby not providing good evidence of any hydrological change around 95 cm as discussed earlier. From 147 to 102 cm core depth a c. 20‰ decrease was recorded for all homologues, potentially indicating an increase in

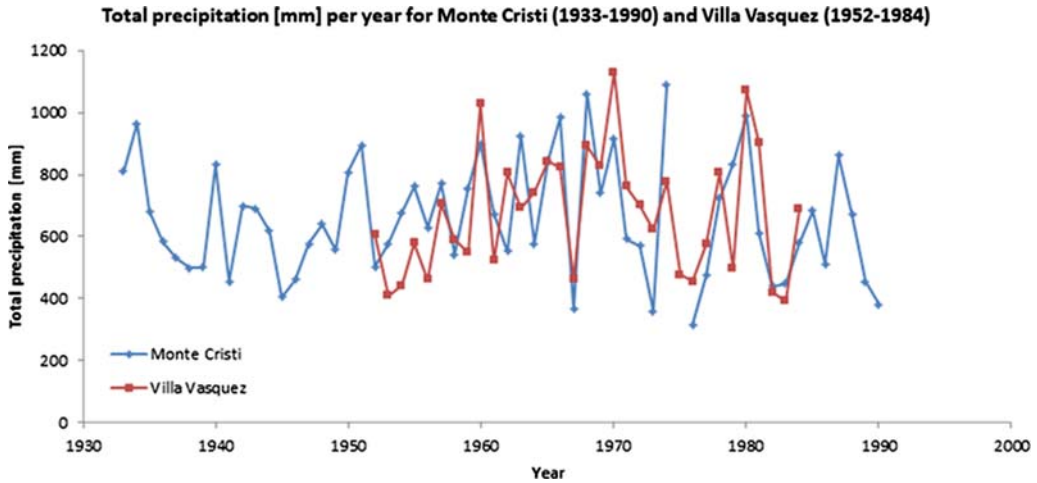

FIGURE 5.4.11 Total annual precipitation (mm) data from two meteorological stations in the province of Monte Cristi (Dominican Republic): Monte Cristi (1933–90) with some missing data in the mid-1970s, and Villa Vasquez (1952–84). *Data obtained from Koninklijk Nederlands Meteorologisch Instituut Climate Explorer (2017a,b).*

precipitation and/or decrease in evaporation. During the elevated carbon content (60–24 cm), probably due to reduced degradation, a (sort of) unimodal peak to its lowest δD values occurs, which could mean increased water availability for plants.

The only other *n*-alkane δD sediment record on Hispaniola and all Caribbean islands is retrieved from Laguna Castilla, a small lake at 976 m asl on the Caribbean side of the Cordillera Central (Fig. 5.4.1) (Lane et al., 2014). Moreover, this is one of the few studies in the tropics that examines compound-specific hydrogen on a decadal timescale. Exact comparison of hydrogen compositions is difficult because of all drivers affecting net fractionation, but patterns and (the direction of) trends in δD values can be compared. Data points since 1500 CE are limited for the Laguna Castilla core; nonetheless no obvious trend toward lower or higher values is visible, as is the case here (Fig. 5.4.10). In the interval 1000–1300 CE, which received the most attention and hence had a higher sampling resolution, a period of increased aridity is observed while also a variability of more than 40‰ is present. Unfortunately, for both Castañuela II and Laguna Castilla sites, such variation could not be translated to a level of change in precipitation and/or evapotranspiration due to the lack of site-specific data clarifying the quantitative relationship between aridity and *n*-alkane δD values (Lane et al., 2014). Based on data from modern soils and lake sediments in Central America, a 40‰ increase would be very significant and could mean a 75% decrease in the ratio between mean annual precipitation and potential evapotranspiration (Douglas et al., 2012).

5.4.4.8 *Observed variability of Castañuela II* n-*alkane δD values*

Precipitation data from two meteorological stations near the city of Monte Cristi (1933–90) and Villa Vasquez (1952–84) show a considerable interannual variability (Fig. 5.4.11). Most of the variation lies between a total of 400 and 1000 mm per year, both stations showing similar results. Also Van Royen (1938) reported large differences between dry and wet years in Monte Cristi (c 500 to >2000 mm/year). The interannual variability is probably caused by El Niño-Southern Oscillation, which disturbs atmospheric circulation and eventually the location and strength of the North Atlantic Subtropical High, leading to abnormally dry summers in the Caribbean (Caffrey et al., 2013). The currently estimated sedimentation rate, based on limited radiocarbon dating, of 0.3–0.5 cm/year implies samples would represent just a couple of years. Assuming this, large interannual fluctuations are representative for the last few centuries; the observed variability in δD values can be just snapshots of wetter and drier years. As mentioned before, evapotranspiration is likely to play a considerable role, causing a precipitation deficit during parts of the year (Izzo et al., 2010). This water deficit will be of great ecological significance (e.g., affecting vegetation composition), but without a local assessment of *n*-alkane δD values from modern plants and sediments/soils (e.g., Douglas et al., 2012) it is hard to say how this is reflected in observed sedimentary δD values.

However, at least two processes potentially complicate the interpretation of *n*-alkane δD values from the Castañuela II sediment core. Throughout the sequence, source appointment of both the studied compound (e.g., *n*-alkane) and the water used by plants is of vital importance for the interpretation of δD values. Evidence from straight-chain lipid biomarker CLDs suggests some possible shifts in vegetation composition, and thus a change in species from which the analysed *n*-alkanes can derive. The apparent fractionation (between source water and lipid) varies across plant species and several studies have found differences between plant lifeforms such as trees, shrubs and grasses (Hou et al., 2007; Sachse et al., 2012). This means that possible changes in δD values of source

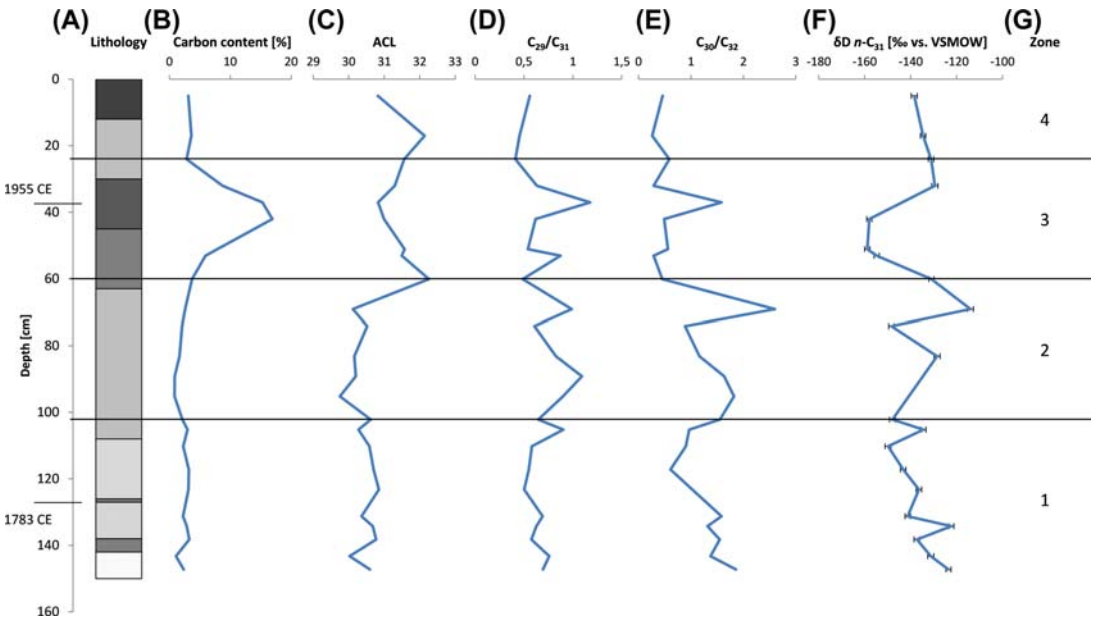

FIGURE 5.4.12 Site Castañuela II (core 1) records for sedimentology, wax lipids indices and compound-specific δD values with depth. (A) Lithology matching the description given in Table 5.4.1 and two calibrated radiocarbon samples. (B) The total carbon content (% of weight). (C) The *n*-alkane average chainlength for odd-numbered homologues in the range $C_{25–35}$. (D) The *n*-alkane ratio C_{29}/C_{31}. (E) The *n*-alcohol ratio C_{30}/C_{32}. (F) Hydrogen-isotopic composition (δD) of *n*-alkane C_{31} (‰ versus Vienna Standard Mean Ocean Water [VSMOW]) with one standard error based on the overall analytical uncertainty per compound plus uncertainty of calibration to the VSMOW scale. (G) Zonation based on qualitative assessment of all studied proxies and calculated indices.

water due to alterations in precipitation/evapotranspiration can be obscured. Especially, fractionation of shrubs and grasses would differ, and a shift between these cannot be ruled out for Castañuela II. Whether a species shift would also significantly impact sedimentary wax lipid δD values in northern Hispaniola should be established first, although this is not easy because of the many variables involved. It requires analysing the hydrogen-isotopic composition of relevant plant parts of all dominant species, as well as the composition of source waters and surface sediments and/or soils, while preferably also changing conditions (e.g., seasonality, interannual variability) are accounted for. Fortunately, such an endeavour can be combined with earlier proposed more elaborate examination of species compositions and their lipid biomarker CLDs, which would all contribute greatly to more robust interpretation of palaeoenvironmental proxies.

Additionally, a flood brings in river water that could have a different isotopic composition compared to direct precipitation, but it is unclear if such an event would ultimately be reflected in sedimentary *n*-alkane δD values. This also raises the question whether the source waters of emergent taxa (meander lake water) and terrestrial plant species (soil water) differ in δD due to evaporative processes. An occasional input of allochthonous water and sediment could be an explanation for the observed *n*-alkane δD

variability in the Castañuela II sequence, which seems a more likely factor than a continuous change in plant species composition.

5.4.5 Palaeoenvironmental reconstruction

Based on an integration of all obtained palaeoenvironmental proxy data, a biomarker zonation is made for the Castañuela II record (Fig. 5.4.12). The breaks between the different zones were determined qualitatively rather than being statistically based. The estimated ages of the zones were based on sedimentation rates calculated from two radiocarbon dated samples (Table 5.4.3), with 0.65 cm/year after and 0.50 cm/year before 1955 CE (39 cm). For the interpretation of proxy data, especially of the sedimentary wax lipids and associated compound-specific deuterium, all previously discussed uncertainties have to be kept in mind – here only the most likely explanations are given.

5.4.5.1 Period 1 c.1740–1830 CE (biomarker zone 1, 147–102 cm, nine samples)

The sedimentology of the bottom section of the Castañuela II core is rather irregular, with alternating layers containing more or less organic matter (Table 5.4.1; Fig. 5.4.12). The very bottom contains more sand, suggesting a different sedimentary environment, whereas the top half of period 1 has more clay. The intervals enriched with organic matter possibly reflect periods with stagnant water and development of aquatic vegetation. The occurrence of varying depositional settings may be due to a dynamic drainage system, during which the river section with the meander is intermittently connected with the main stream channel. In the entire period 1, *n*-alkane C_{31} is clearly dominant, followed by *n*-C_{29} and *n*-C_{33}, while all other chains have a low abundance (Figs 5.4.5 and 5.4.12). For *n*-alcohols the CLD shifts from a dominant *n*-C_{30} followed by equal shares of *n*-C_{28} and *n*-C_{32}, to a more dominant C_{32} at the top of this zone (Figs 5.4.6 and 5.4.12). The projected date at the bottom of this zone (c.1740 CE) is in the second part of the so-called 'Little Ice Age' (LIA, c.1400–1850 CE), which by some has earlier been referred to as a period of increased aridity in the circum-Caribbean region (e.g., Peterson and Haug, 2006; Lane et al., 2011). More recently, the LIA in the Caribbean is believed to be a period of enhanced (effective) rainfall *variability*, with both wet and dry phases on multidecadal timescales (e.g., Burn and Palmer, 2014; Burn et al., 2016). Whether this is also the case for northern Hispaniola is not yet known due to the absence of direct evidence, but possibly the area had increased winter rainfall through storms coming from the north, as suggested by Caffrey et al. (2015). The varying sedimentology (Table 5.4.1) may correspond to decadal rainfall variability, but (independent) more local developments related to human activity and river dynamics could be more important drivers. Based on the preliminary interpretation of *n*-alkane δD values (D enrichment becoming more depleted), the lower valley of the Rio Yaque del Norte experienced a relatively dry period but was becoming more mesic. However, apart from the current uncertainties in the interpretation, this is only compared to more recent times and on a longer term (e.g., the entire Holocene) it might be a relatively wet period.

5.4.5.2 Period 2: c.1830–1910 CE (biomarker zone 2, 102–60 cm, six samples)

The stratigraphy during period 2 is dominated by more clayey deposits with a lamination of brown and grey bands (although less pronounced than during period 1), including some sandy deposits (Table 5.4.1). The mix of studied proxies at the current sampling resolution does not show alternating conditions expected with the observed lamination. As in period 1, the lamination suggests varying depositional conditions related to intermittent river connectivity and possible flooding (i.e., sandy intervals,

deposition in higher energy system). *n*-Alkane C_{31} has lost its dominance and *n*-C_{29} is often equally abundant (Fig. 5.4.12), and the *n*-alcohol CLD has again a dominant *n*-C_{30} followed by prominent *n*-C_{28} and *n*-C_{32} (Fig. 5.4.9). At 95 cm core depth (c.1840s) the plant-derived *n*-alkane signal is almost entirely lost and *n*-C_{17} becomes dominant, indicating enhanced microbial degradation probably during low water levels, yet somehow the *n*-alcohol signal is preserved. A relatively drier climate during early parts of the 1800s has previously been reported for Barbuda (Burn et al., 2016), Jamaica (Burn and Palmer, 2014) and Hispaniola (Lane et al., 2014). Whether precipitation/evaporation patterns were markedly changed in the area surrounding Castañuela II is unknown, because *n*-alkane δD values are unfortunately missing for this section due to the low carbon content. The hydrogen-isotopic composition shows no obvious trend and is not distinctively different than zone 1 (Fig. 5.4.12), although this could be disguised by a shift in plant species composition and/or riverine input.

5.4.5.3 Period 3: c.1910–80 CE (biomarker zone 3, 60–24 cm, six samples)

Zone 3 is marked by a clear increase in organic matter, both reflected in the dark deposits largely consisting of poorly degraded plant remains (in the interval 45–30 cm core depth in particular) and the carbon content surpassing 5% (Table 5.4.1 and Fig. 5.4.12). This sudden change in carbon content, which is followed by a decrease in the top section of the sediment core, indicates a period of improved protection from degradation caused by more reliable higher water levels and/or burial by a sudden influx of sediments. The calibrated age within this zone (1955 CE) and the report from a local landowner make it very likely that at least the latter happened as a consequence of local site developments, for instance, through the construction of the nearby road. Simultaneously, the CLDs of *n*-alkanes and *n*-alcohols show a shift in species composition (Figs 5.4.8 and 5.4.9). For both compound classes, longer homologues become more abundant, which together with a higher $\delta^{13}C$ value could be indicating an increase of C_4 grasses (e.g., Collister et al., 1994; Rommerskirchen et al., 2006; Vogts et al., 2009a). The presence of more grasses could be the results of forest clearance and/or increased human activity in the area, and was also observed in the top section of a sediment core from Laguna Saladilla (Fig. 5.4.1) (Caffrey et al., 2015). The peak in carbon content coincides with the lowest *n*-alkane δD values, also showing some sort of unimodal peak for most homologues, spanning a range of more than 20‰ (Figs 5.4.10 and 5.4.12). This could indicate an increase in precipitation as well as a decrease in evapotranspiration, which both fit more constant higher water levels, although the impact of a shift in sources of water and lipid biomarkers could not be excluded.

5.4.5.4 Period 4: c.1980–2015 (biomarker zone 4, 24–0 cm, three samples)

The dark, carbon-rich deposits of period 4 are topped by dense, light grey clay (Table 5.4.1) that was likely deposited during road construction and/or following surface runoff (partly) due to removal of vegetation. These redeposited materials can be older than or of the same age as underlying deposits. Toward the top, recently deposited materials are present in the form of looser, dark grey and clayey sediment with some plant remains, as if normal sediment and organic matter accumulation has resumed. Compared to period 3 the CLDs of *n*-alkanes and *n*-alcohols have not changed much besides a more abundant *n*-C_{17} alkane at 5 cm (Fig. 5.4.5), likely derived from microbial activity. The lack of change could be caused by redeposition of wax lipids originally formed during period 3, or just indicating that not much has changed in vegetation composition during the last few decades. Similarly, the *n*-alkane δD values do not show an obvious change (Fig. 5.4.10), although compared

to other zones the results among *n*-alkanes are not unequivocal and the number of samples in period 4 is limited.

5.4.6 Conclusions

This case study has demonstrated that the combined application of lipid biomarkers and compound-specific deuterium for palaeoenvironmental research has potential in the dry lowlands of northern Hispaniola. So far, to avoid inaccurate conclusions, no elaborate attempt is made to compare and integrate the results of Castañuela II with studies from Hispaniola and other Caribbean islands due to the current uncertainties surrounding the results, differing approach and focus compared to other studies, and the relatively poor understanding of local climate dynamics and its spatial heterogeneity. Currently, sedimentology and proxy data from the Castañuela II core seemed to primarily show the impact of floodplain dynamics (changing river connectivity) and human activity as opposed to climate. This project served as a starting point for further Caribbean palaeoenvironmental research and highlights its future needs, which should be directed at extending the number of sites and proxies, as well as knowledge about local floodplain dynamics and vegetation compositions, and increased understanding of local determinants of wax lipid biochemistry and their associated hydrogen-isotopic fractionation. Especially, more modern plant biomarker data from the Caribbean are needed to enable application of the VERHIB model – as presented in Section 5.2 – and subsequent meaningful ecological interpretation of observed changes.

References

Acosta Solis, M., 1984. Los páramos andinos del Ecuador. Publicaciones Cientificas MAS, Quito, Ecuador.

Amelung, W., Brodowski, S., Sandhage-Hofmann, A., Bol, R., 2008. Combining biomarker with stable isotope analyses for assessing the transformation and turnover of soil organic matter. Advances in Agronomy 100, 155–250.

Anthelme, F., Jacobsen, D., Macek, P., Meneses, R.I., Moret, P., Beck, S., Dangles, O., 2014. Biodiversity patterns and continental insularity in the tropical High Andes. Arctic Antarctic and Alpine Research 46, 811–828.

Areces-Mallea, A.E., Weakley, A.S., Li, X., Sayre, R.G., Parrish, J.D., Tipton, C.V., Boucher, T., Panagopoulos, N., 1999. A Guide to Caribbean Vegetation Types. The Nature Conservancy, Washington, D.C., United States.

Badewien, T., Vogts, A., Rullkötter, J., 2015. N-Alkane distribution and carbon stable isotope composition in leaf waxes of C3 and C4 plants from Angola. Organic Geochemistry 89, 71–79.

Bakker, J., Moscol, M., Hooghiemstra, H., 2008. Holocene environmental change at the upper forest line in northern Ecuador. The Holocene 18, 877–893.

Bélanger, E., Lucotte, M., Grégoire, B., Moingt, M., Paquet, S., Davidson, R., Mertens, F., Passos, C.J.S., Romana, C., 2015. Lignin signatures of vegetation and soils in tropical environments. Advances in Environmental Research 4, 247–262.

Bellwood, P., 2005. First Farmers. The Origins of Agricultural Societies. Blackwell, Malden, MA, United States of America.

Bi, X., Sheng, G., Liu, X., Li, C., Fu, J., 2005. Molecular and carbon and hydrogen isotopic composition of n-alkanes in plant leaf waxes. Organic Geochemistry 36, 1405–1417.

Bianchi, T.S., Canuel, E.A., 2011. Chemical Biomarkers in Aquatic Systems. Princeton University Press, Oxfordshire, United Kingdom.

Birk, J.J., Dippold, M., Wiesenberg, G.L.B., Glaser, B., 2012. Combined quantification of faecal sterols, stanols, stanones and bile acids in soils and terrestrial sediments by gas chromatography–mass spectrometry. Journal of Chromatography A 1242, 1–10.

Blaga, C.I., Reichart, G.J., Heiri, O., Sinnighe Damsté, J.S., 2009. Tetraether membrane lipid distributions in water-column particulate matter and sediments: a study of 47 European lakes along a north-south transect. Journal of Paleolimnology 41, 523–540.

Bogotá-A, R.G., Groot, M.H.M., Hooghiemstra, H., Lourens, L.J., Van der Linden, M., Berrio, J.C., 2011. Rapid climate change from north Andean Lake Fúquene pollen records driven by obliquity: implications for a basin-wide biostratigraphic zonation for the last 284 ka. Quaternary Science Reviews 30, 3321–3337. https://doi.org/10.1016/j.quascirev.2011.08.003.

Bokhorst, M.P., Duller, G.A.T., Van Mourik, J.M., 2005. Optical dating of a Fimic anthrosol in the southern Netherlands. Journal of Archaeological Science 32, 547–553.

Bol, R., Eriksen, J., Smith, P., Garnett, M.H., Coleman, K., Christensen, B.T., 2005. The natural abundance of 13C, 15N, 34S and 14C in archived (1923-2000) plant and soil samples from the Askov long-term experiments on animal manure and mineral fertilizer. Rapid Communications in Mass Spectrometry 19, 3216–3226.

Bowen, G.J., 2008. Spatial analysis of the intra-annual variation of precipitation isotope ratios and its climatological corollaries. Journal of Geophysical Research 113. D05113.

Brennan, C.W., Verhaak, R.G.W., McKenna, A., Campos, B., Noushmehr, H., Salama, S.R., Zheng, S., Chakravarty, D., Sanborn, J.Z., Berman, S.H., Beroukhim, R., Bernard, B., Wu, C., Genovese, G., Shmulevich, I., Barnholtz-Sloan, J., Zou, L., Vegesna, R., Shukla, S.A., Ciriello, G., Yung, W.K., Zhang, W., Sougnez, C., Mikkelsen, T., Aldape, K., Bigner, D.D., Van Meir, E.G., Prados, M., Sloan, A., Black, K.L., Eschbacher, J., Finocchiaro, G., Friedman, W., Andrews, D.W., Guha, A., Iacocca, M., O'Neill, B.P., Foltz, G., Myers, J., Weisenberger, D.J., Penny, R., Kucherlapati, R., Perou, C.M., Hayes, D.N., Gibbs, R., Marra, M., Mills, G.B., Lander, E., Spellman, P., Wilson, R., Sander, C., Weinstein, J., Meyerson, M., Gabriel, S., Laird, P.W., Haussler, D., Getz, G., Chin, L., TCGA Res Network, 2013. The somatic genomic landscape of glioblastoma. Cell 155, 462–477.

Buggle, B., Zech, M., 2015. New frontiers in the molecular based reconstruction of Quaternary paleovegetation from loess and paleosols. Quaternary International 372, 180–187.

Burn, M.J., Holmes, J., Kennedy, L.M., Bain, A., Marshall, J.D., Perdikaris, S., 2016. A sediment-based reconstruction of Caribbean effective precipitation during the 'Little Ice Age' from freshwater pond, Barbuda. The Holocene 26, 1237–1247.

Burn, M.J., Palmer, S.E., 2014. Solar forcing of Caribbean drought events during the last millennium. Journal of Quaternary Science 29, 827–836.

Burny, J., 1999. Bijdrage tot de historische ecologie van de Limburgse Kempen (1910–1950). Natuurhistorisch Genootschap, Limburg XL11(1), Maastricht, The Netherlands.

Bush, M.B., Alfonso-Reynolds, A.M., Urrego, D.H., Valencia, B.G., Correa-Metrio, A.Y., Zimmermann, M., Silman, M.R., 2015. Fire and climate: contrasting pressures on tropical Andean timberline species. Journal of Biogeography 42, 938–950.

Buytaert, W., Celleri, R., De Bievre, B., Cisneros, F., Wyseure, G., Deckers, J., Hofstede, R., 2006. Human impact on the hydrology of the Andean paramos. Earth-Science Reviews 79, 53–72.

Caffrey, M.A., Horn, S.P., Orvis, K.H., Haberyan, K.A., 2015. Holocene environmental change at Laguna Saladilla, coastal north Hispaniola. Palaeogeography, Palaeoclimatology, Palaeoecology 436, 9–22.

Caffrey, P., Kindberg, L., Stone, C., de Obeso, J., Trzaska, S., Torres, R., Meier, G., 2013. Dominican Republic Climate Change Vulnerability Assessment Report. United States Agency for International Development (USAID), 123 p.

Cano Carmona, E., Veloz Ramirez, A., Cano-Ortiz, A., 2010. Contribution to the biogeography of the Hispaniola (Dominican Republic, Haiti). Acta Botanica Gallica 157, 581–598.

Cano-Ortiz, A., Musarella, C., Piñar, J., Spampinato, G., Veloz, A., Cano, E., 2015. Vegetation of the dry bioclimatic areas in the Dominican Republic. Plant Biosystems 149, 451–472.

Castañeda, I.S., Schouten, S., 2011. A review of molecular organic proxies for examining modern and ancient lacustrine environments. Quaternary Science Reviews 30, 2851–2891.

Castilla-Beltrán, A., Hooghiemstra, H., Hoogland, M.L., Pagán-Jiménez, J., van Geel, B., Field, M.H., Prins, M., Donders, T., Malatesta, E.H., Hung, J.U., 2018. Columbus' footprint in Hispaniola: a paleoenvironmental record of indigenous and colonial impacts on the landscape of the central Cibao Valley, northern Dominican Republic. Anthropocene 22, 66–80.

Chen, Z., Simoneit, B.R.T., Wang, T.-., Huang, W., Yan, D., Ni, Z., Liu, K., 2016. Effects of high temperatures on biomarker ratios during oil-to-gas cracking experiments at two pressures. Organic Geochemistry 101, 108–131. https://doi.org/10.1016/j.orggeochem.2016.08.011.

Clark, J.S., McLachlan, J.S., 2003. Stability of forest biodiversity. Nature 423, 635–638.

Collins, J.A., Carr, A.S., Schefuss, E., Boom, A., Sealy, J., 2017. Investigation of organic matter and biomarkers from diepkloof rock shelter, South Africa: insights into middle stone age site usage and palaeoclimate. Journal of Archaeological Science 85, 51–65.

Collister, J.W., Rieley, G., Stern, B., Eglinton, G., Fry, B., 1994. Compound-specific δ 13C analyses of leaf lipids from plants with differing carbon dioxide metabolisms. Organic Geochemistry 21, 619–627.

Concheri, G., Bertoldi, D., Polone, E., Otto, S., Larcher, R., Squartini, A., 2011. Chemical elemental distribution and soil DNA fingerprints provide the critical evidence in murder case investigation. PLoS One 6, e20222.

Cranwell, P.A., 1984. Lipid geochemistry of sediments from Upton Broad, a small productive lake. Organic Geochemistry 7, 25–37.

Crausbay, S.D., Hotchkiss, S.C., 2012. Pollen-vegetation relationships at a tropical cloud forest's upper limit and accuracy of vegetation inference. Review of Palaeobotany and Palynology 184, 1–13.

Curiale, J.A., 2002. A review of the occurrences and causes of migration-contamination in crude oil. Organic Geochemistry 33, 1389–1400.

D'Anjou, R.M., Bradley, R.S., Balascio, N.L., Finkelstein, D.B., 2012. Climate impacts on human settlement and agricultural activities in northern Norway revealed through sediment biogeochemistry. In: Proceedings of the National Academy of Sciences, USA, vol. 109, pp. 20332–20337.

De Boer, E.J., Tjallingii, R., Vélez, M.I., Rijsdijk, K.F., Vlug, A., Reichart, G., Prendergast, A.L., de Louw, P.G., Florens, F.V., Baider, C., Hooghiemstra, H., 2014. Climate variability in the SW Indian Ocean from an 8000-yr long multi-proxy record in the Mauritian lowlands shows a middle to late Holocene shift from negative IOD-state to ENSO-state. Quaternary Science Reviews 86, 175–189.

De Keyzer, M., 2014. The Common Denominator; the Survival of the Commons in the Late Medieval Campine Area (Ph.D. thesis/masters). University of Antwerp, Department of History, Antwerp, Belgium.

De Rijke, E., Fellner, C., Westerveld, J., Lopatka, M., Cerli, C., Kalbitz, K., De Koster, C., 2015. Determination of n-alkanes in C. annuum (bell pepper) fruit and seed using GC-MS: comparison of extraction methods and application to samples of different geographical origin. Analytical and Bioanalytical Chemistry 407, 5729–5738.

Di Pasquale, G., Marziano, M., Impagliazzo, S., Lubritto, C., De Natale, S., Bader, M.Y., 2007. The Holocene treeline in the northern Andes (Ecuador): first evidence from soil charcoal. Palaeogeography, Palaeoclimatology, Palaeoecology 259, 17–34.

Diefendorf, A.F., Freeman, K.H., Wing, S.L., Graham, H.V., 2011. Production of n-alkyl lipids in living plants and implications for the geologic past. Geochimica et Cosmochimica Acta 75, 7472–7485.

Dinel, H., Schnitzer, M., Meyhus, G.R., 1990. Soil lipids: origin, nature, content, decomposition, and effect on soil physical properties. In: Bollag, J.M., Stotzky, G. (Eds.), Soil Biochemistry. Marcel Dekker Inc., New York, pp. 397–429.

Doorenbosch, M., 2013. Ancestral Heaths; Reconstructing the Barrow Landscape in the Central and Southern Netherlands. Sidestone Press, Leiden, The Netherlands.

Douglas, P.M., Pagani, M., Brenner, M., Hodell, D.A., Curtis, J.H., 2012. Aridity and vegetation composition are important determinants of leaf-wax δD values in southeastern Mexico and Central America. Geochimica et Cosmochimica Acta 97, 24–45.

Dulal, H.B., Shah, K.U., Sapkota, C., 2012. Reducing emissions from deforestation and forest degradation (REDD) projects: lessons for future policy design and implementation. International Journal of Sustainable Development and World Ecology 19, 116–129.

Dungait, J.A.J., Bol, R., Lopez-Capel, E., Bull, I.D., Chadwick, D., Amelung, W., Granger, S.J., Manning, D.A.C., Evershed, R.P., 2010. Applications of stable isotope ratio mass spectrometry in cattle dung carbon cycling studies. Rapid Communications in Mass Spectrometry 24, 495–500.

Durland, W.D., 1922. The forests of the Dominican Republic. Geographical Review 12, 206–222.

Eglinton, G., Hamilton, R.J., 1967. Leaf epicuticular waxes. Science 156, 1322–1335.

Eglinton, T.I., Eglinton, G., 2008. Molecular proxies for paleoclimatology. Earth and Planetary Science Letters 275, 1–16.

FAO, 2006. Guidelines for Soil Description, fourth ed. Food and Agricultural Organization of the United Nations, Rome, Italy.

Feakins, S.J., Sessions, A.L., 2010. Controls on the D/H ratios of plant leaf waxes in an arid ecosystem. Geochimica et Cosmochimica Acta 74, 2128–2141.

Feng, X., Xu, Y., Jaffe, R., Schlesinger, W.H., Simpson, M.J., 2010. Turnover rates of hydrolysable aliphatic lipids in Duke Forest soils determined by compound specific C-13 isotopic analysis. Organic Geochemistry 41, 573–579.

Ficken, K., Li, B., Swain, D., Eglinton, G., 2000. An n-alkane proxy for the sedimentary input of submerged/floating freshwater aquatic macrophytes. Organic Geochemistry 31, 745–749.

Flantua, S.G.A., Blaauw, M., Hooghiemstra, H., 2016a. Geochronological database and classification system for age uncertainties in Neotropical pollen records. Climate of the Past 12, 387–414. https://doi.org/10.5194/cp-12-387-2016.

Flantua, S., Hooghiemstra, H., Vuille, M., Behling, H., Carson, J.F., Gosling, W., Hoyos, I., Ledru, M., Montoya, E., Mayle, F., Maldonado, A., Rull, V., Tonello, M., Whitney, B., González-Arango, C., 2016b. Climate variability and human impact in South America during the last 2000 years: synthesis and perspectives from pollen records. Climate of the Past 12, 483–523.

Flenley, J., 1979. The Equatorial Rain Forest: A Geological History. Butterworths, London, United Kingdom.

French, C.D., Schenk, C.J., 1997. Map Showing Geology, Oil and Gas Fields, and Geologic Provinces of the Caribbean Region.

Gabb, W.M., 1873. On the Topography and Geology of Santo Domingo. M'Calla & Stavely, Philadelphia, United States.

Gao, L., Hou, J., Toney, J., MacDonald, D., Huang, Y., 2011. Mathematical modeling of the aquatic macrophyte inputs

of mid-chain n-alkyl lipids to lake sediments: implications for interpreting compound specific hydrogen isotopic records. Geochimica et Cosmochimica Acta 75, 3781–3791.

Gat, J.R., 1996. Oxygen and hydrogen isotopes in the hydrologic cycle. Annual Review of Earth and Planetary Sciences 24, 225–262.

Giannini, A., Kushnir, Y., Cane, M.A., 2000. Interannual variability of Caribbean rainfall, ENSO, and the Atlantic Ocean. Journal of Climater 13, 297–311.

Gocke, M.I., Kessler, F., van Mourik, J.M., Jansen, B., Wiesenberg, G.L.B., 2016. Paleosols can promote root growth of the recent vegetation – a case study from the sandy soil-sediment sequence Rakt, Netherlands. Soil 2, 537–549.

Griepentrog, M., Eglinton, T.I., Hagedorn, F., Schmidt, M.W.I., Wiesenberg, G.L.B., 2015. Interactive effects of elevated CO_2 and nitrogen deposition on fatty acid molecular and isotope composition of above- and belowground tree biomass and forest soil fractions. Global Change Biology 21, 473–486.

Groot, M.H.M., Bogotá, R.G., Lourens, L.J., Hooghiemstra, H., Vriend, M., Berrio, J.C., Tuenter, E., Van der Plicht, J., Van Geel, B., Ziegler, M., Weber, S.L., Betancourt, A., Contreras, L., Gaviria, S., Giraldo, C., Gonz'alez, N., Jansen, J.H.F., Konert, M., Ortega, D., Rangel, O., Sarmiento, G., Vandenberghe, J., Van der Hammen, T., Van der Linden, M., Westerhoff, W., 2011. Ultra-high resolution pollen record from the northern Andes reveals rapid shifts in montane climates within the last two glacial cycles. Climate of the Past 7, 299–316.

Guhl, E., 1982. Los páramos circundantes de la Sabana de Bogotá. Jardin Botanico 'Jose Celestino Mutus', Bogotá, Colombia.

Günther, F., Mügler, I., Mäusbacher, R., Daut, G., Leopold, K., Gerstmann, U., Xu, B., Yao, T., Gleixner, G., 2011. Response of δD values of sedimentary n-alkanes to variations in source water isotope signals and climate proxies at lake Nam Co, Tibetan Plateau. Quaternary International 236, 82–90.

Hamer, U., Rumpel, C., Dignac, M.-., 2012. Cutin and suberin biomarkers as tracers for the turnover of shoot and root derived organic matter along a chronosequence of Ecuadorian pasture soils. European Journal of Soil Science 63, 808–819.

Haug, G.H., Hughen, K.A., Sigman, D.M., Peterson, L.C., Röhl, U., 2001. Southward migration of the intertropical convergence zone through the Holocene. Science 293, 1304.

Hicks, S., 2006. When no pollen does not mean no trees, Veetation. History Archaeobotany 15, 253–261.

Hofstede, R.G.M., Groenendijk, J.P., Coppus, R., Fehse, J.C., Sevink, J., 2002. Impact of pine plantations on soils and vegetation in the Ecuadorian High Andes. Montain Research Development 22, 159–167.

Hooghiemstra, H., 1984. Vegetational and Climatic History of the High Plain of Bogotá, Colombia., Dissertationes Botanicae, vol. 79. J. Cramer, Vaduz.

Hooghiemstra, H., Agwu, C.O.C., Beug, H.-J., 1986. Pollen and spore distribution in recent marine sediments: a record of NW-African seasonal wind patterns and vegetation belts. Meteor Forschungs-Ergebnisse, C 40, 87–135.

Hooghiemstra, H., Berrio, J.C., Groot, M.H.M., Bogotá, R.G., Olivera, M.M., Gonzállez-Carranza, Z., 2012. The dynamic history of the upper forest line ecotone in the Northern Andes. In: Randall, R.W. (Ed.), Ecotones between Forest and Grassland. Springer New York, New York, NY, pp. 229–246.

Hooghiemstra, H., Olijhoek, T., Hoogland, M., Prins, M., van Geel, B., Donders, T., Gosling, W., Hofman, C., 2018. Columbus' environmental impact in the new world: land use change in the Yaque river valley, Dominican Republic. The Holocene 28, 1818–1835.

Horst, O.H., 1992. Climate and the "encounter" in the Dominican Republic. Journal of Geography 91, 205–210.

Hou, J., D'Andrea, W.J., MacDonald, D., Huang, Y., 2007. Hydrogen isotopic variability in leaf waxes among terrestrial and aquatic plants around Blood Pond, Massachusetts (USA). Organic Geochemistry 38, 977–984.

Hua, Q., Barbetti, M., Rakowski, A.Z., 2013. Atmospheric radiocarbon for the period 1950–2010. Radiocarbon 55, 2059–2072.

Huguet, A., Gocke, M., Derenne, S., Fosse, C., Wiesenberg, G.L.B., 2013. Root-associated branched tetraether source microorganisms may reduce estimated paleotemperatures in subsoil. Chemical Geology 356, 1–10.

Huguet, A., Wiesenberg, G.L.B., Gocke, M., Fosse, C., Derenne, S., 2012. Branched tetraether membrane lipids associated with rhizoliths in loess: Rhizomicrobial overprinting of initial biomarker record. Organic Geochemistry 43, 12–19.

Izzo, M., Rosskopf, C.M., Aucelli, P.P., Maratea, A., Méndez, R., Pérez, C., Segura, H., 2010. A new climatic map of the Dominican Republic based on the Thornthwaite classification. Physical Geography 31, 455–472.

Jansen, B., de Boer, E.J., Cleef, A.M., Hooghiemstra, H., Moscol-Olivera, M., Tonneijck, F.H., Verstraten, J.M., 2013. Reconstruction of late Holocene forest dynamics in northern Ecuador from biomarkers and pollen in soil cores. Palaeogeography, Palaeoclimatology, Palaeoecology 386, 607–619.

Jansen, B., Haussmann, N.S., Tonneijck, F.H., Verstraten, J.M., De Voogt, P., 2008. Characteristic straight-chain lipid ratios as a quick method to assess past forest - páramo transitions in the Ecuadorian Andes. Palaeogeography, Palaeoclimatology, Palaeoecology 262, 129–139.

Jansen, B., Moscol-Olivera, M.C., Tonneijck, F.H., Cleef, A.M., Hooghiemstra, H., Sevink, J., Verstraten, J.M., 2009. Informe final de investigación del programa Reconstrucción del Límite Superior del Bosque en Ecuador (RUFLE), pp. 1–21.

Jansen, B., Nierop, K.G.J., 2009. Me-ketones in high altitude Ecuadorian andisols confirm excellent conservation of plant-specific *n*-alkane patterns. Organic Geochemistry 40, 61–69.

Jansen, B., Nierop, K.G.J., Hageman, J.A., Cleef, A., Verstraten, J.M., 2006a. The straight-chain lipid biomarker composition of plant species responsible for the dominant biomass production along two altitudinal transects in the Ecuadorian Andes. Organic Geochemistry 37, 1514–1536.

Jansen, B., Nierop, K.G.J., Kotte, M.C., De Voogt, P., Verstraten, J.M., 2006b. The application of accelerated solvent extraction (ASE) to extract lipid biomarkers from soils. Applied Geochemistry 21, 1006–1015.

Jansen, B., Nierop, K.G.J., Tonneijck, F.H., Van der Wielen, F.W.M., Verstraten, J.M., 2007. Can isoprenoids in leaves and roots of plants along altitudinal gradients in the Ecuadorian Andes serve as biomarkers? Plant and Soil 291, 181–198.

Jansen, B., Van Loon, E.E., Hooghiemstra, H., Verstraten, J.M., 2010. Improved reconstruction of palaeo-environments through unravelling of preserved vegetation biomarker patterns. Palaeogeography, Palaeoclimatology, Palaeoecology 285, 119–130.

Jansen, B., Wiesenberg, G.L.B., 2017. Opportunities and limitations related to the application of plant-derived lipid molecular proxies in soil science. Soil 3, 211–234.

Janzen, D.H., 1982. Natural history of guacimo fruits (Sterculiaceae: Guazuma ulmifolia) with respect to consumption by large mammals. American Journal of Botany 1240–1250.

Killops, S.D., Frewin, N.L., 1994. Triterpenoid diagenesis and cuticular preservation. Organic Geochemistry 21, 1193–1209.

Kindler, R., Miltner, A., Thullner, M., Richnow, H., Kaestner, M., 2009. Fate of bacterial biomass derived fatty acids in soil and their contribution to soil organic matter. Organic Geochemistry 40, 29–37.

KNMI Climate Explorer (2017) Time series: monthly Monte Cristi GHCN v2 precipitation (all). Koninklijk Nederlands Meteorologisch Instituut (KNMI), retrieved from http://climexp.knmi.nl/getprcpall.cgi?id=someone@somewhere&WMO=78451.3&STATION=MONTE_CRISTI&extraargs, last accessed 28 March, 2017.

KNMI Climate Explorer (2017) Time series: monthly Villa Vasquez GHCN v2 precipitation (all). Koninklijk Nederlands Meteorologisch Instituut (KNMI), retrieved from http://climexp.knmi.nl/getprcpall.cgi?id=someone@somewhere&WMO=78451.7&STATION=VILLA_VASQUEZ&extraargs, last accessed 28 March, 2017.

Kögel-Knabner, I., 2002. The macromolecular organic composition of plant and microbial residues as inputs to soil organic matter. Soil Biology and Biochemistry 34, 139–162.

Kolattukudy, P.E., Croteau, R., Buckner, J.S., 1976. Biochemistry of plant waxes. In: Kolattukudy, P.E. (Ed.), Chemistry and Biochemistry of Natural Waxes. Elsevier, Amsterdam, pp. 289–347.

Körner, C., 1999. Alpine plants: stressed or adapted? In: Press, M.C., Scholes, J.D., Barker, M.G. (Eds.), Physiological Plant Ecology. Blackwell Science Ltd., Oxford, United Kingdom, pp. 297–311.

Körner, C., Basler, D., Hoch, G., Kollas, C., Lenz, A., Randin, C.F., Vitasse, Y., Zimmerman, N.E., 2016. Where, why and how? Explaining the low-temperature range limits of temperate tree species. Journal of Ecology 104, 1076–1088.

Körner, C., Paulsen, J., 2004. A world-wide study of high altitude treeline temperatures. Journal of Biogeography 31, 713–732.

Kramer, C., Gleixner, G., 2006. Variable use of plant- and soil-derived carbon by microorganisms in agricultural soils. Soil Biology and Biochemistry 38, 3267–3278.

Kristen, I., Wilkes, H., Vieth, A., Zink, K., Plessen, B., Thorpe, J., Partridge, T., Oberhänsli, H., 2010. Biomarker and stable carbon isotope analyses of sedimentary organic matter from Lake Tswaing: evidence for deglacial wetness and early Holocene drought from South Africa. Journal of Paleolimnology 44, 143–160.

Laegaard, S., 1992. Influence of fire in the grass páramo vegetation of Ecuador. In: Balslev, H., Luteyn, J.L. (Eds.), Páramo, an Andean Ecosystem under Human Influence. Academic Press, London, pp. 151–170.

Lane, C.S., Horn, S.P., Mora, C.I., Orvis, K.H., 2009. Late-Holocene paleoenvironmental change at mid-elevation on the Caribbean slope of the Cordillera Central, Dominican Republic: a multi-site, multi-proxy analysis. Quaternary Science Reviews 28, 2239–2260.

Lane, C.S., Horn, S.P., Orvis, K.H., Thomason, J.M., 2011. Oxygen isotope evidence of Little Ice Age aridity on the Caribbean slope of the Cordillera central, Dominican Republic. Quaternary Research 75, 461–470.

Lane, C.S., Horn, S.P., Kerr, M.T., 2014. Beyond the mayan lowlands: impacts of the terminal classic drought in the Caribbean Antilles. Quaternary Science Reviews 86, 89–98.

Lavrieux, M., Jacob, J., LeMilbeau, C., Zocatelli, R., Masuda, K., Breheret, J., Disnar, J., 2011. Occurrence of triterpenyl acetates in soil and their potential as chemotaxonomical markers of Asteraceae. Organic Geochemistry 42, 1315–1323.

Lehmann, J., Kleber, M., 2015. The contentious nature of soil organic matter. Nature 528, 60–68.

Li, F.F., Zhang, P.C., Wu, D.P., Xu, Y., Chen, F.Y., Chang, Z.F., Chu, G., Wang, L., Pan, B., Xing, B.S., 2018.

Acid pretreatment increased lipid biomarker extractability: a case study to reveal soil organic matter input from rubber trees after long-term cultivation. European Journal of Soil Science 69, 315–324.

Luo, P., Peng, P., Gleixner, G., Zheng, Z., Pang, Z., Ding, Z., 2011. Empirical relationship between leaf wax n-alkane delta D and altitude in the Wuyi, Shennongjia and Tianshan Mountains, China: implications for paleoaltimetry. Earth and Planetary Science Letters 301, 285–296.

Luong, S., Forbes, S.L., Wallman, J.F., Roberts, R.G., 2018. Monitoring the extent of vertical and lateral movement of human decomposition products through sediment using cholesterol as a biomarker. Forensic Science International 285, 93–104. https://doi.org/10.1016/j.forsciint.2018.01.026.

Luteyn, J.L., 1999. Páramos: A Checklist of Plant Diversity, Geographical Distribution, and Botanical Literature. Memoirs of the New York Botanical Garden, vol. 84. The New York Botanical Garden Press, New York, USA.

Malik, A., Blagodatskaya, E., Gleixner, G., 2013. Soil microbial carbon turnover decreases with increasing molecular size. Soil Biology and Biochemistry 62, 115–118.

Marseille, F., Disnar, J.R., Guillet, B., Noack, Y., 1999. n-alkanes and free fatty acids in humus and Al horizons of soils under beech, spruce and grass in the Massif-Central (Mont-Lozere), France. European Journal of Soil Science 50, 433–441.

Mauqouy, D., Van Geel, B., 2007. Mire and peat macros. In: Elias, S.A. (Ed.), Encyclopedia of Quaternart Science, vol. 3. Elsevier, Amsterdam, The Netherlands, pp. 2315–2336.

Mayle, F.E., Burbridge, R., Killeen, T.J., 2000. Millennial-scale dynamics of Southern Amazonian rain forests. Science 290, 2291–2294. https://doi.org/10.1126/science.290.5500.2291.

Meador, T.B., Zhu, C., Elling, F.J., Könneke, M., Hinrichs, K., 2014. Identification of isoprenoid glycosidic glycerol dibiphytanol diethers and indications for their biosynthetic origin. Organic Geochemistry 69, 70–75.

Mendez-Millan, M., Dignac, M., Rumpel, C., Derenne, S., 2011. Can cutin and suberin biomarkers be used to trace shoot and root-derived organic matter? A molecular and isotopic approach. Biogeochemistry 106, 23–38.

Mendez-Millan, M., Nguyen Tu, T.T., Balesdent, J., Derenne, S., Derrien, D., Egasse, C., Thongo M'Bou, A., Zeller, B., Hatté, C., 2014. Compound-specific ^{13}C and ^{14}C measurements improve the understanding of soil organic matter dynamics. Biogeochemistry 118, 205–223.

Meyers, P.A., 2003. Applications of organic geochemistry to paleolimnological reconstructions: a summary of examples from the Laurentian Great Lakes. Organic Geochemistry 34, 261–289.

Moingt, M., Lucotte, M., Paquet, S., 2016. Lignin biomarkers signatures of common plants and soils of Eastern Canada. Biogeochemistry 129, 133–148.

Moore, P.D., Webb, J.A., Collinson, M.E., 1991. Pollen Analysis. Blackwell, Oxford.

Morales, C., Ortega, T., González, C., Bustillo, E., Rodriguez, P., 2009. Mapa de exposición ante inundaciones en la cuenca de Río Yaque del Norte.

Moscol-Olivera, M.C., Duivenvoorden, J.F., Hooghiemstra, H., 2009. Pollen rain and pollen representation across a forest-páramo ecotone in northern Ecuador. Review of Palaeobotany and Palynology 157, 285–300. https://doi.org/10.1016/j.revpalbo.2009.05.008.

Moscol-Olivera, M.C., Cleef, A.M., 2009a. A phytosociological study of the páramo along two altitudinal transects in northern Ecuador. Phytocoenologia 39, 79–107.

Moscol-Olivera, M.C., Cleef, A.M., 2009b. Vegetation composition and altitudinal distribution of montane rain forests in northern Ecuador. Phytocoenologia 39, 175–204.

Myers, N., 1988. Threatened biotas: "hot-spots" in tropical forests. The Environmentalist 8, 187–208.

Ngosong, C., Gabriel, E., Ruess, L., 2012. Use of the signature Fatty Acid 16:1omega5 as a tool to determine the distribution of arbuscular mycorrhizal fungi in soil. Journal of Lipids 2012, 236807-236807.

Nierop, K.G.J., Jansen, B., 2009. Extensive transformation of organic matter and excellent lipid preservation at the upper, superhumid Guandera páramo. Geoderma 151, 357–369.

Nierop, K.G.J., Tonneijck, F.H., Jansen, B., Verstraten, J.M., 2007. Organic matter in volcanic ash soils under forest and páramo along an Ecuadorian altitudinal transect. Soil Science Society of America Journal 71, 1119–1127.

Oom, S.P., Sibbald, A.M., Hester, A.J., Miller, D.R., Legg, C.J., 2008. Impacts of sheep grazing a complex vegetation mosaic: relating behavior to vegetation change. Agriculture, Ecosystems and Environment 124, 219–228.

Otto, A., Simpson, M.J., 2005. Degradation and preservation of vascular plant-derived biomarkers in grassland and forest soils from Western Canada. Biogeochemistry 74, 377–409.

Pautler, B.G., Sanborn, P.T., Simpson, A.J., Simpson, M.J., 2013. Molecular characterization of organic matter in Canadian Arctic paleosols for paleoecological applications. Organic Geochemistry 63, 122–138.

Peters, K.E., Walters, C.C., Moldowan, J.M., 2005. The Biomarker Guide, 2 ed. Cambridge University Press, Cambridge, United Kingdom.

Peters, T., Braeuning, A., Muenchow, J., Richter, M., 2014. An ecological paradox: high species diversity and low position of the upper forest line in the Andean depression. Ecology and Evolution 4, 2134–2145.

Peterse, F., van der Meer, M.T.J., Schouten, S., Jia, G., Ossebaar, J., Blokker, J., Damste, J.S.S., 2009. Assessment of soil n-alkane delta D and branched tetraether membrane lipid distributions as tools for paleoelevation reconstruction. Biogeosciences 6, 2799–2807.

Peterson, L.C., Haug, G.H., 2006. Variability in the mean latitude of the Atlantic intertropical convergence zone as recorded by riverine input of sediments to the Cariaco basin (Venezuela). Palaeogeography, Palaeoclimatology, Palaeoecology 234, 97–113.

Polissar, P.J., D'Andrea, W.J., 2014. Uncertainty in paleohydrologic reconstructions from molecular δD values. Geochimica et Cosmochimica Acta 129, 146–156.

Powers, L., Werne, J.P., Vanderwoude, A.J., Sinninghe Damsté, J.S., Hopmans, E.C., Schouten, S., 2010. Applicability and calibration of the TEX_{86} paleothermometer in lakes. Organic Geochemistry 41, 404–413.

Prasad, S., Anoop, A., Riedel, N., Sarkar, S., Menzel, P., Basavaiah, N., Krishnan, R., Fuller, D., Plessen, B., Gaye, B., Röhl, U., Wilkes, H., Sachse, D., Sawant, R., Wiesner, M.G., Stebich, M., 2014. Prolonged monsoon droughts and links to Indo-Pacific warm pool: a Holocene record from Lonar Lake, central India. Earth and Planetary Science Letters 391, 171–182.

Price, M., 1999. Global Change in the Mountains. Parthenon, New York.

Pu, Y., Nace, T., Meyers, P.A., Zhang, H., Wang, Y., Zhang, C.L., Shao, X., 2013. Paleoclimate changes of the last 1000 yr on the eastern Qinghai–Tibetan Plateau recorded by elemental, isotopic, and molecular organic matter proxies in sediment from glacial Lake Ximencuo. Palaeogeography, Palaeoclimatology, Palaeoecology 379, 39–53.

Reimer, P.J., Bard, E., Bayliss, A., Beck, J.W., Blackwell, P.G., Bronk Ramsey, C., Buck, C.E., Cheng, H., Edwards, R.L., Friedrich, M., Grootes, P.M., Guilderson, T.P., Haflidason, H., Hajdas, I., Hatté, C., Heaton, T.J., Hoffmann, D.L., Hogg, A.G., Hughen, K.A., Kaiser, K.F., Kromer, B., Manning, S.W., Niu, M., Reimer, R.W., Richards, D.A., Scott, E.M., Southon, J.R., Staff, R.A., Turney, C.S.M., Van der Plicht, J., 2013. IntCal13 and Marine13 radiocarbon age calibration curves 0-50,000 years cal BP. Radiocarbon 55, 1869–1887.

Reimer, P.J., Brown, T.A., Reimer, R.W., 2004. Discussion: reporting and calibration of post-bomb 14C data. Radiocarbon 46, 1299–1304.

Reyna, E., Polonia, A., Pérez, M., 2012. Atlas de Biodiversidad y Recursos Naturales de la República Dominicana. Ministerio de Medio Ambiente y Recursos Naturales, Santo Domingo, Dominican Republic.

Rieley, G., Collier, R.J., Jones, D.M., Eglinton, G., 1991. The biogeochemistry of Ellesmere Lake, U.K. -I: source correlation of leaf wax inputs to the sedimentary lipid record. Organic Geochemistry 17, 901–912.

Rommerskirchen, F., Eglinton, G., Dupont, L., Güntner, U., Wenzel, C., Rullkötter, J., 2003. A north to south transect of Holocene southeast Atlantic continental margin sediments: relationship between aerosol transport and compound-specific δ13C land plant biomarker and pollen records. Geochemistry, Geophysics, Geosystems 4, 1101.

Rommerskirchen, F., Plader, A., Eglinton, G., Chikaraishi, Y., Rullkoetter, J., 2006. Chemotaxonomic significance of distribution and stable carbon isotopic composition of long-chain alkanes and alkan-1-ols in C-4 grass waxes, Organic. Geochemistry 37, 1303–1332.

Sachse, D., Billault, I., Bowen, G.J., Chikaraishi, Y., Dawson, T.E., Feakins, S.J., Freeman, K.H., Magill, C.R., McInerney, F.A., van der Meer, M.T.J., Polissar, P., Robins, R.J., Sachs, J.P., Schmidt, H., Sessions, A.L., White, J.W.C., West, J.B., Kahmen, A., 2012. Molecular paleohydrology: interpreting the hydrogen- isotopic composition of lipid biomarkers from photosynthesizing organisms. Annual Review of Earth and Planetary Sciences 40, 221–249.

Sachse, D., Radke, J., Gleixner, G., 2006. Delta D values of individual n-alkanes from terrestrial plants along a climatic gradient - implications for the sedimentary biomarker record. Organic Geochemistry 37, 469–483.

Salomons, J.B., 1986. Paleoecology of volcanic soils in the Colombian Central Coridillera (Parque National Natural de los Nevados), Dissertationes Botanicae, vol. 95. Borntraeger, Berlin.

Scarre, C. (Ed.), 2013. The Human Past. World Prehistory and the Development of Human Societies. Thames & Hudson, London, United Kingdom.

Schmidt, F., Oberhänsli, H., Wilkes, H., 2014. Biocoenosis response to hydrological variability in Southern Africa during the last 84 ka BP: a study of lipid biomarkers and compound-specific stable carbon and hydrogen isotopes from the hypersaline Lake Tswaing. Global and Planetary Change 112, 92–104.

Schmidt, M.W.I., Torn, M.S., Abiven, S., Dittmar, T., Guggenberger, G., Janssens, I.A., Kleber, M., Koegel-Knabner, I., Lehmann, J., Manning, D.A.C., Nannipieri, P., Rasse, D.P., Weiner, S., Trumbore, S.E., 2011. Persistence of soil organic matter as an ecosystem property. Nature 478, 49–56.

Schouten, S., Forster, A., Panoto, F.E., Damste, J.S.S., 2007. Towards calibration of the TEX86 palaeothermometer for tropical sea surface temperatures in ancient greenhouse worlds. Organic Geochemistry 38, 1537–1546.

Schouten, S., Hopmans, E.C., Damste, J.S.S., 2013. The organic geochemistry of glycerol dialkyl glycerol tetraether lipids: a review. Organic Geochemistry 54, 19–61.

Schreuder, L.T., Beets, C.J., Prins, M.A., Hatte, C., Peterse, F., 2016. Late Pleistocene climate evolution in Southeastern

Europe recorded by soil bacterial membrane lipids in Serbian loess. Palaeogeography, Palaeoclimatology, Palaeoecology 449, 141–148.
Schwab, V.F., Sachs, J.P., 2009. The measurement of D/H ratio in alkenones and their isotopic heterogeneity. Organic Geochemistry 40, 111–118.
Serrano Gine, D., Galarraga Sanchez, R., 2015. The Andean páramo: geographic characterization and state of their environment. An interdisciplinary contribution. Estudios Geográficos 76, 369–393.
Shepherd, T., Griffiths, D.W., 2006. The effects of stress on plant cuticular waxes. New Phytologist 171, 469–499.
Simpson, I.A., Bol, R., Bull, I.D., Evershed, R.P., Petzke, K.J., Dockrill, S.J., 1999. Interpreting early land management through compound specific stable isotope analyses of archaeological soils. Rapid Communications in Mass Spectrometry 13, 1315–1319.
Simpson, M.J., Simpson, A.J., 2012. The chemical ecology of soil organic matter molecular constituents. Journal of Chemical Ecology 38, 768–784.
Sklenar, P., Luyeyn, J.L., Ulloa Ulloa, C., Jorgensen, P.M., Dillon, M.O., 2005. Flora genérica de los páramos; Guia ilustrada de las plantas vasculares, vol. 92. Memoirs of the New York Botanical Garden, New York, United States of America.
Smits, J., Noordijk, J., 2013. Heidebeheer, moderne methoden in e een eeuwenoud landschap. KNNV Uitgeverij, Zeist, The Netherlands.
Sneddon, J., Masuram, S., Richert, J.C., 2007. Gas chromatography mass spectrometry basic principles, instrumentation and selected applications for detection of organic compounds. Analytical Letters 40, 1003–1012.
Spek, T., 2004. Het Drentse Esdorpenlandschap: Een Historisch-Geografiesche Studie. Stichting Matrijs, Utrecth.
Spielvogel, S., Prietzel, J., Kögel-Knabner, I., 2007. Changes of lignin phenols and neutral sugars in different soil types of a high-elevation forest ecosystem 25 years after forest dieback. Soil Biology and Biochemistry 39, 655–668. https://doi.org/10.1016/j.soilbio.2006.09.018.
Street, J.H., Anderson, R.S., Rosenbauer, R.J., Paytan, A., 2013. n-Alkane evidence for the onset of wetter conditions in the Sierra Nevada, California (USA) at the mid-late Holocene transition, ~ 3.0 ka. Quaternary Research 79, 14–23.
Stuiver, M., Reimer, P.J., 1993. Extended 14 C data base and revised CALIB 3.0 14 C age calibration program. Radiocarbon 35, 215–230.
Tactuk, P., Madera, L., García, V., Horacio, Z., González Pérez, I.E., Mora Alcántara, N., Ortiz, L., 2015. Perfiles Estadísticos Provincales. Regiones Cibao Norte-Noroeste.
Tonneijck, F.H., Hageman, J.A., Sevink, J., Verstraten, J.M., 2008. Vertical distribution of SOM in relation to tephra stratification of volcanic soils in Northern Ecuador. Geoderma 144, 231–247.
Tonneijck, F.H., Jansen, B., Nierop, K.G.J., Verstraten, J.M., Sevink, J., De Lange, L., 2010. Towards understanding of carbon stocks and stabilization in volcanic ash soils in natural Andean ecosystems of northern Ecuador. European Journal of Soil Science 61, 392–405.
Tonneijck, F.H., Jongmans, A.G., 2008. The influence of bioturbation on the vertical distribution of soil organic matter in volcanic ash soils: a case study in northern Ecuador. European Journal of Soil Science 59, 1063–1075.
van Bon, L., Affandi, A.J., Broen, J., Christmann, R.B., Marijnissen, R.J., Stawski, L., Farina, G.A., Stifano, G., Mathes, A.L., Cossu, M., York, M., Collins, C., Wenink, M., Huijbens, R., Hesselstrand, R., Saxne, T., DiMarzio, M., Wuttge, D., Agarwal, S.K., Reveille, J.D., Assassi, S., Mayes, M., Deng, Y., Drenth, J.P.H., de Graaf, J., den Heijer, M., Kallenberg, C.G.M., Bijl, M., Loof, A., van den Berg, W.B., Joosten, L.A.B., Smith, V., de Keyser, F., Scorza, R., Lunardi, C., van Riel, P.L.C.M., Vonk, M., van Heerde, W., Meller, S., Homey, B., Beretta, L., Roest, M., Trojanowska, M., Lafyatis, R., Radstake, T.R.D.J., 2014. Proteome-wide analysis and CXCL4 as a biomarker in systemic sclerosis. The New England Journal of Medicine 370, 433–443.
van den Bos, V., Engels, S., Bohncke, S.J.P., Cerli, C., Jansen, B., Kalbitz, K., Peterse, F., Renssen, H., Sachse, D., 2018. Late Holocene changes in vegetation and atmospheric circulation at Lake Uddelermeer (The Netherlands) reconstructed using lipid biomarkers and compound-specific delta D analysis. Journal of Quaternary Science 33, 100–111.
Van der Hammen, T., 1974. The pleistocene changes of vegetation and climate in tropical South America. Journal of Biogeography 1, 3–26.
Van Hengstum, P.J., Donnelly, J.P., Fall, P.L., Toomey, M.R., Albury, N.A., Kakuk, B., 2016. The intertropical convergence zone modulates intense hurricane strikes on the western North Atlantic margin. Scientific Reports 6, 21728.
Van Hengstum, P.J., Donnelly, J.P., Toomey, M.R., Albury, N.A., Lane, P., Kakuk, B., 2014. Heightened hurricane activity on the Little Bahama bank from 1350 to 1650 AD. Continental Shelf Research 86, 103–115.
van Mourik, J.M., Seijmonsbergen, A.C., Jansen, B., 2012. Geochronology of soils and landforms in cultural landscapes on aeolian sandy substrates, based on radiocarbon and optically stimulated luminescence dating (Weert, SE-Netherlands). In: Danuta, M.N. (Ed.), Radiometric Dating. In Tech, Rijeka, Croatia, pp. 75–114.
van Mourik, J.M., Wagner, T.V., De Boer, J.G., Jansen, B., 2016. The added value of biomarker analysis to the

genesis of plaggic anthrosols; the identification of stable fillings used for the production of plaggic manure. Soil 2, 299–310.

van Mourik, J.M., Jansen, B., 2013. The added value of biomarker analysis in palaeopedology; reconstruction of the vegetation during stable periods in a polycyclic drift-sand sequence in SE-Netherlands. Quaternary International 306, 14–23.

Van Royen, W., 1938. A geographical reconnaissance of the cibao of Santo Domingo. Geographical Review 28, 556–572.

Vanholme, R., Demedts, B., Morreel, K., Ralph, J., Boerjan, W., 2010. Lignin biosynthesis and structure. Plant Physiology 153, 895–905.

Vareschi, V., 1970. Flora de los Páramos. Universidad de los Andes, Ediciones del Rectorado, Mérida, Venezuela.

Vasconez, P.M., Medina, G., Hofstede, R., 2001. Los páramos del Ecuador. AbyaYala-Proyecto Páramo, Quito, Ecuador.

Vera, H., 2011. 'Dat me het goed van de ongeboornen niet mag verkoopen'; Gemene gronden in de Meijerij van Den Bosch tussen hertog en hergang 1000–2000. Uitgeverij BOXpress, Oisterwijk, The Netherlands.

Villota, A., Leon-Yanez, S., Behling, H., 2012. Vegetation and environmental dynamics in the Paramo of Jimbura region in the southeastern Ecuadorian Andes during the late Quaternary. Journal of South American Earth Sciences 40, 85–93.

Vogts, A., Moossen, H., Rommerskirchen, F., Rullkötter, J., 2009a. Distribution patterns and stable carbon isotopic composition of alkanes and alkan-1-ols from plant waxes of African rain forest and savanna C3 species. Organic Geochemistry 40, 1037–1054.

Vogts, A., Schefuß, E., Badewien, T., Rullkötter, J., 2012. n-Alkane parameters from a deep sea sediment transect off southwest Africa reflect continental vegetation and climate conditions. Organic Geochemistry 47, 109–119.

Vogts, A., Moossen, H., Rommerskirchen, F., Rullkoetter, J., 2009b. Distribution patterns and stable carbon isotopic composition of alkanes and alkan-1-ols from plant waxes of African rain forest and savanna C-3 species. Organic Geochemistry 40, 1037–1054.

Volkman, J.K., 2005. Sterols and other triterpenoids: source specificity and evolution of biosynthetic pathways. Organic Geochemistry 36, 139–159.

Weijers, J.W.H., Schouten, S., van den Donker, J.C., Hopmans, E.C., Damste, J.S.S., 2007. Environmental controls on bacterial tetraether membrane lipid distribution in soils. Geochimica et Cosmochimica Acta 71, 703–713.

Weijers, J.W.H., Wiesenberg, G.L.B., Bol, R., Hopmans, E.C., Pancost, R.D., 2010. Carbon isotopic composition of branched tetraether membrane lipids in soils suggest a rapid turnover and a heterotrophic life style of their source organism(s). Biogeosciences 7, 2959–2973.

Wille, M., Hooghiemstra, H., Hofstede, R., Fehse, J., Sevink, J., 2002. Upper forest line reconstruction in a deforested area in northern Ecuador based on pollen and vegetation analysis. Journal of Tropical Ecology 18, 409–440.

WNO (World Meteorological Organization), 2017. Dominican Republic. Country Profile Database. Retrieved from: https://www.wmo.int/cpdb/dominican-republic.

Xu, Y., Jaffé, R., 2008. Biomarker-based paleo-record of environmental change for an eutrophic, tropical freshwater lake, Lake Valencia, Venezuela. Journal of Paleolimnology 40, 179–194.

Zeng, F., Xiang, S., Zhang, K., Lu, Y., 2011. Environmental evolution recorded by lipid biomarkers from the Tawan loess-paleosol sequences on the west Chinese Loess Plateau during the late Pleistocene. Environmental Earth Sciences 64, 1951–1963.

Zhang, Z.H., Zhao, M.X., Eglinton, G., Lu, H.Y., Huang, C.Y., 2006. Leaf wax lipids as paleovegetational and paleoenvironmental proxies for the Chinese Loess Plateau over the last 170 kyr. Quaternary Science Reviews 25, 575–594.

Zheng, Y., Xie, S., Liu, X., Zhou, W., Meyers, P.A., 2009. n-alkanol ratios as proxies of paleovegetation and paleoclimate in a peat-lacustrine core in southern China since the last deglaciation. Frontiers of Earth Science in China 3, 445–451.

Zhou, W., Zheng, Y., Meyers, P.A., Jull, A.T., Xie, S., 2010. Postglacial climate-change record in biomarker lipid compositions of the Hani peat sequence, Northeastern China. Earth and Planetary Science Letters 294, 37–46.

CHAPTER

6

Pedogenic provenance analysis

J.M. van Mourik[a,*], S.J. de Vet[b], M.J. Roces Hernandez[c], D.J.G. Braekmans[d]

[a]Institute for Biodiversity and Ecosystem Dynamics (IBED), Faculty of Science, University of Amsterdam, Amsterdam, the Netherlands; [b]Naturalis Biodiversity Center, Leiden, the Netherlands; [c]Universidad Politécnica de Cartagena, Cartagena, Spain; [d]Cranfield Forensic Institute, Cranfield University, Cranfield, United Kingdom

*Corresponding author. j.m.vanmourik@uva.nl

6.1 Introduction

Soils develop in parent materials like slope regolith and sediments. Sometimes the soil archives contain special constituents that can provide relevant information about the pedogenic or geomorphological evolution of a landscape.

A traditional application of provenance analysis is the characterization of the origin of clastic sediments in delta regions, based on the association of heavy minerals. A good example is the reconstruction of the source materials for coversand and driftsand deposits in the southeast Netherlands. The association of heavy minerals extracted from such deposits is similar to the association in the underlying fluvial deposits and points to minerals occurring in weathered hard rock in the river basins of the Rhine and Meuse.

Another example of provenance analysis is the occurrence of a tephra layer in Late Glacial lake deposits on the Gasserplatz (Chapter 3). The tephra originates from an Eifel eruption and is a perfect absolute time marker in the pollen diagram of the deposits.

In the study of the soil archives of the Defensiedijk (southeast Netherlands) there were a number of complications with the interpretation of the radiocarbon ages of buried humous Ah horizons. The radiocarbon age of the oldest buried cambic Podzol in coversand was too young. Biomarker analysis showed that the composition of organic matter in the buried Ah was polluted with decomposed roots of trees, part of the vegetation on a younger overlying driftsand deposit (Chapter 5).

Also, the reconstruction of the provenance of materials, used in stables to produce manure for arable fields where plaggic Anthrosols developed, based on biomarkers is a good example of provenance analysis (Chapter 5).

In archaeology, provenance analysis of ancient ceramic materials has been the scope of various studies over the past decennia. Many of these studies employ geochemical techniques to discriminate sources of ceramic production.

https://doi.org/10.1016/B978-0-444-64108-3.00006-9

In addition, extractions of minerals for the production of ceramics has an impact on the geomorphology of the landscape.

In this chapter we discuss the provenance of extraterrestrial minerals on podzolation in chemically poor coversands (Section 6.2), the extraction of clay for the production of ceramics in Roman Time on the Gutland plateau (Luxembourg) and the impact on geomorphology (Section 6.3).

6.2 Provenance of iron in xeromorphic podzols (Maashorst region, Southeast Netherlands) recognized by scanning electron microscopy-energy-dispersive X-ray spectroscopy analysis

6.2.1 Introduction

Podzolation is the dominant soil-forming process in chemically poor sandy soils in northwestern Europe. It has been well studied how iron concentrations of Podzols are affected by translocation of active iron from eluvial to illuvial horizons and leaching to the aquifer. Iron stocks of Podzols, in contrast, have not been widely studied for comparison purposes of individual soil horizons or between soils. In this study we present an analysis of the iron stocks for a buried carbic Podzol developed in Late Glacial aeolian coversands. Chemical analyses of the active and immobile iron fractions in each of the horizons in both profiles show that more iron has been involved in the podzolation process than the amount which can be derived by chemical weathering of minerals in the overlying soil horizons. This deficit in endogenic iron therefore requires exogenic enrichment to explain the observed iron concentrations during podzolation. The contribution of exogenic iron was studied using micrometeorites as a proxy for atmospheric deposition. These particles of cosmic origins are part of a continuous flux of iron-rich materials into the Earth's atmosphere and they are deposited over time on every square metre of land surface. Their extraction from the ectorganic F horizon of initial Podzols helped to illustrate that atmospheric deposition in the form of aerosol and aeolian (e.g., Sahara) dust, micrometeorites and other hydrolysable particles is a relevant iron contribution in soil development. The requisite active iron for podzolation can therefore be derived from chemical weathering of atmospheric iron sources.

Coversands and driftsands dominate the geomorphology and soil in cultural landscapes in the southeast Netherlands (van Mourik et al., 2012). Coversands are Late Glacial aeolian deposits and driftsands are Holocene remobilized coversands, accumulated into sand covers and inland dunes. The dominant soil-forming process in these chemically poor sands is podzolization.

The iron content of coversand is very low, in the order of $2000 < Fe_2O_3 < 3000$ mg kg^{-1} (Stichting voor Bodemkartering, 1976; de Bakker, 1979) because the sand grains have survived a long history of chemical weathering and fluvial, glacial and finally aeolian transport before their final deposition in coversands. Consequently, the mineral composition is characterized by 90% quartz, 9% feldspars and 1% heavy minerals, mainly garnet, rutile and zirconium (Crommelin, 1964; Bisschops, 1973; Koster, 1978, 2010; Krook, 1997).

In spite of the low concentrations of iron-rich minerals, iron plays a prominent and visible role in primary and secondary soil formation. Several studies pointed to relatively fast podzolation in Late Holocene driftsand deposits and barrows (Chapter 3). The parent material of driftsands and barrows consists of remobilized coversands, preliminary subjected to podzolation and iron leaching until the start of landscape instability, triggered by human activities in the Late Holocene (van Mourik, 2010; Doorenbosch, 2013).

There is, however, a hiatus in the understanding of how much the parent material (i.e., the albic horizons) contributed to the iron enrichment of the underlying spodic horizons. An investigation of the iron stocks in buried xeromorphic Podzols

showed that the total amount of active and immobile iron in the horizons of these soils exceeds the amount of iron that can be released from 'fresh' coversand by chemical weathering (van Mourik and de Vet, 2015). It was suggested that, beside the amount of iron that could be released from iron-containing minerals in coversand, a secondary source of iron must have been active in the Holocene process of podzolation, which explains the total iron stocks in these Podzols. The idea of an exogenic source of iron was inspired by the observation of metallic micrometeorites observed in the Greenland ice cores. The southeast Netherlands is situated in a climatic zone where we may also expect precipitation of micrometeorites.

6.2.1.1 *Case study of profile Herperduin*

For the determination of the iron stocks we selected a polycyclic soil profile in the driftsand landscape HD (Maashorst region in the southeast Netherlands; location Fig. 6.2.1; profile Fig. 6.2.2). The soil was classified as an Arenosol (in driftsands) overlying a xeromorphic carbic Podzol in coversand (ISRIC/FAO, 2006). Sand drifting during the 11th–13th centuries caused by deforestation was responsible for the burial of the Podzol. Sand drifting stabilized during the 19th–20th centuries and a Mormoder humus form (Green et al., 1993) developed.

The buried Podzol is xeromorphic (groundwater table was >150 cm during active podzolation), does not show evidence of severe surface erosion and is well protected from agricultural and industrial pollution during the last few centuries. In summary (van Mourik et al., 2012), soil development in coversand started around 10,000 BP with the formation of an Umbrisol, followed by a period from 9000 to 4000 BP with the formation of Umbric Podzols. During this period, iron was released by hydrolysis and partially translocated from eluvial (E) to illuvial (Bs) horizons and partially leached to the aquifer. However,

FIGURE 6.2.1 Location of profile Herperduin (HD) in the Maashorst area in the southeast Netherlands (Google Earth).

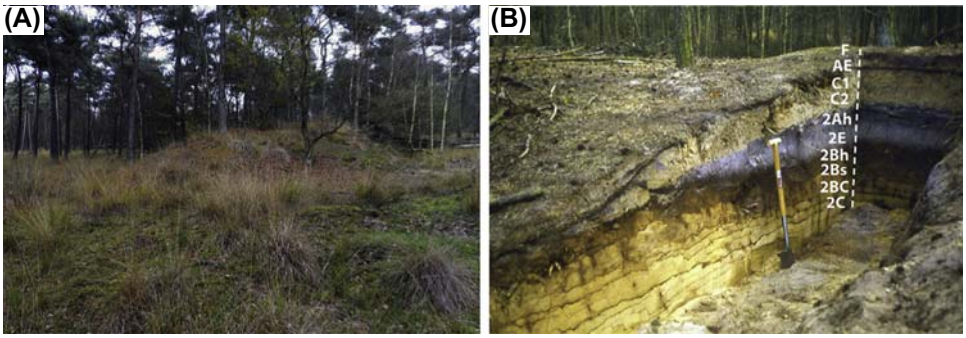

FIGURE 6.2.2 The driftsand landscape at Herperduin is characterized by small plateau dunes (A), presently stabilized under planted pine forest. A profile pit in a plateau dune (B) shows the main soil horizons of the Arenosol with Mormoder humus form in driftsand overlying a carbic Podzol in coversand.

the intensity of hydrolysis in weak acid Umbric Podzols is relatively low. Between 3500 BP and AD 1200 the vegetation degraded from deciduous forest into heath, soil acidification accelerated and the intensity of hydrolysis increased. The active podzolation in coversand stopped after burial by reactivated sand drifting due to the deforestation during the 11th–13th centuries in the immediate surroundings (Vera, 2011). Most of the exposed Podzols in the Maashorst region have been seriously degraded by local land use. In particular, sods digging on the *Calluna* heath since the middle of the 18th century was responsible for a reduction in the thickness of the Ah and E horizons. Buried Podzols in these cultural landscapes can therefore serve as valuable archives of the geoheritage and this makes them crucial for geoecological research.

After stabilization by afforestation, mainly with Scots pines (*Pinus sylvestris*) between 1900 and 1920, initial stages of Podzols, in particular Mormoders, started to develop in the stabilized driftsands. This is well expressed in pollen diagram HD (Fig. 6.2.3).

Zone 1 shows the development of the Mormoder humus form under (planted) pine forest. The pollen concentrations are high. The F horizon consists of decomposing pine needles and grass roots. The thin sections show how blown-in mineral grains are embedded in the organic matrix. Most of these minerals are quartz grains related to sand drifting in the surroundings, but also some minerals cannot be ascribed to local driftsand deposits.

Zone 2 is characterized by high percentages of herbal pollen and low percentages of arboreal pollen. The pollen concentrations are low but rather constant, indicating a syn-sedimentary pollen content in the driftsand deposits. The contrast of the pollen composition with the underlying zone 3 points to sand drifting after deforestation in the surroundings of the former Herper heath.

Zone 3 is characterized by high percentages of arboreal pollen. However, the percentage of Ericaceae indicates the presence of heath in the local vegetation and the Herper heath, and consequently the arboreal pollen originates from trees in the surroundings (see also Chapter 2, Section 2.5). The pollen density curve shows a decrease in the pollen concentrations from the 2Ah horizon to the top of the 2B horizon, indicating pollen infiltration.

Based on the pollen diagram we can conclude that the buried carbic Podzol developed under the heath. Relics of previous phases in soil development are not observable. The Mormoder, developed in stabilized driftsand, is a good

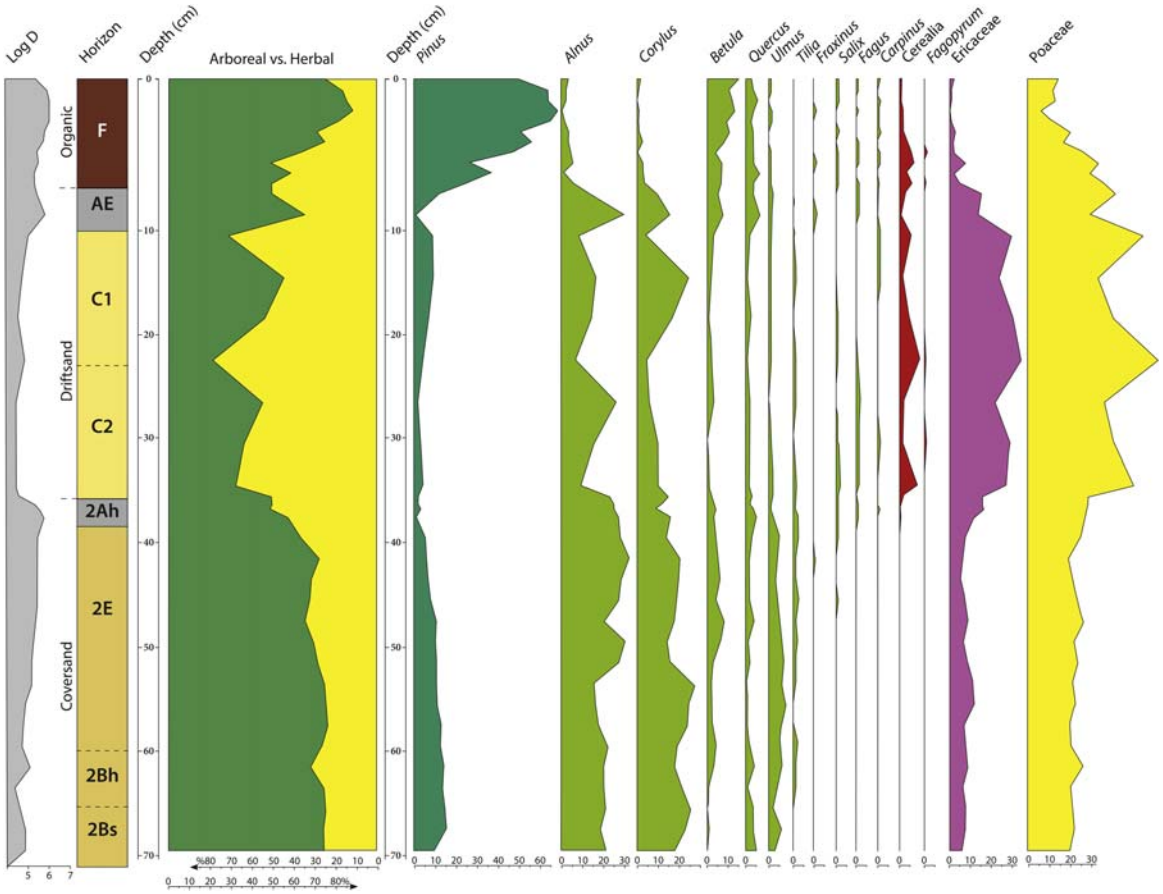

FIGURE 6.2.3 Pollen diagram Herperduin. *After van Mourik, J.M., Odé, B., 2010. Het Herperduin. Geografisch Tijdschrift XXIV, 160–167.*

record of the blowing-in of terrestrial and extra-terrestrial mineral grains during plantation of the pine trees around AD 1920.

6.2.2 Determination of iron stocks in the buried podzol

Determination of iron stocks is based on the distinction of three different iron fractions in the horizons of podzolic soils.

First, the *total iron* concentration in the various soil horizons was determined using the destruction method in HF/H_2SO_4 of Jackson (1958). This concentration represents the sum of iron present in quartz minerals and the total amount of active iron.

Second, the *active iron* fraction includes the iron present in organic complexes and in non-crystalline and crystalline hydrous oxides. The active iron fraction was determined using the citrate-dithionite extraction method of Holmgren (1967), an optimal and highly effective method for the extraction of active iron from soil samples (Ryan and Gschwend, 1991).

Third, the *immobile iron* fraction (present in the crystalline lattice of specific mineral grains such

as feldspars, garnet, rutile and zirconium) can be estimated by subtracting the active iron from the total iron content. This fraction represents the iron not directly available to soil-forming processes and requires substantial chemical weathering of mineral grains for it to be released. In addition to the quantifying of these three iron fractions inside the soil, several descriptive soil parameters have been determined and include the percentage of organic carbon measured by loss of ignition, pH in 0.01 M $CaCl_2$ and the bulk density based on standardized pF rings of 100 cm^3.

The concentrations and stocks of active and immobile iron in the profiles HD are summarized in the Table 6.2.1 (after van Mourik and de Vet, 2015).

Iron, released from mineral grains (e.g., feldspars) by hydrolysis, is the main source of active iron in soils and is available for uptake by vegetation for translocation from the (albic) eluvial to the (spodic) illuviation horizon or can leave the system through leaching with infiltrating rainwater. In many soil systems, active iron is present in organic complexes and in the form of non-crystalline and crystalline hydrous oxides (Scheffer et al., 1979). Studies of soil formation in fluvial sediments have demonstrated that during the Early and Middle Holocene the total concentration of active iron in the soil increased due to iron released by chemical weathering (Alexander, 1974). In contrast, concentrations of active iron during the Late Holocene were found to decrease as a consequence of leaching attributed to soil acidification. In the Maashorst region too, soil development in aeolian sand deposits must have progressed along a comparable developmental pattern. When considering the geographic location of the studied profiles on well-drained coversand ridges, we can thus exclude effects of lateral (upward) iron transport as a source of increased iron, in particular from iron-rich groundwater. The overall translocation of iron in the studied buried Podzols can therefore be characterized as a net downward flux.

The intensity of chemical weathering in the buried Podzols must have been low in the Preboreal, moderate between 9000 and 3500 BP, maximal between 3500 BP and AD 1200 and minimal after burial under driftsand. The concentrations of immobile iron were found to be low in the 2Ah, 2E and 2Bh horizons of the buried Podzols, horizons with a relatively low bulk density. These low values indicate a loss of hydrolysable mineral grains, but at the same time they reflect a rather constant volume of these horizons. The released iron can explain the high concentrations (and stocks) of active iron in the underlying Bs and BC horizons. The total iron concentration of the 2Bs, BC and 2C horizons of the buried Palaeopodzols HD and BBW are rather similar to the concentration found in non-buried xeromorphic Podzols (de Bakker, 1979). However, the top horizons (A, E) of non-buried Podzols have been seriously damaged by ploughing, fertilizing and erosion and are consequently unreliable for the comparison of iron losses of the topsoil and iron precipitation in the spodic Bs and BC horizons.

The Palaeopodzols became inactive after burial under the driftsand deposits. This marks the transition to a new and younger soil sequence, which developed in the driftsand deposits. Sand drifting was an active geomorphological process from AD 1200 to AD 1900. After their recent stabilization, secondary podzolation proceeded for almost 100 years until the present. The source material of these driftsand deposits is derived from previously weathered coversands and is thus composed of the same parent material in which the Palaeopodzols developed. Consequently, the (potential) concentration of immobile iron is similar or somewhat lower than in coversands. Comparison of the concentration of immobile iron in 'fresh' coversand samples (2000–3000 mg kg^{-1}) with the concentration in F horizons of Mormoders shows drastically increased concentrations (10,974 and 19,298 mg kg^{-1}) of immobile iron.

TABLE 6.2.1 Soil properties and Fe stocks of the Herperduin profile per square metre of land surface.

Horizon	Depth (cm)	Volume (m^3)	pH ($CaCl_2$)	Carbon[a] (%)	Bulk density (kg m^{-3})	Active Fe (Fe_2O_3 g kg^{-1})	Immobile Fe (Fe_2O_3 g kg^{-1})	Fe stocks (g per horizon) Active/immobile
F	0–10	0.10	3.45	37.1	290	4.165	19.298	120.8/559.6
AE	10–20	0.10	3.43	0.85	1480	1.708	2.735	252.8/404.8
C1	20–25	0.05	3.63	0.43	1600	1.652	2.590	132.2/207.2
C2	25–40	0.15	4.56	0.11	1530	0.790	2.712	181.3/662.4
2Ah	40–41	0.01	3.88	2.67	1440	0.912	0.131	13.1/1.9
2E1	41–50	0.09	3.52	0.52	1480	0.446	0.734	59.4/97.8
2E2	50–60	0.10	4.02	0.57	1450	0.415	0.694	60.2/21.3
2Bh1	60–65	0.05	3.59	2.09	1330	0.993	0.147	66.0/9.8
2Bh2	65–70	0.05	4.12	3.70	1300	2.425	0.064	159.4/4.2
2Bs1	70–75	0.05	4.23	2.10	1290	14.184	1.278	914.9/82.4
2Bs2	75–85	0.10	4.42	0.78	1280	3.594	2.198	460.0/281.3
2BC	85–100	0.15	4.57	0.34	1420	1.326	2.532	282.4/539.3
2C	>100	n.d.	4.24	0.22	1610	1.035	2.941	n.d. n.d.
Σ 2AEB		0.60						2015.4/1038.0
Original[b]		0.60			~1500		~3.000	~2700.0

[a] *Based on loss of ignition.*
[b] *Values based on expected immobile iron concentrations in unweathered coversands shortly after deposition (Stichting voor Bodemkartering, 1976).*

Evaluation of the observed iron distribution in the investigated Palaeopodzols is subject to two uncertainties. First, the amount of leached active iron to the aquifer during the period of active soil development is unknown; second, some (secondary) illuviation of active iron from the active Mormoder to the Palaeopodzol cannot be excluded. Leaching of iron means an additional amount of (lost) active iron; illuviation from the initial soil in driftsand cannot be substantial in just a century of Mormoder development.

In appreciation of these difficulties we find a notable difference in the total stocks of active and immobile iron present in the 2A, 2E and 2B horizons of the buried Podzols, which exceed the total potential stock of immobile iron that may have been present in 'fresh' coversand deposit before chemical weathering and soil development could have released the iron from these mineral grains. As noted earlier, enrichment with iron supplied by groundwater is excluded as a contributing factor because the buried Podzols are found on well-drained ridges.

Active podzolation stopped in the Palaeopodzols after burial by overriding coversand. Juvenile soil-forming processes in the superposing driftsand play a negligible role in post-burial iron illuviation. Especially, the high iron concentrations of the spodic (Bs) horizons cannot be explained satisfactorily without additional sources of iron added to the soil system.

6.2.3 The identification of micrometeorites embedded in mormoders

The inhibited decomposition of organic matter below *Pinus sylvestris* (HD) and *Quercus robur* (BBW) has led to the formation of humus forms on top of the studied driftsand deposits. Consequently, these ectorganic horizons are unique soil archives that provide useful records on decadal and centennial timespans of potential exogenic iron influx in the form of atmospheric deposition. Notable atmospheric iron sources include aerosol/aeolian dust (frequent Saharan dust events, although generally low in oxides and hydroxides of iron; Caquineau et al., 1998; Journet et al., 2008) and the steady influx of micrometeorites (also known as *cosmic spherules*; Kerridge, 1970; Brownlee, 1985; Taylor et al., 1998, 2000; Maurette, 1991, 2006). Their numbers are dominated by spheruled, iron-rich particles which can provide a continuous supply of iron to the soil and the podzolation process. Global deposition rates of micrometeorites range in the order of annual 2.35 g km^{-2} day^{-1} (Stankowski et al., 2006). Deposition of aerosol/aeolian iron in the North Sea has been estimated at 238 g km^{-2} day^{-1} (GESAMP, 1989). The relative ratio of 1:100 therefore makes micrometeorites a suitable proxy for detecting iron sources arriving in the form of atmospheric deposition.

Micrometeorites are characterized by a black metallic lustre (from magnetite) and vary from 100 to 500 μm in diameter, with typical densities of 3.00–5.8 g cm^{-3} (Murell et al., 1980; Maurette et al., 1987; Taylor et al., 2000; Kearsley et al., 2007; Sauvet et al., 2009). Meteoritic materials also have a unique element composition due to decay of the cosmic radioisotope ^{26}Al to the stable ^{26}Mg. The resulting Mg–Si–Fe ratios of these grains provide a useful discriminative proxy for distinguishing them from terrestrial materials (Taylor et al., 2000; Genge et al., 2005; Gounelle et al., 2009).

Because micrometeorites are more easily identifiable in the ectorganic horizon as atmospherically deposited grains than aerosol dust particles (Caquineau et al., 1998; Journet et al., 2008), we targeted micrometeorites in our analyses to establish if exogenic iron is indeed arriving in the form of atmospheric deposition. Of course, micrometeorites could have been deposited during the whole Holocene on the land surface. In contrast to quartz grains, the metallic micrometeorites are subjected to fast chemical weathering. But we may expect that we can find embedded grains in the not more than 100-year-old Mormoders (Fig. 6.2.4).

FIGURE 6.2.4 Scan of the thin section of the Mormoder, developed in driftsdand, profile Herperduin (45/85 mm).

First, we separated the mineral grains from the organic fraction by drying and sieving and then we concentrated the possible micrometeorites by heavy liquid mineral separation using diiodomethane in an overflow centrifuge (IJlst, 1973). Further refinement of the remaining minerals with grain densities $>3.08\ g\ cm^{-3}$ was achieved in a manual microscope selection based on their ferromagnetic or paramagnetic properties, optical traits and well-rounded to spheruled particle morphologies. The final selection of grains (Fig. 6.2.5) was embedded in epoxy and polished to obtain a fresh cross-section (Fig. 6.2.6) for measuring the elemental composition akin to the approach used by Taylor et al. (1998, 2000).

The chemical characterization of the sectioned grains was performed with a scanning electron microscope (Hitachi S-3500N) coupled to an energy dispersive X-ray detector (Bruker AXS x-Flash Detector 5010, Berlin, Germany). Scanning electron microscopy images of the samples were captured at different magnifications in backscattering electron mode and a working distance of 15 mm. The accelerating voltage and emission current were 15 kV and 72 μA, respectively. Prior to detailed analyses, element mapping using energy-dispersive X-ray spectroscopy (EDX) was carried out with Bruker AXS Microanalysis using EDX which allowed the measurement of the elementary composition of the sample surface of a selected region of interest to produce a preselection of iron-rich particles. For this mapping and semi-quantitative element analyses, EDX spectra were recorded and analysed using the Esprit 1.9.4.3448 software suite. Figs. 6.2.7 and 6.2.8 illustrate this working method.

6.2.4 Sources of the exogenic iron influx

Spheruled, iron-rich micrometeorites are traditionally studied in Antarctic and Arctic environments where their separation from the ice matrix is easily facilitated by the melting of ice (e.g., Murell et al., 1980; Maurette et al., 1987; Taylor et al., 2000; Kearsley et al., 2007; Rochette et al., 2008; Sauvet et al., 2009). However, various studies have also targeted the deposition of these particles in other sedimentary regimes such as deserts and beaches (Freddrikson and Gowdy, 1983; Marvin and Einaudi, 1967), Pacific clays in marine sediments (Murell et al., 1980) and in Mediterranean sediment cores with notably enriched layers of micrometeorites (Cita et al., 1977). Of interest to the study presented here is the work of Stankowski et al. (2006) who illustrated that organic accumulation environments (i.e., peat) can indeed retain detectable records of the atmospheric deposition of micrometeorites, in this case

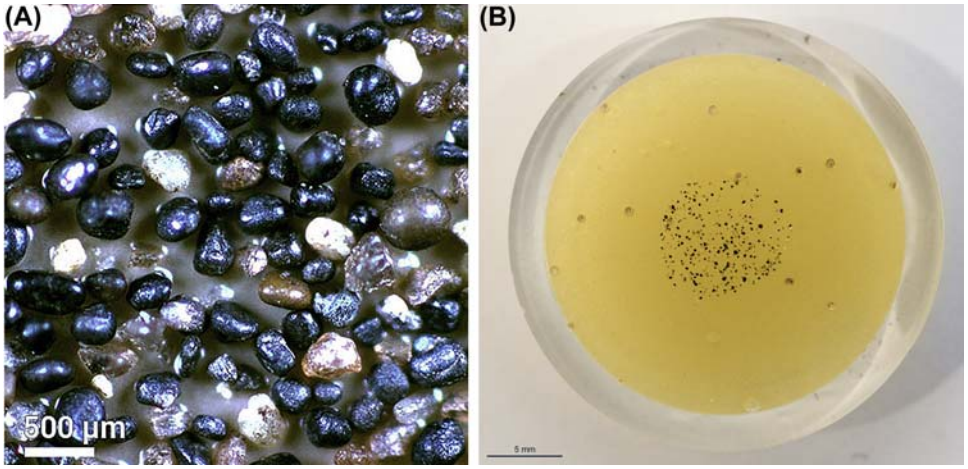

FIGURE 6.2.5 (A) Selected mineral grains after drying, sieving and heavy liquid separation. (B) Selected mineral grains embedded in epoxy and polished.

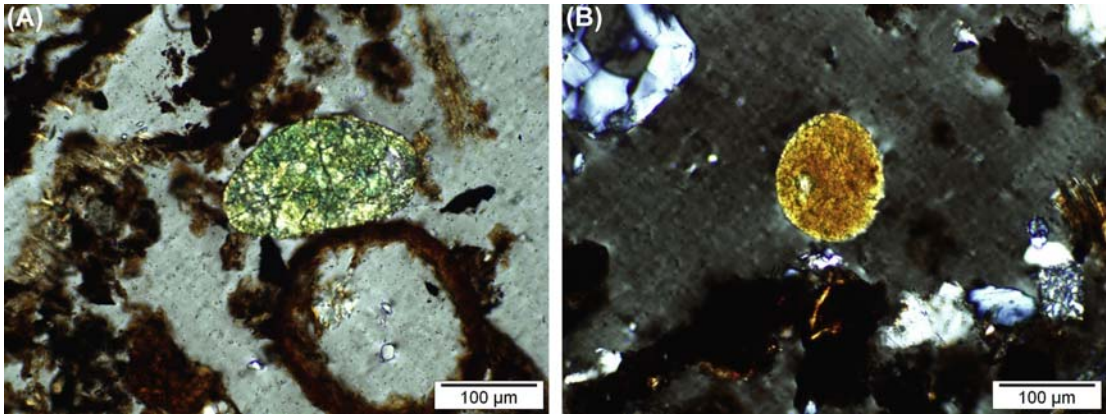

FIGURE 6.2.6 (A) Micrograph of a blown-in exotic olivine mineral in the organic matrix of the F horizon (semi-crossed polarization filters, transmitted light). (B) Micrograph of a blown-in exotic metallic grain in the organic matrix of the F horizon (semi-crossed polarization filters, reflected light).

related to a local iron meteorite impact. While the addition of meteoritic materials to soils may seem exotic, their abundance and deposition on land surfaces has been widely established and studied by various scientific disciplines. However, micrometeorites have never been linked directly to soil or soil development, even though every square metre of the land surface is subject to a continuous influx of micrometeorites. In Fig. 6.2.9 we show that after a strenuous refinement procedure, particles with physicomechanical and compositional properties of micrometeorites can be extracted from the soil. The presence of these grains in the accumulation environment of the ectorganic horizon underlines that exogenic iron via atmospheric deposition delivers iron to the soil system. Using the conservative compositions field (Fig. 6.2.9), the clustering of meteoritic grains

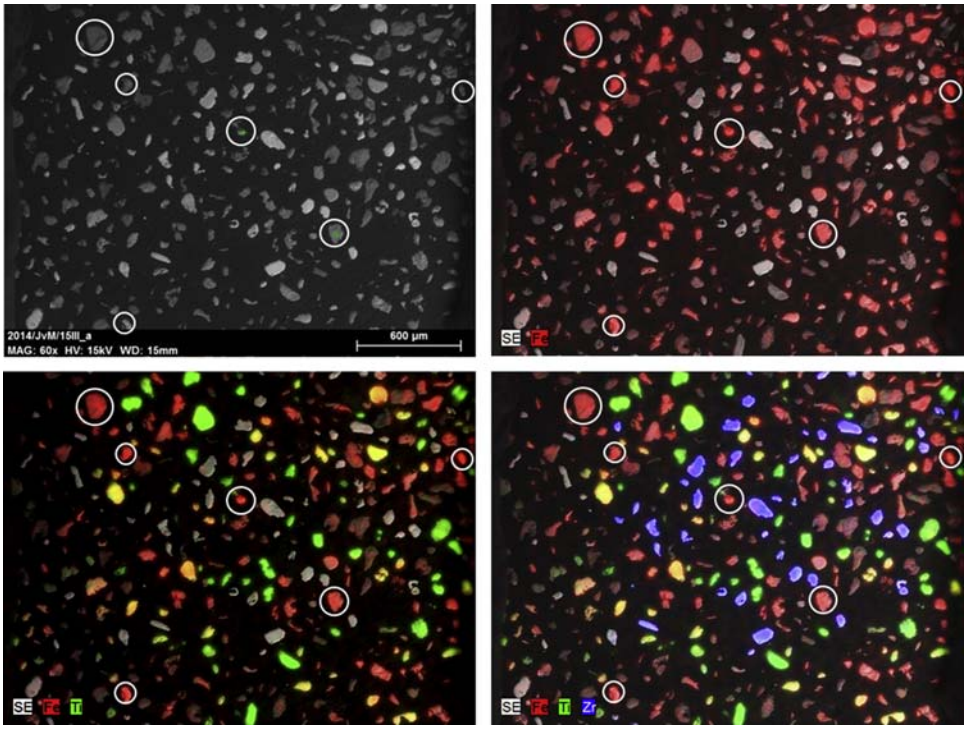

FIGURE 6.2.7 By means of a surface mapping of the elements of interest, mainly iron, we could select, prior to performing the elemental semi-quantitative analysis of X-ray dispersive energies (EDX), the particles whose iron content 'apparently' was high. Subsequently, the selected particles were analysed by EDX.

and the terrestrial grains are found in a ratio of 5: 127.

Obviously, not all grains obtained by the refinement procedures were studied, but the ratio is roughly in line with the expected ratio of micrometeorites and aerosol/aeolian dust. Frontal showers in the northwestern European weather system can provide an effective mechanism for washing such airborne particles out of the atmosphere, which promotes the addition of these grains as iron source to these sandy soils. Concentrated deposition of airborne dust through precipitation may thus make the iron deposition strongly dependent on climatic zones. Tentative results from one of our pilot experiments, where atmospheric deposition was collected to study potential meteorological concentration mechanisms, indeed showed a good correlation of deposition rates of airborne particles with local precipitation patterns. We therefore postulate the idea that for areas with an annual rain surplus the humid and acid microenvironment of the ectorganic horizons can promote a quick release and leaching of iron derived from atmospheric deposition. The observed differences in iron stocks of the studied Podzols may be well explained by this mechanism. The influx from iron, in part from terrestrial (aerosol/aeolian) and to a smaller extent by micrometeoritic, grains therefore plays a significant role in soil development, particularly in the northwestern European coversand district.

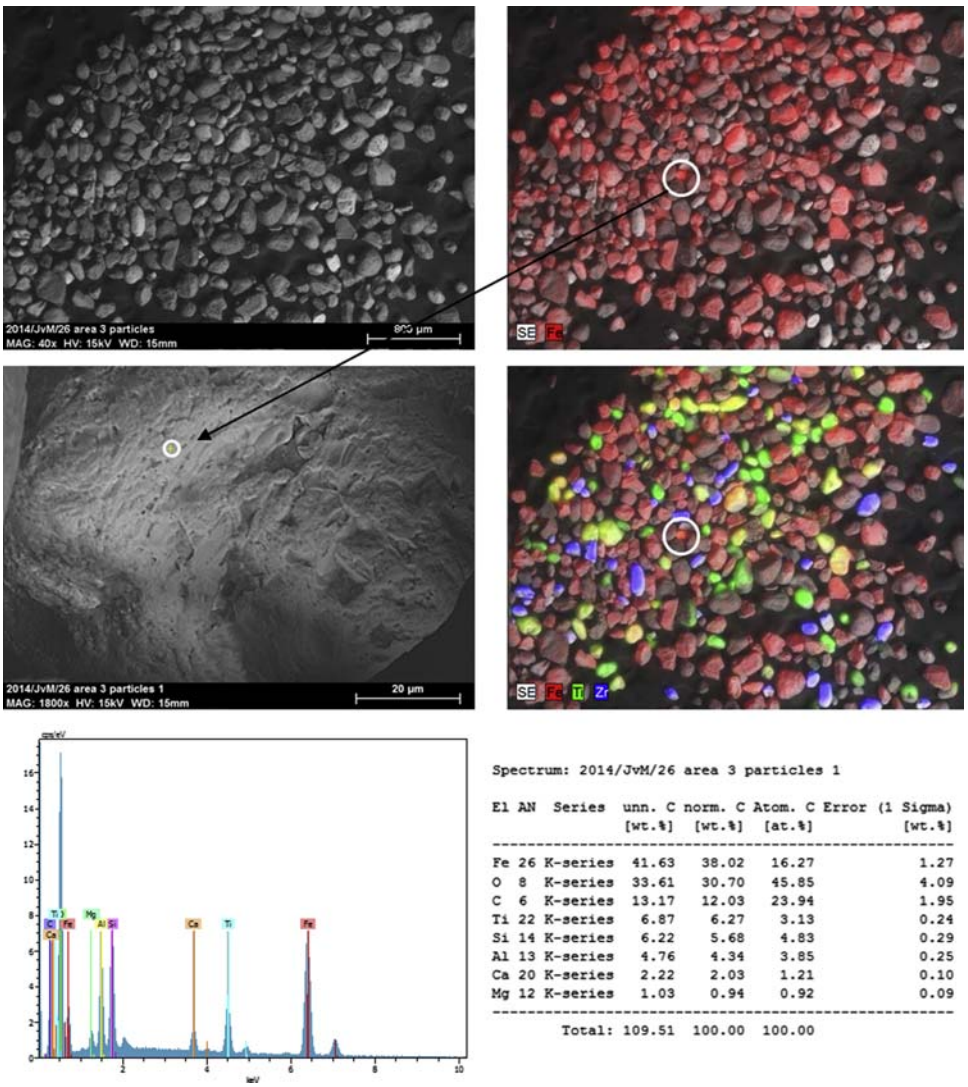

FIGURE 6.2.8 Analysis of the particles selected by surface mapping contained iron but not in all cases was iron presented as the major element. In the particles with major iron content, the percentage varied between 30.83% wt and 54.24% wt. In all cases there was also carbon, oxygen, titanium, sometimes some magnesium and other minor elements such as aluminium, silicon or calcium.

6.2.5 Conclusions

- Iron stocks in podzolic soils have not been widely studied or compared between soils or individual soil horizons. In our study we have provide evidence for a deficit in endogenic iron in buried Podzols developed in coversands in northwestern Europe.
- A detailed comparison of iron fractions in buried Podzols shows that more iron is present in the spodic horizons than can be explained by illuviation of released endogenic

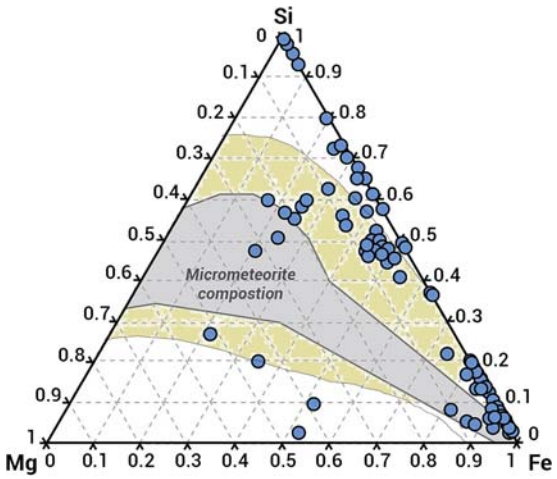

FIGURE 6.2.9 Ternary plot of the high-density minerals from both field sites. The grey areas enclose the compositional field commonly used for identifying micrometeorites, due to their different elemental composition as a result of the decay of radionuclide ^{26}Al to ^{26}Mg in unmetamorphosed materials from space. The conservative compositional field (dark grey) is from Taylor et al. (2000) and Sauvet et al. (2009), while the broader field (light grey) was used by Genge et al. (2005).

iron through chemical weathering of mineral grains from the overlying eluviation horizons. These buried Podzols are groundwater limited and therefore require an external influx via atmospheric deposition in the absence of upward or lateral migration of iron with groundwater.

- We have targeted the deposition of iron-rich micrometeorites as a proxy for exogenic iron influxes because these grains have characteristic traits that allow separation from the bulk of the ectorganic horizon, which tends to accumulate atmospheric deposition.
- These micrometeoritic grains and other hydrolysable iron-rich particles are the likely iron sources that can chemically weather in the humid and acidic soil environment and contribute to the required mobile iron fraction of the soil.

6.3 The provenance of clay for the production of Roman ceramics on the Gutland plateau (Luxembourg)

6.3.1 Introduction

The genesis of mardels, small closed depressions (diameter 10–50 m; depth 1–3 m), has been the subject of much research inside and outside Luxembourg. Poeteray et al. (1984) ascribed the genesis of the majority of the mardels on Keuper marlstone in Luxembourg to subsurface solution of gypsum inclusions, followed by collapse and subsidence of the overlying beds. In Lorraine, Etienne et al. (2011) suggested that the investigated mardels were formed in a relatively short time period between the end of the Iron Age and the Roman Period in a partially deforested, open landscape. Most likely they were manufactured for several possible purposes like clay extraction, soil marling, cattle troughs or fish ponds, but the exact purpose of the diggings remained uncertain. In the Luxembourger mardels (Slotboom and van Mourik, 2015) as well as in those in Lorraine (Etienne et al., 2011) the sedimentary infills could be palynologically dated as post-Roman and consequently the majority of these mardels raised as Gallo-Roman excavations with a post-Roman filling.

Soil research made clear that the origin of the clay trapped in mardels was (and still is) related to the soil processes in weathered marlstone under deciduous forests. The topsoil has a high bioactivity, and dispersed clay in the droppings from earthworms and moles is subjected to soil erosion (Cammeraat, 2006; Cammeraat and Kooijman, 2009). A fraction of the clay, moving downslope to the valleys, is trapped in mardels.

Out of six mardel clusters on the Gutland plateau, one mardel and the surrounding soil was selected for sampling (Fig. 6.3.1). The pollen diagrams of six cores were rather similar and palynologically dates as post-Roman (van

Mourik and Slotboom, 2018, Chapter 2.4). The results of the granular analysis are presented in Table 6.1.1.

Dating of mardel sediments has to be based on palynological time markers because reliable radiocarbon dating is not possible due to the scarcity of organic macro remains and furthermore matter included in colluvial mardel deposits originates from upslope-eroded soil material. Consequently, the results of radiocarbon dating of colluvial deposits will overestimate the real age of the sediments.

Previous research made clear that the development of mardels started with small depressions related to crevasses in the Luxembourger sandstone and subsurface solution of gypsum lenses in the Keuper marl. The depressions are sediment traps and the sediment fillings of mardels on the marls are clayey. Probably, the Romans extracted the clay and enlarged the mardels to quarries. After Roman times the sedimentation of clayey colluvium restarted and resulted in the post-Roman fillings.

Of the suggested applications of mardels by the Romans (Etienne et al., 1911), clay extraction, soil marling, cattle troughs or fish ponds, only clay extraction seems to be realistic for the Gutland plateau. Soil marling of arable fields on the marls is not necessary; cattle troughs and fish ponds are unlikely in the forests on the plateau, considering the many moist valleys in close vicinity.

If the Romans really created mardels by clay extraction, the clay was probably used for the production of ceramics like pottery and tiles. An inventory showed that on the Gutland plateau only two sites were available to collect ceramics in the close vicinity of infilled mardels.

To the west of the Biischtert forest near Michelbouch was the archaeological excavation of a Roman settlement, close to a cluster of mardels in the forest (Figs. 6.3.2 and 6.3.3). The archaeological excavation is documented by Jacoby (2011) and ceramic fragments (Figs. 6.3.6) were provided for analysis. The Michelbouch mardel is located in the Biischtert″ forest (49°48′58″N/6°01′55″E; 357 m above sea level). The forest soil was classified as a stagnic Alisol (clayic) and the soil in the mardel filling as a Stagnosol (clayic, colluvic) (ISRIC-FAO, 2006). The mardel sediments were palynologically dated as post-Roman (van Mourik and Slotboom, 2018).

Close to Savelborn a mardel cluster is situated in the Oussert forest and Kalefeld (Figs. 6.3.4 and 6.3.5). On the archaeological map a Roman tile-works is indicated and here fragments of Roman tiles (Fig. 6.3.7) were sampled for analysis. Mardel Kalefeld, close to the location of the Roman tile-works, is situated in Oustert/Kalefeld (49°48′ 38″N/6°14′40″E; 384 m above sea level) on the Strassen marls in pasture on a smooth slope (3%) close to the local watershed. The Kalefeld pasture was already indicated on the Ferraris map, AD 1775. The properties of the Kalefeld core are rather similar to the Michelbouch core. The colluvial clay layers were deposited under moist conditions on a truncated surface in the Strassen marls.

6.3.2 Aanalysis Provenance through wavelength dispersive-X-ray fluorescence analysis

Provenance analysis of ancient ceramic materials has been the scope of extensive research over the past decennia. Multiple studies employ various geochemical techniques to discriminate sources of ceramic production. It is generally accepted that clay raw materials utilized in the production of ceramic materials have a similar chemical composition which can be used to determine provenance (Hein et al., 2004; Braekmans et al., 2011; Degryse and Braekmans, 2014).

As an analytical technique, X-ray fluorescence (XRF) analysis has played a major role in sourcing ancient ceramics and determining relations with various original clay resources. XRF analysis utilizes the emission of characteristic

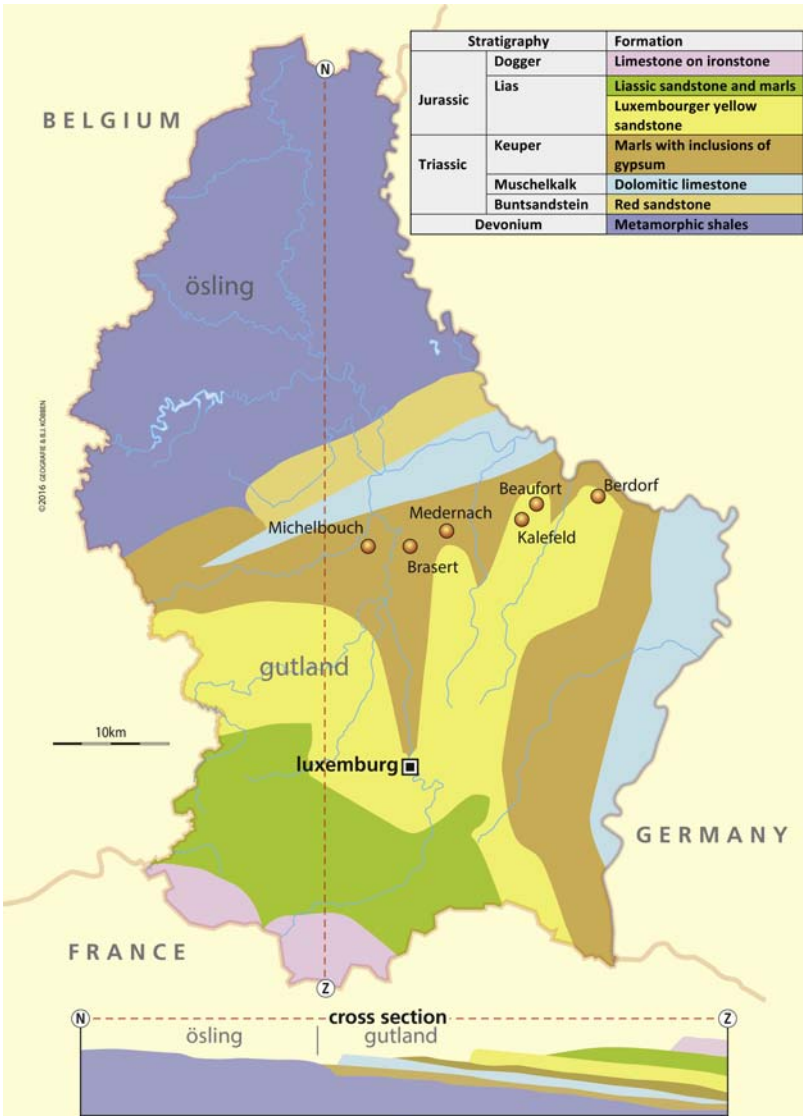

FIGURE 6.3.1 Simplified geological map of Luxembourg with the location of the six sampled mardels.

'secondary' (or fluorescent) X-rays from a material that has been excited by bombarding with high-energy X-rays. The emitted radiation has energies characteristic of the atoms present. The phenomenon is frequently applied to elemental analysis of solids, powders or liquids (Schackley, 2011).

To investigate if the Romans used clay extracted from mardels or the surrounding soil for their ceramic industry we applied wavelength dispersive (WD)-XRF analysis. In this study, 57 samples have been analyzed for their chemical composition: 22 soil samples (Michelbouch, Brasert, Kalefeld, Medernach, Berdorf

FIGURE 6.3.2 Fragment of the topographic map 1:50,000 (Redange, 1955) with the location of the archaeological site (*red arrow*) and the mardels in the Biischtert forest (the sampled mardel is indicated with the *blue arrow*).

and Beaufort), 23 mardel samples (Michelbouch, Kalefeld, Brasert, Medernach, Berdorf and Beaufort) and 12 pieces of ceramics (Biischtert, Kalefeld). Ceramic materials are derived from an Early Roman site located at Biischtert, close to the Michelbouch mardel (Jacoby, 2011), as well as from a supposedly Roman (brick) production facility at Kalefeld. All selected pottery fragments represent only one macroscopic but very common fabric: a frequently attested fine-grained common ware, of apparently local production, for likely jug and jar functionalities. The fabric associated with brick production at Kalefeld is consistently coarser than the pottery fragments, especially regarding the sporadic presence of millimetre-sized particles of lime(-stone). In general the brick fabric has been more thoroughly oxidized compared to the more brown-coloured pottery pieces. Both mardel and soil samples are derived from a small archaeological survey of the area conducted in 2015. All analysed samples were powdered and oven dried at low temperature (70°C) for at least 24 h.

FIGURE 6.3.3 Picture of the sampled mardel in the Biischtert forest. The sample location is indicated with the *red arrow*.

Bulk compositional measurements through WD-XRF analysis were conducted at the X-ray

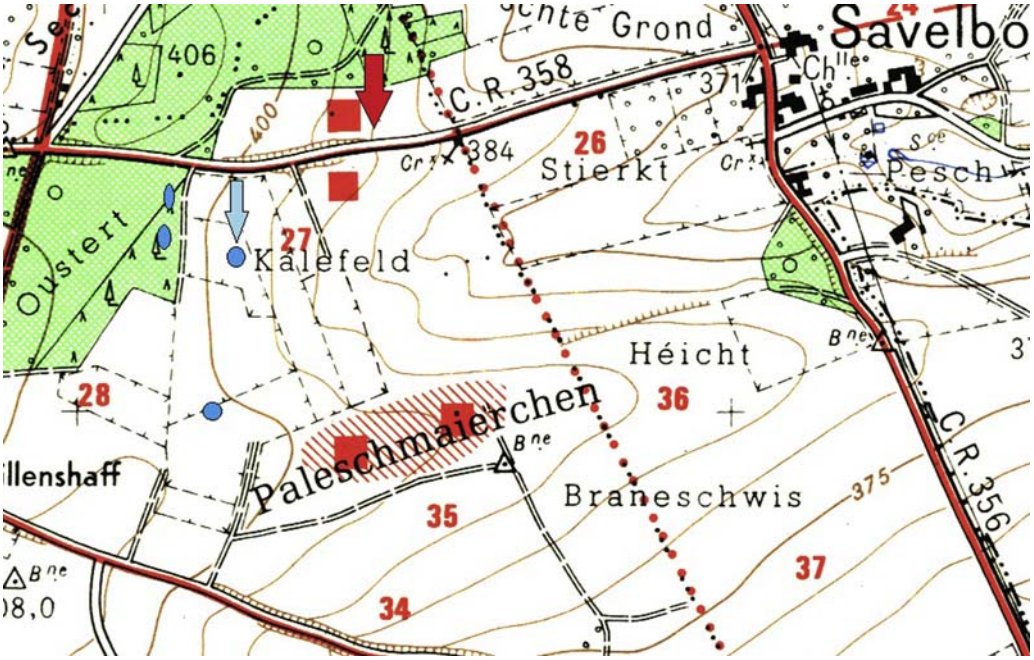

FIGURE 6.3.4 Fragment of the Carte archeologique du Grand-Duche de Luxembourg(1:20,000), Feuille 12, Larochette (legend: Folmer and Krier, 1980) with the mardel cluster Kalefeld/Oustert; the location of the sampled mardel is indicated with the *blue arrow*); the location of the findings of the fragment of the Roman tile-works is indicated with the *red arrow*.

FIGURE 6.3.5 Picture of the sampled mardel Kalefelt (October 2014); sample location indicated with the *red arrow*.

FIGURE 6.3.6 Fragments of Roman pottery collected at the Biischtert excavation close to mardel Biischtert (length of the bar is 1 cm).

FIGURE 6.3.7 Fragments of tiles produced in the relics of the Roman tile-works close to mardel Kalefeld (length of the bar is 1 cm).

facilities of the Materials Science and Engineering Department, Delft University of Technology. The instrumentation used was a Panalytical Axios Max sequential WD-XRF spectrometer and data evaluation was done with SuperQ5.0i/Omnian software. The system is equipped with an Rh anode featuring 4.0 kW operating power, 160 mA tube current and 60 kV excitation. Powder (2 g) was pressed into a tablet with binder (H_3BO_3) and measured in a vacuum. Data were collected for the following major elements: SiO_2, Al_2O_3, Fe_2O_3, MgO, K_2O, TiO_2, CaO, P_2O_5, Na_2O and MnO (expressed as wt%), and minor elements Ba, Zn, Zr, S, Cr, Rb, Ni, Pb, Sr, Nb, Ce, Y and Cu (expressed as parts per million, ppm). Statistical procedures and analyses were conducted in a Statistica software package (version 8.0).

6.3.3 Textures of mardel cores and surrounding soil samples

Table 6.3.1 presents the results of the grain size analyses of samples from mardel colluvium and the surrounding soils. The pH values range from weak acid to neutral, the percentages of organic carbon of the soil samples are relatively low (loss on ignition (LOI) ≈ 2) and of the mardel samples higher (LOI from 1.9 to 10.9). The grain size distributions show the increase of the clay fraction of mardel clay compared with the Bg horizon of the surrounding soils. This reflects the effect of clay dispersion in the soil animal droppings and soil erosion (Cammeraat and Kooijman, 2009). The highest clay percentages were found in the sedimentary infills of the mardels on the Keuper marls.

6.3.4 Geochemical analyses of samples of mardel cores, surrounding soils and ceramic fragments

Chemical analysis by WD-XRF analysis is used as a main technique for defining the potential provenance of the ceramic materials and their consistency with mardel clays (Table 6.3.2 presents the chemical results of all 57 samples). Soils (S samples) and mardels (M samples) are derived from the sites under study: Beaufort (BEAU), Kalefeld (KAL), Medernach (MED), Michelbouch (MICH), Brasert (BRAS) and Berdorf (BER).

The abundances of major and trace elements are fairly consistent for most elements in the ceramic materials. The ceramics attributed to Kalefeld have, however, a systematically higher carbonate content (up to ~16 wt%) and significantly lower MgO, K_2O and Fe_2O_3 values. All analyses from the same locale, i.e., both soil and mardel, are also expected to show similar geochemical values. Nevertheless, consistent variation is present between the uniform ceramic materials and some mardel and soil samples. The compositional analyses from the mardels at Michelbouch and Brasert are very similar and consistent with the chemical values of the ceramics from Biischtert. Generally, the SiO_2 content is higher in both the mardel and soil samples as opposed to the ceramic materials (apart from the Michelbouch mardels). Total

TABLE 6.3.1 Textural analysis of samples of clay from mardels (sample depth 50–60 cm) and surrounding soils (Bg horizon, sample depth 50–60 cm, 50 m upslope to the watershed). Location of the mardel clusters is shown in Fig. 6.3.1.

Geological unit	Lias marlstone						Keuper marlstone					
Location	Berdorf		Beaufort		Kalefeld		Medernach		Brasert		Michelbouch	
Sample	Soil	Mardel	Soil	Mardel	Soil	Mardel	Soil	Mardel	Soil	Mardel	Soil	Mardel
pH (H_2O)	5.2	5.6	7.1	4.7	7.4	5.3	5.6	4.9	6.5	4.4	6.7	7.5
LOI 375°C	2.1	4.9	2.4	4.6	3.6	5.2	1.9	9.6	2.0	10.9	1.9	3.8
Texture fraction	%	%	%	%	%	%	%	%	%	%	%	%
2000–63 μm	16.0	7.0	4.0	5.5	16.5	15.0	4.5	2.5	8.0	2.0	13.0	3.0
63–32 μm	8.5	10.0	5.5	4.5	8.5	7.5	6.5	1.5	3.5	1.5	4.5	3.0
32–16 μm	10.0	8.0	8.0	5.5	8.5	8.0	15.0	3.5	7.0	4.0	6.5	2.0
16–8 μm	9.5	8.5	8.0	6.0	7.0	6.5	11.5	3.0	9.0	4.5	7.0	6.5
8–4 μm	6.5	7.5	8.0	6.0	5.5	5.5	7.5	6.0	11.0	6.0	8.0	8.5
4–2 μm	5.0	7.0	7.0	5.0	6.0	5.0	6.0	6.0	11.0	5.0	7.0	8.5
<2 μm	44.0	51.5	60.0	67.0	47.5	52.5	49.0	77.5	50.0	77.0	53.5	68.5

LOI, Loss on ignition.

Fe_2O_3 content is in general also slightly elevated. The alkalis show uniform concentrations for Na_2O (~0.3 wt%), but are quite variable in K_2O concentrations (from ~1.5 to 3.5 wt%) with the highest values measured in the ceramic materials.

An SiO_2/Al_2O_3 plot (Fig. 6.3.8) is often used as a grain size indicator in geological studies (Dypvik, 1979). A higher proportion of quartz/coarse fractions causes higher SiO_2 values. Clay-based material suitable for ceramic production with good grain size distribution should have a high content in aluminium. This is clearly the case for all Biischtert ceramic samples as well as the mardels from Michelbouch and Brasert. All soil samples have generally higher SiO_2 values and are therefore richer in the sand fraction, which is less ideal and suitable for ceramic production. The Kalefeld ceramics and soils show a different result, and provide systematically lower concentrations of SiO_2 and Al_2O_3 due to the relatively high concentrations of CaO. While the Kalefeld materials are significantly different from the other localities, a close correspondence can be observed between the ceramic and sediment material. A bivariate plot of K_2O versus MgO (Fig. 6.3.9) clearly separates both soil and mardel samples from Beaufort, Kalefeld and Berdorf, excluding them as potential sources for the production of the local ceramics from the site of Biischtert near Michelbouch. While a clear overlap of Biischtert ceramics with all Michelbouch soil and mardel samples can be observed, the Brasert and Medernach samples also show a similar pattern. In this graph the ceramics from Kalefeld show a close connection with the mardels from Kalefeld, Beauford and Berdorf.

A multivariate statistical analysis was conducted to determine group attribution and variability of the soils, mardels and archaeological ceramic samples incorporating both major and trace elemental data. A $\log_{10}$ transformation of the concentration values was conducted to

TABLE 6.3.2 Geochemical composition of all samples (ceramics, mardels and soils) by wavelength dispersive X-ray fluorescence analysis. Major and minor elements are expressed as wt% of oxides, trace elements as ppm.

			Na_2O	MgO	Al_2O_3	SiO_2	P_2O_5	K_2O	CaO	TiO_2	MnO	Fe_2O_3	S	Cr	Ni	Cu	Zn	Rb	Sr	Y	Zr	Nb	Ba	Ce	Nd	Pb
Sample	**Type**	**Location**	**wt%**	**wt%**	**wt%**	**wt%**	**wt%**	**wt%**	**wt%**	**wt%**	**wt%**	**wt%**	**ppm**	**ppm**	**ppm**	**ppm**	**ppm**	**ppm**	**ppm**	**ppm**	**ppm**	**ppm**	**ppm**	**ppm**	**ppm**	**ppm**
Ceramics ($n = 12$)																										
BII-11	Ceramic	Biischtert	0.22	5.55	22.05	57.29	0.22	3.64	0.33	1.16	0.09	8.53	100	151	134	–	402	201	59	–	318	28	788	–	–	68
BII-12	Ceramic	Biischtert	0.17	5.04	22.43	57.65	0.19	3.62	0.36	1.16	0.09	8.56	88	116	126	56	458	183	59	–	333	28	609	342	–	58
BII-13	Ceramic	Biischtert	0.20	5.07	22.39	57.39	0.19	3.69	0.36	1.19	0.09	8.82	84	96	118	56	418	192	59	–	355	21	663	334	–	58
BII-21	Ceramic	Biischtert	0.20	4.41	21.98	58.92	0.14	3.25	0.30	1.10	0.07	9.25	104	151	94	–	337	155	59	39	259	21	1065	350	–	49
BII-22	Ceramic	Biischtert	0.20	3.93	22.37	58.51	0.11	3.23	0.30	1.10	0.07	9.87	80	123	79	40	321	183	59	–	304	21	752	285	–	49
BII-31	Ceramic	Biischtert	0.30	4.23	20.16	60.18	0.12	3.51	0.34	1.02	0.09	9.59	184	137	86	–	313	183	76	39	274	21	985	252	–	68
BII-41	Ceramic	Biischtert	0.29	4.40	21.12	58.72	0.17	3.50	0.25	1.05	0.06	9.62	256	164	71	–	370	183	76	39	267	28	1191	–	–	58
BII-42	Ceramic	Biischtert	0.29	4.24	22.11	58.65	0.13	3.48	0.29	1.06	0.05	8.68	196	130	110	64	386	174	68	–	252	21	492	–	170	39
KALC-1	Ceramic	Kalefeld	0.16	1.66	16.53	55.41	0.43	2.22	16.32	0.99	0.07	6.12	961	140	86	104	92	142	207	–	363	–	–	–	–	63
KALC-2	Ceramic	Kalefeld	0.17	1.70	16.72	55.29	0.47	2.20	15.92	0.98	0.07	6.23	1085	116	110	104	96	137	220	–	355	–	–	–	–	78
KALC-3	Ceramic	Kalefeld	0.15	1.63	16.34	54.91	0.39	2.24	16.71	1.00	0.07	6.01	837	164	63	–	88	146	194	–	370	–	–	–	–	49
KALC-4	Ceramic	Kalefeld	0.16	1.65	16.43	55.06	0.41	2.23	16.51	0.99	0.07	6.07	899	152	75	104	90	144	201	–	366	–	–	–	–	56
Mardel ($n = 23$)																										
BEAU-M1	Mardel	Beaufort	0.20	1.88	19.65	71.15	0.19	2.14	1.31	0.91	0.01	2.24	485	137	55	–	72	101	76	31	304	14	519	–	–	49
BEAU-M2	Mardel	Beaufort	0.21	0.91	21.15	67.96	0.23	2.13	1.37	1.00	1.80	2.62	581	198	94	48	88	128	93	–	392	21	457	–	–	49
BEAU-M3	Mardel	Beaufort	0.20	1.83	21.42	68.49	0.22	2.19	1.38	1.06	0.01	2.60	561	137	126	–	96	128	101	–	341	14	475	293	–	49
BEAU-M4	Mardel	Beaufort	0.23	1.85	21.78	68.48	0.21	2.18	1.30	1.02	0.01	2.56	537	178	86	88	88	119	93	–	355	21	457	–	–	58
BER-M1	Mardel	Berdorf	0.23	2.02	20.70	68.59	0.06	2.30	0.79	1.01	0.01	3.98	120	116	55	447	48	128	85	39	341	21	555	261	–	49
BER-M2	Mardel	Berdorf	0.22	1.75	21.42	68.38	0.05	2.22	0.73	0.92	0.01	3.77	108	116	71	48	56	128	85	–	318	14	385	399	–	58
BER-M3	Mardel	Berdorf	0.22	1.74	21.55	68.48	0.06	2.20	0.74	0.94	0.01	3.64	96	103	63	32	56	119	85	–	296	14	304	252	–	29
BER-M4	Mardel	Berdorf	0.22	1.74	21.55	68.51	0.06	2.19	0.71	0.91	0.01	3.69	112	96	47	40	40	119	85	–	304	21	278	–	–	39
MICH-M1	Mardel	Brasert	0.28	4.96	19.81	61.43	0.07	3.58	0.49	1.04	0.19	7.95	132	103	149	64	121	201	110	39	267	14	877	309	–	97

MICH-M2	Mardel	Brasert	0.25	4.56	22.54	58.41	0.06	3.63	0.57	0.98	0.17	8.63	132	103	102	48	104	210	93	–	252	21	761	–	–	117
MICH-M3	Mardel	Brasert	0.24	4.62	22.51	58.44	0.06	3.54	0.57	0.98	0.17	8.66	136	157	141	96	121	210	101	–	244	21	779	212	–	127
MICH-M4	Mardel	Brasert	0.24	4.60	22.75	58.38	0.06	3.54	0.55	0.97	0.17	8.55	116	123	94	64	88	201	93	–	237	14	689	366	–	156
MED-M1	Mardel	Medernach	0.31	7.02	19.82	63.11	0.11	2.86	0.24	0.89	0.03	5.35	180	137	55	32	80	128	68	24	296	14	654	301	–	29
MED-M2	Mardel	Medernach	0.33	7.28	19.99	62.25	0.07	2.83	0.21	0.94	0.04	5.60	140	68	110	48	88	155	85	–	318	28	519	–	–	–
MED-M3	Mardel	Medernach	0.31	7.29	20.24	62.24	0.07	2.77	0.21	0.91	0.03	5.44	148	116	86	48	96	137	76	–	311	14	636	–	–	–
MED-M4	Mardel	Medernach	0.32	7.34	20.17	62.13	0.07	2.81	0.20	0.88	0.03	5.45	120	103	86	56	96	128	76	–	311	21	573	–	–	–
BRAS-M1	Mardel	Michelbouch	0.26	6.33	21.43	60.55	0.08	3.12	0.45	1.02	0.07	6.49	132	130	94	72	370	165	76	31	244	28	904	–	–	58
BRAS-M2	Mardel	Michelbouch	0.28	6.81	21.36	59.94	0.07	3.25	0.42	0.97	0.07	6.63	124	109	79	80	345	192	76	–	259	21	707	–	–	49
BRAS-M3	Mardel	Michelbouch	0.30	6.81	21.36	59.92	0.07	3.29	0.45	0.97	0.07	6.56	152	96	47	72	370	174	76	–	244	21	716	334	–	49
BRAS-M4	Mardel	Michelbouch	0.29	6.93	21.54	59.69	0.07	3.21	0.41	1.00	0.08	6.59	124	96	55	72	362	174	76	–	259	21	761	358	–	39
KAL-M1	Mardel	Kalefeld	0.16	1.64	19.74	64.15	0.19	2.33	4.60	1.00	0.04	5.54	112	116	86	64	88	137	110	–	289	–	385	244	–	–
KAL-M2	Mardel	Kalefeld	0.18	1.63	20.03	63.56	0.18	2.30	4.56	1.03	0.04	6.05	104	75	79	–	80	128	110	–	311	–	394	–	–	–
KAL-M3	Mardel	Kalefeld	0.17	1.66	20.04	63.81	0.20	2.32	4.68	1.04	0.04	5.51	112	68	102	48	80	128	110	–	296	–	439	293	–	–
Soil (n = 22)																										
BEAU-S1	Soil	Beaufort	0.21	1.92	19.22	71.52	0.07	2.48	0.42	0.88	0.03	2.98	112	96	71	391	56	110	76	31	326	14	475	285	–	68
BEAU-S2	Soil	Beaufort	0.19	1.82	20.25	70.27	0.07	2.50	0.44	0.86	0.04	3.05	100	96	86	–	64	101	76	–	341	14	394	244	–	88
BEAU-S3	Soil	Beaufort	0.19	1.86	20.24	70.42	0.08	2.47	0.42	0.86	0.03	3.01	96	144	94	56	72	110	68	–	333	14	439	–	–	78
BEAU-S4	Soil	Beaufort	0.19	1.83	20.41	70.36	0.08	2.41	0.43	0.85	0.03	2.93	112	123	79	56	72	101	59	–	326	14	376	252	–	68
BER-S1	Soil	Berdorf	0.21	1.53	17.01	71.74	0.07	2.05	0.56	1.05	0.03	5.54	104	130	–	56	48	110	93	39	348	70	448	–	–	49
BER-S2	Soil	Berdorf	0.22	1.41	17.93	71.07	0.07	1.95	0.59	1.01	0.04	5.17	104	75	47	32	64	110	76	–	333	14	403	–	–	58
BER-S3	Soil	Berdorf	0.22	1.42	17.92	71.43	0.06	1.92	0.57	1.03	0.04	5.09	104	96	55	–	48	110	76	–	326	21	448	236	–	88
BRAS-S1	Soil	Brasert	0.27	5.32	21.16	62.49	0.08	3.06	0.44	0.99	0.03	5.86	208	123	63	–	72	165	85	31	341	14	672	228	–	–
BRAS-S2	Soil	Brasert	0.26	5.16	21.62	61.95	0.07	2.97	0.45	1.05	0.03	5.91	204	137	94	–	64	174	85	–	326	21	501	–	–	–
BRAS-S3	Soil	Brasert	0.27	5.13	21.64	62.11	0.07	3.00	0.41	1.05	0.03	5.80	236	130	86	–	88	174	93	–	348	21	528	–	–	29
BRAS-S4	Soil	Brasert	0.26	5.17	21.71	62.15	0.07	3.00	0.42	1.02	0.03	5.63	200	82	94	80	88	165	93	–	326	21	412	317	–	–

Continued

TABLE 6.3.2 Geochemical composition of all samples (ceramics, mardels and soils) by wavelength dispersive X-ray fluorescence analysis. Major and minor elements are expressed as wt% of oxides, trace elements as ppm.—cont'd

			Na_2O	MgO	Al_2O_3	SiO_2	P_2O_5	K_2O	CaO	TiO_2	MnO	Fe_2O_3	S	Cr	Ni	Cu	Zn	Rb	Sr	Y	Zr	Nb	Ba	Ce	Nd	Pb
Sample	**Type**	**Location**	**wt%**	**wt%**	**wt%**	**wt%**	**wt%**	**wt%**	**wt%**	**wt%**	**wt%**	**wt%**	**ppm**	**ppm**	**ppm**	**ppm**	**ppm**	**ppm**	**ppm**	**ppm**	**ppm**	**ppm**	**ppm**	**ppm**	**ppm**	**ppm**
MED-S1	Soil	Medernach	0.32	6.80	18.09	64.81	0.05	2.53	0.14	0.78	0.06	6.21	92	130	47	–	96	119	59	24	259	14	600	–	–	58
MED-S2	Soil	Medernach	0.33	6.63	19.17	63.49	0.06	2.56	0.16	0.81	0.06	6.23	100	89	79	48	80	119	59	24	274	21	430	195	–	49
MED-S3	Soil	Medernach	0.34	6.68	19.57	63.24	0.06	2.54	0.14	0.81	0.06	6.09	96	130	126	56	88	110	68	–	259	21	555	24	–	29
MED-S4	Soil	Medernach	0.33	6.68	19.67	63.55	0.06	2.50	0.14	0.76	0.05	6.04	112	89	94	56	96	110	68	–	267	21	475	–	–	49
MICH-S1	Soil	Michelbouch	0.29	4.37	19.85	65.39	0.08	3.44	0.39	1.02	0.03	4.81	136	164	55	72	281	146	59	31	252	21	761	399	–	58
MICH-S2	Soil	Michelbouch	0.29	4.09	20.10	65.13	0.07	3.41	0.41	1.07	0.04	4.89	156	103	–	48	273	146	68	–	296	21	645	261	–	58
MICH-S3	Soil	Michelbouch	0.29	3.73	18.67	67.53	0.07	3.30	0.41	1.03	0.03	4.71	132	96	86	64	249	155	59	–	267	21	618	138	–	39
KAL-S1	Soil	Kalefeld	0.85	3.28	15.67	53.92	0.38	1.64	14.87	1.04	0.08	7.53	673	103	118	–	121	101	922	–	437	21	2498	–	–	49
KAL-S2	Soil	Kalefeld	0.61	2.74	17.02	52.91	0.32	1.30	15.20	1.04	0.09	8.12	697	109	102	72	112	73	736	–	422	28	1943	–	–	88
KAL-S3	Soil	Kalefeld	0.58	3.05	16.74	51.65	0.31	1.19	16.72	1.05	0.07	7.48	1254	109	–	80	112	64	668	–	489	–	2265	–	–	68
KAL-S4	Soil	Kalefeld	0.01	2.58	16.31	55.68	0.34	1.50	15.40	0.86	0.08	6.77	909	96	–	56	96	91	803	–	400	–	582	–	–	58

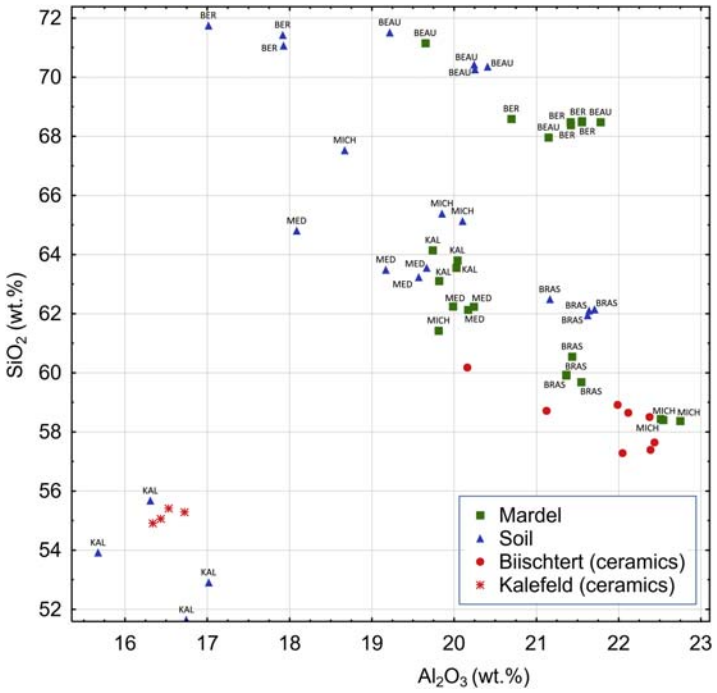

FIGURE 6.3.8 SiO_2/Al_2O_3 plot of the 46 samples.

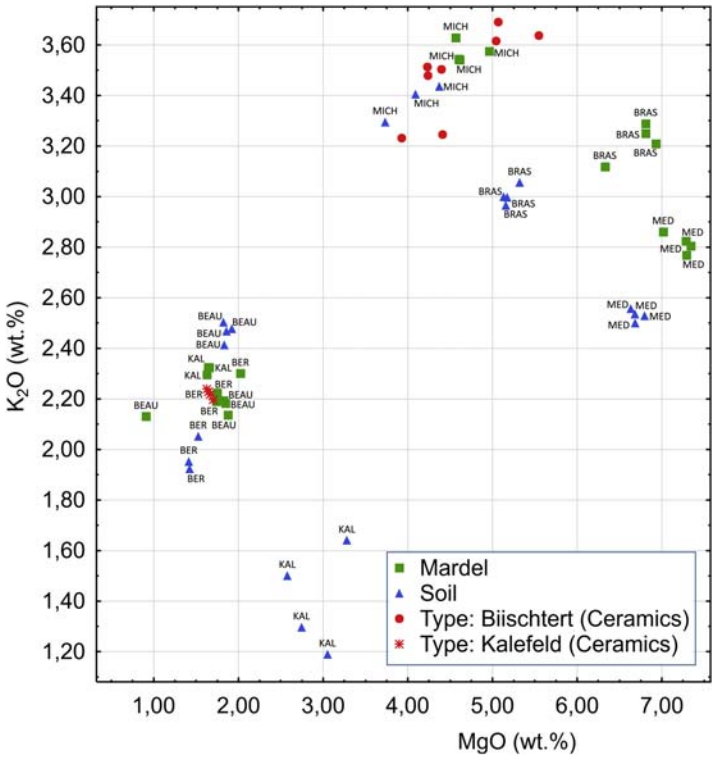

FIGURE 6.3.9 K_2O/MgO plot of the 46 samples.

calculate the principal component analysis scores. Elements SiO_2, CaO, TiO_2, K_2O, Fe_2O_3, MgO, MnO, Na_2O, Al_2O_3, Zr, Zn, Sr, Cr and Rb were retained for this analysis. All samples show low levels of P_2O_5, which signifies restricted post-depositional alterations of the ceramic materials, but was excluded from the statistical analysis.

The first two principal components account for approximately 60% of the variance in the data.

A graphical output of the principal component analysis confirms the presence of at least two distinct groups (Figs. 6.3.10 and 6.3.11). All Biischtert ceramic samples are consistently grouped together, in close correlation with both soils and mardels from especially Michelbouch and Brasser. A clear separation can be observed with the soil and mardel samples from Kalefeld, Berdorf and Beaufort, mainly related to CaO, MgO and SiO_2 content. While less distinct than the previous three sites, the mardel and soil composition from Medernach differentiates from the ceramics mainly in terms of a lower Fe_2O_3 (~5 wt% vs. ~9 wt%) and elevated MgO (~7 wt% vs. 4.5–5.5 wt%) content. The soils and to a lesser extent mardels of Kalefeld are significantly enriched in carbonate and marl content, resulting in a clearly different cluster. Ceramics from Kalefeld are situated between the mardels and soils. Apart from the higher CaO values, the content of MgO, K_2O and Al_2O_3 is consistent with the mardel data obtained from Kalefeld. Based on these observations it can be concluded that the composition of the mardels from Michelbouch and Brasert is consistent with the obtained Biischtert ceramic compositions. While less clear in overlap and apart from the exact CaO content, a consistency can be observed between the Kalefeld ceramics and mardels/soils. Moreover, the mardels of Berdorf, Medernach and Beaufort are significantly different from the other mardel and soil samples. Generally, these latter mardels are especially depleted in MgO content and have significantly lower total Fe values than the other Keuper soils and mardels.

6.3.5 Discussion and conclusions

The aim of this study was to disentangle the man versus nature question about mardel genesis on the Luxembourger Gutland plateau by utilizing geochemical analysis by WD-XRF of various potential source materials for the production of ceramics (samples from mardel deposits and surrounding soils) and finds of Roman ceramics. The results show a consistent pattern of the composition of the Roman ceramics of the Biischtert excavation site with clay samples from the Michelbouch mardels and surrounding soils on the Steinmergelkeuper (also Brasert and Medernach are plausible). A clear distinction and separation can be made with the soils and mardels from Beaufort, Berdorf and Kalefeld. The composition of these clay samples of the Strassen marls is consistently different. The textural properties of the clay samples from the mardels and surrounding soil, however, indicate also potential suitable material for the production of ceramics. This is verification of a match of this source material with ceramic production in the past, by means of a comparison with findings from production sites on the Strassen marls. These ceramic materials represent a very consistent group and production. While exceedingly rich in CaO, the elemental consistency with the mardels and soils from Kalefeld is clear. These ceramics can effectively be discriminated from the Biischtert ceramic production and associated mineral resources.

Based on the results of the WD-XRF analysis we showed the Roman impact on the genesis of mardels and that the traditional theory of the development of Keuper mardels (Slotboom, 1963) can be upgraded as sketched in Fig. 6.3.12. This is an addition to Fig. 2.4.2 (typology of mardels on the Gutland plateau, type A).

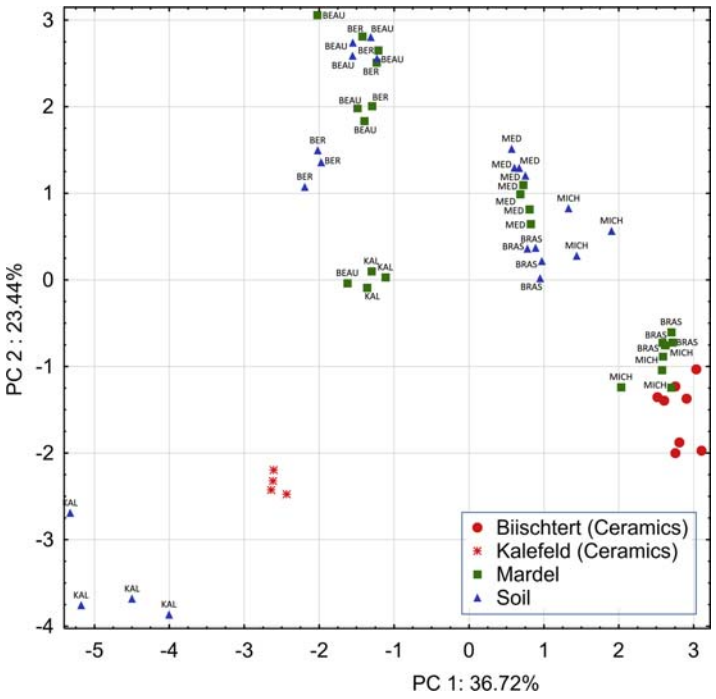

FIGURE 6.3.10 Score plot of principal components 1 and 2 (PC1 vs. PC2), representing 36.72% and 23.44% of total variance.

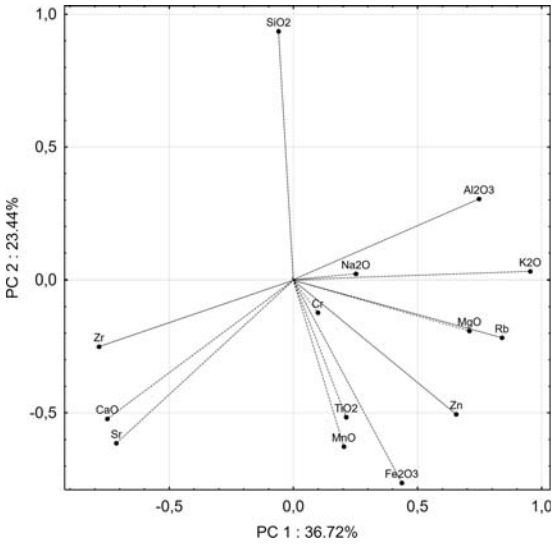

FIGURE 6.3.11 Loading plot of principal components 1 and 2 (PC1 vs. PC2), representing 36.72% and 23.442% of total variance.

The application of WD-XRF analysis on clay samples from mardels and surrounding soils and Roman ceramic fragments led to a number of conclusions:

- Clay from mardels and surrounding soils is an appropriate resource for the production of ceramics.
- Provenance analysis (by WD-XRF analysis) demonstrated the match of the chemical composition of Roman ceramics and clay samples from mardels and surrounding soils. Obviously, the Romans used clay extracted from mardels and surrounding soils to produce ceramics.
- Mardel Michelbouch was developed initially as a natural mardel in Keuper marls (Steinmergelkeuper); the Romans excavated mardel clay (best match between the composition of ceramics and mardel clay); because of clay extraction the mardel reached

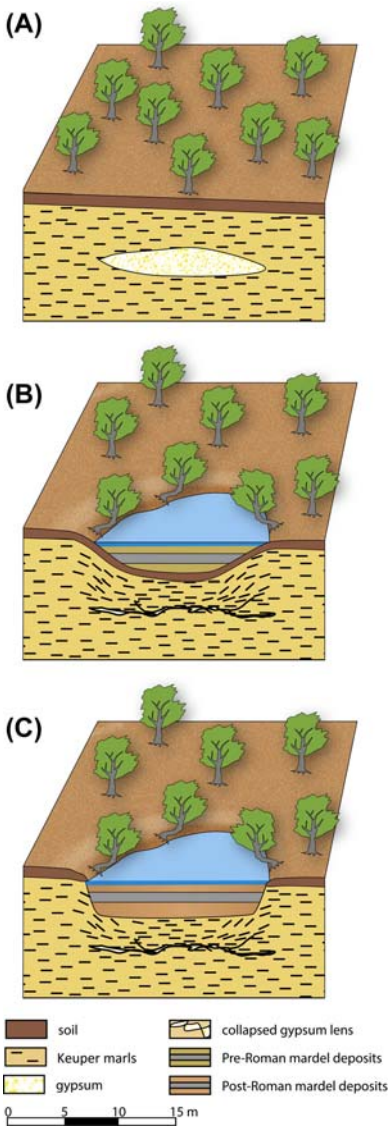

FIGURE 6.3.12 The development of mardels on the Steinmergelkeuper. (A) Initial landscape on the Steinmergelkeuper, with a subsurface gypsum lens. (B) The development of a subsidence basin, caused by dissolution of the gypsum lens, partly filled with pre-Roman clayey colluvium, burying the descended palaeosol. (C) Mardel after Roman clay excavation, filled with post-Roman clayey colluvium, burying the quarry floor.

its current size; and colluvial clay accumulation restarted in the abandoned quarries.

- Mardel Kalefeld (Lias, Strassen marls) is most probably an excavation in a moist clayey soil (best match between the composition of ceramics and soil); moist depressions on the Lias are related to joint patterns in the underlying Luxembourger sandstone; and here clay accumulation restarted in the abandoned quarry.
- The results of the WD-XRF analysis demonstrate the anthropogenic contribution to the genesis of the mardels on the Gutland plateau.

References

Alexander, B., 1974. Extractable iron in relation to soil age on terraces along the Truckee River, Nevada. Soil Science Society of America Journal 38, 121–124.

Bisschops, J.H., 1973. Blad Eindhoven Oost (51 Oost). Toelichtingen bij de geologische kaart van Nederland 1: 50.000. R.G.D., Haarlem, p. 132.

Braekmans, D., Degryse, P., Poblome, J., Neyt, B., Vyncke, K., Waelkens, M., 2011. Understanding ceramic variability: an archaeometrical interpretation of the classical and hellenistic ceramics at düzen tepe and sagalassos (Southwest Turkey). Journal of Archaeological Science 38, 2101–2115.

Brownlee, D.E., 1985. Cosmic dust: collection and research. Annual Review of Earth and Planetary Sciences 13, 147–173.

Cammeraat, L.H., Kooijman, A.M., 2009. Biological control of pedological and hydro-geomorphological processes in a deciduous forest ecosystem. Biologia 64, 428–432.

Cammeraat, L.H., 2006. Luxembourg. In: Boardman, J., Poesen, J. (Eds.), Soil Erosion in Europe. John Wiley and Sons, Chichester, pp. 427–438.

Caquineau, S., Gaudichet, A., Gomes, L., Magonthier, M.-C., Chatenet, B., 1998. Saharan dust; clay ratio as a relevant tracer to assess the origin of soil-derived aerosols. Proceedings of the American Mathematical Society 25, 983–986.

Cita, M.B., Vergnaud-Grazzini, C., Robert, C., Chamley, H., Ciaranfi, N., d'Onfrio, C., 1977. Paleoclimatic record of a long deep sea core from the eastern Mediterranean. Quaternary Research 8, 205–235.

Crommelin, R.D., 1964. A contribution to the sedimentary petrology and provenance of young Pleistocene cover sand in The Netherlands. Geologie en Mijnbouw 43, 389–402.

de Bakker, H., 1979. Major Soils and Soil Regions in the Netherlands. Centre for Agricultural Publishing and Documentation, Wageningen, Netherlands.

Degryse, P., Braekmans, D., 2014. Elemental and isotopic analysis of ancient ceramics and glass. In: Holland, H.D., Turekian, K.K. (Eds.), Treatise on Geochemistry, second ed., vol. 14, pp. 191–207.

Doorenbosch, M., 2013. Ancestral Heaths. Reconstructing the Barrow Landscape in Central and Southern Netherlands. Sidestone Press, Leiden, Netherlands.

Dypvik, H., 1979. Mineralogy and geochemistry of the mesozoic sediments of andøya, Northern Norway. Sedimentary Geology 24, 45–67.

Etienne, D., Ruffaldi, P., Goepp, S., Ritz, F., Georges-Leroy, M., Pollier, B., Dambrine, E., 2011. The origin of closed depressions in Northeastern France: a new assessment. Geomorphology 126, 121–131.

Folmer, N., Krier, J., 1980. Carte archeologique du Grand-Duche de Luxembourg, Feuille, vol. 12. Larochette.

Freddrikson, K., Gowdy, R., 1983. Meteoritic debris from the south Californian desert. Geochimica et Cosmochimica Acta 241–243, 1983.

Genge, M.J., Gileski, A., Grady, M.M., 2005. Chondrules in antarctic micrometeorites. Meteoritics & Planetary Sciences 40, 225–238.

GESAMP, 1989. The atmospheric input of trace species to the world ocean. GESAMP Reports and Studies 38, 111.

Gounelle, M., Chaussidon, M., Morbidelli, A., Barrat, J.-A., Engrand, C., Zolensky, M.E., McKeegan, K.D., 2009. A unique basaltic micrometeorite expands the inventory of solar system planetary crusts. Proceedings of the National Academy of Sciences 106, 6904–6909.

Green, R.N., Towbridge, R.L., Klinka, K., 1993. Towards a Taxonomic Classification of Humus Forms. Forest Science. Monograph 29.

Hein, A., Day, P.M., Cau Ontiveros, M.A., Kilikoglou, V., 2004. Red clays from Central and Eastern Crete: geochemical and mineralogical properties in view of provenance studies on ancient ceramics. Applied Clay Science 24, 245–255. https://doi.org/10.1016/j.clay.2003.07.009.

Holmgren, C.G.S., 1967. A rapid citrate–dithionite extractable iron procedure. Soil Science Society of America Journal 31 (2).

IJlst, L., 1973. A laboratory overflow centrifuge for heavy liquid mineral separation. American Mineralogist 58, 1088–1093.

ISRIC-FAO, 2006. World Reference Base for Soil Recourses 2006. World Soil Resources Reports 103.

Jackson, M.L., 1958. Soil Chemical Analysis. Prentice-Hall Inc.

Jacoby, R., 2011. Chronologie der Aktivitäten in der Biischtert, vol. 10. De Viichter Geschichtsfrënd, pp. 7–10.

Journet, E., Desboeufs, K.V., Caquineau, S., Colin, J.-L., 2008. Mineralogy as a critical factor of dust iron solubility. Geophysical Research Letters 35. https://doi.org/10.1029/2007GL031589.

Kearsley, A.T., Graham, G.A., McDonnell, J.A.M., Taylor, E.A., Drolshagen, G., Chater, R.J., McPhail, D., Burchell, M.J., 2007. The chemical composition of micrometeoroids impacting upon the solar arrays of the Hubble Space Telescope. Advances in Space Research 39, 590–604.

Kerridge, J.F., 1970. Micrometeorite environment at the Earth's orbit. Nature 228, 616–619.

Koster, E.A., 1978. De stuifzanden van de Veluwe, een fysisch geografische studie, vol. 27. Publicatie van het Fysisch Geografisch en Bodemkundig Labortorium van de Universiteit van, Amsterdam.

Koster, E.A., 2010. Origin and development of Late Holocene drift sands. In: Fanta, J., Siepel, H. (Eds.), Inland Drift Sand Landscapes. KNVV Publishing, Zeist, Netherlands, pp. 25–48.

Krook, L., 1997. Het Onderzoek Van Zware Mineralen in Zand. Gea, 1996, nr. 4.

Marvin, U.B., Einaudi, M.T., 1967. Black magnetic spherules from Pleistocene and recent beach sands. Geochimica et Cosmochimica Acta 81, 1871–1884.

Maurette, M., 1991. A collection of diverse micrometeorites recovered from 100 tonnes of Antarctic blue ice. Nature 351, 44–47.

Maurette, M., 2006. Classification of meteorites and micrometeorites. In: Mourette, M. (Ed.), Micrometeorites and the Mysteries of Our Origins. Springer-Verlag Berlin Heidelberg, New York.

Maurette, M., Jehanno, C., Robin, E., Hammer, C., 1987. Characteristics and mass distribution of extraterrestrial dust from the Greenland ice cap. Nature 328, 699–702.

Murell, M.T., Davis, P.A., Nishizumi, K., 1980. Deep-sea spherules from Pacific clay: mass distribution and influx rate. Geochimica et Cosmochimica Acta 44, 2067–2074.

Poeteray, F.A., Riezebos, P.A., Slotboom, R.T., 1984. Rates of Subatlantic lowering calculated from mardel-trapped material (Gutland, Luxembourg). Zeitschrift für Geomorphologie 467–4821, 1984.

Rochette, P., Folco, L., Sauvet, C., van Ginneken, M., Gattacceca, J., Perchiazzi, N., Braucher, R., Harvey, R.P., 2008. Micrometeorites from the transantarctic mountains. Proceedings of the National Academy of Sciences 105, 18206–18211.

Ryan, J.N., Gschwend, P.M., 1991. Extraction of iron oxides from sediments using reductive dissolution by titanium (III). Applied Clay Mineralogy 39, 509–518.

Sauvet, C., Rochette, P., Kars, M., Gattacecca, J., Folco, L., Harvey, R.P., 2009. Statistical properties of the Transantarctic Mountains (TAM) micrometeorite collection. Polar Science 3, 100–109.

Schackley, S., 2011. X-Ray Fluorescence Spectrometry (XRF) in Geoarchaeology. Springer, New York-Dordrecht-Heildelberg-London.

Scheffer, F., Schachtschabel, P., Blume, H.P., Hartige, K.H., Schwertmann, U., 1979. Lehrbuch der Bodenkunde. Ferdinand Enke Verlag, Stuttgart, Germany.

Slotboom, R.T., 1963. Comparative geomorphological and palynological investigation of the pingos (viviers) in the haute fagnes (Belgium) and the mardellen in the Gutland (Luxembourg). Zeitschrift für Geomorphologie 7, 193–231.

Slotboom, R.T., van Mourik, J.M., 2015. Pollen records of mardel deposits; the effects of climatic oscillations and land management on soil erosion in Gutland, Luxembourg. Catena 132, 72–88.

Stankowski, W.T.J., Katrusiak, A., Budzianowski, A., 2006. Crystallographic variety of magnetic spherules from pleistocene and Holocene sediments in the Northern foreland of morasko-meteorite reserve. Planetary and Space Science 54, 60–70.

Stichting voor Bodemkartering, 1976. Bodemkaart Van Nederland Blad 45-oost Met Toelichting 's-Hertogenbosch. Pudoc, Wageningen, Netherlands.

Taylor, S., Lever, J.H., Harvey, R.P., 1998. Accretion rate of cosmic spherules measured at the South Pole. Nature 392, 899–903.

Taylor, S., Lever, J.H., Harvey, R.P., 2000. Numbers, types and composition of an unbiased collection of cosmic spherules. Meteoritics & Planetary Sciences 35, 651–666.

van Mourik, J.M., 2010. Resultaten van het dateringsonderzoek van grafheuvel 39 op de Slabroekse Heide, vol. 72. Archol bv, Leiden, Netherlands, pp. 67–73.

van Mourik, J.M., de Vet, S.J., 2015. Iron stocks of buried Podzols: endogenic iron deficits and potential exogenic enrichment in the Maashorst region, SE Netherlands. Catena 132, 97–104 (2015).

van Mourik, J.M., Odé, B., 2010. Het Herperduin. Geografisch Tijdschrift XXIV, 160–167.

van Mourik, J.M., Slotboom, R.T., 2018. Palynological reconstruction of the effects of Holocene climatic oscillations and agricultural history on soils and landforms in Luxembourg. In: The Luxemburger Gutland Landscape. Springer, pp. 39–72.

van Mourik, J.M., Seijmonsbergen, A.C., Slotboom, R.T., Wallinga, J., 2012. The impact of human land use on soils and landforms in cultural landscapes on aeolian sandy sub-en de rest?.

Vera, H., 2011. 'dat men het goed vande ongeboornen niet mag verkoopen'; Gemene gronden in de Meierij van Den Bosch tussen hertog en hertgang 1000–2000. Uitgeverij BOXpress, Oisterwijk, Netherlands (with English summary).

CHAPTER

7

Phytolith analysis of soil archives: phytoliths in soils of the Netherlands

C.N.H. McMichael, I.K. de Wolf, K. Land*

Institute for Biodiversity and Ecosystem Dynamics, University of Amsterdam, Amsterdam, the Netherlands

***Corresponding author.**

7.1 Introduction

Phytoliths (from the Greek 'plant stone') are rigid, microscopic structures made of silica, found in some plant tissues. Plants take up silica from the soil, whereupon it is deposited within different intracellular and extracellular structures of the plant. Phytoliths survive decomposition and humification of organic tissues and can thus accumulate in the soil. Most of them are part of the textural silt fraction. Although some use 'phytolith' to refer to all mineral secretions by plants, it more commonly refers to siliceous plant remains. Piperno (2006) distinguishes four important stages of phytolith research throughout history.

1. Discovery and exploratory stage (1835–95). The first report on phytoliths was published by a German botanist named Struve in 1835. Later, another German scientist named Christian Gottfried Ehrenberg was one of the leaders in the field of phytolith analysis. He developed the first classification system for phytoliths, and analysed soil samples that were sent to him from all around the world.
2. Botanical phase of research (1895–1936). Phytolith structures in plants gained wide recognition and attention throughout Europe. Research on production, taxonomy and morphology exploded. Detailed notes and drawings on plant families that produce silica structures and morphology within families were published.
3. Period of ecological research (1955–75). First applications of phytolith analysis to palaeoecological work were carried out, mostly in Australia, the United States, the United Kingdom and Russia. Classification systems for differentiation within plant families became popular.
4. Modern period of archaeological and palaeoenvironmental research (1978–present). Archaeobotanists working in the Americas first consider and analyse phytolith assemblages to track prehistoric plant use and domestication. Also, for the first time, phytolith data from pottery are used to track the history of clay procurement and pottery manufacture. Around the same time,

Reading the Soil Archives
https://doi.org/10.1016/B978-0-444-64108-3.00007-0

phytolith data are also used as a means of vegetation reconstruction among palaeoecologists. A much larger reference collection on phytolith morphology within varying plant families is assembled.

5. The promising application of phytolith analysis in (palaeo)pedology. The study of soils and palaeosols in the context of palaeoecological studies was at first based on pollen analysis and absolute dating techniques. However, some palaeosols no longer contain determinable pollen grains, due to chemical and microbial decay of the organic fraction. Phytoliths survive these decomposition processes and this proxy can contribute to the analysis of soil archives.

A good example of a palaeoecological study, based on phytolith analysis of soil samples, was a landscape transect that reconstructed the historical extension of the White Oak Savanna in the Willamette Valley in Oregon (Kirchholtes et al., 2015). Pollen analysis was not an option because of the severe corrosion of the grains and the extremely low pollen concentrations. The history of the Oak Savanna was not recorded in a pollen profile, but diagnostics for the historical presence of the White Oak Savanna were the phytoliths of specific grass species which survived the decomposition processes in the organic horizon. Phytolith analysis is a promising proxy for many questions concerning soil and landscape development. Examples are the identification of plant species involved in soil formation and carbon sequestration in Mormoders, buried Podzols and plaggic Anthrosols, and we will apply the phytolith proxy in the next phase of the study of these soils.

In the next paragraphs we present the results of a pilot study of phytolith analysis in agricultural soils in the Netherlands. This is also a transect study, using samples of the surface of forest soils and agricultural fields. Phytolith analysis is a proxy in development and this study demonstrates the complications concerning the interpretation of phytolith spectra from soil samples. We pay attention to determination and data analysis. The problems in the interpretation of phytolith assemblages are rather similar to the problems discussed regarding soil pollen spectra in Chapter 2. We need to know more about phytolith production and distribution by plant species, infiltration and conservation of phytoliths into the soil. For the determination of phytoliths extracted from soil samples we need further complete global and regional reference bases. In contrast to pollen grains, which are part of aeolian deposition, phytoliths originate from tissues of plants rooting at the site. Consequently, phytolith assemblages of soil samples are normally post-sedimentary but it is also possible that phytoliths that survived humification processes can be involved in aeolian and fluvial erosion and redeposition and can become syn-sedimentary particles in aeolian and fluvial deposits.

7.2 Phytoliths and their function

Phytoliths (silicified cells) are produced by many types of plants for a variety of reasons. They have been shown to support the structure of plant tissues by preventing collapse during periods of drought (Coughenour, 1985). They also function to reduce herbivory from both insects and larger herbivores by limiting access to nutrients (Hunt et al., 2008), or decreasing the digestibility of edible parts of the plant (Reynolds et al., 2009; Massey and Hartley, 2009). Phytoliths can also function to hinder herbivores by wearing down the teeth of grazers (Müller et al., 2014, 2015) or mandibles of insects (Massey and Hartley, 2009).

Phytoliths vary in shape and size and are plant specific. Because of this, many are diagnostic of certain plants at the family, subfamily-, or genus

levels (Piperno, 1985, 2014; Shakoor et al., 2014). As previously mentioned, when plants (or parts of plants) undergo the process of humification, the phytoliths remain, creating a proxy of the vegetation (Shakoor et al., 2014), sometimes even on timescales of millions of years (Rovner, 1971). Because of their ability to identify certain plants and long-term preservation under an array of depositional environments, phytoliths are commonly used in palaeoecological and archaeological reconstructions (Piperno, 2006).

Phytoliths are often combined with other proxies of vegetation, such as pollen in palaeoecological and archaeological reconstructions. The pairing is quite complementary because in lake sediment archives, phytoliths reflect a primarily local vegetation signal (Blinnikov, 2005), whereas pollen reflects both local and regional vegetation (Jackson, 1990; Jackson and Kearsley, 1998; Parshall and Calcote, 2001). Pollen is particularly useful in its ability to identify tree genera. Few tree taxa, however, produce phytoliths or produce phytoliths that are specific at the genus or family level. Grasses and understorey plants produce higher quantities of phytoliths, and ones that are diagnostic at the genus or subfamily level (Shakoor et al., 2014). Grass phytolith composition, however, can also reveal information about forest types even if the trees in the system do not produce phytoliths. For example, certain grass species or the lack of them can be characteristic for certain forest types.

To accurately reconstruct past vegetation change using phytoliths, we need to understand how phytolith assemblages vary between vegetation types. This is most commonly done by comparing phytolith assemblages found in soil surface samples with the modern vegetation found at those sites (Alexandra, 1997; Blinnikov, 2005; Fredlund and Tieszen, 1994; Runge, 1999). These types of studies, however, are lacking in much of Western Europe and particularly in the Netherlands.

7.3 Farming in the Netherlands, a pilot study

A large part of palaeoecological research in the Netherlands is focused on the Quaternary landscape evolution. The impact of human land use on soils and landforms has a long history. On sandy soils the first Neolithic traces of degradation of the natural ecosystems were related to forest grazing and shifting cultivation. Since the Bronze Age, land use intensified and deciduous forests degraded to heaths. Plaggic agriculture dominated from the early Middle Ages until AD 1900 when the invention of chemical fertilizer allowed reclamation of heath to arable land and intensification of crop production (Harms et al., 1987; van Mourik et al., 2012). Nowadays, 1,706,000 ha of the Netherlands consist of agricultural land, which is more than half of the total (CBS et al., 2016). Agricultural soils are soil archives and we will look at the application of phytolith analysis on soil to find a relation between the pollen assemblages and the period of agricultural management since the transition from forest to arable land.

Agricultural soils typically contain fewer phytoliths than soils of forests or grassland due to the harvesting of crops (Haynes, 2017). Most crops are silicon accumulators (Haynes, 2017; Guntzer et al., 2012a,b), meaning that when harvested, most of the silica does not return to the soil in the form of phytoliths (Haynes, 2017). Silica reduction decreases plant growth and yield, resulting in less successful harvests (Savant et al., 1997; Hossain et al., 2001). Silica fertilization often takes place to replenish soils and increase plant growth and yield (Liang et al., 1994), and also creates the possibility for plants to increase the production of phytoliths (de Melo et al., 2010). Yet, repeated harvesting would create a continuous strain on silica supply even with fertilization. Because of this, there is a disturbed silica cycle on

agricultural fields compared to forests (Sommer et al., 2013; Cornelis and Delvaux, 2016) (Fig. 7.3.1).

The primary source of silicon in the cycle (Fig. 7.3.1) is released by chemical weathering (hydrolysis) from silicate minerals in the soil. Hydrolysis is a slow process and consequently plant roots can take up released Si. A second source of silicon available for uptake by plants is dissolved silicon in soil and groundwater. The cycle in a natural vegetation system will be closed by the release of silicon from decomposing litter and decaying roots in the humus form. A part of released silicon by humification can leach to the aquifer, but in agricultural systems silicon leaves the system during harvesting and transport to the food market.

When the effect of crop harvesting on the composition and concentration of phytoliths of samples of agricultural soils is understood, it can help to interpret palaeoecological records of the agricultural history and its effects on landscape development.

The research question of this pilot study is: what is the effect of agricultural practices on the phytolith composition assemblages of soil in cultural landscapes in the Netherlands? To answer this complex question, three different components of this question were investigated:

1. What is the difference in phytolith composition between forest soils and agricultural soils?
2. Does the phytolith association differ when the land is converted recently or when it was converted longer ago?
3. How does the concentration of phytoliths in soils change over a gradient from forest to agricultural land?

It was expected that in forests a relatively high amount of arboreal phytoliths and also grass phytoliths from the undergrowth would be found. In agricultural fields, mainly phytoliths from crops could be found; however, a lower amount of arboreal phytoliths should also be present in the samples. This was expected since ploughing agricultural fields results in a less sequestrated upper layer (0–23 cm) (Guntzer et al., 2012a,b). Because this homogenizes the soil, phytoliths from a few years ago should also be present in the samples, which could be arboreal phytoliths from the trees in the former forest. When fields were converted more than 100 years, the amount of grass and crop phytoliths increased, while the amount of arboreal phytoliths diminished.

Both forest and agricultural soils will not contain many phytoliths. Because trees in temperate climates are known to produce fewer phytoliths (Piperno, 2006), forests are expected to have c.1,000,000 phytoliths per cm^2 (McMichael and Philip, 2019, IBED lab protocols). Fields will have nearly the same but slightly lower concentrations than forests since most crops (including their phytoliths) are harvested. Areas that lie in between forests and agricultural fields will have an intermediate concentration.

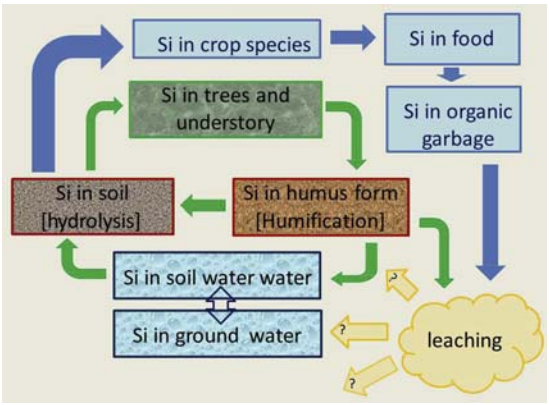

FIGURE 7.3.1 **Silicon cycle in forests and agricultural fields.** Green is the cycle in a forest (Sommer et al., 2013; Cornelis and Delvaux, 2016), and blue is a disturbed cycle in agriculture (Haynes, 2017).

7.4 Methodology

7.4.1 Sampling method

From each of the locations, four soil samples of ≈2 mL were taken, each from just under the litter layer (depth varies with thickness of litter layer, c.0–1 cm depth), totalling 40 samples for agricultural fields. These samples were taken in December/January of 2017/2018. Samples taken on the agricultural field sites had to contain one sample from the adjacent forest, one sample from the area transitioning from forest to field and two from the field.

7.4.2 Site description

The specific sampling locations were determined using the HYDE dataset (Klein Goldewijk et al., 2011). This shows the extent of agriculture across the world (specifically in Europe and the Netherlands) using historical population data. The HYDE model contains maps covering 10,000 BC to AD 2005. For this study, the maps from 1700 to AD 2000 were used and 10 locations were chosen (Fig. 7.4.1).

The locations had to meet the following requirements: there had to be an adjacent forest, the field had to be easily accessible (no fences, for example) and it had to be in the region chosen from the maps.

The Netherlands is to a large extent made up of Quaternary sand, clay and peat deposits (Alterra, 2006). The annual precipitation is c.948 mm per year and the average temperature is 10.9°C (3.8°C in winter and 17.7°C in summer) (CBS et al., 2018). The whole of the Netherlands (and all the locations used in this experiment) has a temperate maritime climate (Table 7.4.1).

The oldest field used in this experiment is near Enschede (Fig. 7.4.2, Gelderland 52.26481/6.91306) and was converted around 1700 (the average temperature in Enschede is 9.1°C and the annual precipitation is 782 mm (AM Online Projects)). On the agricultural field, grass (Poaceae) is grown, and the transition area mainly consists of Poaceae and seedlings of the trees from the adjacent forest. The forest has little undergrowth and mostly *Quercus*, *Sambucus* and *Fagus* (Fig. 7.4.2). The sampling site is located on sandy soil (Alterra, 2006).

The location converted around 1720 is near Plasmolen (Fig. 7.4.3, Limburg 51.75149/5.91623). The area around Plasmolen has an annual precipitation of 771 mm and an average temperature of 9.6°C (AM Online Projects). Here, maize and cereal are grown on the field. The transition area is mostly made up of *Rubus* and *Urtica*. The adjacent forest has almost no undergrowth with the exception of *Pteropsida*; the most common trees are *Acer*, *Fagus*, *Prunus* and *Sambucus*. The sample site is located on a sandy hill (Alterra, 2006).

The location near Groenekan (Fig. 7.4.4, Utrecht 52.12953/5.17421) was converted c.1760; it has a relatively high annual precipitation (802 mm) and an average temperature of 9.3°C (AM Online Projects). The sampling site is on a sand ridge (Alterra, 2006). On the field, cereal is grown (Fig. 7.4.4). In the transition area, mainly Poaceae and *Rubus* are grown and some seedlings of the trees from the forest. The forest has a lot of undergrowth, mainly *Rubus*, and consists of *Quercus*, *Tilia*, *Fagus* and *Sambucus*.

The northernmost sampling site is near Norg (Fig. 7.4.5, Drenthe 53.08249/6.49495), and the agricultural field dates from c.1820. The location near Norg has the lowest average temperature of the selected sites (8.6°C) and its annual precipitation is 790 mm (AM Online Projects). On the field, sugar beet is grown and the transition area is fully covered with Poaceae and *Rubus* (Fig. 7.4.5). The adjacent forest has some undergrowth of *Rubus* and *Pteopsida*. The most common tree is *Sambucus* but there are also *Fagus* and *Prunus*. This sampling site is not on sand

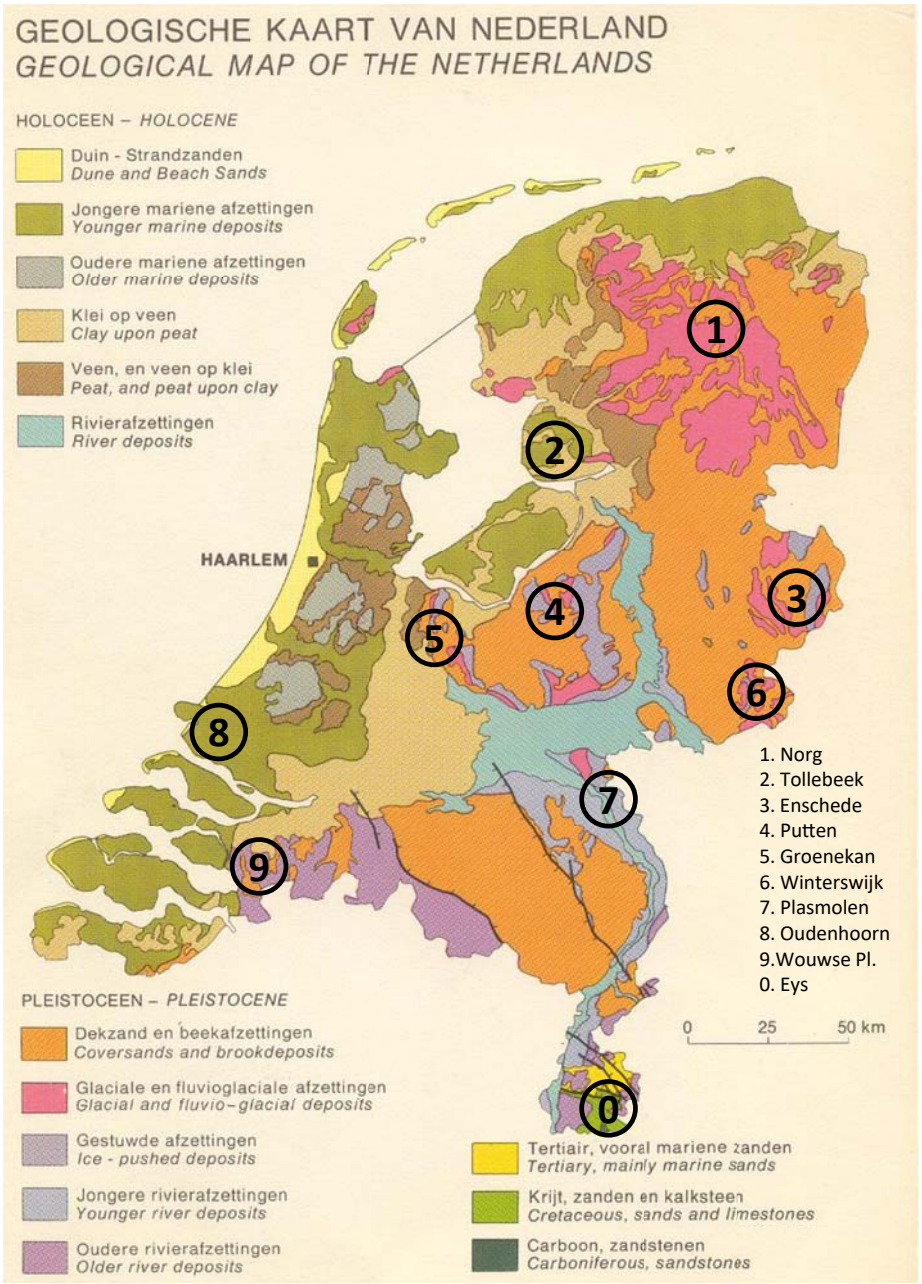

FIGURE 7.4.1 Map of the Netherlands with the sampling locations.

TABLE 7.4.1 Basic information about the locations.

Location (see Fig. 7.4.1)	Year of conversion	Crops grown	Soil texture	Annual rainfall (mm)	Average temperature (°C)
Enschede	1700	Grass	Sand	782	9.1
Plasmolen	1720	Maize, cereal	Sand	771	9.6
Groenkan	1760	Cereal	Sand	802	9.3
Norg	1820	Sugar beet	Peat	790	8.6
Eys	1840	Cereal, maize	Loam	855	9.6
Oudenhoorn	1880	Sugar beet, potato	Sandy clay	766	9.8
Wouwse Plantage	1900	Maize	Sand	781	9.9
Winterswijk	1920	Maize	Sand	784	9.5
Putten	1960	Sugar beet	Sand	790	9.1
Tollebeek	2000	Grass, potato, sugar beet	Sandy clay	782	9.1

like the previous locations but on peat (Alterra, 2006).

Near the border with Belgium lies the location of Eys (Fig. 7.4.6, Limburg 50.82935/5.91673), converted in 1840. This location has a different soil type, namely löss (Alterra, 2006). It is also divergent in its annual precipitation; here it is 855 mm, which is the highest of the selected locations. The average temperature is 9.6°C (AM Online Projects). On this sampling site, mainly maize and cereal are grown. Between the field which was sampled and the transition area/forest there is a small foot and cycle path. Because of the different soil, deviant vegetation occurs in the transition area and the forest. The transition area is mainly made up of *Rubus* but it also has *Anthriscus sylvestris*, *Galium aparine* and *Tilia* seedlings. In the forest there is little undergrowth, and consists of *Galium pumilum* (Fig. 7.4.7), *Pteropsida*, *Arum* and *Hedera*, which is characteristic for this area. The most frequent trees are *Acer*, *Fagus*, *Tilia* and *Quercus*.

FIGURE 7.4.2 Sampling site near Enschede, Gelderland.

FIGURE 7.4.3 Sampling site near Plasmolen, Limburg.

FIGURE 7.4.4 Sampling site near Groenekan, Utrecht.

FIGURE 7.4.6 Sampling site near Eys, Limburg.

In Zuid-Holland near the coast is the sampling site in Oudenhoorn (Fig. 7.4.7, Gelderland 51.82848/4.17300), which was converted around 1880. Oudenhoorn has the lowest annual precipitation with 766 mm. The average temperature is relatively high (9.8°C) (AM Online Projects). This location has a sandy clay soil (Alterra, 2006). In Oudenhoorn, sugar beet and potato are grown alternately. On the transition area, mostly Poaceae are grown and *Vicia cracca*. The forest has a dense undergrowth, mainly consisting of *Urtica*, Poaceae and Rubiaceae. The most common trees are *Quercus*, *Fagus and Sambucus* (Fig. 7.4.8).

One of the more recently converted fields is near the Wouwse Plantage (Fig. 7.4.8, Noord-Brabant 51.47602/4.39351), dating from 1900. The Wouwse Plantage has the highest average temperature (9.9°C) but an average annual precipitation (781 mm) (AM Online Projects). On this location, maize is grown on sandy soil (Alterra, 2006). In between the forest and the field is a border of *Rubus* and Poaceae (Fig. 7.4.9). In the forest, *Prunus* and *Pinus* occur and the undergrowth is mainly made up of *Pteropsida.*

FIGURE 7.4.5 Sampling site near Norg, Drenthe.

FIGURE 7.4.7 Sampling site near Oudenhoorn, Gelderland.

FIGURE 7.4.8 Sampling site near Wouwse Plantage, Noord-Brabant.

FIGURE 7.4.10 Sampling site near Putten, Gelderland.

On the border of Germany and the Netherlands is the sampling site of the field converted in 1920, near Winterswijk (Fig. 7.4.9, Overijssel 52.01461/6.75399). Winterswijk has an average temperature of 9.5°C and an annual precipitation of 784 mm (AM Online Projects). Here also, maize is grown on sandy soil (Fig. 7.4.10) (Alterra, 2006). The vegetation of the transition area and the forest is different from the other locations; the transition area is mainly made up of *Fallopia japonica*, an invasive species from Asia. In the forest, *Vaccinium* and *Convallaria majalis* form the undergrowth under *Prunus*, *Sambucus*, *Quercus* and *Fagus.*

The second most recently converted field (c.1960) is near Putten (Fig. 7.4.10, Gelderland 52.23327/5.68016). This location is on sandy soil (Alterra, 2006). The average temperature of Putten is 9.1°C and the annual precipitation is 790 mm (AM Online Projects). On the field used for the experiment, sugar beet is grown. The transition area has a variety of plants containing *Urtica*, Poaceae, species of Rubiaceae, *Glechoma hederacea* and *Taraxacum officinale.* The

FIGURE 7.4.9 Sampling site near Winterswijk, Overijssel.

FIGURE 7.4.11 Sampling site near Tollebeek, Flevoland.

forest has little undergrowth containing *Rubus* and the most common trees are *Acer*, *Fagus* and *Sambucus*.

The youngest field is near Tollebeek (Fig. 7.4.11, Flevoland 52.68367/5.66603). Tollebeek is in the Noordoostpolder, which used to be part of the Zuiderzee and was reclaimed around 1942. The soil here is made up of sandy clay with a low clay content. Tollebeek has an average temperature of 9.1°C and an annual precipitation of 782 mm (AM Online Projects). On the agricultural field, potato, sugar beet and grass (Poaceae) are grown. The transition area mainly consists of *Taraxacum officinale*, *Anthriscus sylvestris* and *Urtica.* The forest has a rich undergrowth containing *Rubus*, Rubiaceae, *Urtica* and *Glechoma hederacea*. The most common trees are *Acer*, *Fagus* and *Sambucus*.

7.4.3 Laboratory processing of phytoliths

From each sample, 1.0 mL of soil was measured and used for phytolith extraction. To calculate the phytolith concentration (number of phytoliths per mL soil) in each sample, 56,000 microspheres (Microparticles GmbH, Lot: SiO_2-R-L3519-3, ⌀15.29 μm, SD 0.49 μm) were added before the preparation process began. Each sample was then boiled (150°C) in 33% hydroperoxide (H_2O_2) to rid it of all organic material. Samples were then treated with 10% hydrogen chloride (HCl) and potassium permanganate ($KMnO_4$), respectively. Each sample was then decanted and left to settle for 4 h, and the process was repeated multiple times until the samples were clean. The samples were then washed with ethanol (C_2H_6O) and centrifuged another three times. Bromoform (specific gravity 2.3) was then added to each sample to float the phytoliths, after which they were centrifuged for 10 min at 1500 rpm. The flotation causes the phytoliths and microspheres to separate from all other (heavier) material. The solution with only the phytoliths and microspheres was then decanted into a tube with 100% ethanol and centrifuged for 1.5 min at 4500 rpm. The bromoform was then rinsed out with 100% ethanol over multiple centrifuge rounds. Each sample was fixated on a microscope slide with Naphrax.

Phytoliths were identified using the reference collection (in development) at the University of Amsterdam, phytolith reference atlases (Piperno, 2006) and counted using a light microscope (Carl Zeiss 464026). Unknown phytoliths were described and photographed. For each sample, at least 350 phytoliths were counted, but the sample also had to contain at least 200 total grass phytoliths (known as rondels, wavy trapezoids, bilobates, saddles and crosses; Aleman et al., 2014). The percentages of different phytoliths that are present in the samples were also calculated by dividing the number of phytoliths per morphotype by the total number of phytoliths counted. We also counted the silica microspheres in our samples to calculate the concentration of various phytolith types using the following formula:

$$\text{Concentration} = \frac{\text{Total added microspheres} \times \text{counted phytoliths}}{\text{Counted microspheres}} \text{ per mL}$$

7.4.4 Data analysis

The phytolith and vegetation data were analysed using RStudio version 1.0.153 (RStudio Team, 2015). Similarity and dissimilarity

between samples was assessed using detrended correspondence analysis (DCA). Phytolith morphotypes that occurred in fewer than two samples or in less than 5% in total were excluded from the analysis. The analysis was used to look at the differences between vegetation types (agricultural fields, transition areas and forests) and the differences by age of the agricultural fields.

One-way ANOVAs (analysis of variance) were used to determine whether individual phytolith morphotypes were significantly different ($P < .05$) between vegetation types. Before the ANOVAs were performed, outliers (samples that deviated more than 1.5 × interquartile range) were excluded from the data. These ANOVAs were performed for both the concentrations and the percentages of all the morphotypes that were used in the DCA. The same analysis was also performed for the total percentage and concentration of tree phytoliths and grass phytoliths and total concentration of phytoliths. When the ANOVA showed a significant difference, a TukeyHSD test was performed as a post-hoc test. When the assumptions for an ANOVA were not met, a Kruksal–Wallis test was performed with a Dunn test as a corresponding post-hoc test.

7.5 Results

7.5.1 Identification of phytoliths

Fig. 7.5.1 shows a micrograph of phytoliths in a field view at a magnification of 500. The phytoliths can be described and identified using guidelines such as Piperno (2006). In total 19 different phytolith morphotypes were found in all samples. Five of them were recognized as tree phytoliths, eight as grass phytoliths and one as an Asteraceae phytolith. In addition, four unknown phytoliths were detected that are probably arboreal and one of which the origin was unknown (Fig. 7.5.2).

The first unknown tree phytolith morphotype (Fig. 7.5.2A) looks like a sphere with three

FIGURE 7.5.1 Micropicture of phytoliths in the slide of Wouwse Plantage.

inlets evenly distributed over the sphere, its edge has small spikes. The size of this morphotype is approximately 10 nm. It occurred only in the sampling site near Tollebeek. In the forest sample it reached 18.5%, but in the field samples it reached 14.4% and 7.9% and in the transition area sample only 4.1%. The second unknown tree phytolith is similar to a c.80 nm large rectangular rod with small spikes (Fig. 7.5.2B). This phytolith was present in most forest samples (mean percentage = 1.05%) and in some samples from the transition areas (mean percentage = 0.77%) and agricultural fields (mean percentage = 2.98%). In three locations, Tollebeek, Wouwse Plantage and Norg, it does not occur at all.

The third unknown tree phytolith is a messy circle of smaller phytolith fragments. Most of the fragments occur at the edge of the circle; however, there are also some pieces in the middle. The circle is fairly large; approximate size is 80 nm (Fig. 7.5.2C). This morphotype was found in the samples of Eys, Winterswijk, Enschede, Norg and Groenekan, in all three vegetation types.

The fourth tree phytolith (Fig. 7.5.2D) looks like an irregular multifaceted body. The phytolith is large (c.80 nm), just like the previous

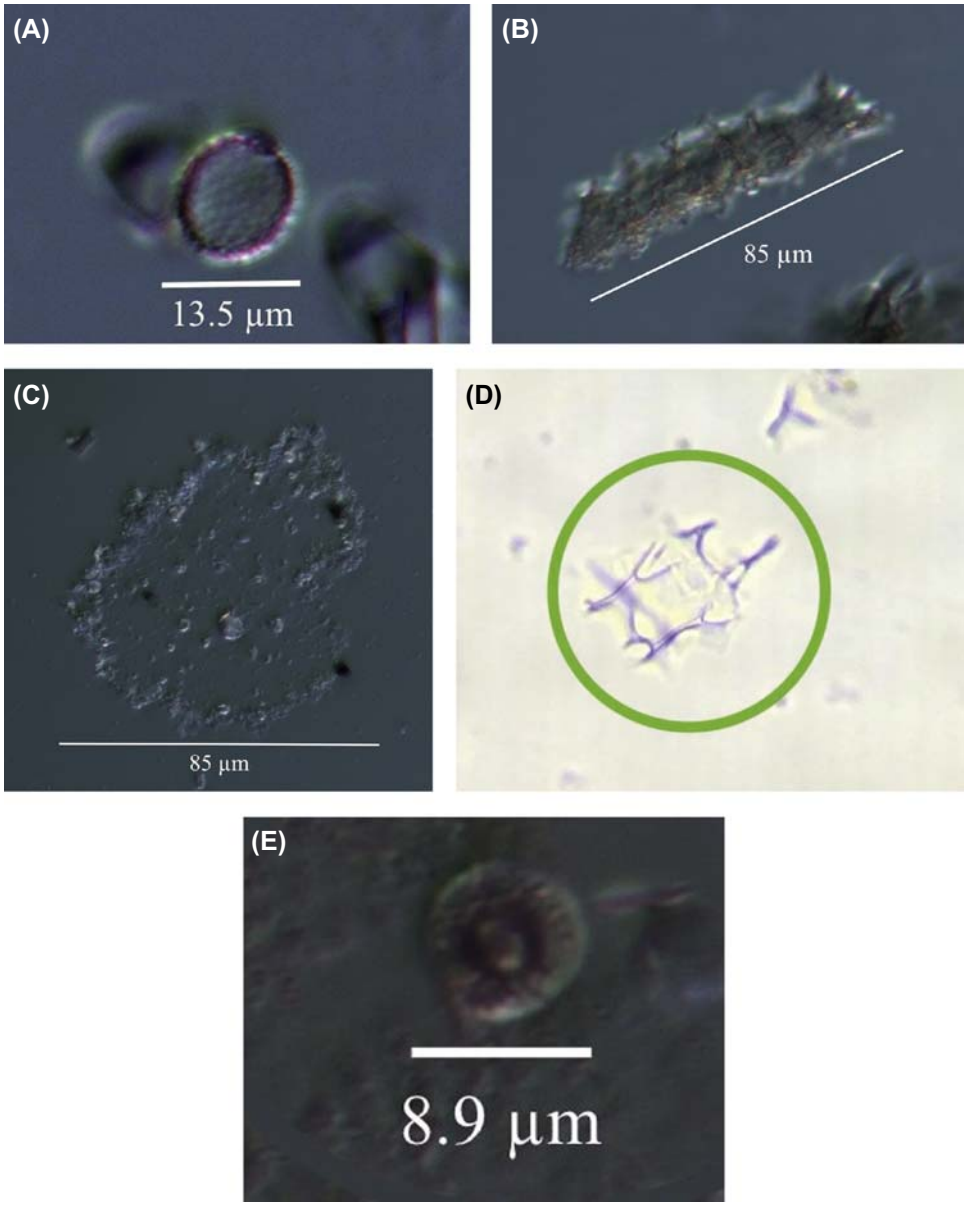

FIGURE 7.5.2 (A–E) Photographs of previously unidentified phytolith types.

unknown phytolith. It was found only in the forest sample of Eys, where it was rare (0.6%).

The last phytolith of unknown origin (Fig. 7.5.2E) is similar to a cell-like sphere; it is a round, regular sphere with smaller circles. Its average size is 10–80 nm and it is present in most forest and transition area samples and some field samples.

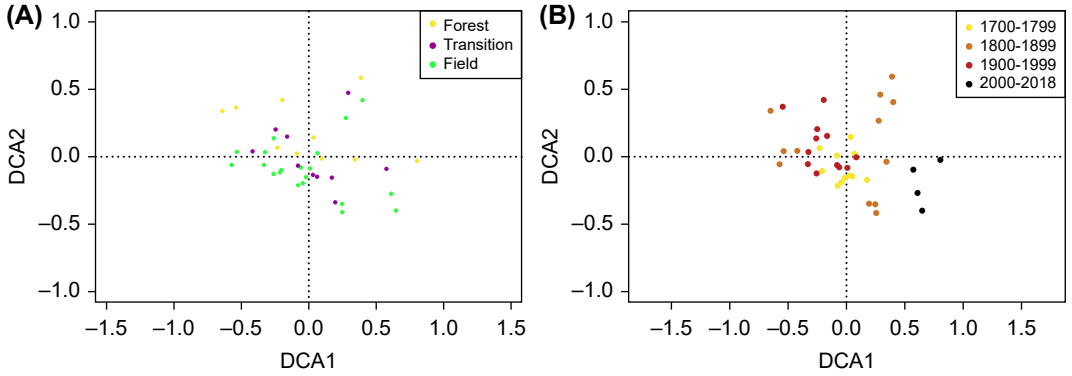

FIGURE 7.5.3 Detrended correspondence analysis (DCA) of the composition of the morphotypes of the phytoliths. (A) Groups based on the vegetation type: forest, transition area or agricultural field. (B) Groups based on the date on which the agricultural fields were converted (1700–99, 1800–99, 1900–99, 2000–18).

7.5.2 Composition of the phytolith associations

In the plot of the DCA with groups based on the vegetation type, two clusters could be seen: forests samples partly separated from the other vegetation types (agricultural fields and transition areas) forming the first cluster, while the other two vegetation types cannot be separated from each other but form the other cluster (Fig. 7.5.3A). When separation is based on the age of the agricultural fields, no clear pattern is visible. Some samples from the same century clustered together; however, the samples from 1800 to 99 do not form a cluster. The different clusters over the centuries also do not show a gradient (Fig. 7.5.3B).

For four of the phytolith types, a significant difference between vegetation types was present: large rugose, small rugose, rondels and wavy trapezoids (Fig. 7.5.4). Both arboreal phytolith types were most present in forest samples. Large rugose had a significantly higher percentage in forest samples (7%) than in samples from agricultural fields (3%) and transition areas (4%) (Forest-Field: $P = .000152$, TukeyHSD, Transition-Forest: $P = .003327$, TukeyHSD). Small rugose also had a relatively high percentage in forest samples (8%) but also in transition areas (7.5%), the proportion in agricultural fields was lower (4%) (Forest-Field: $P = .000069$, TukeyHSD, Transition-Field: $P = .008273$, TukeyHSD). The two morphotypes that pertain to grasses both had a significantly higher percentage in samples from agricultural fields. Rondels had the highest percentage in these samples (45%), while they had a relative low percentage in the forest samples (31%) ($P = .009877$, TukeyHSD); the proportion in the transition areas was not significantly different from both the fields and the forests (40%). Wavy trapezoid percentages were significantly lower in forest samples (6%), which makes them differ from the agricultural fields (14%) and transition areas (15%) (Forest-Field: $P = .004650$, Dunn test, Transition-Forest: $P = .006353$, Dunn test).

Both the total grass phytolith proportion and total tree phytolith proportion showed a significant difference (Fig. 7.5.5). The total grass phytolith proportion was significantly higher in agricultural fields (92%) than in forests (80%) ($P = .002589$, Dunn test). In transition areas the proportion was not significantly different from fields or forests (87%). The difference between

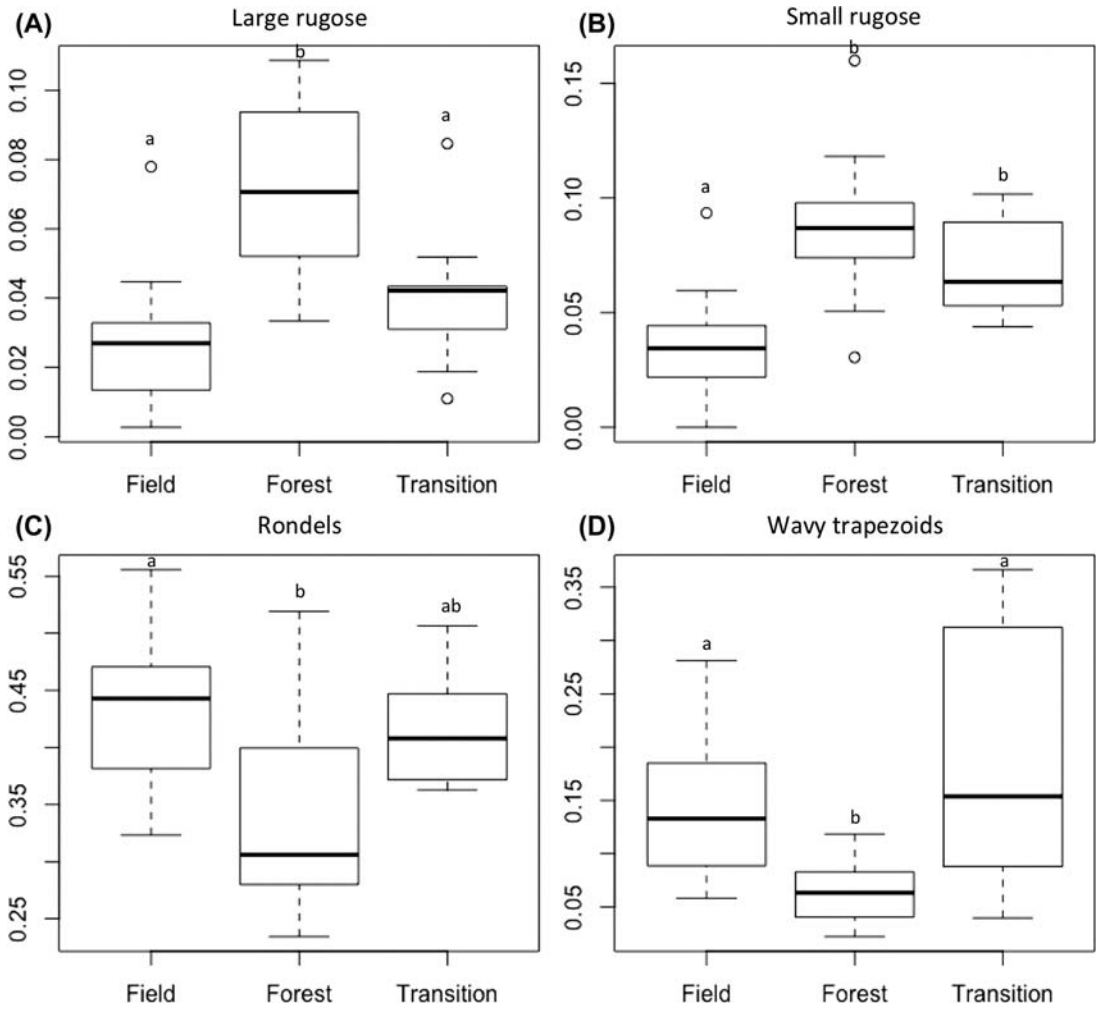

FIGURE 7.5.4 Characteristic proportions of phytoliths per vegetation type. In this figure the proportions of morphotypes of the phytoliths that are significantly different between forest, transition and field are shown. (A) shows large rugose, (B) shows small rugose, (C) shows rondels, (D) shows wavy trapezoids.

the total tree phytolith proportion of agricultural fields (8%) and forests (20%) was significant ($P = .000813$, TukeyHSD). Forest samples were also significantly different from transition areas (12%) ($P = .019480$, TukeyHSD).

A significant correlation was present between the proportion of total tree phytoliths and total number of trees counted in the vegetation surveys ($P = .002584$, Spearman's rank test). A correlation was not present between the proportion of grass phytoliths and percentage of undergrowth cover.

7.5.3 Phytolith concentrations

The DCA did not show a clear separation between the vegetation types (Fig. 7.5.6A). The

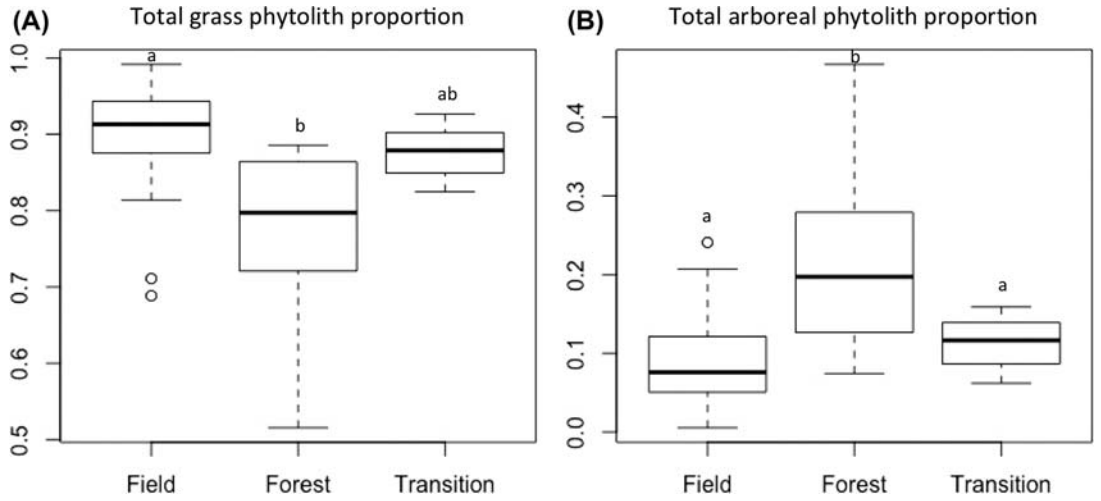

FIGURE 7.5.5 Total grass phytolith proportion and total tree phytolith proportion. This figure shows the total proportion of grass and tree phytoliths for the different vegetation types. In (A), the total grass phytolith proportion is shown; here a significant difference between agricultural fields and forests is present. In (B), the total tree phytolith proportion is shown; the forests differ significantly from both the agricultural fields and the transition areas.

horizontal axis (1) of the DCA explains 16.31% of the separation; the second axis explains 9.38%. It also shows that the age of the agricultural fields had a minor influence on separation; however, there was no clear pattern in this plot (Fig. 7.5.6B). All samples within the same century cluster together, except for the 1800–99 samples; the clusters do not show a gradient, however.

Four of the morphotypes had a significantly different concentration between the vegetation types, namely small rugose, rondels, wavy trapezoids and trilobates (Fig. 7.5.7). Small rugose was present in a significantly higher

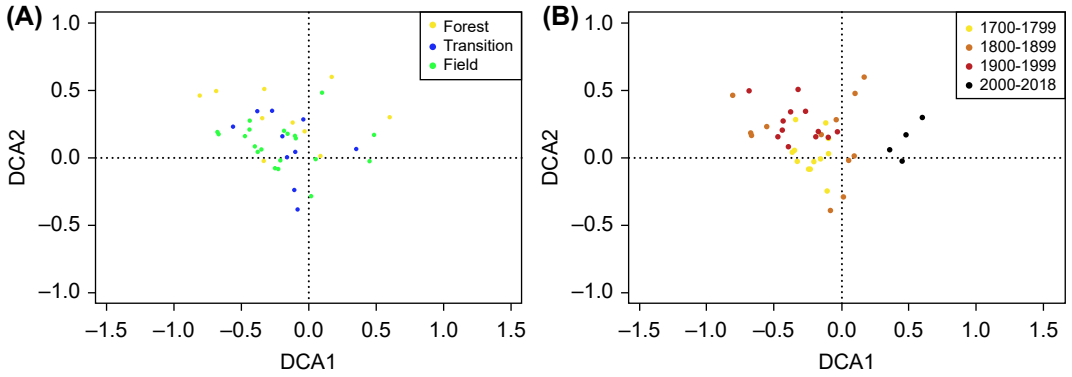

FIGURE 7.5.6 Detrended correspondence analysis (DCA) of the phytolith concentrations. In this plot, the results of the DCA of the concentrations of the phytoliths are shown. In (A), the grouping is based on the vegetation type, forest, transition area or agricultural field. (B) is grouped based on the date on which the agricultural fields were converted. The first axis explains 16.31% of the data; the second axis explains 9.38%.

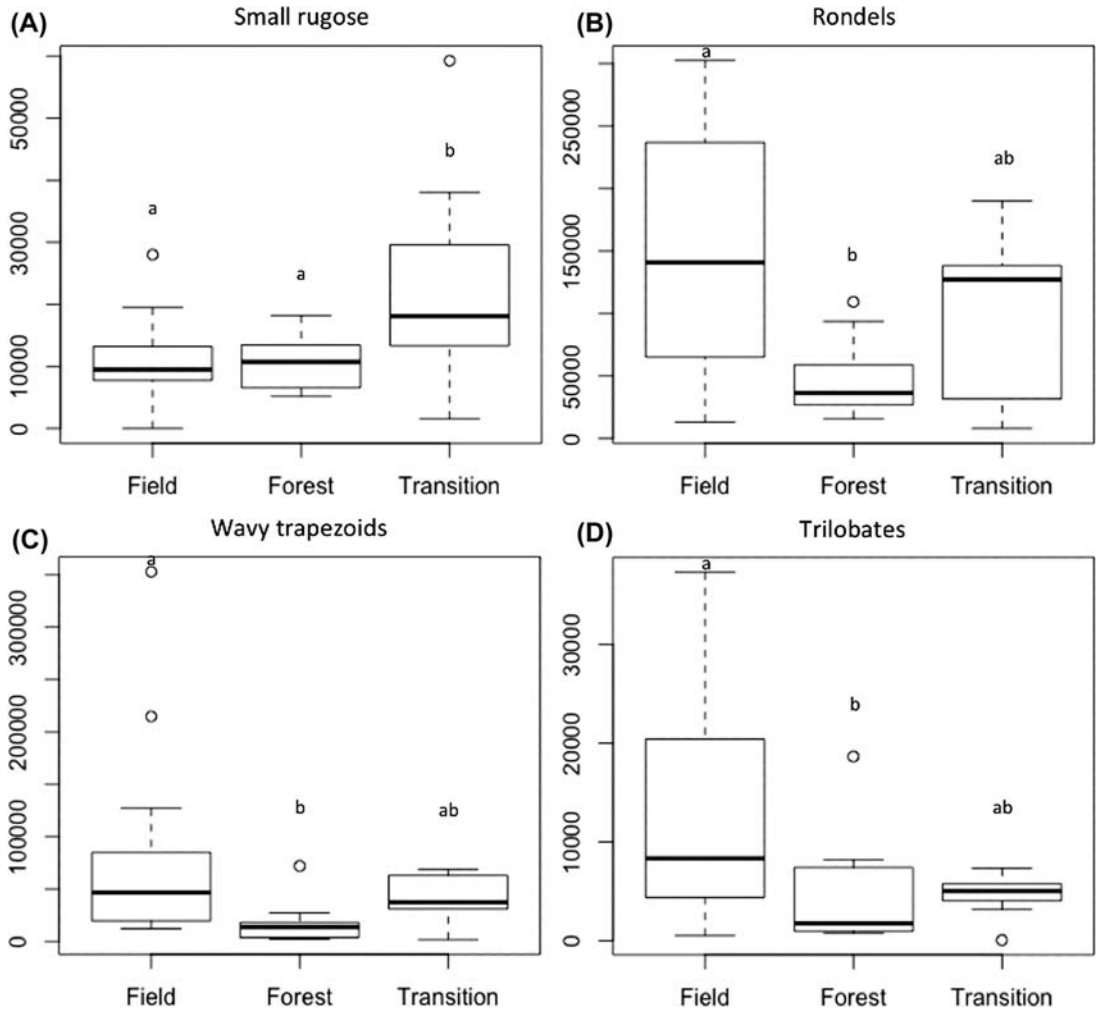

FIGURE 7.5.7 (A–D) Characteristic concentrations of phytolith morphotypes.

concentration in transition areas (c.18,000 phytoliths/mL) than in forests (c.12,000 phytoliths/mL) and agricultural fields (c.10,000 phytoliths/mL) (Transition-Field: $P = .014990$, TukeyHSD, Transition-Forest: $P = .037746$, TukeyHSD). The three grass phytolith types showed the same pattern. A significant difference between agricultural fields and forests is present; however, transition areas did not differ significantly. For rondels, the average concentration in samples from agricultural fields is c.140,000 phytoliths/mL, in forests it is c.40,000 phytoliths/mL and in transition areas it is c.130,000 phytoliths/mL ($P = .011643$, TukeyHSD). For wavy trapezoids, the average concentrations are c.50,000 phytoliths/mL (agricultural fields), c.40,000 phytoliths/mL (transition areas) and c.10,000 phytoliths/mL (forests) ($P = .010655$, TukeyHSD). The average concentrations for trilobates are c.8000 phytoliths/mL

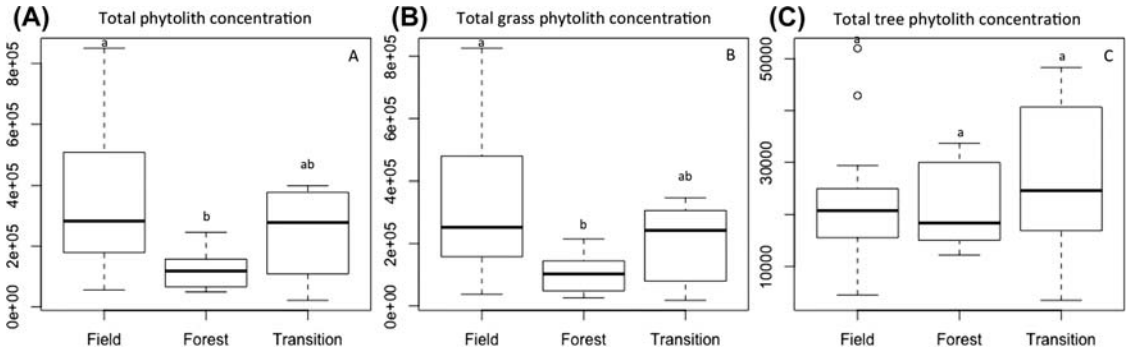

FIGURE 7.5.8 (A–C) Total phytolith concentration and total grass phytolith and tree phytolith concentration.

(agricultural fields), c.5000 phytoliths/mL (transition areas) and c.2500 phytoliths/mL (forests) ($P = .031280$, TukeyHSD).

There is also a significant difference between the total concentration of agricultural fields (c.3,000,000 phytoliths/mL) and forests (c.1,000,000 phytoliths/mL) ($P = .026584$, TukeyHSD) (Fig. 7.5.8). Transition areas do not differ significantly from the other two vegetation types (c.2,900,000 phytoliths/mL). The total grass phytolith concentration had the same significant difference as the total concentration ($P = .022314$, TukeyHSD). The average grass phytolith concentration in agricultural fields is c.3,000,000 phytoliths/mL, in transition areas it is 2,900,000 phytoliths/mL and in forests it is 1,000,000 phytoliths/mL. No significant difference was found between the tree phytolith concentrations.

Between the total grass phytolith concentration and the total percentage undergrowth there was no significant correlation. A correlation was also not found between the total arboreal phytolith concentration and the total number of trees counted.

7.6 Discussion

The phytolith assemblages contain seven previously unidentified phytolith morphotypes and show both expected and unexpected patterns between the soils of the forests, transition and agricultural areas. It was expected that forest soils contain mostly arboreal phytoliths, while agricultural fields would mostly contain grass phytoliths. The concentration of total phytoliths was expected to be highest in forests and lowest in agricultural fields. While significant differences between some phytolith types were as expected, the overall separation in composition and concentration was not as clear as expected.

An explanation for the lack of separation is possibly that in this study strip forests were mostly used. Due to this, these forests could be an inadequate representation for Dutch forests. When the phytolith data of this study are compared with phytolith assemblages from non-disturbed forests, differences between vegetation types become more apparent (Land, 2018) (Fig. 7.6.1). In the study of Land (2018) only forests that have always been forests had been selected. The DCA with both these data showed that a difference between agricultural fields and undisturbed forests is present, which confirms the initial hypothesis that agricultural fields have a different assemblage than forests.

Another possibility is that the geographical location of the samples has an influence on the separation between the samples of this study and the samples of Land (2018). This is, however, unlikely since the locations that are used are all

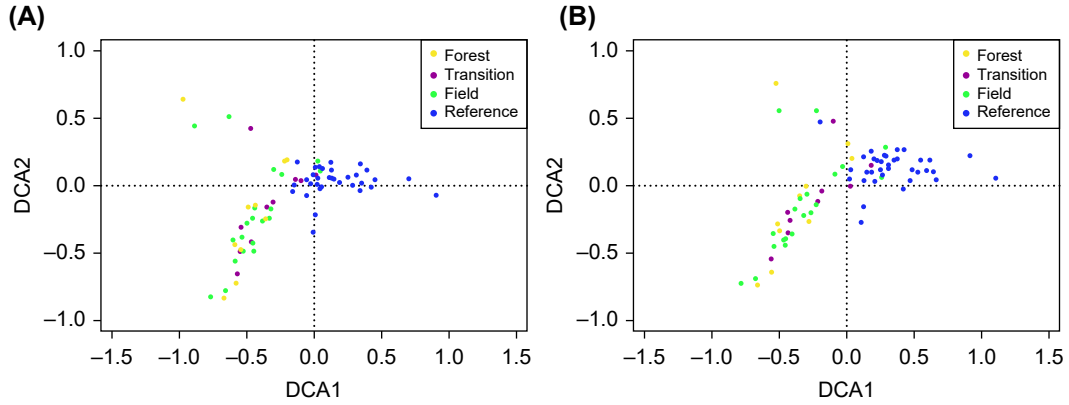

FIGURE 7.6.1 Results of the detrended correspondence analyses (DCAs) with reference data included. In this plot, the results of the DCAs with reference material (samples of undisturbed forests; Land, 2018) are shown. The first DCA (A) shows the assemblage of the samples (percentages of the phytoliths) and the second DCA (B) shows the concentrations. A difference is visible between the reference material and the data of this study.

different from each other except for the location near Norg and the Norgerholt. These locations do not cluster together, which could be an indication that location does not have an influence on separation.

A third factor that could affect the phytolith composition is the composition of the adjacent forest vegetation. An example where this could be the case is the location near Eys, Limburg (Fig. 7.6.2A). In the phytolith composition plot, this location clusters separately from the other locations. Limburg has a quite different soil type than the other locations, leading to a distinctly different vegetation. The main difference between the composition of Eys and the composition of the other locations is the amount of arboreal phytoliths, which is higher than in the other locations.

The number of trees or the composition of the trees in Limburg is from the same as the other locations (Table 7.6.1); however, the undergrowth is quite distinct (Table 7.6.2). Because in the

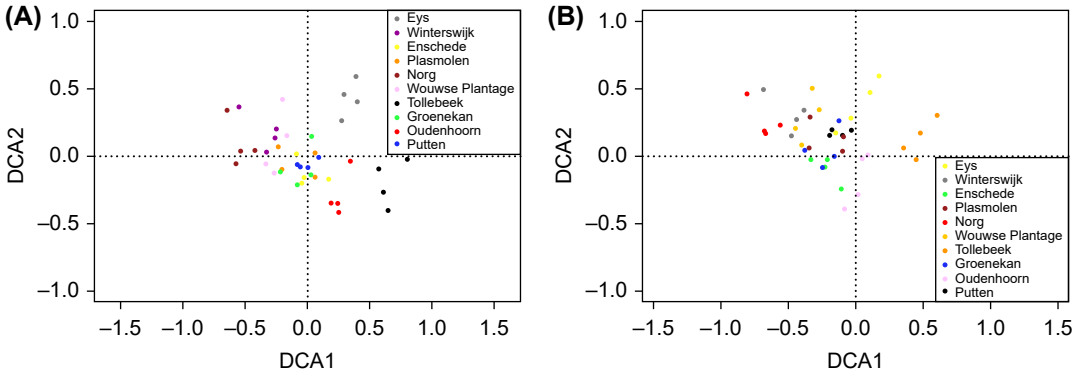

FIGURE 7.6.2 Results of the detrended correspondence analysis (DCA) grouped on location. In (A), the results of the DCA are shown, based on the phytolith type composition. The colours mark the different locations. In (B), the results of the DCA based on the phytolith type concentration are shown.

TABLE 7.6.1 Vegetation surveys of the tree assemblages (in %).

Location	Vegetation type	*Betula* (%)	*Fagus* (%)	*Pinus* (%)	*Sambucus* (%)	*Quercus* (%)	*Acer* (%)	*Tilia* (%)	*Prunus* (%)	Total (%)	Total (number)
Eys	Forest	0.0	37.5	0.0	0.0	12.5	37.5	12.5	0.0	100	8
Eys	Transition	0.0	0.0	0.0	22.2	0.0	22.2	55.6	0.0	100	9
Winterswijk	Forest	0.0	15.4	15.4	23.1	15.4	0.0	0.0	30.8	100	13
Winterswijk	Transition	0.0	0.0	0.0	0.0	0.0	0.0	0.0	0.0	0	0
Enschede	Forest	0.0	21.1	0.0	21.1	52.6	0.0	0.0	5.3	100	19
Enschede	Transition	0.0	0.0	0.0	0.0	0.0	0.0	0.0	0.0	0	0
Plasmolen	Forest	0.0	25.0	0.0	37.5	0.0	25.0	0.0	12.5	100	8
Plasmolen	Transition	0.0	0.0	0.0	50.0	0.0	0.0	0.0	50.0	100	2
Norg	Forest	12.5	0.0	0.0	62.5	0.0	0.0	0.0	25.0	100	8
Norg	Transition	0.0	0.0	0.0	0.0	0.0	0.0	0.0	0.0	0	0
Wouwse Plantage	Forest	0.0	0.0	41.7	8.3	0.0	0.0	0.0	50.0	100	12
Wouwse Plantage	Transition	0.0	0.0	0.0	25.0	0.0	0.0	0.0	75.0	100	4
Tollebeek	Forest	0.0	16.7	0.0	25.0	0.0	58.3	0.0	0.0	100	12
Tollebeek	Transition	0.0	0.0	0.0	0.0	0.0	0.0	0.0	0.0	0	0
Groenekan	Forest	0.0	11.1	0.0	33.3	33.3	0.0	22.2	0.0	100	9
Groenekan	Transition	0.0	0.0	0.0	0.0	0.0	0.0	100.0	0.0	100	1
Oudenhoorn	Forest	0.0	50.0	0.0	12.5	37.5	0.0	0.0	0.0	100	8
Oudenhoorn	Transition	0.0	0.0	0.0	0.0	0.0	0.0	0.0	0.0	0	0
Putten	Forest	0.0	58.8	0.0	17.6	5.9	11.8	0.0	5.9	100	17
Putten	Transition	0.0	0.0	0.0	0.0	0.0	0.0	0.0	0.0	0	0

The last column contains the total numbers of trees found in the sample.

TABLE 7.6.2 Vegetation surveys of the undergrowth (coverage in %).

Location	Vegetation type	*Fagus* (%)	*Narcissus* (%)	*Pinus* (%)	*Quercus* (%)	*Glechoma* (%)	Ranun-culaceae (%)	Asteraceae (%)	Fabaceae (%)	*Urtica* (%)	Apiaceae (%)	Araliaceae (%)	Araceae (%)	Rubiaceae (%)
Eys	Forest	0	0	0	5	0	0	0	0	0	0	10	5	5
Eys	Transition	0	0	0	0	0	0	5	0	2	10	0	0	5
Winterswijk	Forest	0	0	0	0	0	0	0	0	0	0	0	0	0
Winterswijk	Transition	0	0	0	2	0	0	2	0	0	0	0	0	0
Enschede	Forest	0	0	0	5	0	0	0	0	0	0	0	0	0
Enschede	Transition	0	0	0	5	0	0	0	0	0	0	0	0	2
Plasmolen	Forest	2	0	0	0	0	0	0	0	0	0	0	0	0
Plasmolen	Transition	0	0	0	0	0	0	0	0	25	0	0	0	0
Norg	Forest	0	0	0	0	0	0	0	0	0	0	0	0	0
Norg Wouwse	Transition	0	0	0	0	0	0	0	0	0	0	0	0	0
Plantage Wouwse	Forest	0	0	0	0	0	0	0	0	0	0	0	0	0
Plantage	Transition	0	0	0	1	0	0	0	0	0	0	0	0	0
Tollebeek	Forest	30	0	0	0	5	0	0	0	30	0	0	0	5
Tollebeek	Transition	0	0	0	0	5	35	20	0	7.5	10	0	0	0
Groenekan	Forest	0	0	0	0	0	0	0	0	0	2	0	0	0
Groenekan	Transition	0	0	0	2	0	0	0	0	2	0	0	0	0
Oudenhoorn	Forest	0	0	0	0	0	0	0	0	10	0	0	0	10
Oudenhoorn	Transition	0	0	0	0	0	0	0	1	0	0	0	0	0
Putten	Forest	0	1	1	0	0	0	0	0	0	0	0	0	0
Putten	Transition	0	0	0	0	2	0	5	1	0	0	0	0	0

forest where the sample was taken only a low undergrowth cover is present and that undergrowth is not known to have a high phytolith production, this could lead to increased arboreal phytolith percentage.

A different location that clustered separately from the other location in the DCA based on the phytolith type concentration was Tollebeek, Flevoland (Fig. 7.6.2). Tollebeek might be different from the other locations because it used to be under water until 80 years ago. Because of this, these samples mostly contained diatoms and not phytoliths. While it can be used as a representation for a younger agricultural field, there was no previous old forest or it might not have been a forest at all before, which leads to variation between this site and the other sites.

Another problem that occurred when selecting the locations was that the used dataset was based on the average amount of agricultural fields in a grid, which means that it might not be precise enough to base the age of fields on. This could affect the pattern in the composition and concentration when looking at the age of the agricultural fields. However, since the different centuries still somewhat cluster together this might not be the case. Another explanation for the lack of pattern in the different locations is that, perhaps due to ploughing, the disturbance of the phytolith composition made by converting forest to agricultural fields is a singular event instead of a process that takes a few years.

The increase in phytolith concentration that was found in the samples of agricultural fields was unexpected; a decrease in total phytolith concentration in these samples was expected. Two explanations can be given for this. The first is that harvesting has less of an effect than previously thought. This is, however, unlikely since previous research indicates that a decrease in phytoliths occurs when crops are harvested (Sommer et al., 2013; Cornelis and Delvaux, 2016). The second, more likely, explanation is that the fields are fertilized and that this fertilization has a large effect on the amount of phytoliths in the soil. Evidence for this is that the differences in concentration between the fields are large (Fig. 7.6.2A); this indicates that some fields are fertilized and some are not. It could also be an indication for different fertilization methods (Hossain et al., 2001; Mecfel et al., 2007; Rodgers-Gray and Shaw, 2004); however, further research will be needed to come to a conclusion. When all factors are combined, it can, however, be concluded that they do correctly display the Si-cycle and the effects of agriculture as depicted in the conceptual diagram of Fig. 7.3.1.

From this study it can be concluded that agricultural disturbance has an effect on the phytolith composition of the soil. Areas that are converted to agricultural fields have a different phytolith composition than forests, meaning that they can be recognized in palaeoecological records. Also, it is important for these records to take into account that regional differences have an effect on the differences in phytolith composition. This means that, while agricultural fields can be recognized, different regions can also be recognized by their phytolith composition.

7.7 Conclusions

Based on these results, it can be concluded that differences in phytolith association of soils under different vegetation types are present. Aside from that, a difference between regions is present as well. The differences in the assemblage and the concentration of phytoliths in the samples were probably not influenced by the age of the agricultural fields.

This study is just a pilot study and further research is needed to enable conclusions on changes in the landscape of the Netherlands in relation to agricultural development. Crucial is the creation of a reference base of phytoliths,

present in plants that occur in forests, grasslands and agricultural crops in the region or even in Europe as a whole. This pilot shows that phytolith analysis is a potentially promising proxy for many geoecological studies based on information from soil archives.

References

Aleman, J.C., Canal-Subitani, S., Favier, C., Bremond, L., 2014. Influence of the local environment on lacustrine sedimentary phytolith records. Palaeogeography, Palaeoclimatology, Palaeoecology 414, 273–283.

Alexandra, A., 1997. Content and distribution of phytoliths in the main types of soils in Eastern Europe. In: Pinilla, A., Juan-Tresserras, J., Machado, M.J. (Eds.), First European Meeting on Phytolith Research. Editorial CSIC-CSIC Press, p. 15.

Alterra, W.U., 2006. Grondsoortenkaart. WUR. https://www.wur.nl/nl/show/Grondsoortenkaart.htm.

AM Online Projects , Climate-Data.org. Available: Climate-Data.org [accessed 2018, 07-01].

Blinnikov, M.S., 2005. Phytoliths in plants and soils of the interior Pacific Northwest, USA. Review of Palaeobotany and Palynology 135, 71.

CBS (Centraal Bureau voor de Statistiek), 2016. Den Haag, PBL Planbureau voor de Leefomgeving, Den Haag, RIVM Rijksinstituut voor Volksgezondheid en Milieu. Bilthoven & en Wageningen University and Research, Wageningen, 16-12-2016-last update, Land- en tuinbouw: ruimtelijke spreiding, grondgebruik en aantal bedrijven, 1980-2015. http://www.clo.nl/indicatoren/nl2119-agrarisch-grondgebruik.

CBS, PBL, RIVM, WUR, 2018. Meteorologische gegevens, 1990–2017 (Indicator 0004, Versie 20, 17 Mei 2018). http://www.clo.nl/indicatoren/nl0004-meteorologische-gegevens-in–nederland.

Cornelis, J., Delvaux, B., 2016. Soil processes drive the biological silicon feedback loop. Functional Ecology 30, 1298–1310.

Coughenour, M.B., 1985. Graminoid responses to grazing by large herbivores: adaptations, exaptations, and interacting processes. Annals of the Missouri Botanical Garden 72, 852–863.

de Melo, S.P., Monteiro, F.A., De Bona, F.D., 2010. Silicon distribution and accumulation in shoot tissue of the tropical forage grass *Brachiaria brizantha*. Plant and Soil 336, 241–249.

Fredlund, G.G., Tieszen, L.T., 1994. Modern phytolith assemblages from the North American great plains. Journal of Biogeography 21, 321–335.

Guntzer, F., Keller, C., Meunier, J., 2012a. Benefits of plant silicon for crops: a review. Agronomy for Sustainable Development 32, 201–213.

Guntzer, F., Keller, C., Poulton, P.R., McGrath, S.P., Meunier, J., 2012b. Long-term removal of wheat straw decreases soil amorphous silica at Broadbalk, Rothamsted. Plant and Soil 352, 173–184.

Harms, W., Stortelder, A., Vos, W., 1987. Effects of intensification of agriculture on nature and landscape in the Netherlands. In: Wolman, M.G., Fournier, F.G.A. (Eds.), Land Transformation in Agriculture. John Wiley & Sons, New York, pp. 357–379.

Haynes, R.J., 2017. The nature of biogenic Si and its potential role in Si supply in agricultural soils. Agriculture, Ecosystems and Environment 245, 100–111.

Hossain, K.A., Horiuchi, T., Miyagawa, S., 2001. Effects of silicate materials on growth and grain yield of rice plants grown in clay loam and sandy loam soils. Journal of Plant Nutrition 24, 1–13.

Hunt, J., Dean, A., Webster, R., Johnson, G., Ennos, A., 2008. A novel mechanism by which silica defends grasses against herbivory. Annals of Botany 102, 653–656.

Jackson, S.T., 1990. Pollen source area and representation in small lakes of the northeastern United States. Review of Palaeobotany and Palynology 63, 53–76.

Jackson, S.T., Kearsley, J.B., 1998. Quantitative representation of local forest composition in forest-floor pollen assemblages. Journal of Ecology 86, 474–490.

Kirchholtes, R.P., van Mourik, J.M., Johnson, B.R., 2015. Phytoliths as indicators of plant community change: a case study of the reconstruction of the historical extent of the oak savanna in the Willamette Valley Oregon, USA. Catena 132, 89–96.

Klein Goldewijk, K., Beusen, A., de Vos, M., van Drecht, G., 2011. The HYDE 3.1 spatially explicit database of human induced land use change over the past 12,000 years. Global Ecology and Biogeography 20, 73.

Land, K., 2018. Phytolith Composition of Dutch Forests (Bachelor thesis). IBED, University of Amsterdam, Amsterdam.

Liang, Y.C., Ma, T.S., Li, F.J., Feng, Y.J., 1994. Silicon availability and response of rice and wheat to silicon in calcareous soils. Communications in Soil Science and Plant Analysis 25, 2285–2297.

Massey, F.P., Hartley, S.E., 2009. Physical defences wear you down: progressive and irreversible impacts of silica on insect herbivores. Journal of Animal Ecology 78, 281–291.

McMichael, C.N.H., Philip, A., 2019. Quantifying Phytolith Concentrations along an Elevational Gradient in 2 Neotropical Soils and Sediments. Intern report, IBED, University of Amsterdam, Amsterdam.

Mecfel, J., Hinke, S., Goedel, W.A., Marx, G., Fehlhaber, R., Bäucker, E., Wienhaus, O., 2007. Effect of silicon fertilizers

on silicon accumulation in wheat. Journal of Plant Nutrition and Soil Science 170, 769–772.

Müller, J., Clauss, M., Codron, D., Schulz, E., Hummel, J., Fortelius, M., Kircher, P., Hatt, J., 2014. Growth and wear of incisor and cheek teeth in domestic rabbits (*Oryctolagus cuniculus*) fed diets of different abrasiveness. Journal of Experimental Zoology Part A: Ecological Genetics and Physiology 321, 283–298.

Müller, J., Clauss, M., Codron, D., Schulz, E., Hummel, J., Kircher, P., Hatt, J., 2015. Tooth length and incisal wear and growth in Guinea pigs (*Cavia porcellus*) fed diets of different abrasiveness. Journal of Animal Physiology and Animal Nutrition 99, 591–604.

Parshall, T., Calcote, R., 2001. Effect of pollen from regional vegetation on stand-scale forest reconstruction. The Holocene 11, 81–87.

Piperno, D.R., 1985. Phytolith analysis and tropical paleoecology: production and taxonomic significance of siliceous forms in New World plant domesticates and wild species. Review of Palaeobotany and Palynology 45, 185–228.

Piperno, D.R., 2006. Phytoliths: A Comprehensive Guide for Archaeologists and Paleoecologists. Rowman, Altamira.

Piperno, D.R., 2014. Phytolith Analysis: An Archaeological and Geological Perspective. Elsevier, Amsterdam.

Reynolds, O.L., Keeping, M.G., Meyer, J.H., 2009. Silicon-augmented resistance of plants to herbivorous insects: a review. Annals of Applied Biology 155, 171–186.

Rodgers-Gray, B., Shaw, M., 2004. Effects of straw and silicon soil amendments on some foliar and stem-base diseases in pot-grown winter wheat. Plant Pathology 53, 733–740.

Rovner, I., 1971. Potential of opal phytoliths for use in paleoecological reconstruction. Quaternary Research 1, 343–359.

RStudio Team, 2015. RStudio: Integrated Development Environment for R, 1.0, 153 edn. RStudio, Inc., Boston, MA.

Runge, F., 1999. The opal phytolith inventory of soils in central Africa—quantities, shapes, classification, and spectra. Review of Palaeobotany and Palynology 107, 23–53.

Savant, N.K., Datnoff, L.E., Snyder, G.H., 1997. Depletion of plant-available silicon in soils: a possible cause of declining rice yields. Communications in Soil Science and Plant Analysis 28, 1245–1252.

Shakoor, S., Bhat, M., Mir, S., 2014. Phytoliths in plants: a review. Research and Reviews: Journal of Botanical Sciences 3, 10–24.

Sommer, M., Jochheim, H., Höhn, A., Breuer, J., Zagorski, Z., Busse, J., Barkusky, D., Meier, K., Puppe, D., Wanner, M., 2013. Si cycling in a forest biogeosystem. Biogeosciences 10, 4991.

van Mourik, J.M., Seijmonsbergen, A.C., Slotboom, R.T., Wallinga, J., 2012. The impact of human land use on soils and landforms in cultural landscapes on aeolian sandy substrates (Maashorst, SE Netherlands). Quaternary International 265, 74–89.

This page intentionally left blank

CHAPTER

8

Can geodiversity help to save the soil archives?

A.C. Seijmonsbergen[a,*], J.A.M. van den Ancker[b], P.D. Jungerius[b], S.J. Norder[a,c]

[a]Theoretical and Computational Ecology (TCE), University of Amsterdam, Amsterdam, the Netherlands; [b]Geoheritage NL, Ede, the Netherlands; [c]Centre for Ecology, Evolution and Environmental Changes (cE3c)/Azorean Biodiversity Group, Faculdade de Ciências, Universidade de Lisboa, Lisboa, Portugal

*Corresponding author.

8.1 Introduction

Palaeosols, soils that are no longer influenced by active soil-forming processes, are windows on the past: they contain information about landscape development, soil diversity and cultural heritage. Palaeosols are fossil soils that have been buried by volcanic, aeolian, colluvial, glacial, anthropogenic or other depositional processes (Chaopricha and Marín-Spiotta, 2014). They play an important role in the reconstruction of past, long- and short-term soil-forming processes, and they reflect former climatic conditions, parent material, topographic conditions, levels of organic activity (Jenny, 1994) and human activities (Richter, 2007). Often, most palaeosols contain important scientific and cultural information, not only about pedogenic processes, but also on the geomorphological development of former landscapes, including land use and land cover changes. They are part of the 'soil archive' and reflect past environmental and societal conditions. Deciphering soil archives is facilitated by new analytical techniques such as optical stimulated luminescence dating of sand (Chapter 4), phytolith analysis (Chapter 7) and biomarkers of palaeosols (Chapter 5), in parallel with traditional soil analysis techniques such as soil micromorphology (Chapter 1), soil pollen analysis (Chapter 2) and radiocarbon dating (Chapter 3). These techniques substantially improve our knowledge of the soil archive and open up new ways to quantify soil diversity, landscape dynamics, spatiotemporal patterns of soil loss and past human–soil interactions. The soil studies described in previous chapters emphasize the human impact on soil loss rates and the contribution of historic land use to building the soil archive.

Reading the Soil Archives
https://doi.org/10.1016/B978-0-444-64108-3.00008-2

The soil archive includes the past and present soils in the landscape, but can also comprise a collection of stored soil specimens, aiming to provide facilities and protocols for conserving the long-term scientific value of soil specimens and associated soil data (Karssies and Wilson, 2015). Without protection, the natural soil archives in a landscape are exposed to natural degradation processes or threatened by land use and land cover changes. The cultural heritage value, stored in palaeosols, could be irreversibly lost.

A major challenge in the conservation of palaeosols is that their spatial distribution is largely unknown. A reason is that palaeosols are inadequately developed in the current soil classification systems (Krasilnikov and García Calderón, 2006): soil scientists categorize the current soil types based on recent soil-forming processes and neglect buried palaeosols. Soil classification systems in general focus on the actual soil and ignore the polycyclic dimension. In contrast to descriptions of geological key localities of litho- and biostratigraphic importance, which are protected worldwide, descriptions of key soil profiles and related collections of soil samples are mainly managed by national soil surveys. For example, the Australian national soil archive (National Soil Archive, 2019) stores >75,000 soil samples, taken from 9500 sites in Australia. This archive is saved behind 'closed doors' and a digital counterpart is accessible through the Australian Soil Resource Information System (Australian Soil Resource Information System, 2019). In addition to physically stored soil profile samples and profiles, digital global repositories exist, such as the SoilGrids database (Hengl et al., 2014), the Harmonized World Soil Database (Fischer et al., 2008), the ISRIC-WISE Global Soil Profile data soil database (Batjes, 2009) and, for Europe, the LUCAS system (Orgiazzi et al., 2018).

Fortunately, the current anthropogenic pressures and soil conditions may be manipulated to slow down soil loss threats and thus promote preservation (Davidson and Wilson, 2006). Therefore the distribution of valuable soils should be known to ensure that efficient legislation can promote, support and secure the soil archive in the landscape for future generations. However, implementation of such legislation is challenging because it involves complex trade-offs between the cultural, provisioning, supporting and regulating services that the soil provides. The contribution of actively forming soils to economic sectors such as agriculture, forestry and mineral extraction sometimes hampers the adoption of legislation that aims to protect the soil archive. This emphasizes the need for science-based, transparent and widely applicable strategies for the identification, mapping and monitoring of soil erosion-prone areas, which may serve as input to support soil conservation initiatives from local to national and global scales. The distribution and intensity of soil erosion should ideally be monitored in a transferable, transparent and repeatable way, based on consistent indicators for soil degradation in the context of the landscape.

While the conservation of palaeosols is still in its infancy, palaeosols are sometimes indirectly protected by measures aimed at protecting the bio- and geodiversity in landscapes. Soil, including palaeosols, is one of the components of geodiversity. Viewing palaeosols in the wider context of geodiversity might facilitate the conservation of these archives of human–environment interactions. The key question we aim to address in this final chapter is how palaeosols and the soil archive can be preserved. To address this question, we adopt a landscape approach and view the protection of palaeosols in the wider context of geodiversity and geoheritage conservation. We present examples of the relationships between soils and geodiversity and give an overview of major threats to soils and palaeosols. Finally, using the European Union as a case study, we highlight policy measures to support sustainable use and management of soils.

8.2 Soils are part of nature's diversity

Nature's diversity can be divided into biodiversity, which is not further discussed here, and geodiversity. While nature conservation policies still mainly emphasize the conservation of biodiversity (Gordon et al., 2017), geodiversity is increasingly seen as a useful concept in nature conservation (Hjort et al., 2015). We here define geodiversity, geoheritage and geoconservation:

- *Geodiversity* is the natural range (diversity) of geological (rocks, minerals, fossils), geomorphological (landform, processes), hydrological (lakes, rivers) and soil features. It includes their assemblages, relationships, properties, interpretations and systems (Gray, 2013).
- *Geoheritage* is those parts of geodiversity that are specifically identified as having conservation significance, i.e., that have some specific value to human society and therefore ought to be conserved, particularly if they are threatened by human activities and could therefore be lost or damaged (Gray, 2013).
- *Geoconservation* is the practice of conserving, enhancing and promoting awareness of those features and underlying processes of geodiversity that have significant scientific, educational, cultural, aesthetic or ecological value (Gordon et al., 2018).

The definition of geodiversity by Gray (2013) not only refers to the natural components of geodiversity at a landscape scale, but also to sites and elements of natural and/or cultural importance. Geosites and geoheritage elements can be assigned certain values in relation to the scientific, touristic and/or educational functions they represent for society, or because they are part of the quality of our daily living environment. The unique educational quality of palaeosols is that they reflect periods of landscape formation and historical information of changing land use and land cover in cultural systems. Many European and international organizations are actively promoting the inventory and conservation of geoheritage elements (see Section 8.4). Transparent, science-based methodologies are needed that describe soil development in historical and contemporaneous cultural systems to advance understanding of how soils are fixated to become palaeosols, and what their values are in relation to geoheritage at different spatial scales.

Soil diversity, i.e., the variety of soil types, soil physical, biological, and chemical processes across a landscape, is part of geoheritage and geoconservation (Fig. 8.2.1). When referring to soils, soil diversity, soil heritage and soil conservation can be used. Although soil conservation is at the moment limited to activities to combat soil erosion and land degradation, caring for soil heritage and soil diversity, including information in palaeosols, is part of soil conservation.

8.3 Soil formation in natural and cultural systems

Soils form the foundation of human societies (Montgomery, 2007), because they shape the conditions for agriculture and human settlement. The relation between society and soils is two directional: people also modify the soil to suit their needs. Therefore soils should not only be viewed as the outcome of geophysical and bioclimatic processes, but as co-produced by human–environment interactions in the past and present (Fig. 8.3.1). This section will review soil-forming factors and the erosion rates in natural and cultural systems to address the potential of natural and cultural soils to be preserved as palaeosols.

8.3.1 Natural soil systems

The potential of soils to become preserved as palaeosols depends on the rate of soil formation relative to soil loss rates. Under steady-state

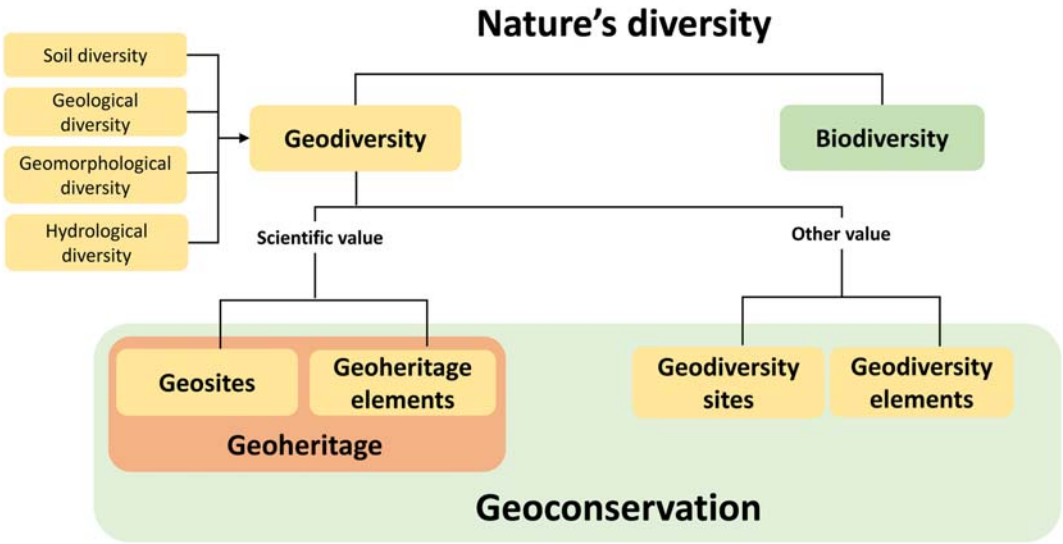

FIGURE 8.2.1 Conceptual relations between nature's diversity, geodiversity, geoheritage and geoconservation and subdivision therein. Here, we regard four components (soil, geology, geomorphology and hydrology) as part of geodiversity. Geoheritage elements include cultural values, connection to archaeology and biodiversity. Geodiversity elements include specific aspects of soil, geology, geomorphology and/or hydrology. *After Brilha, J. 2016. Inventory and quantitative assessment of geosites and geodiversity sites: a review. Geoheritage 8, 119–134.*

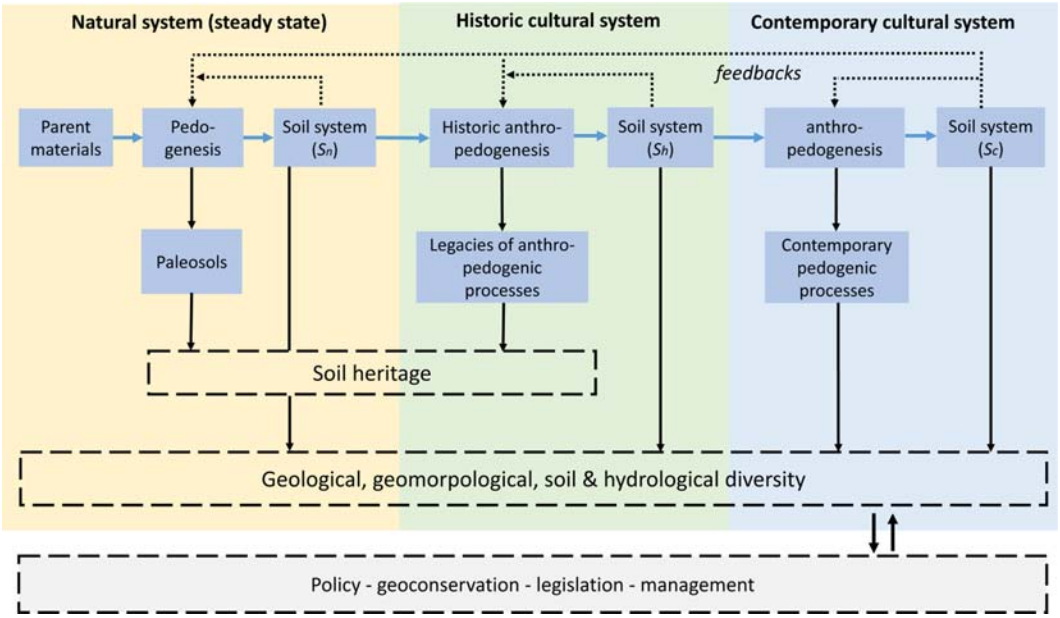

FIGURE 8.3.1 Diagram illustrating the formation a soil heritage as the result of soil-forming processes under natural conditions, historic and contemporary cultural systems. In natural and historic cultural systems, palaeosols build a specific part of the soil heritage. *After Richter, D.D.B., 2007. Humanity's transformation of earth's soil: pedology's new frontier. Soil Science 172, 957–967.*

conditions, there is a balance between the production of parent material through the process of weathering and the removal of soil through baseline soil loss rates. The steady-state system can temporarily be disturbed by natural hazards such as landslides, volcanic eruptions and flooding events, forest fires and drought periods, which may lead to local or regional increase in soil loss rates. Soils are traditionally viewed as being dependent on five soil-forming factors (Jenny, 1994): climate, topography, biota, parent material and time. The important contribution of human activities to soil formation was later recognized (Yaalon and Yaron, 1966). In a study on 18 non-agricultural areas in North America, Europe, Australia and Zimbabwe, soil formation rates were found to range between 0.02 and 1.27 ton/ha/year (Verheijen et al., 2009). In a similar study by Wakatsuki and Rasyidin (1992), soil formation rates varied between 0.37 and 1.29 ton/ha/year, with higher rates being mentioned for Japan (5.7 ton/ha/year), in a high-precipitation situation. Extremely low values are reported for basaltic parent material of 0.004 ton/ha/year in a semi-arid area in Australia. At the other side of the equation, erosion rates under natural conditions also show wide variation. The geological erosion rates increase from gently sloping lowland landscapes of ancient continental cratons ($<10^{-4}$ to 0.01 mm/year), to moderate gradient hillslopes of soil-mantled terrain (0.001−1 mm/year) and steep tectonically active alpine topography (0.1 to >10 mm/year) (Montgomery, 2007). The natural disturbances in steady-state natural soil systems are exceeded in historical times by human activities. For example, conventional agricultural practices increase soil loss rates with one to two orders of magnitude above rates of soil formation and long-term geological erosion rates (Montgomery, 2007). As a result, the effects of land use and land cover change in historic and contemporary cultural systems have drastically transformed the steady-state soils (Fig. 8.3.1).

8.3.2 Historic and contemporary cultural soil systems

As a result of human activities, new soils are formed and existing soils are altered by pre-existing soil processes, or sometimes entirely novel processes (Ellis, 2011). Yaalon and Yaron (1966) recognize four ways in which humans transform the soil by modifying topographical features (terracing, land levelling, dam construction), hydrological factors (drainage, irrigation, flooding), chemical factors (fertilizers, irrigation, clay marling) and by cultivation (deforestation, ploughing, shifting cultivation, grazing). The contribution of human activities to soil formation has been referred to as *metapedogenesis* (Yaalon and Yaron, 1966) or *anthropedogenesis* (Richter, 2007, Fig. 2). In prehistoric times, human activities already significantly altered the soil (Dotterweich, 2013). The plaggen soils of northwest Europe are an excellent example of soils formed by anthropedogenesis: people enriched these soils with organic matter and nutrients, a process which commenced 3000 years ago (Blume and Leinweber, 2004). When we consider the historical evolution of soil erosion at a global scale, three phases can be identified (Mcneill and Winiwarter, 2004): the first phase started around 2000 BCE when early civilizations advancing beyond the expanded river valleys converted the forested mountain slopes. The second phase lasted from the 16th into the 19th centuries, and was triggered by the invention of sharper ploughshares that could cut through the topsoil of the extensive grasslands in Eurasia and the Americas. The end of the Second World War marked the start of the third and most recent phase, in which mechanization and

agricultural expansion further accelerated soil erosion. Although the impact of human activities on the soil has a long history, both its rate and spatial extent have increased over the last millennia. Given the strong association between soil loss and land use change (Vanwalleghem et al., 2017), modelling soil loss on data on historical land conversions might give an indication of the extent to which human activities affected the soil in the past (Norder et al., 2017).

Both biophysical and anthropogenic soil-forming processes are stopped after burial by younger parent material, and palaeosols are formed. Such palaeosols may contain traces of (pre-)historic land use patterns and practices, such as: enrichment or depletion of organic matter and nutrients, changes in erosion or sedimentation rates, plough or spade marks and substances, including charcoal, plant and animal remains, chemicals or artefacts (Certini and Scalenghe, 2011; Ellis, 2011). Palaeosols are windows on the past and often will contain crucial information about the presence of human activities in the course of history. For example, the presence of soil phosphorus in the form of phosphate generally indicates human activities in the past (Eidt, 1977). Although palaeosols contain useful information for reconstructing past human–landscape interactions, most palaeosols are affected by present-day human activities. An overview of threats to soils and palaeosols and an inventory of location and intensity of such threats should help support policies for conservation actions.

8.4 Threats to soils and palaeosols as elements of geodiversity

Soils are a component of geodiversity and threats to geodiversity also pose a threat to soils. The main threats to geodiversity are listed in Table 8.4.1, along with a set of indicators that can be used to monitor changes in the status of geodiversity. Urban expansion, deforestation, agricultural practices, water use and mining activities put pressure on ecosystems' landscapes and soils and the services they provide.

To efficiently protect soil heritage (Fig. 8.3.1), it is crucial to gain an overview of threats to soils and palaeosols and instruments available to address those threats. There is a wide range of processes that threaten soils and palaeosols (Table 8.4.1), for example: soil loss by water or wind, organic matter decline, compaction, sealing, salinization and desertification. *Soil organic matter (SOM) decline* is basically the reduction of SOM. The modelled global loss of soil organic carbon, based on input from global soil databases, presents alarming levels of soil organic carbon losses when compared relatively to the original conditions (Stoorvogel et al., 2017). In many regions, *susceptibility to compaction*, a physical process that mainly affects porosity and permeability, is a main threat. The decline in *soil biodiversity* is mostly related to deterioration of soil quality parameters that affect the soil organisms, for example, by using pesticides and fertilizers in agricultural systems. Another threat is *soil sealing*, which is the transformation of open natural, semi-natural and/or agricultural areas into residential or infrastructural areas. For example, in 2006, almost 100,000 km^2 (2.3%) of land within Europe was sealed (Gardi et al., 2015). Artificial surfaces like roads and buildings cover soils and could therefore potentially contribute to the formation of palaeosols, hosting the future soil archive of contemporaneous landscapes. However, covering the soil with impermeable surfaces inhibits soil functions and ecosystem services which affects the water infiltration capacity of the soil and could increase the urban heat island effect (European Environment Agency, 2011). In many countries, *salinization* is the increase in salts in soils as the result of both natural processes and mismanagement, for example, related to irrigation. Salinization often occurs in parallel with the process of *desertification*, which is defined as land

TABLE 8.4.1 Overview of threats to soils and palaeosols.

Threats to geodiversity	Meaning for soils and/or palaeosols	Indicators
Ignorance	Lack of awareness of soils as archives of the past, as records of scientific and cultural heritage	Absence of legislation, no educational initiatives, no inventory of geosites or protected areas
Infrastructure and urban expansion	Urban sprawl and the interconnected infrastructure irreversibly destroy the soil, set back soil development or transform natural soils into anthrosols	Soil sealing; land levelling; infrastructure; impervious surfaces; mining
Agriculture	Irrigation, drainage and fertilizers will change original soil development, which will be overprinted by younger and different soil development; bare soil is exposed to rainfall; acceleration of soil erosion	Changing soil quality; soil biology; soil extraction; soil organic carbon; nutrient depletion, use of fertilizers and pesticides; levelling of subtle landforms/topography; soil harvesting
Water management	Coastal and inland regulation of surface and groundwater levels, construction of dikes and the training of rivers influence natural soil development in adjacent areas; soil erosion may increase	Canals; ditches; dikes; groundwater change; sediment transfer to rivers/lakes
Extraction of rare earth and construction materials	Surface mining activities cause irreversible loss of topsoil and parent material, which is sometimes replaced by materials in which new soils may develop	Land take, sand and clay extraction, loss of landforms, land levelling; deposition of quarry spoil and mine tailings; pollution
Afforestation and deforestation	Deforestation may lead to accelerated soil erosion and loss of characteristic forest soils and soil quality; afforestation may set back soil development: soils related to open grasslands and semi-natural terrains are turned into young soils	Changes in biomass, change in land use/land cover, normalized differential vegetation index, change in soil quality; loss of subtle landforms; obscure visibility and accessibility
Recreation and tourism	Activities such as skiing, mountain biking, trekking, hiking, climbing	Footpath erosion, gullying, slope instability, landscape fragmentation

After Ronchi, S., Salata, S., Arcidiacono, A., Piroli, E., Montanarella, L. 2019. Policy instruments for soil protection among the EU member states: a comparative analysis. Land Use Policy 82, 763–780; Wunder, S., Kaphengst, T., Frelih-Larsen, A., McFarland, K., Albrecht, S. 2018. Implementing SDG Target 15.3 on "Land Degradation Neutrality". Environmental Research of the Federal Ministry for the Environment, Nature Conservation, Building and Nuclear Safety, Report No. (UBA-FB) 002587/ENG, 58 pp; Schrodt, F., Bailey, J.J., Kissling, W.D., Rijsdijk, K.F., Seijmonsbergen, A.C., van Ree, D., Hjort, J. 2019. To advance sustainable stewardship, we must document not only biodiversity but geodiversity. Proceedings of the National Academy of Sciences 116, 16155–16158. https://www.pnas.org/content/116/33/16155.

degradation in arid, semi-arid and dry sub-humid areas as the result of climatic variations and human activities. Both salinization and desertification are mainly concentrated in the Mediterranean region. Particularly in hilly and mountainous member states, *landsliding* and related *flood hazards* can seriously contribute to soil loss. *Diffuse pollution* and *soil contamination* sites are threats that are difficult to assess, often due to the absence of the location of polluted sites on a European scale. Diffuse soil pollution occurs from the use of fertilizers and pesticides in an agricultural context, whereas contaminated sites often relate to (illegal) waste dumps of varying origin. Finally, the natural reserves of soil micronutrients such as zinc become increasingly depleted, leading to alarming deficiencies in people, livestock and crops (Platform Agriculture, Innovation & Society, 2012).

8.4.1 Case study: soil loss and erosion rates in the European Union

Arguably, of all the threats to soils and palaeosols, soil erosion by water or wind has the highest impact. Soil degradation – and more specifically, soil loss – now receives increasing attention from scientists and policymakers. For example, the Common Agricultural Policy (CAP) of the European Union and the Sustainable Developments Goals (SDGs) seek to reach Zero Net Land Degradation targets by 2030. The SDGs (e.g., no. 15: Life on Land) identify soils as a crucial resource for sustainable development and they promote the protection of soil resources to achieve zero land degradation by 2030 (Keesstra et al., 2016). To achieve these goals, we need to know where soil loss is most severe, and where valuable soil resources are located. Recent studies on the spatial distribution and volumes of soil loss by running water indicate that there is an extraordinarily high variability in erosion rates. The net amount of soil loss in a given site is the difference between all processes that detach and remove soil material, and those processes that deliver and deposit new material (García-Ruiz et al., 2015). In many locations there is an imbalance between soil formation and soil erosion, reducing soil quality in terms of physical, chemical and biological aspects. The physical and chemical state of soil properties within Europe is assessed every 3 years (Orgiazzi et al., 2018) to extract policy-relevant statistics related to the effect of land management on soil characteristics. In addition to these physical and chemical soil properties, the European Union has published the free Global Soil Biodiversity Atlas (Orgiazzi et al., 2016) which maps the geographical distribution of soil biodiversity and some of its major threats. However, while the spatial distribution of some threats such as erosion by water or wind are known at large scales (e.g., Borelli et al., 2016), the contribution of the fine-scale soil erosion processes, such as overland flow, crop harvesting, rill formation, gullying, tillage erosion and piping, remain largely unexplored at larger extents. These erosion processes are often studied on a local scale, using specific measurement techniques, and could therefore be difficult to upscale or extrapolate to a European level, because such projections do not incorporate offsite effects such as deposition and loss of soil quality resulting from agricultural practices.

A common method to scale up to a European level is by applying the Universal or the Revised Universal Soil Loss Equation (Wischmeier and Smith, 1978; Renard et al., 1997): $E = R * K * LS * C * P$, where E = soil loss in ton/ha/year, R = rainfall-runoff erosivity in MJ mm/ha/h/year, K = erosion sensitivity factor based on texture and organic matter (Renard et al., 1997; Panagos et al., 2015), LS = slope length factor (unitless), C = crop factor and P = supporting practice. On a European scale (Fig. 8.4.1), hotspots of soil erosion by water, with values exceeding 10 ton/ha/year, are found in the Alps, southern Spain, large parts of Italy (especially Sardinia), Greece and Scotland, northern Sweden and eastern European countries. Intermediate levels of erosion are located across the hilly areas of central Europe, while low soil erosion numbers are mostly found in the formerly glaciated areas in Finland and Sweden in Scandinavia, the northern lowland area of Germany and Poland, the Netherlands, the United Kingdom and Ireland. The lowest mean annual soil loss rates are found in Finland (0.06 ton/ha/year), Estonia (0.21 ton/ha/year) and the Netherlands (0.27 ton/ha/year), while the highest values are found in Italy (8.46 ton/ha/year), followed by Slovenia (7.43 ton/ha/year) and Austria (7.19 ton/ha/year) (Panagos et al., 2016). The mean soil loss rate in the European Union is estimated to be 2.46 ton/ha/year. Panagos et al. (2016) found that interventions in the context of the CAP reduced overall soil loss by 9.5% during the last

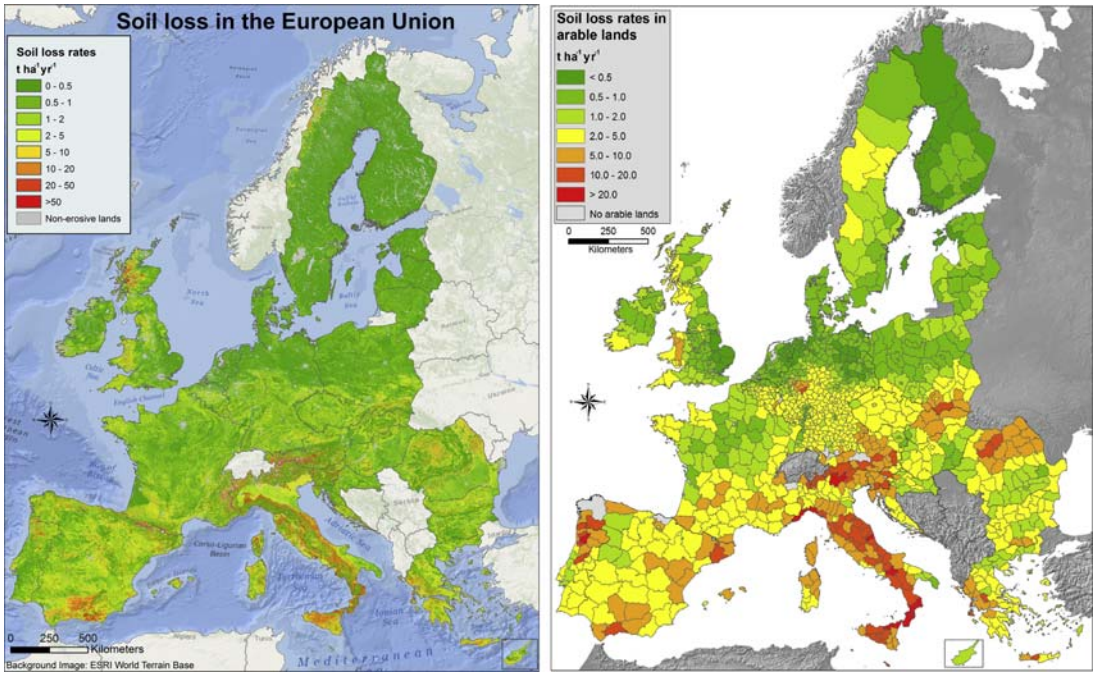

FIGURE 8.4.1 Soil loss in Europe. *Left*: Modelled soil loss by water using the Revised Universal Soil Loss Equation. *Right*: Soil loss rates in arable land (Panagos et al., 2015).

decade. Predictions of rainfall erosivity for Europe based on climate scenarios and soil erodibility show an average increase of 10%–20% soil loss by the year 2050, with the most sensitive regions to be found in northwestern Europe and the Alps (Panagos et al., 2016).

Soil loss rates in Europe (Fig. 8.4.1) in many places exceed reported soil formation rates. Verheijen et al. (2009) took field measurements across Europe and found these rates to vary from <0.05 ton/ha/year in the French Alps to 0.39 ton/ha/year in the Pyrenees. It is evident that the European Union is confronted with a net loss of soils in the contemporary cultural systems. Especially in the Mediterranean member states (Italy, Spain and Greece), countries with a particularly rich soil heritage, uncontrolled erosion may lead to irreversible destruction of the soil archive.

8.5 Soil conservation

Recently, it has been recognized by the Intergovernmental Science-Policy Platform on Biodiversity and Ecosystem Services (IPBES) that land degradation is a major environmental problem that affects natural and cultivated socio-ecosystems, with negative consequences for the well-being of least 3.2 billion people (IPBES, 2018). Land degradation, especially soil degradation, is a complex issue, which is influenced by many external processes and disturbances that affect the physical, chemical and biological reduction of soil quality. To prevent the soil archive being irreversibly destroyed and to improve sustainable use of soils, harmonized legislation is needed at national, European and global scales.

8.5.1 Soil protection in the European member states

The Soil Thematic Strategy (European Commission, 2012) forms the basis of the EU Soil Directive of 2006, the official law on soils. The EU Thematic Soil Strategy has four pillars, namely awareness raising, research, integration and legislation. Outside the European member states, countries such as Norway also have national legislation that prevents building on its best agricultural soils. This is similar to locally implemented legislation within the EU member states (Table 8.5.1) which developed numerous acts, decrees or other legislation and/or directives that limit, for example, the amount of fertilizers on soils to prevent leaching of nitrogen and phosphate to ground- and surface waters. Often, these rules are only indirectly related to soil, for example, via legislation related to agricultural practices, hydrology (surface and groundwater), spatial planning or in relation to forests. For this reason the European Union tried to develop harmonized communal soil legislation, which was regarded as a major step toward uniform regulations for soils, sustainable soil management and cleaning up soil pollution in all countries within the European Union. Most member states supported the proposal for a Soil Framework Directive as a legally binding component of the EU Soil Thematic Strategy. However, while it was endorsed by the EU Parliament in 2007, it was blocked by a minority of countries. They argued that existing national soil legislation and financial and administrative aspects were not sufficiently considered in the proposal (Ronchi et al., 2019). Because the proposal was never accepted, the process of harmonizing soil legislation within the EU has come to a standstill. As a result, soils are currently not legally protected at the EU level against any adverse use, and in many countries soils are therefore not protected at all. Nonetheless, many member states do support the CAP strategic plans (Table 8.5.1), which aim to prevent and mitigate soil degradation processes in agricultural areas by increasing or maintaining SOM and soil biodiversity, and to reduce the erosion, contamination and compaction of soils (Ronchi et al., 2019). In addition, soil conservation is also indirectly included in the Environmental Action Programme for 2020 (European Commission, 2014). It states that by 2020, land should be managed sustainably, soils should be adequately protected and the remediation of contaminated sites should be well under way.

8.5.2 Global geoconservation initiatives

While large tracts of soils remain unprotected at both European and global scales, in some specific areas, soils and palaeosols are conserved because they are part of protected geodiversity areas. A successful attempt to globally protect significant geoheritage and geodiversity is through the establishment of the United Nations Educational, Scientific and Cultural Organization (UNESCO) Global Geoparks (UGGs). A geopark is a territory with clearly defined boundaries that includes a particular geological heritage and a sustainable territorial economic development strategy. A geopark must comprise a certain number of geological sites of particular importance in terms of their scientific quality, rarity, aesthetic appeal or educational value. Within Europe, there are currently 73 geoparks within 24 countries (European Geoparks Network, 2019). Since 2001, UNESCO has awarded the status of 'Global Geopark' to 140 areas. These parks are defined as 'single unified geographical regions where sites and landscapes of international geological significance are managed with a holistic concept of protection, education and sustainable development' (UNESCO, 2015). UNESCO has defined clear admission procedures and criteria for newly established geoparks. Four fundamental features should be included in a UGG, namely: geological heritage of international value, comprehensive

TABLE 8.5.1 Soil threats and relevant soil policy legislation for each EU member state. Main soil threats: 1 = water erosion, 2 = wind erosion, 3 = soil sealing 4 = salinization, 5 = landslides/flooding, 6 = loss of soil biodiversity, 7 = desertification, 8 = compaction, 9 = contamination, 10 = SOM decline (arable/peatlands).

Country	Threats	Relevant soil policy legislation
Austria	1, 5, 9	National laws on environmental protection, improving biodiversity and landscape management; regional governmental instruments
Belgium	10	CAP-related measures; Wallonia Agricultural Code; Manure Action Plan; maintaining soil organic matter; Waste Resource Plan
Bulgaria	2, 5, 10	National Soil Act to prevent soil degradation; national law for remediation of contaminated sites, agricultural activity and topsoil removal; national action plan for sustainable land management and combatting desertification
Croatia	1, 5, 8	National laws for managing the natural area
Cyprus	4	National action plan to combat desertification
Czech Republic	10	Rural development plan; several national laws to regulate fertilizer use, agricultural land and monitor changes
Denmark	2, 10	Regulative tools/Acts; CAP measures; protecting natural areas; taxation of pesticides
Estonia	8	Estonian Environmental Strategy includes development of integrated soil policy, an adequate monitoring system, raising awareness for land owners and sustainable soil use
Finland	8, 9, 10	Governmental Development Programme for the Organic Product Sector and Objectives 2020; national programme on soil remediation under state waste management system; promoting sustainable agricultural practices
France	1, 5, 6, 9, 10	Several 'codes' on planning, environment, rural areas and forests; instruments for fiscal and regulatory measures related to soils
Germany	3, 5, 6, 9, 10	National instruments aimed directly at soil conservation such as the National Forest Soil Inventory and a soil information system for monitoring; Federal Soil Protection Act, Building Code and National Sustainable Development Strategy
Greece	1, 3, 4, 5, 6, 7, 10	National legislative proposal for soil protection (soil pollution, inventory of contaminated sites); national action plan for combatting desertification
Hungary	4, 8, 10	National law to regulate agricultural practices; CAP measures; regulations for fertilizer use; Fourth National Environmental Remediation Plan; Strategy for Sustainable Development; National Climate Change Strategy; Soil Information and Monitoring System
Ireland	6, 10	Soil strategy for Ireland under development; Irish Soil Information System
Italy	1, 3, 4, 5, 6, 9, 10	CAP regulation; National Strategy for Climate Change Adaptation; Environmental Code; National Biodiversity Strategy; landslide inventories; Decree on Sewage Sludge and Regional Waste Management Plans
Latvia	8, 10	National Resources Tax Law; Environmental Policy Strategy; General Regulation for the Planning, Use and Building of the Territory; CAP measures
Lithuania	8, 9, 10	Law on Environmental Impact Assessment; National Strategy on Sustainable Development; Programme on Water Pollution Reduction from Agricultural Sources: Environmental Protection Requirements for Manure and Slurry Management: Law on Protected Areas

(*Continued*)

TABLE 8.5.1 Soil threats and relevant soil policy legislation for each EU member state. Main soil threats: 1 = water erosion, 2 = wind erosion, 3 = soil sealing 4 = salinization, 5 = landslides/flooding, 6 = loss of soil biodiversity, 7 = desertification, 8 = compaction, 9 = contamination, 10 = SOM decline (arable/peatlands).—cont'd

Country	Threats	Relevant soil policy legislation
Luxembourg	3, 6, 9, 10	CAP measures; Rural Development Programme; regulatory measures for the use of nitrogen fertilizers and sewage sludge; Loi du 19 décembre 2008 relative à l'eau; the National Environmental Soil Monitoring Initiative; the National Environmental Land Cover Monitoring Database
Malta	1, 3, 9	CAP-related measures; National Environment Policy; Strategic Plan for Environment and Development; Nitrates Action Programme Malta
Netherlands	3, 6, 8, 9, 10	CAP and directives to prevent contamination from the use of fertilizers and nitrates; Soil Protection Act; Environmental Protection Act; Soil Quality Decree; Water Act
Poland	8, 9, 10	CAP (Greening and Cross-Compliance Standards); Code of Good Agricultural Practices; law on forests; Environmental Protection Law; Nature Conservation Act; Act on Preventing and Remedying Damage to the Environment
Portugal	9	Law on the Use of Sewage Sludge on Agricultural Soils; Law on the Distribution, Sale and Application of Plant Protection Products for Professional Use and the Manual of Agricultural Good Practices; Water Law
Romania	4, 5, 6, 8, 10	Decision on the Assessment of the Effects of Certain Public and Private Projects on the Environment; Environmental Impact Assessment (EIA) Directive; Law on Afforestation of Degraded Land
Slovakia	9, 10	CAP (Greening and Cross-Compliance Standards); National Soil Protection Act; Monitoring of Environment (Partial Monitoring System − Soil)
Slovenia	1, 5, 9, 10	CAP measures (Greening and Cross-Compliance Standards); Agricultural Land Act; Water Act and Delegated Regulations for Erosion, Flooding and Landslides
Spain	3, 4, 5, 6, 7, 8, 9, 10	CAP (Greening and Cross-Compliance Standards); Royal Decree to Decommission Petroleum-Product Tanks; Decree on Protecting Waters from Pollution by Nitrates Derived from agricultural sources; State Framework Plan for Waste Management; Law for Integrated Pollution Prevention and Control; Forestry Law/Strategy
Sweden	2, 10	CAP instruments of Greening, Cross-Compliance Standards and the Rural Development Programme; Strategy for Sustainable Land Use
United Kingdom	5, 6, 10	CAP (e.g., Greening Payment Requirements or Cross-Compliance Standards); UK Forestry Standard; Catchment Sensitive Farming Programme, Soil Indicators for Scottish Soils; Wales Glastir Monitoring and Evaluation Programme; Land Strategy for Northern Ireland; Agricultural Land (Removal of Surface Soil) Act; Nitrate Pollution Prevention Regulations; the Pesticides Control Legislation or the Sludge (Use in Agriculture) Regulations

CAP, Common Agricultural Policy.
Compiled from Ronchi, et al. 2019. Policy instruments for soil protection among the EU member states: a comparative analysis. Land Use Policy 82, 763–780.

management, public visibility and networking with other geoparks. For recent and new candidates, a long list of criteria is rated in the application forms that include amongst others scientific-, educational-, touristic- and management-related fulfilments, clearly addressing geodiversity and geoheritage with the objective to raise awareness amongst citizens

and promote sustainable tourism. Soils are included in the application procedure as part of geodiversity (UNESCO, 2016).

Another important milestone is the UNESCO World Heritage Convention (WHC) (https://whc.unesco.org/en/convention/) that was established in 1972 and aims to preserve cultural heritage by making strong links to nature conservation. By including many partners from the private and public sectors, UNESCO is actively expanding its list of World Heritage Sites (WHS). Such sites must be of outstanding universal value and meet at least 10 criteria, which are defined in the operational guidelines (WHC, 2019) for the implementation of the WHC. Approximately 1100 WHS have been recognized across 167 countries and the list is growing. Although soils are not a main target, they are mentioned in many of the WHS-related documents and thus contribute to saving the soil archive in the landscape and its related cultural heritage.

The successfulness of soil protection on a global scale is indirectly affected by setting targets that, over a certain period, can be reached by the combined action of individual countries via, for instance, the Millennium Development Goals (MDGs), the UN SDGs and legislation set by the Environmental Law Programme of the International Union for Conservation of Nature (IUCN). The MDGs, which were initiated in 2000, recognized 8 goals and 18 measurable targets, which was followed from 2015 to 2030 by the adoption of an Agenda for Sustainable Development, which includes the 17 SDGs and its 169 associated targets. Several of these SDGs include soil-related targets. As an example, the second SDG 'zero hunger' is closely related to the production of food, therefore closely related to soil fertility, which underpins the need to protect soils and mitigate/reverse soil loss. In the IPBES report the relevance of land degradation is linked to all SDGs (IPBES, 2018). The UGGs also contribute to meeting the SDGs, with special focus on goals 1, 4, 5, 8, 11, 12, 13 and 17 (UNESCO, 2019). Since 1948, the IUCN has been a global authority on the status of the natural world and the measures to safeguard it (https://www.iucn.org/about). Soil science experts actively contribute to specialist groups to assist individual countries with soil conservation, desertification and reforming agriculture legislation. Hannam and Boer (2004), as part of the IUCN Environmental Law Programme, proposed legislation to promote the sustainable use of soils. These global initiatives open the way for the protection of soils and palaeosols from a geodiversity perspective. Geodiversity can support the mapping of valuable areas within a cultural landscape, which we illustrate by a case on geodiversity in the Netherlands.

8.5.3 Case study: geodiversity in the Netherlands

In the Netherlands there is a long tradition to raise agricultural production and to reclaim and drain land. The associated land use and land cover changes have changed geodiversity. Currently, expert-based and semi-quantitative methods using weighting and ranking criteria are in development to objectively value geodiversity (Zwolinski et al., 2018). For example, Maas and Wolfert (1997) prepared cell-based categorized maps of earth scientific value, based on rarity and geogenetic characteristics, extracted from the digital geomorphological map of the Netherlands. Geodiversity index maps are composed of sub-indices that also include soil diversity. For the Netherlands (Fig. 8.5.1) a geodiversity index was calculated based on soil diversity, geological diversity, geomorphological diversity and hydrological diversity (Ten Vreegelaar, 2015). In ArcGIS10.4, a fishnet of 1 km cells was created for which the soil diversity sub-index was derived based on the number of soil types per grid cell. Using the Jenks natural breaks classification (Jenks, 1967), we divided the result into five classes,

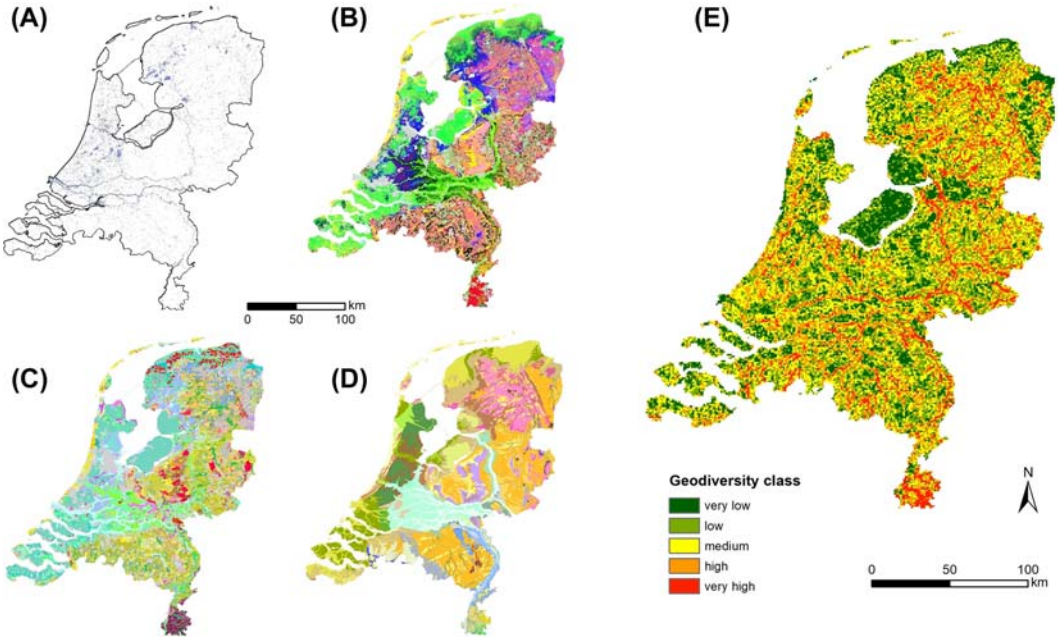

FIGURE 8.5.1 Geodiversity index map (map E) of the Netherlands, which is based on the summed variety of hydrology (map A), soil types (map B), geological formations (map C) and landforms (map D), categorized into five classes ranked from very low to very high in 500 m grid cells (Ten Vreegelaar, 2015).

ranging from very low, low, moderate, high and very high. Similarly, we included other components of geodiversity – the geomorphological map of the Netherlands (Publieke Dienstverlening op de Kaart [a]) and the hydrological map of the Netherlands (Publieke Dienstverlening op de Kaart [b]), which resulted in a geodiversity map of the Netherlands (Fig. 8.5.1). It has been recognized that geodiversity is generally increasing with increasing age of the subsurface (Seijmonsbergen et al., 2018), mainly attributed to the fact that soil development and geomorphogenesis are time dependent. For example, the 'Hondsrug' UGG (https://www.dehondsrug.nl/) is relatively geodiverse, which is largely related to its soil and geogenetic age variation. In the Dutch historic cultural landscape, human-induced disturbances (e.g., drainage and plaggen) have resulted in widely available landscape fragmentation that affected existing soils and initiated the formation of palaeosols. In this context, it should be realized that both natural and anthropogenic disturbances of the landscape may increase soil diversity (van Mourik et al., 2012). Index-based maps have great potential to objectively identify areas of potential landscape-wide conservation value, but expert-based site information is often necessary to fully understand and describe the soils and palaeosols.

8.6 Examples of historic and contemporary cultural soil systems

In previous chapters, multiple well-illustrated examples of plaggen soils and palaeosols in the Netherlands have been presented. Here, we show examples of two contrasting historical landscapes with different ecosystem services and functions, and highlight how soils have been co-produced by human and natural

processes. The first is a high-montane area in western Austria that has been transformed from a traditional grassland/pasture landscape into an environment for skiing and recreational use. The second example is a historic cultural landscape on the island of Tenerife (Spain) that has been transformed from a landscape with extensive agricultural terraces into a mixture of abandoned and modernized terraces.

8.6.1 Soils under pressure by tourism

The municipality of Lech in Vorarlberg, Austria, is surrounded by expanding skiing resorts in a high alpine landscape that is underlain by a wide variety of geological formations and genetically diverse landforms, stemming from the last glacial maximum to the recent Holocene. The presence of areas underlain by naked gypsum karst has created a characteristic (sub) surface hydrology and soils that contribute to a unique geodiverse landscape in the region (Fig. 8.6.1). The area is a naturally protected area at the level of the 'Bundesland' (province). The gypsum underlain area is threatened by soil compaction, soil degradation and chemical and physical alteration of the topsoils, due to treatment with chemicals and machinery on the ski slopes. The transition from traditional use as grasslands and pastures to a touristic and recreational landscape threatens not only the soils in the area, but the entire surrounding geodiversity (Seijmonsbergen et al., 2014). As a measure of raising awareness, a hiking route through the doline clusters has been created that informs tourists of the geological formation of gypsum, and the process of mountain building and landscape development, caused by a solution of gypsum and its relation to hydrology, soils and unique vegetation (Krieg and Waldegger, 1985).

8.6.2 Soils under pressure of changing land use in Tenerife

Tenerife island is part of the Canary archipelago and has a distinct elevation gradient from sea level to the El Teide volcanic peak at 3718 m a.s.l., only 15 km from the coast. The island was first colonized by the Guanches approximately 2000–2500 years ago (Atoche, 2008), and conquered by the Castilians at the end of the 15th century. While population growth over the subsequent centuries was relatively gradual, it rapidly accelerated around the end of the 19th century (Instituto Canario de Estadística, 2017). Population growth, exacerbated by the tourism boom in the mid-1970s, resulted in a drastic expansion of urban areas. Since the island was first colonized, it went through several phases of land use and land cover change. This has influenced the distribution and quality of the natural soils as well as the geodiversity of the volcanic slopes. Over the last 500 years deforestation of the coniferous forest (Corona Forestal) continued until the mid-1950's, after which a reforestation program was started. However, most deforested slopes were reshaped into terraced slopes by erecting stone walls to get rid of the volcanic boulders and rocks on the newly created agricultural fields, thereby creating clear boundaries. This reshaping of the land interfered with the natural drainage and stopped sediment transfer along slopes because the original soils were completely reworked and levelled. An irrigation system was constructed that negatively influenced the natural aquifers. Via so-called 'gallerias' the deeper groundwater reservoirs were tapped for irrigating the agricultural fields. The gallerias were originally rather shallow, but nowadays they penetrate more than 4 km into the rock formations to reach the lowered groundwater reservoir. At the same time, the relatively nutrient- and organically poor soils were

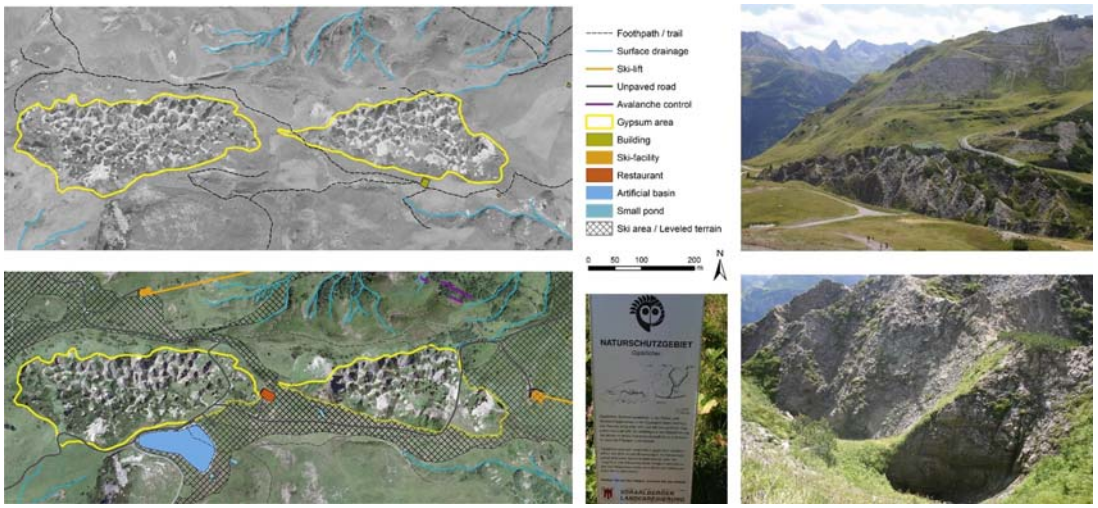

FIGURE 8.6.1 Changing land use is a threat to soils and geodiversity near the ski resort of Lech in Vorarlberg, Austria. The upper left panel is a panchromatic air photo from the nineteen fifties detailing the situation of the protected gypsum dolines in the landscape (*photos right*). The 2009 true colour imagery in the lower left panel shows how the area has changed for touristic skiing purposes (Seijmonsbergen et al., 2014). The sign (*centre*) addresses the conservation status (Naturschutzgebiet) under the local legislation of the 'Land Vorarlberg'.

enriched by transporting enormous amounts of organic topsoil from the Pleistocene remnants of the Laurasilva forests to the terraced landscape. In addition, pine needles were regularly harvested from the coniferous forest and transported to the lower terraces. Before 1954 (the establishment of the Canadas National Park), lapilli was mined from local volcanic cones, and also transported to lower terraces, because lapilli could retain water in the topsoil while preventing evaporation. After 1954, local sources are still used to mine pumice and lapilli for use on modernized terraces. The traditional agricultural terraces have largely been abandoned, which has triggered the recovery of the soils, because the lack of maintenance forces the terrace walls to collapse over time (Fig. 8.6.2), which allows renewed transfer of nutrients and sediments. Soil formation starts to redevelop, which can be monitored from the relatively rapid changes in SOM over time. Fig. 8.6.2 presents preliminary results from SOM percentages taken from terrace clusters of young (0–10 years), intermediate (11–25 years) and old (>25 years) age of abandonment. It is shown that initially SOM is still available in young, recently abandoned terrace clusters, which is due to the remnants of agricultural crops (Fig. 8.6.3). Over time, these crops disappear, while a recovery of local grasses and shrubs on the abandoned terraces is responsible for an increase in SOM. The lower central graph illustrates that the number of terrace wall collapses increases with age of abandonment.

Over the last 15–20 years, new modern terraces appear in the landscape nearby rich communities such as Vilaflor, which still have access to irrigation water, which is now distributed either by drop irrigation or sprinkler installations. These modern terrace walls can be several metres high and are often constructed from locally mined pumice rocks and filled with relics from older, abandoned terraces, and lapilli and pumice as a topsoil cover for the cultivation of potatoes (Fig. 8.6.3).

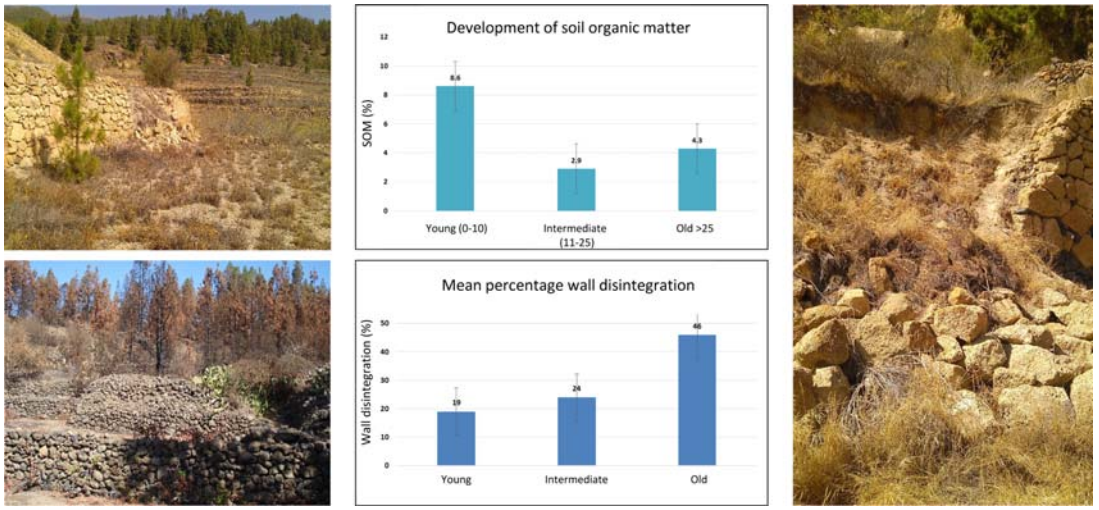

FIGURE 8.6.2 *Left*: Abandoned agricultural terraces. *Centre*: Results of soil organic matter (SOM) percentages from terrace clusters of young (0–10 years), intermediate (11–25 years) and old (>25 years) age of abandonment. *Right*: Collapsed terrace wall.

FIGURE 8.6.3 Modern agricultural terraces on Tenerife island are changing slope profiles and convert natural soils into anthrosols, which are topped by a layer of lapilli for the growth of potatoes near Vilaflor village.

8.7 Conservation of soils

The history of human–soil interactions goes back several millennia. Soil conservation strategies have been implemented in traditional agriculture since prehistoric times (Denevan, 1995) to prevent soil loss. The construction of agricultural terraces is an example of a soil conservation practice that was already used at least 4000 years ago to prevent soil loss (Dotterweich, 2013). From the end of the 18th century onward, scholars started focusing their efforts on soil conservation (Dotterweich, 2013). Initially, the main objective of soil conservation measures was to maintain soil fertility and agricultural productivity. This is also evident from the concept of soil quality, which traditionally emphasized mainly the aspects related to productivity. However,

over the last few decades, the definition of soil quality has widened to include other aspects such as: ecosystem services, ecosystem functions, intrinsic values, and uniqueness (Warkentin, 1995; Bünemann et al., 2018). The ecosystem services that soils provide to society can be divided into four categories (Millennium Ecosystem Assessment, 2005; Gray, 2013; Addhikari and Hartemink, 2016): provisioning, regulating, cultural, and supporting services (Fig. 8.7.1).

The ecosystem services might aid in the development of criteria for which soils should be prioritized in conservation. Criteria are different for soils and palaeosols because the services provided by palaeosols are primarily cultural services. Across the globe, palaeosols differ not only in the value of cultural services they provide, but their persistence is also threatened to a different degree. Palaeosols also differ in their rarity; this feature cannot be translated into a general rule in which palaeosols deserve higher conservation priority. In some cases a palaeosol might deserve priority because it shows unique features of past human–environment interactions. In other cases an archetypal palaeosol that has aspects that are typical of past human–environment interactions in a certain period or landscape might deserve particular priority. Some palaeosols might be common in one country but rare on a global scale. One might be inclined to suggest that uniqueness should always be considered at the highest scale possible (global or transnational). However, in practice, this will always be a trade-off. Therefore the decision by which palaeosols should be conserved partly depends on the type of cultural services they provide, and who the beneficiaries are.

We suggest a subdivision in soil categories according to their function from a soil heritage perspective. Since these soils have national and also European and global importance, the best way to protect them is to include them in a wider landscape perspective such as national parks, or in global protected areas such as UGGs, although examples exist outside of such (potential) park sites. In Table 8.7.1 the five soil categories worthy of protection, including a short description, are shown. Ultimately, the idea is to create a 'soil heritage database' in line with the proposal of the European Parliament that urged the European Commission in 2007 "to draw up, in cooperation with the Member States and the competent regional authorities, a scientific soil catalogue which should include the nature of the soil, its biography, health and vulnerability, degradation and erosion processes

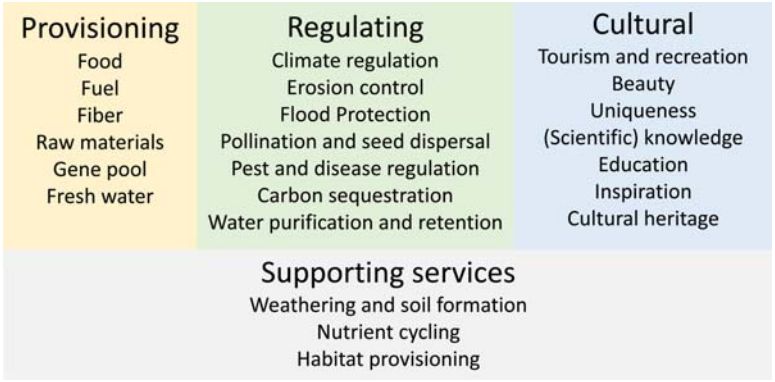

FIGURE 8.7.1 Ecosystem services provided by the soil. *Based on Millenium Ecosystem Assessment. 2005. Ecosystems and Human Well-Being- Synthesis. Summary for Decision-Makers, 24pp; Gray et al., 2013; Addhikari, K. Hartemink, A.E. 2016. Linking soils to ecosystem services — a global review. Geoderma 262, 101–111.*

TABLE 8.7.1 Soil categories worthy of protection.

Soil protection category	Description	Potential function
Benchmark soils	Natural undisturbed soils. They represent zero-influence situations necessary to specify the deviation of a specific soil from its 'steady state' and its natural origin, to study soil resilience and sustainable soil use.	Control sites for accelerated soil erosion, deterioration of organic matter, soil sealing, compaction, salinization, pollution and other adverse processes
Soil catenas and palaeosols	Soil series that represent distinct soil processes in periods of age development, related to, e.g., (glacio)isostatic uplift in relation to time	Scientific data on soil development under various conditions of climatic, tectonic or otherwise varying abiotic conditions; soil heritage
(Sustainable) cultural heritage soils	Soils related to specific historic events or related to traditional cultural and natural elements in the landscape; examples are the European plaggen soils, the 'cultura mixta' in Toscane, Italy, and the dehesa soils in Spain	Cultural soil heritage; soil conservation; geoconservation
Natural heritage soils	These are soils that have already been designated a special status because of their special natural heritage value; examples are old forest soils and driftsand parabolic dunes that carry the eldest forest relics of Europe	Natural heritage conservation; nature conservation
Soils in nature areas	Soils in balance with the landscape and that sustain biodiversity and healthy ecosystem functions	Nature conservation and management, including its flora and fauna

and contaminated areas, recognising the existence of high-value soils (in terms of agriculture, geology, ecology, history or the countryside) and the need to draw up recommendations for their conservation and sustainable use".

Many approaches to value the abiotic part of nature already exist. Literature reviews (Reynard et al., 2009; Brilha, 2016, 2018; Seijmonsbergen et al., 2014) show that many researchers use a number of robust criteria to value geodiversity and soil geoheritage. A common approach is to weight areas into classes of very low to very high geoconservation potential based on criteria such as frequency of occurrence, disturbance and vulnerability (Seijmonsbergen et al., 2014). Table 8.7.2 presents a list of selected criteria and their explanations in valuing geodiversity and soil heritage.

Modern societies should aim at a sustainable use of resources by safeguarding geodiversity. Apart from the protection of scientifically interesting benchmark soil profiles, soil diversity, soil biodiversity and many other soil heritage aspects should be included. Soil conservation and soil conservational organizations should include the protection of natural, cultural and benchmark soil systems for scientific, educational, ecological, recreational and landscape quality purposes.

Soil conservation approaches can be divided into three categories (Table 8.7.3): advisory/educational, regulatory/fiscal, inventory/monitoring. The practical implementations of these approaches are different for the conservation of soils and palaeosols. Approaches to conserve active soil, such as measures to reduce soil loss, can indirectly contribute to the conservation of

TABLE 8.7.2 Criteria commonly used in valuing geodiversity and soil heritage.

Value	Explanation/example
Cultural	Landforms and landscapes that are associated with cultural history: Patterns of enclosure, traditional land use, archaeology, traditional building materials, folklore and religion
Aesthetic	The visual appeal of landscapes, geotourism, the effect on health, potential for recreational uses and artistic inspiration
Ecological	The abiotic world is the basis for, e.g., biodiversity
Functional	The role of soil and substrates in providing platforms, storage, burial sites, pollution control and nutrients, as well as geosystem and ecosystem functions
Economic	The current or potential use of soils for agriculture, forestry, tourism and recreation, construction and other industrial materials, fossils
Scientific	The use of the abiotic world to provide information on the history of the earth, the evolution of life, landscape evolution and climate change
Educational	The potential opportunities for raising awareness, for field education and training

After Reynard, E., Coratza, P., Regolini-Bissig, G., 2009. International Conference on Geomorphology. Geomorphosites. München, Verlag Dr Friedrich Pfeil; Brilha, J. 2016. Inventory and quantitative assessment of geosites and geodiversity sites: a review. Geoheritage, 8, 119–134., Brilha, J. 2018. Geoheritage: inventories and evaluation. In: Reynard, E., Brilha, J. (Eds). Geoheritage. Chennai: Elsevier, 67–86; Seijmonsbergen, A., de Jong, M. G. G., de Graaff, L. W. S., Anders, N. S. 2014. Geodiversität von Vorarlberg und Liechtenstein/Geodiversity of Vorarlberg and Liechtenstein. (Bristol-Schriftenreihe; No. 41). Bern: Haupt.

TABLE 8.7.3 Overview of conservation approaches and targets for various scales.

Conservation approach	Soils	Palaeosols
Advisory/ educational	Development and implementation of policies, strategies and charters, e.g., related to soil conservation, retention of topographic character, restoration of former topography, sustainable use of georesources Influencing political decision-makers at all levels	Public involvement in practical activities, education about values of soils as part of our geoheritage Television programmes on geoheritage Preparation of books and leaflets promoting the use of geodiversity and geoheritage in spatial planning Provision of museum and visitor centre displays on soil- and geodiversity Developing and use of social media such as apps and Twitter for highlighting and promoting soil heritage and geodiversity
Regulatory/ fiscal	Harmonizing taxes, grants and subsidies for the sustainable management of land Enforcement and imposition of suitable penalties for non-compliance	Conservation laws that include geodiversity and geoheritage Introducing geoconservation and geoheritage into land use planning regulations, environmental impact assessment procedures
Inventory/ monitoring	Identifying regional threats to soil conservation Developing spatially explicit models of different threats (soil compaction, salinization, soil loss, etc.)	Identifying and designating protected geoheritage areas and sites Designation of European geoheritage sites and parks Monitoring geodiversity and geoheritage

underlying palaeosols. It will not always be the most effective approach to conserve the rich archive that is stored in palaeosols. In contrast, connecting to already established approaches for the conservation of geodiversity and geoheritage could be more effective in protecting palaeosols.

8.8 Concluding remarks and outlook

Soils are part of geodiversity and the product of soil-forming processes in past and contemporary cultural systems. People have modified soils for hundreds and sometimes thousands of years. Both the rate and the spatial scale of human activities on the soil have substantially increased. Landscapes have been modified by historical and contemporaneous agricultural and cultural systems, which is reflected in soil diversity and the soil archives stored in palaeosols. It should be realized that soils are dynamic entities, and conservation and management should focus on fixating soils and on the preconditions for soil processes to occur.

Soils in Europe are threatened over large areas by a variety of degradation processes. These threats are characterized by a high geographic heterogeneity and relate to climatic variation, differences in underlying substratum and land use and land cover. Both active soil and palaeosols are negatively affected by soil loss. The majority of these soils have functional and/or economic values (Table 8.7.2). Clearly, the protection of these soils is most effective through overarching legislation on national and supranational scales (Table 8.5.1) and can effectively be monitored using standardized methods such as soil loss modelling. The effects of remediation measures should be monitored.

There are numerous local areas or sites that host important benchmark soils or palaeosols of outstanding value. These soils have cultural, scientific and educational values. The identification, mapping and documentation of these soils is a necessity, because their spatial distribution is still largely incomplete.

Ideally, soils should be protected at various scales, from local, national to European and global scales. This requires harmonization of valuation criteria for legislation and protection. The existing global soil maps could be part of such an organizational infrastructure.

The inclusion of soil heritage in national and international protected areas such as UGGs would greatly benefit the protection of soil archives. UGGs strongly contribute to raising awareness, education and conservation of the soil archive within the concept of geodiversity.

Actions are needed that lead to consistent and harmonized legislation to protect soils and geodiversity from local to transnational levels (cf. Matthews, 2014). Lack of awareness and understanding that soil and land degradation is a serious problem is a major barrier. Science-based and publicly available information is needed to allow policymakers, land managers and consumers to make decisions that promote sustainable soil use. This includes the conservation of soils that form the foundation of our societies, as well as conservation of palaeosols in which our collective heritage is recorded. Scientists should be challenged and contribute to actions needed to protect soils and geodiversity.

References

Addhikari, K., Hartemink, A.E., 2016. Linking soils to ecosystem services — a global review. Geoderma 262, 101–111.

Australian Soil Resource Information System (ASRIS). http://www.asris.csiro.au/.

Atoche, P., 2008. Las culturas protohistóricas canarias en el contexto del desarrollo cultural mediterráneo: propuesta de fasificación. In: González, R., López, F., Peña, V. (Eds.), Los Fenicios Y El Atlántico. Centro de Estudios Fenicios y Púnicos, Madrid, pp. 317–344.

Batjes, N.H., 2009. Harmonized soil profile data for applications at global and continental scales: updates to the WISE database. Soil Use and Management 25, 124–127. https://doi.org/10.1111/j.1475-2743.2009.00202.x (suppl.

information: https://www.isric.org/sites/default/files/isric_report_2008_02.pdf.
Blume, H.-P., Leinweber, P., 2004. Plaggen soils: landscape history, properties, and classification. Journal of Plant Nutrition and Soil Science 167, 319–327. https://doi.org/10.1002/jpln.200420905.
Borelli, P., van Oost, Meusburger, K., Alewell, C., Lugato, E., Panagos, P., 2016. A step towards a holistic assessment of soil degradation in Europe: coupling on-site erosion with sediment transfer and carbon fluxes. Environmental Research 161, 291–298.
Brilha, J., 2016. Inventory and quantitative assessment of geosites and geodiversity sites: a review. Geoheritage 8, 119–134.
Brilha, J., 2018. Geoheritage: inventories and evaluation. In: Reynard, E., Brilha, J. (Eds.), Geoheritage. Elsevier, Chennai, pp. 67–86.
Bünemann, E.K., Bongiorno, G., Bai, Z., Rachel, Creame, A.E., de Deyn, G., de Goede, R., Fleskens, L., Geissen, V., Kuyper, T.W., Mäder, P., Pulleman, M., Sukkel, W., van Groenigen, J.W., Brussaard, L., 2018. Soil quality – a critical review. Soil Biology and Geochemistry 120, 105–125.
Certini, G., Scalenghe, R., 2011. Anthropogenic soils are the golden spikes for the Anthropocene. The Holocene 21, 1269–1274.
Chaopricha, N.T., Marín-Spiotta, E., 2014. Soil burial contributes to soil organic carbon storage. Soil Biology and Biochemistry 69, 251–264.
Davidson, D.A., Wilson, C.A., 2006. An Assessment of Potential Soil Indicators for the Preservation of Cultural Heritage. Report of: School of Biological and Environmental Science, University of Stirling, Stirling, p. 49.
Denevan, M., 1995. Prehistoric agricultural methods as models for sustainability. Advances in Plant Pathology 11, 21–43.
Dotterweich, M., 2013. The history of human-induced soil erosion: geomorphic legacies, early descriptions and research, and the development of soil conservation – a global synopsis. Geomorphology 201, 1–34.
European Commission, 2012. Report from the commission to the European parliament, the council, the European economic and social committee and the committee of the regions. The Implementation of the Soil Thematic Strategy and Ongoing Activities. https://eur-lex.europa.eu/legal-content/EN/TXT/PDF/?uri=CELEX:52012DC0046&from=EN.
European Commission, 2014. Environment Action Programme to 2020. http://ec.europa.eu/environment/action-programme/.
European Environment Agency, 2011. Air Quality in Europe – 2011 Report. EEA Technical Report no.12, 86 pp..
European Geoparks Network 2019, 2019. http://www.europeangeoparks.org/.
Eidt, R.C., 1977. Detection and examination of anthrosols by phosphate analysis. Science 197, 1327–1333.
Ellis, E.C., 2011. Anthropogenic transformation of the terrestrial biosphere. Philosophical Transactions of the Royal Society A 369, 1010–1035.
Fischer, G., Nachtergaele, F., Prieler, S., van Velthuizen, H.T., Verelst, L., Wiberg, D., 2008. Global Agro-Ecological Zones Assessment for Agriculture (GAEZ 2008). IIASA, Laxenburg, Austria and FAO, Rome, Italy.
García-Ruiz, J.M., Beguería, S., Nadal-Romero, E., González-Hidalgo, J.C., Lana-Renault, N., Sanjuán, Y., 2015. A meta-analysis of soil erosion rates across the world. Geomorphology 239, 60–173.
Gardi, C., Panagos, P., van Liedekerke, M., Bosco, C., de Brogniez, D., 2015. Land take and food security: assessment of land take on the agricultural production in Europe. Journal of Environmental Planning and Management 58, 898–912.
Gordon, J.E., Crofts, R., Díaz-Martínez, E., Woo, K.S., 2017. Enhancing the role of geoconservation in protected area management and nature conservation. Geoheritage 10, 191–203. https://doi.org/10.1007/s12371-017-0240-5.
Gordon, J.E., Crofts, R., Díaz-Martínez, E., Woo, K.S., 2018. Geoheritage conservation and environmental policies: retrospect and prospect. In: Reynard, E., Brilha, J. (Eds.), Geoheritage. Elsevier, Chennai, pp. 213–235.
Gray, M., 2013. Geodiversity: Valuing and Conserving Abiotic Nature, second ed. John Wiley & Sons, Ltd, p. 508.
Hannam, I., Boer, B., 2004. Drafting Legislation for Sustainable Soils: A Guide. IUCN, Gland, Switzerland and Cambridge, UK, p. x+100.
Hengl, T., Mendes de Jesus, J., MacMillan, R.A., Batjes, N.H., Heuvelink, G.B.M., et al., 2014. SoilGrids1km — global soil information based on automated mapping. PLoS One 9 (8), e105992. https://doi.org/10.1371/journal.pone.0105992.
Hjort, J., Gordon, J.E., Gray, M., Hunter, M.L., 2015. Why geodiversity matters in valuing nature's stage. Conservation Biology Journal 29, 630–639.
Instituto Canario de Estadística, 2017. Estadística de la Evolución Histórica de la Población. http://www.gobiernodecanarias.org/istac/temas_estadisticos/demografia/poblacion/cifrascensales/C00025A.html.
IPBES (Intergovernmental Science-Policy Platform on Biodiversity and Ecosystem Services), 2018. The Assessment Report on Land Degradation and Restoration. Summary for Policymakers. IPBES secretariat, Bonn, Germany, 44pp.
Jenks, G.F., 1967. The data model concept in statistical mapping. International Yearbook of Cartography 7, 186–190.
Jenny, H., 1994. Factors of Soil Formation. A System of Quantitative Pedology. Dover Press, New York. Reprint (first

published in 1941), Online: https://www.soilandhealth.org/wp-content/uploads/01aglibrary/010159.Jenny.pdf.

Karssies, L., Wilson, P., 2015. Soil archives: supporting research into soil changes. IOP Conference Series: Earth and Environmental Science 25, 1–4. https://doi.org/10.1088/1755-1315/25/1/012021.

Keesstra, S.D., Bouma, J., Wallinga, J., Tittonell, P., Smith, P., Cerdà, A., Montanarella, L., Quinton, J.N., Pachepsky, Y., van der Putten, W.H., Bardgett, R.D., Moolenaar, S., Mol, G., Jansen, G., Fresco, L.O., 2016. The significance of soils and soil science towards realization of the United Nations sustainable development goals. Soil 2, 111–128.

Krasilnikov, P., García Calderón, N.E., 2006. A WRB-based buried palaeosol classification. Quaternary International 156–157, 176–188. https://doi.org/10.1016/j.quaint.2006.05.009.

Krieg, W., Waldegger, H., 1985. Die Lecher "Gipslöcher" in naturkundlicher Sicht. Montfort 37, 84–100. Bregenz.

Maas, G.J., Wolfert, H.P., 1997. Aardkundige Waarden in Nederland. Rapport 498. DLO-Staring Centrum, Wageningen, p. 88.

Matthews, T.J., 2014. Integrating geoconservation and biodiversity conservation: theoretical foundations and conservation recommendations in a European Union context. Geoheritage 6, 57–70.

Mcneill, J.R., Winiwarter, V., 2004. Breaking the sod: humankind, history and soil. Science 304, 1627–1629.

Millenium Ecosystem Assessment, 2005. Ecosystems and Human Well-Being- Synthesis. Summary for Decision-Makers, 24pp.

Montgomery, D.R., 2007. Soil erosion and agricultural sustainability. Proceedings of the National Academy of Sciences United States of America 104, 13268–13272.

National Soil Archive, 2019. https://www.csiro.au/en/Do-business/Services/Enviro/Soil-archive.

Norder, S.J., Seijmonsbergen, A.C., van Loon, E.E., Tatayah, V., Kamminga, A.T., Rijsdijk, K.F., 2017. Assessing temporal couplings in social–ecological island systems: historical deforestation and soil loss on Mauritius (Indian Ocean). Ecology and Society 22, 29.

Orgiazzi, A., Ballabio, C., Panagos, P., Jones, A., Fernández-Ugalde, O., 2018. LUCAS Soil, the largest expandable soil dataset for Europe: a review. European Journal of Soil Science 69, 140–153. https://doi.org/10.1111/ejss.12499.

Orgiazzi, A.R.D., Bardgett, E., Barrios, V., Behan-Pelletier, M.J.I., Briones, J.L., Chotte, G.B., de Deyn, P., Eggleton, N., Fierer, T., Fraser, K., Hedlund, S., Jeffrey, N.C., Johnson, A., Jones, E., Kandeler, N., Kaneko, P., Lavelle, P., Lemanceau, L., Miko, L., Montanarella, F.M., de Souza Moreira, K.S., Ramirez, S., Scheu, B.K., Singh, J., Six, W.H., van der Putten, W.H., Wall, D.H. (Eds.), 2016. Global Soil Biodiversity Atlas. European Commission, Publications Office of the European Union, Luxembourg.

Panagos, P., Borelli, P., Poesen, J., Ballabio, C., Lugato, E., Meusburger, K., Montanarello, L., Alewell, C., 2015. The new assessment of soil loss by water erosion in Europe. Environmental Science and Policy 54, 438–447.

Panagos, P., Imeson, A., Meusburger, K., Borelli, P., Poesen, J., Alewell, C., 2016. Soil conservation in Europe: wish or reality? Soil Degradation and Development 27, 1547–1551.

Platform Agriculture, Innovation & Society, 2012. Scarcity of Micronutrients in Soil, Feed, Food, and Mineral Reserves. https://www.iatp.org/sites/default/files/scarcity_of_micronutrients.pdf.

Publieke Dienstverlening Op de Kaart (n.d. a). Dataset: Geomorfologische kaart van Nederland, schaal 1: 50 000. Online: https://www.pdok.nl/introductie/-/article/geomorfologischekaart-1-50-000.

Publieke Dienstverlening Op de Kaart (n.d. b). Dataset: hydrografie – netwerk RWS. Online: https://www.pdok.nl/introductie/-/article/hydrografie-netwerk-rws-inspire-geharmoniseerd-.

Renard, K.G., Foster, G.R., Weesies, G.A.,D., McCool, D.K., Yoder, D.C., 1997. Predicting Soil Erosion by Water: A Guide to Conservation Planning with the Revised Universal Soil Loss Equation (RUSLE). Agriculture Handbook 703. U.S. Department of Agriculture, Washington, D.C., USA.

Reynard, E., Coratza, P., Regolini-Bissig, G., 2009. International Conference on Geomorphology. Geomorphosites. Verlag Dr Friedrich Pfeil, München.

Richter, D.D.B., 2007. Humanity's transformation of earth's soil: pedology's new frontier. Soil Science 172, 957–967.

Ronchi, S., Salata, S., Arcidiacono, A., Piroli, E., Montanarella, L., 2019. Policy instruments for soil protection among the EU member states: a comparative analysis. Land Use Policy 82, 763–780.

Schrodt, F., Bailey, J.J., Kissling, W.D., Rijsdijk, K.F., Seijmonsbergen, A.C., van Ree, D., Hjort, J., et al., 2019. To advance sustainable stewardship, we must document not only biodiversity but geodiversity. Proceedings of the National Academy of Sciences 116, 16155–16158. https://www.pnas.org/content/116/33/16155.

Seijmonsbergen, A., de Jong, M.G.G., de Graaff, L.W.S., Anders, N.S., 2014. Geodiversität von Vorarlberg und Liechtenstein/Geodiversity of Vorarlberg and Liechtenstein. Bern, Haupt (Bristol-Schriftenreihe; No. 41).

Seijmonsbergen, A.C., Guldenaar, J., Rijsdijk, K.F., 2018. Exploring Hawaiian long-term insular geodiversity dynamics. Landform Analysis 35, 31–43. https://doi.org/10.12657/landfana.035.007.

Stoorvogel, J.J., Bakkenes, M., Temme, A.J., Batjes, N.H., Ten Brink, B.J., 2017. S-world: a global soil map for

environmental modelling. Land Degradation and Development 28, 22–33. https://doi.org/10.1002/ldr.2656.

Ten Vreegelaar, M., 2015. Developing a Geodiversity Index for the Netherlands. Unpublished BSc thesis. Universiteit van Amsterdam, Amsterdam, 42 pp.

UNESCO, 2015. Statutes of the International Geoscience and Geoparks Programme. Retrieved 8-3-2019 from: https://unesdoc.Unesco.org/ark:/48223/pf0000260675.

UNESCO, 2016. Evaluation Document A - Self Evaluation. Downloaded 1-4-2019. Retrieved from: http://www.Unesco.org/new/en/natural-sciences/environment/earth-sciences/Unesco-global-geoparks/application-process/.

UNESCO, 2019. http://www.unesco.org/new/en/natural-sciences/environment/earth-sciences/unesco-global-geoparks/sustainable-development-goals/.

van Mourik, J.M., Seijmonsbergen, A.C., Slotboom, R.T., Wallinga, J., 2012. Impact of human land use on soils and landforms in cultural landscapes on aeolian sandy substrates (Maashorst, SE-Netherlands). Quaternary International 265, 74–89.

Vanwalleghem, T., Gómez, J.A., Infante Amate, J., González de Molina, M., Vanderlinden, K., Guzmán, G., Laguna, A., Giráldez, J.V., 2017. Impact of historical land use and soil management change on soil erosion and agricultural sustainability during the Anthropocene. Anthropocene 17, 13–29.

Verheijen, F.G.A., Jones, R.J.A., Rickson, R.J., Smith, C.J., 2009. Tolerable versus actual soil erosion rates in Europe. Earth-Science Reviews 1–4, 23–38. https://doi.org/10.1016/j.earscirev.2009.02.003.

Wakatsuki, T., Rasyidin, A., 1992. Rates of weathering and soil formation. Geoderma 52, 251–263.

Warkentin, B.P., 1995. The changing concept of soil quality. Journal of Soil and Water Conservation 3, 226–228.

Wischmeier, W.H., Smith, D.D., 1978. Predicting Rainfall Erosion Losses: A Guide to Conservation Planning. Agriculture Handbook 537. US Department of Agriculture, Washington, DC.

World Heritage Centre, 2019. Operational Guidelines for the Implementation of the World Heritage Convention. UNESCO World Heritage Centre, Paris, France, 177 pp.

Wunder, S., Kaphengst, T., Frelih-Larsen, A., McFarland, K., Albrecht, S., 2018. Implementing SDG Target 15.3 on "Land Degradation Neutrality". Environmental Research of the Federal Ministry for the Environment, Nature Conservation, Building and Nuclear Safety, p. 58. Report No. (UBA-FB) 002587/ENG.

Yaalon, D.H., Yaron, B., 1966. Framework for manmade soil changes: an outline of metapedogenesis. Soil Science 102, 272–277.

Zwoliński, Z., Najwer, A., Giardino, M., 2018. Methods for assessing geodiversity. In: Reynard, E., Brilha, J. (Eds.), Geoheritage. Elsevier, pp. 27–52.

Index

'*Note:* Page numbers followed by "t" indicate tables, "f" indicate figures and "b" indicate boxes.'

S

T

U

This page intentionally left blank

DEVELOPMENTS IN **QUATERNARY SCIENCE 18**
SERIES EDITOR: JAAP J.M. VAN DER MEER

READING THE SOIL ARCHIVES

UNRAVELING THE GEOECOLOGICAL CODE OF PALAEOSOLS AND SEDIMENT CORES

EDITED BY
JAN M. VAN MOURIK AND JAAP J.M. VAN DER MEER

Reading the Soil Archives: Unraveling the Geoecological Code of Palaeosols and Sediment Cores provides details of new techniques for understanding geological history in the form of quantitative pollen analyses, soil micromorphology, radiocarbon dating, optically stimulated luminescence dating and biomarker and phytolith analysis. It presents the genesis of cultural landscapes, based on multiproxy analysis of palaeosols and integration of geomorphological, pedological and archaeological research results, which can be a model for geoecological landscape studies.

Beginning with analytical methods for interpreting soil archives, *Reading the Soil Archives* examines methods for reconstructing the landscape genesis. It presents strengths and weaknesses of the applications, especially in relation to the data from case studies in the Netherlands. The final chapter of the book addresses landscape evolution in different cultural periods. Reading the Soil Archives offers an integrated approach to geoecological knowledge that is valuable to students and professionals in Quaternary science, physical geography, soil science, archaeology, historical geography and land planning and restructuring.

Jan van Mourik has published extensively on the topic of soils as a record of the past, including serving as Guest Editor for the Quaternary International special issue "Soils as a Record of the Past".

Jaap van der Meer previously served as series editor for the Developments in Quaternary Science series. His research areas of interest include glacial dynamics, sedimentology and the Arctic and Antarctic.

ISBN 978-0-444-64108-3
9 780444 641083

ELSEVIER elsevier.com/books-and-journals